Государственное образовательное учреждение
высшего профессионального образования
**«Томский государственный университет
систем управления и радиоэлектроники»**

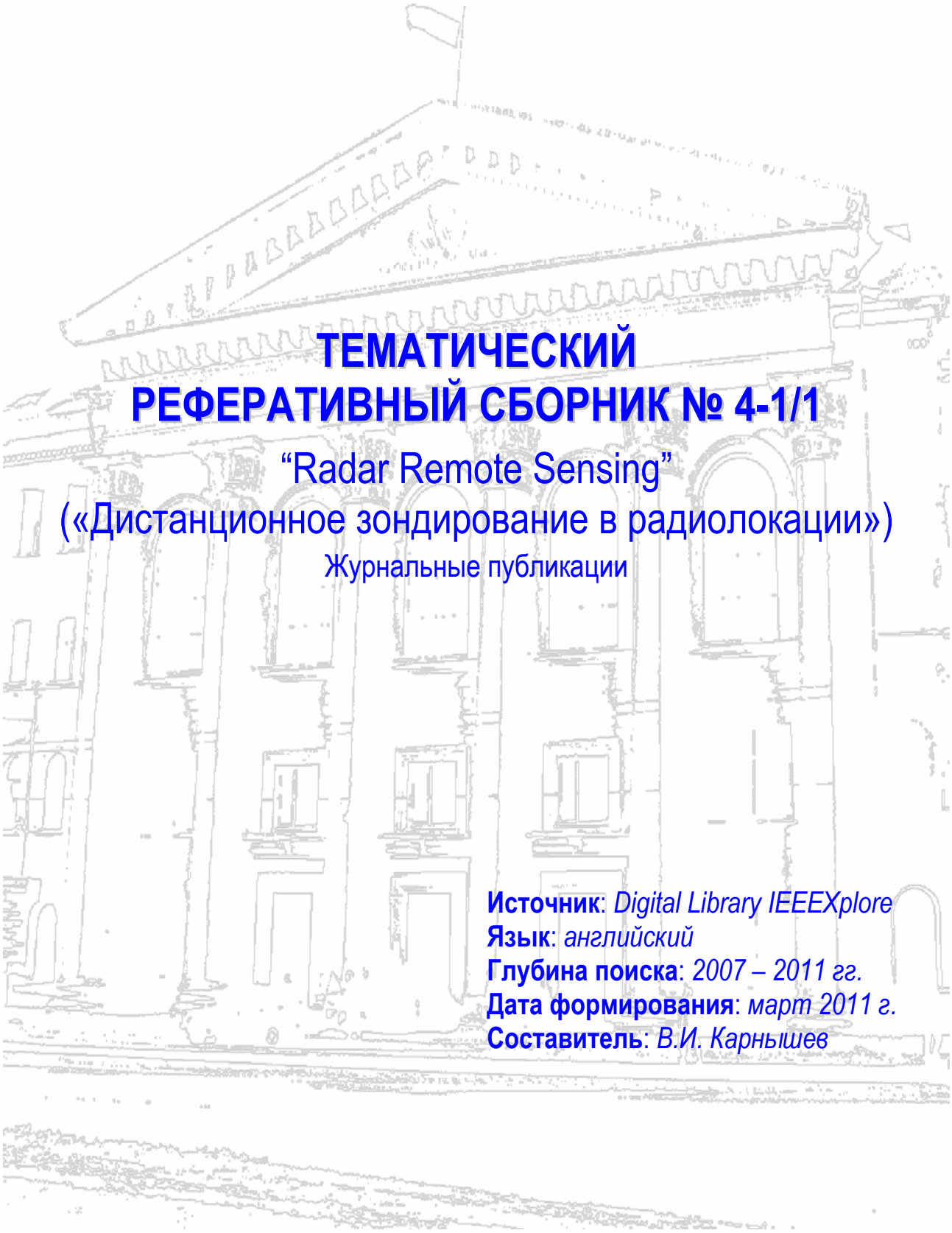

# ТЕМАТИЧЕСКИЙ РЕФЕРАТИВНЫЙ СБОРНИК № 4-1/1

## “Radar Remote Sensing”
## («Дистанционное зондирование в радиолокации»)

Журнальные публикации

**Источник**: *Digital Library IEEEXplore*
**Язык**: *английский*
**Глубина поиска**: *2007 – 2011 гг.*
**Дата формирования**: *март 2011 г.*
**Составитель**: *В.И. Карнышев*

**Томск – 2011**

# ТЕМАТИЧЕСКИЙ РЕФЕРАТИВНЫЙ СБОРНИК № 4-1/1

**"Radar Remote Sensing"**

**(«Дистанционное зондирование в радиолокации»)**

Журнальные публикации

## "Rice Crop Monitoring in South China With RADARSAT-2 Quad-Polarization SAR Data"

This letter presents preliminary results of an attempt to monitor rice crop growth using RADARSAT-2 quad polarization synthetic aperture radar (SAR) data. Three RADARSAT-2 quad-polarization SAR images are collected from transplanting to rice crop harvesting. Ground truth data, such as rice height and biomass, are measured during RADARSAT-2 data acquisition in Hainan Province, South China. The correlation between backscattering coefficient and rice growth parameters is analyzed, and then, a rice field mapping method with quad polarization SAR image is developed. Experiments show that an HV or VH image backscattering coefficient exhibits the best correlation with rice age after transplantation. Furthermore, the HV or VH image is also more suitable for retrieving rice growth parameters, such as rice height and dry biomass, for FQ4 RADARSAT-2 SAR data. The ratio image of HH/VV possesses high separability required to distinguish rice crop from banana, forest, and river. Results indicate that RADARSAT-2 quad polarization SAR data presented enormous potential for monitoring rice crop growth. [J1]

## "Exploiting MIMO SAR Potentialities With Efficient Cross-Track Constellation Configurations for Improved Range Resolution"

In this paper, an innovative technique is presented for synthetic aperture radar (SAR) ground range resolution improvement using multiple transmit and receive platforms with adequate cross-track displacement. Using orthogonal waveforms, which occupy the same bandwidth in the range frequency domain, for the different platforms of the constellation, a multiple-input-multiple-output SAR system is configured. The proposed technique allows one to achieve a maximum theoretical range resolution improvement factor that is significantly greater than the number of operating SAR sensors by jointly exploiting both mono- and bistatic acquisitions. This can be exploited to obtain a ground range resolution that is much higher than the resolution corresponding to the frequency bandwidth transmitted by the single platform. After illustrating the proposed technique and its system requirements, a simulated data set is used to show the effectiveness of the proposed approach. [J2]

## "Application of a Simple Adaptive Estimator for an Atmospheric Doppler Radar"

A simple method for estimating parameters of the Doppler spectrum of atmospheric signals is described. The method is based on an adaptive filter processing that has been widely used in telecommunications but rarely applied in measurements using atmospheric radars. The method has been tested using both synthetic and real data obtained by the radar profiler-Transportable Atmospheric Radar (TARA)-and the weather radar-International Research Centre for Telecommunications and Radar (IRCTR) Drizzle Radar (IDRA)-both developed by IRCTR. The method is compared with the traditional pulse-pair method and fast Fourier transform (FFT)-based methods, as well as with the IRCTR FFT-based method implemented in the TARA and IDRA processing including an additional noise clipping stage. The tests have demonstrated high efficiency of the adaptive filtering estimator under low signal-to-noise ratio conditions. The applicability of adaptive estimations in radar meteorology and the limitations associated with a sample length are discussed. [J3]

## "Approaches for Compression of Super-Resolution WSR-88D Data"

Weather radar products from the U.S. National Weather Service (NWS) are used by the government and private sectors. Very high resolution radar data are increasingly being utilized in real time. However, the bandwidth needed to transmit these data (termed level-II super-resolution data) from the radar to the destination site is a limiting issue. General-purpose compression programs are not tuned to the properties of weather radar data. As the NWS continues to upgrade the capabilities of radar network, the amount of data will continue to increase. As a result, compression is of vital interest to keep down maintenance, storage, and transmission costs. A method for lossless compression of these data on a radial-by-radial basis focusing on the delta (difference) between range bins of super-resolution radar data is presented and is called super-resolution delta compression (SRDC). There are several specialized aspects of SRDC that are based on the properties of weather radar data. SRDC

was tested on level-II reflectivity product data from several S-band Doppler weather radars in the NWS network and was compared with two general-purpose compression programs and a different weather-radar-specific compression approach. The results show that the newly developed SRDC yield is approximately 17% better than the next best approach and approximately 47% better than only preprocessed radials. [J4]

## "Coherence, Polarization, and Statistical Independence in Cloude-Pottier's Radar Polarimetry"

The Cloude-Pottier radar polarimetry paradigm, which is understood as the spectral decomposition theorem of the target coherency matrix plus the classification technique based on the triad of parameters given by entropy, alpha angle, and anisotropy, has become a very well-established methodology for treating high-resolution polarimetric radar images, particularly those obtained with synthetic aperture radar (SAR) sensors. This methodology is revisited here from the standpoint of the coherence and polarization theory and their mutual relationship, in the light of the interest aroused once again after Wolf's article on this subject in 2003. Despite its success in terms of acceptance by the SAR community, the Cloude-Pottier paradigm relies on the arguable assumption that different scattering mechanisms can be separated by diagonalizing the aforementioned coherency matrix and then assigning each corresponding eigenvector to one of the independent scattering mechanisms. Our main statement in this paper is that the coherency matrix illustrates the behavior of the target from the point of view of polarization and not of full coherence, which would justify this assumption, even if only partially. Therefore, it is not rigorous to identify each eigenvector of this decomposition with a distinct scattering mechanism. Cloude and Pottier argue that the eigendecomposition of the coherency matrix outperforms other target decomposition theorems due to its uniqueness. It is also suggested that this very uniqueness, together with the orthogonality of the eigenvectors, supports the injective mapping between scattering mechanisms and eigenvectors that was first assumed based on statistical independence. With the aim of providing a comprehensive overview of the problem, we discuss some important concepts with regard to both field and target coherency matrices. In addition, we revise the concepts of entropy, alpha angle, and anisotropy as defined by the aforementioned authors, which are-- also a central part of this paradigm and which have played an important role in SAR image classification since its introduction. Again, some disagreement is found with the meaning of these parameters as they have been discussed so far. [J5]

## "Ground Moving Targets Imaging Algorithm for Synthetic Aperture Radar"

It is well known that the motion of a target induces range migration, especially for high-resolution synthetic aperture radar (SAR) systems. Ground moving target imaging necessitates the correction of the unknown range migration. To finely refocus a moving target, one must accurately obtain the motion parameters for compensating the target trajectory. However, in practice, these parameters usually cannot be precisely estimated. This paper proposes a new imaging approach for ground moving targets without a priori knowledge of their motion parameters. In the devised method, the azimuth compression function is constructed in range frequency domain, which can eliminate the coupling effect between range and azimuth. Theoretical analysis confirms that the methodology can precisely focus targets without interpolation procedure. The effectiveness of the proposed imaging technique is demonstrated by both simulated and real airborne SAR data. [J6]

## "A Cluster-Analysis-Based Efficient Multibaseline Phase-Unwrapping Algorithm"

Multibaseline phase unwrapping is a critical processing procedure of multibaseline synthetic aperture radar interferometry (InSAR). It has an advantage over single-baseline phase unwrapping in discontinuous-terrain-height estimation. In this paper, the pixels' combination information of multiple InSAR interferograms with different baseline lengths is deeply investigated, and the term ambiguity vector is proposed to represent a pixel's ambiguity number of multiple interferograms. It is also revealed that pixels with the same ambiguity vector have an exclusive pattern among them. A fast cluster-analysis (CA)-based method is proposed for multibaseline phase unwrapping. In this method, all pixels are first clustered into different groups according to their patterns, and then, information of the cluster center is used to unwrap the phases of pixels group by group. Simulation results are shown to verify the effectiveness, efficiency, and noise robustness of CA multibaseline phase-unwrapping method. [J7]

## "Comparison of Ocean-Surface Winds Retrieved From QuikSCAT Scatterometer and Radarsat-1 SAR in Offshore Waters of the U.S. West Coast"

In this letter, we generate a temporal/spatial matchup data set between QuikSCAT scatterometer and RADARSAT-1 synthetic aperture radar (SAR) wind products in offshore waters along the U.S. West Coast. Analysis of the resulting three-year database shows that, in general, the wind products from both sensors have characteristics similar to those reported in the literature. Then, we perform an error analysis in the space domain and find that there is significant discrepancy between the two wind products as the matchup points move closer

to the coast. The root-mean-square error (rmse) and standard deviation (STD) between the two data sets increases markedly for points matched within about 100 km of the coastline. Beyond 100 km, the rmse, STD, and systematic bias become small and stable. In addition, an empirical relationship between QuikSCAT and SAR winds in coastal region is proposed. Thus, the bias and errors should be taken into account if the standard operational QuikSCAT wind products are used for forcing models in the coastal ocean. [J8]

## "Combination of Advanced Inversion Techniques for an Accurate Target Localization via GPR for Demining Applications"

We used advanced ground-penetrating radar (GPR) inversion techniques for detecting landmines in laboratory conditions. The radar data were acquired with a calibrated vector network analyzer combined with an off-ground monostatic horn antenna, thereby setting up a stepped-frequency continuous-wave radar. Major antenna effects and interactions with the soil and targets were filtered out using frequency-dependent complex antenna transfer functions. The proposed strategy first exploits inversion approaches that are able to give an accurate characterization of the antenna-soil interaction and a reliable estimate of the soil permittivity. The outcomes of this first phase are at the basis of the application of a microwave tomographic approach based on the Born approximation to achieve the imaging of the subsurface. The algorithms were applied for imaging three landmines of different sizes and buried at different depths in sand. Although the radar system was off the ground, the results showed that it was possible to reconstruct all mines, including a shallow plastic mine as small as 5.6 cm in diameter. This last mine was invisible in the raw radar data, and the use of common GPR imaging techniques did not lead to satisfactory results. The proposed integrated method shows great promise for shallow subsurface imaging in a demining context, particularly because it automatically provides accurate information on the shallow soil dielectric permittivity. [J9]

## "Edge Enhancement Algorithm Based on the Wavelet Transform for Automatic Edge Detection in SAR Images"

This paper presents a novel technique for automatic edge enhancement and detection in synthetic aperture radar (SAR) images. The characteristics of SAR images justify the importance of an edge enhancement step prior to edge detection. Therefore, this paper presents a robust and unsupervised edge enhancement algorithm based on a combination of wavelet coefficients at different scales. The performance of the method is first tested on simulated images. Then, in order to complete the automatic detection chain, among the different options for the decision stage, the use of geodesic active contour is proposed. The second part of this paper suggests the extraction of the coastline in SAR images as a particular case of edge detection. Hence, after highlighting its practical interest, the technique that is theoretically presented in the first part of this paper is applied to real scenarios. Finally, the chances of its operational capability are assessed. [J10]

## "Focusing of Medium-Earth-Orbit SAR With Advanced Nonlinear Chirp Scaling Algorithm"

The signal processing of the medium-Earth-orbit synthetic aperture radar (SAR) is more challenging than that of the current low-Earth-orbit SAR because the imaging geometry is more complicated, and the range and azimuth variances are more severe. This paper deals with these imaging problems in three aspects. First, an advanced hyperbolic range equation (AHRE) is proposed for the first time, which is more precise for a spaceborne SAR than the conventional hyperbolic range equation (CHRE). Second, the point target spectrum based on the AHRE is analytically derived, which is useful for developing efficient SAR processing algorithms. Third, the well-known nonlinear chirp scaling (NLCS) algorithm is modified according to this new spectrum, and the so-called AHRE-based advanced NLCS (A-NLCS) algorithm is established. The simulation results validate the correctness of our method for L-band SAR systems at altitudes from 1000 to 10000 km with an azimuth resolution around 3 m. It is also shown that the A-NLCS algorithm has better performance than the CHRE-based algorithms in longer integration time cases. Therefore, we recommend the A-NLCS algorithm for a spaceborne SAR with a lower frequency, finer resolution, and higher satellite altitude. [J11]

## "A New Three-Dimensional Imaging Algorithm for Airborne Forward-Looking SAR"

In this letter, a new 3-D imaging algorithm is proposed for forward-looking synthetic aperture radar based on the imaging geometry and the characteristic of the echo signal. The key point of the proposed algorithm is the introduction of the nonlinear frequency modulation scaling in along-track processing to obtain accurate focusing. As the method needs only Fourier transform and multiplication operations, it is computationally efficient. Simulations with point scatterers are used to validate the method. [J12]

## "Unsupervised Extraction of Flood-Induced Backscatter Changes in SAR Data Using Markov Image Modeling on Irregular Graphs"

The near real-time provision of precise information about flood dynamics from synthetic aperture radar (SAR) data is an essential task in disaster management. A novel tile-based parametric thresholding approach under the generalized Gaussian assumption is applied on normalized change index data to automatically solve the three-class change detection problem in large-size images with small class a priori probabilities. The thresholding result is used for the initialization of a hybrid Markov model which integrates scale-dependent and spatiocontextual information into the labeling process by combining hierarchical with noncausal Markov image modeling. Hierarchical maximum a posteriori (HMAP) estimation using the Markov chains in scale, originally developed on quadtrees, is adapted to hierarchical irregular graphs. To reduce the computational effort of the iterative optimization process that is related to noncausal Markov models, a Markov random field (MRF) approach is defined, which is applied on a restricted region of the lowest level of the graph, selected according to the HMAP labeling result. The experiments that were performed on a bitemporal TerraSAR-X StripMap data set from South West England during and after a large-scale flooding in 2007 confirm the effectiveness of the proposed change detection method and show an increased classification accuracy of the hybrid MRF model in comparison to the sole application of the HMAP estimation. Additionally, the impact of the graph structure and the chosen model parameters on the labeling result as well as on the performance is discussed. [J13]

## "A Sparse Aperture MIMO-SAR-Based UWB Imaging System for Concealed Weapon Detection"

A high-resolution imaging system based on the combination of ultrawideband (UWB) transmission, multiple-input-multiple-output (MIMO) array, and synthetic aperture radar (SAR) is suggested and studied. Starting from the resolution requirements, spatial sampling criteria for nonmonochromatic waves are investigated. Exploring the decisive influence of the system's fractional bandwidth (instead of previously claimed aperture sparsity) on the imaging capabilities of sparse aperture arrays, a MIMO linear array is designed based on the principle of effective aperture. For the antenna array, an optimized UWB antenna is designed allowing for distortionless impulse radiation with more than 150% fractional bandwidth. By combining the digital beamforming in the MIMO array with the SAR in the orthogonal direction, a high-resolution 3-D volumetric imaging system with a significantly reduced number of antenna elements is proposed. The proposed imaging system is experimentally verified against the conventional 2-D SAR under different conditions, including a typical concealed-weapon-detection scenario. The imaging results confirm the correctness of the proposed system design and show a strong potential of the MIMO-SAR-based UWB system for security applications. [J14]

## "The Glacier and Land Ice Surface Topography Interferometer: An Airborne Proof-of-Concept Demonstration of High-Precision Ka-Band Single-Pass Elevation Mapping"

As part of the NASA International Polar Year activities, a Ka-band cross-track interferometric synthetic aperture radar (SAR) recently demonstrated high-precision elevation swath mapping capability. This proof-of-concept instrument was achieved by interfacing two Ka-band slotted-waveguide antennas in a cross-track geometry and Ka-band electronics with the Jet Propulsion Laboratory's L-band uninhabited aerial vehicle SAR. Deployed on the NASA Gulfstream III, initial engineering flights in March and April 2009 marked the first airborne demonstration of single-pass cross-track interferometry at Ka-band. Results of a preliminary interferometric assessment indicate height precisions that, for a 3 m Ч 3 m posting, range from 30 cm in the near range to 3 m in the far range and greater than 5 km of swath over the urban areas imaged. The engineering flights were followed by a comprehensive campaign to Greenland in May 2009 for ice-surface topography mapping assessment. Toward that end, coordinated flights with the NASA Wallops Airborne Topographic Mapper lidar were conducted in addition to establishing ground calibration sites at both the Summit Station of the National Science Foundation and the Swiss Camp of the Cooperative Institute for Research in the Environmental Sciences. Comparisons of the radar-derived elevation measurements with both in situ and lidar data are planned for a subsequent paper; however, at this stage, a single data example over rugged ice cover produced a swath up to 7 km with the desired height precision as estimated from interferometric correlation data. While a systematic calibration, including assessment and modeling of biases, due to penetration of the electromagnetic waves into the snow cover has not yet been addressed, these initial results indicate that we will exceed our system requirements. [J15]

## "Exploration of Subsidence Estimation by Persistent Scatterer InSAR on Time Series of High Resolution TerraSAR-X Images"

Ground subsidence is a major concern for land use planning and engineering risk assessment. This paper explores subsidence detection by the persistent scatterer (PS) interferometric synthetic aperture radar (InSAR) technique using the multitemporal high resolution spaceborne SAR images. We first describe the mathematical models and the data reduction procedures of the PS solution. The experiments of subsidence detection are then carried out over the Jinghai County in Tianjin (China) which has been sinking due to overuse of groundwater. The time series of high resolution SAR images collected by the X-band radar sensor onboard the satellite

TerraSAR-X (TSX) are utilized for the PS detection, PS networking and subsidence estimation. The experimental results demonstrate that the high resolution of TSX SAR images can dramatically increase the PSs' density and coverage extent, especially in the built-up areas. Subsidence values can be extracted on the individual objects like buildings, street lamps and manhole covers, and on the linear engineering structures like the Jinghu high-speed railway. The PS InSAR with short radar wavelength (3.1 cm) is quite sensitive to ground displacement in the radar line-of-sight direction, and the derived subsidence measurements are in good agreement with the in situ data taken by optical leveling. [J16]

## "Backscatter 2- Lidar Validation for Atmospheric Differential Absorption Lidar Applications"

A 2-μm backscatter lidar system has been developed by utilizing tunable pulsed laser and infrared phototransistor for the transmitter and the receiver, respectively. To validate the system, the 2-μm atmospheric backscatter profiles were compared to profiles obtained at 1 and 0.5 μm using avalanche photodiode and photomultiplier tube, respectively. Consequently, a methodology is proposed to compare the performance of different lidar systems operating at different wavelengths through various detection technologies. The methodology is based on extracting the system equivalent detectivity and comparing it to that of the detectors, as well as the ideal background detectivity. Besides, the 2-μm system capability for atmospheric CO2temporal profiling using the differential absorption lidar (DIAL) technique was demonstrated. This was achieved by tuning the laser at slightly different wavelengths around the CO2R22 absorption line in the 2.05-μm band. CO2temporal profiles were also compared to in situ measurements. Preliminary results indicated average mixing ratios close to 390 ppm in the atmospheric boundary layer with 3.0% precision. The development of this system is an initial step for developing a high-resolution, high-precision direct-detection atmospheric CO2DIAL system. A successful development of this system would be a valuable tool in obtaining and validating global atmospheric CO2measurements. [J17]

## "Multilevel Local Pattern Histogram for SAR Image Classification"

In this letter, we propose a theoretically and computationally simple feature for synthetic aperture radar (SAR) image classification, the multilevel local pattern histogram (MLPH). The MLPH describes the size distributions of bright, dark, and homogenous patterns appearing in a moving window at various contrasts; these patterns are the elementary properties of SAR image texture. The MLPH is a very powerful descriptor of SAR images because it captures both local and global structural information. Additionally, it is robust to speckle noise. Experiments on a TerraSAR-X data set demonstrate that MLPH significantly outperforms four other widely used features in SAR image classification. [J18]

## "Possibilistic Soil Roughness Identification for Uncertainty Reduction on SAR-Retrieved Soil Moisture"

Soil roughness plays an essential role in the reflection of the incoming radar signal at the soil surface and is, therefore, highly important in the retrieval of the soil moisture information from the backscattered radar signal. However, soil roughness, generally described by means of the root mean square (rms) height and the correlation length, remains difficult to measure correctly and is, furthermore, found to be highly variable. In order to overcome these difficulties, Verhoest et al. suggested the use of possibility distributions to reflect possible values of roughness parameters for a given roughness state of an agricultural field. These distributions were then further used to retrieve the soil moisture information. Nevertheless, as they estimated the possibility distributions by brute force, without taking into account any interactivity between the roughness parameters, rather wide distributions of retrieved soil moisture content were obtained. This paper first tries to independently estimate the possibility distributions for both roughness parameters on the basis of a synthetically generated roughness data set. Next, the interactivity between the rms height and the correlation length is taken into account through the identification of a joint possibility distribution by means of a possibilistic clustering algorithm. When applied to actual synthetic aperture radar data, the results show that a narrower, i.e., more specific, possibility distribution of the soil moisture content is obtained when the possibilistic retrieval procedure is performed based on the joint possibility distributions. [J19]

## "Efficient Electromagnetic Imaging of an Artificial Infiltration Process in the Vadose Zone Using Cross-Borehole Radar"

Cross-borehole ground-penetrating radar (GPR) has been widely used to characterize the shallow subsurface and to monitor hydrogeologic processes. To investigate an infiltration process in the vadose zone, an artificial groundwater infiltration test was conducted in Nagaoka, Japan. Time-lapse cross-borehole GPR data were collected using zero-offset profiling (ZOP) mode. The infiltration process was observed as a variation of GPR traveltimes, which can be transformed into a dielectric constant, and further converted to volumetric water

content. A standard ZOP analysis, for which all first arrivals are assumed to be direct waves, results in an underestimation of the dielectric constant because of the existence of critically refracted waves. This letter presents an efficient algorithm using the maximum first-cycle amplitude to approximately determine the traveltime of direct arrival, deriving a dielectric constant model more accurately than the standard ZOP analysis from ZOP data. Tests on synthetic and real field data show that the proposed approach is effective in building accurate water content profile without iterative calculations as in the standard ZOP analysis. [J20]

## "On the Generation of Late ERS Deformation Time Series Through Small Doppler and Baseline Subsets Differential SAR Interferograms"

In this letter, we investigate the potential of the small baseline subset (SBAS) differential synthetic aperture radar interferometry (DInSAR) technique to produce consistent deformation time series by using data sets of SAR images with high Doppler centroid (DC) frequencies. To cope with this issue properly, we exploited an archive of SAR scenes acquired by the European Remote Sensing 2 (ERS-2) sensor after the February 2000 three-gyroscope navigation mode failure. Our approach is oriented toward the long-term investigation of large-scale displacements with low spatial resolution (about 100 Ч 100 m) by processing sets of SAR images without discarding scenes depending on their DC values. Our analysis involves a set of descending SAR data frames from 1992 to 2007 relevant to the Napoli (Italy) bay area. Comparison with contemporaneous Global Positioning System measurements clearly confirms the effectiveness of the proposed approach. [J21]

## "Physical Limitations on Detecting Tunnels Using Underground-Focusing Spotlight Synthetic Aperture Radar"

This paper examines the feasibility of underground-focusing spotlight synthetic aperture radar (UF-SL-SAR) systems for tunnel detection applications. A general formulation is reviewed for generating UF-SL-SAR imaging by using multiple frequencies across a wide band and by focusing in space to subsurface points using well-known ray refraction at the nominal ground surface. A full-wave finite-difference frequency-domain model is used to consider wave propagation in realistic soil with loss- and frequency-dependent dielectric constant and a randomly rough ground surface, both of which serve to obscure and distort the returned tunnel target signal. Imaging results are presented for two representative soil scenarios: dry sand and moist clay loam. Considering the ground surface ray refraction for focusing greatly improves the SAR image relative to conventional SAR focusing at the ground surface. Using UF-SL-SAR, a small shallow tunnel is reasonably imaged for the sand case, despite the roughness of the ground interface. However, for higher conductivity moist clay loam, the clutter from the rough surface overwhelms the significantly attenuated target signal, which must propagate through the lossy intervening soil. It is demonstrated that, despite ideal focusing, the tunnel is successfully imaged only for the sand case. [J22]

## "Building Detection From One Orthophoto and High-Resolution InSAR Data Using Conditional Random Fields"

Today's airborne SAR sensors provide geometric resolution in the order well below half a meter. Many features of urban objects become visible in such data. However, layover and occlusion issues inevitably arise in urban areas complicating automated object detection. In order to support interpretation, SAR data may be analyzed using complementary information from maps or optical imagery. In this paper, an approach for building detection in urban areas based on object features extracted from high-resolution interferometric SAR (InSAR) data and one orthophoto is presented. Features describing local evidence as well as context information are used. Buildings are detected by classification of those feature vectors within a Conditional Random Field (CRF) framework. Although as graphical model similar to Markov Random Fields (MRF), CRFs have the advantage of incorporating global context information, of relaxing the conditional independence assumption between features, and of a more general integration of observations. We show that, first, CRFs perform well in comparison to Maximum Likelihood classifiers and MRFs. Second, the combined use of optical and InSAR features may improve detection results. [J23]

## "Three-Dimensional SAR Focusing From Multipass Signals Using Compressive Sampling"

Three-dimensional synthetic aperture radar (SAR) image formation provides the scene reflectivity estimation along azimuth, range, and elevation coordinates. It is based on multipass SAR data obtained usually by nonuniformly spaced acquisition orbits. A common 3-D SAR focusing approach is Fourier-based SAR tomography, but this technique brings about image quality problems because of the low number of acquisitions and their not regular spacing. Moreover, attained resolution in elevation is limited by the overall acquisitions baseline extent. In this paper, a novel 3-D SAR data imaging based on Compressive Sampling theory is presented. It is shown that since the image to be focused has usually a sparse representation along the

elevation direction (i.e., only few scatterers with different elevation are present in the same range-azimuth resolution cell), it suffices to have a small number of measurements to construct the 3-D image. Furthermore, the method allows super-resolution imaging, overcoming the limitation imposed by the overall baseline span. Tomographic imaging is performed by solving an optimization problem which enforces sparsity through ℓ1-norm minimization. Numerical results on simulated and real data validate the method and have been compared with the truncated singular value decomposition technique. [J24]

## "An Interpolated Phase Adjustment by Contrast Enhancement Algorithm for SAR"

Phase adjustment by contrast enhancement (PACE) is an autofocus algorithm that is capable of performance that is unattainable by conventional techniques. It is a nonparametric method that requires no constraints on the type of phase error to be measured. The algorithm does not require special data culling techniques or the presence of isolated scatterers. However, the drawback of PACE algorithm is that the number of estimated variables is very large; it leads to a long computational time. The azimuth sampling frequency is commonly much bigger than the bandwidth of phase error in SAR image so that we can estimate part of the phase error variables and then obtain the whole variables by interpolation; this induces the interpolated phase adjustment by contrast enhancement (IPACE) algorithm. The IPACE algorithm can remarkably reduce the computational time while maintaining the accuracy. This letter has derived the detailed processing of IPACE, and the results of the experiments using real SAR data are presented to show the validity of the proposed algorithm. [J25]

## "Polarimetric Decomposition Over Glacier Ice Using Long-Wavelength Airborne PolSAR"

In recent years, there has been increased interest in using synthetic aperture radar (SAR) to study and monitor glaciers and ice sheets for glaciological and climate change research. However, due to the medium's complexity, SAR backscattering from ice remains poorly understood, including the relative importance of scattering from surface and volume layers and also dependences on frequency and glacier zone. Extreme weather conditions can result in quickly changing surface conditions influencing backscatter signatures while leaving the underlying volume of interest unchanged. Surface and volume components must thus be separated in order to infer information regarding the properties of the ice volume. This paper describes a three-component scattering model to decompose polarimetric SAR (PolSAR) images of glacier ice. Total backscatter is modeled as the incoherent summation of surface, volume, and sastrugi (wind-induced feature) components. The proposed model adapts and extends the Freeman and Durden decomposition for an ice volume scenario in which the volume is a dielectric medium. Forms of the model for both random and oriented volumes are considered, and a new oriented sastrugi component is introduced which is able to explain backscatter behavior between different winter scenes. Validation is performed with airborne PolSAR data at L- and P-band collected using the E-SAR system of the German Aerospace Center over the Austfonna ice cap in Svalbard, Norway, as part of the ICESAR campaign. [J26]

## "Scattering and Doppler Spectral Analysis for Two-Dimensional Linear and Nonlinear Sea Surfaces"

Two-dimensional linear and second-order Creamer [Creamer (2)] nonlinear sea-surface models are combined with the second-order small-slope approximation method to comparatively study the electromagnetic scattering and the Doppler spectral characteristics from sea surfaces. Due to nonlinear hydrodynamics, the bistatic normalized radar cross section (NRCS) calculated from Creamer (2) surfaces is slightly larger than its linear surface counterpart for scattering angles departing from the specular direction, and the Creamer (2) surface backscattering coefficient increases as well for wind direction angles around upwind and downwind, whereas, for the crosswind direction, it is interesting to note that the observations are contrary. However, as was pointed out by Toporkov in a 1-D surface case, the effect of the nonlinear surface model on the average NRCS is minute. In particular, the Doppler spectra of the backscattered echoes are compared for the linear and Creamer (2) surfaces at various incident angles. It is seen, as expected, that the Doppler shifts and spectral widths of 2-D Creamer (2) surfaces exhibit different features compared with those of the linear surfaces, agreeing with the 1-D cases. However, for larger incident angles, the Doppler spectral broadening for Creamer (2) surfaces is not as severe as was reported in previous 1-D studies that used full Creamer model. The reason for this discrepancy appears to be the reduced nature of the Creamer (2) approximation. Moreover, studies of the Doppler characteristics for different wind directions demonstrate that nonlinear effects become weaker as the wind direction varies from upwind to crosswind. [J27]

## "SPEC Method-A Fine Coregistration Method for SAR Interferometry"

There is increasing demand for landscape acquisition using interferometric synthetic aperture radar for frequent Earth observation. Making an accurate digital elevation model (DEM) from an interferogram is often seriously

affected by a mass of singular points (SPs) included in the interferogram. The origin of a type of SPs lies in inaccurate coregistration in making the interferogram. However, there have not been any method more effective than affine transformation based on cross correlation. Numerous research works have aimed at how to process the SPs resulting in the coregistration. In this paper, contrarily, we propose an additional method of local and nonlinear coregistration which employs the number of SPs as the evaluation criterion. This method provides us with an interferogram to generate a more accurate DEM. Experiments demonstrate that, with the proposed method, we can obtain a DEM having higher signal-to-noise ratios. [J28]

## "An Improved Scheme for Target Discrimination in High-Resolution SAR Images"

To design a highly automatic and practical method for target discrimination in synthetic aperture radar images, we propose in this paper an improved scheme consisting of the framework and algorithms for target discrimination. Our main contribution in this scheme comprises four aspects. First, an integrative frame sequentially combining the algorithm based on feature extraction and the knowledge of target group has been presented. Second, three new features for target discrimination have been introduced. Third, a genetic algorithm-based feature-selection algorithm has been presented. The results show that this algorithm can evaluate the goodness-of-feature better. Finally, to improve the accuracy of the discriminator, we have designed a weighted quadratic distance discriminator, which has been observed to improve the performance of target discrimination. We have analyzed the performance of the proposed scheme comprehensively and specifically using some measured data, and carried out comparisons of the existing algorithms. The results show that the proposed scheme could improve the application ability in target discrimination. [J29]

## "A Novel Radar Waveform for Monostatic Ionosonde"

Monostatic radar, whether using interpulse or intrapulse coded pulse trains, will suffer from the blind zones caused by eclipsing. This letter proposes a novel biphase interpulse coded radar waveform using diverse Pulse Repetition Intervals (PRIs) instead of a consistent PRI within each coherent processing interval (CPI). This waveform can achieve long unambiguous range, high-range resolution and high Doppler resolution without blind zones, and is specially suitable for a monostatic ionosonde. [J30]

## "X-, C-, and L-Band DInSAR Investigation of the April 6, 2009, Abruzzi Earthquake"

This letter compares the coseismic deformation maps obtained from different synthetic aperture radar (SAR) sensors using the well-known differential SAR interferometry technique. In particular, four deformation maps have been obtained from X-, C-, and L-band SAR sensors onboard COSMO-SkyMed, Envisat, and ALOS satellite missions correspondingly. The test case is the April 6,2009, earthquake (Mw= 6.3). This seismic event struck a densely populated region of the Apennines and was felt all over Central Italy. The SAR data set is rather inhomogeneous, since it includes interferograms with three different wavelengths, four acquisition geometries, different spatial resolutions, variable temporal and spatial baselines, and differently emphasized signal noise. However, we find that the detected displacements are highly comparable. The outcome of this work is that, even though such differences have an impact on the properties of the interferograms, the displacements can be measured with an overall discrepancy of about half the value of the shortest wavelength (COSMO-SkyMed) data set. [J31]

## "Fast Raw-Signal Simulation of Extended Scenes for Missile-Borne SAR With Constant Acceleration"

Fast raw-signal simulation is of considerable value for missile-borne synthetic aperture radar (SAR) algorithm development. On the basis of the two-dimensional (2-D) Fourier simulation method for stripmap SAR, we present a fast echo simulation method suitable for missile-borne SAR diving with constant acceleration. The analytical expression for the 2-D signal spectrum is derived and then converted to a stripmap one. Simulation results for a point target and a real scene demonstrate its validity and effectiveness. [J32]

## "Mapping Three-Dimensional Surface Deformation by Combining Multiple-Aperture Interferometry and Conventional Interferometry: Application to the June 2007 Eruption of Kilauea Volcano, Hawaii"

Surface deformation caused by an intrusion and small eruption during June 17-19, 2007, along the East Rift Zone of Kilauea Volcano, Hawaii, was three-dimensionally reconstructed from radar interferograms acquired by the Advanced Land Observing Satellite (ALOS) phased-array type L-band synthetic aperture radar (SAR) (PALSAR) instrument. To retrieve the 3-D surface deformation, a method that combines multiple-aperture interferometry (MAI) and conventional interferometric SAR (InSAR) techniques was applied to one ascending and

one descending ALOS PALSAR interferometric pair. The maximum displacements as a result of the intrusion and eruption are about 0.8, 2, and 0.7 m in the east, north, and up components, respectively. The radar-measured 3-D surface deformation agrees with GPS data from 24 sites on the volcano, and the root-mean-square errors in the east, north, and up components of the displacement are 1.6, 3.6, and 2.1 cm, respectively. Since a horizontal deformation of more than 1 m was dominantly in the north-northwest-south-southeast direction, a significant improvement of the north-south component measurement was achieved by the inclusion of MAI measurements that can reach a standard deviation of 3.6 cm. A 3-D deformation reconstruction through the combination of conventional InSAR and MAI will allow for better modeling, and hence, a more comprehensive understanding, of the source geometry associated with volcanic, seismic, and other processes that are manifested by surface deformation. [J33]

## "Robust Extraction of Urban Area Extents in HR and VHR SAR Images"

This work is devoted to analyze the performance and adapt the parameters requested for the operational use of a methodology aimed at urban extent extraction. The procedure, initially proposed in a reduced version in a previous paper, has been expanded and improved to make it useful with different HR and VHR radar sensors, and extensive comparison of the results in many different parts of the world have been considered. [J34]

## "Ocean Wave Integral Parameter Measurements Using Envisat ASAR Wave Mode Data"

An empirical algorithm to retrieve integral ocean wave parameters such as significant wave height (SWH), mean wave period, and wave height of waves with period larger than 12 s (H12) from synthetic aperture radar (SAR) images over sea surface is presented. The algorithm is an extension to the Envisat Advanced SAR (ASAR) wave mode data based on the CWAVE approach developed for ERS-2 SAR wave mode data and is thus called CWAVE_ENV (CWAVE for Envisat). Calibrated ASAR images are used as the only source of input without needing prior information from an ocean wave model (WAM) as the standard algorithms used in weather centers. This algorithm makes SAR an independent instrument measuring integrated wave parameters like SWH and mean wave period to altimeter quality. A global data set of 25 000 pairs of ASAR wave mode images and collocated reanalysis WAM results from the European Centre for Medium-Range Weather Forecasts (ECMWF) is used to tune CWAVE_ENV model coefficients. Validation conducted by comparing the retrieved SWH to in situ buoy measurements shows a scatter index of 0.24 and 0.16 when compared to the ECMWF reanalysis WAM. Two case studies are presented to evaluate the performance of the CWAVE_ENV algorithm for high sea state. A North Atlantic storm during which SWH is above 18 m as observed by SAR and Radar Altimeter simultaneously is analyzed. For an extreme swell case that occurred in the Indian Ocean, the potential of using SWH measurements from ASAR wave mode data derived by the CWAVE_ENV algorithm is demonstrated. [J35]

## "Seismic Source Quantitative Parameters Retrieval From InSAR Data and Neural Networks"

The basic idea of this paper relies on the concurrent exploitation of the capabilities of neural networks (NNs) and SAR interferometry (InSAR) for the characterization of a seismic source and the estimation of its geometric parameters. When a moderate-to-strong earthquake occurs, we can apply the InSAR technique to compute a differential interferogram. The earthquake is generated by an active seismogenic fault having its own specific geometry. The corresponding differential interferogram contains, in principle, information concerning the geometry of the seismic source that the earthquake comes from. To perform the inversion operation, a novel approach based on NNs is considered. This requires the generation of a statistically significant number of synthetic interferograms necessary for the network training phase. Each of them corresponds to a different combination of fault geometric parameters. After the training, the network is ready to perform, in real time, the inversion on new differential interferograms. This paper illustrates such a methodology and its validation on a set of experimental data. [J36]

## "Land Geophysical Parameters Retrieval Using the Interference Pattern GNSS-R Technique"

In the past years, the scientific community has placed a special interest in remotely sensing soil moisture and vegetation parameters. Radiometry and radar techniques have been widely used for years. Global Navigation Satellite Systems opportunity signals Reflected (GNSS-R) over the earth's surface are younger, but they have already shown their potential to perform these observations. This paper presents a GNSS-R technique, based on Global Positioning System (GPS) measurements, that allows the retrieval of several geophysical parameters from land surfaces. This technique measures the power of the interference signal between the direct GPS signal and the reflected one after scattering over the land, so it is called Interference Pattern Technique (IPT). This paper presents the results obtained after applying the IPT for topography, soil moisture, and vegetation height retrievals over vegetation-covered soils. [J37]

## "An Internal Calibration Scheme for Polarimetric Synthetic Aperture Radar System"

Two important aspects of internal calibration of polarimetric synthetic aperture radar are discussed, i.e., system gain calibration and individual transmit/receive module (TRM) calibration. System gain variation is measured, utilizing the internal calibration loop. A dual-channel TRM gain and phase calibration is carried out using orthogonal phase coding, where a signal of individual TRM is phase encoded according to a set of orthogonal codes in order to be separated from the composite calibration signal of all TRMs. Calibration results are developed both theoretically and through simulation in the case of TRM failure. Error introduced by phase-shifter toggling inaccuracy is discussed. A cross talk model is used to investigate the effect of imperfect isolation between the two polarization channels of each TRM on the calibration error. [J38]

## "Time-Series InSAR Applications Over Urban Areas in China"

In this study, we present the results achieved within the Dragon project, a cooperation program between the European Space Agency (ESA) and the National Remote Sensing Center of China (NRSCC), about monitoring subsidences and landslides in urban areas, analyzing cities growth and measuring the deformation of big man-made structures. Among the processed areas, we report here the main results we obtained in the test sites of Shanghai, Tianjin, Badong, and Three Gorges Dam. The techniques that have been used to process the data are original SAR interferometry (InSAR), Permanent Scatterers (PS-InSAR), Quasi-PS InSAR (QPS-InSAR), and a combination of coherent-uncoherent analysis. The results show that time-series InSAR techniques allow us to extract ground information with high spatial density and thus help us understanding the impact of urban development on terrain movements. [J39]

## "Semiempirical Calibration of the Integral Equation Model for SAR Data in C-Band and Cross Polarization Using Radar Images and Field Measurements"

The estimation of surface soil parameters (moisture and roughness) from synthetic aperture radar (SAR) images requires the use of well-calibrated backscattering models. The objective of this letter is to extend the semiempirical calibration of the backscattering integral equation model (IEM) initially proposed by Baghdadi for HH and VV polarizations to HV polarization. The approach consisted in replacing the measured correlation length by a fitting/calibration parameter so that model simulations would closely agree with radar measurements. This calibration in C-band covers radar configurations with incidence angles between 24 and 45.8. Good agreement was found between the backscattering coefficient provided by the SAR and that simulated by the calibrated version of the IEM. [J40]

## "The Effect of Orientation Angle Compensation on Coherency Matrix and Polarimetric Target Decompositions"

The polarization orientation angle (OA) of the scattering media affects the polarimetric radar signatures. This paper investigates the effects of orientation compensation on the coherency matrix and the scattering-model-based decompositions by Freeman-Durden and Yamaguchi et al. The Cloude and Pottier decomposition is excluded, because entropy, anisotropy, and alpha angle are roll invariant. We will show that, after orientation compensation, the volume scattering power is consistently decreased, while the double-bounce power has increased. The surface scattering power is relatively unchanged, and the helicity power is roll invariant. All of these characteristics can be explained by the compensation effect on the nine elements of the coherency matrix. In particular, after compensation, the real part of the (HH-VV) · HV* correlation reduces to zero, the intensity of cross-pol |HV| always reduces, and |HH-VV| always increases. This analysis also reveals that the common perception that OA compensation would make a reflection asymmetrical medium completely reflection symmetric is incorrect and that, contrary to the general perception, the four-component decomposition does not use the complete information of the coherency matrix. Only six quantities are included-one more than the Freeman-Durden decomposition, which explicitly assumes reflection symmetry. [J41]

## "Global CALIPSO Observations of Aerosol Changes Near Clouds"

Several recent studies have found that clouds are surrounded by a transition zone of rapidly changing aerosol optical properties and particle size. Characterizing this transition zone is important for better understanding aerosol-cloud interactions and aerosol radiative effects, and also for improving satellite retrievals of aerosol properties. This letter presents a statistical analysis of a monthlong global data set of Cloud-Aerosol Lidar and Infrared Pathfinder Satellite Observation (CALIPSO) lidar observations over oceans. The results show that the transition zone is ubiquitous over all oceans and extends up to 15 km away from clouds. They also show that near-cloud enhancements in backscatter and particle size are strongest at low altitudes, slightly below the top of the nearest clouds. Also, the enhancements are similar near illuminated and shadowy cloud sides, which confirms that the asymmetry of Moderate Resolution Imaging Spectroradiometer reflectances found in an earlier

study comes from 3-D radiative processes and not from differences in aerosol properties. Finally, the effects of CALIPSO aerosol detection and cloud identification uncertainties are discussed. The findings underline the importance of accounting for the transition zone to avoid potential biases in studies of satellite aerosol products, aerosol-cloud interactions, and aerosol direct radiative effects. [J42]

## "Comparison of Backscattering Models at L-Band for Growing Corn"

The impact of incoherent and coherent formulations on estimates of terrain backscatter (σterrain0) at L-band for a growing season of corn is examined. The average root mean square difference (RMSD) between the two formulations over the growing season ranged between 3-4 dB, with higher RMSDs at HH polarization (pol), indicating the presence of coherent effects. In the incoherent model, the direct scattering from stems was the primary mechanism, while in the coherent formulation, the interactions between the stems and soil were the primary mechanisms due to the coherent effects. Both incoherent and coherent formulations estimated equally high sensitivities of σterrain0to soil moisture (SM) during early stage under low vegetation conditions. During the early and mid stages, the σterrain0estimated by both formulations exhibited higher sensitivities during dry conditions than wet conditions. In contrast, during the reproductive stage, the σterrain0by the incoherent formulation was more sensitive to the SM at wet conditions than at dry conditions. Based upon the ALOS/SMAP accuracy for σterrain0, the incoherent formulation exhibited the highest sensitivity during the early stage with detection of SM changes as low as 2 vol% for dry condition, whereas the coherent formulation exhibited the highest sensitivity during the mid stage with detection of SM changes as low as 2.5 vol%. The results of this study suggest that the coherent effects should be considered for defining accuracy of SM estimation algorithms for corn at L-band. [J43]

## "A New Improved Step Transform Algorithm for Highly Squint SAR Imaging"

In this letter, a new improved step transform (IST) algorithm is developed for highly squint stripmap synthetic aperture radar (SAR) imaging. Different from the previous step transform algorithms, such as the time-varying step transform algorithm, the new algorithm compensates the cubic phase term and the phase term caused by the varying chirp rate using estimation of the target position focused in the coarse-resolution fast Fourier transform, and these undesirable phase terms can be compensated more appropriately. The algorithm can process SAR imaging under a squint angle of up to 75° in X-band. Simulation results show that the IST algorithm is effective. [J44]

## "Enhanced Dictionary-Based SAR Amplitude Distribution Estimation and Its Validation With Very High-Resolution Data"

In this letter, we address the problem of estimating the amplitude probability density function (pdf) of single-channel synthetic aperture radar (SAR) images. A novel flexible method is developed to solve this problem, extending the recently proposed dictionary-based stochastic expectation maximization approach (developed for a medium-resolution SAR) to very high-resolution (VHR) satellite imagery, and enhanced by introduction of a novel procedure for estimating the number of mixture components, that permits to reduce appreciably its computational complexity. The specific interest is the estimation of heterogeneous statistics, and the developed method is validated in the case of the VHR SAR imagery, acquired by the last-generation satellite SAR systems, TerraSAR-X and COSMO-SkyMed. This VHR imagery allows the appreciation of various ground materials resulting in highly mixed distributions, thus posing a difficult estimation problem that has not been addressed so far. We also conduct an experimental study of the extended dictionary of state-of-the-art SAR-specific pdf models and consider the dictionary refinements. [J45]

## "Classification of Tropical Vegetation Using Multifrequency Partial SAR Polarimetry"

This letter presents a case study addressing the comparison between different synthetic aperture radar (SAR) partial polarimetric options for tropical-vegetation cartography. These options include compact polarization (CP), dual polarization (DP), and alternating polarization (AP). They are all derived from fully polarimetric (FP) SAR data acquired by the airborne SAR (AIRSAR) sensor over the French Polynesian Tubuai Island. The classification approach is based on the support vector machine algorithm and is further validated by several ground surveys. For a single frequency band, FP data give significantly better results than any other partial polarimetric configuration. Among the partial polarimetric architectures, the CP mode performs best. In addition, the DP mode shows better performance than the AP mode, highlighting the value of the polarimetric differential phase. The combination of different frequency bands (P-, L-, and C-bands) holds the most significant improvement: The multifrequency diversity adds generally more information than the multipolarization diversity. A noticeable result is the major contribution of the C-band at VV polarization (the only polarization available at C-band with the AIRSAR data set used in this letter) to the classification performance, due to its ability to

discriminate between Pinus and Falcata. [J46]

## "Using Doppler Spectra to Separate Hydrometeor Populations and Analyze Ice Precipitation in Multilayered Mixed-Phase Clouds"

Multimodality of cloud radar Doppler spectra is used to partition cloud particle phases and separate distinct ice populations in the radar sample volume, thereby facilitating the analysis of individual ice showers in multilayered mixed-phase clouds. A 35-GHz cloud radar located at Barrow, Alaska, during the Mixed-Phase Arctic Cloud Experiment collected the Doppler spectra. Data from a pair of collocated depolarization lidars confirmed the presence of two liquid cloud layers reported in this letter. Both of these cloud layers were embedded in ice precipitation yet maintained their liquid. The spectral separation of the ice precipitation yielded two distinct ice populations: the ice initiated within the two liquid cloud layers and the ice precipitation formed in the higher cloud layers. The comparisons of ice fall velocity-versus-radar reflectivity relationships derived for distinct showers reveal that a single relationship does not properly represent the ice showers during this period. [J47]

## "Impact of Soil Structure on Microwave Volume Scattering Evaluated by a Two-Dimensional Numerical Model"

Soil volumetric structure is an important parameter for tillage operation. The aim of this paper is to assess whether volume characteristics can be inferred from radar measurements. A 2-D numerical model (the 2DSCAT model) was developed based on a numerical solver using a time-domain finite-element method to solve Maxwell's equations. Perfectly matched layers were implemented as well as a near- to far-field transformation. A focused incident beam was generated by adapting the boundary conditions. To represent the soil structure, a simulator was developed describing the soil as biphasic media (fine earth and clods). Clods were represented by randomly deformed ellipses, with randomly determined dimensions, locations, and orientations. The model performed successfully, as evaluated against exact analytical solutions available for an infinite perfectly conducting cylinder and the reflection of flat semi-infinite media. The model was then evaluated against measurements made by an X-band FM continuous-wave radar on a box filled with dry clods of different sizes. The effect of the clod size on the backscattering power was very well reproduced, showing the potential of using a 2-D numerical model to understand microwave-backscattering patterns from cloddy soils. Analysis of the volume scattering shows that this phenomenon can be mostly hidden in the scatter diagram by surface scattering when the latter occurred. However, the volume scattering gives a stronger residual signal in time because of propagation through the medium. Thus, time studies of the scattering signal provide further information about volume heterogeneities. [J48]

## "DOMUS: DOppler MUltiple-Scattering Simulator"

Multiple scattering (MS) strongly affects CloudSat's W-band cloud-profiling radar (CPR) reflectivity when the satellite is overpassing moderate and heavy precipitation systems. With the upcoming deployment of W-band Doppler radars in space-Earth Clouds, Aerosols, and Radiation Explorer's CPR in primis-and the goal of retrieving vertical motions within convective systems, there is an urgent need to assess the impact of MS onto the Doppler signatures. A Monte Carlo code capable of simulating the reflectivity enhancement due to higher orders of scattering has been extended to include the Doppler effects. This paper presents the main guidelines for the inclusion of the Doppler analysis into the Monte Carlo scheme. To our knowledge, this simulator is the first one capable of simulating realistic Doppler signals in the presence of MS. The case studies are first presented in uniform beam-filling conditions for the profiles extracted from a cloud-resolving model simulation of deep convection (i.e., 1-D profiles are used to characterize a stratified atmosphere). The simulations demonstrate that, at ranges where MS contributions affect the overall radar signal, two main features appear as the following: 1) The Doppler spectrum tends to broaden with increasing MS enhancement, adding up to the single-scattering (SS) Doppler fading due to the satellite motion; and 2) the mean Doppler of the backscattered signal departs from the mean Doppler determined by the combined effect of the vertical-wind and hydrometeor-terminal velocities at all range bins below the altitude where the MS contribution significantly overcomes the SS. The simulator can be run in nonuniform-beam-filling conditions as well (i.e., a 3-D field is used to characterize the atmosphere at scales smaller than the radar resolution). With its cutting-edge capabilities, it provides a unique tool for the evaluation of the performances of the upcoming high-frequency spaceborne Doppler radars. [J49]

## "Validation of Microwave Tomographic Inverse Scattering Approach via Through-the-Wall Experiments in Semicontrolled Conditions"

This letter presents experimental verification of a tomographic through-the-wall radar imaging technique by exploiting real data measurements of 3-D scenes carried out under semicontrolled conditions. More specifically,

the 3-D reconstructions are obtained by a linear inverse scattering algorithm and a sliced approach. This strategy ensures fast data processing and allows quick investigation of a very large spatial region. The effectiveness of the imaging scheme is shown for both a single-target scene and a scene with multiple targets at different depths. [J50]

## "Electromagnetic Modeling of Breaking Waves at Low Grazing Angles With Adaptive Higher Order Hierarchical Legendre Basis Functions"

At low grazing angles (LGA), sophisticated electromagnetic scattering of sea surfaces may give rise to complicated surface-current distribution. Therefore, for the multilevel fast multipole algorithm (MLFMA) with the Rao-Wilton-Glisson basis function, the sea scatterer must be meshed fine enough to ensure the precision of the scattering at LGA, which brings huge computational costs. The higher order hierarchical Legendre vector basis functions can bring a great reduction of the unknowns and sparsification of the impedance matrix. The MLFMA with higher order hierarchical Legendre basis functions is applied in the electromagnetic-scattering approach of 3-D breaking water wave crests at LGA for the first time. In addition, an adaptive-order technique is also introduced for the first time in describing the currents which can achieve accurate results and maximally reduce the computational costs from some case analysis. It has been investigated in analyzing the vertically (VV) and horizontally (HH) polarized scattering of profiles of the LONGTANK breaking waves. "Sea-spike" phenomenon has been demonstrated at LGA. [J51]

## "Automatic Urban Water-Body Detection and Segmentation From Sparse ALSM Data via Spatially Constrained Model-Driven Clustering"

Identifying hydrological features is important for urban planning and disaster assessment. Data spatial resolution poses challenges in automatic processing. In this letter, we present a novel spatially constrained model-driven clustering method that automatically detects and delineates water bodies in an urban area using airborne laser swath mapping (ALSM) data and imagery. Our method analyzes the modality of the sparseness histogram to decide the existence of water body, followed by clustering. Using the sparseness, clusters are decided by selecting candidate sites. In the iteration of clustering process, new sites are recruited within a close spatial vicinity of the boundary sites. Experiments were conducted using data sets from the city of New Orleans. Our method demonstrated superior robustness regardless of the density of ALSM sample and data discrepancy and very competitive accuracy in comparison with manual tracing, with an overall accuracy above 98%. [J52]

## "Radar Imaging Simulation for Urban Structures"

With the recent advent of very high resolution (VHR) spaceborne synthetic aperture radar (SAR) sensors such as TerraSAR-X and COSMO-SkyMed, the potential to use SAR simulators is increasing. In this letter, we propose a novel radar imaging simulator that is relatively simple to implement and that finds a balance between accuracy and efficiency. The main goal of the proposed method is to obtain a precise simulation of the geometry of objects in SAR images rather than a detailed radiometric simulation. The simulator is based on an extended ray-tracing procedure to determine which surfaces of a generic object contribute to the backscatter. The backscatter contributions are calculated by means of a Lambertian-specular mixture model. The simulator has already been employed successfully in a methodology for 3-D reconstruction of man-made objects from single detected VHR SAR imagery. Here, we illustrate its work on two rather different structures, a rectangular gable-roof building and an Egyptian pyramid. [J53]

## "Combination of Direct and Double-Bounce Ground Responses in the Homogeneous Oriented Volume Over Ground Model"

Complex interferometric coherence expressions for the homogeneous (random or oriented) volume-over-ground model are originally derived in a simplified way by neglecting one of the two possible contributions of the ground response: direct return from the ground surface or double-bounce interaction with stems or trunks. The influence of these depends on both system and scene parameters, and in many cases, none of them should be ignored a priori. Therefore, a more general formulation accounting for the simultaneous presence of both ground contributions should be developed. This letter derives this formulation and analyzes the combined effect of both ground returns on the complex coherences. In addition, the implications for a subsequent inversion procedure based on this model are also discussed. [J54]

## "Modeling PSInSAR Time Series Without Phase Unwrapping"

In this paper, we propose a least-squares-based method for multitemporal synthetic aperture radar interferometry that allows one to estimate deformations without the need of phase unwrapping. The method

utilizes a series of multimaster wrapped differential interferograms with short baselines and focuses on arcs at which there are no phase ambiguities. An outlier detector is used to identify and remove the arcs with phase ambiguities, and a pseudoinverse of the variance-covariance matrix is used as the weight matrix of the correlated observations. The deformation rates at coherent points are estimated with a least squares model constrained by reference points. The proposed approach is verified with a set of simulated data. [J55]

## "Focusing of Tandem Bistatic-Configuration Data With Range Migration Algorithm"

A bistatic range migration algorithm (RMA) based on an exact analytical bistatic point-target (PT) spectrum in the tandem configuration is proposed in this letter. For the conventional geometry-based bistatic formula method, the derived spectrum is only a quasi-analytical one because a variable called half-quasi-bistatic angle (HQBA) is not exactly analytically expressed. The key step of the proposed algorithm is to deduce an analytical HQBA in the tandem configuration, and thus, an exact analytical closed-form PT spectrum is acquired. Based on this analytical spectrum, a bistatic RMA is presented. It is demonstrated that this algorithm can handle the bistatic tandem configuration with extremely large baseline/range ratio and can also be applied to wide-swath imaging. [J56]

## "InSAR Deformation Time Series Using an -Norm Small-Baseline Approach"

Satellite synthetic aperture radar interferometry (InSAR) is an invaluable tool for land displacement monitoring. Improved access to time series of satellite data has led to the development of several innovative multitemporal algorithms. Small baseline (SB) is one such time-series InSAR method, based on combining and inverting a set of unwrapped interferograms for surface displacement. Two-dimensional unwrapping of sparse data sets is a challenging task, and unwrapping errors can lead to incorrectly estimated deformation time series. It is well known that L1-norm is more robust than L2-norm cost function minimization if the data set has a large number of outlying points. In this paper, we present an L1-norm-based SB method using an iteratively reweighted least squares algorithm. We show that the displacement phase of both synthetic data, as well as a real data set that covers the San Francisco Bay area, is recovered more accurately than with L2-norm solutions. [J57]

## "Bias Correction and Doppler Measurement for Polarimetric Phased-Array Radar"

This paper discusses ways to avoid and/or mitigate biases in polarimetric variables inherent to agile-beam planar phased-array radars. Two bias-avoiding schemes produce unbiased estimates of the polarimetric backscattering covariance matrix which are then combined into bias-free polarimetric variables. One concerns full polarimetric measurements and calls for adjusting the amplitudes and phases of the array elements so that the transmitted field equals that generated by a mechanically steered polarimetric weather radar antenna; this is followed by an additional adjustment of the received fields. The second scheme is also applicable to full polarimetric measurements but involves adjustments only of the received fields. Crucial to both schemes is decoupling of the Doppler effects from the terms of the covariance matrix. It is a significant part of the bias issue that had not been previously addressed. A scheme to reduce bias applicable to nondepolarizing media (i.e., diagonal backscattering matrix) is also addressed; it calls for multiplication of the fields received by each dipole as opposed to a combination of multiplication and addition required for full correction. The schemes are applied to the alternate transmission and simultaneous reception polarimetric mode and the simultaneous transmission and simultaneous reception mode. [J58]

## "Unsupervised Classification of SAR Images Using Markov Random Fields and Model"

This letter deals with synthetic aperture radar (SAR) data classification in an unsupervised way. Many models have been proposed to fit SAR data (K, Weibull, Log-normal, etc.), but none of them are flexible enough to model all kinds of surfaces (particularly when there are urban areas present in the image). Our main contribution is the application of a statistical model G0in a classification process which is shown to be able to model areas with different degrees of heterogeneity. The quality of the classification obtained by mixing this model and a Markovian segmentation is high. We use an iterative conditional estimation method to estimate the parameters of the proposed model. [J59]

## "Altimeter-Derived Ocean Wave Period Using Genetic Algorithm"

It is known that wave period can be estimated from altimeter measurements of wave height, wind speed, radar backscatter cross section, etc., using empirical relationship. Of late, the data adaptive approach of neural networks has been used to derive wave period from altimeter data, and it has been shown that the technique appears to be superior compared to the empirical approaches. Another powerful data adaptive approach of genetic algorithm has been advocated more recently in oceanographic studies. Although primarily used for forecasting time series, the algorithm can be tuned to find a relationship between input and output variables. In

the present work, this algorithm has been used to find estimates of wave period from altimeter-observed parameters, and the performance of the algorithm has been found to be quite satisfactory. It has been also found that the introduction of wave age leads to significant enhancement of the accuracy of the estimate. [J60]

## "Remote Sensing of Volcanic Ash Cloud During Explosive Eruptions Using Ground-Based Weather RADAR Data Processing [JIn the Spotlight]"

The ash ejected into the atmosphere by the Eyjafjalla Icelandic volcano during its recent eruption posed such a threat to flights over much of Europe that the ensuing cancellations resulted in an unprecedented disruption of the European commercial air transportation system. Volcanic ash is not only a significant hazard to aircraft operations but also to public safety from volcanic ash fall at the surface. Given the significance of the hazards posed by volcanic ash, timely detection and tracking of the erupted ash cloud is essential to a successful warning process, particularly during and immediately following an eruptive event. In this article, we will discuss ground-based radar (radio detection and ranging) data processing for ash cloud remote sensing pointing to the physical basis of retrieval algorithms and an example of their application. [J61]

## "Foreword to the Special Issue on the 2009 International Geoscience and Remote Sensing Symposium (IGARSS '09)"

The nine papers in this special issue were originally presented at the 2009 International Geoscience and Remote Sensing Symposium (IGARSS '09), held at the University of Cape Town, Rondebosch, South Africa, from July 12 to 17. [J62]

## "On the Use of Anisotropic Covariance Models in Estimating Atmospheric DInSAR Contributions"

Stochastic models are often used to describe the spatial structure of atmospheric phase delays in differential interferometric synthetic aperture radar (DInSAR) data. Synthetic aperture radar interferograms often exhibit anisotropic atmospheric signals. In view of this, the use of anisotropic models for atmospheric phase estimation is increasingly advocated. However, anisotropic models lead to increased computational complexity in estimating the correlation function parameters with respect to the isotropic case. Moreover, the performance is degraded when dealing with DInSAR techniques involving only a few sparse points usable for computations, as in the case of persistent scatterer interferometry applications, particularly when this estimation has to be done in an automated way on many interferograms. In the present work, we propose some observations about the actual advantage given by anisotropic modeling of atmospheric phase in the case of sparse-grid point-target DInSAR applications. Through analysis of simulated data, we observe that an improvement in the performances of kriging reconstruction approaches can be obtained only when sufficient sampling densities are available. In critical sampling conditions, automated methods with reasonable computational cost may improve their performance if external information on the atmospheric phase screen field is available. [J63]

## "On the Discrimination of Radar Signatures of Atmospheric Gravity Waves and Oceanic Internal Waves on Synthetic Aperture Radar Images of the Sea Surface"

Synthetic aperture radar (SAR) images acquired over the ocean frequently show sea wave-like patterns that have wavelengths well above those of ocean surface waves and that are sea surface signatures of oceanic internal waves (OIWs) or of atmospheric gravity waves (AGWs). However, it is often difficult to decide whether they result from the first or the second kind of waves, which has led many investigators to misinterpret SAR images of the sea surface. Based on solitary wave and radar imaging theories of AGWs and OIWs, we present criteria that help distinguish between them. However, there are cases where these criteria, which are based solely on the shape and structure of the features visible on the SAR images, yield ambiguous results. In these cases, one must resort to additional information on the generation of AGWs and OIWs, which are listed in this paper. [J64]

## "Electromagnetic Land Surface Classification Through Integration of Optical and Radar Remote Sensing Data"

We present a nonhierarchical electromagnetic (EM) land surface classification method through the integration of satellite multispectral high-resolution optical and polarized radar images of central Alberta near the Saskatchewan border. We implement a conventional supervised land surface classification method and a principal component analysis to a QuickBird image. The EM properties are then assigned to the classified surfaces to produce hierarchical EM land classification maps. To further classify a hierarchical EM surface (i.e., dielectric constant), we calculate the root-mean-square surface height with a Shuttle Radar Topography Mission 3-arc-second digital elevation model and the temperatures from a thermal band of a Landsat-5 Thematic

Mapper image. We also calculate the backscattering coefficients from the Advanced Land Observing Satellite Phased Array L-band Synthetic Aperture Radar image. Using these estimated values, we calculate the intrinsic weighting factors with the Dubois (1995) model for less vegetated land areas and the Ulaby (1986) model for open water areas. By applying these weighting factors to the hierarchical EM surface, we generate a nonhierarchical higher resolution EM surface map of the study area. [J65]

## "Radar detection based on compound-gaussian model with inverse gamma texture"

The coherent radar detection against a background of compound-Gaussian clutter with inverse gamma texture is studied and three detectors: One-step generalised likelihood ratio test (1S-GLRT), maximum a posteriori GLRT (MAP-GLRT) and two-step GLRT (2S-GLRT) are proposed. The detectors have the same structure with their test statistics and modified thresholds, respectively, related to the scale and the shape parameters of the texture, which can also be formulated in a matched filter (MF) form. Subsequently, the performance assessments are given by their probability of detection and probability of false alarm. The authors find that the probability of false alarm is dependent on the shape parameter, meaning the detectors have no CFAR property. When the shape parameter and the number of the integrated radar pulses satisfy certain condition, it has no relation with the shape parameter and then the detectors have CFAR property. Finally, simulation results show that: (i) 1S-GLRT and MAP-GLRT have the same performance for fixed probability of false alarm and 2S-GLRT bears slightly bad performance; (ii) the performance of 1S-GLRT is much closer to the adaptive coherence estimator (ACE) and is better than that of the Kelly GLRT and (iii) the 1S-GLRT is robust when parameter estimation errors exist. [J66]

## "The Seafloor: A Key Factor in Lidar Bottom Detection"

The environmental factors that determine the ability of airborne lidar bathymetry (ALB) to detect the seafloor are not well understood; however, water clarity is often considered the single factor for detection. A comparison of data from two different ALB systems (LADS-MKII and SHOALS-3000) of a small area offshore Gerrish Island, Maine, USA shows a striking correlation (95% overlap) in areas of no bottom detection that is independent of the tide status, the date of collection and the orientation of the survey flight. The laser measurements from the two ALB systems are compared to acoustic measurements of depth, seafloor slope, and backscatter from a Kongsberg EM3002 echosounder. The comparison shows that in water depths deeper than 7 m, there is a close correlation between the ALB detection patterns and bottom features. The study results indicate that lack of bottom detection by ALB does not necessarily indicate that water depths deeper than the surrounding areas have lidar strong bottom detection. No bottom detection in the study area actually reflects a change in bottom characteristics. [J67]

## "Two-Frequency Radar Experiments for Sounding Glacier Ice and Mapping the Topography of the Glacier Bed"

We performed airborne experiments using 150- and 450-MHz radars to measure ice thickness on the Greenland ice sheet. Our objectives were to investigate to what degree surface clutter obscures the basal echo when airborne measurements are made at different elevations and at different frequencies. We also explored interferometric techniques for processing the data to form swath measurements of ice thickness. We found that surface clutter was minimal for either frequency when operated at low aircraft elevations (500 m above the ice sheet surface) or over benign regions of the ice sheet. Because signal-to-clutter ratios were favorable, we found that we could retrieve the swath measurements of ice thickness at both frequencies using an interferometric technique. At high elevation, surface clutter degraded the 150-MHz signal, but the nadir ice thickness was still retrievable. The basal return in high-elevation 450-MHz data was detectable only after additional beam-steering techniques were applied to the data to reduce the surface clutter signal. Results suggest that interferometric cross-track ice-thickness measurements can be successfully made given a sufficient number of antenna elements driven at either 150 or 450 MHz and flown at both high and low elevations over the interior ice sheet. [J68]

## "Ship Surveillance With TerraSAR-X"

Ship detection is an important application of global monitoring of environment and security. In order to overcome the limitations by other systems, surveillance with satellite synthetic aperture radar (SAR) is used because of its possibility to provide ship detection at high resolution over wide swaths and in all weather conditions. A new X-band radar onboard the TerraSAR-X (TS-X) satellite gives access to spatial resolution as fine as 1 m. In this paper, first results on the combined use of TS-X ship detection, automatic identification system (AIS), and satellite AIS (SatAIS) is presented. The AIS system is an effective terrestrial method for tracking vessels in real time typically up to 40 km off the coast. SatAIS, as a space-based system, allows almost global coverage for monitoring of ships since not all ships operate their AIS and smaller ships are not equipped with AIS. The

system is considered to be of cooperative nature. In this paper, the quality of TS-X images with respect to ship detection is evaluated, and a first assessment of its performance for ship detection is given. The velocity of a moving ship is estimated using complex TS-X data. As test cases, images were acquired over the North Sea, Baltic Sea, Atlantic Ocean, and Pacific Ocean in Stripmap mode with a resolution of 3 m at a coverage of 30 km 100 km. Simultaneous information on ship positions was available from TS-X and terrestrial as well as SatAIS. First results on the simultaneous superposition of SatAIS and high-resolution radar images are presented. [J69]

## "Modeling the Configuration of HF Electrical Antennas for Deep Bistatic Subsurface Sounding"

In the frame of the European Space Agency's 2016 ExoMars mission, the Electromagnetic Investigation of the SubSurface (EISS) ground-penetrating radar has been designed and developed to perform deep soundings of the Martian subsurface from the surface. The EISS is designed to take advantage of the potential for bistatic radar investigations of the Martian subsurface between the fixed station (Lander) and the mobile platform (rover) and to characterize the 3-D structure and stratigraphy of the subsurface at depths ranging from 100 m to a few kilometers out to a 1-km radius around the lander. The EISS makes use of an electric dipole antenna made of two identical 35-m resistively loaded monopoles to transmit (and also receive in a monostatic mode) the high-frequency signal. However, the EISS's most innovative capability is its potential for bistatic operation, made possible by the accommodation of a small magnetic sensor on the rover (as initially planned for the ExoMars mission) which can measure the magnetic field (all three components) of the received waves whatever the direction and orientation of the rover. The aim of this paper is to show that the two monopoles of the antenna must be deployed on the surface in nearly opposite directions but not aligned to ensure good volume coverage around the transmitter. This paper is based on Finite Difference in Time Domain (FDTD) electromagnetic simulations. The simulated data have been used to study the impact of the angle between these two monopoles on the instrument performance. [J70]

## "Mapping Soil Moisture Using RADARSAT-2 Data and Local Autocorrelation Statistics"

The purpose of this study is to evaluate the capability of surface radar backscatter models to estimate soil moisture over agricultural fields from fully polarimetric RADARSAT-2 C-band synthetic aperture radar (SAR) responses. For validation purposes, ground measurements over 44 sampling sites in eastern Ontario, Canada were carried out in the spring of 2008 simultaneously with satellite data acquisitions. Soil moisture retrieval was accomplished using two semi-empirical scattering models (Dubois and Oh) and the SAR image backscatter. Discrepancies between measured radar backscatter coefficients and those predicted by the models were previously reported, requiring correction factors to reduce biases associated with these semi-empirical approaches. Soil moisture was estimated by explicitly solving the two backscatter equations of the Dubois model, and using a look-up table (LUT) approach applied to the Oh model. Results showed that the Oh model in a cross-polarization (HH-HV) and Dubois in a co-polarization (HH-VV) inversion scheme provide the best estimates. These model configurations were implemented to produce multi-date soil moisture maps for the eastern Ontario site. To expand the range of validity of these soil moisture estimates, the maps produced by the Dubois and Oh models were uniquely combined. These estimates of absolute soil moisture were then used to derive spatial patterns of near-surface moisture content using the Getis statistic. The Getis statistic maps provide meaningful spatial information, demonstrating the potential of combining the Getis statistic and RADARSAT-2 data in predicting soil moisture conditions. [J71]

## "NL-InSAR: Nonlocal Interferogram Estimation"

Interferometric synthetic aperture radar (SAR) data provide reflectivity, interferometric phase, and coherence images, which are paramount to scene interpretation or low-level processing tasks such as segmentation and 3-D reconstruction. These images are estimated in practice from a Hermitian product on local windows. These windows lead to biases and resolution losses due to the local heterogeneity caused by edges and textures. This paper proposes a nonlocal approach for the joint estimation of the reflectivity, the interferometric phase, and the coherence images from an interferometric pair of coregistered single-look complex (SLC) SAR images. Nonlocal techniques are known to efficiently reduce noise while preserving structures by performing the weighted averaging of similar pixels. Two pixels are considered similar if the surrounding image patches are "resembling." Patch similarity is usually defined as the Euclidean distance between the vectors of graylevels. In this paper, a statistically grounded patch-similarity criterion suitable to SLC images is derived. A weighted maximum likelihood estimation of the SAR interferogram is then computed with weights derived in a data-driven way. Weights are defined from the intensity and interferometric phase and are iteratively refined based both on the similarity between noisy patches and on the similarity of patches from the previous estimate. The efficiency of this new interferogram construction technique is illustrated both qualitatively and quantitatively on synthetic and true data. [J72]

## "Impact of DEM-Assisted Coregistration on High-Resolution SAR Interferometry"

Image alignment is a crucial step in synthetic aperture radar (SAR) interferometry. Interferogram formation requires images to be coregistered with an accuracy of better than a few tenths of a resolution cell to avoid significant loss of phase coherence. In conventional interferometric precise coregistration methods for full-resolution SAR data, a 2-D polynomial of low degree is usually chosen as warp function, and the polynomial parameters are estimated through least squares fit from the shifts measured on image windows. In case of rough topography or long baselines, the polynomial approximation may become inaccurate, leading to local misregistrations. These effects increase with spatial resolution of the sensor. An improved elevation-assisted image-coregistration procedure can be adopted to provide better prediction of the offset vectors. This approach computes pixel by pixel the correspondence between master and slave acquisitions by using the orbital data and a reference digital elevation model (DEM). This paper aims to assess the performance of this procedure w.r.t. the "standard" one based on polynomial approximation. Analytical relationships and simulations are used to evaluate the improvement of the DEM-assisted procedure w.r.t. the polynomial approximation as well as the impact of the finite vertical accuracy of the DEM on the final coregistration precision for different resolutions and baselines. The two approaches are then evaluated experimentally by processing high-resolution SAR data provided by the COnstellation of small Satellites for the Mediterranean basin Observation (COSMO/SkyMed) and TerraSAR-X missions, acquired over mountainous areas in Italy and Tanzania, respectively. Residual-range pixel offsets and interferometric coherence are used as quality figure. [J73]

## "Linear Feature Detection in Polarimetric SAR Images"

Recently, the use of linear features for processing remote-sensing images has shown its importance in applications. Unfortunately, traditional linear feature detection methods rely heavily on the image's local information which makes them vulnerable to the presence of noise in the image. This problem becomes particularly difficult for synthetic aperture radar (SAR) image applications where SAR images are corrupted by speckle noise. In order to overcome this problem, we propose a novel method that processes the polarimetric synthetic aperture radar (Pol-SAR) images by combining the multiscale image analysis with polarimetric information in a new fashion. A two-scale approach is adopted here. On a coarse level, the coarse regions of the linear features are extracted by a curvelet transform from a speckle noise reduced image obtained by the polarimetric whitening filter. On a fine level, we develop a fuzzy polarimetric detector to accurately locate the linear features inside the regions. The effectiveness of the proposed method is demonstrated using simulated Pol-SAR data acquired from both EMISAR and Convair-580 systems. [J74]

## "Differential Absorption Lidar to Measure Subhourly Variation of Tropospheric Ozone Profiles"

A tropospheric ozone Differential Absorption Lidar system, developed jointly by The University of Alabama in Huntsville and the National Aeronautics and Space Administration, is making regular observations of ozone vertical distributions between 1 and 8 km with two receivers under both daytime and nighttime conditions using lasers at 285 and 291 nm. This paper describes the lidar system and analysis technique with some measurement examples. An iterative aerosol correction procedure reduces the retrieval error arising from differential aerosol backscatter in the lower troposphere. Lidar observations with coincident ozonesonde flights demonstrate that the retrieval accuracy ranges from better than 10% below 4 km to better than 20% below 8 km with 750-m vertical resolution and 10-min temporal integration. [J75]

## "Mode Effect on Direct Wave in Single-Hole Borehole Radar"

In this paper, we investigate the influence of radar sonde eccentricity on a direct wave between a transmitting and a receiving antenna in a single-hole borehole radar measurement. We analyze the direct wave using an analytical method with the approximated solution of branch cut integrals and that of residues of poles. According to our calculation, at high frequencies above 200 MHz, guided waves, which are caused by the poles, play a vital role in the direct wave. We found that the most important pole is the HE11mode one, which is excited only when the antenna is eccentered in the borehole. We show that this causes artificial noise in the moving average subtraction, which is a common signal processing method used to remove the direct wave. In a laboratory experiment with a ground plane, we confirmed the excitation of the guided waves when the antenna was eccentered. In field experiments in granite, we conducted a special experiment, in which the location and rotation of the radar sonde were controlled mechanically. We found the excitation of the HE11mode at high frequencies when the sonde was noncentered by 1.7 cm in a borehole. These effects are also predicted in a theoretical analysis. [J76]

## "A Microphysics-Based Simulator for Advanced Airborne Weather Radar Development"

Incorporating dual-polarized operation and microphysics-based processing is becoming a challenge to future scientific and commercial airborne weather radars. This paper introduces a Monte Carlo simulation-based approach to address the theoretical basis and uncertainties of hydrometeor scattering along with sensor platform properties. Detailed characterizations of mixed-phase aviation hydrometeor hazards (rain, snow, hail, and mixtures) and the impact of melting on polarimetric radar signature at X-band frequency are discussed. A "single resolution cell" Monte Carlo dual-polarization variable simulation technique is described and then applied in different radar scanning scenarios based on numeric weather prediction model output weather fields. The produced dual-polarization signatures of an X-band array radar for different scan scenarios are analyzed. [J77]

## "An Improved Quality-Guided Phase-Unwrapping Algorithm Based on Priority Queue"

Phase unwrapping is one of the key problems in reconstructing the elevation map of a scene from interferometric synthetic aperture radar or interferometric synthetic aperture sonar (InSAS) data. In this letter, an improved quality-guided phase-unwrapping algorithm is proposed, which depends on the quality value and its surrounding quality information to guide the path of unwrapping more accurately. In order to design highly efficient quality-guided algorithm, a guided map deduced from the quality map is introduced and taken as the new quality map which the quality-guided algorithm should completely depend on. A quantized quality-guided method is designed, which adopts the quantized new quality map and the priority queue designed to optimize the process of unwrapping. The quantized quality map establishes the relation between the quality values and the indexes of array, which can save the time of inserting one pixel into the priority queue according to its integral quality value. Priority queue keeps all the pixels by their quantized quality in a nondecreasing order by maintaining the doubly linked lists in an increasing order. An optimized strategy is used to accelerate the process of finding the pixel with the highest quality value in the priority queue. Tests performed on real InSAS data and simulated interferograms confirm the accuracy and efficiency of the proposed algorithm, and the improved algorithm is suitable for our real-time processing InSAS system. [J78]

## "An Improved Radon-Transform-Based Scheme of Doppler Centroid Estimation for Bistatic Forward-Looking SAR"

For high-quality synthetic aperture radar (SAR) processing, Doppler centroid estimation is an essential procedure. An incorrect Doppler centroid would cause a loss of SNR, an increase in the azimuth ambiguity level, a shift in the location of the target, etc. An improved Radon-transform-based Doppler centroid estimation scheme of bistatic forward-looking SAR is proposed in this letter. First, this scheme performs edge detection on the range-compressed data and then does the coarse and fine Radon transforms to estimate the Doppler centroid. Simulations and real-data experiments validate the effectiveness of this method. [J79]

## "Unsupervised Spatiotemporal Mining of Satellite Image Time Series Using Grouped Frequent Sequential Patterns"

An important aspect of satellite image time series is the simultaneous access to spatial and temporal information. Various tools allow end users to interpret these data without having to browse the whole data set. In this paper, we intend to extract, in an unsupervised way, temporal evolutions at the pixel level and select those covering at least a minimum surface and having a high connectivity measure. To manage the huge amount of data and the large number of potential temporal evolutions, a new approach based on data-mining techniques is presented. We have developed a frequent sequential pattern extraction method adapted to that spatiotemporal context. A successful application to crop monitoring involving optical data is described. Another application to crustal deformation monitoring using synthetic aperture radar images gives an indication about the generic nature of the proposed approach. [J80]

## "Adaptive Model-Based Decomposition of Polarimetric SAR Covariance Matrices"

Previous model-based decomposition techniques are applicable to a limited range of vegetation types because of their specific assumptions about the volume scattering component. Furthermore, most of these techniques use the same model, or just a few models, to characterize the volume scattering component in the decomposition for all pixels in an image. In this paper, we extend the model-based decomposition idea by creating an adaptive model-based decomposition technique, allowing us to estimate both the mean orientation angle and a degree of randomness for the canopy scattering for each pixel in an image. No scattering reflection symmetry assumption is required to determine the volume contribution. We examined the usefulness of the proposed decomposition technique by decomposing the covariance matrix using the National Aeronautics and Space Administration/Jet Propulsion Laboratory Airborne Synthetic Aperture Radar data at the C-, L-, and P-bands. The randomness and mean orientation angle maps generated using our adaptive decomposition significantly improve the physical interpretation of the scattering observed at the three different frequencies. [J81]

## "A Novel Imaging Method for Fast Rotating Targets Based on the Segmental Pseudo Keystone Transform"

Fast rotating targets such as gimbaled antennas or propeller blades may cause migration through resolution cells (MTRC) of the high-resolution range profile during the imaging time, which makes the inverse synthetic aperture radar image smeared. To solve this problem, a novel imaging method for fast rotating targets is proposed in this paper. The method is based on the segmental pseudo Keystone transform, which is designed to realize MTRC correction. The fast realization is achieved by employing the discrete match Fourier transform, which makes the algorithm feasible and simple. Experiments with simulated radar data demonstrate the performance of the proposed method. [J82]

## "New method for generating site-specific clutter map for land-based radar by using multimodal remote-sensing images and digital terrain data"

By using multimodal remote-sensing images and digital terrain data of the environment, this study presents a new method for generating the clutter map specific to the selected land radar site and the radar's operating parameters. In the proposed method, the estimation of backscattering from the environment involves extrapolation of the airborne radar remote-sensing image to provide the baseline values, classification of multispectral remote-sensing satellite images to provide a detailed description of terrain types, use of digital terrain elevation data with the land radar position and height to provide local grazing angles and a terrain visibility map and use of the digital topographic map to provide the geometric reference for all data sets. Using actual remote-sensing images and digital terrain data acquired from a real environment with various terrain features, the clutter map generated by the proposed method for land-based radar is compared with that generated by the competitive modelling method. The accuracy of the proposed method is demonstrated based on the differences with respect to the actual clutter measurements using a different airborne radar-sensing configuration. [J83]

## "Complex Permittivity of Volcanic Rock and Ash at Millimeter Wave Frequencies"

Millimeter wave radar has shown to be of great use in the field of volcanology in terrain mapping applications. One area less studied to date is its use in ash cloud monitoring applications. In order for this to be realized, a quantitative study of the dielectric properties of volcanic rock and ash is required. In this letter, we present a method for accurately determining the complex dielectric permittivity of volcanic samples using a quasi-optical technique on the pellets of pulverized rock and present the results obtained. When averaged across our sample set, the results show agreement with those obtained by previous authors for both the permittivity of the volcanic material at lower frequencies and the permittivity of other rocks at millimeter wave frequencies. The results also show good levels of consistency between the multiple splits of each sample. In order to relate the measurements of the porous collections of ash to a continuous rock equivalent that is needed for use in the distributed target radar equation, mixing formulas are required. A measurement technique is presented for validating the mixing formulas using pressed pellets and loose ash. Bojttcher's formula is found to be both accurate and sufficient for our purposes and is used further to relate our measurements to the continuous rock equivalents. These equivalents show that, for andesitic ash, the radar reflectivity factor may be taken to be an average value of $K= |(\varepsilon-1)/(\varepsilon + 2)|2= 0.39 \pm 0.03$, showing no measurable deviation from that reported previously at frequencies of up to 19 GHz. [J84]

## "Standard Deviation of Spatially Averaged Surface Cross Section Data From the TRMM Precipitation Radar"

We investigate the spatial variability of the normalized radar cross section of the surface (NRCS or $\sigma 0$) derived from measurements of the Tropical Rainfall Measuring Mission (TRMM) Precipitation Radar (PR) for the period from 1998 to 2009. The purpose of this letter is to understand the way in which the sample standard deviation (SSD) of the $\sigma 0$data changes as a function of spatial resolution, incidence angle, and surface type (land/ocean). The results have implications regarding the accuracy by which the path-integrated attenuation (PIA) from precipitation can be inferred by the use of surface-scattering properties. [J85]

## "Consistent Clustering of Radar Reflectivities Using Strong Point Analysis: A Prelude to Storm Tracking"

An image segmentation algorithm using an alternating erosion/dilation technique called strong point analysis (SPA) is introduced for general-purpose feature detection. The ability to associate and group pixels with the salient features of an image allows computers to consider images not as an array of values but as a collection of objects. This enables other algorithms to perform advanced tasks, such as tracking an object in a time series of

images. The qualitative needs for proper tracking of storm cells in radar images are discussed. To test SPA for those qualities, radar reflectivity images from three S-band weather radars were used. The algorithm is demonstrated to identify features fairly consistently over a time series of images, as well as exhibiting well-behaved changes to its output with respect to changes to the algorithm's input parameters. [J86]

## "Pattern-Based Accuracy Assessment of an Urban Footprint Classification Using TerraSAR-X Data"

Assessing the accuracy of land-cover classifications is a major challenge in remote sensing. This is mostly due to the absence of geometrically and thematically highly resolved, reliable, area wide, and up-to-date reference data. This study focuses on a multifaceted accuracy assessment of an urban footprint classification derived from a single-polarized TerraSAR-X image in stripmap mode for the city of Padang in Indonesia. For this purpose, a pixel-based approach was used to identify the urbanized and nonurbanized areas. As reference, a geometrically and thematically highly resolved, accurate, and detailed 3-D city model is available. Based on this data, the classification result is assessed by basic methodologies-square measures and error matrix. Beyond that, the accuracy of the urban footprint classification is analyzed in dependence of the physical structure of the complex urban landscape-defined by built-up density and building volumes. Results reveal that the accuracy of classification results varies in dependence of the structural characteristics of the particular urban environment. Furthermore, the study shows what is thematically mapped by an urban footprint classification. [J87]

## "Experimental Study on Radiometric Performance of Synthetic Aperture Radiometer HUT-2D-Measurements of Natural Targets"

This paper describes the analysis of L-band radiometric measurement data gathered with the synthetic aperture radiometer HUT-2D during several ground-based and airborne measurement campaigns. The radiometric data are analyzed from the instrument's performance point of view, aiming to verify the theoretical performance of an instrument of this kind and to assess the performance of the HUT-2D radiometer system in particular. The data sets considered for the study consist of measurements of well-known natural targets, such as cosmic background radiation, and measurements of pure water scenes, the brightness temperature of which is possible to model based on in situ measurements. We define four figures of merit, which are applicable for synthetic aperture radiometers. These are radiometric resolution, image bias, pixel-to-pixel random error, and temporal stability. Then, we use the selected data sets to assess these in the case of HUT-2D. The experimental results are discussed and compared to the theoretical values, where applicable. Also, we discuss possibilities to improve the presented performance. The main results of this paper are the consolidated performance parameters of the HUT-2D instrument. We study and discuss the properties of the error components related to the technology in a general level, and study the scalability of the errors as a function of the measured targets. In particular, the stability of the direction-dependent error component is pointed out, and a mitigation guideline is proposed. [J88]

## "Numerical Simulations of Borehole Radar Detection for Metal Ore"

We perform a finite-difference time-domain numerical simulation for metal ore detection by borehole radar. The ore-body model is a practical Ni-Cu-Pt one which is a magmatic deposit located in Sudbury, Canada. We design three boreholes along a cross section perpendicular to the geological strike of the formation which is composed of overburden, ore zone, iron formation, peridotite, granite gneiss, and sediments. We analyze the simulated borehole radar profiles and find that some interfaces could be detected. The ore zone is very absorptive to electromagnetic wave. By combined interpretation of the data from several boreholes, the azimuth ambiguity of the borehole radar could be overcome with some a priori geological information, and the geological structure could be delineated clearly. [J89]

## "Imaging Geodesy-Toward Centimeter-Level Ranging Accuracy With TerraSAR-X"

In this paper, we report on experiments to measure large-scale Earth surface displacements, such as those caused by solid Earth tides, with centimeter-level accuracy using TerraSAR-X radar images. With two totally different approaches, corner reflectors and image correlation techniques, we show the clear interrelation between the radar range measurements and the projection of the solid Earth tide motion vector onto the radar line of sight. Pixel location accuracies of up to 2.6-cm standard deviation can be achieved after a single calibration. We further demonstrate that solid Earth tides and tropospheric water vapor variations are the largest sources of ranging error if not compensated for. Alternatively, tropospheric water vapor can be estimated with centimeter accuracy using our proposed technique of synthetic aperture radar (SAR) image correlation and solid Earth motion compensation by the existing models. We also consider ionospheric delays which improve the results marginally in the X-band. Our results show the best ranging accuracies so far reported for spaceborne radar amplitude images and make TerraSAR-X-together with our simple compensation methodology-suitable for the

imaging of centimeter-level Earth displacements. Absolute measurements of volcanoes or glaciers are possible without the use of ground equipment and without the use of SAR interferometry, thus avoiding the associated problems of phase ambiguity, phase unwrapping, and reference points. [J90]

## "Hierarchical Segmentation of Polarimetric SAR Images Using Heterogeneous Clutter Models"

In this paper, heterogeneous clutter models are used to describe polarimetric synthetic aperture radar (PolSAR) data. The KummerU distribution is introduced to model the PolSAR clutter. Then, a detailed analysis is carried out to evaluate the potential of this new multivariate distribution. It is implemented in a hierarchical maximum likelihood segmentation algorithm. The segmentation results are shown on both synthetic and high-resolution PolSAR data at the X- and L-bands. Finally, some methods are examined to determine automatically the "optimal" number of segments in the final partition. [J91]

## "Cross-Range Scaling Algorithm for ISAR Images Using 2-D Fourier Transform and Polar Mapping"

This paper proposes a new method that solves the problem of inverse synthetic aperture radar image cross-range scaling by estimating the rotational velocity (RV) using the expansion-rotation-scale relationship between two range-Doppler (RD) images. This method is composed of three steps. The first step is preprocessing to construct 2-D Fourier transform images and initial polar-mapped images. In this step, two RD images are 2-D Fourier transformed to avoid the necessity of finding the rotation center; then, the transformed images are polar mapped with identical polar grids to convert rotation into translation in the θ-direction only. The second step is a coarse search that finds the angular shift that provides the maximum correlation between two polar images. The angular shift found is used as the initial relative rotation angle (RA), and the initial relative scaling factor (RSF) is calculated using the RV which is equal to the angular shift divided by the time delay between the images. The third step is the optimization of the relative RA using the Nelder-Mead approach, with the RSF updated using the relative RA derived during each iteration. In simulations using a Mig-25 aircraft, composed of ideal point scatterers, and the measured data from a Boeing 747-400, the targets were properly rescaled in the range-cross-range domain due to the accurate estimation of the RV. [J92]

## "A Foreground/Background Separation Framework for Interpreting Polarimetric SAR Images"

In this letter, we present a novel foreground/background separation (FBS) framework for interpreting polarimetric synthetic aperture radar (PolSAR) images. The FBS framework takes the spatial relations between pixels into consideration and incorporates the advantages of pairwise dissimilarity-based grouping schemes. The FBS method can separate specific targets and objects from the background, which is essential in an interpretation system. Multiple FBS operations can be integrated to interpret PolSAR images, flexibly fusing various inherent features of PolSAR data. Several PolSAR data sets are used to verify the proposed approach. [J93]

## "Three-Dimensional GPR Ray Tracing Based on Wavefront Expansion With Irregular Cells"

A new ray-tracing method in 3-D heterogeneous isotropic media is proposed based on the bilinear travel-time interpolation and wavefront group marching method (GMM). In this method, an irregular cell discretization scheme is used to accurately describe arbitrarily undulant interfaces in a model. The ray tracing is carried out by forward-backward processing. In the forward step, the travel time in an irregular cell is expressed in terms of the bilinear interpolation of the known travel times on the cell's surfaces. Then, the wavefront is evolved from the source to the whole computational domain by using the newly developed travel-time solver and the fast wavefront expansion GMM. In the backward step, each ray path is traced from the receiver by finding the intersection points of potential ray propagation vectors with the surfaces of the relevant cells. The same travel-time solver is used to compute the candidate intersection points on all surfaces of each relevant cell, and the point with the minimum travel time is selected as a ray point from which the similar step is continued until the sources are found. Several numerical experiments are presented to demonstrate that the new algorithm is accurate, efficient, and robust. [J94]

## "Investigation on Doppler Shift and Bandwidth of Backscattered Echoes From a Composite Sea Surface"

In the general framework of the second-order small-slope approximation (SSA) (SSA-II), Doppler shifts of backscattered fields from time-varying sea surfaces are predicted at small and moderate incidence angles. The composite sea surface is modeled as a superposition of large-scale gravity waves and small-scale ripples. Here, the elevation of the large-scale surface component, on which each small facet travels along a closed orbit under the condition of the first-order approximation, is described by the coordinates of the small facets. The predicted

Doppler shifts are compared with the results obtained by the small perturbation method (SPM), the geometrical optics method, the first-order SSA (SSA-I), and the two-scale scattering method (TSM). We can find that the predicted Doppler shifts for SPM and SSA-I in copolarized configuration are insensitive to the polarization state. However, the results obtained by SSA-II are consistent with those obtained by TSM and yield significant differences between HH and VV polarizations. Spectrum bandwidth is mainly induced by sea-surface orbit motions. In this paper, the formula of the spectrum bandwidth for the scattered echoes from the composite sea surface is also derived on the basis of TSM. The predicted bandwidths are compared with the Monte Carlo simulated results and the measured data. Furthermore, the dependences of the Doppler shift and the bandwidth on the parameters, such as the polarization, wind speed, radar frequency, etc., are also discussed. [J95]

## "Incoherent Scatter Spectral Theories-Part II: Modeling the Spectrum for Modes Propagating Perpendicular to"

Incoherent scatter (IS) spectral models for collisional and magnetized F-region plasmas are developed based on a general framework described in part I of this paper and on the statistics of simulated particle trajectories. In the simulations, a Langevin update equation is used to describe the motion of charge carriers undergoing Coulomb collisions. It is shown that random displacements of oxygen ions in the F-region can be characterized as a Brownian-motion process with Gaussian distributed displacement vectors. Electron displacements, on the other hand, are non-Brownian, and their statistics exhibit a dependence on the magnetic aspect angle. A numerical library of characteristic functions of electron displacements was constructed from the simulation data obtained for a set of plasma parameters typical of the equatorial F-region. Spectral models for the IS radar signals from F-region heights are constructed with one-sided Fourier transforms of the characteristic functions of electron and ion displacements. The models are valid at all magnetic aspect angles, including the zero aspect angle that corresponds to radar observations perpendicular to the ambient geomagnetic field . [J96]

## "Detection of Ships in Marine Environments by Square Integration Mode and Multilayer Perceptrons"

A novel method for detecting ships in marine environments is presented in this paper. For this purpose, the information contained in the marine images obtained by a measuring and monitoring marine system is used. The ship detection is done by multilayer perceptrons (MLPs). In the first approach, the MLP processes the information extracted from the images using horizontal or vertical integration modes. However, if a suitable combination of these integration modes is done, better detection performances are achieved. Therefore, the use of an improved integration mode is proposed, which is based on a square shape. These modes are also used in a commonly used detector, the cell averaging constant false alarm rate (CA-CFAR) detector, which is taken as reference in our experiments. The comparison of the performances of both detectors shows how the MLP-based detector outperforms the CA-CFAR detector in all the cases under study. This comparison is based on objective (probabilities of false alarm and detection) and subjective estimations of their performances. The MLP-based detector also presents another advantage, particularly when the square integration mode is considered: high-performance robustness against changes in the marine environmental conditions. [J97]

## "Multitemporal Image Change Detection Using Undecimated Discrete Wavelet Transform and Active Contours"

In this paper, an unsupervised change detection method for satellite images is proposed. Owing to its robustness against noise, the undecimated discrete wavelet transform is exploited to obtain a multiresolution representation of the difference image, which is obtained from two satellite images acquired from the same geographical area but at different time instances. A region-based active contour model is then applied to the multiresolution representation of the difference image for segmenting the difference image into the "changed" and "unchanged" regions. The proposed change detection method has been conducted on two types of image data sets, i.e., the synthetic aperture radar images and the optical images. The change detection results are compared with several state-of-the-art techniques. The extensive simulation results clearly show that the proposed change detection method consistently yields superior performance. [J98]

## "Incoherent Scatter Spectral Theories-Part I: A General Framework and Results for Small Magnetic Aspect Angles"

A general framework for the incoherent scatter radar spectral theories is presented in terms of the generalized Nyquist theorem, Kramers-Kronig relations, and the characteristic functions of random charge-carrier displacements in the ionosphere. Specific spectral models for typical ionospheric conditions are derived and discussed. The discussions focus on the effect of Coulomb collisions in magnetized plasmas, which is a topic of current interest treated in further detail in the companion paper by the authors, as well as on different

combinations of physical principles that can be invoked in the derivation of incoherent scatter spectral models. [J99]

## "Radio frequency interference cancellation for sea-state remote sensing by high-frequency radar"

High-frequency surface wave radar (HFSWR) has been widely adopted as a useful remote-sensing tool for sea-state monitoring. There are limitations to the performance because of various unwanted clutters and interferences that contaminate radar signals. Among all types of unwanted signals, radio frequency interference (RFI) is dominant since the frequency bands 3??30 MHz, the operation range of HFSWR, are shared by many radio services. If RFI occupies the areas in the Doppler spectrum that are essential for the estimation of oceanographic parameters, for example, wind speed, current speed, wave height etc., it will significantly reduce the quality of the data. The characteristics of RFI in time, space and Doppler domains are analysed for sea-state monitoring, and a robust and general signal processing method consisting of image recognition, segmentation processing and subspace projection for cancellation of RFI is proposed. The effectiveness of this approach is validated using data obtained with the Pisces HF radar, which is a high-performance radar developed for long-range wave measurement, operating in the lower half of the HF band (5??10 MHz). [J100]

## "Polarization Phase Difference Analysis for Selection of Persistent Scatterers in SAR Interferometry"

In this letter, we propose a technique for selecting persistent scatterers (PSs) based on their polarization phase difference (PPD). We analyze a normalized PPD between HH and VV channels averaged over a temporal set of images and select pixels that demonstrate predominantly even or odd bounce scattering properties. We compare selected scatterers to PSs selected by applying an amplitude dispersion threshold as suggested by a standard PS interferometry (PSI) approach and show that both methods are complementary. However, the proposed approach can be potentially used on a small set of synthetic aperture radar (SAR) images, which can be beneficial in the early stage of data acquisition. We apply the proposed technique to produce a deformation map for the San Francisco region from six quad-pol RADARSAT-2 SAR images acquired during 2008-2009. The coverage and the precision of the produced deformation map are higher than if it was calculated with the standard PSI technique applied to the same data set. [J101]

## "Model-Based Estimation of Forest Canopy Height in Red and Austrian Pine Stands Using Shuttle Radar Topography Mission and Ancillary Data: A Proof-of-Concept Study"

In this paper, accurate tree stand height retrieval is demonstrated using C-band Shuttle Radar Topography Mission (SRTM) height and ancillary data. The tree height retrieval algorithm is based on modeling uniform tree stands with a single layer of randomly oriented vegetation particles. For such scattering media, the scattering phase center height, as measured by SRTM, is a function of tree height, incidence angle, and the extinction coefficient of the medium. The extinction coefficient for uniform tree stands is calculated as a function of tree height and density using allometric equations and a fractal tree model. The accuracy of the proposed algorithm is demonstrated using SRTM and TOPSAR data for 15 red pine and Austrian pine stands (TOPSAR is an airborne interferometric synthetic aperture radar). The algorithm yields root-mean-square (rms) errors of 2.5-3.6 m, which is a substantial improvement over the 6.8-8.3-m rms errors from the raw SRTM minus National Elevation Dataset Heights. [J102]

## "Statistical Linear Destriping of Satellite-Based Pushbroom-Type Images"

This paper introduces a new self-calibration destriping technique for pushbroom-type satellite imaging systems. Self-calibration means that no specific training data are required. It is based on the statistical estimation of each detector gain from the observed image, assuming a linear response. Both theoretical and practical behaviors are studied. Our technique is shown to outperform simpler techniques based on column averages in terms of gain estimation precision while keeping the computational cost within admissible limits. [J103]

## "Mutual-Information-Based Registration of TerraSAR-X and Ikonos Imagery in Urban Areas"

The launch of high-resolution remote sensing satellites like TerraSAR-X, WorldView, and Ikonos has benefited the combined application of synthetic aperture radar (SAR) and optical imageries tremendously. Specifically, in case of natural calamities or disasters, decision makers can now easily use an old archived optical with a newly acquired (postdisaster) SAR image. Although the latest satellites provide the end user already georeferenced and orthorectified data products, still, registration differences exist between different data sets. These differences need to be taken care of through quick automated registration techniques before using the images in different applications. Specifically, mutual information (MI) has been utilized for the intricate SAR-optical registration

problem. The computation of this metric involves estimating the joint histogram directly from image intensity values, which might have been generated from different sensor geometries and/or modalities (e.g., SAR and optical). Satellites carrying high-resolution remote sensing sensors like TerraSAR-X and Ikonos generate enormous data volume along with fine Earth observation details that might lead to failure of MI to detect correct registration parameters. In this paper, a solely histogram-based method to achieve automatic registration within TerraSAR-X and Ikonos images acquired specifically over urban areas is analyzed. Taking future sensors into a perspective, techniques like compression and segmentation for handling the enormous data volume and incompatible radiometry generated due to different SAR-optical image acquisition characteristics have been rightfully analyzed. The findings indicate that the proposed method is successful in estimating large global shifts followed by a fine refinement of registration parameters for high-resolution images acquired over dense urban areas. [J104]

## "IceSynth II: Synthesis of SAR Sea-Ice Imagery Using Region-Based Posterior Sampling"

A novel method for synthesizing synthetic aperture radar (SAR) sea-ice imagery named IceSynth II is presented. A Markov random field model is assumed, and a conditional sampling approach is used to learn local conditional posterior probability distributions on a regional basis. Synthetic SAR sea-ice images and the associated ground-truth segmentations are generated using a region-based posterior sampling approach. Experimental results using single-polarization RADARSAT-1 and dual-polarization RADARSAT-2 SAR sea-ice imagery provided by the Canadian Ice Service show that IceSynth II is capable of producing SAR sea-ice imagery that is more realistic than existing approaches. The synthesized images are well suited for performing systematic and reliable objective evaluation of SAR sea-ice image segmentation methods. [J105]

## "Performance Metrics for Single-Photon Laser Ranging"

Airborne laser swath mapping systems collect thousands of range measurements per second, enabling high-resolution surface mapping. Low-signal-to-noise-ratio (LSNR) detection techniques allow for implementation of light detection and range (LIDAR) instrumentation aboard platforms with stringent power, size, and weight restrictions. The University of Florida has developed the coastal area tactical-mapping system, which is a prototype LSNR LIDAR system that is capable of single-photon laser ranging. Laser pulses of 532 nm, 3.5 ??J, and 480 ps are transmitted at 8 kHz, with the outgoing footprint split into a 10 ?? 10 array of elements. Backscattered photons are imaged back onto separate anodes of a multistop microchannel plate photomultiplier tube. A 2-GHz event timer processes returns over the array. Ranges for known targets are accumulated for repeated laser shots, and statistical analysis is applied to evaluate performance metrics that are related to minimum separation distance, bathymetric mapping depth, and atmospheric scattering. An LSNR detection paradigm based on Poisson statistics has enabled topographic target detection and shallow-water bathymetry. Quantitative results are used to draw conclusions about feature detection in topographic and bathymetric mapping scenarios. [J106]

## "Contrast-Optimization-Based Range-Profile Autofocus for Polarimetric Stepped-Frequency Radar"

One of the main benefits brought by the use of fully polarimetric radars is the ability to identify scattering mechanisms, which are related to the target physical properties. One of the most critical problems in synthetic range-profile reconstruction is the distortion induced by the target motion. Radial target velocity and acceleration generate second- and third-order phase terms in the received signal, which produce range shift and point-spread-function smearing. The distortions induced by the target motion produce, as a consequence, a signal-to-noise ratio loss. Recently, a method based on contrast maximization has been proposed in order to compensate target radial motions using single-polarization data. In this paper, an extension of such an algorithm is proposed that exploits fully polarimetric data in order to improve the target radial motion compensation. [J107]

## "Application of a Multiseed-Based Clustering Technique for Automatic Satellite Image Segmentation"

The problem of classifying an image into different homogeneous regions is viewed as a task of clustering the pixels in the intensity space. In this letter, a newly developed genetic clustering technique is used for automatically segmenting remote sensing satellite images. Each cluster is divided into several small hyperspherical subclusters, and the centers of all these small subclusters are encoded in a chromosome to represent the whole clustering. For assigning points to different clusters, these local subclusters are considered individually. For the purpose of objective function evaluation, these subclusters are merged appropriately to form a variable number of global clusters. A newly proposed point-symmetry-distance-based cluster validity index, Symindex, is used as a measure of the validity of the corresponding segment. The effectiveness of the proposed technique compared to a fuzzy C-means clustering technique, a recently proposed GAPS clustering with Sym-

index-based method, and a subtractive clustering technique is demonstrated in identifying different land cover regions from two numeric image data sets and a remote sensing image of a part of the city of Kolkata. [J108]

## "TerraSAR-X Instrument Operations Rooted in the System Engineering and Calibration Project"

This paper presents the TerraSAR-X instrument operations embedded into the Instrument Operations and Calibration Segment. Special focus is on the data-take (DT) command generation. The command generation for standard DTs is discussed, and the nonnominal DT commanding is described for several examples which demonstrate the flexibility of both the TerraSAR-X instrument and the instrument operations system on-ground. [J109]

## "A Backscatter Modeling for River Ice: Analysis and Numerical Results"

A microwave backscatter model was developed to help provide an understanding of the interaction of a radar signal with the different ice types formed on natural freshwater bodies. This model was based on the radiative transfer theory, which is solved by the doubling matrix method. This numerical method provides an explanation for scattering effects due to volume, boundaries, boundary-volume interactions and interactions between layers. Three ice types were analyzed: columnar ice, frazil ice, and snow ice. Simulations with the model proved that the radar response from river ice cover depends on both ice-cover boundaries. The shape and distribution of air inclusions within the different ice types seem to have a significant impact on their contributions to the total response. The presence of tubular air inclusions within columnar ice causes an increase in the total response as a result of a double-bounce scattering. Small spherical and closed air inclusions within snow ice and frazil ice generate significant backscattering at high frequencies due to volume and surface-volume scattering. A further increase in the ice-cover thickness with air inclusions also causes increased scattering. Superposing two or more of these ice types causes considerable multiple scattering between layers. Finally, radar ice measurements collected over the Athabasca River were employed to further validate the model, and satisfactory results were obtained. [J110]

## "Focus FMCW SAR Data Using the Wavenumber Domain Algorithm"

The combination of frequency-modulation continuous-wave (FMCW) technology and synthetic aperture radar (SAR) promises a lightweight, cost-effective, and high-quality imaging sensor for remote sensing. However, the long signal duration time leads to the failure of the conventional start/stop approximation of the pulsed SAR. In this paper, a signal model is proposed to address the effects of the continuous motion during the transmit time on the echoed signal. Based on the model, an analytical point target reference spectrum is derived. From the spectrum, it will be seen that the continuous motion introduces an additional range-azimuth coupling term and a range walk term compared with the conventional pulsed SAR. The range walk term is well known, whereas the foregoing range-azimuth coupling term is formulated for the first time in the FMCW SAR community. For the squint and spotlight modes, these range walk and range-azimuth coupling terms might significantly degrade the image quality. In this paper, based on the proposed analytical signal model, we further discuss the application of the wavenumber domain algorithm for the FMCW SAR data. In addition, different approximations of the Stolt mapping are made to highlight the effect of the range-dependent higher-order range-azimuth coupling terms on the 2-D impulse responses. Finally, X-band simulated experiments and Ka-band real FMCW SAR data are used to validate the signal model and the processing method. [J111]

## "Final TerraSAR-X Calibration Results Based on Novel Efficient Methods"

TerraSAR-X is a satellite mission for scientific and commercial applications operating a highly flexible X-band synthetic aperture radar (SAR) instrument with a multitude of different operation modes. As product quality is of crucial importance, the success or failure of the mission depends essentially on the method of calibrating TerraSAR-X in an efficient way during commissioning the entire system in a restricted time. Only then, product quality and the correct in-orbit operation of the entire SAR system can be ensured. This paper describes the in-orbit calibration method for TerraSAR-X and dedicated activities performed during the commissioning phase as well as final results derived from all calibration procedures. [J112]

## "Advanced Land Observing Satellite (ALOS) and Monitoring Global Environmental Change"

The Advanced Land Observing Satellite (ALOS) was developed for detailed observation of the Earth's surface and frequent monitoring of global environmental changes, using high-resolution optical (visible and near infrared push-broom) and active microwave sensors (L-band synthetic aperture radar). ALOS has four mission objectives: cartography, regional observations, disaster observations, and resource exploration. It has been operational since its launch in January 24, 2006, and is acquiring a large amount of land-surface data supported by the Ka-band intersatellite communication system that downlinks to ground receiving stations. A global

systematic acquisition strategy is implemented for all three sensors to enable consistent data collection over all land areas on a repetitive basis. Through its three sensors, acquisition strategy, and communication infrastructure, the ALOS mission is aimed to contribute to monitoring water, carbon, and global climate change. In this paper, we describe ALOS and its contribution to global environmental monitoring. [J113]

## "Terrain Modeling From Lidar Range Data in Natural Landscapes: A Predictive and Bayesian Framework"

The Earth's topography, including vegetation and human-made features, reduced to a virtual 3-D representation is a key geographic layer for any extended development or risk management project. Processed from multiple aerial images or from airborne lidar systems, the 3-D topography is first represented as a point cloud. This paper deals with the generation of digital terrain models (DTMs) in natural landscapes. We present a global methodology for estimating the terrain height by deriving a predictive filter paradigm. Under the assumption that the terrain topography (elevation and slope) is regular in a neighboring system, a predictive filter combines linearly the predicted topographic values and the effective measured values. In this paper, such a filter is applied to 3-D lidar data which are known to be of high elevation accuracy. The algorithm generates an adaptive local geometry wherein the elevation distribution of the point cloud is analyzed. Since local terrain elevations depend on the local slope, a predictive filter is first applied on the slopes and then on the terrain elevations. The algorithm propagates through the point cloud following specific rules in order to optimize the probability of computing areas containing terrain points. Considered as an initial surface, the previous DTM is finally regularized in a Bayesian framework. Our approach is based on the definition of an energy function that manages the evolution of a terrain surface. The energy is designed as a compromise between a data attraction term and a regularization term. The minimum of this energy corresponds to the final terrain surface. The methodology is discussed, and some conclusive results are presented on vegetated mountainous areas. [J114]

## "Micro-Doppler Effect Analysis and Feature Extraction in ISAR Imaging With Stepped-Frequency Chirp Signals"

The micro-Doppler (m-D) effect induced by the rotating parts or vibrations of the target provides a new approach for target recognition. To obtain high range resolution for the extraction of the fine m-D signatures of an inverse synthetic aperture radar target, the stepped-frequency chirp signal (SFCS) is used to synthesize the ultrabroad bandwidth and reduce the requirement of sample rates. In this paper, the m-D effect in SFCS is analyzed. The analytical expressions of the m-D signatures, which are extracted by an improved Hough transform method associated with time-frequency analysis, are deduced on the range-slow-time plane. The implementation of the algorithm is presented, particularly in those extreme cases of rotating (vibrating) frequencies and radii. The simulations validate the theoretical formulation and robustness of the proposed m-D extraction method. [J115]

## "Automatic Correction of Range Migration in SAR Imaging"

A new technique is developed for the automatic correction of range migration in synthetic aperture radar imaging. In the range-Doppler domain, samples at a Doppler frequency constitute a Doppler slice. It is noted that, when there is no range migration, the Doppler slices have similar envelopes, i.e., the envelope of one Doppler slice roughly equals the envelope of another Doppler slice multiplied by a constant. Thus, range migration can be corrected by shifting the Doppler slices such that their envelopes are similar. The technique applies even when the radar moves irregularly or the target is moving. [J116]

## "Fore and Aft Channel Reconstruction in the TerraSAR-X Dual Receive Antenna Mode"

The TerraSAR-X satellite is a high-resolution synthetic aperture radar (SAR) system launched in June 2007 which provides the option to split the antenna in along-track direction and sample two physical channels separately. Modern SARs are equipped with active phased array antennas and multiple channels. In order to keep costs low, TerraSAR-X uses the redundant receiver unit for the second channel such that fore and aft channel signals are combined by a hybrid coupler to form sum and difference channel data. The dual receive antenna (DRA) mode can either be used to acquire along-track interferometric data or to acquire signals with different polarizations at the same time (Quad-Pol). Fore and aft channel reconstruction is necessary if ground moving target indication (GMTI) algorithms such as the displaced phase center antenna technique or along-track interferometry shall be applied, and in order to separate the horizontally and vertically polarized received signal components. The proposed approach uses internal calibration pulses from different calibration beams in order to estimate and compensate the hardware impact. The theoretical framework together with the results from the experimental data evaluation for the fore and aft channel reconstruction of the TerraSAR-X DRA mode are presented. The impact of the receive hardware transformation matrix estimation accuracy on errors in the reconstructed fore and aft channel image data is studied, and first examples on the GMTI capability of the

TerraSAR-X DRA mode are given. [J117]

## "Investigation of Ocean Surface Wave Refraction Using TerraSAR-X Data"

As a scientific and technological continuation of the X-band Synthetic Aperture Radar (X-SAR) and Shuttle Radar Topography Mission (SRTM) missions, the new X-SAR, namely, TerraSAR-X (TSX), was launched on June 15, 2007. Since then, it has provided numerous high-quality data over land and ocean operationally. In this paper, surface wave refraction and diffraction are investigated using TSX imagery acquired over the coast of Terceira island situated in the North Atlantic. Peak wavelength and wave direction are determined by SAR 2-D image spectra. They are compared to measurements of X-band marine radar and results of the WAve prediction Model (WAM). Significant wave height in the near-shore shallow water region is estimated from TSX Spotlight mode data following the wave refraction laws and using the developed XWAVE empirical algorithm. Image spectra of the TSX subscenes in the full-coverage region are given to investigate significant changes of wave direction and length. By analyzing another TSX image acquired in StripMap mode, a shadow zone in the lee side of Terceira island is identified. It is influenced jointly by wave refraction and diffraction. Furthermore, a cross-sea pattern revealed in the image spectra is investigated. The cross sea is generated by the diffracted wave rays from the northern and southern coasts of the island. Less wave directional spreading for the cross-sea situation is observed as well when compared to the image spectra at the origin of diffraction. [J118]

## "Reconstruction of GPR Signals by Spectral Analysis of the SVD Components of the Data Matrix"

This letter considers the problem of reconstructing total-time responses from noisy data collected by ground-penetrating radar (GPR). The well-known singularity expansion method (SEM)-a theory-for late-time response representation is generalized to establish a matrix model (data matrix)representing total-time responses of radar scattering waveforms. Using singular value decomposition of the data matrix-an intermediate processing technique, we present an approach to model-order determination and successfully reconstruct the total-time responses. The model order is quantitativelyselected by spectral analysis of left singular vectors of the data matrix and of the emitted waveform. The most important discoveries in this letter are as follows: (1) the GPR upper frequency can be used as a criterion for the selection of left singular vectors of the data matrix, and (2) the left singular vectors of the data matrix, which should not be neglected, tend to be predominantly low-pass functions and also provide valuable information for model-order determination. [J119]

## "Covariance Estimation for dInSAR Surface Deformation Measurements in the Presence of Anisotropic Atmospheric Noise"

We study anisotropic spatial autocorrelation in differential synthetic aperture radar interferometric (dInSAR) measurements and its impact on geophysical parameter estimations. The dInSAR phase acquired by the satellite sensor is a superposition of different contributions, and when studying geophysical processes, we are usually only interested in the surface deformation part of the signal. Therefore, to obtain high-quality results, we would like to characterize and/or remove other phase components. A stochastic model has been found to be appropriate to describe atmospheric phase delay in dInSAR images. However, these phase delays are usually modeled as being isotropic, which is a simplification, because InSAR images often show directional atmospheric anomalies. Here, we analyze anisotropic structures and show validation results using both real and simulated data. We calculate experimental semivariograms of the dInSAR phase in several European Remote Sensing satellite-1/2 tandem interferograms. Based on the theory of random functions (RFs), we then fit anisotropic variogram models in the spatial domain, employing Mate??rn- and Bessel-family correlation functions in nested models to represent complex dInSAR covariance structures. The presented covariance function types, in the statistical framework of stationary RFs, are consistent with tropospheric delay models. We find that by using anisotropic data covariance information to weight dInSAR measurements, we can significantly improve both the precision and accuracy of geophysical parameter estimations. Furthermore, the improvement is dependent on how similar the deformation pattern is to the dominant structure of the anisotropic atmospheric signals. [J120]

## "TerraSAR-X Mission Planning System: Automated Command Generation for Spacecraft Operations"

On June 15, 2007, TerraSAR-X was successfully launched from Baikonur, Kazakhstan. On board TerraSAR-X, a high-resolution X-band synthetic aperture radar (SAR) instrument is being operated as the primary payload. The user community requesting SAR products is composed of commercial and scientific partners as documented in a public-private-partnership agreement. The operations of the TerraSAR-X bus as well as payload operations are performed by the Mission Operations Segment (MOS). The Mission Planning System (MPS), which is a part of the MOS, has been designed to handle complex payload and standard bus operations in an automated manner. The purpose of this paper is to describe the concepts and the TerraSAR-X realization of the MPS. [J121]

## "Topographic Mapping of the German Tidal Flats Analyzing SAR Images With the Waterline Method"

The waterline method is used to derive the topography of the tidal flats along the German coast by evaluation of synthetic aperture radar (SAR) images. A series of about 70 European Remote Sensing Satellites SAR images of the German Bight taken at different water levels within four years is analyzed to detect the borderline between tidal flats and adjacent water areas using a wavelet-based edge-detection algorithm. After geocoding, the waterlines are combined with the corresponding water levels to represent the topography on an irregularly spaced grid. The water levels are taken from a numerical tide model and corrected with the measured gauge data. Interpolation of these data into a regular grid yields a topographic map of the intertidal zone. While the general practicability of this method has been demonstrated in previous studies for smaller test areas, this paper is the first attempt to generate maps of a large area on a yearly basis. [J122]

## "An Estimation Method for InSAR Interferometric Phase Based on MMSE Criterion"

In this paper, we propose a method based on minimum mean squared error (mmse) criterion to estimate synthetic aperture radar interferometry (InSAR) interferometric phase. In this method, the cross-correlation coefficient vector with large coregistration error is given first, and then, the cost function under the mmse criterion is used to estimate the InSAR interferometric phase. The method can auto-coregister the SAR images and reduce the interferometric phase noise simultaneously. Theoretical analysis and computer simulation results show that the method can provide an accurate estimate of the terrain interferometric phase (interferogram) even when the coregistration error reaches 1 pixel. [J123]

## "Statistical Analysis of a High-Resolution Sea-Clutter Database"

This paper presents the statistical analysis of an experimental high-resolution sea-clutter database, collected with a high-resolution Ka-band radar at the south coast of Spain. The main motivation of this paper has been to check the validity of the available theoretical models for high-resolution sea-clutter against data corresponding to a range resolution of centimeters. The overall amplitude probability density function (pdf), the compatibility with a compound representation, and the average spectral behavior of the data are analyzed in detail. Results clearly show the suitability of the compound Gaussian model and, more precisely, that the empirical pdf is well modeled by the generalized Kdistribution with log-normal texture. A close agreement has also been found between the estimated clutter spectral density and a power-law model. [J124]

## "Estimating River Depth From Remote Sensing Swath Interferometry Measurements of River Height, Slope, and Width"

The Surface Water and Ocean Topography (SWOT) mission is a swath mapping radar interferometer that would provide new measurements of inland water surface elevation (WSE) for rivers, lakes, wetlands, and reservoirs. SWOT WSE estimates would provide a source of information for characterizing streamflow globally and would complement existing in situgage networks. In this paper, we evaluate the accuracy of river discharge estimates that would be obtained from SWOT measurements over the Ohio river and eleven of its major tributaries within the context of a virtual mission (VM). SWOT VM measurements are obtained by using an instrument measurement model coupled to simulated WSE from the hydrodynamic model LISFLOOD-FP, using USGS streamflow gages as boundary conditions and validation data. Most model pixels were estimated two or three times per 22-day orbit period. These measurements are then input into an algorithm to obtain estimates of river depth and discharge. The algorithm is based on Manning's equation, in which river width and slope are obtained from SWOT, and roughness is estimated a priori.SWOT discharge estimates are compared to the discharge simulated by LISFLOOD-FP. Instantaneous discharge estimates over the one-year evaluation period had median normalized root mean square error of 10.9%, and 86% of all instantaneous errors are less than 25%. [J125]

## "Sonar Measurements in Ship Wakes Simultaneous With TerraSAR-X Overpasses"

A pilot experiment was conducted in the period from April to June 2008 in the Straits of Florida near Port Everglades, Florida, in order to study the dynamics of far wakes of ships. In this experiment, a small boat with downward-looking sonar made ??snakelike?? sections through wakes of ships of opportunity during the TerraSAR-Xoverpasses. The ship and its parameters (length, speed, course, etc.) were identified utilizing an automated identification system. The sonar responded to the clouds of microbubbles generated in the ship wake by the propulsion system and ship-hull turbulence. The ship wakes were traced in the sonar signal typically from 10 to 30 min after the ship's passage. A preliminary analysis of the measurements suggests that the visibility of the centerline ship wake in synthetic aperture radar (SAR) images is correlated with the presence of microbubbles in the wake. This supports the hypothesis that natural surfactants scavenged and brought to the

surface by rising bubbles play an important role in the wake visibility in SAR. The influence of the wind-wave field on the ship wake, as well as the effect of screening of the wind-wave field by the ship's hull, adds another level of complexity to wake patterns observed in SAR images. [J126]

## "The TerraSAR-X Mission and System Design"

This paper describes the TerraSAR-X mission concept within the context of a public-private partnership (PPP) agreement between the German Aerospace Center (DLR) and the industry. It briefly describes the PPP concept as well as the overall project organization. This paper then gives an overview of the satellite design and the corresponding ground segment, as well as the main mission parameters. After a short introduction to the scientific and commercial exploitation scheme, this paper finally focuses on the mission accomplishments achieved so far during the ongoing mission. [J127]

## "One-Dimensional Mirrored Interferometric Aperture Synthesis"

Aperture synthesis technique can provide high spatial resolution without requiring very large and massive real aperture. However, for a large aperture synthesis system, which will involve hundreds of antennas and thousands of correlators, system and its calibration are very complicated. In this letter, mirrored interferometric aperture synthesis (MIAS) is proposed, which can achieve the same spatial resolution as a large traditional aperture synthesis system but needs fewer antennas. First, the imaging principle of MIAS is presented. A new concept, named Cosine Visibility, is proposed to replace the visibility function used in traditional aperture synthesis. The relationship between the brightness temperature and the cosine visibility is a Cosine Transform. Inverse Cosine Transform can be applied to reconstruct the image of brightness temperature. Then, an example for MIAS is given, and a method is proposed to handle the problems of baselines missing and the rank defect associated with the underdetermined linear equations which relate the cross correlation between signals collected by pairs of antennas with the cosine visibility. Moreover, MIAS with a small array can provide higher and higher spatial resolution by combining more and more linear equations with the help of adjusting the distance from the array to the reflector. The simulation results demonstrate the validity of MIAS and the improvement of spatial resolution. The study in this letter provides a means to reduce the complexity of system and calibration of large traditional aperture synthesis systems. [J128]

## "Polarimetric Characterization and Temporal Stability Analysis of Urban Target Scattering"

This paper studies the polarimetric-dispersion properties of urban targets and their evolution along time in terms of the geometrical configuration. The relations between target geometry and the scattering behavior have been defined through the analysis of large stacks of simulated images. Scattering maps and synthetic aperture radar (SAR) images have been synthesized with the numerical tool GRaphical Electromagnetic COmputing SAR for different qualitative models of two real buildings. Ground-based SAR (GB-SAR) data acquired in a subsidence measurement campaign has been used to assess the simulator's realism. These data have permitted the identification of the critical simulation parameters and their range of recommended values for realistic simulations. In the context of very high resolution images, the results derived from this study may be crucial for making progress in urban-image postprocessing. As the different resolution cells comprise few scattering centers showing a quasi-deterministic scattering behavior, nonprobabilistic models based on target's geometry seem more suited for scattering modeling. In these models, the geometry-scattering (GS) links precisely inferred from simulated images can be very important. In addition to change detection and land classification, GS models may help in improving the interpretation of subsidence results with differential interferometry. Certainly, new processing algorithms can be developed exploiting the available scattering data with more physical sense. In addition, they can take more advantage of the fine resolution and polarimetric capabilities of the new sensors, like TerraSAR-X or RADARSAT-2. [J129]

## "SAR Calibration Aided by Permanent Scatterers"

We propose a calibration method suitable for a set of repeated synthetic aperture radar (SAR) acquisitions that uses both absolute calibrated devices (such as corner reflectors) and stable targets identified in the scene [the permanent scatterers (PSs)]. Precisely, the role of the PS is to extend the initial calibration sequence by monitoring the radiometric stability of the system throughout the whole mission life span. At a first step, this paper approaches the problem of PS-based normalization by an iterative maximum-likelihood method that exploits the stack of complex interferometric SAR images. Two solutions are given based on different assumptions on the PS phases. As a second step, the merging of these estimates with the available calibration information is discussed. Results achieved by experimental acquisitions are shown in two different SAR systems: 1) a C-band spaceborne SAR and 2) a Ku-band ground-based SAR. [J130]

## "Noise-Related Radiometric Correction in the TerraSAR-X Multimode SAR Processor"

Synthetic aperture radar (SAR) image intensity is disturbed by additive system noise. During SAR focusing, pattern corrections that are adapted to the characteristics of the wanted signal, but not to the characteristics of the noise, influence the spatial distribution of the noise power. Particularly in the case of ScanSAR, a distinct residual noise pattern in low backscatter areas results. This necessitates a noise-adapted radiometric correction of the focused image for almost all applications except interferometry. In this paper, we thoroughly investigate this topic. Based on signal theoretical and stochastic considerations, we develop a radiometric correction scheme. Simulations and the application of the algorithm to TerraSAR-X datatakes support the theoretical results. [J131]

## "PolInSAR Statistical Analysis and Coherence Optimization Using Fractional Lower Order Statistics"

In this letter, the polarimetric synthetic aperture radar (SAR) interferometry (PolInSAR) statistical model is studied using the alpha-stable distribution. Based on this model, a vector coherence formulation using fractional lower order statistics is proposed. This vector coherence is the generalization of the vector coherence in the paper of Cloude and Papathanassiou when the PolInSAR data are non-Gaussian and conform to the symmetrical form of the alpha-stable distribution. The standard coherence optimization method in the aforementioned paper is modified based on this generalized vector coherence. Results were demonstrated using a small L-band PolInSAR data set and suggest that this proposed coherence optimization method reduces artifacts in the optimized phases in certain areas. [J132]

## "Multipolarization Microwave Scattering Model for Sahelian Grassland"

A coherent scattering formulation is developed for radar remote sensing of Sahelian grassland. This African vegetation is mainly composed of annual grass and shrubs. In the proposed procedure, first, a temporalmodel for generation of grass and shrub structures, which includes important realistic botanical information, is implemented. Because we develop a coherent scattering model, preserving the relative position of plant elements in a statistical manner as accurately as possible is very important. Shrubs are reproduced using cylindrical elements which represent trunks, branches, and thin green stems that function as leaves for these shrubs. Their crown shape is highly irregular, but for the most part can be encompassed in an ellipsoidal or cylindrical volume; on the other hand, the grass is represented as a set of cylindrical stalks and blade leaves. The scattered power from each grass element is added because multiple scattering among adjacent elements can be neglected at microwave frequencies. We calculate the soil scattering using the Integral Equation Method and neglect the soil volume scattering which may become significant for dry soil condition at high incidence angles. Backscatter statistics are acquired via a Monte Carlo simulation over a large number of realizations. The accuracy of the model is verified using measured data acquired by the C-band environmental satellite advanced synthetic aperture radar instrument at different incident angles. [J133]

## "Fast Alternatives to for Polarimetric SAR"

The polarimetric entropy (H) and the alpha angle (α) are two important parameters for analyzing polarimetric synthetic aperture radar data. However, for some special cases, the unstableness of the alpha angle is found; in addition, time consumption for extracting both the parameters will become quite tedious for very large images by pixelwise eigendecomposition. To overcome these shortcomings, a fast algorithm to calculate the polarimetric entropy and two new parameters are proposed in this paper. The first parameter has similar properties to the alpha angle but is stable; the second also behaves similar to the polarimetric entropy. More importantly, both new parameters can be derived very quickly. Like the unsupervised Hα classification, the image can also be classified based on the two new parameters. The NASA/JPL AIRSAR L-band data of San Francisco are applied in the experiment. [J134]

## "Building Height Retrieval From VHR SAR Imagery Based on an Iterative Simulation and Matching Technique"

Experimental airborne synthetic aperture radar (SAR) systems achieve spatial resolutions of approximately 10 cm, whereas the new spaceborne very high spatial resolution (VHR) SAR sensors onboard the TerraSAR-X and COSMO-SkyMed satellites achieve spatial resolutions down to 1 m. In VHR SAR data, features from individual urban structures (i.e., buildings) can be identified by their characteristic settings in urban settlement patterns. In this paper, we present a novel concept for the height estimation of generic man-made structures from single detected SAR data. The proposed approach is based on the definition of a hypothesis on the height of the building and on the simulation of a SAR image for testing that hypothesis. A matching procedure is applied between the estimated and the actual SAR image in order to test the height hypothesis. The process is iterated

for different height assumptions until the matching function is optimized, and thus, the building height is estimated. The efficiency of the proposed method is demonstrated on a set of 40 flat- and gable-roof buildings using two submeter VHR airborne and two 1-m resolution TerraSAR-X SAR scenes all acquired from the same residential area in Dorsten, Germany. The results show that, in the absence of string disturbing effects, the method is able to estimate the height of flat- and gable-roof buildings in the submeter data to the order of a meter, while the accuracy for the meter resolution spaceborne data is lower but still sufficient to estimate the number of floors of a building. [J135]

## "Radar-Coding and Geocoding Lookup Tables for the Fusion of GIS and SAR Data in Mountain Areas"

Synthetic aperture radar (SAR) image orthorectification induces an important alteration of information due to the side-looking geometry of SAR acquisition. In high-relief areas, the difficulty is increased by the foldover effect: The images acquired with low incidence angles cannot be registered by a bijective transformation like polynomial transformations, as usually proposed by conventional software. In this letter, a simple and efficient method, fitted to geocoded data and SAR images, is introduced to propose a generic coregistration tool that takes SAR geometry into account without requiring the exact sensor model, specific parameters, and precise navigation data. This method is based on a simulated SAR image and on the computation of lookup tables (LUTs) that represent the coordinate transform from one geometry to the other. Results are presented on a high-relief area in the Alps, where satellite and airborne SAR images are used for glacier evolution monitoring. A comparison to other sensor-independent approaches has been performed, showing that the proposed approach performs better in mountain areas. The resulting LUTs allow merging SAR data with the georeferenced data, either in ground geometry by orthorectifying the SAR information or in radar geometry by the inverse transformation, namely, radar-coding data from a geographic information system, to improve the analysis of SAR images and the result interpretation. [J136]

## "4-D SAR Imaging: The Case Study of Rome"

Four-dimensional synthetic aperture radar (SAR) imaging, also known as differential SAR tomography, is a new research topic in the framework of coherent multitemporal/multibaseline SAR processing that extends the interferometry concept. Four-dimensional SAR imaging-based processing could improve the capability of ground-scatterer monitoring with respect to classical differential interferometric SAR processing. The first results on the applicability of such an advanced tomographic SAR processing to real spaceborne data were recently discussed in the literature. In this letter, we present the results of an experiment with a data set that demonstrates the potentialities of this new technique for monitoring complex targets, such as infrastructures. [J137]

## "Interferometric Microrelief Sensing With TerraSAR-X-First Results"

The meter-scale ground resolution of TerraSAR-X spotlight images promises for the first time the 3-D detection of landforms and landform changes on the microrelief scale from a satellite-based remote sensing system. Using repeat-pass pairs of high-resolution spotlight images, this paper analyzes the spatial variation of coherence on the micro- and mesorelief scale and demonstrates the high potential as well as some limitations of this approach for digital elevation model generation, geomorphological mapping, and geomorphic-change detection in contrasting landscapes of the coastal desert of southern Peru. [J138]

## "Experimental Verification of SAR-GMTI Improvement Through Antenna Switching"

Recently, theoretical investigations have shown that switching between parts of the transmit and/or receive aperture in a pulse-to-pulse cycle may improve the ground moving target indication (GMTI) performance of a two-channel radar system. This paper intends to verify these findings experimentally for the switching concept for the first time. Accordingly, six different GMTI modes were implemented in the system PAMIR (phased-array multifunctional imaging radar) of the Fraunhofer Institute for High Frequency Physics and Radar Techniques (Fraunhofer FHR) including three switching modes. An experiment was conducted using six cooperative vehicles following a predefined scenario to compare the GMTI performance and, in particular, the positioning accuracy of the different GMTI modes. The results of this experiment as well as the underlying signal processing are presented in this paper. The analysis is based on a multilook constant false-alarm rate detection scheme. Due to the heterogenous nature of the considered scene, the well-known test statistic for homogeneous terrain had to be extended accordingly, and a novel test statistics is proposed. [J139]

## "On a Novel Approach Using MLCC and CFAR for the Improvement of Ship Detection by Synthetic Aperture Radar"

Multilook cross correlation (MLCC) is a useful technique in extracting the images of ships embedded in heavy sea clutter by synthetic aperture radar (SAR). In the ship detection experiment in 2006 by Phased Array L-band Synthetic Aperture Radar (PALSAR) on board the Advanced Land Observing Satellite, we applied MLCC to PALSAR data in order to extract small fishing boats. The result was that some boats were detected by thresholding MLCC coherence images under favorable conditions. However, it was also found that the threshold method was not suitable to automatically determine the threshold levels corresponding to the desired false alarm rate (FAR) values. In order to overcome this problem and to improve the accuracy of ship detection by MLCC, we propose a new and simple technique of MLCC-constant FAR (CFAR) or gamma-CFAR. In this method, CFAR is applied to interlook coherence images produced by MLCC. We tested this method using simulation and PALSAR data and then found out substantial improvement in signal-to-noise ratio and FAR in comparison with the coherence image alone. In this letter, we summarize the MLCC-CFAR algorithm and the experimental results. [J140]

## "Segmentation of SAR Intensity Imagery With a Voronoi Tessellation, Bayesian Inference, and Reversible Jump MCMC Algorithm"

This paper presents a region-based approach to segmentation of the satellite synthetic aperture radar (SAR) intensity imagery. The approach is based on a Voronoi tessellation, the Bayesian inference, and the reversible jump Markov chain Monte Carlo (RJMCMC) algorithm. By Voronoi tessellation, the approach partitions a SAR image into a set of polygons corresponding to the components of the segmented homogenous regions. Each polygon is assigned a label to indicate a homogeneous region. The labels for all the polygons form a label field, which is characterized by an improved Potts model. The intensities of pixels in each polygon are assumed to satisfy identical and independent gamma distributions in terms of their label. Following the Bayesian paradigm, the posterior distribution that characterizes the SAR image segmentation can be obtained up to the integration constant. Then, a RJMCMC scheme is designed to simulate the posterior distribution and estimate its parameters. Finally, an optimal segmentation is obtained by the maximum a posteriori algorithm. The results obtained on both real Radarsat-1/2 and simulated SAR intensity images show that our approach works well and is very promising. [J141]

## "Single and Multipolarimetric SAR Tomography of Forested Areas: A Parametric Approach"

In this paper, a technique is described for the tomographic characterization of forested areas through multiple synthetic aperture radar (SAR) observations, based on either single or multipolarimetric acquisitions. This technique is based on the idea of characterizing the Fourier spectrum of the multibaseline data as being constituted by two effective scattering centers displaced along the vertical direction, plus the associated decorrelation terms. As a result, SAR tomography will be formulated as the problem of detecting the number of scattering centers within the resolution cell, estimating the parameters that describe their spatial structure, and evaluating the associated backscattered powers. Parameter estimation is carried out through the covariance matching estimation technique, which provides an asymptotically optimal solution. The results of an experiment performed on a real P-band multibaseline fully polarimetric data set relative to the forested site of Remningstorp, Sweden, are reported. [J142]

## "Soil Moisture Effect on Thermal Infrared (8-13-μm) Emissivity"

Thermal infrared (TIR) emissivities of soils with different textures were measured for several soil moisture (SM) contents under controlled conditions using the Box method and a high-precision multichannel TIR radiometer. The results showed a common increase of emissivity with SM at water contents lower than the field capacity. However, this dependence is negligible for higher water contents. The highest emissivity variations were observed in sandy soils, particularly in the 8-9-μm range due to water adhering to soil grains and decreasing the reflectance in the 8-9-μm quartz doublet region. Thus, in order to model the emissivity dependence on soil water content, different approaches were studied according to the a priori soil information. Soil-specific relationships were provided for each soil texture and different spectral bands between 8 and 13 μm, with determination coefficients up to 0.99, and standard estimation errors in emissivity lower than ± 0.014. When considering a general relationship for all soil types, standard estimation errors up to ±0.03 were obtained. However, if other soil properties (i.e., organic matter, quartz, and carbonate contents) were considered, along with soil water content, the general relationship predicted TIR emissivities with a standard estimation error of less than ±0.008. Furthermore, the study showed the possibility of retrieving SM from TIR emissivities with a standard estimation error of about ±0.08 m3. m-3. [J143]

## "Delineation of Urban Footprints From TerraSAR-X Data by Analyzing Speckle Characteristics and Intensity Information"

With a spatial resolution of up to 1 m, the German radar satellite TerraSAR-X (TSX) has significantly increased the usability of spaceborne synthetic aperture radar (SAR) imagery in the context of urban applications. This paper presents an approach toward the semiautomated detection of built-up areas (BAs) based on single-polarized TSX images. The proposed methodology includes a specific preprocessing of the SAR data and an automated image analysis procedure. The preprocessing focuses on the analysis of local speckle characteristics in order to provide a texture layer that highlights BAs. In the context of an object-oriented image analysis, this texture layer is used along with the original intensity information to automatically extract settlements. The technique is tested on the basis of 12 TSX scenes covering representative urban agglomerations distributed throughout the world. Overall, accuracies between 76% and 96% for the derived city footprints demonstrate the high potential of both the TSX imagery and the proposed analysis approach in detecting BAs. In order to demonstrate the robustness and transferability of the image analysis concept, we finally transferred the classification strategy from the object-oriented domain to a more general and simplified pixel-based approach. [J144]

## "Benchmarking High-Resolution Global Satellite Rainfall Products to Radar and Rain-Gauge Rainfall Estimates"

This paper presents an in-depth investigation of the error properties of two high-resolution global-scale satellite rain retrievals verified against rainfall fields derived from a moderate-resolution rain-gauge network (25-30-km intergage distances) covering a region in the midwestern U.S. (Oklahoma Mesonet). Evaluated satellite retrievals include the NASA Tropical Rainfall Measuring Mission multisatellite precipitation analysis and the National Oceanic and Atmospheric Administration Climate Prediction Center morphing technique. The two satellite products are contrasted against a rain-gauge-adjusted radar rainfall product from the WSR-88D network in continental U.S. This paper presents an error characterization of the Mesonet rainfall fields based on an independent small-scale, but very dense (100-m intergage distances), rain-gauge network (named Micronet). The Mesonet error analysis, although significantly lower than the corresponding error statistics derived for the satellite and radar products, demonstrates the need to benchmark reference data sources prior to their quantitative use in validating remote sensing retrievals. In terms of the remote sensing rainfall products, this paper provides quantitative comparisons between the two satellite estimates and the most definitive rain-gauge-adjusted radar rainfall estimates at corresponding spatial and temporal resolutions (25 km and 3 hourly). Error quantification presented herein includes zero- (rain detection probability and false alarm), first- (bias ratio), and second-order (root mean square error and correlation) statistics as well as an evaluation of the spatial structure of error at warm and cold seasons of 2004 and 2006. [J145]

## "Motion Parameter Estimation in the SAR System With Low PRF Sampling"

A novel approach to motion parameter estimation with low pulse repetition frequency (PRF) sampling based on compressed sensing (CS) theory is introduced. As is known to us, when PRF is less than the Doppler spectrum bandwidth, moving targets suffer both Doppler centroid frequency ambiguity and Doppler spectrum ambiguity. Under this condition, the traditional parameter estimation method in the Doppler domain is out of action. The key of this letter converts motion parameter estimation in the synthetic aperture radar system with low PRF sampling into solving an optimization equation based on CS theory. Because moving targets in the scene can be regarded as sparse signals after clutter cancellation, an optimization algorithm based on CS theory is proposed to reconstruct sparse signals and meanwhile estimate the along-track velocities and azimuth positions of moving targets. Considering the fact that range cell migration of moving targets is not subject to PRF limitations, Radon transform is adopted to obtain unambiguous across-track velocities and range positions. Results on simulation and real data are provided to show the effectiveness of this method. [J146]

## "Phase Spectrum of Signals in Ground-Penetrating Radar Applications"

The phase structure of ground-penetrating radar (GPR) signals operating on the basis of a stepped-frequency continuous wave (SFCW) is extracted to obtain additional information about the physical properties of buried objects. The phase structure is obtained from a signal-phase-frequency spectrum by applying the discrete Fourier transform to signals on the output of an SFCW georadar quadrature phase detector. We show that the phase gradient of a phase-frequency spectrum of signals reflected from underground layers and buried objects is determined by their electrical properties. We represent a signal phase structure during the georadar movement along the ground surface as an image of phase isolines (lines corresponding to the phase shift of n2??). We show that the spatial variability of isolines is determined by a medium physical property change or by the presence of inhomogeneous objects. [J147]

## "Accurate UWB Radar Three-Dimensional Imaging Algorithm for a Complex Boundary Without

## Range Point Connections"

Ultrawide-band pulse radars have immeasurable potential for a high-range-resolution imaging in the near field and can be used for noncontact measurement of industrial products with specular or precision surfaces, such as reflector antenna or aircraft fuselage, or identifying and locating the human body in security systems. In our previous work, we developed a stable and high-speed 3-D imaging algorithm, Envelope, which is based on the principle that a target boundary can be expressed as inner or outer envelopes of spheres, which are determined using antenna location and observed ranges. Although Envelope produces a high-resolution image for a simple shape target that may include edges, it requires an exact connection for observed ranges to maintain the imaging quality. For complex shapes or multiple targets, this connection becomes a difficult task because each antenna receives multiple echoes from many scattering points on the target surface. This paper proposes a novel imaging algorithm without range point connection to accomplish high-quality and flexible 3-D imaging for various target shapes. The algorithm uses an accurate estimation for the direction of arrival using signal amplitudes and realizes direct mapping from observed ranges to target points. Several comparative studies of conventional algorithms clarify that our proposed method accomplishes accurate and reliable 3-D imaging even for complex or multiple boundaries. [J148]

## "Change Detection in Satellite Images Using a Genetic Algorithm Approach"

In this letter, we propose a novel method for unsupervised change detection in multitemporal satellite images by minimizing a cost function using a genetic algorithm (GA). The difference image computed from the multitemporal satellite images is partitioned into two distinct regions, namely, ??changed?? and ??unchanged,?? according to the binary change detection mask realization from the GA. For each region, the mean square error (MSE) between its difference image values and the average of its difference image values is calculated. The weighted sum of the MSE of the changed and unchanged regions is used as a cost value for the corresponding change detection mask realization. The GA is employed to find the final change detection mask with the minimum cost by evolving the initial realization of the binary change detection mask through generations. The proposed method is able to produce the change detection result on the difference image without a prioriassumptions. Change detection results are shown on multitemporal Advanced Synthetic Aperture Radar images acquired by the ESA/Envisat satellite and on multitemporal optical images acquired by the Landsat multispectral scanner. The comparisons with the state-of-the-art change detection methods are provided. [J149]

## "Foreword to the Special Issue on TerraSAR-X: Mission, Calibration, and First Results"

The 34 papers in this special issue provide an overview of the TerraSAR-X mission, commissioning phase, calibration, data processing, and applications. [J150]

## "Scaling the 3-D Image of Spinning Space Debris via Bistatic Inverse Synthetic Aperture Radar"

In 3-D inverse synthetic aperture radar (ISAR) imaging of spinning space debris, the image obtained via the available algorithm is modified by a scaling factor. Determined by the angle between the spinning vector and the radar line of sight, this factor cannot be estimated by a monostatic radar in a short imaging interval. This letter derives the bistatic ISAR (Bi-ISAR) geometry and signal model for 3-D imaging of space debris. Then, a 3-D image scaling algorithm is introduced based on the connections between the mono- and bistatic echoes of the same scatterer. Numeric simulations have proved the validity of the proposed algorithm. [J151]

## "Simulation and Analysis of Human Micro-Dopplers in Through-Wall Environments"

We present a simulation methodology for generating micro-Doppler radar signatures of humans moving behind walls. The method combines primitive-based modeling of humans with finite-difference time-domain (FDTD) simulation of walls. Realistic motions of humans are generated from computer animation data. The time-varying human radar cross section is simulated using the primitive-based prediction technique. The scattered returns of humans behind walls are then simulated by a hybrid of the human simulation model with the through-wall propagation data generated from FDTD. The resulting simulator is used to investigate the effects of walls of both homogeneous and inhomogeneous types on human micro-Dopplers. It is found that while through-wall propagation affects the magnitude response of the Doppler spectrogram in the form of attenuation and fading, it only introduces very minor distortions on the actual Doppler frequencies from the body parts. This is corroborated by measurement data collected using a Doppler radar, as well as by a point-scatterer analysis of refraction and multipath introduced by walls. [J152]

## "The TerraSAR-X Satellite"

TerraSAR-X is a versatile synthetic aperture radar (SAR) satellite with active phased array antenna technology and represents the backbone of the German national radar Earth observation mission. With its large variety of different SAR imaging modes and its high operational flexibility, TerraSAR-X ideally serves the scientific community and users from the industrial sector and governmental institutions. The innovative satellite system design combines the rich experience from past German and European SAR space missions like X-SAR, SRTM, ERS 1 and 2, and Envisat combined with state-of-the-art Earth observation bus technology as used, e.g., on the CHAMP and GRACE satellites. [J153]

## "An Iterative Least Square Approach to Elastic-Lidar Retrievals for Well-Characterized Aerosols"

An iterative least square method is presented for estimating the solution to the lidar equation. The method requires knowledge of the backscatter values at a boundary point for all channels and a priori defined relationships between backscatter, extinction, and mass-fraction concentration for all scattering components. The lidar equation is formulated in vector form, and a solution is computed using an iterative least square technique. The solution is stable for signals with extremely low signal-to-noise ratios and for signals at ranges far beyond the boundary point. The solution can be applied to lidar signals with an arbitrary number of wavelengths and scattering components. [J154]

## "Automatic Extraction of Traffic Flows Using TerraSAR-X Along-Track Interferometry"

Spaceborne synthetic aperture radar (SAR) offers great potential for the measurement of ground traffic flows. A SAR with multiple receiving apertures aligned in flight direction repeatedly images the same ground area with a short time lag. This allows for an effective detection of moving ground objects, whose range variation translates into an interferometric phase signal between the receiving channels. The high-resolution German SAR satellite TerraSAR-X offers several ways to create multiple along-track apertures. We exploit this to demonstrate satellite-based traffic-flow measurements using along-track interferometry (ATI) and Displaced Phase Center Array techniques. In this paper, we address the usage of different TerraSAR-X ATI modes for data acquisition and describe an automatic near-real-time processing chain for the extraction of traffic information. The performance of this TerraSAR-X traffic processor is significantly driven by incorporating a prioriknowledge of road networks. We present examples of automatic traffic detection as well as empirical evaluations thereof using different kind of reference data. [J155]

## "Three-Dimensional Imaging via Wideband MIMO Radar System"

The 3-D inverse synthetic aperture radar imaging fast maneuvering targets is an active research area in the past decades. Planar antenna arrays are used to avoid the motion compensation algorithms but at the cost of increasing the hardware complexity. In this letter, to reduce the hardware complexity of the imaging system, a wideband multiple-input multiple-output system with two perpendicular linear arrays is suggested. In contrast to the existing 3-D imaging methods with planar antenna arrays, with the proposed method, the lower hardware complexity is achieved by many additive virtual array elements. Simulations based on synthetic data are provided for testing the proposed method. [J156]

## "Spatial-Temporal Variability of Great Slave Lake Levels From Satellite Altimetry"

The study of lake-level variability of five selected areas across Great Slave Lake (GSL) using satellite altimetry is presented. Data from Topex/Poseidon (TP) and Jason-1 (J1) missions at GSL for the ice-free seasons of 1993-2002 and 2002-2008, respectively, reveal lower performance of J1 for areas closer to 20 km from the coastline compared to 10 km for TP. A calculated bias of 6.99 cm was subtracted to J1 range since TP has better tracking of shoreline waters and lower data rejection. High correlation coefficients for the relative rate of change between lake altimetry heights (LAHs) and corresponding gauge data for Yellowknife Bay and Hay River support the use of LAH changes as effective indicators of variability at GSL. Differences in LAH between the five areas indicate a nonuniform slope which we relate more to variability of the surface water temperature distribution than wind effects. The deeper and colder areas are associated to the least change of LAH gradient through time; therefore, they represent ideal areas to study interannual climate variability. A potential correlation between areas with higher variability in LAH gradients and higher changes in modeled surface water temperatures during the 2003 ice free season is observed. [J157]

## "Toward SMOS L4 SSS Products: Improving L3 SSS With Auxiliary SSS Data"

The Soil Moisture and Ocean Salinity (SMOS) mission will provide for the first time satellite observations of sea-surface salinity (SSS). At level 3 (L3) of the SMOS processing chain, a large amount of SSS data obtained by the satellite will be summarized in gridded products with the aim of synthesizing the information and reducing the error of individual SSS observations. A further improvement of SSS maps could come from the combination of

L3 products with auxiliary SSS data from Argo buoys, ships of opportunity, or moored oceanographic stations. In this paper, we investigate the benefits of combining SMOS data with different auxiliary data sets. We show that the greatest error reductions come from the increase in the spatial-data coverage, even if the temporal coverage is scarce. Conversely, redundant information (i.e., many observations close to each other) or very localized measurements, even if they have a high temporal resolution, do not provide a significant improvement of the SSS products. We show that the most useful auxiliary data in terms of improving the analysis accuracy are those obtained in areas where SMOS data are noisier or, as a second choice, where the SSS field has a large variance. We also show that for areas with the same error in the L3 product (whatever the source of those errors is), it is more advisable to place the auxiliary observations in areas with longer correlation length scales. [J158]

## "The Geometric-Distortion Correction Algorithm for Circular-Scanning SAR Imaging"

The image formation scheme for circular-scanning synthetic aperture radar includes generating a set of focused subimages and the followed mosaiking processing. However, due to the particular acquisition geometry and irregular motion of the radar platform, the inevitable geometric distortions in the subimages are necessary to be corrected. In this letter, a 2-D geometric-distortion correction algorithm based on projection transformation between the scatterers and the images is presented, in condition of focusing the subimages using a linear range-Doppler algorithm. The point target simulation and real circular-scanning data implementation results are provided to demonstrate the validity of the proposed method. [J159]

## "TerraSAR-X Antenna Calibration and Monitoring Based on a Precise Antenna Model"

The high flexibility and tight accuracy requirements of modern spaceborne synthetic aperture radar (SAR) systems require innovative technologies to calibrate and process SAR images. To perform accurate pattern correction during SAR processing, an antenna model can be used to derive the multitude of different antenna beams generated by active antenna steering. The application of such an antenna model could be successfully demonstrated for the TerraSAR-X mission, launched in 2007. The methodology and the results of the in-orbit verification with an achieved accuracy of better than ??0.2 dB are reviewed in this paper in detail, showing its outstanding accuracy. Additionally, the results of the antenna pattern long-term monitoring are described, pointing out the high stability of the system. [J160]

## "An Autonomous Interference Detection and Filtering Approach Applied to Wind Profilers"

An autonomous interference detection and filtering algorithm has been developed for removing the interference bands generated in the Doppler spectra of mesosphere-stratosphere-troposphere (MST) radar signals. The technique, implemented with the MST radar at Gadanki (13.5?? N, 79?? E), is based on identifying interferencelike band signals using a statistical signal variance approach for fixing the amplitude threshold, through which detecting the interference frequency and designing an adaptable notch filter to filter the undesired frequency bands are done. Signals received from the MST radar are sometimes contaminated with interference signals received from other objects or generated within the system through arcing of high-power devices. Multiple interference bands with different characteristics are observed in the power spectra, which contaminate the wind information and other atmospheric signals. The autonomous interference detection and filtering algorithm is applied to various cases, and it is found that the interference signals could effectively be removed, leaving behind the original signals. By this approach, the effective number of signal samples obtained is increased, which helps one to improve the temporal resolution. [J161]

## "Influence of Atmospheric Path Delay on the Absolute Geolocation Accuracy of TerraSAR-X High-Resolution Products"

Two coupled investigations of TerraSAR-X (TSX) high-resolution data are described in this paper: geometric validation, and estimation of the tropospheric path delay using measurements of corner reflectors (CRs) placed at different altitudes but nearly identical ranges. The CRs were placed within Alpine and valley sites in Switzerland, where terrain diversity provides ideal territory for geometric validation studies. Geometric validation was conducted using slant-range complex products from the spotlight and stripmap (SM) modes in ascending and descending configurations. Based on the delivered product annotations, the CR image positions were predicted, and these predictions were compared to their measuredimage positions. To isolate path delays caused by the atmosphere, six TSX SM scenes ( ~ 35 x 50 km) were examined containing four identical CRs with the same ranges and an altitude difference of ~ 3000 m. The CR arrangement made it possible to verify the annotated TSX atmospheric path delay by comparing the predicted slant range with the slant range obtained by measuring the reflector image coordinates. Range differences between the high- and low-altitude reflectors helped to quantify small variations in the path delay. Both SM and spotlight TSX products were verified to meet

the specified accuracy requirements, even for scenes with extreme terrain variations, in spite of the simplicity of the atmospheric model currently integrated into the processor. Small potential improvements of the geolocation accuracy through the implementation of more comprehensive atmospheric modeling were demonstrated. [J162]

## "Evidence of Rainfall Signatures on X-Band Synthetic Aperture Radar Imagery Over Land"

Five spaceborne X-band synthetic aperture radars (X-SARs) are nowadays operating, and several more will be launched in the coming years. These X-SAR sensors, able to image the Earth's surface at metric resolution, may provide a unique opportunity to measure rainfall over land with spatial resolution of about a few hundred meters due to the moving-target degradation effects. This work is devoted to experimentally demonstrate this X-SAR capability, which can also be exploited to correct synthetic aperture radar (SAR) imagery for rainfall attenuation effects. Several case studies, selected from TerraSAR-X (TSX) overpasses over Europe and the southern U.S. in 2008, are qualitatively analyzed in terms of rainfall signatures. Visual validation of these rainfall SAR signatures is carried out by using available data from ground-based weather radars. A detailed data analysis for the case study of Hurricane ??Gustav?? on September 2, 2008, is carried out to assess a quantitative correlation among X-SAR response and near-surface precipitation rain rate. Two simplified empirical inversion algorithms, based on statistical regression and probability matching, are developed to retrieve rain rate from TSX cross-track ground-range measurements. The TSX-retrieved rain fields are compared to those estimated from the Next Generation Weather Radar (NEXRAD) in Mobile (Alabama, U.S.), showing a root-mean-square error less than 15 mm/h and a correlation of about 0.7. [J163]

## "Improving Land Cover Class Separation Using an Extended Kalman Filter on MODIS NDVI Time-Series Data"

It is proposed that the normalized difference vegetation index time series derived from Moderate Resolution Imaging Spectroradiometer satellite data can be modeled as a triply (mean, phase, and amplitude) modulated cosine function. Second, a nonlinear extended Kalman filter is developed to estimate the parameters of the modulated cosine function as a function of time. It is shown that the maximum separability of the parameters for natural vegetation and settlement land cover types is better than that of methods based on the fast Fourier transform using data from two study areas in South Africa. [J164]

## "Development of the TanDEM-X Calibration Concept: Analysis of Systematic Errors"

The TanDEM-X mission, result of the partnership between the German Aerospace Center (DLR) and Astrium GmbH, opens a new era in spaceborne radar remote sensing. The first bistatic satellite synthetic aperture radar mission is formed by flying TanDEM-X and TerraSAR-X in a closely controlled helix formation. The primary mission goal is the derivation of a high-precision global digital elevation model (DEM) according to High-Resolution Terrain Information (HRTI) level 3 accuracy. The finite precision of the baseline knowledge and uncompensated radar instrument drifts introduce errors that may compromise the height accuracy requirements. By means of a DEM calibration, which uses absolute height references, and the information provided by adjacent interferogram overlaps, these height errors can be minimized. This paper summarizes the exhaustive studies of the nature of the residual-error sources that have been carried out during the development of the DEM calibration concept. Models for these errors are set up and simulations of the resulting DEM height error for different scenarios provide the basis for the development of a successful DEM calibration strategy for the TanDEM-X mission. [J165]

## "TerraSAR-X SAR Processing and Products"

The TerraSAR-X mission was launched in June 2007. After successful completion of the commissioning phase, the mission entered its operational phase in January 2008. Since that time, TerraSAR-X provides the scientific remote sensing community and commercial customers with high-quality spaceborne synthetic aperture radar (SAR) data products. The intention of this paper is to present the SAR data processing concept and the comprehensive portfolio of products reflecting the instrument's diverse imaging capabilities together with options of processing and achieved product quality as well as the essentials of SAR processing. Furthermore, it shall also provide details on how to fully exploit the precision of the TerraSAR-X products. [J166]

## "Coherency Matrix Estimation of Heterogeneous Clutter in High-Resolution Polarimetric SAR Images"

This paper presents an application of the recent advances in the field of spherically invariant random vector (SIRV) modeling for coherency matrix estimation in heterogeneous clutter. The complete description of the polarimetric synthetic aperture radar (POLSAR) data set is achieved by estimating the span and the normalized

coherency independently. The normalized coherency describes the polarimetric diversity, while the span indicates the total received power. The main advantages of the proposed fixed-point (FP) estimator are that it does not require any a prioriinformation about the probability density function of the texture (or span) and that it can directly be applied on adaptive neighborhoods. Interesting results are obtained when coupling this FP estimator with an adaptive spatial support based on the scalar span information. Based on the SIRV model, a new maximum-likelihood distance measure is introduced for unsupervised POLSAR classification. The proposed method is tested with both simulated POLSAR data and airborne POLSAR images provided by the Radar Ae?? roporte?? Multi-Spectral d'Etude des Signatures system. Results of entropy/alpha/anisotropy decomposition, followed by unsupervised classification, allow discussing the use of the normalized coherency and the span as two separate descriptors of POLSAR data sets. [J167]

## "Capon- and APES-Based SAR Processing: Performance and Practical Considerations"

This paper discusses the use of Capon's minimum-variance method (MVM) and Amplitude and Phase EStimation (APES) spectral-estimation algorithms to synthetic aperture radar range-azimuth focusing. The rationale of the algorithms is discussed. An implementation of a Capon or APES processing chain is explained, and processing parameters such as chip-image size, resampling factor, and diagonal loading are discussed. For multichannel cases, a joint-processing approach is presented. A set of Monte Carlo simulations are described and used to benchmark Capon- and APES-based processing against conventional matched-filter-based approaches. Both methods improve the resolution and reduce sidelobes. APES yields generally better estimates of amplitude and phase than Capon but with worse resolution. Results with RADARSAT-2 quad-polarization data over Barcelona are used to qualitatively study the real-life performance of these algorithms. [J168]

## "Modeling Envisat RA-2 Waveforms in the Coastal Zone: Case Study of Calm Water Contamination"

Radar altimeters have so far had limited use in the coastal zone, the area with most societal impact. This is due to both lack of, or insufficient accuracy in the necessary corrections, and more complicated altimeter signals. This letter examines waveform data from the Envisat RA-2 as it passes regularly over Pianosa (a 10-km2island in the northwestern Mediterranean). Forty-six repeat passes were analyzed, with most showing a reduction in signal upon passing over the island, with weak early returns corresponding to the reflections from land. Intriguingly, one third of cases showed an anomalously bright hyperbolic feature. This feature may be due to extremely calm waters in the Golfo della Botte (northern side of the island), but the cause of its intermittency is not clear. The modeling of waveforms in such a complex land/sea environment demonstrates the potential for sea surface height retrievals much closer to the coast than is achieved by routine processing. The long-term development of altimetric records in the coastal zone will not only improve the calibration of altimetric data with coastal tide gauges but also greatly enhance the study of storm surges and other coastal phenomena. [J169]

## "Assessment of the Stereo-Radargrammetric Mapping Potential of TerraSAR-X Multibeam Spotlight Data"

TerraSAR-X can acquire image data in various resolutions down to a range of about 1 m. Moreover, the sensor can operate at various imaging beams and thus acquire image data at different off-nadir viewing angles. These circumstances led to a stimulation of the traditional stereo-mapping approach, as TerraSAR-X image pairs became available in high resolution and in various geometric dispositions. With respect to 3-D surface mapping, TerraSAR-X stereo data processing, therefore, is a serious alternative to synthetic aperture radar interferometry, which can be addressed as the evolving mapping technique of the last decade. Within the TerraSAR-X science program of the German Aerospace Center (DLR), high-resolution multibeam data sets in Spotlight mode were acquired for several Austrian test sites. In general, three images were obtained from either ascending or descending orbits. In order to exploit the 3-D mapping accuracy of TerraSAR-X, stereo-radargrammetric mapping techniques were applied to the data sets, thereby utilizing stereo pairs as well as multi-image data sets in various dispositions. This paper focuses on one of the selected test sites and refers to the issues of 2-D and 3-D mapping-accuracy assessment as well as to surface model and vegetation-height-model generation. Validation of these products was widely restricted to visual analysis due to the lack of adequate high-quality reference products. [J170]

## "HF Radio-Frequency Interference Mitigation"

The dense radio-frequency interference (RFI) distributed on the spectrum in the high-frequency band greatly degrades the performance of radio systems and makes it urgent to find an effective and speedy method to eliminate the interferences. The interference mitigation method introduced in this letter is implemented before any further signal processing. It reconstructs the interference by the exactly estimated frequency, amplitude, and

phase parameters in the signal spectrum and then subtracts the artificial interference from the input time-domain complex signal. The procedure steps of the method are illustrated in detail. The data stream of continuous oblique-incident ionospheric detection has been processed effectively and rapidly in real time. Several delay-Doppler ionograms severely contaminated by RFI are selected and presented. Comparisons of the original and mitigated ionograms and the signal-to-noise ratio (SNR) data show that the RFIs are eliminated perfectly and that the SNR is greatly improved. [J171]

## "Signal Processing for Improved Detection of Trapped Victims Using UWB Radar"

Detection of trapped victims using ultrawideband radar is considered a highly challenging task due to multiple unknown parameters and generally very low signal-to-noise-and-clutter ratio (SNCR) conditions. In this paper, we propose a novel detection algorithm which is designed for detection of periodic motion caused by, e.g., respiratory motion of the victim for low SNCR conditions. The aim is to separate the respiratory-motion response of a trapped victim from nonstationary clutter originating from moving objects in the scene of interest. The algorithm performs stationary-clutter removal, high-level noise, and nonstationary-clutter suppression, indicates presence of the trapped victim, and estimates its range. The performance of the algorithm is investigated, both by means of simulation and experimental verification. The results show improved detection capabilities in low SNCR over an existing algorithm proposed by Zaikov et al. [J172]

## "Signatures of ERS-Envisat Interferometric SAR Coherence and Phase of Short Vegetation: An Analysis in the Case of Maize Fields"

Interferometric observations between the European Remote Sensing, ERS-2, synthetic aperture radar (SAR) and the Envisat Advanced SAR (ASAR) are unique since they are characterized by a short repeat-pass interval (28 min) and a perpendicular baseline of approximately 2 km. In vegetated areas, this configuration should preserve from strong temporal decorrelation and enhance the sensitivity of coherence and SAR interferometric (InSAR) phase to volumes with small heights. This assumption could be tested with the data acquired during the dedicated ERS-Envisat Tandem mission on October 15, 2007, over the Seeland region, Switzerland. Five maize fields and one sunflower field presented lower coherence and offsets of the interferometric phase, i.e. height, with respect to neighboring bare fields. To gain understanding on the interferometric signatures, the interferometric water cloud model was used to simulate coherence and InSAR height for the maize fields. Both the coherence and the InSAR height present clear dependence upon vegetation height and exhibit strong consistency. Simulations showed that the modeled coherence and InSAR height are most sensitive to the two-way attenuation and the temporal coherence of the vegetation. The best correspondence between the observed and modeled InSAR parameters was obtained with two-way attenuation values between 2 and 4 dB/m (corresponding to an extinction between 1 and 2 dB/m) and high temporal coherence of the vegetation (above 0.6), with this being due to the very stable conditions of the weather during the 28-min interval between image acquisitions. [J173]

## "Estimation and Error Analysis of Woody Canopy Leaf Area Density Profiles Using 3-D Airborne and Ground-Based Scanning Lidar Remote-Sensing Techniques"

Vertical profiles of the leaf area density (LAD) of a Japanese zelkova canopy were estimated by combining airborne and portable ground-based light detection and ranging (lidar) data and using a voxel-based canopy profiling method. The profiles obtained by the two types of lidars complemented each other, eliminating blind regions and yielding more accurate LAD profiles than could be obtained by using each type of lidar alone. In the combined results, the mean absolute errors (MAEs) of LAD ranged from 0.20 to 0.42 m2m-3, and the mean absolute percentage errors (MAPEs) of the leaf area index (LAI) ranged from 22.3% to 27.2%, for ground areas from 4 to 32 m2, respectively. A laser beam coverage index ?? incorporating the lidar's beam settings and a beam attenuation factor was proposed. This index showed general applicability to explain the LAD estimation error for LAD measurements using different types of lidars and with different beam settings. Parts of the LAD profiles that were underestimated even when data from both lidars were combined were interpolated by using a Gaussian function. The interpolation yielded improved results for ground areas of 16 and 32 m2; the respective MAEs of LAD were 0.17 and 0.11 m2m-3, and the respective MAPEs of LAI were 8.0% and 9.4%. The proposed method improves lidar-derived LAD estimation and is adapted to broadleaved canopies. The index ?? was tested against an actual canopy scenario and could be used to determine appropriate lidar measurement settings when data from different sources of lidar data are combined to estimate LAD profiles. [J174]

## "Effect of Target Moisture on Laser Scanner Intensity"

We have studied the effect of moisture on the backscatter reflectance of mineral aggregate (such as sand and gravel) targets that are used as reflectance standards in airborne laser scanning intensity calibration. Target

moisture has turned out to be a crucial factor when using external reference targets (either commercial or naturally available at the measurement site). The most common targets used thus far are different types of gravel and sand, which emphasizes the role of moisture because of the long time required for drying. We carried out laboratory and field experiments to find out how moisture affects the performance of these targets as reference standards. We found that even small amount of moisture has a crucial effect on target reflectance properties: The backscattered reflectance decreases strongly up to 10% gravimetric water content, after which the reflectance level mostly remains constant. The moisture effect has to be further studied and taken into account in the retrieval and calibration of laser scanner intensity data acquired in moist conditions. We also demonstrate a practical method of deriving the surface backscattered reflectance at different moisture contents with a digital camera. [J175]

## "Numerical Backscattering Analysis for Rough Surfaces Including a Cloddy Structure"

In recent years, the presence of a new type of agricultural-surface tillage used for the sowing of wheat and corn has been observed with increasing frequency. It illustrates less roughly ploughed soils, with a greater quantity of small clods distributed over the soil surface. In this paper, a new description of such rough agricultural surfaces is proposed. It is based on a composite model, including a classical surface represented by an exponential correlation function, together with a random cloddy structure. This description enables volumetric structures to be introduced over the soil's surface. A numerical moment-modeling method, based on integral equations, is used to evaluate the contribution of clods to the radar backscattering behavior of agricultural surfaces. It is found that the presence of clods explains the very small correlation lengths which are often found in cloddy agricultural fields. The classical approach, in which the surface is described by a correlation function only based on two statistical parameters, rms height and correlation length, overestimates the backscattering coefficients when compared with an approach that includes the clods. This overestimation is often observed with real radar data for such fields. [J176]

## "Application of TerraSAR-X Data for Emergent Oil-Spill Monitoring"

Synthetic aperture radar (SAR) signals can propagate through hazardous weather and atmospheric conditions with heavy cloud cover, volcanic dust, snow, or rain. The all-weather capabilities of SARs have attracted significant interest in remote sensing communities, since serious environmental disasters such as oil spills have been highly ??elusive?? to optical sensors, making visible spectrum data vulnerable to rapidly changing atmospheric conditions. In this paper, we discuss the technical functionalities of TerraSAR-X from the emergency response perspective, describing its technical abilities in terms of a damping ratio, radiometric accuracy, and noise level with reference to the actual Hebei Spirit oil-spill incident that occurred on the west coast of the Korean peninsula in December 2007. The damping ratios estimated from the TerraSAR-X data as a function of Bragg wavenumber for various wind speeds indicate that TerraSAR-X data can be effectively used to identify oil-spill areas with acceptable accuracy. We also received ERS-2, ENVISAT, RADARSAT-1, and ALOS PALSAR data for this oil-spill event, not simultaneously but with varying time delays. The processing results for the multitemporal data sets obtained from the X- and C-band SAR systems are useful since they can be used to determine the near-real-time migration of spilt oil. The results of the current study indicate that there are distinct advantages of using X-band TerraSAR-X data for oil-spill detection compared to the data obtained at other available frequencies. [J177]

## "The May 12, 2008, (Mw 7.9) Sichuan Earthquake (China): Multiframe ALOS-PALSAR DInSAR Analysis of Coseismic Deformation"

A destructive (Mw 7.9) earthquake affected the Sichuan province (China) on May 12, 2008. The seismic event ruptured approximately 270 km of the Yingxiu-Beichuan fault and about 70 km of the Guanxian-Anxian fault. Surface effects were suffered over a wide epicentral area (about 300 km E-W and 250 km N-S). We apply the differential synthetic aperture radar interferometry (DInSAR) technique to detect and measure the surface displacement field, using a set of ALOS-PALSAR L-band SAR images. We combine an unprecedented high number of data (25 frames from six adjacent tracks) to encompass the entire area which has coseismically displaced. The resulting mosaic of differential interferograms covers an overall area of about 340 km E-W and 240 km N-S. We investigate the source of the Sichuan earthquake by modeling the DInSAR data. The geometry and position of the fault parameters are inferred by a nonlinear inversion, followed by a linear inversion to retrieve the relative slip distribution. Our results show two different source mechanisms for the 145-long Yingxiu-Beichuan fault and for the 105-long Beichuan-Qingchuan fault. Both faults are characterized by slip concentrations of up to 8 m. [J178]

## "Bistatic Scattering of GPS Signals Off Arctic Sea Ice"

This paper evaluates the potential of a global positioning system (GPS) bistatic radar for the retrieval of information concerning the presence and condition of sea ice cover. For this purpose, the permittivityand roughnessof a ground scattering target at L-band are extracted from reflected GPS waveforms collected from an airborne platform using the Kirchhoff approximation for the surface cross section. The retrieved GPS estimates are then evaluated against collocated measurements of surface roughness obtained from a lidar profiler and a reference classification of sea ice types inferred from a multisensor data set that includes polarimetric microwave emissions, RADARSAT backscatter, and Moderate Resolution Imaging Spectroradiometer infrared/visible imagery. [J179]

## "A Two-Dimensional Spectrum for General Bistatic SAR Processing"

This letter derives a 2-D point target spectrum for general bistatic synthetic aperture radar (SAR). For the bistatic configuration, the contributions of the transmitter and the receiver to the overall instantaneous Doppler are unequal due to the different slant range histories. In this letter, an instantaneous Doppler contribution ratio is proposed to represent the difference between the instantaneous Doppler contributions of the transmitter and the receiver, which varies with instantaneous Doppler and range frequency. Then, the 2-D spectrum is obtained by using the stationary phase principle and Taylor series expansion for general bistatic SAR. The accuracy of the spectrum is verified with a point target simulation of different general bistatic configurations. [J180]

## "ISAR Imaging for Avian Species Identification With Frequency-Stepped Chirp Signals"

Imaging an avian target by inverse synthesis aperture radar (ISAR) is a novel and important technological approach of solving the problem of avian detection. However, the ISAR images of birds obtained with the conventional range-Doppler algorithm could be contaminated due to serious micro-Doppler effects, which are generated by the birds' flapping wings. In this letter, a novel imaging method of birds is proposed, which is simple to comprehend and operate, and avoids lots of complications and computation burdens. In the method, the moving status of bird is identified first via finding the variety of moving average values of the cross-correlation coefficient of the adjacent high-resolution range profiles. The usage of moving average values is attributed to the characters of the bird's flapping. The parts of respective flapping spectrogram can then be eliminated, and the parts of the residual spectrogram, i.e., the respective gliding spectrogram, can be connected to prepare for the cross-compression. In this letter, the minimum waveform entropy criterion and genetic algorithm are employed in the spectrogram connection to compensate the phase error. Finally, the feasibility and effectiveness of the methods are verified by simulation results. [J181]

## "Uncertainties in Ice-Sheet Altimetry From a Spaceborne 1064-nm Single-Channel Lidar Due to Undetected Thin Clouds"

In support of the Ice, Cloud, and land Elevation Satellite (ICESat)-II mission, this paper studies the bias in surface-elevation measurements caused by undetected thin clouds. The ICESat-II satellite may only have a 1064-nm single-channel lidar onboard. Less sensitive to clouds than the 532-nm channel, the 1064-nm channel tends to miss thin clouds. Previous studies have demonstrated that scattering by cloud particles increases the photon-path length, thus resulting in biases in ice-sheet-elevation measurements from spaceborne lidars. This effect is referred to as atmospheric path delay. This paper complements previous studies in the following ways: First, atmospheric path delay is estimated over the ice sheets based on cloud statistics from the Geoscience Laser Altimeter System onboard ICESat and the Moderate Resolution Imaging Spectroradiometer (MODIS) onboard Terra and Aqua. Second, the effect of cloud particle size and shape is studied with the state-of-the-art phase functions developed for MODIS cirrus-cloud microphysical model. Third, the contribution of various orders of scattering events to the path delay is studied, and an analytical model of the first-order scattering contribution is developed. This paper focuses on the path delay as a function of telescope field of view (FOV). The results show that reducing telescope FOV can significantly reduce the expected path delay. As an example, the average path delays for FOV= 167 ??rad (a 100-m-diameter circle on the surface) caused by thin undetected clouds by the 1064-nm channel over Greenland and East Antarctica are illustrated. [J182]

## "A Physically Based Screen for Precipitation Over Complex Surfaces Using Passive Microwave Observations"

Physically based passive microwave precipitation retrievals are difficult to develop over land because high nonuniform land emissivity values are difficult to distinguish from those of clouds. This paper uses an empirical approach to determine the covariance of emissivity at different microwave window channels and relies on this covariance to estimate the portion of the observed brightness temperatures that may be attributable to rainfall. One year (2006) of global cloud-free surface emissivity values were retrieved using data sets from multiple instruments on NASA's Aqua satellite. Correlations between the emissivities at different channels were

developed for use in an empirical model within an optimal estimation retrieval. The optimal estimation retrieves surface temperature, total column water vapor, cloud water, and the emissivity at the 10.7-GHz horizontally polarized channel. From this retrieval and the covariance of emissivities, the 89.0-GHz brightness temperature at both polarizations can be estimated. Significant differences between the observed and retrieved high-resolution brightness temperatures are used to screen for precipitation, and results are compared to ground-based radar data for several study regions representing a variety of land surface types in the U.S. The Heidke Skill Score is used to determine the robustness of this methodology and, in all cases, demonstrates at least some increase in skill relative to random chance. [J183]

## "Alternative Methodologies for the Internal Quality Control of Parallel LiDAR Strips"

Light Detection and Ranging (LiDAR) systems have been widely adopted for the acquisition of dense and accurate topographic data over extended areas. Although the utilization of this technology has increased in different applications, the development of standard methodologies for the quality control (QC) of LiDAR data has not followed the same trend. In other words, a lack in reliable, practical, cost-effective, and commonly acceptable QC procedures is evident. A frequently adopted procedure for QC is comparing the LiDAR data to ground control points. Aside from being expensive, this approach is not accurate enough for the verification of horizontal accuracy, unless specifically designed LiDAR targets are used. This paper is dedicated to providing accurate, economical, and convenient internal QC procedures for the evaluation of LiDAR data, which is captured from parallel flight lines. The underlying concept of the proposed methodologies is that, in the absence of systematic and random errors in system parameters and measurements, conjugate surface elements in overlapping strips should perfectly match each other. Consistent incompatibilities and the quality of fit between conjugate surface elements in overlapping strips can be used to detect systematic errors in the system parameters/measurements and to evaluate the noise level in the LiDAR point cloud, respectively. Experimental results from real data demonstrate that all the proposed methods, with one exception, produce compatible estimates of systematic discrepancies between the involved data sets, as well as good quantification of inherent noise. [J184]

## "Monitoring Subglacial Volcanic Eruption Using Ground-Based C-Band Radar Imagery"

The microphysical and dynamical features of volcanic clouds, due to Plinian and sub-Plinian eruptions, can be quantitatively monitored by using ground-based microwave weather radars. In order to demonstrate the unique potential of this remote sensing technique, a case study of a subglacial volcanic eruption, occurred in Iceland in November 2004, is described and analyzed. Volume data, acquired by a C-band ground-based weather radar, are processed to automatically classify and estimate ash particle concentration. The ash retrieval physical-statistical algorithm is based on a backscattering microphysical model of fine, coarse, and lapilli ash particles, used within a Bayesian classification and optimal regression algorithm. A sensitivity analysis is carried out to evaluate the overall error budget and the possible impact of nonprecipitating liquid and ice cloud droplets when mixed with ash particles. The evolution of the Icelandic eruption is discussed in terms of radar measurements and products, pointing out the unique features, the current limitations, and future improvements of radar remote sensing of volcanic plumes. [J185]

## "TerraSAR-X Data for Burn Severity Evaluation in Mediterranean Forests on Sloped Terrain"

TerraSAR-X (TSX) dual-polarized synthetic aperture radar (SAR) data from a test site in Spain have been investigated to determine the relationship between forest burn severity and SAR backscatter. The role of the local incidence angle on the backscatter coefficient has been also studied. Burn severity was estimated by means of composition burn index plots and the remotely sensed differenced normalized burn ratio index. To infer the potential of the TSX data for burn severity assessment, the determination coefficients obtained from linear regression analysis have been used. At horizontal transmit horizontal receive (HH) polarization, backscatter increased for slopes oriented toward the sensor and areas affected by high burn severity, whereas, at horizontal transmit vertical receive (HV) polarization, higher backscatter occurred for slopes oriented away from the sensor in areas of low burn severity. The dependence of the backscatter coefficient on topography for areas affected by forest fire has been confirmed. The HH backscatter presented a clear descending trend with the increase in local incidence angle, whereas the HV backscatter presented an ascending trend. The determination coefficients showed that, at HH polarization, better estimates of burn severity are obtained at low local incidence angles, whereas, for HV polarization, the best estimates are obtained at high local incidence angles. The dual-polarized X-band SAR data showed potential for burn severity estimation in the Mediterranean environment if local incidence angle is accounted for. [J186]

## "ML-Based Fringe-Frequency Estimation for InSAR"

This letter focuses on estimating the local fringe frequency of the interferometric phase, under the hypothesis of superficial scattering. Starting from the formulation of the maximum-likelihood estimator, a new simplified estimator is derived. Due to computational efficiency and robustness versus model errors, the resulting estimator is suited for large data processing in the presence of model uncertainty. Furthermore, such an estimator can be straightforwardly extended to the multi-baseline case, resulting in the possibility to estimate the terrain slope with great accuracy. An application to real data is presented, based on a multi-baseline ENVISAT data set. [J187]

## "InSAR Coherence-Decomposition Analysis"

The phase coherence in synthetic aperture radar interferometry is often used in classification algorithms to detect possible temporal changes of the imaged terrain. However, in mountain areas, the interferometric coherence is also sensitive to the slight variations of the acquisition geometry. In this letter, we propose a very simple but effective method to separate the temporal decorrelation from the geometrical one. Assuming the imaged terrain can be modeled as a distributed target, the geometrical coherence can be estimated by exploiting a topographic model and the sensor acquisition parameters. The discrepancy between the geometrical coherence and the observed one can then be ascribed to temporal changes. Moreover, in presence of pointlike targets, the hypothesis of distributed terrain is no longer valid, and higher values of the observed coherence with respect to the synthetic geometrical one can be used to detect such targets. The proposed approach allows then in mountain areas the following conditions: (1) a simple and very fast rough estimation of the temporal coherence, and (2) the identification of pointlike targets using just two images. The method has been applied and tested in the Badong (China) site using European Remote Sensing satellite tandem data. [J188]

## "Processing of Sliding Spotlight and TOPS SAR Data Using Baseband Azimuth Scaling"

This paper presents an efficient phase preserving processor for the focusing of data acquired in sliding spotlight and Terrain Observation by Progressive Scans (TOPS) imaging modes. They share in common a linear variation of the Doppler centroid along the azimuth dimension, which is due to a steering of the antenna (either mechanically or electronically) throughout the data take. Existing approaches for the azimuth processing can become inefficient due to the additional processing to overcome the folding in the focused domain. In this paper, a new azimuth scaling approach is presented to perform the azimuth processing, whose kernel is exactly the same for sliding spotlight and TOPS modes. The possibility to use the proposed approach to process data acquired in the ScanSAR mode, as well as a discussion concerning staring spotlight, is also included. Simulations with point targets and real data acquired by TerraSAR-X in sliding spotlight and TOPS modes are used to validate the developed algorithm. [J189]

## "Focusing Bistatic SAR Data in Airborne/Stationary Configuration"

This paper presents a frequency-domain-based focusing algorithm for the bistatic synthetic aperture radar (BiSAR) data in airborne/stationary configuration. In this bistatic configuration, only the moving platform contributes to the azimuth modulation, whereas the stationary platform introduces a range offset (RO) to the range migration trajectories of targets at the same range. The offset is determined by the azimuth position of different targets with respect to the stationary platform. Since the RO is position dependent, monostatic SAR imaging algorithms are not able to focus the bistatic data collected in this configuration. In this paper, an analytical bistatic point-target reference spectrum is derived, and then, a frequency-domain-based algorithm is developed to focus the bistatic data. It uses an interpolation-free wavenumber-domain algorithm as a basis and performs a range-variant interpolation to correct the position-dependent RO in the image domain after coarse focusing. The proposed algorithm is validated by the simulated data and the real BiSAR data acquired by the Forschungsgesellschaft fu??r Angewandte Naturwissenschaften's airborne SAR system, PAMIR, in December 2007. In this BiSAR experiment, an X-band transmitter was stationary operated on a hill with PAMIR as the receiver mounted on a Transall C-160. [J190]

## "Climatology of the Aerosol Extinction-to-Backscatter Ratio from Sun-Photometric Measurements"

The elastic lidar equation contains two unknown atmospheric parameters, namely, the particulate optical extinction and backscatter coefficients, which are related through the lidar ratio (i.e., the particulate-extinction-to-backscatter ratio). So far, independent inversion of the lidar signal has been carried out by means of Raman lidars (usually limited to nighttime measurements), high-spectral-resolution lidars, or scanning elastic lidars under the assumption of a homogeneously vertically stratified atmosphere. In this paper, we present a procedure to obtain the lidar ratio at 532 nm by a combined Sun-photometer-aerosol-model inversion, where the viability of the solution is largely reinforced by assimilating categorized air-mass back-trajectory information. Thus, iterative lidar-ratio tuning to reconstruct the Sun-photometric aerosol optical depth (AOD) is additionally constrained by the air-mass back trajectories provided by the hybrid single-particle Lagrangian integrated-trajectory model. The

retrieved lidar ratios are validated with inversions of lidar data based on the Klett-Fernald-Sasano algorithm and with the Aerosol Robotic Network (AERONET)-retrieved lidar ratios. The estimated lidar ratios concur with the AERONET-retrieved lidar ratios and with those of the well-known KFS inversion constrained with Sun-photometric AOD values and embedded single-scattering models. The proposed method can be applied to routinely extract climatological values of the lidar ratio using measurements of direct solar irradiance (more numerous than those of sky radiance). [J191]

## "A New Slant-Range Velocity Ambiguity Resolving Approach of Fast Moving Targets for SAR System"

This paper describes an ambiguity resolving approach for slant-range velocity estimation which utilizes the wideband characteristic of the transmitted signal (multiple wavelengths). Based on the wavelength dual-wavelength radar data. Then, two effective approaches are introduced to focus the moving target no matter the Doppler ambiguity exists or not. The slant-range velocity is estimated by the number of azimuth cell displacements between the two focused images. Both imaging methods have different properties and advantages. A performance analysis is made, and deleterious factors in practice are analyzed in detail. The effectiveness of the unambiguous slant-range velocity estimation approach is demonstrated with the use of simulated and real data. [J192]

## "Radio Frequency Tomography for Tunnel Detection"

Radio frequency (RF) tomography is proposed to detect underground voids, such as tunnels or caches, over relatively wide areas of regard. The RF tomography approach requires a set of low-cost transmitters and receivers arbitrarily deployed on the surface of the ground or slightly buried. Using the principles of inverse scattering and diffraction tomography, a simplified theory for below-ground imaging is developed. In this paper, the principles and motivations in support of RF tomography are introduced. Furthermore, several inversion schemes based on arbitrarily deployed sensors are devised. Then, limitations to performance and system considerations are discussed. Finally, the effectiveness of RF tomography is demonstrated by presenting images reconstructed via the processing of synthetic data. [J193]

## "Validation and Calibration of ASCAT Using CMOD5.n"

The Advanced Scatterometer (ASCAT) onboard the Metop-A satellite became operational shortly after launch in 2006, and an absolute calibration using three transponders was achieved in November 2008. In this paper, we describe how the CMOD5.n ocean backscatter geophysical model function (GMF), which was derived using data from previous scatterometers onboard the European Remote Sensing 1 and 2 satellites (ERS-1 and ERS-2), was used to derive backscatter bias correction factors. The purpose is to remove the bias between ASCAT backscatter data and the CMOD5.n GMF output which allows these data to be used in place of ERS data in existing wind processing algorithms. The ASCAT Wind Data Processor, developed at the Royal Netherlands Meteorological Institute (KNMI), applies the bias correction factors to ASCAT data and uses CMOD5.n to retrieve wind vectors in order to produce an operational wind product. This resulted in a stable and high-quality ASCAT wind product since February 2007. We validate this product by comparing it to the European Centre for Medium-range Weather Forecasts (ECMWF) winds and buoy measurements. The bias correction factors indicate that ASCAT data and the GMF differ by roughly 0.3 dB below 55 ?and up to 0.8 dB above 55 ?. A possible explanation lies in CMOD5.n which has been poorly validated in this incidence angle regime. Validation of ASCAT data using the ocean calibration method confirms this result and also indicates that bias-corrected data are everywhere within 0.3 dB of CMOD5.n. The wind product validation shows an rms error of 1.3 m ?s-1in wind speed and 16 ?in wind direction when compared to ECMWF winds. This is better than the results achieved using ERS scatterometer data. Against buoy winds, we find an rms error wind component error of approximately 1.8 m ?s-1. These results show that the ASCAT wind product is of high quality and satisfies its wind component accuracy requirement of-- 2 m ?s-1. [J194]

## "Equivalence Analysis of Accuracy of Geolocation Models for Spaceborne InSAR"

There are two main geolocation models for spaceborne synthetic aperture radar (SAR) interferometry (InSAR): range Doppler (RD) and direct geocoding (DG) models. The RD model gets the target position by combining and solving the Doppler equation, slant-range equation, and the modified Earth model equation. The DG location model gets the target position through its 3-D coordinates by the Doppler equation and two slant-range equations. Usually, the geolocation accuracy analyses of these two models are discussed separately. It is confused which one is more precise and we should use during InSAR system designing. This paper deduced and compared the geolocation accuracies of these two models in the same frame-matrix. According to the matrix theory, the explicit expressions of the geolocation uncertainty of RD and DG models were deduced through the

use of parameters in matrix form. After defining a new slant-range plane coordinate system, the precision of RD geolocation model and that of geocoding location model were compared quantificationally. It was presented that the geolocation uncertainty formulas between RD and DG models were the same. Then, the conclusion that these two models would lead to the same precision in geolocation measurement was obtained. At last, computer simulation results were employed to confirm the mathematical analysis. [J195]

## "Unifying Experiment Design and Convex Regularization Techniques for Enhanced Imaging With Uncertain Remote Sensing Data-Part II: Adaptive Implementation and Performance Issues"

The unified descriptive experiment design regularization (DEDR) method from a companion paper provides a rigorous theoretical formalism for robust estimation of the power spatial spectrum pattern of the wavefield scattered from an extended scene observed in the uncertain remote sensing (RS) environment. For the considered here imaging synthetic aperture radar (SAR) application, the proposed DEDR approach is aimed at performing, in a single optimized processing, SAR focusing, speckle reduction, and RS scene image enhancement and accounts for the possible presence of uncertain trajectory deviations. Being nonlinear and solution dependent, the optimal DEDR estimator requires rather complex signal processing operations ruled by the fixed-point iterative implementation process. To simplify further the processing, in this paper, we propose to incorporate the descriptive regularization via constructing the projections onto convex sets that enable us to factorize and parallelize the reconstructive image processing over the range and azimuth coordinates, design a family of such regularized easy-to-implement iterative algorithms, and provide the relevant computational recipes for their application to fractional imaging SAR. We also comment on the adaptive adjustment of the DEDR operational parameters directly from the actual speckle-corrupted scene images and demonstrate the effectiveness of the proposed adaptive DEDR techniques. [J196]

## "Unifying Experiment Design and Convex Regularization Techniques for Enhanced Imaging With Uncertain Remote Sensing Data-Part I: Theory"

This paper considers the problem of high-resolution remote sensing (RS) of the environment formalized in the terms of a nonlinear ill-posed inverse problem of estimation of the power spatial spectrum pattern (SSP) of the wavefield scattered from an extended remotely sensed scene via processing the discrete measurements of a finite number of independent realizations of the observed degraded data signals [single realization of the trajectory signal in the case of synthetic aperture radar (SAR)]. We address a new descriptive experiment design regularization (DEDR) approach to treat the SSP reconstruction problem in the uncertain RS environment that unifies the paradigms of maximum likelihood nonparametric spectral estimation, descriptive experiment design, and worst case statistical performance optimization-based regularization. Pursuing such an approach, we establish a family of the DEDR-related SSP estimators that encompass a manifold of algorithms ranging from the traditional matched filter to the modified robust adaptive spatial filtering and minimum variance beamforming methods. The theoretical study is resumed with the development of a fixed-point iterative DEDR technique that incorporates the regularizing projections onto convex solution sets into the SSP reconstruction procedures to enforce the robustness and convergence. For the imaging SAR application, the proposed DEDR approach is aimed at performing, in a single optimized processing, adaptive SAR focusing, speckle reduction and RS scene image enhancement, and accounts for the possible presence of uncertain trajectory deviations. [J197]

## "Applying the Freeman-Durden Decomposition Concept to Polarimetric SAR Interferometry"

In this paper, the Freeman-Durden polarimetric decomposition concept is adapted to polarimetric SAR interferometry (PolInSAR) data. The covariance matrix obtained from PolInSAR observations is decomposed into the three scattering mechanisms matrices proposed by Freeman and Durden for polarimetric SAR (PolSAR) data. The objective is to describe each interferometric cross correlation as the sum of the contributions corresponding to direct, double-bounce, and random volume scattering processes. This procedure enables the retrieval not only of the magnitude associated with each mechanism but also of their location along the vertical dimension of the scene. One of the most important features of this algorithm is the potential to isolate more accurately the direct and volume contributions which usually cannot be correctly separated by means of PolSAR measurements. In addition, it is also possible to distinguish between direct scattering responses originated either at ground or produced by upper layers of vegetation. The proposed algorithm has been tested with simulated data from PolSARProSim software, laboratory data from maize and rice samples, and airborne data from a test site with different scenarios. [J198]

## "Huber-Markov Model for Complex SAR Image Restoration"

This letter presents the despeckling of single-look complex (SLC) synthetic aperture radar (SAR) images using nonquadratic regularization. The objective function consists of an image model, a gradient, and a prior model.

The Huber-Markov random field (HMRF) models the prior. A numerical solution is achieved through extensions of half-quadratic regularization methods using complex-valued SAR data. The proposed method using the HMRF prior together with nonquadratic regularization shows the superior results on SLC synthetic and actual SAR images. [J199]

## "Hypothesis Testing in Speckled Data With Stochastic Distances"

Images obtained with coherent illumination, as is the case of sonar, ultrasound-B, laser, and synthetic aperture radar, are affected by speckle noise which reduces the ability to extract information from the data. Specialized techniques are required to deal with such imagery, which has been modeled by the G0distribution and, under which, regions with different degrees of roughness and mean brightness can be characterized by two parameters; a third parameter, which is the number of looks, is related to the overall signal-to-noise ratio. Assessing distances between samples is an important step in image analysis; they provide grounds of the separability and, therefore, of the performance of classification procedures. This paper derives and compares eight stochastic distances and assesses the performance of hypothesis tests that employ them and maximum likelihood estimation. We conclude that tests based on the triangular distance have the closest empirical size to the theoretical one, while those based on the arithmetic-geometric distances have the best power. Since the power of tests based on the triangular distance is close to optimum, we conclude that the safest choice is using this distance for hypothesis testing, even when compared with classical distances as Kullback-Leibler and Bhattacharyya. [J200]

## "Road Network Extraction in VHR SAR Images of Urban and Suburban Areas by Means of Class-Aided Feature-Level Fusion"

In this paper, we propose to combine two road extractors from very high resolution synthetic aperture radar scenes: one more successful in rural areas and one explicitly designed for urban areas. In order to get the best combination of both, a rapid mapping filter for discriminating rural and urban scenes is utilized. Finally, the results are fused on a feature level and connected by means of a network optimization. The approach is tested and evaluated on TerraSAR-X data containing complex urban areas and urban-rural fringe scenes. [J201]

## "Analysis of Gable-Roofed Building Signature in Multiaspect InSAR Data"

The spatial resolution of state-of-the-art synthetic aperture radar sensors enables the structure analysis of urban areas. The appearance of buildings in magnitude images in settlements is dominated by the effects of the inherent oblique scene illumination. In urban residential districts, salient pairs of parallel lines of bright magnitude are often caused by direct reflection and double-bounce signal at gable-roofed buildings. In this letter, the magnitude and interferometric phase signature of gable-roofed buildings are discussed to extract reliable building features for reconstruction. The analysis contains signature changes by varying illumination and building geometry. The presented approach is aiming at the reconstruction of gable-roofed buildings by a knowledge-based analysis considering the discussed effects. The reconstruction results are assessed by using a high-resolution LIDAR surface model as ground truth. [J202]

## "Gibbs Random Field Models for Model-Based Despeckling of SAR Images"

Synthetic aperture radar (SAR) images are affected by multiplicative noise called speckle. This noise makes automatic image classification and image interpretation difficult. Thus, many methods have been developed to remove speckle from SAR images while preserving the useful information of the scene such as texture and geometry. In this letter, a comparison between three different despeckling methods based on a Bayesian approach and Gibbs random fields is made. The used methods are Gauss-Markov random field (GMRF) and autobinomial modeling, which operate in the image domain, and the GMRF approach, which operates in the wavelet domain. Our methods are evaluated with synthetic and real SAR data (TerraSAR-X images). The experimental results show that, with these three methods, the speckle is well removed while structures are preserved; quantitative measures show that the autobinomial method provides the best smoothness and sharpness criteria in real SAR data, while the wavelet-based method generates the smallest bias. [J203]

## "Despeckling of TerraSAR-X Data Using Second-Generation Wavelets"

This letter presents the despeckling of synthetic aperture radar (SAR) images within the bandelet and contourlet domains. A model-based approach is presented for the despeckling of SAR images. The speckle-reduced estimate is found using the first-order Bayesian inference, and the best model's parameters are estimated using the second-order Bayesian inference. Synthetic and real images are used for evaluating the qualities of the despeckling methods. The experimental results showed that the combination of Bayesian inference and bandelet transform outperforms the contourlet-based despeckling algorithm using synthetic data and objective

measurements. [J204]

## "Analysis of Optical Properties of Saharan Dust Derived From Dual-Wavelength Aerosol Retrievals From CALIPSO Observations"

Since its first collection of data in June of 2006, the Cloud and Aerosol LIdar with Orthogonal Polarization (CALIOP) lidar instrument aboard the CALIPSO satellite has observed numerous Saharan dust events over West Africa and the Atlantic, predominantly from late May through early September. Due to CALIOP's sensitivity to polarization at 532 nm, the depolarization arising from scattering from the nonspherical dust particles serves as an independent means of discrimination between dust and other aerosol species. In addition to being an important and frequently observed class of aerosol, the Saharan dust provides an excellent basis for the evaluation of elastic-scatter lidar retrieval techniques. The Constrained Ratio Aerosol Model-fit (CRAM) method is one such technique, which applies aerosol modeling constraints in order to limit the ambiguity inherent in aerosol retrievals from elastic-scatter lidar. This letter, in addition to investigating the overall scattering properties of Saharan dust, highlights various retrieval approaches useful in determining the scattering properties of aerosols, as observed by the CALIOP instrument. Herein, we attempt to arrive at an improvement in the dust aerosol model used within CRAM. [J205]

## "Coarse-to-Fine Approach for Urban Area Interpretation Using TerraSAR-X Data"

With the launch of the German TerraSAR-X system in June 2007, a new generation of high-resolution spaceborne synthetic aperture radar (SAR) data is available, which should facilitate the interpretation of urban environments. Our overall objective in this letter is to provide a semiautomatic tool for urban area interpretation using SAR data. We propose in this letter to fuse different automatic object extractors in order to provide more reliable pieces of interpretation. Our fusion is a coarse-to-fine approach. First, a segmentation of the image is performed to partition the scene into regions having similar properties. The second step consists in detecting bright and dark linear structures which are, in general, linked to the presence of buildings and roads (main classes in urban areas), respectively. The last step gives the final image interpretation using contextual knowledge. Evaluation of the proposed approach in mapping urban areas was carried out using real TerraSAR-X data over the city of Las Vegas in the U.S. [J206]

## "Evaluation of TerraSAR-X Observations for Wetland InSAR Application"

This paper assesses the potential of using spaceborne X-band synthetic aperture radar (SAR) data for monitoring water-level changes over wetlands. Our analysis is based on three sets of TerraSAR-X (TSX) observations acquired over South Florida's Everglades wetlands during an eight-month period in 2008. The first set was acquired in single HH polarization stripmap mode over our northern study area, consisting of managed wetlands and urban environments. The second set was acquired in dual-polarization stripmap mode over the western half of the same area, consisting mostly of managed wetlands. The third set was also acquired with dual-polarization stripmap mode over our southern study area, consisting of natural flow freshand salt-water wetlands in the southern Everglades. The first data set was used for a proof-of-concept study to verify that X-band data can generate coherent interferograms in wetland areas. Interferometric processing of this data set shows a high level of coherence (> 0.35) over both wetland and urban regions, maintaining interferometric phase in all three interferograms spanning 11 days. Surprisingly, phase is maintained over some of the wetlands even for interferograms spanning 33 days. The other two data sets were used to evaluate interferometric coherence of all four polarization modes and to determine dominant scattering mechanism in each wetland environment. Our results show high coherence values (> 0.4) in all polarization modes, with highest values in HH, then VV, and lowest in HV or VH. Interferograms calculated from multipolarization data show very similar fringe patterns regardless of the polarization type, suggesting that the phase information in all polarization data reflects water-level changes in wetlands and that volume scattering may be less important than commonly believed. We also used the two multipolarization data sets to conduct the Pauli decomposition, finding a strong dependence of scattering mechanism on vegetation t--ype. The high interferometric coherence level of all polarization data suggests that a significant part of the X-band scattered signal interacts with lower sections of the vegetation (trunks and branches), because scattering from wind-affected canopies cannot support such a high coherence level. The high spatial resolution of TSX, combined with its 11-day repeat orbit, makes this X-band sensor surprisingly suitable for wetland interferometric SAR applications. [J207]

## "Derivation and Discussion of the SAR Migration Algorithm Within Inverse Scattering Problem: Theoretical Analysis"

The analysis of synthetic aperture radar (SAR) migration developed by Gilmore has been refined within the context of the inverse scattering problem, particularly the distorted-wave Born approximation (DWBA). The SAR

migration algorithm can be deduced from the DWBA-based inversion formulation when the following assumptions are satisfied: 1) homogeneous and nonfrequency-dependent background medium; 2) the exploding source model; and 3) the well-resolved targets described by an orthogonal relation derived in this paper. In addition, the other contributions of this paper are as follows: 1) The removal of the ??2term has been clarified by the derived orthogonal relation; 2) a scale factor that balances the near-far field has been derived; and 3) a novel SAR migration algorithm for the imaging of targets embedded in a layered medium has been proposed. [J208]

## "Segmentation and Classification of Polarimetric SAR Data Using Spectral Graph Partitioning"

A new approach for segmentation and classification of polarimetric synthetic aperture radar (POLSAR) data is proposed based on spectral graph partitioning. Since automated analysis techniques are often challenged due to the noisy properties of POLSAR data, human experts are employed to aid in the interpretation of such data in an operational setting. Humans can improve the performance of segmentation and classification of POLSAR data, because their vision system can apply cognitive skills that are not easy to incorporate into an automated system. The motivation for this paper is to incorporate some of these human perceptual skills into the computer algorithms. A framework that has recently emerged in computer vision for solving grouping problems with perceptually plausible results-spectral graph partitioning-is customized for POLSAR data. Segmentation is performed using the contour information in a region-based setting with the aid of spatial proximity. This is followed by a classification step performed through graph partitioning based on similarities of the mean coherence matrices obtained for each segment. Using the proposed approach, the results achieved are superior to the Wishart classifier. Automated parameter selection procedures are under development. This framework also suggests a way to accommodate different representations of polarimetric data and combine them with other information sources (e.g., optical imagery and digital elevation models). [J209]

## "Compensation of Faraday Rotation in Multipolarization Scatterometry"

Spaceborne remote sensors operating at L-band and lower frequencies can significantly be affected by Faraday rotation (FR) as their signals pass through the Earth's ionosphere. A method of compensating for FR in multipolarization scatterometry is introduced, which utilizes an ancillary estimate of the FR angle to retrieve corrected polarized scattered powers. Simulation results are presented to demonstrate the behavior of the FR correction process when radar speckle, instrument errors, and errors in the ancillary FR angle estimate are introduced. [J210]

## "Monitoring of Snow-Cover Properties During the Spring Melting Period in Forested Areas"

As spaceborne C-band synthetic aperture radar (SAR) observations are used for monitoring the snow cover during the spring melt period, temporal changes in backscatter from forest cover disturb the mapping of snow cover. This paper presents an analysis of snow backscattering properties in eight test areas situated around weather stations. Test areas represent open and forested landscapes in Northern Finland. Analyses are carried out using an extensive multitemporal ERS-2 C-band SAR data set from the snow melt period. We validate the following topics: 1) forest backscattering model for forest compensation; 2) Helsinki University of Technology (TKK) fractional snow-covered area (SCA) method with in situobservations; and 3) inversion of a combined forest/snow/ground backscattering model in an application to yield estimates of the relative changes of snow wetness during full snow cover conditions. The results show that the semiempirical TKK backscattering model describes the average C-band backscattering properties of all test regions well as a function of forest stem volume. Comparison of SCA estimation results with available ground-truth data also shows a good performance. The retrieved relative snow wetness values agree well with temperature observations. [J211]

## "Ray-Tracing Simulation Techniques for Understanding High-Resolution SAR Images"

In this paper, a simulation concept is presented for creating synthetic aperture radar (SAR) reflectivity maps based on ray tracing. Three-dimensional models of man-made objects are illuminated by a virtual SAR sensor whose signal is approximated by rays sent through the model space. To this end, open-source software tools are adapted and extended to derive output data in SAR geometry followed by creating the reflectivity map. Rays can be followed for multiple reflections within the object scene. Signals having different multiple reflection levels are stored in separate image layers. For evaluating the potentials and limits of the simulation approach, simulated reflectivity maps and distribution maps are compared with real TerraSAR-X images for various complex man-made objects like a skyscraper in Tokyo, the Wynn Hotel in Las Vegas, and the Eiffel Tower in Paris. The results show that the simulation can provide very valuable information to interpret complex SAR images or to predict the reflectivity of planned SAR image acquisitions. [J212]

## "Three-Dimensional Coherent Radar Backscatter Model and Simulations of Scattering Phase

## Center of Forest Canopies"

A 3-D coherent radar backscatter model for forest canopies was developed and used to improve the understanding of synthetic aperture radar (SAR) interferometric data. The model was based on a realistic 3-D spatial structure of a forest stand, in which every scatterer has its deterministic location. A backscattering signal from a scatterer was mapped into a pixel according to its range or signal time delay. The range or the time delay also determines the phase of the scattered field. All scattering matrices within a pixel were coherently added to yield the total backscattering field of the pixel. The coherent radar backscatter model takes into account not only the scattering contribution from the scatterers in the forest canopy but also the direct backscattering of the ground surface. Forest stands with three different spatial structures were simulated using L-system and field measurements. The number and sizes of trees in these forest stands were identical, but the 2-D arrangements of the trees were different. The interferometric SAR (InSAR) signals of these scenes were simulated using the 3-D coherent SAR model, and the heights of scattering phase centers were estimated from the simulated InSAR data. The results reported in this paper show that the spatial structures of vegetation play an important role in the location of the scattering phase center. The height of scattering phase center depends on canopy height, attenuation of canopy, and the gaps within the canopy. This paper shows that the spatial structure needs to be considered when the InSAR data are used for the estimation of forest structural parameters. [J213]

## "A Novel Autofocusing Approach for Real-Time Through-Wall Imaging Under Unknown Wall Characteristics"

A novel real-time through-wall imaging (TWI) algorithm with autofocusing ability in the presence of wall ambiguities is proposed in this paper. The spectrum Green's function is employed to formulate the TWI algorithm, where the fast Fourier transform can be used to reconstruct the image in a very short computation time. The complex scattering process due to the presence of the wall is automatically included in the imaging formulation through the multilayer Green's function. The autofocusing is achieved by introducing a time factor in the TWI formulation to get a dynamic image at different focusing time. The image at the time instant when the defined entropy is minimized is stored as the output of the TWI result. Simulation results show that the proposed method can provide high-quality focused image in a short computation time regardless of the estimated value of the wall parameters. [J214]

## "SAR Image Despeckling Using Edge Detection and Feature Clustering in Bandelet Domain"

To effectively preserve the edges of a synthetic aperture radar (SAR) image when despeckling, an algorithm with edge detection and fuzzy clustering in the translation-invariant second-generation bandelet transform (TIBT) domain is proposed in this letter. A Canny operator is first utilized to detect and remove edges from the SAR image. Then, TIBT and fuzzy C-mean clustering are employed to decompose and despeckle the edge-removed image, respectively. Finally, the removed edges are added to the reconstructed image. The algorithm suggests each coefficient in high-frequency subbands as the clustering feature, proposes a calculation method of the best clustering number, and defines the signal and noise in the clustering results. Experimental results show that the visual quality and evaluation indexes outperform the other methods with no edge preservation. The proposed algorithm effectively realizes both despeckling and edge preservation and reaches the state-of-the-art performance. [J215]

## "Gaussian Process Approach to Buried Object Size Estimation in GPR Images"

Recently, a promising pattern-recognition system has been presented to deal with the extraction of buried-object characteristics in ground-penetrating-radar images. In particular, it allows the detecting of buried objects by means of a search method based on genetic algorithms and the recognizing of the material type of the identified objects through a classification approach based on support vector machines. In this letter, we propose to extend the processing capabilities of this system by addressing the issue of the detected buried-object size estimation. This problem is viewed as a regression issue where it is aimed at reproducing the relationship between a set of opportunely extracted features and the object size. For such purpose, it is formulated within a Gaussian process (GP) regression approach. A detailed experimental study is reported, showing encouraging object-size-estimation accuracies even when buried objects are close to each other. [J216]

## "Scattering Model for a Pine Tree Employing VIE With a Broadband MLFMA and Comparison to ICA"

In this paper, we present accurate calculations of electromagnetic wave scattering from a high-detail pine tree model, which includes also the needles. We have deployed a volume integral equation (VIE) model, which takes into account high-order reflections between all scatterers, even between single needles. The pine tree is modeled as a realistic collection of dielectric cylinders. With the help of our calculations, we assess the

importance of multiple scattering inside the pine canopy and the contribution of the needles to the scattering. We compare our calculations with a much simpler model output to determine the validity conditions for simplified approaches. As the simpler model, we use an infinite cylinder approximation (ICA) model which uses a truncated cylinder approximation and takes into account only the first-order reflections from single cylinders. Both models are bistatic, fully coherent, and fully polarimetric models suitable in calculating the scattering from a large and general collection of dielectric cylinders. Our results show that, for the C-band calculations, the VIE model output differs significantly from the simple ICA model output, indicating the importance of the higher order scattering between the needles and branches. However, for the L-band, the accurate VIE model gives similar results as the ICA model, indicating that, in this case, the higher order scattering between the needles can be neglected. [J217]

## "ISAR Imaging of Maneuvering Target Based on the L-Class of Fourth-Order Complex-Lag PWVD"

In inverse synthetic aperture radar (ISAR) imaging of a maneuvering target, the received signal in a range bin can be characterized as a multicomponent polynomial phase signal (PPS) after motion compensation. The traditional discrete Fourier transform algorithm is not appropriate in analyzing the PPS. In this paper, the L-class of a fourth-order complex-lag polynomial Wigner-Ville distribution (PWVD) is presented to generate a high-resolution time-frequency distribution (TFD) for the multicomponent PPS. For a signal with polynomial phase up to order four (this is accurate enough in ISAR imaging), the cross-terms between different components can be reduced by the convolution in the frequency domain of the L-class of the fourth-order complex-lag PWVD. The new TFD is used in the ISAR imaging of the maneuvering target, and high-quality instantaneous ISAR images are obtained. Results of simulated and real data demonstrate the effectiveness of the method above. [J218]

## "The TerraSAR-X Ground Segment"

TerraSAR-X, the first national German remote-sensing satellite, was launched on June 15, 2007. It carries an X-band high-resolution synthetic aperture radar (SAR) instrument featuring imaging modes like StripMap, ScanSAR, and, particularly, SpotLight in a variety of different polarization modes. Primary mission goal is the provision of both science and commercial users with a variety of products from advanced SAR modes. The TerraSAR-X Ground Segment, which is provided by the German Aerospace Center (DLR), constitutes the central element for controlling and operating the TerraSAR-X satellite, for calibrating its SAR instrument, and for archiving the SAR data, as well as generating and distributing the basic data products. This paper depicts the ground-segment layout and describes its major elements. The ordering and product-generation workflow is presented. It introduces the applied prelaunch integration, testing, verification, and validation approach, a major key to the completion not only of the SAR technical-verification program but also the operational qualification of the ground segment itself within the commissioning phase. [J219]

## "Working Together for Better Student Learning: A Multi-University, Multi-Federal Partner Program for Asynchronous Learning Module Development for Radar-Based Remote Sensing Systems"

Students are not exposed to enough real-life data. This paper describes how a community of scholars seeks to remedy this deficiency and gives the pedagogical details of an ongoing project that commenced in the Fall 2004 semester. Fostering deep learning, this multiyear project offers a new active-learning, hands-on interdisciplinary laboratory program in which engineering, geoscience, and meteorology students are encouraged to participate actively. Storms, tornadoes, and hazardous weather cause damage and loss that could be minimized through enhanced radar technologies and longer warning lead times. To study these topics, the program has generated a unique, interdisciplinary research-oriented learning environment that will train future engineers and meteorologists in the full set of competencies needed to take raw radar data and transform them into meaningful interpretations of weather phenomena. [J220]

## "TerraSAR-X Instrument Calibration Results and Extension for TanDEM-X"

Spaceborne remote sensing with synthetic aperture radar (SAR) has become an essential source of high-resolution and continuous Earth observation. Modern satellites like the German TerraSAR-X system provide state-of-the-art radar images with respect to operating flexibility and imaging quality. The outstanding performance of TerraSAR-X image products is achieved by an innovative calibration approach that minimizes systematic antenna and instrument characteristics. The active phased array X-band antenna is fed by 384 transmit/receive modules for electronic beam steering and shaping in the azimuth and elevation direction. The flexible radar instrument hosts an internal calibration system which guarantees the high radiometric stability of all SAR products. New techniques for antenna performance control have been successfully implemented, setting a high standard for next-generation SAR missions. This paper summarizes all essential calibration results of TerraSAR-X that cover internal instrument behavior. Furthermore, we give an outlook on the required bistatic

calibration techniques for the future TanDEM-X mission that faces additional performance challenges when calibrating two TerraSAR-X satellites flying in close formation. [J221]

## "Estimation of Forest Structure, Ground, and Canopy Layer Characteristics From Multibaseline Polarimetric Interferometric SAR Data"

This paper concerns forest parameter retrieval from polarimetric interferometric synthetic aperture radar (PolInSAR) data considering two layers, one for the ground under the vegetation and one for the volumetric canopy. A model is designed to combine a physical model-based polarimetric decomposition with the random-volume-over-ground (RVoG) PolInSAR parameter inversion approach. The combination of a polarimetric scattering media model with a PolInSAR RVoG vertical structure model provides the possibility to separate the ground and the volume coherency matrices based on polarimetric signatures and interferometric coherence diversity. The proposed polarimetric decomposition characterizes volumetric media by the degree of polarization orientation randomness and by the particle scattering anisotropy. Using the full model enhances the estimation of the vertical forest structure parameters by enabling us to estimate the ground-to-volume ratio, the temporal decorrelation, and the differential extinction. For forest vegetation observed at L-band, this model accounts for the ground topography, forest and canopy layer heights, wave attenuation in the canopy, tree morphology in the form of the angular distribution and the effective shapes of the branches, and the contributions from the ground level consisting of surface scattering and double-bounce ground-trunk interactions, as well as volumetric understory scattering. The parameter estimation performance is evaluated on real airborne L-band SAR data of the Traunstein test site, acquired by the German Aerospace Center (DLR)'s E-SAR sensor in 2003, in both single- and multibaseline configurations. The retrieved forest height is compared with the ground-truth measurements, revealing, for the given test site, an average root-mean-square error (rmse) of about 5 m in the repeat-pass configuration. This implies an improvement in rmse by over 2 m in comparison to the pure coherence-based RVoG PolInSAR parameter inversion. [J222]

## "Bistatic TerraSAR-X/F-SAR Spaceborne-Airborne SAR Experiment: Description, Data Processing, and Results"

We report about the first X-band spaceborne-airborne bistatic synthetic aperture radar (SAR) experiment, conducted early November 2007, using the German satellite TerraSAR-X as transmitter and the German Aerospace Center's (DLR) new airborne radar system F-SAR as receiver. The importance of the experiment resides in both its pioneering character and its potential to serve as a test bed for the validation of nonstationary bistatic acquisitions, novel calibration and synchronization algorithms, and advanced imaging techniques. Due to the independent operation of the transmitter and receiver, an accurate synchronization procedure was needed during processing to make high-resolution imaging feasible. Precise phase-preserving bistatic focusing can only be achieved if time and phase synchronization exist. The synchronization approach, based on the evaluation of the range histories of several reference targets, was verified through a separate analysis of the range and Doppler contributions. After successful synchronization, nonstationary focusing was performed using a bistatic backprojection algorithm. During the campaign, stand-alone TerraSAR-X monostatic as well as interoperated TerraSAR-X/F-SAR bistatic data sets were recorded. As expected, the bistatic image shows a space-variant behavior in spatial resolution and in signal-to-noise ratio. Due to the selected configuration, the bistatic image outperforms its monostatic counterpart in almost the complete imaged scene. A detailed comparison between monostatic and bistatic images is given, illustrating the complementarity of both measurements in terms of backscatter and Doppler information. The results are of fundamental importance for the development of future nonsynchronized bistatic SAR systems. [J223]

## "A Contribution of Polarimetry to Satellite Differential SAR Interferometry: Increasing the Number of Pixel Candidates"

This letter presents a general method for increasing the number of pixel candidates, those selected for processing in advanced differential SAR interferometry, by means of the exploitation of the polarimetric information provided by new satellite sensors. The algorithm is formulated for two different criteria of selection: the average coherence over the stack of interferograms and the amplitude dispersion index of the stack of images. Experimental results obtained with dual-pol images of TerraSAR-X over an urban area have demonstrated the expected improvement. The number of pixel candidates for an arbitrary threshold is 60% higher than that for single-pol data when using the average coherence and three times higher when using the dispersion index. The approach has also been compared to a selection based on a set of conventional channels (the copolar linear channels and the first two Pauli ones), showing a slight improvement for coherence selection and an important one for amplitude dispersion selection. [J224]

## "Soil Surface Water Content Estimation by Full-Waveform GPR Signal Inversion in the Presence of Thin Layers"

We analyzed the effect of shallow thin layers on the estimation of soil surface water content using full-waveform inversion of off-ground ground penetrating radar (GPR) data. Strong dielectric contrasts are expected to occur under fast wetting or drying weather conditions, thereby leading to constructive and destructive interferences with respect to surface reflection. First, synthetic GPR data were generated and subsequently inverted considering different thin-layer model configurations. The resulting inversion errors when neglecting the thin layer were quantified, and then, the possibility to reconstruct these layers was investigated. Second, laboratory experiments reproducing some of the numerical experiment configurations were conducted to assess the stability of the inverse solution with respect to actual measurement and modeling errors. Results showed that neglecting shallow thin layers may lead to significant errors on the estimation of soil surface water content(????>0.03 m3/m3), depending on the contrast. Accounting for these layers in the inversion process strongly improved the results, although some optimization issues were encountered. In the laboratory, the proposed full-waveform method permitted to reconstruct thin layers with a high resolution up to 2 cm and to retrieve the soil surface water content with an rmse less than 0.02 m3/m3, owing to the full-waveform inverse modeling. These results suggest that the proposed GPR approach is promising for field-scale mapping of soil surface water content of nondispersive soils with low electrical conductivity and for instances when soil layering is encountered. [J225]

## "Segmentation of ISAR Images of Targets Moving in Formation"

This paper proposes a new method to separate inverse synthetic aperture radar (ISAR) images using the range-Doppler algorithm when multiple targets fly closely spaced in a formation. This method is composed of three steps. The first step is an initial range-Doppler imaging of the whole set of targets to obtain a ??bulk?? image. In this step, range profiles are aligned using a new cost function, which is the sum of the amplitudes of the pixels lying along a polynomial that models the trajectory of the bulk image. To reduce the probability of incorrectly aligning high-amplitude pixels from different targets, pixel amplitudes are converted to binary form: A number ?? of pixels with the greatest amplitudes are identified in the bulk range profile, and their amplitudes are converted to one; the amplitudes of the remaining pixels are converted to zero. This process gives each of the ? ? pixels the same weight on the cost function. Then, phase adjustment is used to coarsely separate targets in a 2-D image. The second step is the separation of the bulk image into component images using a window of the target size. The third step is a second range-Doppler imaging, in which each ISAR image is enhanced using range alignment and phase adjustment. Simulations using three targets composed of point scattering centers prove that the proposed method can effectively segment three targets flying in a formation. [J226]

## "Coherent MapDrift Technique"

A new parametric autofocus technique with a high accuracy of flight-parameter estimation dedicated to strip-mode synthetic aperture radar (SAR) systems is presented. Most of the known autofocus techniques require high-reflectivity targets (man-made targets) to obtain a properly focused SAR image. The technique proposed in this paper allows flight parameters to be estimated effectively, even for a low-contrast scene (e.g., forests, fields, small paths, etc.). The autofocus technique is based on well-known MapDrift (MD) principles. The presented technique is a coherent one, which allows flight parameters to be estimated more precisely than in the other well-known parametric technique referred to as classical MD. The presented technique allows flight parameters to be estimated with accuracy that is independent of the initial velocity error. It can be used for real-time processing for both Earth imaging and moving-target indication. [J227]

## "Mapping of Different Sea Ice Regimes Using Images From Sentinel-1 and ALOS Synthetic Aperture Radar"

Airborne C- and L-band synthetic aperture radar (SAR) images were acquired for three test sites over different sea ice regimes around Svalbard in March 2007, complemented by optical imagery, environmental data, and ice observations. One objective was to use the high-resolution low-noise radar data for investigations on the technical performance of European Space Agency's Sentinel-1 mission for sea ice mapping, the other to assess the potential gain of additional use of L-band SAR data currently available from Advanced Land Observing Satellite (ALOS). The airborne SAR images were employed to simulate data products resembling the interferometric wide-swath mode (IWSM) of Sentinel-1 and ALOS PALSAR fine resolution mode (FRM) in order to quantify the information loss due to the higher noise level and coarser spatial resolution. At the IWSM noise level, zones of deformation, level ice, and new ice can be well separated at like-polarization. At cross-polarization, the noise level is too high for a robust automated classification including thin ice, but deformed and level ice can be discriminated. PALSAR FRM is on average better suited to distinguish deformed and level ice over all ice regimes. It was worse for separating new from thicker level ice at two test sites. For the third test site with very few patches of new ice, the PALSAR FRM showed larger intensity contrasts between new and level ice

than Sentinel-1 IWSM. The spatial resolution provided by the IWSM and FRM is sufficient to identify most ice features and types without ambiguities. Typical characteristics of the imaged ice regimes are described. [J228]

## "Assessing Ionospheric Influence on L-Band SAR Data: Implications on Coseismic Displacement Measurements of the 2008 Sichuan Earthquake"

Ionospheric contributions to the phase of L-band synthetic aperture radar (SAR) signals put severe limitations on ground displacement measurements retrieved by either differential SAR interferometry or radar amplitude-image offsets. Such contributions result in an ionospheric phase screen on the differential interferogram and in directional fluctuations in the relative position of azimuth pixels on offsets maps. In this letter, we propose a procedure for estimating and removing ionospheric contributions to surface displacement measurements derived from L-band SAR data. We test the procedure on SAR data from the May 28, 2008 Sichuan Earthquake. The applied corrections allow both a clearer interpretation of the surface rupture and a more accurate measurement of the surface displacement, which has important implications in earthquake modeling based on L-band SAR data. [J229]

## "Ultrawideband Chirp Scaling Algorithm"

A new version of chirp scaling (CS), the so-called ultrawideband (UWB) CS (UCS), is proposed in this letter. UCS aims at UWB synthetic aperture radar (SAR) systems utilizing large fractional bandwidth and wide antenna beamwidth associated with a wide integration angle. Furthermore, it is also valid for SAR systems with special characteristics such as ground-moving-target-indication SAR systems with a very high pulse repetition frequency. [J230]

## "Nonuniform Ground Motion Monitoring With TerraSAR-X Persistent Scatterer Interferometry"

In the past, the application of Persistent Scatterer Interferometry (PSI) was primarily possible in the case of slow (less than a few centimeters per year) uniform movements. In this paper, we show how PSI permits the monitoring of relatively fast (including rates up to > 50 cm/year) and nonuniform movements using TerraSAR-X repeat observations over deep-level mining. To enable this, parts of the PSI methodology were adapted to the special characteristics of the example studied. Apart from a description of the methodology used and the result achieved, error considerations and a validation of the result with in situ measurements are included. [J231]

## "A Bistatic SAR Raw Data Simulator Based on Inverse Algorithm"

A synthetic aperture radar (SAR) raw data simulator is an important tool for testing the system parameters and the imaging algorithms. In this paper, a scene raw data simulator based on an inverse ω-kalgorithm for bistatic SAR of a translational invariant case is proposed. The differences between simulations of monostatic and bistatic SAR are also described. The algorithm proposed has high precision and can be used in long-baseline configuration and for single-pass interferometry. Implementation details are described, and plenty of simulation results are provided to validate the algorithm. [J232]

## "Forest Modeling For Height Inversion Using Single-Baseline InSAR/Pol-InSAR Data"

The Random Volume over Ground (RVoG) model has been extensively applied to polarimetric synthetic aperture radar interferometry (Pol-InSAR) data for forest height inversion. The model assumes forest as a homogeneous volume of randomly oriented particles characterized by a constant extinction but does not take into account the forest vertical heterogeneity, to which interferometric coherence is sensitive. In order to integrate vertical heterogeneity in forest models, two complementary models, which take into consideration the forest natural structure, are investigated through analysis of volume interferometric coherence. The first model assumes a vertically varying extinction in the volume layer, and the second model considers predominant contributions localized in a finite height interval, modeled as a Gaussian-distributed backscatter. The two forest models are compared with constant extinction RVoG in the coherence and interferometric phase aspects. Finally, the contribution of these new models for forest height inversion using the Pol-InSAR technique is discussed in the context of a two-layer ground + canopy medium. [J233]

## "Deep Ice Stratigraphy and Basal Conditions in Central West Antarctica Revealed by Coherent Radar"

We discuss results from a high-sensitivity, multichannel, very high frequency, and surface-based radar depth sounder/imager. The instrument was used to map deep internal layers and characterize basal conditions over a 240- km2grid in the vicinity of the West Antarctic Ice Sheet Divide ice core site. The ice thickness at the core site was found to be about 3470 m, and we detected internal layers to within 350 m of the ice/bed interface.

Radar-detected layer stratigraphy does not show evidence of flow-induced disturbances that might complicate the depth-age relationship and the interpretation of climate history preserved in the ice. We also found that bed reflectivity over the region varies by more than 30 dB. Approximately 15 dB of this variability appears to be the result of transitions from a frozen to a thawed bed in a number of places. The remainder probably results from changes in bed roughness. Our data are important for planning drilling to the bed, as well as providing constraints and boundary conditions for regional ice-flow models. [J234]

## "Segmentation and Reconstruction of Polyhedral Building Roofs From Aerial Lidar Point Clouds"

This paper presents a solution framework for the segmentation and reconstruction of polyhedral building roofs from aerial LIght Detection And Ranging (lidar) point clouds. The eigenanalysis is first carried out for each roof point of a building within its Voronoi neighborhood. Such analysis not only yields the surface normal for each lidar point but also separates the lidar points into planar and nonplanar ones. In the second step, the surface normals of all planar points are clustered with the fuzzy k-means method. To optimize this clustering process, a potential-based approach is used to estimate the number of clusters, while considering both geometry and topology for the cluster similarity. The final step of segmentation separates the parallel and coplanar segments based on their distances and connectivity, respectively. Building reconstruction starts with forming an adjacency matrix that represents the connectivity of the segmented planar segments. A roof interior vertex is determined by intersecting all planar segments that meet at one point, whereas constraints in the form of vertical walls or boundary are applied to determine the vertices on the building outline. Finally, an extended boundary regularization approach is developed based on multiple parallel and perpendicular line pairs to achieve topologically consistent and geometrically correct building models. This paper describes the detail principles and implementation steps for the aforementioned solution framework. Results of a number of buildings with diverse roof complexities are presented and evaluated. [J235]

## "Field Investigations of Ku-Band Radar Penetration Into Snow Cover on Antarctic Sea Ice"

Monitoring long-term, large-scale changes in the Antarctic sea ice thickness is not currently possible due to the sampling constraints of the ship-based and airborne observations which comprise most of the available thickness data. Satellite radar altimetry has been used to measure sea ice thickness variability in the Arctic where it is assumed that the highest amplitude radar return originates from the snow/ice interface as the Arctic snow is cold and dry; however, this may not be the case in the Antarctic due to more complex snow stratigraphy caused by warmer winter temperatures and frequent snow flooding. We present the first measurements of radar penetration into snow cover on Antarctic sea ice in the Ku-band at which satellite radar altimeters operate. Data were taken using a sled-borne radar on sea ice off East Antarctica during September and October 2007. Radar data and field measurements of snow density, thickness, wetness, and layers were taken over a range of locations including snow packs with flooding, hard crusts, and icy layers. Detailed snow pit studies showed that the snow/ice interface was the dominant scattering surface only for snow without morphological features or flooding. Analysis of transect data showed that the mean depth of the dominant scattering surface of the radar was only around 50% of the mean measured snow depth, indicating that the dominant scattering surface was not always the snow/ice interface for the Antarctic sea ice surveyed. [J236]

## "UWB Through-Wall Imaging Based on Compressive Sensing"

To achieve high-resolution 2-D images, through-wall imaging (TWI) radar with ultra-wideband and long antenna arrays faces considerable technical challenges such as a prolonged data collection time, a huge amount of data, and a high hardware complexity. This paper presents a novel data acquisition scheme and an imaging algorithm for TWI radar based on compressive sensing (CS), which states that a signal having a sparse representation can be reconstructed from a small number of nonadaptive randomized projections by solving a tractable convex program. Instead of measuring all spatial-frequency data, a few samples, by employing an overcomplete dictionary, are sufficient to obtain reliable target space images even at high noise levels. Preliminary simulated and experimental results show that the proposed algorithm outperforms the conventional delay-and-sum beamforming method even though many fewer CS measurements are used. [J237]

## "Analysis of Local Variation of Soil Surface Parameters With TerraSAR-X Radar Data Over Bare Agricultural Fields"

The objective of this paper is to analyze the sensitivity of very high resolution TerraSAR-X radar data taken over bare soils to surface soil parameters and to study the spatial variability of these parameters at a fine scale (within a field plot). The relationship between the backscattering coefficient and the soil's parameters (moisture, surface roughness, texture, and local topography) was examined by means of four satellite images, as well as ground truth measurements, of each of the three agricultural plots, recorded during several field campaigns in

the winter and spring of 2008. TerraSAR images demonstrate high potential for the identification of local variations of roughness and texture. An approach for the estimation of local moisture is proposed using an empirical method adapted to the scale of an individual field. The results show that, by using TerraSAR-X data to study bare agricultural fields, local variations in soil moisture can be retrieved with a root-mean-square error of 0.05 cm3??cm-3. [J238]

## "TerraSAR-X System Performance Characterization and Verification"

This paper presents results from the synthetic aperture radar (SAR) system performance characterization, optimization, and verification as carried out during the TerraSAR-X commissioning phase. Starting from the acquisition geometry and instrument performance, fundamental acquisition parameters such as elevation beam definition, range timing, receiving gain, and block adaptive quantization setting are presented. The verification of the key performance parameters-ambiguities, impulse-response function, noise, and radiometric resolution-is discussed. ScanSAR and Spotlight particularities are described. [J239]

## "Instrument-Based Noncontact Doppler Radar Vital Sign Detection System Using Heterodyne Digital Quadrature Demodulation Architecture"

In this paper, we present a fast solution to build a Doppler radar system for noncontact vital sign detection (VSD) using instruments that are generally equipped in radio-frequency and communication laboratories. This paper demonstrates the feasibility of conducting research on VSD in ordinary radio-frequency laboratories. The system is designed with a heterodyne digital quadrature demodulation architecture that helps mitigate quadrature channel imbalance and eliminate the complicated dc offset calibration required for arctangent demodulation. Moreover, its tunable carrier frequency helps select different optimal frequencies for different human objects. Two sets of extensive experiments have been carried out in the laboratory environment with a self-designed 2.4-GHz patch antenna array and a 1-18-GHz broadband antenna. The test results are satisfactory: for a 0-dBm transmit power, the detection range can be extended to 2.5 m with accuracy higher than 80%. The system is also capable of detecting vital signs in the presence of different obstructions between the subject and the antenna. [J240]

## "TOPS Imaging With TerraSAR-X: Mode Design and Performance Analysis"

This paper reports about the performed investigations for the implementation of the wide-swath TOPS (Terrain Observation by Progressive Scan) imaging mode with TerraSAR-X (TSX). The TOPS mode overcomes the limitations imposed by the ScanSAR mode by steering the antenna along track during the acquisition of a burst. In this way, all targets are illuminated with the complete azimuth antenna pattern, and, thus, scalloping is circumvented, and an azimuth dependence of signal-to-noise ratio and distributed target ambiguity ratio (DTAR) is avoided. However, the use of electronically steered antennas leads to a quantization of the steering law and a nonideal pattern for squinted angles (grating lobes and main lobe reduction). The former provokes spurious peaks, while the latter introduces slight scalloping and DTAR deterioration. These effects are analyzed and quantified for TSX, and a TOPS system design approach is presented. Next, the requirements concerning interferometry are investigated. Finally, several results are shown with the TSX data, including a comparison between the TOPS and the ScanSAR modes and the reporting of the first TOPS interferometric results. [J241]

## "On the Doppler Spreading Effect for the Range-Instantaneous-Doppler Technique in Inverse Synthetic Aperture Radar Imagery"

Inverse synthetic aperture radar (ISAR) is an all-weather radar technique which may generate high-resolution images of noncooperative targets. The standard range-Doppler algorithm (RDA) is usually employed for image generation. However, the images obtained with RDA are usually blurred because of the relative motion between radar and target. As a consequence, motion compensation techniques should be used to improve the imagery quality. The range-instantaneous-Doppler (RID) technique based on time-frequency transforms has been proposed for obtaining a sequence of focused ISAR images without the need of using motion compensation techniques. However, in this letter, it is clearly shown that the migration of the target scatterers in slant range indirectly induces Doppler spreading of the scatterers' point spread function in each of the ISAR images obtained by the RID technique. This Doppler spreading means blurring. It is important to highlight that the migration in slant range may be caused not only by the radial component of the translational motion but also by the rotational motion. The application of motion compensation techniques prior to the use of the RID technique allows us to mitigate the Doppler spreading, as shown here both for simulated and live data acquired by a high-resolution coherent radar. [J242]

## "Flood Detection in Urban Areas Using TerraSAR-X"

Flooding is a major hazard in both rural and urban areas worldwide, but it is in urban areas that the impacts are most severe. An investigation of the ability of high-resolution TerraSAR-X synthetic aperture radar (SAR) data to detect flooded regions in urban areas is described. The study uses a TerraSAR-X image of a one-in-150-year flood near Tewkesbury, U.K., in 2007, for which contemporaneous aerial photography exists for validation. The German Aerospace Center (DLR) SAR end-to-end simulator (SETES) was used in conjunction with airborne scanning laser altimetry (LiDAR) data to estimate regions of the image in which water would not be visible due to shadow or layover caused by buildings and taller vegetation. A semiautomatic algorithm for the detection of floodwater in urban areas is described, together with its validation using aerial photographs. Of the urban water pixels that are visible to TerraSAR-X, 76% were correctly detected, with an associated false positive rate of 25%. If all the urban water pixels were considered, including those in shadow and layover regions, these figures fell to 58% and 19%, respectively. The algorithm is aimed at producing urban flood extents with which to calibrate and validate urban flood inundation models, and these findings indicate that TerraSAR-X is capable of providing useful data for this purpose. [J243]

## "TerraSAR-X Commissioning Phase Execution Summary"

This paper provides an overview of the TerraSAR-X commissioning phase (CP). The overall CP planning and preparation is presented. The strategy for data-take (DT) command generation is discussed, and statistical reports summarize the acquired CP DTs. An overview summary on the main results in the different characterization and verification areas is provided together with synthetic aperture radar image examples. [J244]

## "Efficient Wavenumber Domain Focusing for Ground-Based SAR"

We present an efficient focusing algorithm for synthetic aperture radar (SAR) data acquired in short bursts by a geometry with a large range spread, i.e., the case of ground-based (GB) SAR. The usual approach for focusing GB SAR data is the polar formatting algorithm, whose computational complexity, however, is quite relevant due to the nonseparability of the kernel. In this letter, we introduce a different format for the focused data, namely, the range-angular domain. Such format keeps the benefit of the polar format that samples data close to the resolution, but allows for the design of a separable kernel in the wavenumber domain. The proposed kernel exploits a modified Stolt interpolation and an efficient space-varying resampling. Results of processing on both simulated and real data are presented. [J245]

## "Multi-Instrument Calibration Method Based on a Multiwavelength Ocean Surface Model"

A-Train platforms offer the possibility of measuring the same physical parameters using active and passive instruments, to improve our understanding of geophysical processes in the Earth system. In this letter, a new calibration approach is developed using active [Cloud-Aerosol Lidar and Infrared Pathfinder Satellite Observation (CALIPSO) lidar and CloudSat radar] and passive [Advanced Microwave Scanning Radiometer for the Earth Observing System (AMSR-E)] instruments. The parameters of an existing oceanic surface model are first adjusted to give consistent sea surface scattering properties for CALIPSO and CloudSat observations. Revisiting the lidar/radar data analysis procedure using this model, as well as sea surface wind speed, the temperature and water vapor products of the microwave radiometer (AMSR-E) allowed one to refine the calibration factors for both lidar and radar observations in a coherent approach. This study also improves other applications such as the retrieval of atmospheric attenuation from aerosols at optical wavelengths. [J246]

## "PolSAR Data Segmentation by Combining Tensor Space Cluster Analysis and Markovian Framework"

We present a new segmentation method for the fully polarimetric synthetic aperture radar (PolSAR) data by coupling the cluster analysis in the tensor space and the Markov random field (MRF) framework. The PolSAR data are usually obtained as a set of 3 ?? 3 Hermitian positive definite polarimetric covariance matrices, which do not form a Euclidean space. If we regard each matrix as a tensor, the PolSAR data space can be represented as a Riemannian manifold. First, the mean shift algorithm is extended to the manifold to cluster such tensors. Then, under the MRF framework, the data energy term is defined by the memberships of all tensors in all the clusters, and the smoothness energy term is defined according to the cluster overlap rates. These parameters regarding the cluster analysis are computed under the Riemannian framework. The total energy is minimized using a graph-cut-based optimization to achieve the segmentation results. The effectiveness of the proposed method is verified using real fully PolSAR data and synthetic images. [J247]

## "First Analysis of TerraSAR-X Along-Track InSAR-Derived Current Fields"

We present the first analysis of surface current fields derived from TerraSAR-X along-track interferometric

synthetic aperture radar (along-track InSAR, ATI) data. The images were acquired over the mouth of the Elbe river (Germany) during six satellite overpasses in spring and summer 2008, using the experimental "aperture switching" mode of TerraSAR-X. In this mode, the phased-array synthetic aperture radar (SAR) antenna is split into two halves for receiving, but in contrast to the "dual receive antenna" mode, which uses two independent receivers in parallel, a single receiver is multiplexed to process signals from the two antenna halves in an alternating manner at a doubled pulse repetition frequency. The effective ATI baseline is on the order of 0.8 m. The SAR/ATI raw data processing is described in another paper in this issue. This paper focuses on the conversion of the basic interferograms into line-of-sight surface current fields, which includes an elimination of ship signatures, identification, and correction (as far as possible) of imaging artifacts, additional filtering and smoothing, and a subtraction of contributions of wave motions to detected velocities according to a theoretical model. We evaluate the quality of the results by comparison with current fields from a numerical flow model and with available in situdata. The ATI performance of TerraSAR-X is found to be basically consistent with theoretical expectations. After applying the same data processing algorithms to all six images, mean differences between TerraSAR-X-derived currents and reference currents in our main test area range from -0.11 to + 0.08 m/s in five of the six cases with one outlier at +0.42 m/s. The spatial current variations within the TerraSAR-X-derived current fields are consistent with the model in three cases, but unrealistically strong variations across the images are found in the other three cases. We attribute this to shortcomings of our preliminary raw data processi--ng algorithms, which can probably be fixed after some more detailed analysis and testing. The results obtained so far encourage us to believe that our internal performance goal of a typical current measuring accuracy of 0.1 m/s at an effective spatial resolution better than 1 km can be met. [J248]

## "A Novel Strategy for the Surface Current Determination From Marine X-Band Radar Data"

This letter deals with the sea state monitoring starting from marine radar images in the X-band. For such a topic, one of the key factors affecting the reliability of reconstruction procedure is the determination of the equivalent surface current that also accounts for the velocity of a moving ship. In this letter, we propose a method to evaluate the surface current, particularly for large values. The reliability of the proposed procedure is shown by a numerical analysis with synthetic data. Subsequently, we present some preliminary results with experimental data collected by a radar on a moving ship. [J249]

## "Minimum Entropy via Subspace for ISAR Autofocus"

In this letter, a novel approach to autofocus for inverse synthetic aperture radar (ISAR) imaging called minimum entropy via subspace autofocus is presented. This scheme uses the weighted signal subspace to express the phase errors left in the echoes after range-bin alignment and estimates the optimal weights sequentially via an optimization algorithm based on an entropy minimization principle, and its robustness and convergence can be ensured by the optimization method. Both the theoretical analysis and processing results of the real ISAR data have confirmed the feasibility of this new scheme. [J250]

## "Assessment of TerraSAR-X Products with a New Feature Extraction Application: Monitoring of Cylindrical Tanks"

There is no doubt that retrieving observed scene features is one of the most interesting and challenging activities in all fields of remote sensing: The successful extraction of scene parameters may not only mean the success of the adopted procedure but also the success of a prediction model, an image product, a sensor project, or even an entire mission. This paper is partly concerned with this. The mission, the sensor, and the products at issue are the TerraSAR-X; the feature retrieval approach is the deterministic model-based approach already tested on E-SAR images and now in phase of improvement and testing on high-resolution TerraSAR-X images. Together with assessing the performances of TerraSAR-X products, this paper deals with a new application which, until now, has not received enough attention even if being worth of it: monitoring of big tanks in suburban or urban areas. Detailed discussion concerning the most suitable product for this kind of application is accompanied by retrieval results carried out on recently acquired TerraSAR-X images. [J251]

## "Remote Survey of the Leaning Tower of Pisa by Interferometric Sensing"

The Leaning Tower of Pisa, one of the world-famous architectural marvels of Italian heritage, needs continuous surveying to assess its stability. In this letter, remote-sensing equipment recently developed by the authors, based on the principle of microwave radar interferometry, has been experimented to measure the frequency response of the Tower without requiring any contact with its structure. Wind and human traffic were used as natural excitation sources, allowing the natural frequencies of the first vibration mode of the Tower to be measured in the north-south and in the west-east directions. Modal shapes of the Tower vibrations were also obtained from data acquired by the radar. [J252]

## "APC Trajectory Design for "One-Active" Linear-Array Three-Dimensional Imaging SAR"

This paper discusses the antenna phase center trajectory (APCT) design for the "one-active" linear-array 3D imaging SAR (LASAR). First, we discuss the principle of the one-active LASAR and demonstrate its feasibility by experiment. To describe the 3D spatial resolution of the one-active LASAR, the relationship between the 3D ambiguity function (AF) of the one-active LASAR and the system parameters is discussed in detail. Based on the analysis, we divide the APCT design into three topics: the direction of the linear array, the length of the linear array, and the switching mode of the active element [named as antenna phase center function (APCF)]. On the first topic, we conclude that, when the range, along-track, and cross-track directions are orthogonal to each other, the ambiguity region of the one-active LASAR attains minimum, and the 3D spatial resolution can be separated into the range, along-track, and cross-track resolutions. On the second topic, we find that the cross-track resolution is determined by the length of the linear array and the frequency of the carrier. To ensure that the length of the linear array is acceptable, the carrier should be W-band wave or millimeter wave. On the third topic, the effect of APCF is researched, and we find that both the periodic APCF and the pseudorandom APCF can produce 3D resolution, except for the periodic rectangle APCF. For the pseudorandom APCF and the periodic APCF with short period, the cross-range 2D AF is or can be approximated as the product of two 1D AFs in the along- and cross-track directions. Finally, the distribution of the pseudorandom APCF is optimized by the Lagrange multiplier method under the minimum variance criterion, and we find that, when the pseudorandom APCF obeys the parabolic distribution, the cross-range 2D AF is optimal. [J253]

## "Multichannel InSAR Building Edge Detection"

In this paper, the problem of building edge detection in synthetic aperture radar images is addressed. A new stochastic approach based on local Gaussian Markov random field (LGMRF) is proposed. The algorithm finds the edges of buildings starting from the estimation of the hyperparameters of the LGMRF model. The hyperparameters are seen as an indicator of the spatial correlation between adjacent pixels. The procedure is applied on interferometric data, using single-channel and multichannel configurations. The algorithm has been tested on simulated and real data, providing good results in both cases. [J254]

## "Simultaneous Observation of Lunar Radar Sounder and Laser Altimeter of Kaguya for Lunar Regolith Layer Thickness Estimate"

Simultaneous observations of Lunar Radar Sounder (LRS) and Laser ALTimeter (LALT) of Kaguya, a Japanese lunar exploration project, were carried out for the purpose of mapping regolith layer thickness of the Moon. Nadir surface echo of a high-frequency (5 MHz) pulse of LRS interferes the shallow (<; 10 m) subsurface echo from the bottom of the regolith layer, which subsequently makes the apparent surface be detected at a range deviated from the actual surface range, while the actual surface range is optically detected by LALT. Regolith layer thickness information is retrieved from this range difference after an inversion process. So far, four major maria on the near side of the Moon (Maria Tranquillitatis, Serenitatis, Imbrium, and Oceanus Procellarum) have been investigated, and the mean regolith layer thicknesses of the four maria were found to be about the same, ranging from 6.3 to 6.9 m. However, spatial distribution of areal regolith thickness appears different in eastern maria from western maria, which implies a difference of the growth history of the regolith layer. [J255]

## "On the Potential of Kinematic GPR Surveying Using a Self-Tracking Total Station: Evaluating System Crosstalk and Latency"

In this paper, we present an efficient kinematic ground-penetrating radar (GPR) surveying setup using a self-tracking total station (TTS). This setup combines the ability of modern GPR systems to interface with Global Positioning System (GPS) and the capability of the employed TTS system to immediately make the positioning information available in a standardized GPS data format. Wireless communication between the GPR and the TTS system is established by using gain variable radio modems. Such a kinematic surveying setup faces two major potential limitations. First, possible crosstalk effects between the GPR and the positioning system have to be evaluated. Based on multiple walkaway experiments, we show that, for reasonable field setups, instrumental crosstalk has no significant impact on GPR data quality. Second, we investigate systematic latency (i.e., the time delay between the actual position measurement by TTS and its fusion with the GPR data) and its impact on the positional precision of kinematically acquired 2-D and 3-D GPR data. To quantify latency for our kinematic survey setup, we acquired forward-reverse profile pairs across a well-known subsurface target. Comparing the forward and reverse GPR images using three fidelity measures allows determining the optimum latency value and correcting for it. Accounting for both of these potential limitations allows us to kinematically acquire high-quality and high-precision GPR data using off-the-shelf instrumentation without further hardware modifications. Until now, these issues have not been investigated in detail, and thus, we believe that our findings have significant implications also for other geophysical surveying approaches. [J256]

## "Detection of Moving Targets by Focusing in UWB SAR-Theory and Experimental Results"

Moving-target detection in ultrawideband (UWB) synthetic aperture radar (SAR) is associated with long integration time and must accommodate azimuth focusing for reliable detection. This paper presents the theory on detection of moving targets by focusing and experimental results on single-channel SAR data aimed at evaluating the detection performance. The results with respect to both simulated and real data show that the ability to detect moving targets increases significantly when applying the proposed detection technique. The improvement in signal-to-clutter noise ratio, which is a basic requisite for evaluating the performance, reaches approximately 20 dB, using only single-channel SAR data. This gain will be preserved for the case of multichannel SAR data. The reference system for this study is the airborne UWB low-frequency SAR Coherent All RAdio BAnd Sensing II. [J257]

## "Angular Backscatter Variation in L-Band ALOS ScanSAR Images of Tropical Forest Areas"

Scanning synthetic aperture radar (ScanSAR) systems provide continuous information over large areas, but for effective use of such products in tropical forest, the decrease of radar backscatter with large variation of incidence angles requires attention. This letter analyzes the dependence of radar backscatter on incidence angle for L-band ScanSAR images of tropical forest. We investigated and modeled the angular backscatter effect per land-cover class in three ScanSAR images of the Colombian Orinoco. We found that there is an evident effect of incidence angle on radar backscatter, depending on land-cover class, moisture content, and physical structure of the reflecting targets. To normalize the angular backscatter variation, we proposed two methods. The first one applies a cosine correction estimated through linear regression. The second one models the radar backscatter of flooded forest considering second-order signal interactions. The model explains the observed backscatter of flooded forest areas in the rainy season (R2that is larger than 0.77). [J258]

## "A New CFAR Ship Detection Algorithm Based on 2-D Joint Log-Normal Distribution in SAR Images"

The characteristic difference between targets and clutter is analyzed. Considering the ship target's gray intensity distribution and its shape difference compared to the clutter, in this letter, a new algorithm is presented based on correlation. The algorithm utilizes the strong gray intensity correlation in the ship target; also, the joint gray intensity distribution using 2-D joint log-normal distribution of a pixel with neighboring pixels in the clutter is modeled, which can be used for correlation-based joint constant false alarm rate detection. Using this algorithm, the false alarms caused by speckle and local background nonhomogeneity can be greatly reduced. The detection performance is much better. [J259]

## "Analysis of Spatial Similarities Between NEXRAD and NLDAS Precipitation Data Products"

Precipitation is one of the key inputs for hydrological modeling. Although the Multisensor Precipitation Estimator (MPE) from NEXRAD (Next Generation Radar) and the NLDAS (North American Land Data Assimilation System) precipitation data have been extensively used in various hydrological and climatic studies, there has been no systematic investigation of the spatial similarities and differences between them, based on long-term time series data over a large spatial region. In this study, six years of hourly and daily precipitation time series data from NEXRAD and NLDAS were investigated for their spatial similarities, over a subregion of the Ohio River basin. Three spatial metrics were used: Cohen's Kappa coefficient, Forecast Quality Index (FQI), and displacement-based Forecast Quality Measure (FQM). The three metrics were also applied to the two data products after stratification by season (warm, cold). Results show that significant differences exist between NEXRAD MPE and NLDAS. Analyses and discussions are presented on possible causes of the dissimilarities. In addition, results show that a single metric cannot adequately represent their spatial characteristics. The three metrics are complementary to each other and, when used jointly, can provide a more complete picture of the similarities and differences between the two precipitation products. However, if a single metric is desired, then a more comprehensive one needs to be developed to effectively account for magnitude, distance, shape, and neighborhood effects. [J260]

## "Mapping of Sand Layer Thickness in Deserts Using SAR Interferometry"

This paper presents an interferometric synthetic aperture radar (InSAR) system to map the bedrock topography underneath the sand in deserts and arid areas. This is anticipated to greatly increase the efficiency of oil field and ground water exploration as well as environmental and archaeological studies. The proposed system consists of two InSAR subsystems, one operating at Ka-band to map the sand topography and the other operates in the VHF band to map the subsurface topography. The different issues associated with InSAR processing for subsurface mapping are discussed. It is shown that conventional InSAR processing produces

unacceptable error in height estimation since it does not account for the refraction and the different propagation velocity in the sand. Thus, a new inversion algorithm is developed which can be used to accurately estimate the bedrock topography for arbitrary sand and bedrock geometries. A sensitivity analysis is then presented to show the effect of the different systematic and random errors. The inversion algorithm is verified experimentally for flat sand case using a scaled model that was implemented in the lab. [J261]

## "A General Characterization for Polarimetric Scattering From Vegetation Canopies"

Current polarimetric model-based decomposition techniques are limited to specific types of vegetation because of their assumptions about the volume scattering component. In this paper, we propose a generalized probability density function based on the nth power of a cosine-squared function. This distribution is completely characterized by two parameters; a mean orientation angle and the power of the cosine-squared function. We show that the underlying randomness of the distribution is only a function of the power of the cosine-squared function. We then derive the average covariance matrix for various different elementary scatterers showing that the result has a very simple analytical form suitable for use in model-based decomposition schemes. [J262]

## "Clear-Cut Detection in Swedish Boreal Forest Using Multi-Temporal ALOS PALSAR Backscatter Data"

An extensive dataset of images acquired by the Advanced Land Observing Satellite (ALOS) Phased Array type L-band Synthetic Aperture Radar (PALSAR) is investigated for clear-cut detection in the county of Vajsterbotten, Sweden. Strong forest/non-forest contrast and temporal consistency were found for the Fine Beam Dual HV-polarized backscatter in summer/fall. In consequence of a clear-cut between image acquisitions, the HV-backscatter dropped in most cases between 2 and 3 dB. Thus, a simple thresholding algorithm that exploits the temporal consistency of time series of HV-backscatter measurements has been developed for clear-cut detection. The detection algorithm was applied at pixel level to ALOS PALSAR strip images with a pixel size of 50 m. The performance of the detection algorithm was tested with three different threshold values (2.0, 2.5 and 3.0 dB). The classification accuracy increased from 57.4% to 78.2% for decreasing value of the threshold. Conversely, the classification error increased from 3.0% to 9.7%. For about 90% of the clear-felled polygons used for accuracy assessment the proportion of pixels correctly detected as clear-felled was above 50% when using a threshold value of 2.0 dB. For the threshold values of 2.5 and 3.0 dB the corresponding figures were 80% and 65%, respectively. The total area classified as clear-felled during the time frame of the ALOS PALSAR data differed by 5% compared to an estimate of notified fellings for the same period of time when using a detection threshold of 2.5 dB. The performance of the simple detection algorithm is reasonable when aiming at detecting clear-cuts, whereas there are shortcomings in terms of delineation. [J263]

## "A Wireless Soil Moisture Smart Sensor Web Using Physics-Based Optimal Control: Concept and Initial Demonstrations"

This paper introduces a new concept for a smart wireless sensor web technology for optimal measurements of surface-to-depth profiles of soil moisture using in-situ sensors. The objective of the technology, supported by the NASA Earth Science Technology Office Advanced Information Systems Technology program, is to enable a guided and adaptive sampling strategy for the in-situ sensor network to meet the measurement validation objectives of spaceborne soil moisture sensors. A potential application for this technology is the validation of products from the Soil Moisture Active/Passive (SMAP) mission. Spatially, the total variability in soil-moisture fields comes from variability in processes on various scales. Temporally, variability is caused by external forcings, landscape heterogeneity, and antecedent conditions. Installing a dense in-situ network to sample the field continuously in time for all ranges of variability is impractical. However, a sparser but smarter network with an optimized measurement schedule can provide the validation estimates by operating in a guided fashion with guidance from its own sparse measurements. The feedback and control take place in the context of a dynamic physics-based hydrologic and sensor modeling system. The overall design of the smart sensor web-including the control architecture, physics-based hydrologic and sensor models, and actuation and communication hardware-is presented in this paper. We also present results illustrating sensor scheduling and estimation strategies as well as initial numerical and field demonstrations of the sensor web concept. It is shown that the coordinated operation of sensors through the control policy results in substantial savings in resource usage. [J264]

## "A New Strategy to Estimate Local Fringe Frequencies for InSAR Phase Noise Reduction"

A new approach is presented to estimate the fringe frequencies in interferometric synthetic aperture radar (InSAR) phase image. A first-order model is usually used for fringe frequency estimation, but in steep regions or low-correlation regions, it often fails. In this letter, a prefiltered interferogram, obtained by the slope-compensated

or conventional mean filter, is divided into small patches and unwrapped separately. Subsequently, we differentiate the local-phase-unwrapping results to obtain the fringe frequencies. Furthermore, the invalid fringe frequencies are eliminated by a statistical threshold. Finally, the interferogram is filtered by compensating the estimated fringe frequencies in the averaging window of the mean filter. The proposed method can obtain continuous fringe frequency estimation, and it is not constrained by the first-order model. The effectiveness of the proposed approach is verified by the simulated and real InSAR data. [J265]

## "An Analytical Method of Updating the Range Derivatives and a Simple Image Registration Method for the MSR-Based Range Doppler Algorithm"

Based on the method of series reversion, Neo developed a quite accurate range Doppler algorithm (RDA). In performing this RDA, the range derivatives need to be updated along the range. In this letter, first, we will give an analytical method to update the range derivatives for this RDA. The proposed method mainly exploits two points the first is the introduction of a reference vector on the ground plane of the bistatic geometry, and the second is the use of the principle of series reversion. Second, based on this new method of updating the range derivatives, we present a simple image registration method for mapping the focused image onto the ground plane, which needs a 1-D interpolation only in the range direction. Third, a motion compensation method is also proposed. [J266]

## "Polarimetric SAR Data in Land Cover Mapping in Boreal Zone"

This paper compares ALOS PALSAR fully polarimetric and dual-polarized data in the application area of land cover mapping. To assure versatile comparison of the data, different classification methods and different features of data are used. Two of the classification methods used are based on supervised classification and two on unsupervised classification. Polarimetric data are used in three ways: (1) as fully polarimetric data; (2) features calculated from fully polarimetric data; and (3) intensity data of selected channels. Combinations of six (water, field, sparse forest, dense forest, peat land, and urban areas), five, four, and three classes were used for classification. Fully polarimetric data gave better results (87.5%-84.7% with three classes; open land areas, forest, and water) than intensity data only (83.6%-78.6%), but the differences in the overall accuracies between the methods were not more than 7.6%. Kappa coefficients of agreement are moderate for all the classifications. Supervised classification can be expected to perform better than unsupervised classification, given that the training areas can be selected accurately. Dual polarization data were found to be an attractive alternative in cases where fully polarimetric data are not available or it is of low resolution. With intensities of selected polarimetric features, it was possible to obtain a high classification accuracy as with fully polarimetric data. This also opens possibilities for nonspecialist users to benefit from polarimetric information in classification. [J267]

## "Interferometric SAR Extended Coherence Calculation Based on Fractional Lower Order Statistics"

A polarimetric synthetic aperture radar (SAR) coherence calculation method based on fractional lower order statistics (FLOS) was proposed in Bian's paper. In this letter, we apply this approach to the coherence calculation for interferometric SAR (InSAR) and provide a detailed analysis. An L-band InSAR data set is used to provide comparative results between the coherence derived in the traditional manner and that based on FLOS. In the areas around strong scatterers, the coherence is found to be biased due to the deviation of the statistical model from Gaussian when using the traditional coherence calculation. However, the coherence based on FLOS largely reduces this bias. From the experimental results using the InSAR data, we found that this method reduces the artifacts in the traditional coherence calculation method. The removal of bias due to sample estimation is also discussed. [J268]

## "A New Vector Waveform Inversion Algorithm for Simultaneous Updating of Conductivity and Permittivity Parameters From Combination Crosshole/Borehole-to-Surface GPR Data"

We have developed a new full-waveform groundpenetrating radar (GPR) multicomponent inversion scheme for imaging the shallow subsurface using arbitrary recording configurations. It yields significantly higher resolution images than conventional tomographic techniques based on first-arrival times and pulse amplitudes. The inversion is formulated as a nonlinear least squares problem in which the misfit between observed and modeled data is minimized. The full-waveform modeling is implemented by means of a finite-difference time-domain solution of Maxwell's equations. We derive here an iterative gradient method in which the steepest descent direction, used to update iteratively the permittivity and conductivity distributions in an optimal way, is found by cross-correlating the forward vector wavefield and the backward-propagated vectorial residual wavefield. The formulation of the solution is given in a very general, albeit compact and elegant, fashion. Each iteration step of our inversion scheme requires several calculations of propagating wavefields. Novel features of the scheme compared to previous full-waveform GPR inversions are as follows: 1) The permittivity and conductivity

distributions are updated simultaneously (rather than consecutively) at each iterative step using improved gradient and step length formulations; 2) the scheme is able to exploit the full vector wavefield; and 3) various data sets/survey types (e.g., crosshole and borehole-to-surface) can be individually or jointly inverted. Several synthetic examples involving both homogeneous and layered stochastic background models with embedded anomalous inclusions demonstrate the superiority of the new scheme over previous approaches. [J269]

## "A Neural Network Technique for Improving the Accuracy of Scatterometer Winds in Rainy Conditions"

We exhibit a technique for improving wind accuracy in Ku-band ocean wind scatterometers in the presence of rain. The technique is autonomous in that it only makes use of measurements made by the scatterometer itself, so that no colocation of an external data set (e.g., rain radiometers) is required to perform the correction. The only inputs to the technique are the normalized radar cross-section measurements for each wind vector cell, the cross-track distance of the cell as a proxy for measurement geometry, and the nominal retrieved wind vector for the cell without rain correction. This last input is used to avoid modifying winds not contaminated by rain. The technique was applied to QuikSCAT data for the month of January 2008, resulting in a marked improvement to rainy data. For data that were determined to be rain contaminated by the Jet Propulsion Laboratory rain flag, the rms speed error with respect to National Data Buoy Center buoy winds improved from 8.9 to 3.5 m/s for colocations within 25 km. The rms speed error in rain also improved when compared with the European Centre Medium-Range Weather Forecast winds from 7 to 3 m/s. Data that were not flagged as rain contaminated were not significantly changed, despite the fact that the technique does not make use of the rain flag. The technique was able to distinguish between rain-contaminated wind cells and rain-free wind cells and to substantially improve the wind speed accuracy of the former using QuikSCAT data alone without recourse to any external information about the extent of the rain. [J270]

## "Flexible Dynamic Block Adaptive Quantization for Sentinel-1 SAR Missions"

The letter introduces a novel quantizer suited for medium to high-resolution synthetic aperture radar (SAR) systems, like the forthcoming SENTINEL-1 SAR. The Flexible Dynamic Block Adaptive Quantization (FDBAQ) extends the concept of the Block Adaptive Quantization (BAQ), used in spaceborne SAR since the Magellan mission, by adaptively tuning the quantizer rate according to the local signal-to-noise-ratio (SNR). A design is presented aiming to optimize the average bit-rate, while constraining the minimum SNR. FDBAQ optimized performance is then evaluated using backscatter maps derived from ENVIronment SATellite (ENVISAT) data. [J271]

## "A Simple Moment Method of Forest Biomass Estimation From Non-Gaussian Texture Information by High-Resolution Polarimetric SAR"

A simple method is described to estimate forest biomass by high-resolution polarimetric synthetic aperture radar (SAR). The method is based on the regression analysis between the measured biomass from the ground survey and the second intensity moment of the non-Gaussian texture in the cross-polarized L-band SAR images. The SAR data used in the analysis were acquired by the airborne polarimetric interferometric SAR over the coniferous forest in Hokkaido, Japan. The regression analysis was first carried out, and a model function was derived to relate the intensity moment and the measured biomass in 19 forest stands. Using this model function, the biomass values were estimated and compared with those of 21 different stands with known biomass. The average accuracy of the moment model was found to be 85%, which is similar to that of the previous K -distribution model. The advantage of this method over the distribution-based model is that there is no need to search a specific distribution function which fits best to the image texture. [J272]

## "Radiometric Calibration of the Advanced Wind Scatterometer Radar ASCAT Carried Onboard the METOP-A Satellite"

The Advanced Wind Scatterometer (ASCAT) is a six-beam spaceborne radar instrument designed to measure wind fields over the oceans. An ASCAT instrument is carried by each of the three METOP satellites. The ASCAT calibration strategy is described and detailed results are presented concerning the radiometric calibration achieved. [J273]

## "Velocity Estimation and Range Shift Compensation for High Range Resolution Profiling in Stepped-Frequency Radar"

In this letter, a novel radial velocity estimation and range shift compensation algorithm is proposed for high-range resolution profiling of moving targets in stepped-frequency (SF) radar. Compared to traditional methods,

this algorithm is based on a more precise signal model, and can therefore achieve much higher estimation accuracy. Furthermore, the range shift problem caused by target motion can be resolved without alterations to the radar waveform. The performance of this algorithm is demonstrated using simulated and experimental results. [J274]

## "Evaluation of Aerial Remote Sensing Techniques for Vegetation Management in Power-Line Corridors"

This paper presents an evaluation of airborne sensors for use in vegetation management in power-line corridors. Three integral stages in the management process are addressed, including the detection of trees, relative positioning with respect to the nearest power line, and vegetation height estimation. Image data, including multispectral and high resolution, are analyzed along with LiDAR data captured from fixed-wing aircraft. Ground truth data are then used to establish the accuracy and reliability of each sensor, thus providing a quantitative comparison of sensor options. Tree detection was achieved through crown delineation using a pulse-coupled neural network and morphologic reconstruction applied to multispectral imagery. Through testing, it was shown to achieve a detection rate of 96%, while the accuracy in segmenting groups of trees and single trees correctly was shown to be 75%. Relative positioning using LiDAR achieved root-mean-square-error (rmse) values of 1.4 and 2.1 m for cross-track distance and along-track position, respectively, while direct georeferencing achieved rmse of 3.1 m in both instances. The estimation of pole and tree heights measured with LiDAR had rmse values of 0.4 and 0.9 m, respectively, while stereo matching achieved 1.5 and 2.9 m. Overall, a small number of poles were missed with detection rates of 98% and 95% for LiDAR and stereo matching. [J275]

## "A Novel UWB Sampling Receiver and Its Applications for Impulse GPR Systems"

A novel ultrawideband (UWB) synchronous receiver for a UWB radar system is presented. The developed receiver is the first to employ a sampling phase detector, which integrates a step recovery diode and a pair of Schottky diodes, to sample the UWB signal of a radar, enabling the miniaturization of the design. It achieves a 6-GHz sampling bandwidth, a dynamic range of more than 50 dB, and low harmonic distortion of the output baseband signal. The receiver's down-converted IF signals closely match with their original shape, demonstrating its good performance to reconstruct the microwave signals from a receiving antenna. These IF signals can be converted to digital signals by a low-cost A/D. For verification, the performance of the UWB receiver is tested through the experiments of buried steels at different thicknesses in the sand when it is applied to the ground-penetrating radar (GPR). The results show that the GPR system has good horizontal resolution and large detection depth. Therefore, this GPR system is very attractive and effective for applications of short-range and high-resolution detection. [J276]

## "A Qualitative Inverse Scattering Method for Through-the-Wall Imaging"

Imaging methods that are able to detect targets located behind a wall and monitor their motion have recently gained an increasing attention. To pursue this aim, we propose a qualitative inverse scattering approach based on the linear sampling method, which is a computationally effective nonapproximated shape-reconstruction strategy. In particular, we describe the formulation of the method for the through-the-wall scenario for both the case of static and dynamic targets. The results of a numerical analysis are reported as a preliminary assessment of the achievable performances. [J277]

## "An Array Error Estimation Method for Constellation SAR Systems"

In practice, unavoidable array errors, consisting of phase and position errors, significantly degrade the performance of constellation synthetic aperture radar (SAR) systems. Therefore, methods are required to estimate these errors. In constellation SAR systems, the clutter spectrum components within a Doppler bin can be used as calibration sources with known directions. In this letter, it is observed that the steering vectors of the spectrum components in one Doppler bin are conjugate with those of the spectrum components in its contrary Doppler bin on condition that each SAR operates in side-looking mode and its nominal left coordinate is zero, which is easy to realize. We obtain a new phase error estimation method based on this observation. An array error estimation method, which estimates phase and position errors simultaneously, is proposed via combining the new phase error estimation method with the least squares method for estimating position errors. The advantages of the proposed method include its capability to directly estimate phase and position errors without joint iteration between the estimations of phase and position errors; thus, it performs well, while the conventional method behaves unstably because it may converge to a local optimal solution, when position errors are large. Furthermore, mathematical analysis indicates that the proposed method has less computational load. In addition, computer simulations show that it performs better than the conventional method. The only cost is that it employs twice as many Doppler bins as the conventional method does, which is endurable because there are numerous

Doppler bins. [J278]

## "RFI Suppression in Ultrawideband SAR Using an Adaptive Line Enhancer"

In this letter, we propose an approach to suppress radio-frequency interference (RFI) in ultrawideband (UWB) low-frequency synthetic aperture radar (SAR). According to the proposal, RFI is suppressed by using an adaptive line enhancer controlled by the normalized least mean square algorithm. The approach is tested successfully on real UWB low-frequency SAR data. In order to keep the computational burden down, possible ways to integrate the RFI suppression approach into SAR imaging algorithms are also suggested. [J279]

## "Noniterative Super-Resolution Technique Combining SVA With Modified Geometric Mean Filter"

We propose a super-resolution algorithm that combines spatially variant apodization (SVA) with a modified geometric mean filter to improve the resolution of synthetic aperture radar (SAR) images and reduce sidelobes simultaneously. This method does not require iterative calculation. The efficacy of the proposed algorithm is verified by simulation with point targets and in experiments with a real SAR image. The proposed method improved resolution by 40% compared to SVA and phase-extension inverse filtering. [J280]

## "Effect of Rain Attenuation on Range Weighting in Weather Radar"

The amplitude analysis of radar signals from rain is refined. Uniform rain return details with amplitude weighting due to 1) range gate straddle losses and 2) rain attenuation within the processed range cell, both respectively and in nonlinear resultant conditions, are considered. The resulting factor is small in magnitude, except in heavy rain and short wavelengths. The factor has a data-dependent analytic form, without a known analytic inverse. A quantitative solution for the reflectivity factor may employ numerical look-up tables parameterized in specific attenuation single parameter coefficients and range gate width. [J281]

## "The Surface Water and Ocean Topography Mission: Observing Terrestrial Surface Water and Oceanic Submesoscale Eddies"

The elevation of the ocean surface has been measured for over two decades from spaceborne altimeters. However, existing altimeter measurements are not adequate to characterize the dynamic variations of most inland water bodies, nor of ocean eddies at scales of less than about 100 km, notwithstanding that such eddies play a key role in ocean circulation and climate change. For terrestrial hydrology, in situ and spaceborne measurements of water surface elevation form the basis for estimates of water storage change in lakes, reservoirs, and wetlands, and of river discharge. However, storage in most inland water bodies, e.g., millions of Arctic lakes, is not readily measured using existing technologies. A solution to the needs of both surface water hydrology and physical oceanography communities is the measurement of water elevations along rivers, lakes, streams, and wetlands and over the ocean surface using swath altimetry. The proposed surface water and ocean topography (SWOT) mission will make such measurements. The core technology for SWOT is the Ka-band radar interferometer (KaRIN), which would achieve spatial resolution on the order of tens of meters and centimetric vertical precision when averaged over targets of interest. Average revisit times will depend upon latitude, with two to four revisits at low to mid latitudes and up to ten revisits at high latitudes per ~20-day orbit repeat period. [J282]

## "A Lossless Compression Algorithm for SAR Amplitude Imagery Based on Modified Quadtree Coding of Bit Plane"

A lossless compression algorithm for synthetic aperture radar (SAR) amplitude images based on modified quadtree bit-plane coding is proposed. First, a SAR amplitude image is divided into independent bit planes, and then, the probability of bit "0" is computed and compared with the predefined threshold in order to select the optimal block size for each bit plane. Finally, a modified quadtree coding method is adopted to encode each block data. Additionally, the computing method of predefined threshold is also addressed in this letter. The experimental results show that the proposed method outperforms previous methods for all SAR images of the test sets; an average 0.895-bpp decrease in bit rate was observed when compared with JPEG-LS. [J283]

## "Phase Unwrapping by Markov Chain Monte Carlo Energy Minimization"

Phase unwrapping (PU) is a process to obtain the absolute value of a phase field from the wrapped one. Ideally, without phase noise, singularity, and aliasing problems, the phase information can be unwrapped easily. However, the phase data are always contaminated by noise and discontinuities, making the PU process more complicated. Hence, a suitable PU algorithm is required to address the problems appropriately. Markov Chain Monte Carlo (MCMC) Energy Minimization is usually used to partially remove phase noise. In this letter, the

MCMC energy minimization that yields the unwrapped phase is shown. Furthermore, the capability of the proposed method to unwrap simulated and actual InSAR phase images is also demonstrated (Fujiyama Mount). [J284]

## "A Noniterative Approach for the Quick Alignment of Multistation Unregistered LiDAR Point Clouds"

A novel approach for aligning multistation unregistered Light Detection and Ranging (LiDAR) point clouds is presented in this letter. It is designed to find the rigid rotations and translations between two data sets using hybrid conjugate features, including points, lines, planes, and groups of points. In addition, the proposed solution is expressed in a closed form, meaning that neither an initial alignment nor an iterative computation is required. Based on the numerical results from a real case study, it has been demonstrated that the proposed approach is capable of giving an efficient and reliable alignment solution. With the aforementioned advantages, the proposed technique can not only be directly implemented in a general analysis of LiDAR surveying data but will also particularly benefit those applications where classical point-based iterative analysis approaches are not practically feasible (e.g., an application without a sufficient number of connecting points). [J285]

## "Spectroscopic Calibration Correlation of Field and Lab-Sized Fluorescence LIDAR Systems"

A method has been developed to correlate spectral signatures obtained with various fluorescence LIght Detection And Ranging (LIDAR) systems. A calibrated fluorescence reference target was used to calibrate the spectral response of the LIDAR transmitter channels and obtain their transfer functions. Two LIDAR systems have been spectrally characterized, and corrected signatures for two bioaerosols are presented. The first LIDAR system is the Standoff Integrated Bioserosol Active Hyperspectral Detection field LIDAR developed by Defence R&D Canada. This standoff system uses a 351-nm pulsed laser in a monoaxial design. The second system is a lab-sized aerosol chamber designed to characterize fluorescent aerosols under controlled environmental conditions. The chamber was designed according to classical short-range biaxial LIDAR principles, with the purpose of duplicating the results obtained with field LIDAR systems. Aerosols generated within the chamber are probed by a 355-nm pulsed laser, and autofluorescence spectra are measured with a spectrometer and an intensified charge-coupled device camera. This chamber is used to collect the reference spectra of various fluorescing aerosols and simulants of biological agents. One of the main objectives in using this chamber is to produce and compile a library of instrument-free fluorescing spectra that can be transferred to other LIDAR-based bioaerosol sensors with known optical transfer functions. [J286]

## "Obtaining Accurate Ocean Surface Winds in Hurricane Conditions: A Dual-Frequency Scatterometry Approach"

We describe a method for retrieving winds from colocated Ku- and C-band ocean wind scatterometers. The method utilizes an artificial neural network technique to optimize the weighting of the information from the two frequencies and to use the extra degrees of freedom to account for rain contamination in the measurements. A high-fidelity scatterometer simulation is used to evaluate the efficacy of the technique for retrieving hurricane force winds in the presence of heavy precipitation. Realistic hurricane wind and precipitation fields were simulated for three Atlantic hurricanes, Katrina and Rita in 2005 and Helene in 2006, using the Weather Research and Forecasting model. These fields were then input into a radar simulation previously used to evaluate the Extreme Ocean Vector Wind Mission dual-frequency scatterometer mission concept. The simulation produced high-resolution dual-frequency normalized radar cross-section (NRCS) measurements. The simulated NRCS measurements were binned into 5 x 5 km wind cells. Wind speeds in each cell were estimated using an artificial neural network technique. The method was shown to retrieve accurate winds up to 50 m/s even in intense rain. [J287]

## "HFSW Radar Model: Simulation and Measurement"

High-frequency surface-wave (HFSW) radars are usually used to remotely measure oceanographic parameters. These systems can also potentially detect targets beyond the conventional microwave radar coverage. In this paper, the backscattered Doppler spectrum made up of the sea clutter, ship echoes, and the background noise has been modeled. Taking into account the propagation and the signal-processing effects, a range-Doppler image has been generated. This model can be used for different purposes like the (theoretical) evaluation of detection performance. This paper gives an overview of the theoretical elements for modeling the backscatter signal. The processing effects on the range-Doppler image and the time-evolving target signature are also introduced. Some of the simulated elements and the obtained range-Doppler images are compared with real data. Finally, from this model, the detection capabilities of HFSW radars are evaluated. [J288]

## "Estimation of the Backscatter Vertical Profile of a Pine Forest Using Single Baseline P-Band (Pol-

## )InSAR Data"

The vertical backscatter profile of a pine forest constituted by stands of different height is inverted from a single baseline P-band Pol-InSAR data in order to identify scatterers in the canopy. The proposed approach uses the Gaussian vertical backscatter profile model, which associates an interferometric coherence expression to a vertical scatterers' distribution characterized by relative standard deviation and elevation. The methodology, which uses in situmeasurements of forest height and unbiased ground level estimation, is applied to HV and VV channels, providing accuracy given sufficiently low ground-to-canopy power ratios. Inverted backscatter profiles show maximum power converging toward the basis of the tree crown on highest forests, where the largest branches are located, indicating the high sensitivity of P-band measurements to the forest structure and to the vertical biomass distribution. Over lower stands with larger tree densities, the power peak is located in the upper part of the canopy, which can be explained by a stronger attenuation in the canopy. [J289]

## "An Evaluation of the ALOS PALSAR L-Band Backscatter-Above Ground Biomass Relationship Queensland, Australia: Impacts of Surface Moisture Condition and Vegetation Structure"

Focusing on woody vegetation in Queensland, Australia, the study aimed to establish whether the relationship between Advanced Land Observing Satellite (ALOS) Phased Array L-band SAR (PALSAR) HH and HV backscattering coefficients and above ground biomass (AGB) was consistent within and between structural formations (forests, woodlands and open woodlands, including scrub). Across these formations, 2781 plot-based measurements (from 1139 sites) of tree diameters by species were collated, from which AGB was estimated using generic allometric equations. For Queensland, PALSAR fine beam dual (FBD) 50 m strip data for 2007 were provided through the Japanese Space Exploration Agency's (JAXA) Kyoto and Carbon (K&C) Initiative, with up to 3 acquisitions available for each Reference System for Planning (RSP) paths. When individual strips acquired over Queensland were combined, `banding' was evident within the resulting mosaics, with this attributed to enhanced L-band backscatter following rainfall events in some areas. Reference to Advanced Microwave Scanning Radiometer-EOS (AMSR-E) data indicated that strips with enhanced L-band backscatter corresponded to areas with increased effective vegetation water content (kg m-2) and, to a lesser extent, soil moisture (g cm-3). Regardless of moisture conditions, L-band HV topographically normalized backscattering intensities backscatter (σfo) increased asymptotically with AGB, with the saturation level being greatest for forests and least for open woodlands. However, under conditions of relative maximum surface moisture, L-band HV and HH σfowas enhanced by as much as 2.5 and 4.0 dB respectively, particularly for forests of lower AGB, with this resulting in an overall reduction in dynamic range. The saturation level also reduced at L-band HH for forests and woodlands but remained similar for open woodlands. Differences in the rate of increase in bo--th L-band HH and HV σfowith AGB were observed between forests and the woodland categories (for both relatively wet and dry conditions) with these attributed, in part, to differences in the size class distribution and stem density between non-remnant (secondary) forests and remnant woodlands of lower AGB. The study concludes that PALSAR data acquired when surface moisture and rainfall are minimal allow better estimation of the AGB of woody vegetation and that retrieval algorithms ideally need to consider differences in surface moisture conditions and vegetation structure. [J290]

## "Signal level Simulator for netted text radar waveforms evaluation"

When evaluating the performances of radar waveforms, it is crucial to understand how the signal is affected by multiple interactions with the environment and the system hardware. Analysis of complex radar systems, such as multistatic and netted designs (see Figure 1) is often intractable without the application of a dedicated radar simulation system. Recent research into radar simulation has focused primarily on synthetic aperture radar (SAR) systems [1] and is not entirely applicable to traditional radar systems concerned with the location and tracking of remote targets. A complete simulator has been designed for the accurate simulation of raw returns in complex, multistatic, and netted radars, and is applicable to pulsed and continuous wave (CW) systems, and both active and passive radar systems. The Flexible Simulator for Multistatic Radars (FERS) can be used to simulate radar systems with arbitrary waveforms and arbitrary numbers of receivers, transmitters, and scatterers. Herein, algorithms for the simulation of raw radar return signals are presented, based on interpolation and modification of the transmitted signal and modeling of the radar hardware and environment. The algorithms are expected to be especially valuable for the simulation of emerging radar technologies, such as Passive Coherent Location (PCL) [2], netted radar and phased array radar. Preliminary results, presented herein, suggest that these algorithms can simulate physical systems with excellent accuracy. [J291]

## "Simulating X-Band Interferometric Height in a Spruce Forest From Airborne Laser Scanning"

The aim of this study is to use airborne laser scanning (ALS) data to simulate synthetic aperture radar interferometry (InSAR) elevation data [digital elevation model (DEM)] from the spatial distribution of scatterers. A Shuttle Radar Topography Mission X-band DEM data set and an ALS data set from a spruce-dominated forest

area are used. A 3-D grid of voxels is made from the spatial distribution of ALS first echoes. The slant angle penetration rate of the SAR microwaves (PSAR) is simulated to be a function of the vertical ALS penetration rate (PALS), i.e., PSAR= PALS4. The InSAR DEM and heights above the ground are fairly well reproduced by the simulator. A total least squares regression model between the simulated and measured InSAR DEMs has an R2value of 0.99 and a slope of 1: 1. By subtracting the ALS-based terrain heights (digital terrain model), we obtained InSAR heights, which were reproduced with an R2value of 0.78, a slope of 0.96, and a root-mean-square error of 2.3 m. With the simulator, it was demonstrated how a disturbance event would affect the InSAR height. Unfortunately, the relationship was curvilinear and concave, which means that the method is not very sensitive to weak disturbances. This might be partly overcome by using a more vertical incidence angle of the SAR microwaves. The simulator might be used for validation or ground truthing of the InSAR data, as well as gaining understanding of how vegetation changes affect the InSAR data. [J292]

## "Iterative Bayesian Retrieval of Hydrometeor Content From X-Band Polarimetric Weather Radar"

Dual-polarized weather radars are capable to detect and identify different classes of hydrometeors, within stratiform and convective storms, exploiting polarimetric diversity. Among the various techniques, a model-supervised Bayesian method for hydrometeor classification, tuned for S- and X-band polarimetric weather radars, can be effectively applied. Once the hydrometeor class is estimated, the retrieval of their water content can also be statistically carried out. However, the critical issue of X-band radar data processing, and in general of any attenuating wavelength active system, is the intervening path attenuation, which is usually not negligible. Any approach aimed at estimating hydrometeor water content should be able to tackle, at the same time, path attenuation correction, hydrometeor classification uncertainty, and retrieval errors. An integrated iterative Bayesian radar algorithm (IBRA) scheme, based on the availability of the differential phase measurement, is presented in this paper and tested during the International H2O Project experiment in Oklahoma in 2002. During the latter campaign, two dual-polarized radars, at S- and X-bands, were deployed and jointly operated with closely matched scanning strategies, giving the opportunity to perform experimental comparisons between coincident measurements at different frequencies. Results of the IBRA technique at X-band are discussed, and the impact of path attenuation correction is quantitatively analyzed by comparing hydrometeor classifications and estimates with those obtained at S-band. The overall results in terms of error budget show a significant improvement with respect to the performance with no path attenuation correction. [J293]

## "Discrete Almost-Symmetric Wave Packets and Multiscale Geometrical Representation of (Seismic) Waves"

We discuss a multiscale geometrical representation of (seismic) waves through a decomposition into wave packets. Wave packets can be thought of as certain localized "fat" plane waves. Here, we construct discrete almost-symmetric 3-D wave packets by using the unequally spaced fast Fourier transform. The resulting discrete transform is unitary, implying that the reconstruction operator is simply the adjoint of the decomposition operator. Another relevant aspect of the discretization scheme is the appearance of parameters that control the tiling of the phase space that corresponds with the dyadic parabolic decomposition, preserving the relative parabolic scaling while adapting to the physical problem at hand. We consider applications in exploration and global seismology, in particular for higher dimensional data regularization, seismic map migration, denoising, directional regularity analysis, and feature extraction. [J294]

## "Tomographic SAR Inversion by -Norm Regularization-The Compressive Sensing Approach"

Synthetic aperture radar (SAR) tomography (TomoSAR) extends the synthetic aperture principle into the elevation direction for 3-D imaging. The resolution in the elevation direction depends on the size of the elevation aperture, i.e., on the spread of orbit tracks. Since the orbits of modern meter-resolution spaceborne SAR systems, like TerraSAR-X, are tightly controlled, the tomographic elevation resolution is at least an order of magnitude lower than in range and azimuth. Hence, super-resolution reconstruction algorithms are desired. The high anisotropy of the 3-D tomographic resolution element renders the signals sparse in the elevation direction; only a few pointlike reflections are expected per azimuth-range cell. This property suggests using compressive sensing (CS) methods for tomographic reconstruction. This paper presents the theory of 4-D (differential, i.e., space-time) CS TomoSAR and compares it with parametric (nonlinear least squares) and nonparametric (singular value decomposition) reconstruction methods. Super-resolution properties and point localization accuracies are demonstrated using simulations and real data. A CS reconstruction of a building complex from TerraSAR-X spotlight data is presented. [J295]

## "Estimating surface water flow speeds using time-frequency methods"

Synthetic aperture radar (SAR) image formation implicitly assumes that the backscattered returns arise from

stationary isotropic targets. When objects move during the SAR integration time, signal anomalies appear that distort, displace and smear moving targets in the image. Although these anomalies degrade the image, they provide the information that allows analysis of the underlying target motion. Joint time-frequency analysis (JTFA) exploits these signal anomalies to estimate the motion of typical point targets. However, the weak, transient returns from water surface scatterers complicate standard JTFA estimates of water surface speeds. A time-frequency representation is applied based on the Capon-s spectral estimation technique that allows joint analysis of multiple azimuth lines, thereby increasing the signal-to-clutter ratio of weak scatterers. The authors compare the time-frequency estimate, employing single-phase-centre SAR data, to along-track interferometric SAR estimates of the same flow and show that both the methods produce comparable results. The authors derive the JTFA equations and estimate water surface speed for data collected at a specific imaging geometry. This study highlights the feasibility of using a single-phase-centre SAR system to determine the motion of slow moving distributed targets representative of water flow. [J296]

## "Synthetic Aperture Radar for Earth Observation from a Lunar Base: Performance and Potential Applications"

Starting from the reborn international interest in lunar exploration and the widely documented need for hyper-accurate measurements of Earth crustal dynamics, at a high revisit frequency and on a global scale, the idea of a Moon-based interferometric synthetic aperture radar (SAR) is presented. After introducing models to describe synthetic antenna formation and discussing key issues of a Moon-based radar for Earth remote sensing, a preliminary system design and performance analysis are conducted. Quantitative results are presented in terms of achievable resolutions and needed radar parameters. Although the Moon-based observatory requires technical solutions and a budget that likely make its realization distant, a comparison with currently planned spaceborne interferometric systems shows that it offers height measurement accuracies at a level and with a frequency not achievable otherwise. [J297]

## "Mapping Subsurface Geology in Sahara Using L-Band SAR: First Results From the ALOS/PALSAR Imaging Radar"

Within the framework of Kyoto & Carbon Initiative of the Japanese Space Agency (JAXA), we used JERS-1 and ALOS/PALSAR radar images to build regional and continental scale mosaics of Sahara. The unique capability of L-band SAR to map subsurface structures in arid areas revealed previously unknown geological features: craters, faults, paleo-rivers. The latter are of particular interest for water resource detection in arid regions. [J298]

## "Using ALOS/PALSAR and RADARSAT-2 to Map Land Cover and Seasonal Inundation in the Brazilian Pantanal"

The Brazilian Pantanal is a large continuous tropical wetland with large biodiversity and many threatened habitats. The interplay between the distribution of vegetation, the hydrology, the climate and the geomorphology nourishes and sustains the large diversity of flora and fauna in this wetland, but it is poorly understood at the scale of the entire Pantanal. This study uses multi-temporal L-band ALOS/PALSAR and C-band RADARSAT-2 data to map ecosystems and create spatial-temporal maps of flood dynamics in the Brazilian Pantanal. First, an understanding of the backscattering characteristics of floodable and non-floodable habitats was developed. Second, a Level 1 object-based image analysis (OBIA) classification defining Forest, Savanna, Grasslands/Agriculture, Aquatic Vegetation and Open Water cover types was achieved with accuracy results of 81%. A Level 2 classification separating Flooded from Non-Flooded regions for five temporal periods over one year was also accomplished, showing the interannual variability among sub-regions in the Pantanal. Cross-sensor, multi-temporal SAR data was found to be useful in mapping both land cover and flood patterns in wetland areas. The generated maps will be a valuable asset for defining habitats required to conserve the Pantanal biodiversity and to mitigate the impacts of human development in the region. [J299]

## "Polarimetric Scattering Similarity Between a Random Scatterer and a Canonical Scatterer"

In this letter, we propose a novel parameter to measure the scattering similarity between a random scatterer and a canonical scatterer. Compared with the similarity parameter proposed by Yang, the novel parameter not only has some advantages, such as its independence of the spans of a coherence matrix, but also can be applied directly in the case of a random scatterer made up of multiscattering centers. As an example, the novel parameter is adopted to extract some scattering characteristics of a target. With the full polarimetric L-band airborne synthetic aperture radar data, we illustrate the veracity of the novel parameter in measuring scattering similarity and its application in terrain classification. [J300]

## "Simultaneous Observations and Analysis of Severe Storms Using Polarimetric X-Band SAR and

## Ground-Based Weather Radar"

Recent advances in synthetic aperture radar (SAR) technology have revived meteorological applications with this type of radar. SARs are designed for surface imaging, but now that several X-band multipolarization SAR satellites are in orbit, the attenuation and backscatter caused by precipitation can be better studied. The results presented here demonstrate some of the possibilities by analyzing observations from dual-polarization (HH, VV) TerraSAR-X (TSX) acquisitions over central Florida surrounding severe storms in August 2008. Simultaneous to the SAR acquisitions, WSR-88D ground weather radars in Melbourne and Tampa Bay, FL, collected reflectivity and radial velocity data; the observed strong precipitation cells from convective storms are colocated with severe attenuation in the corresponding SAR images. The observations from SAR measurements are explained quantitatively by converting ground radar reflectivity into spaceborne radar attenuation via a theoretical model. In addition, polarization analysis comparing the SAR image to two additional TSX acquisitions 11 days apart and without rain provides an indication of storm-induced propagation effects on X-band SAR. Specifically, the copolar ratio Z_dr and the copolar correlation differences exhibit behavior that is better explained by the precipitation impact versus surface changes. Multiple regions with varying ground cover, including urban, and storm characteristics are analyzed to highlight the complexity of meteorological research using SAR while revealing a potential use of the technology to investigate the storm structure. [J301]

## "Image Autocoregistration and Interferogram Estimation Using Extended COMET-EXIP Method"

In this paper, an extended COvariance Matching Estimation Techniques-Extend Invariance Principle (COMET-EXIP) method is proposed to estimate interferometric synthetic aperture radar or interferometric synthetic aperture sonar (InSAS) interferometric phase in the presence of large coregistration errors, even up to one pixel. First, the extended COMET-EXIP method is presented for the application of joint-pixel-model-based interferogram estimation, through choosing a novel "unstructured model" in terms of the parameters to be estimated and decoupling the interesting parameters from the uninteresting "nuisance parameters." Then, a fast algorithm of COMET-EXIP is proposed for the interferometric phase estimation. Finally, the ambiguity problem of the COMET-EXIP method is solved without introducing performance degradation. The simulated data and real data from the trial InSAS and X-SAR are used to verify the validity of the method. The results show that the method is robust for a wide range of signal-to-noise ratio and has a good performance on both fringe preserving and noise suppressing. In addition, the same computational speed level of the proposed method as that of the pivoting mean filtering is very attractive. [J302]

## "Requirement on Antenna Cross-Polarization Isolation for the Operational Use of C-Band SAR Constellations in Maritime Surveillance"

The issue of antenna cross-polarization isolation has been previously discussed for the design of fully polarimetric synthetic aperture radars (SARs). Dual-polarized antennas with cross-polarization isolation that is better than -30 dB are desirable for more convenient polarimetric data calibration since measurements of antenna crosstalk (magnitude and phase) variations with incidence angle are not required. For an antenna with significant polarization crosstalk, it is still possible to retrieve pure polarization measurements of HH, HV, VH, and VV provided that the four corresponding received voltages are measured. However, it is not possible to recover from cross-polarization contamination for single- or dual-polarization measurements. Therefore, it is important to set up a minimum requirement on dual-polarized antenna isolation so that single- and dual-polarization applications are not unduly affected. In this letter, the minimum requirement on cross-polarization antenna isolation is investigated for operational use of C-band SARs in maritime surveillance applications. Calibrated polarimetric RADARSAT-2 data are used to simulate single- and dual-polarization data with cross-polarization contamination for a dual-polarized antenna with cross-polarization isolation ranging from -20 to -35 dB. It is shown that the cross-polarization HV (or VH) channel can be significantly affected, particularly at steep incidence angles. As a result, key applications that require the use of pure HV, such as ship detection and wind-speed measurements, are significantly affected. A requirement for a minimum of -30-dB antenna isolation is established. Antennas with cross-polarization isolation better than -35 dB are desirable for reliable exploitation of HV data at steep incidence angles. [J303]

## "Predicting Small Target Detection Performance of Low-SNR Airborne Lidar"

Recent technological advances in the performance of small micro-lasers and multi-channel multi-event photo-detectors have enabled the development of experimental airborne lidar (light detection and ranging) systems based on a low-SNR (LSNR) paradigm. Due to dense point spacing (tens of points per square meter) and sub-decimeter range resolution, LSNR lidar can likely enable detection of meter-scale targets that would go unnoticed by traditional lidar technology. Small vehicle obstructions and other similar targets in the beach and littoral zones are of particular interest, because of LSNR lidar's applicability to the near-shore environment and the general desire to improve detection of antivehicle and antipersonnel obstacles in the coastal zone. A target detection

procedure is presented that exploits the detailed information available from LSNR lidar data while diminishing the effect of spurious noise events. Consideration is given to detection in both topographic and bathymetric scenarios. Data sets for target detection analysis are supplied by a numerical sensor simulator developed at the University of Florida. Target detection performance is evaluated as a function of environmental characteristics, such as water clarity and depth, and system parameters, specifically transmitted pulse energy and laser pulse repetition frequency. Analysis of results with regards to consideration for future system design is discussed. [J304]

## "Improving Discrimination of Savanna Tree Species Through a Multiple-Endmember Spectral Angle Mapper Approach: Canopy-Level Analysis"

Differences in within-species phenology and structure are controlled by genetic variation, as well as topography, edaphic properties, and climatic variables across the landscape, and present important challenges to species differentiation with remote sensing. The objectives of this paper are as follows: 1) to evaluate the classification performance of a multiple-endmember spectral angle mapper (SAM) classification approach in discriminating ten common African savanna tree species and 2) to compare the results with the traditional SAM classifier based on a single endmember per species. The canopy spectral reflectance of the tree species ( Acacia nigrescens, Combretum apiculatum, Combretum imberbe, Dichrostachys cinerea, Euclea natalensis, Gymnosporia buxifolia, Lonchocarpus capassa, Pterocarpus rotundifolius, Sclerocarya birrea, and Terminalia sericea) was extracted from airborne hyperspectral imagery that was acquired using the Carnegie Airborne Observatory system over Kruger National Park, South Africa, in May 2008. This study highlights three important phenomena: 1) Intraspecies spectral variability affected the discrimination of savanna tree species with the SAM classifier; 2) the effect of intraspecies spectral variability was minimized by adopting the multiple-endmember approach, e.g., the multiple-endmember approach produced a higher overall accuracy (mean of 54.5% for 20 bootstrapped replicates) when compared to the traditional SAM (mean overall accuracy = 20.5%); and 3) targeted band selection improved the classification of savanna tree species (the mean overall percent accuracy is 57% for 20 bootstrapped replicates). Higher overall classification accuracies were observed for evergreen trees than for deciduous trees. [J305]

## "Generating Large-Scale High-Quality SAR Mosaic Datasets: Application to PALSAR Data for Global Monitoring"

This paper proposes a mosaicking algorithm to produce large-scale radiometrically and geometrically calibrated Synthetic Aperture Radar (SAR) datasets as a base for environmental monitoring of terrestrial biospheric and cryospheric changes. Features of the proposed method are thematic inclusion of a) long-strip processing of the SAR data, b) ortho-rectification and slope correction using a digital elevation model, c) suppression of differences in intensity between neighboring strips, and d) preparation of metadata (e.g., dates from launch, local incidence angle, radar shadow, layover, and valid/invalid data) to support dataset interpretation. The performance of the proposed method is evaluated using Advanced Land Observing Satellite (ALOS) Phased Array type L-band SAR (PALSAR) mosaics for Southeast Asia, Australia, and Africa. [J306]

## "PALSAR Wide-Area Mapping of Borneo: Methodology and Map Validation"

This paper describes the operational radar mapping processing chain developed and steps taken to produce a provisional wide-area PALSAR forest and land cover map covering Borneo for the year 2007, compliant with emerging international standards (CEOS guidelines, FAO LCCS). A Bayesian approach based on (unsupervised) mixture modeling followed by Markov Random Field (MRF) classification has been selected for its suitability and flexibility to deal with a situation where ground truth is sparse and sometimes ambiguous. The methodology is based on the classification of Fine Beam Single (FBS) and Fine Beam Dual (FBD) polarization (path) image pairs. To cover Borneo the equivalent of 554 standard images is required. Qualitative and quantitative validation results and findings are reported. The final overall accuracy assessment result shows the demonstration map product is in 85.5% full agreement with the independent reference dataset and in 7.8% 'partial agreement'. The accuracy achieved is widely considered adequate, a very promising result for a sub-continental high resolution map based on just single-year radar data. Approaches for further improvement of the accuracy of less accurately classified thematic classes such as grassland, cropland and shrubland are suggested. This work has been undertaken in part within the framework of the ALOS Kyoto & Carbon Initiative. [J307]

## "The Kyoto & Carbon Initiative-A Brief Summary"

The Kyoto & Carbon (K&C) Initiative is an international collaboration led by the Japan Aerospace Exploration Agency (JAXA) that revolves primarily around the Advanced Land Observing Satellite (ALOS) Phased Arrayed L-band SAR (PALSAR). The Initiative builds on the experience gained from the Global Rain Forest Mapping (GRFM) and Global Boreal Forest Mapping (GBFM) projects [1], [2], in which SAR data from the Japanese Earth

Resources Satellite (JERS-1) were used to generate consistent image mosaics over the entire tropical and boreal zones of Earth. While the GRFM and GBFM projects were undertaken already in the mid 1990s, they demonstrated the utility of L-band SAR data for mapping and monitoring forest and wetland areas and the importance of providing spatially and temporally consistent satellite acquisitions for regional-scale monitoring and surveillance. [J308]

## "First experimental demonstration of a photonic band gap channel-drop filter at 240 GHz"

We have designed, fabricated, and tested a novel photonic band gap (PBG) channel-drop filter (CDF) operating at around 240 GHz. A PBG CDF is a device that allows the channeling of selected frequencies from continuous spectra into separate waveguides through select defects in a PBG structure. It is compact and configurable, and thus, it can be employed for millimeter-wave spectrometry with applications in communications, radio astronomy, and radar receivers for remote sensing and nonproliferation. In this paper we present the design, modeling, and fabrication methods used to produce a silicon-based PBG CDF, and demonstrate its ability to filter the frequency of 240 GHz with a linewidth of approximately 1 GHz and transmission of 25 dB above background. [J309]

## "Ortho-Rectification and Slope Correction of SAR Data Using DEM and Its Accuracy Evaluation"

This paper proposes an accurate ortho-rectification and slope correction method for Synthetic Aperture Radar (SAR) images using a digital elevation model (DEM). Since SAR observation is performed in the squint condition, the image is distorted both geometrically and radiometrically (e.g., through foreshortening, range and azimuth shift, layover, radiometric modulation associated with slope, and shadowing). Furthermore, the pixel height cannot be retrieved directly even when orbital data are accurate. The proposed method calculates the geometric and radiometric distortion components from a comparative process between the DEM-based Simulated SAR Image (DSSI) and the SAR slant range image. When applied to Advanced Land Observing Satellite (ALOS) Phased Array Type L-band SAR (PALSAR) data, the geometric accuracy of the ortho-rectified SAR image at the off-nadir angle of 34.3° was high, with a Root Mean Square Error (RMSE) of 11.9 m when evaluated against Ground Control Points (GCPs) deployed globally. The slope correction effectively reduced the radiometric variation caused by the terrain height variation. The proposed method can be applied to a range of SAR data to support a diversity of applications. [J310]

## "Coherent Detection of Swerling 0 Targets in Sea-Ice Weibull-Distributed Clutter Using Neural Networks"

The detection of Swerling 0 targets in movement in sea-ice Weibull-distributed clutter by neural networks (NNs) is presented in this paper. Synthetic data generated for typical sea-ice Weibull parameters reported in the literature are used. Due to the capability of NNs for learning the statistical properties of the clutter and target signals during a supervised training, high clutter reduction rates are achieved, reverting on high detection performances. The proposed NN-based detector is compared with a reference detector proposed in the literature that approximates the Neyman-Pearson (NP) detector. The results presented in the paper allow empirically demonstrating how the NN-based detector outperforms the detector taken as reference in all the cases under study. It is achieved not only in performance but also in robustness with respect to changes in sea-ice Weibull-distributed clutter conditions. Moreover, the computational cost of the NN-based detector is very low, involving high signal processing speed. [J311]

## "Backscattering and Statistical Information Fusion for Urban Area Mapping Using TerraSAR-X Data"

With the launch of the German TerraSAR-X system, a new generation of high-resolution spaceborne SAR data is available. This opens new perspectives and challenges for the automatic interpretation of urban environments. In fact, a rich information content, previously hidden or not clearly distinguishable in low resolution images such as urban structures (small buildings, vehicles, etc), is now disclosed. However, only proper approaches are able to retrieve automatically this new detailed information. This paper provides solutions for the semi-automatic interpretation and mapping of urban areas using the high resolution provided by TerraSAR-X data. Our solutions take into the increase, with the high resolution, of the visibility of some man-made structures whose scattering response has improved with the high frequency X-band SAR sensor carried by the TerraSAR-X system. They are mainly based on two steps. Firstly, we extract and describe two kinds of information: backscattering and statistical. Secondly, we propose to use information fusion techniques where intelligence has been introduced and enhanced in the way the different information is processed or treated, so that accurate mapping of urban areas could be reached. This mapping is performed through semantic categorization and retrieval of the different scene contents. Promising improvements and real progress toward automatic urban area mapping have been achieved using TerraSAR-X data. [J312]

## "Random Walk Approach for Wave Propagation through Atmospheric Layers for DInSAR Applications"

The accuracy and reliability of the measured differential path in satellite synthetic aperture radar (SAR) interferometry are strongly affected by the uncertainty in the estimation of the atmospheric contribution. Changes in the physical parameters of the medium, due to turbulence layers or gas concentrations, induce slight variations in the curvature of the propagation path that finally generate an overall disturbance term that is usually comparable, or even larger, than the displacement to be observed. A stochastic model for the three dimensional path field is derived by considering a plane wave propagating in a random layered medium. In the vertical direction a piecewise-linear walk, made by straight ray subpaths, is assumed, wherein the length of each path (thickness of the layer) and the number of paths are modelled as random variables. Along the horizontal plane mutual interactions among cells are defined through an interaction equation that closely resembles typical competitions in biological evolution models. The resulting parametric model is fitted with observations from the residual atmosphere, as measured after topographic removal in SAR images, and results are shown. [J313]

## "Eco-Hydrological Characterization of Inland Wetlands in Africa Using L-Band SAR"

Maps describing the eco-hydrology of inland wetland systems in Africa are needed to identify and implement appropriate adaptive management plans related to land use and land cover. Many African countries lack regional baseline information on the temporal extent, distribution and characteristics of wetlands. This information is provided here in the form of maps which characterize two wetland sites of international importance in Malawi and Mozambique. Multi-temporal L-band Synthetic Aperture Radar (SAR) datasets are combined with Landsat Thematic Mapper and ASTER images, digital elevation models, and vegetation species data to provide information on wetland ecology and hydrology. These data were used as input to a hybrid, Decision Tree classifier and a Principal Components Analysis classification approach to produce maps depicting the spatial distribution of vegetation species and characterizing the wetland dynamics. The maps exhibit classification accuracies of 89% and 84% for the two sites respectively. The L-band SAR datasets have proved to be an essential information source in the production of these maps due to (i) frequent cloud cover/smoke which reduces the temporal coverage of optical data, and (ii) a systematic observation strategy and frequent image acquisition which enables characterization of the flood dynamics at a high temporal resolution. [J314]

## "Corrections to "An Array Error Estimation Method for Constellation SAR Systems" [JOct 10 731-735]"

In the above titled paper (ibid., vol. 7, no. 4, pp. 731-735, Oct. 10), there are errors in Section IV which are corrected here. [J315]

## "The First-Order High Frequency Radar Ocean Surface Cross Section for an Antenna on a Floating Platform"

The first-order high frequency surface wave radar (HFSWR) cross section of the ocean surface is derived for the case of the transmitting and receiving antenna being mounted on a floating, but otherwise fixed, ocean platform. It is assumed that the sway component of the platform or barge motion is responsible for observed differences in the cross section compared to that for the fixed antenna case. Based on earlier work, a general expression for the bistatically received first-order electric field, which consists of a two-dimensional spatial convolution, is presented and reduced to integral form. Then, it is assumed that the surface can be described by a Fourier series whose coefficients are zero-mean Gaussian random variables, and from there the analysis proceeds for the backscatter case. The integrals are taken to the time domain, with the source field being that of a barge-mounted omnidirectional vertically polarized pulsed dipole antenna. Subsequently, the first-order monostatic radar cross section is developed and found to consist of Bessel functions. Simulation results for the new cross section are also provided to show the effects of barge motion under different sea states and operating frequencies. It is seen that the results have important implications in the application of HFSWR technology to ocean remote sensing. [J316]

## "An End-to-End Error Model for Classification Methods Based on Temporal Change or Polarization Ratio of SAR Intensities"

This paper aims at defining the expression of the probability of error of classification methods using a synthetic aperture radar (SAR) intensity ratio as a classification feature. The two SAR intensities involved in this ratio can be measurements from different dates, polarizations, or, also possibly, frequency bands. Previous works provided a baseline expression of the probability of error addressing the two-class problem with equal a prioriclass probabilities and no calibration error. This study brings up a novel expression of the error, providing the

possibility to assess the effect of class probabilities and calibration errors. An extended expression is described for the n-class problem. The effect of calibration errors such as channel gain imbalance, radiometric stability, and crosstalk is assessed in the general case. The results indicate that, for the applications under study, channel gain imbalance is usually not a decisive parameter, but radiometric stability is more critical in methods based on the temporal change. Crosstalk has a negligible effect in the case of copolarizations. The impacts of other system parameters, such as ambiguity ratio, time-lapse between repeat-pass orbits, spatial resolution, and number of looks, are illustrated through a set of assumptions on the backscattering values of the considered classes. The model is validated by comparing some of its outputs to experimental results calculated from the application of rice fields mapping methods on real data. This error model constitutes a tool for the design of future SAR missions and for the development of robust classification methods using existing SAR instruments. [J317]

## "Passive Coherent Location as Cognitive Radar"

Cognitive Radar describes a generic radar system that is capable of adapting its transmission waveforms and cooperation with other sensors in order to achieve superior detection, recognition, and tracking of targets. For example, the sensors of a cognitive radar system might use the illumination signals to carry broadcast data, allowing the sharing of target information. Herein, we postulate that it would be possible to implement a cognitive version of Passive Coherent Location (PCL) which has much in common with the broad cognitive radar concept, but adapts only to the waveforms it senses in the environment, and exploits those that are most useful to it for target detection. In addition, it would model the terrain to improve coverage and provide countermeasures against direct signal saturation. By its name, PCL does not transmit, but relies on emissions from other radiating systems, such as broadcast services, other radars, cellular radio, WiFi, and so on. It is clear that such a system, consisting of multiple, cooperating receivers, can achieve excellent performance in the presence of deliberate jamming, difficult terrain, and attempts at target stealth. In the civilian radar domain, the technology offers opportunities for bandwidth conservation. [J318]

## "Time-Reversal Ground-Penetrating Radar: Range Estimation With Cramйr-Rao Lower Bounds"

In this paper, first, a new range-estimation technique using time reversal (TR) for ground-penetrating-radar (GPR) applications is presented. The estimator is referred to as the TR/GPR range estimator. The motivation for this paper comes from the need of accurately estimating the location of underground objects such as landmines or unexploded ordinance for safe clearance. Second, the Cramer-Rao lower bound (CRLB) for the performance of the TR/GPR range estimator is derived and compared with the CRLB for the conventional matched filter (MF). The CRLB analysis shows that the TR/GPR range estimator has the potential to achieve higher accuracy in estimating the location of the target than that of the conventional MF estimator. Third, the proposed TR/GPR estimator is tested using finite-difference time-domain simulations, where the surface-based reflection GPR is modeled using an electromagnetic transverse-magnetic (TM) mode formulation. In our simulations, the TR/GPR estimator outperforms the conventional MF approach by up to 5-dB reduction in mean square error at signal-to-noise ratios ranging from -20 to 20 dB for dry-soil environments. [J319]

## "Model-Based Weather Radar Remote Sensing of Explosive Volcanic Ash Eruption"

Microphysical and dynamical features of volcanic ash clouds can be quantitatively monitored by using ground-based microwave weather radars. These systems can provide data for determining the ash volume, total mass, and height of eruption clouds. In order to demonstrate the unique potential of this microwave active remote-sensing technique, the case study of the eruption of Augustine Volcano in Alaska in January 2006 is described and analyzed. Volume scan data, acquired by a NEXRAD WSR-88D S-band ground-based weather radar, are processed to automatically classify and estimate eruptive cloud particle concentration. The numerical results of the coupled model Z-reflectivity from Active Tracer High resolution Atmospheric Model (ATHAM), including particle aggregation processes and simulation of radar reflectivity from the ATHAM microphysical model, are exploited to train the inversion algorithm. The volcanic ash radar retrieval based on the ATHAM algorithm is a physical-statistical approach based on the backscattering microphysical model of volcanic cloud particles (hydrometeors, ash, and aggregates), used within a Bayesian classification and optimal regression algorithm. A sensitivity analysis is carried out to evaluate the overall error budget. The evolution of the Augustine eruption is discussed in terms of radar measurements and products, pointing out the unique features, the current limitations, and future improvements of radar remote sensing of volcanic plumes. [J320]

## "Radiometric, Geometric, and Image Quality Assessment of ALOS AVNIR-2 and PRISM Sensors"

The Advanced Land Observing Satellite (ALOS) was launched on January 24, 2006, by a Japan Aerospace Exploration Agency (JAXA) H-IIA launcher. It carries three remote-sensing sensors: 1) the Advanced Visible and

Near-Infrared Radiometer type 2 (AVNIR-2); 2) the Panchromatic Remote-Sensing Instrument for Stereo Mapping (PRISM); and 3) the Phased-Array type L-band Synthetic Aperture Radar (PALSAR). Within the framework of ALOS Data European Node, as part of the European Space Agency (ESA), the European Space Research Institute worked alongside JAXA to provide contributions to the ALOS commissioning phase plan. This paper summarizes the strategy that was adopted by ESA to define and implement a data verification plan for missions operated by external agencies; these missions are classified by the ESA as third-party missions. The ESA was supported in the design and execution of this plan by GAEL Consultant. The verification of ALOS optical data from PRISM and AVNIR-2 sensors was initiated 4 months after satellite launch, and a team of principal investigators assembled to provide technical expertise. This paper includes a description of the verification plan and summarizes the methodologies that were used for radiometric, geometric, and image quality assessment. The successful completion of the commissioning phase has led to the sensors being declared fit for operations. The consolidated measurements indicate that the radiometric calibration of the AVNIR-2 sensor is stable and agrees with the Landsat-7 Enhanced Thematic Mapper Plus and the Envisat MEdium-Resolution Imaging Spectrometer calibration. The geometrical accuracy of PRISM and AVNIR-2 products improved significantly and remains under control. The PRISM modulation transfer function is monitored for improved characterization. [J321]

## "Resolution Enhancement for Inversed Synthetic Aperture Radar Imaging Under Low SNR via Improved Compressive Sensing"

The theory of compressed sampling (CS) indicates that exact recovery of an unknown sparse signal can be achieved from very limited samples. For inversed synthetic aperture radar (ISAR), the image of a target is usually constructed by strong scattering centers whose number is much smaller than that of pixels of an image plane. This sparsity of the ISAR signal intrinsically paves a way to apply CS to the reconstruction of high-resolution ISAR imagery. CS-based high-resolution ISAR imaging with limited pulses is developed, and it performs well in the case of high signal-to-noise ratios. However, strong noise and clutter are usually inevitable in radar imaging, which challenges current high-resolution imaging approaches based on parametric modeling, including the CS-based approach. In this paper, we present an improved version of CS-based high-resolution imaging to overcome strong noise and clutter by combining coherent projectors and weighting with the CS optimization for ISAR image generation. Real data are used to test the robustness of the improved CS imaging compared with other current techniques. Experimental results show that the approach is capable of precise estimation of scattering centers and effective suppression of noise. [J322]

## "Estimating Surface Water Speeds With a Single-Phase Center SAR Versus an Along-Track Interferometric SAR"

Synthetic aperture radar (SAR) single-aperture systems are designed to image fixed scenes. Dual-antenna along-track interferometric (ATI) SAR systems are designed to detect moving targets and estimate their motion parameters. Although SAR systems are not designed to characterize moving targets, for localized targets, such as vehicles or ships, this problem has been addressed in the literature with some success. Distributed moving targets are hard to characterize, even for ATI systems. Estimating surface water speeds is an ideal example of this since the water returns are generated from weak returns randomly distributed in both time and space. The question asked here is can one measure surface water speeds with a single-phase center SAR system? The answer presented is a qualified yes, with the aid of an upper bound on the water speed, but not with the same accuracy as an ATI system. This upper bound and the collection geometry provide design criteria for the filtering of the phase information. Time-frequency (TF) methods provide another speed estimate as well as a rough profile of the speed across the water channel. A robust nonparametric TF method was developed and applied to estimate the speed. Comparisons between the ATI estimate and single-phase estimates are made using data from an X-band ATI-SAR system. [J323]

## "Improved Estimators of Faraday Rotation in Spaceborne Polarimetric SAR Data"

Spaceborne polarimetric synthetic aperture radar systems operating at lower frequencies, such as P-band, are significantly affected by Faraday rotation (FR). A new set of FR estimators is derived from the off-diagonal terms in the measured covariance matrix of a distributed target. These estimators have a phase ambiguity of period, instead of /2 as for the published estimators, and this ambiguity can be completely resolved for arbitrarily large values of FR using total electron content maps derived from Global Navigation Satellite System measurements. Simulations show that one of the new estimators has particularly high resistance to system noise and channel amplitude imbalance but greater sensitivity to channel phase imbalance than the published estimators. Hence, the expected values of residual system distortion after calibration may affect the choice of estimator. [J324]

## "L-band array for ground-based remote sensing of volcanic eruptions"

In this study, an L-band array for ground-based remote sensing of volcanic eruptions will be presented. The proposed array configuration was created using a particular class of microstrip elements, namely shorted rectangular patch (SRP) antennas, with improved directivity arranged in a 6Ч6 array with high inter-element spacing. This solution allowed high directivity, while grating lobe effects were mitigated by the element factor. The array was developed for use with volcano Doppler radar (Voldorad), a volcanological Doppler radar used to remotely sense summit eruptions of Mt. Etna in Sicily, where the prototype Voldorad is now located. The main features of the SRP and the design principles of the array will be presented, along with simulated and measured results. [J325]

## "Scattering From Nonlinear Gravity Waves: The "Choppy Wave" Model"

To progress in the understanding of the impact of nonlinear wave profiles in scattering from sea surfaces, a nonlinear model for infinite-depth gravity waves is considered. This model, termed as the "Choppy Wave" Model (CWM), is based on horizontal deformation of a linear reference random surface. It is numerically efficient and enjoys explicit second-order statistics for height and slope, which makes it well adapted to a large family of scattering models. We incorporate the CWM into a Kirchhoff or small-slope approximation and derive statistical expressions for the corresponding incoherent cross section. We insist on the importance of "undressing" the wavenumber spectrum to generate a nonlinear surface with a prescribed spectrum. Interestingly, the inclusion of nonlinearities is found to be practically compensated by the spectral undressing process; an effect which might be specific to the CWM and needs to be investigated in the framework of fully nonlinear models. Accordingly, the difference between the respective normalized radar cross section is rather small. The most noticeable changes are faster azimuthal variations and a slight increase of the radar returns at nadir. A statistical analysis of sea clutter in the framework of a two-scale model is also performed at large but nongrazing incidence. It shows a pronounced polarization dependence of the distribution of large backscattered amplitudes, the tail being much larger in horizontal polarization and for small resolution cell. Surface nonlinearities are shown to increase the tail of the amplitude distribution, as expected. Less obviously, their relative impact is found lesser in horizontal polarization. This raises the question of the actual contribution of nonlinearities in radar sea spikes at nongrazing angles. [J326]

## "A Novel Strategy for Radar Imaging Based on Compressive Sensing"

Radar data have already proven to be compressible with no significant losses for most of the applications in which it is used. In the framework of information theory, the compressibility of a signal implies that it can be decomposed onto a reduced set of basic elements. Since the same quantity of information is carried by the original signal and its decomposition, it can be deduced that a certain degree of redundancy exists in the explicit representation. According to the theory of compressive sensing (CS), due to this redundancy, it is possible to infer an accurate representation of an unknown compressible signal through a highly incomplete set of measurements. Based on this assumption, this paper proposes a novel method for the focusing of raw data in the framework of radar imaging. The technique presented is introduced as an alternative option to the traditional matched filtering, and it suggests that the new modes of acquisition of data are more efficient in orbital configurations. In this paper, this method is first tested on 1-D simulated signals, and results are discussed. An experiment with synthetic aperture radar (SAR) raw data is also described. Its purpose is to show the potential of CS applied to SAR systems. In particular, we show that an image can be reconstructed, without the loss of resolution, after dropping a large percentage of the received pulses, which would allow the implementation of wide-swath modes without reducing the azimuth resolution. [J327]

## "Geodetically Accurate InSAR Data Processor"

We present a new interferometric synthetic aperture radar (InSAR) processing approach that capitalizes on the precise orbit tracking that is available with modern radar satellites. Our method uses an accurate orbit information along with motion-compensation techniques to propagate the radar echoes to positions along a noninertial virtual orbit frame in which the location and focusing equations are particularly simple, so that images are focused without requiring autofocus techniques and are computed efficiently. Motion compensation requires two additional focus correction phase terms that are implemented in the frequency domain. If the images from an interferometric pair or stack are all computed along the same reference orbit, flat-Earth topographic correction is not needed, and image coregistration is simplified, obviating many difficulties that are often encountered in InSAR processing. We process several data sets collected by the ALOS PALSAR instrument and find that the geodetic accuracy of the radar images is 10-20 m, with up to 20 m of additional image distortion needed to align 100 km Ч 100 km scenes with reference digital elevation models. We validated the accuracy by using both known radar corner reflector locations and by the registration of the interferograms with digital maps. The topography-corrected interferograms are free from all geometric phase terms, and they clearly show the

geophysical observables of crustal deformation, atmospheric phase, and ionospheric phase. [J328]

## "Feature Selection in AVHRR Ocean Satellite Images by Means of Filter Methods"

Automatic retrieval and interpretation of satellite images is critical for managing the enormous volume of environmental remote sensing data available today. It is particularly useful in oceanography and climate studies for examination of the spatio-temporal evolution of mesoscalar ocean structures appearing in the satellite images taken by visible, infrared, and radar sensors. This is because they change so quickly and several images of the same place can be acquired at different times within the same day. This paper describes the use of filter measures and the Bayesian networks to reduce the number of irrelevant features necessary for ocean structure recognition in satellite images, thereby improving the overall interpretation system performance and reducing the computational time. We present our results for the National Oceanographic and Atmospheric Administration satellite Advanced Very High Resolution Radiometer (AVHRR) images. We have automatically detected and located mesoscale ocean phenomena of interest in our study area (North-East Atlantic and the Mediterranean), such as upwellings, eddies, and island wakes, using an automatic selection methodology which reduces the features used for description by about 80%. Finally, Bayesian network classifiers are used to assess classification quality. Knowledge about these structures is represented with numeric and nonnumeric features. [J329]

## "Role of Land-Water Classification and Manning's Roughness Parameter in Space-Borne Estimation of Discharge for Braided Rivers: A Case Study of the Brahmaputra River in Bangladesh"

The proposed Surface Water and Ocean Topography (SWOT) mission will provide global, space-based estimates of water elevation, its temporal change, and its spatial slope for terrestrial water bodies. Using derivations of water slope from the Shuttle Radar Topography Mission (SRTM) elevation data, river bathymetry and Manning's equation, the potential of SWOT for discharge estimation of large braided rivers in humid climates, such as the Brahmaputra river, was found to be promising (Jung, in Earth Surface Processes and Landforms, 2010). In this study we extend the work on assessing SWOT for braided rivers to understand the sensitivity of two river hydraulic parameters to discharge estimation: 1) section factor (AR2/3) derived from land-water classification and in situ river bathymetry and 2) Manning's roughness coefficient. For braided rivers, the first parameter, is intimately dependent on how braided rivers are classified of the multiple channels (water) and in-stream braided bars (land) that consequently dictates the accuracy of wetted perimeter and area of flow estimation from water elevation data. We show that the use of the minimum water elevation data at a river cross section minimizes estimation of section factor which consequently minimizes outlier discharge estimation reported in the Jung study. We also show that by treating roughness coefficient "flexible" as a calibration parameter, discharge estimation from SRTM elevation data can be further improved through trial and error manual optimization. Our sensitivity study illustrates the value of treating section factor and roughness coefficient as calibration parameters for data assimilation systems that use SWOT observables to estimate river discharge in braided rivers. [J330]

## "Sensitivity of X-, C-, and L-Band SAR Backscatter to Burn Severity in Mediterranean Pine Forests"

Synthetic aperture radar (SAR) data at X-, C-, and L-bands have been investigated to determine the relationship between backscatter and forest burn severity over three sites in Spain. The dependence of SAR backscatter on local incidence angle and environmental conditions has been analyzed. At HH and VV polarizations, the backscatter increased with burn severity for X- and C-bands, whereas it decreased for L-band. Cross-polarized (HV) backscatter decreased with burn severity for all frequencies. Determination coefficients were used to quantify the relationship between radar backscatter and burn severity for given intervals of local incidence angle. For X- and C-band copolarized data, higher determination coefficients were observed for slopes oriented toward the sensors, whereas for cross-polarized data, the determination coefficients were higher for slopes oriented away from the sensor. At L-band, the association strength of cross-polarized data to burn severity was high for all local incidence angles. C- and L-band cross-polarized backscatter showed better potential for burn severity estimation in the Mediterranean environment when the local incidence angle is accounted for. The small dynamic range observed for X-band data could hinder its use in forests affected by fires. [J331]

## "Impact of Radarsat-2 SAR Ultrafine-Mode Parameters on Stereo-Radargrammetric DEMs"

The new high-resolution mode of Radarsat-2 was evaluated for digital elevation model (DEM) generation using stereo-radargrammetry with Toutin's 3-D physical model as part of the Canadian Space Agency's programs. In addition, the impact of radar parameters on stereo-extracted DEMs was evaluated. Three stereo pairs using

different radar parameters (resolutions; HH and VV polarizations; slant and ground range; image spacing) from ultrafine-mode Radarsat-2 data acquired over a test site north of Quebec City, Canada, were formed to generate DEMs, which were thus compared to 15-cm-accurate lidar elevation data. Results showed a good accuracy for the three stereo-extracted DEMs: less than 0.8 m for the horizontal positioning and around 3 m (1) for the elevation on bare soils, with small 3-D biases (2-3 m). The HH stereo pair in slant-range format slightly but consistently achieved the best results. [J332]

## "Very High Resolution Spaceborne SAR Tomography in Urban Environment"

Synthetic aperture radar tomography (TomoSAR) extends the synthetic aperture principle into the elevation direction for 3-D imaging. It uses stacks of several acquisitions from slightly different viewing angles (the elevation aperture) to reconstruct the reflectivity function along the elevation direction by means of spectral analysis for every azimuth-range pixel. The new class of meter-resolution spaceborne SAR systems (TerraSAR-X and COSMO-Skymed) offers a tremendous improvement in tomographic reconstruction of urban areas and man-made infrastructure. The high resolution fits well to the inherent scale of buildings (floor height, distance of windows, etc.). This paper demonstrates the tomographic potential of these SARs and the achievable quality on the basis of TerraSAR-X spotlight data of urban environment. A new Wiener-type regularization to the singular-value decomposition method-equivalent to a maximum a posteriori estimator-for TomoSAR is introduced and is extended to the differential case (4-D, i.e., space-time). Different model selection schemes for the estimation of the number of scatterers in a resolution cell are compared and proven to be applicable in practice. Two parametric estimation algorithms of the scatterers' elevation and their velocities are evaluated. First 3-D and 4-D reconstructions of an entire building complex (including its radar reflectivity) with very high level of detail from spaceborne SAR data by pixelwise TomoSAR are presented. [J333]

## "Large-Area Classification and Mapping of Forest and Land Cover in the Brazilian Amazon: A Comparative Analysis of ALOS/PALSAR and Landsat Data Sources"

Information on the distribution of tropical forests is critical to decision-making on a host of globally significant issues ranging from climate stabilization and biodiversity conservation to poverty reduction and human health. The majority of tropical nations need high-resolution, satellite-based maps of their forests as the international community now works to craft an incentive-based mechanism to compensate tropical nations for maintaining their forests intact. The effectiveness of such a mechanism will depend in large part on the capacity of current and near-future Earth observation satellites to provide information that meets the requirements of international monitoring protocols now being discussed. Here we assess the ability of a state-of-the-art satellite radar sensor, the ALOS/PALSAR, to support large-area land cover classification as well as high-resolution baseline mapping of tropical forest cover. Through a comprehensive comparative analysis involving twenty separate PALSAR- and Landsat-based classifications, we confirm the potential of PALSAR as an accurate (>90%) source for spatially explicit estimates of forest cover based on data and analyses from a large and diverse region encompassing the Xingu River headwaters in southeastern Amazonia. Pair-wise spatial comparisons among maps derived from PALSAR, Landsat, and PRODES, the Brazilian Amazon deforestation monitoring program, revealed a high degree of spatial similarity. Given that a long-term data record consisting of current and future spaceborne radar sensors is now expected, our results point to the important role that spaceborne imaging radar can play in complementing optical remote sensing to enable the design of robust forest monitoring systems. [J334]

## "Validation of the ASAR Global Monitoring Mode Soil Moisture Product Using the NAFE'05 Data Set"

The Advanced Synthetic Aperture Radar (ASAR) Global Monitoring (GM) mode offers an opportunity for global soil moisture (SM) monitoring at much finer spatial resolution than that provided by the currently operational Advanced Microwave Scanning Radiometer for the Earth Observing System and future planned missions such as Soil Moisture and Ocean Salinity and Soil Moisture Active Passive. Considering the difficulties in modeling the complex soil-vegetation scattering mechanisms and the great need of ancillary data for microwave backscatter SM inversion, algorithms based on temporal change are currently the best method to examine SM variability. This paper evaluates the spatial sensitivity of the ASAR GM surface SM product derived using the temporal change detection methodology developed by the Vienna University of Technology. This evaluation is made for an area in southeastern Australia using data from the National Airborne Field Experiment 2005. The spatial evaluation is made using three different types of SM data (station, field, and airborne) across several different scales (1-25 km). Results confirmed the expected better agreement when using point (Rstation= 0.75) data as compared to spatial (RPLMR, 1 km= 0.4) data. While the aircraft-ASAR GM correlation values at 1-km resolution were low, they significantly improved when averaged to 5 km (RPLMR, 5 km= 0.67) or coarser. Consequently, this assessment shows the ASAR GM potential for monitoring SM when averaged to a spatial resolution of at least 5 km. [J335]

## "Measurement of Ionospheric TEC in Spaceborne SAR Data"

The propagation of spaceborne radar signals operating at L-band frequency or below can be seriously affected by the ionosphere. At high states of solar activity, Faraday rotation (FR) and signal path delays disturb radar polarimetry and reduce resolution in range and azimuth. While these effects are negligible at X-band, FR and the frequency-dependent path delays can become seriously problematic starting at L-band. For quality assurance and calibration purposes, existing L-band or potential spaceborne P-band missions require the estimation of the ionospheric state before or during the data take. This paper introduces two approaches for measuring the ionospheric total electron content (TEC) from single-polarized spaceborne SAR data. The two methods are demonstrated using simulations. Both methods leverage knowledge of the frequency-dependent path delay through the ionosphere: The first estimates TEC from the phase error of the filter mismatch, while the second gauges path-delay differences between up and down chirps. FR, mean (direct current) offsets, and noise contributions are also considered in the simulations. Finally, possibilities for further methodological improvements are discussed. [J336]

## "Interferometric Synthetic Aperture Radar (SAR) Missions Employing Formation Flying"

This paper presents an overview of single-pass interferometric Synthetic Aperture Radar (SAR) missions employing two or more satellites flying in a close formation. The simultaneous reception of the scattered radar echoes from different viewing directions by multiple spatially distributed antennas enables the acquisition of unique Earth observation products for environmental and climate monitoring. After a short introduction to the basic principles and applications of SAR interferometry, designs for the twin satellite missions TanDEM-X and Tandem-L are presented. The primary objective of TanDEM-X (TerraSAR-X add-on for Digital Elevation Measurement) is the generation of a global Digital Elevation Model (DEM) with unprecedented accuracy as the basis for a wide range of scientific research as well as for commercial DEM production. This goal is achieved by enhancing the TerraSAR-X mission with a second TerraSAR-X like satellite that will be launched in spring 2010. Both satellites act then as a large single-pass SAR interferometer with the opportunity for flexible baseline selection. Building upon the experience gathered with the TanDEM-X mission design, the fully polarimetric L-band twin satellite formation Tandem-L is proposed. Important objectives of this highly capable interferometric SAR mission are the global acquisition of three-dimensional forest structure and biomass inventories, large-scale measurements of millimetric displacements due to tectonic shifts, and systematic observations of glacier movements. The sophisticated mission concept and the high data-acquisition capacity of Tandem-L will moreover provide a unique data source to systematically observe, analyze, and quantify the dynamics of a wide range of additional processes in the bio-, litho-, hydro-, and cryosphere. By this, Tandem-L will be an essential step to advance our understanding of the Earth system and its intricate dynamics. Enabling technologies and techniques are described in detail. An ou--tlook on future interferometric and tomographic concepts and developments, including multistatic SAR systems with multiple receivers, is provided. [J337]

## "Three-Component Model-Based Decomposition for Polarimetric SAR Data"

An improved three-component decomposition for polarimetric synthetic aperture radar (SAR) data is proposed in this paper. The reasons for the emergence of negative powers in the Freeman decomposition have been analyzed, and three corresponding improvements are included in the proposed method. First, the deorientation process is applied to the coherency matrix before it is decomposed into three scattering components. Then, the coherency matrix with the maximal polarimetric entropy, i.e., the unit matrix, is used as the new volume-scattering model instead of the original one adopted in the Freeman decomposition. A power constraint is also added to the proposed three-component decomposition. The E-SAR polarimetric data acquired over the Oberpfaffenhofen area in Germany are applied in the experiment. The results show that the pixels with negative powers are totally eliminated by the proposed decomposition, demonstrating the effectiveness of the new model. [J338]

## "An Efficient and Flexible Statistical Model Based on Generalized Gamma Distribution for Amplitude SAR Images"

In the context of synthetic aperture radar (SAR) image processing and applications, the precise modeling of statistical knowledge is a crucial problem. In this paper, an efficient and flexible statistical model, called generalized Gamma Rayleigh (G??R) distribution, for amplitude SAR images is proposed by assuming a two-sided generalized Gamma distribution for the real and imaginary parts of the complex SAR backscattered signal. It is shown that the Rayleigh and recently proposed generalized Gaussian Rayleigh distributions can be regarded as special cases of G??R distribution. Considering that the probability density function estimation problem is formulated as a parameter estimation one for the parametric statistical analysis of SAR images, a two-stage estimator based on second-kind cumulants is derived for the parameters of G??R distribution. Furthermore,

experimental results on several actual SAR images are given to demonstrate the validity and flexibility of the proposed model. [J339]

## "RF Tomography for Below-Ground Imaging of Extended Areas and Close-in Sensing"

Three extensions to radio-frequency (RF) tomography for imaging of voids under wide areas of regard are presented. These extensions are motivated by three challenges. One challenge is the lateral wave, which propagates in proximity of the air-earth interface and represents the predominant radiation mechanism for wide-area surveillance, sensing of denied terrain, or close-in sensing. A second challenge is the direct-path coupling between transmitters (Txs) and receivers (Rxs), that affects the measurements. A third challenge is the generation of clutter by the unknown distribution of anomalies embedded in the ground. These challenges are addressed and solved using the following strategies: 1) A forward model for RF tomography that accounts for lateral waves expressed in closed form (for fast computation); 2) a strategy that reduces the direct-path coupling between any Tx-Rx pair; and 3) an improved inversion scheme that is robust with respect to noise, clutter, and high attenuation. A finite-difference time domain simulation of a scenario representing close-in sensing of a denied area is performed, and reconstructed images obtained using the improved and the classical models of RF tomography are compared. [J340]

## "Modified Kirchhoff Migration for UWB MIMO Array-Based Radar Imaging"

In this paper, the formulation of Kirchhoff migration is modified for multiple-input-multiple-output (MIMO) array-based radar imaging in both free-space and subsurface scenarios. By applying the Kirchhoff integral to the multistatic data acquisition, the integral expression for the MIMO imaging is explicitly derived. Inclusion of the Snell's law and the Fresnel's equations into the integral formulation further expends the migration technique to subsurface imaging. A modification of the technique for strongly offset targets is proposed as well. The developed migration techniques are able to perform imaging with arbitrary MIMO configurations, which allow further exploration of the benefits of various array topologies. The proposed algorithms are compared with conventional diffraction stack migration on free-space synthetic data and experimentally validated by ground-penetrating radar experiments in subsurface scenarios. The results show that the modified Kirchhoff migration is superior over the conventional diffraction stack migration in the aspects of resolution, side-lobe level, clutter rejection ratio, and the ability to reconstruct shapes of distributed targets. [J341]

## "Ship Detection Using TerraSAR-X Images in the Campos Basin (Brazil)"

The very large extent of the Brazilian coast (~8000 km) and the growing maritime vessel traffic demand that research be made on ancillary methods to monitor and control ship's traffic in national waters. An important tool for this purpose is the use of orbital synthetic aperture radar (SAR) imagery, particularly due to its ability to work day and night and to suffer almost no interference of cloud coverage. In this letter, we investigate some ship detection concepts, as applied to TerraSAR-X (TSX) ScanSAR images (16-m resolution), in VV and HH polarization. Ocean clutter statistical parameters are estimated, and the Kolmogorov-Smirnov test is used to verify the goodness of fit for the K-distribution to TSX images. A constant false alarm rate (CFAR) target detection algorithm is developed, and its performance is verified. Incidence angle, CFAR's window size, and probability of false alarm influence are further analyzed. [J342]

## "Temperature-Dependable Microwave Dielectric Model for an Arctic Soil"

Dielectric measurements of an organic-rich permafrost soil over the range from 1.0 to 16 GHz and from -30??C to +25??C are presented. The measured shrub soil contains up to 90% organic matter and is the first soil of this composition for which the soil dielectric has been characterized. The measurements were fitted to the generalized refractive mixing dielectric model (GRMDM) recently proposed by Mironov et al., which combines the complex refractive indexes for the major components of the soil. These components were found to be the solid content, bound water, transient bound water, liquid capillary water, and moistened ice water. The dielectric properties of the frequency-dispersive components are each described by their own Debye relaxation spectrum. The GRMDM has been modified to incorporate the temperature dependence of the Debye parameters. The phase transformation of the soil water components at the freezing temperature is taken into account. As a result, a temperature-dependable GRMDM (TD GRMDM) has been developed, including model parameters which have a physical interpretation. This TD GRMDM predicts the dielectric for this soil in the whole range of moistures, frequencies, and temperatures measured. The model prediction errors are on the same order as that of dielectric measurements. The model proposed is the first of its kind to provide a physical basis for radar and radiothermal remote sensing algorithms that retrieve the freeze/thaw state and the volumetric moisture in the upper layer of an Arctic soil. [J343]

## "Dual-Tree Complex Wavelet Transform Based SAR Despeckling Using Interscale Dependence"

In this paper, a dual-tree complex wavelet transform (DTCWT) based despeckling algorithm is proposed for synthetic aperture radar (SAR) images, considering the significant dependences of the wavelet coefficients across different scales. The DTCWT has the advantage of improved directional selectivity, approximate shift invariance, and perfect reconstruction over the discrete wavelet transform. The wavelet coefficients in each subband are modeled with a bivariate Cauchy probability density function (PDF) which takes into account the statistical dependence among the wavelet coefficients. Mellin transform of two dependent random variables is utilized to estimate the dispersion parameter of the bivariate Cauchy PDF from the noisy observations. This method is faster and effective when compared to that of the earlier techniques on numerical integration. Within this framework, we propose a new method for despeckling SAR images employing a maximum a posteriori estimator. Experimental results show that the proposed method based on bivariate Cauchy prior achieves better performance in terms of equivalent number of looks, peak signal-to-noise ratio, and Pratt's figure of merit. [J344]

## "Radar Imaging From Geosynchronous Orbit: Temporal Decorrelation Aspects"

Synthetic aperture radar imaging from geosynchronous orbit has significant potential advantages over conventional low-Earth orbit radars, but it also has challenges to overcome. The baseline mission we consider is an L-band geosynchronous passive (bistatic) radar achieving a spatial resolution of about 100 m with an integration time of 8 h. The atmosphere changes its structure on timescales of minutes to hours, and this has to be compensated if useful images are to be provided. The analysis shows that ionospheric delay is the major source of temporal decorrelation; other effects, such as tropospheric delay and Earth tides, have to be dealt with but appear to be easier to handle. [J345]

## "Multichannel Azimuth Processing in ScanSAR and TOPS Mode Operation"

Due to a system-inherent limitation, conventional synthetic aperture radar (SAR) is incapable of imaging a wide swath with high geometric resolution. This restriction can be overcome by systems with multiple receive channels in combination with an additional digital signal processing network. So far, the application of such digital beamforming algorithms for high-resolution wide-swath SAR imaging has been restricted to multichannel systems in stripmap operation. However, in stripmap mode, the overall azimuth antenna length restricts the achievable swath width, thus preventing very wide swaths as requested by future SAR missions. Consequently, new concepts for ultrawide-swath imaging are needed. A promising candidate is a SAR system with multiple azimuth channels being operated in burst mode. This paper analyzes innovative ScanSAR and Terrain Observation by Progressive Scans (TOPS) system concepts with regard to multichannel azimuth processing. For this, the theoretical analyses, performance figures, and SAR signal processing, which had previously been derived for multichannel stripmap mode, are extended to systems operating in burst modes. The investigations reveal that multichannel ScanSAR systems enable the imaging of ultrawide swaths with high azimuth resolution and compact antenna lengths. These considerations are embedded in a multichannel ScanSAR system design example to demonstrate its capability to image an ultrawide swath of 400 km with a high geometric resolution of 5 m. In a next step, this system is adapted to TOPS mode operation, including an innovative "staircase" multichannel processing approach optimized for TOPS. [J346]

## "ADS-Based Guidelines for Thinned Planar Arrays"

We propose an analytical technique based on almost difference sets (ADSs) for thinning planar arrays with well controlled sidelobes. The method allows one to synthesize bidimensional arrangements with peak sidelobe levels (PSLs) predictable and deducible from the knowledge of the array aperture, the filling factor, and the autocorrelation function of the ADS at hand. The numerical validation, concerned with both small and very large apertures, points out that the expected PSL values are significantly below those of random arrays and comparable with those from different sets (DSs) although obtainable in a wider range of configurations. [J347]

## "Comparison of Radar Waveforms for a Low-Power Vertical-Incidence Ionosonde"

Vertical-incidence (VI) ionosonde is a kind of high-frequency radar. The sounding waveform is an important characteristic for measurement by ionosondes. This letter compares, both theoretically and practically, four different biphase-coded pulse compression radar waveforms which can be employed in the Wuhan Ionosphere Comprehensive Sounding System at VI sounding, including interpulse-coded m sequence, interpulse-coded Wolfman-Goutelard sequence, intrapulse-coded Barker sequence, and intrapulse-coded complementary sequence pairs. The experimental results demonstrate that among the four waveforms, the intraphase-coded complementary-sequence pairs have the best performance. [J348]

## "Two Novel Bayesian Multiscale Approaches for Speckle Suppression in SAR Images"

Speckle suppression is a prerequisite for many synthetic aperture radar (SAR) image-processing tasks. Previously, we introduced a Bayesian-based speckle-suppression method that employed the 2-D generalized autoregressive conditional heteroscedasticity (2D-GARCH) model for wavelet coefficients of log-transformed SAR images. Based on this method, we propose two new Bayesian speckle-suppression approaches in this paper. In the first approach, we introduce a new heteroscedastic model, i.e., the 2D-GARCH Mixture (2D-GARCH-M) model, as an extension of the 2D-GARCH model. This new model can capture the characteristics of wavelet coefficients. Also, the 2D-GARCH-M model introduces additional flexibility in the model formulation in comparison with the 2D-GARCH model, which results in better characterization of SAR image subbands and improved restoration in noisy environments. Then, we design a Bayesian estimator for estimating the clean-image wavelet coefficients based on 2D-GARCH-M modeling. In the second approach, the logarithm of an image is analyzed by means of the curvelet transform instead of wavelet transform. Then, we study the statistical properties of curvelet coefficients, and we demonstrate that the 2D-GARCH model can capture the characteristics of curvelet coefficients, such as heavy tailed marginal distribution, and the dependences among them. Consequently, under the 2D-GARCH model, we design a Bayesian estimator for estimating the clean-image curvelet coefficients. Finally, we compare these methods with other denoising methods applied on artificially speckled and actual SAR images, and we verify the performance improvement in utilizing the new strategies. [J349]

## "Identification of Dry and Rainy Periods Using Telecommunication Microwave Links"

Microwave links are widely used for wireless data exchange, particularly between base stations of mobile phone networks. Because of the range of frequencies used for data transmission, the link signal is attenuated when rainfall occurs along the link path. This attenuation can be related to the path-averaged rain rate. A critical issue in this procedure is the ability to separate the attenuation due to rainfall from the attenuation occurring during dry periods. This letter presents a technique to separate dry and rainy periods and to estimate a time-varying attenuation baseline using path-integrated attenuation measurements from operational telecommunication microwave links. Dry and rainy periods are separated by analyzing the local variability of the link signal. The attenuation baseline is estimated in real time through the classification into dry and rainy periods. The method is applied to four different links and ten different rain events. Measurements from a nearby C-band weather radar are used to evaluate the performance of the algorithm. The new method performs well, identifying about 92% of all rainy periods, 86% of all dry periods, and 93% of the total rain amount on average. [J350]

## "Corrections to “Signal Processing for Improved Detection of Trapped Victims Using UWB Radar” [JApr 10 2005-2014]"

In the above paper (this issue, pp. 2005-2014), there is an error in the top line of the right column, page 2010, which is corrected in this paper. [J351]

## "The Rough Surface Impulse Response of a Pulse-Limited Altimeter With an Elliptical Antenna Pattern"

This letter describes the impulse response of a pulse-limited altimeter with an elliptical antenna pattern from a uniformly rough surface inclined at an angle to a sphere or, equivalently, from spherical surface and mispointed antenna. An integral for the impulse response is given, and analytic forms for the special cases of a mispointed circular antenna and a nadir-pointed elliptical antenna are derived. An analytic approximation for the case of small ellipticity and small surface gradient (or mispointing) are also given. The letter is illustrated with numerical examples that show the general effect of ellipticity on the impulse response. It also shows that in the practical case of the elliptical CryoSat-2 satellite SIRAL antenna, the analytic approximation is sufficiently accurate to provide a correction for the ellipticity for CryoSat-2 echoes from the ocean surface. [J352]

## "Single-Pass Bistatic SAR Interferometry Using Fixed-Receiver Configurations: Theory and Experimental Validation"

In this paper, bistatic interferometry using fixed-receiver configurations is addressed both theoretically and experimentally. The analytical expressions for interferometric phase and height sensitivity are derived, and a full interferometric processing chain for digital elevation model (DEM) generation is presented. The derived expressions are general, and they can be applied to two possible acquisition geometries: backscatteringand forward scattering. The theoretical developments are complemented with experimental results done with the bistatic receiver Synthetic Aperture radar Bistatic Receiver for INterferometric Applications. The obtained DEMs are compared with a DEM from the Shuttle Radar Topography Mission and a digital terrain model from the Institut Cartografic de Catalunya. The comparison allows one to validate the results and demonstrate to which particular features of the scene that the bistatic radar is sensitive. [J353]

## "Definition of ICESat Selection Criteria for Their Use as Height References for TanDEM-X"

The TanDEM-X satellite synthetic aperture radar (SAR) mission, which is the result of the partnership between the German Aerospace Center (DLR) and Astrium GmbH, has the goal to deliver a high-precision global digital elevation model (DEM). The X-band SAR interferometry-derived DEMs contain absolute and relative height errors that have to be minimized with the help of height references in order to achieve the specified accuracies. ICESat laser altimetry data are suited for this task, due to their accuracy and global distribution. In order to gain experience in the comparison between a radar-derived DEM and ICESat GLA14 elevation data, an X-band DEM was acquired over a test region with the experimental airborne radar system of DLR in Oberpfaffenhofen. Additionally, a laser DEM of the area was used to verify the height accuracy claimed by previously published ICESat studies over different terrain types and after applying different selection threshold criteria. The analyses described in this paper are the basis for the definition of a suitable global ICESat selection strategy and include the computation of the density of selected ICESat samples over the Earth. These aspects are crucial for a successful TanDEM-X DEM generation. [J354]

## "The Importance of Soil Moisture and Soil Structure for InSAR Phase and Backscatter, as Determined by FDTD Modeling"

In this paper, we introduce a finite-difference time-domain simulator that accurately models the interaction of microwaves with realistic soils, specifically from spaceborne interferometric synthetic aperture radar (InSAR). The modeled soils are characterized by surface roughness, correlation length, bulk moisture content, vertical moisture gradient, and small air-filled-void content. Simulation results include both backscatter and interferometric phase, and we are particularly interested in assessing the potential of the latter as a proxy for soil moisture. We find that differences in homogeneous bulk moisture result in only small phase differences (< 5?). In contrast, combinations of vertical moisture gradients and small air-filled voids, which may typically exist in more realistic soils, can produce phase changes > 30? for HH and > 50? for VV when the soil moisture is varied from 3% to 30% in the uppermost 2 cm of the soil. Phase changes of this magnitude are easily detectable by spaceborne InSAR techniques. While a strong phase response to a change in mean bulk moisture is common to vertical moisture gradient and small air-filled-void cases, their corresponding backscatter responses are very different. A vertical moisture gradient makes the backscatter response dramatically flatter compared with the case of uniform moisture; in contrast, the introduction of air-filled voids barely alters the backscatter. Thus, it may be possible to infer near-surface soil-structure parameters such as vertical gradients or fractions of voids and inhomogeneities from combined SAR phase and backscatter data. Future SAR sensors could be optimized for this purpose. Prior theoretical work based on the assumption of vertically uniform soil-moisture distributions may need to be adjusted, and the lack of a theory that accommodates more complex soil structures may explain why backscatter inversions have yet to result in a viable operational system. [J355]

## "A Polarimetric Target Detector Using the Huynen Fork"

The contribution of synthetic aperture radar polarimetry in target detection is described and found to add valuable information. A new target detection methodology that makes novel use of the polarization fork of the target is described. The detector is based on a correlation procedure in the target space, and other target representations (e.g., Huynen parameters or ?? angle) can be employed. The mathematical formulation is general and can be applied to any kind of single target; however, in this paper, the detection is optimized for the odd and even bounces (the first two elements of the Pauli scattering vector) and for the oriented dipoles. Validation against real data shows significant agreement with the expected results based on the theoretical description. [J356]

## "Sequential Track Initialization with Page's Test"

A new track initialization method for remote sensing systems that uses the amplitudes of the measurements to provide some statistical separation between true and false contacts is presented. In the proposed method the data are partitioned into Hough transform bins, and Page's test is performed on the data in each bin. The new method embodies the best ideas of existing sequential and batch methods, exploits both the amplitude and the temporal information in the data, and minimizes the average latency for initializing target tracks for a specified false track initialization rate. Analytic performance predictions for the proposed method for the Swerling I signal model with Poisson clutter are developed and compared with the theoretical performance of a commonly used "M of N" method. The new method provides substantial improvement in the false track initialization rate and the average latency for initializing target tracks. [J357]

## "Dual-Polarization C-Band Radar Observations of Sea Ice in the Amundsen Gulf"

Polarimetric observations of sea ice from synthetic aperture radar can, in principle, assist in sea-ice classification and ice-water discrimination. In this paper, we use dual-polarization ground-based scatterometer observations of sea ice to assess the potential value of spaceborne dual-polarization observations of sea ice for operational ice analysis, focusing on C-band and, in particular, the contribution of the HV backscatter coefficient and HH/VV polarization ratios. Results show that signature variability resulting from frost flowers, ice deformation, and snow cover can overwhelm systematic differences between younger ice types, up to first-year thin. As a result of this and noise floor limitations of spaceborne sensors, the HV backscatter coefficient makes visual ice type and open water discrimination easier only below about 30?? incidence angle. The HH/VV ratio is less impacted by the noise floor of spaceborne sensors but retains similar ambiguities for sea-ice classification. [J358]

## "Evaluation of Ozone Analyses From UARS MLS Assimilation by BASCOE Between 1992 and 1997"

We present the analyses of UARS MLS ozone data obtained by the Belgian Assimilation System for Chemical ObsErvations (BASCOE). This system, based on the 4D-var method, is dedicated to the assimilation of stratospheric chemistry observations. It uses a 3-D Chemical Transport Model (3D-CTM) including 57 chemical species with explicit calculation of stratospheric chemistry. The CTM is driven by ECMWF ERA-40 analyses of winds and temperature, with a horizontal grid of 3.75 in latitude by 5 in longitude, and with 37 pressure levels from the surface to 0.1 hPa. BASCOE has assimilated UARS MLS observations acquired during the period 1992-1997. We discuss how BASCOE is able to reproduce MLS data, and we evaluate the BASCOE analyses with respect to independent observations from UARS HALOE, ozonesondes, and ground-based lidars. An excellent agreement is found with independent observations (bias usually less than 10%), except in the lowermost stratosphere and in the Antarctic ozone hole. The performances of BASCOE ozone analyses are also compared to those of two other long-term ozone reanalyses; namely, ERA-40 and ERA-Interim, both from ECMWF. Finally, sensitivity test based on BASCOE free model runs suggest that ozone analyses during the ozone hole period would be greatly improved by driving BASCOE with the dynamical fields of the new ECMWF reanalyses ERA-Interim. This work is part of the Stratospheric Ozone Profile Record service raised by the GMES Service Element PROMOTE. [J359]

## "Dry-Wet Bedrock Interface Detection by Radio Echo Sounding Measurements"

In this paper, a method to distinguish a wet or dry bedrock-ice interface is proposed. It is based on the analysis of radio echo sounding (RES) measurements, a widely employed method for determining bedrock topography in Antarctica. In particular, the RES system has played an important role in subglacial lake exploration and hydrogeological studies at the bedrock-ice interface. Recently, bedrock characterization has been improved through the analysis of the power of radar echoes. Signal power depends on bedrock reflectivity and its specific physical condition. In this paper, a linear model describing the loss term (internal ice absorption) is proposed. This model, together with other known quantities, contributes toward an assessment of power variation of bedrock reflectivity in order to determinate wet and dry bedrock interfaces in the Dome C region in Antarctica. [J360]

## "Earthquake Damage Assessment of Buildings Using VHR Optical and SAR Imagery"

Rapid damage assessment after natural disasters (e.g., earthquakes) and violent conflicts (e.g., war-related destruction) is crucial for initiating effective emergency response actions. Remote-sensing satellites equipped with very high spatial resolution (VHR) multispectral and synthetic aperture radar (SAR) imaging sensors can provide vital information due to their ability to map the affected areas with high geometric precision and in an uncensored manner. In this paper, we present a novel method that detects buildings destroyed in an earthquake using pre-event VHR optical and post-event detected VHR SAR imagery. The method operates at the level of individual buildings and assumes that they have a rectangular footprint and are isolated. First, the 3-D parameters of a building are estimated from the pre-event optical imagery. Second, the building information and the acquisition parameters of the VHR SAR scene are used to predict the expected signature of the building in the post-event SAR scene assuming that it is not affected by the event. Third, the similarity between the predicted image and the actual SAR image is analyzed. If the similarity is high, the building is likely to be still intact, whereas a low similarity indicates that the building is destroyed. A similarity threshold is used to classify the buildings. We demonstrate the feasibility and the effectiveness of the method for a subset of the town of Yingxiu, China, which was heavily damaged in the Sichuan earthquake of May 12, 2008. For the experiment, we use QuickBird and WorldView-1 optical imagery, and TerraSAR-X and COSMO-SkyMed SAR data. [J361]

## "Tropical Cyclone Intensity Estimated From Wide-Swath SAR Images"

Due to the relatively small amount of in situdata available for the open oceans, remote sensing techniques take

an important role in the retrieval of geophysical information, particularly during extreme events. The work presented here aims at the improvement of prediction of cyclone intensity using synthetic aperture radar (SAR) images. A new method to measure the hurricane intensity using SAR images, in combination with a parametric Holland-type model of wind speed, is presented. The algorithm is based on a least square minimization of the difference between the parametric model results and the SAR measurement. The radius of the maximum wind speed, required as input for the minimization procedure, is estimated from the SAR image using wavelet analysis. Information on wind direction is extracted from the SAR image through analysis of image features caused by boundary layer rolls. The root-mean-square error of the suggested method has been validated to be equal to 3.9 m/s. The study is based on a data set of wide-swath SAR images of about 400 km ?? 400 km coverage, acquired by the European Envisat satellite, over tropical cyclones. As a case study, hurricane Katrina is investigated in detail. A total of five tropical cyclone images will be used to validate the results of the new algorithm. [J362]

## "Coseismic Horizontal Offsets and Fault-Trace Mapping Using Phase Correlation of IRS Satellite Images: The 1999 Izmit (Turkey) Earthquake"

On August 17, 1999, a strong earthquake (Mw ?? 7.4) occurred along the western sector of the North Anatolian Fault system in Turkey. The epicenter was located near the city of Izmit, 50 km east of Istanbul. Previous works determined the coseismic surface displacements by satellite synthetic aperture radar (SAR) interferometry (InSAR) and satellite optical-image correlation. In 1999, the highest spatial resolution orbiting camera was the panchromatic sensor (PAN), a 5.8-m pixel sensor (SPOT 2 was a 10-m pixel sensor) onboard the Indian Remote Sensing (IRS) satellite. We propose to apply a new phase-correlation method to PAN images to study the coseismic rupture due to the Izmit earthquake. The phase-correlation method does not need phase unwrapping and was proved to be robust under a wide variety of circumstances. Image correlometry deals with the quantification of the subpixel offsets over the whole image, allowing displacement measurement with an accuracy that is proportional to the pixel size. We measured the near-field deformations exploiting two geometrically corrected IRS images with similar look angles. A quality check of the derived offset map was performed by comparison with GPS benchmarks and SPOT offsets. The results show that IRS PAN images can be correlated to derive coseismic slip offsets due to a large earthquake (and to map its fault trace). [J363]

## "Physical Meaning of Bistatic Polarimetric Parameters"

A generalization of the polarization theory to bistatic scattering had shown that coherent scattering mechanisms are characterized by six bistatic fork parameters. The purpose of this paper is to try again to assign physical properties to these parameters as it was done in the monostatic case by Huynen. Our conclusions are validated with COSMO (Coherent Scattering Model) model and BABI (Base BIstatique) measurements. [J364]

## "A New Method of Deriving Spectrum for Bistatic SAR Processing"

The formulation of a point target spectrum is a key step in deriving synthetic aperture radar focusing algorithms, which exploits the processing efficiency of the frequency domain. However, the existence of a double-square root in the bistatic range equation makes it difficult to find an exact analytical solution for the 2-D spectrum. In this letter, according to the idea of function optimal approach, we derive a new 2-D point target spectrum on the basis of Legendre polynomial expansion, which is more exact than the existing spectra during the synthetic aperture time. [J365]

## "Cold Regions Hydrology High-Resolution Observatory for Snow and Cold Land Processes"

Snow is a critical component of the global water cycle and climate system, and a major source of water supply in many parts of the world. There is a lack of spatially distributed information on the accumulation of snow on land surfaces, glaciers, lake ice, and sea ice. Satellite missions for systematic and global snow observations will be essential to improve the representation of the cryosphere in climate models and to advance the knowledge and prediction of the water cycle variability and changes that depend on snow and ice resources. This paper describes the scientific drivers and technical approach of the proposed Cold Regions Hydrology High-Resolution Observatory (CoReH2O) satellite mission for snow and cold land processes. The sensor is a synthetic aperture radar operating at 17.2 and 9.6 GHz, VV and VH polarizations. The dual-frequency and dual-polarization design enables the decomposition of the scattering signal for retrieving snow mass and other physical properties of snow and ice. [J366]

## "Correcting Airborne Laser Scanning Intensity Data for Automatic Gain Control Effect"

The intensity data recorded by airborne laser scanning (ALS) systems are useful for several applications, e.g., automatic point classification, change detection, and environmental studies. Before the intensity values can be

used for any specific application, it has to be calibrated for atmospheric effect, range, energy loss, and incidence angle. Some ALS systems use automatic gain control (AGC). AGC is useful for getting laser returns even from low-reflectance surfaces (e.g., dark roofs), but it also changes the recorded intensity during the data acquisition, even within one surface type. This means that the same asphalt road might have totally different intensity values depending on the surrounding environment, which has affected the state of the AGC level. Therefore, it is important to correct the intensity values to neglect the effect of AGC in order to be able to get a normalized intensity value, which is only affected by the target characteristics. A first approach to correct the intensity values for AGC is reported in this letter. The same area was flown with AGC on and off, which allowed the modeling to take place. The results showed that the model produces values that agreed with an R2of 0.76 to the intensities obtained when AGC was turned off. [J367]

## "Sparsity and Compressed Sensing in Radar Imaging"

Remote sensing with radar is typically an ill-posed linear inverse problem: a scene is to be inferred from limited measurements of scattered electric fields. Parsimonious models provide a compressed representation of the unknown scene and offer a means for regularizing the inversion task. The emerging field of compressed sensing combines nonlinear reconstruction algorithms and pseudorandom linear measurements to provide reconstruction guarantees for sparse solutions to linear inverse problems. This paper surveys the use of sparse reconstruction algorithms and randomized measurement strategies in radar processing. Although the two themes have a long history in radar literature, the accessible framework provided by compressed sensing illuminates the impact of joining these themes. Potential future directions are conjectured both for extension of theory motivated by practice and for modification of practice based on theoretical insights. [J368]

## "Terrestrial Quadstatic Interferometric Radar Observations of Mars"

A new technique for resolving the ambiguity inherent in delay-Doppler radar observations of Mars has been developed and implemented using a suite of data collected during 2001, 2003, and 2005 oppositions. New recording systems, processing techniques, and, most importantly, the addition of a fourth receiving telescope allow for the high-resolution mapping of Mars' radar properties. In this paper, we develop a maximum likelihood method to probabilistically estimate the contributions to the received radar signal from the ambiguous resolution cells. Our delay-Doppler interferometric radar observations are designed to map the radar properties of Mars surface while disregarding the historically typical goal of measuring topography, instead using Mars' topography as a prioriknowledge. Example data from the September 27, 2003 observation over Mars' southern highlands, including Ma'adim Vallis and Gusev Crater, and the June 7, 2001 observation crossing Terra Meridiani are presented to demonstrate the effectiveness of the technique. Analysis of these observations predicted a root-mean-square (rms) roughness, or slopes, for the Mars Exploration Rover (MER) Spirit landing site of 1.80?? ?? 0.75??. Similarly, analysis of the Gusev Crater landing site of MER Opportunity predicted rms slopes of 1.1?? ? ? 0.1??. Both predictions were validated by analysis of in siturover images. [J369]

## "Low-Frequency Limit of Unified Models for Backscattering From Oceanlike Surfaces"

In the context of electromagnetic-wave backscattering from oceanlike surfaces, by using the first two orders of unified models, like the small slope approximation and the local curvature approximation, we recently proposed an original technique to reduce the number of numerical integrations to two for easier numerical implementation. In this letter, this technique is simplified in the low-frequency limit, allowing us to bring a correction to the first-order small perturbation method. [J370]

## "MST Radar Signal Processing Using Cepstral Thresholding"

The cepstrum thresholding approach for variance reduction is applied to estimate the spectrum of mesosphere-stratosphere-troposphere radar data, which are complex. Unlike in a real data case, where the cepstral values are real, for complex signals, cepstral values will be complex. We propose two different thresholding approaches: 1) applying a threshold independently for real and imaginary values of cepstral estimates and 2) threshold application to the modulus of cepstral estimates. Reductions of the total variance of the estimated spectra using the aforementioned two threshold approaches have been tested with simulated data. Finally, the algorithm has been applied to the practical atmospheric radar data to estimate the wind parameters through the computation of Doppler shift. Results have been validated using simultaneous Global Positioning System sonde data. [J371]

## "The Impact of Radar Incidence Angle on Soil-Moisture-Retrieval Skill"

The impact of measurement incidence angle (θ) on the accuracy of radar-based surface soil-moisture (Θs) retrievals is largely unknown due to discrepancies in theoretical backscatter models as well as limitations in the availability of sufficiently extensive ground-based Θsobservations for validation. Here, we apply a data-

assimilation-based evaluation technique for remotely sensed Θsretrievals that does not require ground-based soil-moisture observations to examine the sensitivity of skill in surface Θsretrievals to variations in θ. Past results with the evaluation approach have shown that it is capable of detecting relative variations in the anomaly correlation coefficient between remotely sensed Θsretrievals and ground-truth soil-moisture measurements. Application of the evaluation approach to the Vienna University of Technology (TU Wien) European Remote Sensing (ERS) scatterometer Θsdata set over regional-scale ( ~ 10002km2) domains in the Southern Great Plains and southeastern (SE) regions of the U.S. indicate a relative reduction in correlation-based skill of 23% to 30% for Θsretrievals obtained from far-field (θ>50°) ERS observations relative to Θsestimates obtained at θ <; 26°. Such relatively modest sensitivity to θ is consistent with Θsretrieval noise predictions made using the TU-Wien ERS Water Retrieval Package 5 backscatter model. However, over moderate vegetation cover in the SE domain, the coupling of a bare soil backscatter model with a "vegetation water cloud" canopy model is shown to overestimate the impact of θ on Θsretrieval skill. [J372]

## "Context-Dependent Multisensor Fusion and Its Application to Land Mine Detection"

We present a novel method for fusing the results of multiple land mine detection algorithms which use different sensors, features, and different classification methods. The proposed multisensor/multialgorithm fusion method, which is called context-dependent fusion (CDF), is motivated by the fact that the relative performance of different sensors and algorithms can vary significantly depending on the mine type, geographical site, soil and weather conditions, and burial depth. CDF is a local approach that adapts the fusion method to different regions of the feature space. The training part of CDF has two components: context extraction and algorithm fusion. In context extraction, the features used by the different algorithms are combined and used to partition the feature space into groups of similar signatures, or contexts. The algorithm fusion component assigns a degree of worthiness to each detector in each context based on its relative performance within the context. To test a new alarm using CDF, each detection algorithm extracts its set of features and assigns a confidence value. Then, the features are used to identify the best context, and the degrees of worthiness of this context are used to fuse the individual confidence values. Results on large and diverse ground-penetrating radar and wideband electromagnetic data collections show that the proposed method can identify meaningful and coherent clusters and that different expert algorithms can be identified for the different contexts. Typically, the contexts correspond to groups of alarm signatures that share a subset of common features. Our extensive experiments have also indicated that CDF outperforms all individual detectors and the global fusion that uses the same method to assign aggregation weights. [J373]

## "SAR and Multispectral Image Fusion Using Generalized IHS Transform Based on a Trous Wavelet and EMD Decompositions"

In the intensity hue saturation (IHS) based image fusion, the enhancement of the spatial information often leads to the distortion of the information in the spectral domain. In this paper, a spectral preserve fusion method is developed by introducing aГ‚Вї trous wavelet transform (AWT) and empirical mode decomposition (EMD) into one generalized IHS transform, which extends panchromatic sharpening of low-resolution multispectral images (LRMIs) through detail injection to the fusion of LRMIs and synthetic aperture radar imagery (SARI). The original LRMIs are first transformed into one low-resolution intensity component (LRIC) and the details from the SARI are abstracted using AWT. The LRIC and the approximation image of the SARI are fused through an intrinsic mode functions based model. Subsequently, high RIC produced through an inverse AWT is then substituted for the old one. High RMIs are obtained through an inverse IHS transform. Experiments reveal that this approach performs better than the AWT and IHS-AWT-based methods in preserving the spectral information of the LRMIs. The performance of the image fusion is examined both visually and quantitatively. [J374]

## "Monitoring Dry, Wet, and No-Snow Conditions From Microwave Satellite Observations"

Possible climate warming in northern latitudes will affect stream flow in watersheds dominated by snowmelt. It is important to detect early snowmelt conditions for applications to flood forecasting and monitoring fresh water stored in snow cover. This letter presents a study to demonstrate the potential of combined active and passive microwave spaceborne observations for monitoring global to regional snow cover on a daily basis. The proposed approach uses the temporal gradient of two parameters: 1) the Ku-band QuikSCAT scatterometer backscattering coefficient variation for snow wetness detection and 2) a dual-frequency emissivity index (Δ t) derived from the Defense Meteorological Satellite Program Special Sensor Microwave Imager brightness temperatures for snow line detection. This approach takes into account the land cover derived from satellite data on a pixel-by-pixel basis. The evolution of the backscatter and Δ tsignatures throughout the winter-spring seasonal snow cycle is compared with in situ snow and air temperature measurements and with the snow-cover maps derived from high-resolution satellite data over Eastern Canada. The results show the high potential of this approach for historical analysis, as well as for day-to-day prospective investigation (forecasting). [J375]

## "An ISAR Imaging Method Based on MIMO Technique"

With the inverse synthetic aperture radar (ISAR) imaging model, targets should move smoothly during the coherent processing interval (CPI). Since the CPI is quite long, fluctuations of a target's velocity and gesture will deteriorate image quality. This paper presents a multiple-input-multiple-output (MIMO)-ISAR imaging method by combining MIMO techniques and ISAR imaging theory. By using a special M-transmitter N-receiver linear array, a group of Morthogonal phase-code modulation signals with identical bandwidth and center frequency is transmitted. With a matched filter set, every target response corresponding to the orthogonal signals can be isolated at each receiving channel, and range compression is completed simultaneously. Based on phase center approximation theory, the minimum entropy criterion is used to rearrange the echo data after the target's velocity has been estimated, and then, the azimuth imaging will finally finish. The analysis of imaging and simulation results show that the minimum CPI of the MIMO-ISAR imaging method is 1/MNof the conventional ISAR imaging method under the same azimuth-resolution condition. It means that most flying targets can satisfy the condition that targets should move smoothly during CPI; therefore, the applicability and the quality of ISAR imaging will be improved. [J376]

## "Aquarius and Remote Sensing of Sea Surface Salinity from Space"

Aquarius is an L-band radiometer and scatterometer instrument combination designed to map the salinity field at the surface of the ocean from space. The instrument is designed to provide global salinity maps on a monthly basis with a spatial resolution of 150 km and an accuracy of 0.2 psu. The science objective is to monitor the seasonal and interannual variation of the large scale features of the surface salinity field in the open ocean. This data will promote understanding of ocean circulation and its role in the global water cycle and climate. Aquarius is the primary instrument on the Aquarius/SAC-D mission which is a partnership between the space agencies in the USA (NASA) and Argentina (CONAE). Launch is scheduled for late in 2010. [J377]

## "Compressive Stepped-Frequency Continuous-Wave Ground-Penetrating Radar"

Data acquisition speed is an inherent problem of stepped-frequency continuous-wave (SFCW) radars, which may discourage further usage and development of this technology. We propose an emerging paradigm called compressed sensing (CS) to overcome this problem. In CS, a signal can be reconstructed exactly based on only a few samples below the Nyquist rate. Accordingly, the data acquisition speed can be increased significantly. A novel design of an SFCW ground-penetrating radar (GPR) with high acquisition speed is proposed and evaluated. Simulation by a monocycle waveform and actual measurement by a vector network analyzer at a GPR test range indicate the applicability of the proposed system. [J378]

## "Passive and Active L-Band Microwave Observations and Modeling of Ocean Surface Winds"

L-band microwave backscatter and brightness temperature of sea surfaces acquired using the Passive/Active L-band Sensor during the High Ocean Wind campaign are reported in terms of their dependence on ocean surface wind speed and direction. We find that the L-band VV, HH, and HV radar backscatter data increase by 6-7 dB from 5 to 25 m/s wind speed at a 45° incidence angle. The data suggest the validity of Phased Array type L-band Synthetic Aperture Radar (PALSAR) HH model function between 5 and 15 m/s wind speeds, but show that the extrapolation of PALSAR model at above 20 m/s wind speeds overpredicts A0and a1coefficients. There is wind direction dependence in the radar backscatter with about 4 dB differences between upwind and crosswind observations at 24 m/s wind speed for VV and HH. The passive brightness temperatures show about a 5-K change for TVand a 7-K change for THfor a wind speed increasing from 5 to 25 m/s. Circle flight data suggest a wind direction response of about 1-2 K in TVand THat 14 and 24 m/s wind speeds. The L-band microwave data show excellent linear correlation with the surface wind speed with a correlation better than 0.95. The results support the use of L-band radar data for estimating the wind-driven excess brightness temperature of sea surfaces. The data also support the applications of L-band microwave signals for high-resolution (kilometer scale) observation of ocean surface winds under high wind conditions (10-28 m/s). [J379]

## "C-Band Polarimetric Backscattering Signatures of Newly Formed Sea Ice During Fall Freeze-Up"

A study of the polarimetric backscattering response of newly formed sea ice types under a large assortment of surface coverage was conducted using a ship-based C-band polarimetric radar system. Polarimetric backscattering results and physical data for 40 stations during the fall freeze-up of 2003, 2006, and 2007 are presented. Analysis of the copolarized correlation coefficient showed its sensitivity to both sea ice thickness and surface coverage and resulted in a statistically significant separation of ice thickness into two regimes: ice less than 6 cm thick and ice greater than 8 cm thick. A case study quantified the backscatter of a layer of snow infiltrated frost flowers on new sea ice, showing that the presence of the old frost flowers can enhance the

backscatter by more than 6 dB. Finally, a statistical analysis of a series of temporal-spatial measurements over a visually homogeneous frost-flower-covered ice floe identified temperature as a significant, but not exclusive, factor in the backscattering measurements. [J380]

## "CALIOP Aerosol Subset Processing for Global Aerosol Transport Model Data Assimilation"

A system for processing Cloud-Aerosol Lidar with Orthogonal Polarization (CALIOP) satellite-based 0.532 and 1.064 elastic and polarization lidar datasets for global aerosol transport model assimilation is described. A method for constructing one-degree along-track and cloud-free signal composite averages, consistent with Navy Aerosol Analysis and Prediction System (NAAPS) model gridding, using CALIOP Level 1B attenuated backscatter and Level 2 cloud boundary-height products is outlined. Optimal vertical resolutions and relative signal uncertainties for the composite signal averages are described for both day and nighttime measurement scenarios. Depolarization profiles are described for the 0.532 channel as well as attenuated color ratio profiles using 0.532 and 1.064 attenuated backscatter measurements. Constrained by NAAPS model aerosol optical depths, processed attenuated backscatter profiles are inverted to solve for extinction and backscatter coefficients, their ratio, and extinction coefficient profiles which serve as the basis for data assimilation. [J381]

## "Automatic Extraction of Control Points for the Registration of Optical Satellite and LiDAR Images"

A novel method for automatic extraction of control points for the registration of optical images with Light Detection And Ranging (LiDAR) data is proposed. It is based on transformation-invariant detection of salient image disks (SIDs), which determine the location of control points as the centers of the corresponding image fragments. The SID is described by a feature vector, which, in addition to the coordinates and diameter, includes intensity descriptors and region shape characteristics of the image fragment. SIDs are effectively extracted using multiscale isotropic matched filtering-a visual attention operator that indicates image locations with high-intensity contrast, homogeneity, and local shape saliency. This paper discusses the extraction of control points from both natural landscapes and structured scenes with man-made objects. Registration experiments conducted on QuickBird imagery with corresponding LiDAR data validated the proposed approach. [J382]

## "Improved Hurricane Ocean Vector Winds Using SeaWinds Active/Passive Retrievals"

The SeaWinds scatterometer, onboard the QuikSCAT satellite, infers global ocean vector winds (OVWs); however, for a number of reasons, these measurements in hurricanes are significantly degraded. This paper presents an improved hurricane OVW retrieval approach, known as Q-Winds, which is derived from combined SeaWinds active and passive measurements. In this technique, the effects of rain are implicitly included in a new geophysical model function, which relates oceanic brightness temperature and radar backscatter measurements (at the top of the atmosphere) to the surface wind vector under both clear sky and in the presence of light to moderate rain. This approach extends the useful wind speed measurement range for tropical cyclones beyond that exhibited by the standard SeaWinds Project Level-2B (L2B) 12.5-km wind vector algorithm. A description of the Q-Winds algorithm is given, and examples of OVW retrievals are presented for the Q-Winds and L2B 12.5-km algorithms for ten hurricane overpasses in 2003-2008. These data are also compared to independent surface wind vector estimates from the National Oceanic and Atmospheric Administration Hurricane Research Division's objective hurricane surface wind analysis technique known as H*Wind. These comparisons suggest that the Q-Winds OVW product agrees better with independently derived H^ Wind analysis winds than does the conventional L2B OVW product. [J383]

## "Automated Polar Ice Thickness Estimation From Radar Imagery"

This paper focuses on automating the task of estimating Polar ice thickness from airborne radar data acquired over Greenland and Antarctica. This process involves the identification and accurate selection of the ice sheet's surface location and interface between the ice sheet and the underlying bedrock for each measurement. Identifying the surface and bedrock locations in the radar imagery enables the computation of ice sheet thickness, which is important for the study of ice sheets, their volume, and how they may contribute to global climate change. The time-consuming manual approach requires sparse hand-selection of surface and bedrock interfaces by several human experts, and interpolating between the selections to save time. Two primary methods have been studied in this paper, namely, edge-based and active contour. Results are evaluated and presented using the metrics of time requirements and accuracy. Automated ice thickness estimation results from 2006 and 2007 Greenland field campaigns illustrate that the edge-based approach offers faster processing (seconds compared to minutes), but suffers from a lack of continuity and smoothness aspects that active contours provide. The active contour approach is more accurate when compared to ground truth selections provided by human experts, and has proven to be more robust to image artifacts. It is shown that both techniques offer advantages which could be integrated to yield a more effective system. [J384]

## "The Soil Moisture Active Passive (SMAP) Mission"

The Soil Moisture Active Passive (SMAP) mission is one of the first Earth observation satellites being developed by NASA in response to the National Research Council's Decadal Survey. SMAP will make global measurements of the soil moisture present at the Earth's land surface and will distinguish frozen from thawed land surfaces. Direct observations of soil moisture and freeze/thaw state from space will allow significantly improved estimates of water, energy, and carbon transfers between the land and the atmosphere. The accuracy of numerical models of the atmosphere used in weather prediction and climate projections are critically dependent on the correct characterization of these transfers. Soil moisture measurements are also directly applicable to flood assessment and drought monitoring. SMAP observations can help monitor these natural hazards, resulting in potentially great economic and social benefits. SMAP observations of soil moisture and freeze/thaw timing will also reduce a major uncertainty in quantifying the global carbon balance by helping to resolve an apparent missing carbon sink on land over the boreal latitudes. The SMAP mission concept will utilize L-band radar and radiometer instruments sharing a rotating 6-m mesh reflector antenna to provide high-resolution and high-accuracy global maps of soil moisture and freeze/thaw state every two to three days. In addition, the SMAP project will use these observations with advanced modeling and data assimilation to provide deeper root-zone soil moisture and net ecosystem exchange of carbon. SMAP is scheduled for launch in the 2014-2015 time frame. [J385]

## "Height Retrieval of Isolated Buildings From Single High-Resolution SAR Images"

Detection of man-made structures in urban areas, in terms of both geometric and electromagnetic features, from a single, possibly high resolution (HR), synthetic aperture radar (SAR) image is a highly interesting open challenge. Within this framework, a possible approach for the extraction of some relevant parameters, describing the shape and materials of a generic building, is proposed here. The approach is based on sound electromagnetic models for the radar returns of each element of the urban scene. A fully analytical representation of electromagnetic returns from the scene constituents to an active microwave sensor is employed. Some possible applications of feature extractions from real SAR images, based on the aforementioned approach, have already been presented in the literature as first examples of potentiality of a model-based approach, but here, the overall theory is analyzed and discussed in depth, to move to general considerations about its soundness and applicability, and the efficiency of further applications may be derived. For the sake of conciseness, although the proposed approach is general and can be applied for the retrieval of different scene parameters (in principle, anyone contributing to the radar return), we focus here on the extraction of the building height, and we assume that the other parameters are either a prioriknown (e.g., electromagnetic properties of the materials) or have been previously retrieved from the same SAR image (e.g., building length and width). An analysis of the sensitiveness of the height retrieval to both model inaccuracies and errors on the knowledge of the other parameters is performed. Some simulation examples accompany and validate the solution scheme that we propose. [J386]

## "Correction to "A New Vector Waveform Inversion Algorithm for Simultaneous Updating of Conductivity and Permittivity Parameters From Combination Crosshole/Borehole-to-Surface GPR Data""

In the above titled paper (ibid., vol. 48, no. 9, pp. 3391-3407, Sep. 10), there is an error in equation (A-5). The correct form is presented here. [J387]

## "RADARSAT-2 and Coastal Applications: Surface Wind, Waterline, and Intertidal Flat Roughness"

RADARSAT-2 is a follow-up to RADARSAT-1 and is an all weather Earth observation satellite with fully polarimetric imaging capability. The synthetic aperture radars (SARs) onboard both RADARSATs are C-band imaging radars and they are well suited for Earth's ecosystem monitoring and maritime surveillance, because of the near polar orbit and their unique all weather imaging capability, independent of solar illumination. In this paper, RADARSAT-2 is first introduced and several applications of various modes of SAR data to coastal zone problems are discussed, including the coastal surface wind, waterline mapping, and polarimetric SAR data inversion for topographic and geological parameters of tidal flats. Coastal zones, the important interface between the land and the ocean, where a large proportion of the world's population inhabits, continuously change and evolve. The dynamic interaction of coastal winds, coupled with the coastal waves and currents, continuously erode rocks and land mass, and move and deposit various sediments on a continuous basis, along with the tides. Estimation of wind speeds and directions in coastal areas are empirically formulated and can further be improved with the available fully polarimetric data from RADARSAT-2. The water line mapping critically depends on the SAR frequency, or the wavelength of the SAR data used, and RADARSAT-2 SAR data using C-band should map waterlines more accurately than the longer wavelength L- or P-band SAR systems. The roughness parameters and partial information on the tidal flat compositions can be obtained from fully polarimetric SAR

data. Some results obtained from NASA AIRSAR(2000) L-band data and RADARSAT-2(2008) C-band data do not fully agree with field measurements and further investigation is in progress. The inversion of polarimetric SAR data is a very complex problem and critically depends on the SAR signal frequency and model functions. RADARSAT-2 is an imaging radar, which is very flexible and powerfu--l tool for potential coastal zone applications. Key RADARSAT-2 features and potential coastal zone application capabilities are also briefly reviewed. [J388]

## "The ICESat-2 Laser Altimetry Mission"

Satellite and aircraft observations have revealed that remarkable changes in the Earth's polar ice cover have occurred in the last decade. The impacts of these changes, which include dramatic ice loss from ice sheets and rapid declines in Arctic sea ice, could be quite large in terms of sea level rise and global climate. NASA's Ice, Cloud and Land Elevation Satellite-2 (ICESat-2), currently planned for launch in 2015, is specifically intended to quantify the amount of change in ice sheets and sea ice and provide key insights into their behavior. It will achieve these objectives through the use of precise laser measurements of surface elevation, building on the groundbreaking capabilities of its predecessor, the Ice Cloud and Land Elevation Satellite (ICESat). In particular, ICESat-2 will measure the temporal and spatial character of ice sheet elevation change to enable assessment of ice sheet mass balance and examination of the underlying mechanisms that control it. The precision of ICESat-2's elevation measurement will also allow for accurate measurements of sea ice freeboard height, from which sea ice thickness and its temporal changes can be estimated. ICESat-2 will provide important information on other components of the Earth System as well, most notably large-scale vegetation biomass estimates through the measurement of vegetation canopy height. When combined with the original ICESat observations, ICESat-2 will provide ice change measurements across more than a 15-year time span. Its significantly improved laser system will also provide observations with much greater spatial resolution, temporal resolution, and accuracy than has ever been possible before. [J389]

## "A Novel Hierarchical Method of Ship Detection from Spaceborne Optical Image Based on Shape and Texture Features"

Ship detection from remote sensing imagery is very important, with a wide array of applications in areas such as fishery management, vessel traffic services, and naval warfare. This paper focuses on the issue of ship detection from spaceborne optical images (SDSOI). Although advantages of synthetic-aperture radar (SAR) result in that most of current ship detection approaches are based on SAR images, disadvantages of SAR still exist, such as the limited number of SAR sensors, the relatively long revisit cycle, and the relatively lower resolution. With the increasing number of and the resulting improvement in continuous coverage of the optical sensors, SDSOI can partly overcome the shortcomings of SAR-based approaches and should be investigated to help satisfy the requirements of real-time ship monitoring. In SDSOI, several factors such as clouds, ocean waves, and small islands affect the performance of ship detection. This paper proposes a novel hierarchical complete and operational SDSOI approach based on shape and texture features, which is considered a sequential coarse-to-fine elimination process of false alarms. First, simple shape analysis is adopted to eliminate evident false candidates generated by image segmentation with global and local information and to extract ship candidates with missing alarms as low as possible. Second, a novel semisupervised hierarchical classification approach based on various features is presented to distinguish between ships and nonships to remove most false alarms. Besides a complete and operational SDSOI approach, the other contributions of our approach include the following three aspects: 1) it classifies ship candidates by using their class probability distributions rather than the direct extracted features; 2) the relevant classes are automatically built by the samples' appearances and their feature attribute in a semisupervised mode; and 3) besides commonly used shape and texture features, a new texture operator, i.e., loca--l multiple patterns, is introduced to enhance the representation ability of the feature set in feature extraction. Experimental results of SDSOI on a large image set captured by optical sensors from multiple satellites show that our approach is effective in distinguishing between ships and nonships, and obtains a satisfactory ship detection performance. [J390]

## "GNSS-Derived Path Delay: An Approach to Compute the Wet Tropospheric Correction for Coastal Altimetry"

This letter presents an innovative method for computing the wet tropospheric correction for altimetry measurements in the coastal regions, where the measurements from the microwave radiometers (MWRs) onboard altimetric missions become invalid. The method, called Global Navigation Satellite System (GNSS)-derived Path Delay, gives an estimation of the correction, along with the associated mapping error, from the combination of independent zenith wet delay (ZWD) values obtained from the tropospheric delays derived at a network of coastal GNSS stations, from the MWR measurements acquired before land degradation, and from the European Centre for Medium-Range Weather Forecasts Deterministic Atmospheric Model. The wet tropospheric

correction is estimated at each altimeter point with an invalid MWR value using a linear space-time objective analysis technique that takes into account the spatial and temporal variability of the ZWD field and the accuracy of each data set used. The method was applied in the South West European region for the whole Envisat data series, and the results are presented here. The uncertainty of the wet-delay estimates is below 1 cm, provided they are obtained for points at distances shorter than ~ 50 km from a GNSS station, and/or valid MWR measurements are available for the estimation. The method can be implemented globally and foster the use of satellite altimetry in coastal studies. [J391]

## "A Monte Carlo Study of Altimeter Pulse Returns and the Electromagnetic Bias"

The electromagnetic (EM) bias is an important error term in sea-surface height estimation from satellite radar altimetry. While the EM bias has been studied extensively, previous studies have utilized hydrodynamic and EM models that require an a priori separation of the sea surface into "long" and "short" waves that are then treated separately. This paper presents a study of the EM bias that avoids this decomposition by employing a Monte Carlo procedure with numerical nonlinear hydrodynamic simulations coupled with numerical physical-optics methods for EM scattering from the sea surface. Due to the computational complexity of the approach, only long-crested surfaces (i.e., 2-D scattering problems) are considered. The formulation of the physical-optics model utilized is presented, along with a derivation of the standard Brown model for the long-crested surface case for comparison. The simulated pulse returns generally are in good agreement with the Brown model using the specular surface height probability density function. However, the influence of the EM frequency on the EM bias obtained is much smaller than that reported from satellite observations. Predicted biases are also examined as the range of length scales included in the surface profile is varied, in order to determine any apparent cutoff or length-scale separations that occur. It is found that the bias continues to increase as additional short waves are included in the surface spectrum, although a saturation occurs for surface length scales shorter than the EM wavelength. [J392]

## "Development and Initial Observation of High-Resolution Volume-Scanning Radar for Meteorological Application"

A new high-resolution Doppler radar, called Ku-band broadband radar (BBR), with fast scanning capability for meteorological application has been developed. Due to the new system design, the BBR can accurately measure the radar reflectivity factor with a range resolution of several meters and a time resolution of 55 s per volume scan from the nearest range of 50 m to 15 km for 10-W power using pulse compression. In this paper, the basic concepts, configuration, and signal processing of the BBR are described. In the initial observation, the observation accuracy of reflectivity is evaluated using Joss-Waldvogel disdrometer (JWD). As a result, the reflectivity of the BBR is in fairly good agreement with that of JWD. In addition, in the spiral observation, a fine structure of a thunderstorm obtained by the BBR is presented. [J393]

## "Experimental Determination of the Sea Correlation Time Using GNSS-R Coherent Data"

The feasibility of the Global Navigation Satellite Signal Reflectometry (GNSS-R) techniques has been proven for remote determination of sea state. When using GNSS-R techniques, coherent integration time is limited by the correlation time of the surface under observation which, in the case of the ocean, depends on sea state. In this letter, a new technique to retrieve the sea correlation time at L-band using GNSS-R coherent data is presented along with experimental results. [J394]

## "Bistatic SAR Experiments With PAMIR and TerraSAR-X-Setup, Processing, and Image Results"

The spatial separation of the transmitter and the receiver in bistatic synthetic aperture radar (SAR) enables a variety of data acquisition geometries to achieve benefits like the increased information content of bistatic SAR data. In the case of hybrid bistatic SAR constellations where the transmitter is spaceborne and the receiver is onboard an aircraft, one has to deal with a huge discrepancy between platform velocities. This paper presents bistatic spaceborne/airborne SAR experiments, where the radar satellite TerraSAR-X is used as a transmitter and the airborne SAR sensor Phased Array Multifunctional Imaging Radar (PAMIR) of the Fraunhofer Institute for High Frequency Physics and Radar Techniques (FHR) is used as a receiver. Both sensors are equipped with phased-array antennas, which offer the possibility of beam steering and could be used for the first time for the "double sliding spotlight mode." In this mode, the space- and airborne sensors operate with different sliding factors (ratio between footprint and platform velocity). The performance of two different experiments is analyzed, and the novel double sliding spotlight mode is presented. This paper describes the experimental setups, the synchronization system, and the data acquisition. The image results were processed by a modified backprojection algorithm and a frequency-domain algorithm. The analysis of the final bistatic images comprises the spatial resolution and the scattering behavior of selected objects. Parts of the bistatic SAR images are

compared with the corresponding monostatic images of PAMIR and TerraSAR-X. It will be shown that hybrid bistatic SAR is a worthwhile and helpful addition to current monostatic SAR. [J395]

## "Practical applications of UWB technology"

Use of ultra-wideband (UWB) technology in various areas for remote sensing of the objects at short distances are considered. As an illustration UWB radar, in medicine and in psychophysiology, for remote measuring of patient's beating of the pulse and respiration is shown. The opportunity of UWB technology application in the other areas is described, including measuring of liquid levels, definition of a position of people in buildings, and position of people in woodlands. [J396]

## "ICESat Geolocation Validation Using Airborne Photography"

NASA's ICESat satellite launched in January of 2003, carrying the Geoscience Laser Altimeter. During the initial phase of this mission, many validation procedures were implemented to verify the accuracy associated with a variety of altimetry-derived data products. Of specific interest was the need to validate the geodetic position of the ICESat footprints, which is a convolution of laser-pointing determination, satellite position, and ranging measurements. This paper describes the methodology and implementation of one effort using aerial photography to image the laser spots on the surface during a satellite overflight. The spot locations are determined based on the relative positions of accurately placed geodetic infrared-emitting markers within the overflight area and apparent in the aerial photograph. One specific overflight opportunity captured six successive ICESat footprints with the airborne camera system. The mean geolocation predictions of those spots using the ground fiducial placement in the image provide a data product validation to better than 3.1-m rms on the surface with an estimated accuracy of ??3.6 m when compared to the ICESat solution. These results are within the ICESat mission requirement of 4.5 m on the surface (1.5-arcsecond pointing knowledge) for geodetic position determination. [J397]

## "Surface-Wavefield Estimation From Coherent Marine Radars"

One major impediment to using marine radars for real-time shipboard measurements of evolving ocean wavefields is the uncertainty in the transfer function that relates the radar cross section to sea-surface height. In this letter, a more direct approach is proposed to infer nonlinear sea-surface heights by using radial-velocity measurements from coherent marine radars. The radial velocities are initially integrated along range lines to obtain a scalar potential function. The velocity potential field is then differentiated with respect to time to yield the sea-surface height. Numerical simulations have been conducted to evaluate the sensitivity of the proposed scheme to sampling errors and noise. Under idealized conditions, the results demonstrate that the sea-surface elevation can be reliably estimated from the radial-velocity field provided that the antenna-rotation period is much smaller than a characteristic wave period. [J398]

## "Decorrelation of L-Band and C-Band Interferometry Over Vegetated Areas in California"

Temporal decorrelation is one of the main limitations for recovering interseismic deformation along the San Andreas Fault system using interferometric synthetic aperture radar. To assess the improved correlation properties of L-band with respect to C-band, we analyzed L-band Advanced Land Observation Satellite (ALOS) interferograms with a range of temporal and spatial baselines over three vegetated areas in California and compared them with corresponding C-band European Remote Sensing Satellite (ERS) interferograms. Over the highly vegetated Northern California forests in the Coast Range area, ALOS remains remarkably well correlated over a 2-year period, whereas an ERS interferogram with a similar temporal and spatial baseline lost correlation. In Central California near Parkfield, we found a similar pattern in decorrelation behavior, which enabled the recovery of a fault creep and a local uplifting signal at L-band that was not apparent at C-band. In the Imperial Valley in Southern California, both ALOS and ERS have low correlation over farmlands. ALOS has lower correlation over some sandy surfaces than ERS, probably due to low signal-to-noise ratio. In general, L-band interferograms with similar seasonal acquisitions have higher correlation than those with dissimilar season. For both L- and C-band, correlation over vegetated areas decreases with time for intervals less than 1 year and then remains relatively constant at longer time intervals. The decorrelation time for L-band is more than 2 years in the forest in California whereas that for C-band is less than 6 months. Overall, these results suggest that L-band interferograms will reveal near-fault interseismic deformation once sufficient data become available. [J399]

## "Single-Range Image Fusion for Spinning Space Debris Radar Imaging"

In this letter, a novel single-range image fusion method for radar imaging of spinning space debris with dimensions smaller than the radar range resolution is proposed. On the assumption that the target consists of isolated isotropic scattering centers, a 2-D image can be obtained using single-range unit cross-range echo

data, which have a theoretical resolution of a quarter of a wavelength. The proposed approach is computationally efficient particularly for smaller sized targets, as the total rotational angle is divided into four small sections, allowing for easier processing of each region. Moreover, the proposed method can be used to directly obtain an image in Cartesian coordinates, unlike current algorithms where images are obtained in a polar format, requiring reformatting to the Cartesian grid. The validity of the proposed approach is confirmed using numerical simulations. [J400]

## "On the Role of Phase Stability in SAR Multibaseline Applications"

This paper is meant to present a statistical analysis of the role of propagation disturbances (PDs), such as those due to atmospheric disturbances or to residual platform motion, in multibaseline synthetic aperture radar (SAR) interferometry (InSAR) and tomography (T-SAR) applications. The analysis will consider both pointlike and distributed targets in such a way as to cover all the cases that are relevant in the applications. In order to provide a tool for the evaluation of the impact of PDs on the analysis of an arbitrary scenario, a definition of signal-to-noise ratio (SNR) will be introduced that accounts for both the presence of PDs and the characteristics of the imaged scene. In the case of pointlike targets, it will be shown that such definition of SNR allows reusing well known results following after the Neyman-Pearson theory, thus providing a straightforward tool to asses phase-stability requirements for the detection and localization of multiple pointlike targets. In the case of distributed targets, instead, it will be provided a detailed analysis of the random fluctuations of the reconstructed scene as a function of the extent of the PDs, of the vertical structure of the imaged scene, and of the number of looks that are employed. Results from Monte Carlo simulations will be presented that fully support the theoretical developments within this paper. The most relevant conclusion of this paper is that the impact of PDs is more severe in the case where the imaged scene is characterized by a complex vertical structure or when multiple pointlike targets are present. As a consequence, it follows that the T-SAR analyses require either a higher phase stability or a more accurate phase calibration with respect to InSAR analyses. Finally, an example of phase-stability analysis and phase calibration of a real data set will be shown, based on a P-band data set relative to the forest site of Remningstorp, Sweden. [J401]

## "Optimal Waveform Design for Improved Indoor Target Detection in Sensing Through-the-Wall Applications"

This paper deals with waveform design for improved detection and classification of targets behind walls and enclosed structures. The target impulse response is incorporated in an optimum design of the transmitted waveform which aims at maximizing the signal-to-interference and noise ratio (SINR) at the receiver output. The interference represents signal-dependent clutter which, along with the wall, degrades the receiver performance compared to the free-space and zero-clutter case. Computer simulations show sensitivity of the optimum waveform to target orientation but depict an SINR enhancement over chirped waveform radar emissions at all aspect angles. Numerical electromagnetic modeling is used to provide the impulse response of typical indoor stationary targets, namely, tables, chairs, and humans. [J402]

## "Performance Study of a Cross-Frequency Detection Algorithm for Pulsed Sinusoidal RFI in Microwave Radiometry"

An analysis of the performance of a cross-frequency detection algorithm for pulsed sinusoidal radio frequency interference (RFI) is performed. The performance obtained is compared with that of pulse and kurtosis detection methods that have been previously reported. The results of the study show that the cross-frequency algorithm provides good performance in detecting pulsed sinusoidal RFI at high duty cycles, including the case of continuous sinusoidal interference. The use of the cross-frequency algorithm requires choice of a detection threshold that in practice can be estimated using measured data. The effect of this threshold estimation on the detector performance is also examined. [J403]

## "Topographic Correction for ALOS PALSAR Interferometry"

L-band synthetic aperture radar (SAR) interferometry is very successful for mapping ground deformation in densely vegetated regions. However, due to its larger wavelength, the capacity to detect slow deformation over a short period of time is limited. Stacking and small baseline subset (SBAS) techniques are routinely used to produce time series of deformation and average deformation rates by reducing the contribution of topographic and atmospheric noise. For large sets of images that are presently available from C-band European Remote Sensing Satellites (ERS-1/2) and Environmental Satellite (ENVISAT), the standard stacking and SBAS algorithms are accurate. However, the same algorithms are often inaccurate when used for processing of interferograms from L-band Advanced Land Observing Satellite Phased Array type L-band SAR (ALOS PALSAR). This happens because only a limited number of interferograms is acquired and also because of large spatial baselines often

correlated with the time of acquisition. In this paper two techniques are suggested that can be used for removing the residual topographic component from stacking and SBAS results, thereby increasing their accuracy. [J404]

## "Numerical Simulation of the Wind-Stress Effect on SAR Imagery of Far Wakes of Ships"

Centerline wakes of ships in synthetic aperture radar (SAR) images were modeled in 2-D with the computational fluid dynamics (CFD) software Fluent and a radar-imaging algorithm. We initialized the model with a pair of vortices generated by a ship hull and applied wind stress perpendicular to the ship wake. Results of the CFD simulation using a nonhydrostatic model have demonstrated ship-wake asymmetry with respect to the wind-stress direction relative to the ship course. Due to the wind stress, flow convergence increased on the upwind side of the centerline wake and reduced on the downwind side of the wake. The radar-imaging algorithm processed with the surface velocity field produced by the CFD model revealed ship-wake asymmetry relative to the wind direction. These results are qualitatively consistent with SAR images from the TerraSAR-X satellite and representative statistics of photographic images of the ship wake collected from a volunteer observing ship. [J405]

## "Multistatic and MIMO Distributed ISAR for Enhanced Cross-Range Resolution of Rotating Targets"

In this paper, we present a new technique to exploit the data acquired simultaneously by multiple radar sensors carried by multiple air platforms to increase the cross-range resolution of inverse synthetic aperture radar (ISAR) images of rotating targets. This distributed ISAR technique is devised for two different cases: 1) multiple-input-multiple-output (MIMO) case with each platform carrying an active radar that transmits and receives RF waveforms and 2) multistatic case with a single platform carrying an active radar (transmitting and receiving) and the remaining platforms equipped with passive sensors (namely, receiving only). The processing chain proposed for the distributed ISAR is shown, together with the results obtained against simulated ISAR data for both the MIMO and the multistatic cases. The performance analysis shows that the proposed technique is able to provide an increase of the cross-range resolution up to the number of platforms in the multistatic case and even higher in the MIMO case, if the platforms are properly located. This is of great benefit in applications where the target rotation angle is insufficient to guarantee the desired resolution. A typical case is the imaging of ship targets with rotation induced by the sea swell structure under low sea state conditions. To make the results appealing for practical application, the performance degradation is also analyzed arising from errors in the knowledge of both the target rotation motion and the acquisition geometry. Experimental data collected by a ground-based radar operating together with a rotating platform are processed by following the presented distributed ISAR technique to validate the proposed approach. [J406]

## "Imaging of Fractal Profiles"

In this paper, a model for radar images of fractal (topologically 1-D) profiles is introduced. A twofold approach is followed: on one hand, we analytically solve the problem whenever small-slope profiles are in order; on the other hand, we present a partly analytical and partly numerical setup to cope with the general-slope case. By means of the analytical approach, we evaluate in closed form both the structure function and the power density spectrum of the radar signal. An appropriately smoothed (physical) fractional Brownian model (fBm) process is employed; its introduction is justified by the finite sensor resolution. A fractal scattering model is employed. It is shown that for a fractal profile modeled as an fBm stochastic process, the backscattered signal turns out to be strictly related to the associated fractional Gaussian noise process if a small-slope regime for the observed profile can be assumed. In the analytical-numerical framework, a profile with prescribed fractal parameters is first synthesized; then, fractal scattering methods (applicable to wider slope regimes with respect to the previous case) are employed to compute the signal backscattered toward the sensor. Finally, the power density spectrum of the acquired radar image is estimated. The obtained spectra are favorably compared with the theoretical results, and a parametric study is performed to assess the overall method behavior. [J407]

## "Potentials and Limitations of Moon-Borne SAR Imaging"

Moon exploitation is among the next space mission priorities. Earth observation (EO), which is traditionally implemented on artificial lower Earth orbit satellites, can be, in principle, extended to the platform constituted by the natural Earth satellite. With this regard, we investigate the features related to the EO by a possible Moon-borne synthetic aperture radar system in terms of imaging characteristics and potential applications, as well as of expected limitations. [J408]

## "Code-Division Multiple Transmission for High-Speed UWB Radar Imaging With an Antenna Array"

The ultrawideband (UWB) radar is a promising high-resolution 3-D imaging technique for near targets. We have

developed a high-speed imaging algorithm, SEABED, for a UWB pulse radar, a key real-time imaging technology. When the algorithm is applied to UWB, antenna scanning for data acquisition takes significantly longer than calculating the SEABED algorithm itself. This presents a serious problem for the real-time application of UWB radar. In this paper, we use pseudonoise (PN) sequences as the transmitting waveforms, while the original work on the SEABED algorithm assumed impulsive short-wave pulses. Using PN sequences enables us to simultaneously transmit signals with multiple antennas, eliminating the need to scan antennas. We demonstrate that the proposed radar system works well using random sequences to suppress direct waves, which is critical in achieving high speeds for imaging. [J409]

## "Statistical Characteristics of the Global Surface Current Speeds Obtained From Satellite Altimetry and Scatterometer Data"

Near-real time ocean surface currents derived from satellite altimeter (JASON-1, GFO, ENVISAT) and scatterometer (QSCAT) data on 1deg times 1deg resolution for world oceans (60deg S to 60deg N) are available online as ldquoOcean Surface Current Analyses-Real Time (OSCAR).rdquo The probability distribution function (PDF) of the current speeds (omega), constructed from global OSCAR data from 1992 to 2008, satisfies the two-parameter Weibull distribution reasonably well, and such a PDF has little seasonal and interannual variations. Knowledge on PDF of omega will improve the ensemble horizontal flux calculation, which contributes to the climate studies. [J410]

## "Automatic Model-Based Estimation of Boreal Forest Stem Volume From Repeat Pass C-band InSAR Coherence"

C-band repeat pass interferometric synthetic aperture radar coherence can provide high-accuracy estimates of boreal forest stem volume in spite of environmental dependence. Typically, the retrieval methods require a data set of insitumeasurements for training the model linking coherence to stem volume. The drawback is the need for such data and the incapacity to take into account spatial variations of environmental conditions. Here, we demonstrate a model training method that does not require reference data. For the investigated case, the relative root mean square error of stem volume is 18% or as good as obtained using the traditional training method with insitudata. [J411]

## "Automatic Detection of Terrain Surface Changes After Wenchuan Earthquake, May 2008, From ALOS SAR Images Using 2EM-MRF Method"

A method of two-threshold expectation maximum and Markov random field is presented to automatic detection of terrain surface changes after the Wenchuan earthquake, on May 12, 2008, using multitemporal ALOS PALSAR images. As an example in the Beichuan area, three kinds of terrain surface changes, i.e., scattering enhanced, reduced, and no-changed, are automatically detected and classified. By using the tool of Google Earth, the surface change situation after the earthquake can be shown in multiazimuth views as an animated cartoon. The detection and classification are also compared with optical photographs. [J412]

## "Measurements of Dielectric Constant of Volcanic Ash Erupted From Five Volcanoes in Japan"

The dielectric properties of volcanic ash from five volcanoes in Japan were measured by using the transmission/reflection coaxial line method of a network analyzer, in a frequency range from 3 to 13 GHz. The measured permittivity of powdered ash was then converted to that of solid ash (dense rock equivalent) with the aid of effective medium theory. The values of solid-ash relative permittivities for the five volcanoes revealed that they were in a relatively narrow range. Their real part was generally in a range from five to six in magnitude, while their imaginary part was in a range from 0.08 to 0.18. [J413]

## "Genetic-Algorithm-Based Parameter Estimation Technique for Fragmenting Radar Meteor Head Echoes"

Meteoroid fragmentation presents a serious problem for Doppler estimation using Fourier transform techniques. Radar returns from multiple closely spaced bodies traveling at nearly identical speeds result in an interference pattern which makes it difficult to estimate properties of individual bodies by traditional techniques. Here, we present a genetic-algorithm-based procedure to determine the properties of the individual fragments, such as relative scattering cross section, speed, and deceleration. The radar meteor observations presented here were made using the Poker Flat (Alaska) Incoherent Scatter Radar operating at 449.3 MHz. [J414]

## "A Fast and Accurate Far-Field Pseudopolar Format Radar Imaging Algorithm"

A novel imaging algorithm to be used under the condition of having an image scene in the far field of a linear radar aperture is presented. This is an application scenario that is drastically different from those of spaceborne and airborne synthetic aperture radar (SAR) systems, which has not been properly addressed to date. The technique is particularly tailored for a stepped-frequency continuous wave (CW) or frequency-modulated CW radar. The radar aperture must be linear and can be formed either with a physical or synthetic array. With the suggested method, the radar reflectivity of the image scene is obtained through an interpolation-free series expansion, where only 2-D fast Fourier transforms of the frequency-domain backscatter data are required. The resulting image is sampled on a ldquopolarlikerdquo or pseudopolar grid, which is introduced to simplify the formulation. The main advantages of this method are its extremely low computational cost and the high accuracy of the resulting imagery. The technique is extensively validated both with numerical simulations and two ground-based SAR data sets. Last but not least, numerical simulations show that this technique can be used with an ultrawideband radar of 1 GHz of bandwidth. [J415]

## "Estimation of Sahelian-Grassland Parameters Using a Coherent Scattering Model and a Genetic Algorithm"

In this paper, the applicability of a procedure for retrieval of vegetation parameters using a coherent scattering model that considers the botanical properties of Sahelian grassland and a stochastic optimization algorithm is studied. This African vegetation is mainly composed of shrubs and grass. Since the coherent scattering model is computationally time-consuming, a simplified empirical model is constructed by fitting of simulation results obtained by the scattering model. Inputs to the empirical model are the sensitive parameters that, for the studied class of vegetation, are the soil moisture content, grass density, and grass moisture content. The model outputs are the polarimetric backscattering coefficients as a function of the incidence angle. Employing the empirical model and a genetic algorithm, a search routine is implemented to estimate the biophysical parameters of the African vegetation from a data set of backscattering coefficients. The estimation of Sahelian-grassland parameters using the set of C-band HH-polarized measured data shows that this procedure achieves good agreement with the ground-truth data. [J416]

## "A Study of UWB FM-CW Radar for the Detection of Human Beings in Motion Inside a Building"

A study of an ultrawideband frequency-modulated continuous-wave radar with an extended frequency sweep from 0.5 to 8 GHz is presented. It has been applied to through-the-wall human detection. This work presents the modeling of wall attenuation followed by real measurements. The radar system is presented, and trials of human being tracking are shown. This radar will enable large stand-off distance capabilities and dasiadasiain-depthpsilapsila building detection. [J417]

## "Empirically Adopted IEM for Retrieval of Soil Moisture From Radar Backscattering Coefficients"

The integral equation model (IEM) is considered as a promising algorithm for soil moisture retrieval from active microwave data over bare soil and sparsely vegetated conditions. However, the soil dielectric constant is implicitly embedded in the complicated IEM; inversion of soil moisture is often accomplished through iteration and is thus computationally expensive, particularly when it is applied to retrieve soil moisture from active microwave data on a large scale. To simplify the inversion process of soil moisture directly from the active microwave data, basic math functions were adopted to fit the simulation results of the original IEM so that the radar backscattering coefficient becomes an explicit function of soil dielectric constant or the soil dielectric constant is an explicit function of radar backscattering coefficient. Soil moisture is then calculated directly from radar backscattering coefficient without iteration. We called this model empirically adopted IEM (EA-IEM). The accuracy of the EA-IEM to the original IEM and its applicability are analyzed through three processes: model intercomparison, sensitivity analysis, and model comparison with insitumeasurements. The average differences of backscattering coefficients between the EA-IEM and the original IEM are 0.14 dB for HH-polarization and 0.12 dB (Gaussian correlation function) and 0.2 dB (exponential correlation function) for VV-polarization. The sensitivity of soil moisture variation is examined under the consideration of absolute and relative calibration errors. A comparison between the soil moisture estimated and the measurements is performed, and the root-mean-square (rms) error is found to be 3.4%, suggesting that the EA-IEM performs well in these real cases. All these analyses indicate that the EA-IEM is a good representative of the original IEM and can be used to retrieve soil moisture under the tested range of model parameters: incidence angles between 10degand 60--deg, soil dielectric constants between 4 and 42, surface rms height from 4 to 31 mm, and correlation length from 50 to 250 mm. [J418]

## "An Efficient Method for Performance Monitoring of Active Phased Array Antennas"

Modern synthetic aperture radars (SARs) are equipped with active phased array antennas to electronically

generate various antenna beams. The TerraSAR-X satellite is a high resolution SAR system launched in June 2007. Its active phased array X-band antenna hosts 384 transmit/receive modules (TRMs) for controlling the electronic beam steering in azimuth and elevation direction. The precise modeling of the antenna performance is only possible if the actual characteristics of each individual TRM are monitored. TerraSAR-X has been equipped with an innovative characterization mode based on a coding technique, which is the so-called pseudonoise gating method. The individual and simultaneous characterization of all TRMs is realized under most realistic conditions with power supply loads like in nominal radar operation. For the first time, this novel technique has been applied on a spaceborne SAR system. [J419]

## "Model-Based Compensation of Topographic Effects for Improved Stem-Volume Retrieval From CARABAS-II VHF-Band SAR Images"

A limiting factor that has been identified for stem-volume retrieval in coniferous forests using VHF synthetic aperture radar is that the backscatter varies depending on ground topography. On sloping ground, the backscatter from a forest is reduced, since the dominant ground-trunk double-bounce scattering mechanism is changed. This leads to underestimation of stem volume, and the variations caused by topography can obscure real variations in stem volume. By using multiple images acquired with different flight headings and combining the image information with ground-topography data in a model-based inversion method, we are able to compensate for the ground-topography influence on the backscatter. The inversion method is based on image segmentation and the optimal estimation method. Using four or more images from the CARABAS-II system and a coarse digital elevation model with 50-m horizontal grid, the stem volume can be retrieved with an average root-mean-square error (rmse) of less than 60 m3ha-1for stem volumes in range of 80-700 m3ha-1(in terms of above-ground biomass, this is equivalent to an rmse of less than 40 ton ldr ha-1over the range of 50-400 ton ldr ha-1). The retrieval accuracy is similar to that previously obtained for similar forests standing on flat and horizontal ground. [J420]

## "Exploitation of Ship Scattering in Polarimetric SAR for an Improved Classification Under High Clutter Conditions"

This paper evaluates the potentialities of polarimetric ship scattering for basing classification methods that provide reasonable performance within cluttered scenes. Both simulated and airborne polarimetric synthetic aperture radar (SAR) images have been used to validate the conclusions of a previous phenomenological study. Numerical simulations have been carried out with GRECOSAR, a polarimetric interferometric SAR simulation tool that is able to process highly complex targets with a fast and accurate radar-cross-section prediction module. A representative set of scenarios has been defined, which includes various realistic ship models, sea states, and imaging geometries. In all of them, a two-scale sea surface model precisely accounting for sea-ship interaction and sea clutter has been added. The analysis of different images has shown that, with an adequate spatial resolution, ships may be characterized by a particular spatial arrangement and polarization state distribution of dominant scattering centers. This feature has allowed one to propose a new classification algorithm, which shows a promising behavior after various preliminary tests. In this paper, the performance of this technique is further evaluated with realistic clutter. The results show that robust classification is possible even in highly cluttered scenes if quad-pol imagery is available. On the contrary, in low clutter conditions, the usage of less restrictive solutions, like circular dual-pol schemes, is feasible and may still get an acceptable performance. [J421]

## "Water Level Estimation and Reduction of Hydraulic Model Calibration Uncertainties Using Satellite SAR Images of Floods"

Exploitation of river inundation satellite images, particularly for operational applications, is mostly restricted to flood extent mapping. However, there lies significant potential for improvement in a 3-D characterization of floods (i.e., flood depth maps) and an integration of the remote-sensing-derived (RSD) characteristics in hydraulic models. This paper aims at developing synthetic aperture radar (SAR) image analysis methods that go beyond flood extent mapping to assess the potential of these images in the spatiotemporal characterization of flood events. To meet this aim, two research issues were addressed. The first issue relates to water level estimation. The proposed method, which is an adaptation to SAR images of the method developed for water level estimation using flood aerial photographs, is composed of three steps: (1) extraction of flood extent limits that are relevant for water level estimation; (2) water level estimation by merging relevant limits with a Digital Elevation Model; and (3) constraining of the water level estimates using hydraulic coherence concepts. Applied to an ENVISAT image of an Alzette River flood (2003, Grand Duchy of Luxembourg), this provides plusmn54-cm average vertical uncertainty water levels that were validated using a sample of ground surveyed high water marks. The second issue aims at better constraining hydraulic models using these RSD water levels. To meet this aim, a "traditional" calibration using recorded hydrographs is completed via comparison between simulated and RSD water levels.

This integration of the RSD characteristics proves to better constrain the model (i.e., the number of parameter sets providing acceptable results with respect to observations has been reduced). Furthermore, simulations of a flood event of a different return period (2007) using the model calibrated for the 2003 flood event shows the reliability of the latter for flood forecasting. [J422]

## "Comparison of TRMM TMI and PR Version 5 and 6 Precipitation Data Products Under Cyclonic Weather Conditions"

In 2004, the Tropical Rainfall Measuring Mission (TRMM) Science Project released a newer version of precipitation products, i.e., version 6 (V6), from its various instruments. The V6 data products are expected to be more accurate than the previous version 5 (V5). In this letter, we have attempted to analyze V5 and V6 products from two primary sensors on the TRMM, namely, the TRMM Microwave Imager (TMI) and the Precipitation Radar (PR), to unravel the quality of the V6 products vis-a-vis that of the V5 products. It is found that there are significant changes in the TMI-derived precipitation values, but the TMI brightness temperature (Tb) has not undergone any change from V5 to V6. Thus, the retrieval algorithm must have undergone some changes from V5 to V6. While the total number of TMI raining pixels is nearly unchanged, V5 moderate rain events (1-5 mm ldr h-1) are more often classified as low rain events (< 1 mm ldr h-1) in V6. Thus, TMI-based precipitation shows larger bias, particularly at low to moderate rain rates than that in V5. This results in a depression in the average Tb at around 2 mm ldr h-1in the Tb-rain-rate relationship with V6 measurements, which is implausible. This dip in average Tb value further complicates the Tb-rain-rate relationship by showing a continuous rise in Tb with rain rate, which is again implausible. On the other hand, PR-based rain rates have not undergone much change from V5 to V6. The relationship between Tb from TMI and rain rate from PR also does not show any anomalous behavior. [J423]

## "Two-Dimensional Spectrum Matched Filter Banks for High-Speed Spinning-Target Three-Dimensional ISAR Imaging"

In this letter, a 3-D inversed synthetic aperture radar imaging algorithm for targets in high-speed spinning is proposed based on 2-D spectrum matched filter (MF) banks. Each spectrum MF bank yields a focused slice for its corresponding scatterers. By extracting the spatial parameters from all slices, the 3-D image of the target can be constructed. Numeric simulation confirms the validity of the algorithm. [J424]

## "Tropical-Forest-Parameter Estimation by Means of Pol-InSAR: The INDREX-II Campaign"

This paper addresses the potential and limitations of polarimetric synthetic aperture radar (SAR) interferometry (Pol-InSAR) inversion techniques for quantitative forest-parameter estimation in tropical forests by making use of the unique data set acquired in the frame of the second Indonesian Airborne Radar Experiment (INDREX-II) campaign-including Pol-InSAR, light detection and ranging (LIDAR), and ground measurements-over typical Southeast Asia forest formations. The performance of Pol-InSAR inversion is not only assessed primarily at L- and P-band but also at higher frequencies, namely, X-band. critical performance parameters such as the ldquovisibility of the groundrdquo at L- and P-band as well as temporal decorrelation in short-time repeat-pass interferometry are discussed and quantitatively assessed. Inversion performance is validated against LIDAR and ground measurements over different test sites. [J425]

## "Potential of Estimating Soil Moisture Under Vegetation Cover by Means of PolSAR"

In this paper, the potential of using polarimetric SAR (PolSAR) acquisitions for the estimation of volumetric soil moisture under agricultural vegetation is investigated. Soil-moisture estimation by means of SAR is a topic that is intensively investigated but yet not solved satisfactorily. The key problem is the presence of vegetation cover which biases soil-moisture estimates. In this paper, we discuss the problem of soil-moisture estimation in the presence of agricultural vegetation by means of L-band PolSAR images. SAR polarimetry allows the decomposition of the scattering signature into canonical scattering components and their quantification. We discuss simple canonical models for surface, dihedral, and vegetation scattering and use them to model and interpret scattering processes. The performance and modifications of the individual scattering components are discussed. The obtained surface and dihedral components are then used to retrieve surface soil moisture. The investigations cover, for the first time, the whole vegetation-growing period for three crop types using SAR data and ground measurements acquired in the frame of the AgriSAR campaign. [J426]

## "Using a Ground-Based SAR Interferometer and a Terrestrial Laser Scanner to Monitor a Snow-Covered Slope: Results From an Experimental Data Collection in Tyrol (Austria)"

In this paper, we report on an experimental activity aimed at investigating the potential of two terrestrial remote-

sensing techniques, namely, ground-based SAR (GB SAR) interferometry and terrestrial laser scanning, in order to retrieve snow-depth (SD) measurements in mountainous regions. Terrestrial laser scanning is a more consolidated technique based on the measurement of the optical (near infrared) reflectivity, and it is affected by the surface of the snow layer: a temporal data sequence allows us to estimate the absolute SD variation. Recent use of SAR interferometry to evaluate snow-mass characteristics is based on relating the measured interferometric phase shift to a change in the snow mass. Interferometric GB SAR measurements and terrestrial laser scanner scans were collected together with pointwise conventional measurements of physical snow parameters during the winters of 2005/2006 and 2006/2007. The experiment was carried out in the Wattener Lizum, a high Alpine area at about 2000-m elevation north of the main ridge of the Austrian Alps in Tyrol. Notwithstanding the difficulty of providing both lengthy data record in dry snow conditions and detailed knowledge of the observed snow characteristics, the obtained results confirmed the presence of a clearly measurable interferometric phase variation in relation to the growing height of the snow layer. A comparison of the SD maps obtained through the two techniques shows differences partly due to the different nature of the two observations. [J427]

## "Microwave Signature of the Greenland Ice Sheet at Ku- and S-Bands"

This letter is focused on the microwave signature characterization of the Greenland ice sheet. Such characterization is carried out by exploiting the S- and Ku-band brightness temperatures measured by the radar altimeter RA-2 when it operates as a radiometer during the ENVISAT Commissioning Phase for the purpose of calibrating the receiver. Despite the poor radiometric resolution and the calibration issues, this activity represented a unique opportunity to gather brightness temperatures at frequencies that are not available from current spaceborne microwave radiometers. The analysis of the passive RA-2 data investigates the influence of terrain height and of the temperature of the snow layers on the brightness temperatures at RA-2 bands. The effect of the different penetration depths of the electromagnetic radiation at S- and Ku-bands is also pointed out. Measurements from the Advanced Microwave Scanning Radiometer for the Earth Observing System are used to complement the data provided by RA-2 and to verify their reliability. [J428]

## "A Model-Spectrum-Based Flattening Algorithm for Airborne Single-Pass SAR Interferometry"

An effective method is proposed to remove the flat-Earth phase (i.e., flattening) in airborne single-pass interferometric synthetic aperture radar (InSAR) imaging. Two conventional flattening methods, namely, the orbit-equation algorithm and the fringe-frequency algorithm, are used for comparison. The orbit-equation algorithm is theoretically accurate, but the orbit ephemeris that it requires is maybe inaccurate or even unknown. The fringe-frequency algorithm is effective in spaceborne InSAR flattening, but in airborne cases, a phase trend will remain in the residual interferogram with this method. To overcome these limitations, this letter presents a novel flattening algorithm by combining the two conventional methods for airborne single-pass InSAR flattening. By exploiting a reasonable model of the flat-Earth phase and the spectrum information of the practical interferogram, the proposed algorithm is able to flatten the interferogram accurately without knowledge of the airplane trajectory (except for the airplane height). Finally, some experimental results demonstrate the effectiveness of the proposed flattening algorithm. [J429]

## "ISAR Imaging of a Ship Target Using Product High-Order Matched-Phase Transform"

Inverse synthetic aperture radar (ISAR) imaging of a ship target is very important compared with the plane target, and the imaging condition of the ship target is more complicated than that of the plane target due to the complexity of the ship's movement. In this letter, the received signal of a ship target is modeled as a multicomponent cubic phase signal, and the product high-order matched-phase transform is proposed to estimate the parameters of each component. Then, the instantaneous ISAR images can be obtained. Results of real data demonstrate the effectiveness of the new method proposed. [J430]

## "Bathymetric Retrieval From Hyperspectral Imagery Using Manifold Coordinate Representations"

In this paper, we examine the accuracy of manifold coordinate representations as a reduced representation of a hyperspectral imagery (HSI) lookup table (LUT) for bathymetry retrieval. We also explore on a more limited basis the potential for using these coordinates for modeling other in water properties. Manifold coordinates are chosen because they are a data-driven intrinsic set of coordinates, which naturally parameterize nonlinearities that are present in HSI of water scenes. The approach is based on the extraction of a reduced dimensionality representation in manifold coordinates of a sufficiently large representative set of HSI. The manifold coordinates are derived from a scalable version of the isometric mapping algorithm. In the present and in our earlier works, these coordinates were used to establish an interpolating LUT for bathymetric retrieval by associating the representative data with ground truth data, in this case from a Light Detection and Ranging (LIDAR) estimate in

the representative area. While not the focus of the present paper, the compression of LUTs could also be applied, in principle, to LUTs generated by forward radiative transfer models, and some preliminary work in this regard confirms the potential utility for this application. In this paper, we analyze the approach using data acquired by the Portable Hyperspectral Imager for Low-Light Spectroscopy (PHILLS) hyperspectral camera over the Indian River Lagoon, Florida, in 2004. Within a few months of the PHILLS overflights, Scanning Hydrographic Operational Airborne LIDAR Survey LIDAR data were obtained for a portion of this study area, principally covering the beach zone and, in some instances, portions of contiguous river channels. Results demonstrate that significant compression of the LUTs is possible with little loss in retrieval accuracy. [J431]

## "Near Real-Time Orthorectification and Mosaic of Small UAV Video Flow for Time-Critical Event Response"

A method for real-time mosaic of video flow acquired by a small low-cost unmanned aerial vehicle (UAV) has been presented in this paper. The basic procedures of real-time mosaic are as follows: (1) Each video frame is resampled and orthorectified using a developed mathematical model, which can simultaneously solve the video camera's interior orientation parameters and the exterior orientation parameters of each video frame; (2) each orthorectified video frame is mosaicked at real time. A test field located in Picayune, Mississippi, has been established for testing our method. Sixty-minute video data were collected using the UAV and were processed using the proposed method. The results demonstrated that each video frame can be geo-orthorectified and mosaicked together to produce a 2-D planimetric mapping at near real time. Accuracy of the mosaicked video images (2-D planimetric map) is approximately 1-2 pixels, when compared to 55 checkpoints, which were measured by differential GPS surveying. [J432]

## "Recent Retreat of Wilkins Ice Shelf Reveals New Insights in Ice Shelf Breakup Mechanisms"

The disintegration of various ice shelves on the Antarctic Peninsula has demonstrated their vulnerability and impacts on tributary glaciers. A satellite image of Wilkins Ice Shelf (WIS) from July of 2007 reveals the formation of a large new double fracture, accompanied by numerous small fractures. We show that bending stresses induced by buoyancy forces were responsible for fracture formation. On February 28-29, 2008, an area of about 425 km2broke up at a narrow connection of the WIS to one of its confining islands. In contrast to Larsen B Ice Shelf, melt ponds that drain into crevasses played no role in this breakup process. A further breakup of 160 km2in the same area occurred on May 30-31, 2008 and documented that breakup can occur during austral winter. Radar images reveal a frozen surface, which demonstrates that in this breakup, surface melt water did not play a role. We conclude that ice shelves with strong thickness contrasts carry potential for disintegration. The fact that the WIS experienced two breakup events under two widely contrasting surface conditions (one during the melt season and one during winter) reveals that there may be several reasons for the disintegration of ice shelves that operate under differing circumstances. [J433]

## "Cassini RADAR Sequence Planning and Instrument Performance"

The Cassini RADAR is a multimode instrument used to map the surface of Titan, the atmosphere of Saturn, the Saturn ring system, and to explore the properties of the icy satellites. Four different active mode bandwidths and a passive radiometer mode provide a wide range of flexibility in taking measurements. The scatterometer mode is used for real aperture imaging of Titan, high-altitude (around 20 000 km) synthetic aperture imaging of Titan and Iapetus, and long range (up to 700 000 km) detection of disk integrated albedos for satellites in the Saturn system. Two SAR modes are used for high- and medium-resolution (300-1000 m) imaging of Titan's surface during close flybys. A high-bandwidth altimeter mode is used for topographic profiling in selected areas with a range resolution of about 35 m. The passive radiometer mode is used to map emission from Titan, from Saturn's atmosphere, from the rings, and from the icy satellites. Repeated scans with differing polarizations using both active and passive data provide data that can usefully constrain models of surface composition and structure. The radar and radiometer receivers show very good stability, and calibration observations have provided an absolute calibration good to about 1.3 dB. Relative uncertainties within a pass and between passes can be even smaller. Data are currently being processed and delivered to the planetary data system at quarterly intervals one year after being acquired. [J434]

## "Efficient Directional Gaussian Smoothers"

Linear and nonlinear filters, including morphological operators, play a significant role in the processing of remote sensing imagery. In particular, smoothing filters have been extensively used for noise removal and image restoration. In applications where linear and shift-invariant filters can be effectively employed, filtering is computationally efficient if implemented in transform domains. Nevertheless, in remote sensing applications, it is essential that smoothing filters be capable of handling missing and erroneous data without loss of information. In

such cases, filtering requires the involvement of logical operations in order to determine which pixels should be used for processing, and thus takes the form of a nonlinear operator. Hence, transform-based methods cannot be used. Still, in applications where large volumes of data need to be processed, it is greatly desired that fast filtering algorithms are used. This letter introduces a computationally efficient spatial-domain-based implementation which is partially separable and steerable. The technique is general, and its efficiency has been demonstrated on weather radar data. It is shown that the proposed filtering approach is significantly faster compared to a recently introduced separable filter implementation. [J435]

## "Sparse Two-Dimensional Phase Unwrapping Using Regular-Grid Methods"

Phase unwrapping is usually defined as the reconstruction of a function sampled on a spatial grid given its value modulo 2pi. Phase unwrapping is a key step in image reconstruction in many imaging techniques including interferometric synthetic aperture radar (InSAR). In recent years, many new methods have been developed to exploit the presence of coherent or persistent scattering points for extracting deformation signatures in regions where the conventional InSAR fails. These techniques often yield measurements that are only poorly sampled spatially, yet these sparse data must still be unwrapped if we are to be able to extract useful geophysical information. The conventional well-sampled 2-D phase unwrapping problem based on phase residues is fairly well understood, and many novel techniques involving geometry and network flow concepts have been implemented successfully to date. For sparse data, residues may be computed over the Delaunay triangulation of the data points, but published algorithms meet with limited success when the sparse data are unwrapped. The advantages of modern unwrapping methods applicable to well-sampled data are often lost when sparse data are analyzed. In this letter, we show that a nearest neighbor interpolation scheme allows powerful and existing 2-D solvers to be applied to sparse data. We present results using both simulated and real data sets to illustrate our method. [J436]

## "Omega-k Algorithm for Airborne Forward-Looking Bistatic Spotlight SAR Imaging"

For flexibility and cost reduction, the forward-looking bistatic spotlight synthetic aperture radar (FL-BSSAR) which uses the side-looking transmitter and the forward-looking receiver has been studied recently. For the FL-BSSAR imaging, we introduce a modified omega-k algorithm. Specifically, using rotation and shifting of the receiver path and resampling of the transmitter path, we convert the FL-BSSAR into the side-looking BSSAR. Then, we modify the matched filter and Stolt interpolation using the principle of the stationary phase to obtain the SAR image. Simulation results show that the modified omega-k algorithm enhances the image quality. [J437]

## "Rain Observations by a Multifrequency Dual-Polarized Radiometer"

During the Convective and Orographically Induced Precipitation Study, advanced microwave radiometer for rain identification has continuously acquired measurements at the Atmospheric Radiation Measurement Mobile Facility in the Black Forest from the beginning of August until December 2007. The radiometer has six channels measuring in horizontal and vertical polarizations at 10.65, 21.0, and 36.5 GHz. Rainy events have been selected out of the entire database according to collocated gauges and, subsequently, analyzed. Measured brightness temperatures and (vertical-horizontal) polarization differences are interpreted by comparing with radiative transfer simulations, which account for the presence of nonspherical particles in preferential orientation. Measurements confirm the importance of the polarization signal for separating the effect introduced by non-Rayleigh scatterers and, therefore, the rain from the cloud component. More quantitative interpretation of the signal requires a better understanding of the role played by melting particles and an identification of the 3-D structure of the precipitating system under observation. Both aspects will be tackled in the near future by exploiting the synergy with a coinstalled micro rain radar. [J438]

## "A Particle Filter Approach for InSAR Phase Filtering and Unwrapping"

This paper presents a new phase-unwrapping (PU) algorithm for SAR interferometry that makes use of a particle filter (PF) to perform simultaneously noise filtering and PU. The formulation of this technique provides independence from noise statistics and is not constrained by the nonlinearity of the problem. In addition, an enhanced variant of this method combining a PF with artificial-intelligence search strategies and an omnidirectional local phase estimator, based on the mode of the power spectral density, is also presented. Results obtained with synthetic and real data show a significant improvement with respect to other conventional unwrapping algorithms in some situations. [J439]

## "High-Resolution Three-Dimensional Imaging of Spinning Space Debris"

Since space debris could post a significant threat to orbiting objects around the Earth, their reorganization, measurement, and catalogue are of great importance. This paper establishes a 3-D inverse synthetic aperture

radar (ISAR) imaging geometry and signal model for space debris. Then, a 3-D imaging algorithm is proposed to realize coherent imaging in the range-slow-time domain. This algorithm is based on the complex-valued back-projection transform according to the spinning nature of space debris. The simulation results for both point scattering and continuous targets have proved the validity of the proposed algorithm. [J440]

## "A Matched-Filter-Bank-Based 3-D Imaging Algorithm for Rapidly Spinning Targets"

For rapidly spinning targets, such as the rotating ground radar antenna, helicopter blades, spinning space debris, etc., the scatterers on the target may rotate for several periods in the observation time. Since the range and Doppler information of these scatterers are no longer constant, the conventional range-Doppler-based imaging algorithms are invalid. Meanwhile, 3-D imaging is necessary to obtain additional information for the spinning target. However, the available interferometric inverse synthetic radar (ISAR) and snapshot 3-D imaging algorithms do not work well since they require low target spinning speed. In this paper, a matched-filter-bank-based 3-D imaging algorithm for rapidly spinning targets is proposed, based on target motion features. This algorithm utilizes the rapidly rotating turntable model of the ISAR target instead of the slow rotating one. First, 2-D image slices of the target are obtained from the output of the matched filter bank by changing matching parameters. Then, a series of 2-D image slices are combined to form the 3-D target image. Since this algorithm applies to the monostatic radar system, it is easy to implement in practical applications. Both the theoretical derivation and the simulation results have proved the validity of the proposed algorithm. [J441]

## "Focusing of Airborne Synthetic Aperture Radar Data From Highly Nonlinear Flight Tracks"

Standard focusing of data from synthetic aperture radar (SAR) assumes a straight recording track of the sensor platform. Small nonlinearities of airborne platform tracks are corrected for during a motion-compensation step while maintaining the assumption of a linear flight path. This paper describes the processing of SAR data acquired from nonlinear tracks, typical of sensors mounted on small aircraft or drones flying at low altitude. Such aircraft do not fly along straight tracks, but the trajectory depends on topography, influences of weather and wind, or the shape of areas of interest such as rivers or traffic routes. Two potential approaches for processing SAR data from such highly nonlinear flight tracks are proposed, namely, a patchwise frequency-domain processing and mosaicking technique and a time-domain back-projection-based technique. Both are evaluated with the help of experimental data featuring tracks with altitude changes, a double bend, a 90deg curve, and a linear flight track. In order to assess the quality of the focused data, close-ups of amplitude images are compared, impulse response functions of a point target are analyzed, and the coherence is evaluated. The experimental data were acquired by the German Aerospace Center's E-SAR L-band system. [J442]

## "Predicting Topographic and Bathymetric Measurement Performance for Low-SNR Airborne Lidar"

Government and commercial airborne light detection and ranging (lidar) systems have enabled extensive measurements of the Earth's surface and land cover over the past decade. There is much interest, however, in employing smaller lidar systems that require less power to enable sensing from small unmanned aerial vehicles or satellites. Technological advances in the performance of small microlasers and photodetector sensitivity have recently enabled the development of experimental airborne lidar systems with low signal-to-noise ratios (LSNRs). Recent government and academic prototypes have indicated that LSNR airborne lidars could significantly increase the fidelity of terrain reconstruction over what is possible with existing conventional lidars. Thus, there is a need to build up a modeling capability for such systems in order to aid in future system and mission design. A numerical sensor simulator has been developed to model the expected returns from LSNR microlaser altimeter systems and predict their performance. Both optical and signal processing system components are considered, along with other factors, including atmospheric effects and surface conditions. Topographic (solid Earth) and bathymetric (littoral zone) measurement scenarios are considered. The analysis of topographic simulation data focuses on the effect of solar noise on SNR and elevation accuracy while bathymetric performance is evaluated with regard to water depth and scan angle for different water clarities. The mission conditions chiefly responsible for limiting the performance of LSNR lidar are discussed in detail, along with suggestions for further algorithm development and system performance evaluation. [J443]

## "Characteristic Polarization States Estimation in an Ultrawideband Context: A Frequency Approach"

The concept of characteristic polarization states (CPSs) is extended to an ultrawideband (UWB) context. This is achieved by a sparse representation of the target UWB scattering spectrum by a set of frequency bands associated with the target natural resonance modes. The polarization description involves using the average power within each resonant frequency band to derive the Kennaugh power matrix and, subsequently, a set of CPSs using the Lagrangian optimization procedure. To validate this, preliminary feature sets are formed by extracting robust information from each derived CPS and then implementing a correlation measure criterion from

which the relationships between these preliminary feature sets as a function of resonance order are established. These relationships are invariant to range and target orientation about the radar-target direction and are robust to noise. [J444]

## "Narrow-Band Interference Suppression for SAR Based on Complex Empirical Mode Decomposition"

Narrow-band interference (NBI) is a common interference source in synthetic aperture radar (SAR) imaging. Its existence will degrade the imaging quality greatly. Based on detailed analysis on the characteristics of NBI, this letter proposes a new NBI suppression algorithm using the complex empirical mode decomposition (CEMD) method. In this algorithm, echoes that include NBI are recognized in the time domain first. Then, these echoes are decomposed into a number of intrinsic mode functions (IMFs) via the CEMD. After that, IMFs that correspond to NBI are subtracted from the echoes by thresholding. Finally, well-focused SAR imagery can be obtained from the separated target echoes using traditional SAR imaging algorithms. The effective data loss in this algorithm is smaller than other NBI suppression approaches. In addition, this algorithm is robust to time-varying NBI. Imaging results of measured data have proved the validity of this algorithm. [J445]

## "SAR Images of Rooms and Buildings Based on FDTD Computer Models"

This paper presents synthetic aperture radar (SAR) images of rooms and buildings based on numerical simulations, with application to sensing through the wall (STTW) scenarios. We use the finite-difference time-domain modeling technique to compute the radar return from configurations of increasing complexity, where humans and furniture objects are placed in a room. We apply SAR image formation techniques and analyze the images obtained for various wall materials, aspect angles, and radar parameters. We investigate the multipath propagation issues relevant to STTW imaging radar and discuss the radar parameter tradeoff based on image quality. We also look at images obtained in cross-polarization, demonstrating how this radar operational mode can achieve significant clutter rejection. The phenomenological results obtained in this paper can be used as guidance by radar engineers in order to optimize the performance of STTW SAR imaging systems. [J446]

## "High-Frequency EM Characterization of Through-Wall Building Imaging"

A high-frequency asymptotic technique based on the Uniform Geometric Theory of Diffraction (UTD) is employed for building interior imaging. The analysis is implemented using a ray-tracing technique to account for multiple scattering interactions in a building, along with a set of heuristic diffraction coefficients for dielectric wedges and corners. Imaging of the synthetic aperture radar data is carried out by the conventional fast Fourier transform method to transform to the downrange domain, and combined with a coherent near-zone imaging function for cross-range. Comparisons with experimental data for a scaled-down building model are given to demonstrate the suitability and efficacy of our analysis for through-wall building imaging. The UTD ray mechanisms account for the dominant scattering features observed in the image. [J447]

## "A Time-Series Approach to Estimate Soil Moisture Using Polarimetric Radar Data"

Electromagnetic scattering from a rough surface is a function of both surface roughness and dielectric constant of the scattering surface. Therefore, in order to estimate soil moisture of a bare surface accurately from radar measurements, the effects of surface roughness must be compensated for properly. Several algorithms have been developed to estimate soil moisture from a polarimetric radar image, all with limited ranges of applicability. No theoretical algorithm has been reported to retrieve volumetric soil moisture of a vegetated surface. In this paper, we examine a different approach to estimate soil moisture that exploits the fact that the backscattering cross section from a natural object changes over short timescales mainly due to variations in soil moisture. We develop a model function that expresses copolarized backscattering cross sections (sigmahhand sigmavv) in terms of volumetric soil moisture using L-band experimental data for both bare and vegetated surfaces. In order to estimate soil moisture, two unknowns in the model function must be determined. We propose a viable approach to determine these two unknowns using combined radiometer and radar data. This time-series approach also provides a framework to utilize aprioriknowledge on soil moisture to improve the retrieval accuracy of volumetric soil moisture. We demonstrate that this time-series algorithm is a simple and robust way to estimate soil moisture for both bare and vegetated surfaces. [J448]

## "On the Combination of Multisensor Data Using Meta-Gaussian Distributions"

With the ever-increasing number and diversity of Earth observation satellites, it steadily becomes more important to be able to analyze compound data sets consisting of different types of images acquired by different sensors. In this paper, we examine different ways of obtaining joint distributions of such images, and we propose a method that enables incorporation of correlations between images while keeping a good fit to the marginal distributions.

The approach basically consists of two steps. First, the marginal densities are specified. Based on this specification, each marginal variable is transformed to a normal distributed variable. The joint distribution of the transformed variables is assumed to be multivariate normal. Transforming back to the original scale gives a joint distribution with dependence, where the initial marginal distributions are preserved. The parameters of the new joint distribution can be estimated. The focus is on marginal distributions that are Gamma, K, or Gaussian, although any distribution could be considered. The joint distributions produced by the transformation method can be used in supervised classification of radar and optical images. Results obtained for a set of four-look synthetic aperture radar (SAR) images, as well as a combination of SAR and optical images, are presented. [J449]

## "Impact of Hillslope-Scale Organization of Topography, Soil Moisture, Soil Temperature, and Vegetation on Modeling Surface Microwave Radiation Emission"

Microwave radiometry will emerge as an important tool for global remote sensing of near-surface soil moisture in the coming decade. In this modeling study, we find that hillslope-scale topography (tens of meters) influences microwave brightness temperatures in a way that produces bias at coarser scales (kilometers). The physics underlying soil moisture remote sensing suggests that the effects of topography on brightness temperature observations are twofold: 1) the spatial distribution of vegetation, moisture, and surface and canopy temperature depends on topography and 2) topography determines the incidence angle and polarization rotation that the observing sensor makes with the local land surface. Here, we incorporate the important correlations between factors that affect emission (e.g., moisture, temperature, and vegetation) and topographic slope and aspect. Inputs to the radiative transfer model are obtained at hillslope scales from a mass-, energy-, and carbon-balance-resolving ecohydrology model. Local incidence and polarization rotation angles are explicitly computed, with knowledge of the local terrain slope and aspect as well as the sky position of the sensor. We investigate both the spatial organization of hillslope-scale brightness temperatures and the sensitivity of spatially aggregated brightness temperatures to satellite sky position. For one computational domain considered, hillslope-scale brightness temperatures vary from approximately 121 to 317 K in the horizontal polarization and from approximately 117 to 320 K in the vertical polarization. Including hillslope-scale heterogeneity in factors effecting emission can change watershed-aggregated brightness temperature by more than 2 K, depending on topographic ruggedness. These findings have implications for soil moisture data assimilation and disaggregation of brightness temperature observations to hillslope scales. [J450]

## "Polarimetric Backscattering Coefficients of Flooded Rice Fields at L- and C-Bands: Measurements, Modeling, and Data Analysis"

The polarimetric backscattering coefficients (vv-, hh-, hv-, and vh-polarizations) of a flooded rice field are measured using L- and C-band ground-based polarimetric scatterometers. These measurements were made during the rice growth cycle, i.e., from the transplanting period to the harvest period (May to October 2006), to understand the feasibility of modeling and estimating rice growth. We also collected ground truth data that include fresh and dry biomasses, plant height, leaf area index, and leaf size. To study the incidence angle effect, the scatterometer data were collected at four different incidence angles, i.e., 30deg, 40deg, 50deg, and 60deg. In this paper, we show that the backscattering coefficients of a rice field can accurately be modeled using the radiative transfer theory. We also demonstrate that a polarimetric scatterometer is an effective tool for estimating rice growth. The hh-polarized backscattering coefficient is more sensitive to rice growth than its vv-polarization counterpart. The polarimetric ratio can be used to estimate rice growth accurately. [J451]

## "Assessment of Glacier Volume Change Using ASTER-Based Surface Matching of Historical Photography"

Glaciated regions are known to be particularly sensitive to climate change. Historical archives of glacier volume change are important, as they provide context for present-day changes. Although photogrammetric archives exist for many regions, their usefulness is often limited by a lack of contemporary ground control. High quality digital elevation models (DEMs) underpin a range of change analysis activities. This paper presents a cost-effective solution which utilizes Advanced Spaceborne Thermal Emission and Reflection Radiometer (ASTER) DEMs as control for the scaling and orientation of archival data sets. Instead of relying upon ground-control points, a robust surface matching algorithm is employed to automatically determine the transformation required to register two overlapping DEMs. Through application to the Slakbreen glacier system in Svalbard, Norway, the strategy is assessed by first matching an ASTER DEM to a fixed lidar reference surface. This demonstrates that ASTER DEMs are effectively correct in scale, supporting their use as a control surface. The second stage of the research implements this by matching an aerial photogrammetric DEM to an ASTER reference surface. Resultant volumetric and annual elevation change rates are compared to those derived from lidar data, which are considered in this paper as a truth data set. ASTER-based matching produced a mean annual elevation change rate of -4.12 ma-1, compared to a value of -4.11 ma-1derived from the lidar data. In volumetric terms, this

equates to a difference of 0.6%. A major advantage of this approach is the near-global coverage offered by ASTER data and the opportunity that this presents for remote glacial change analysis over regional extents. [J452]

## "Radar Volume Backscatter From Spatially Extended Geophysical Targets in a "Slice" Approach"

This paper presents an assessment of the radar backscatter from a spatially extended geophysical target (SEGT) based on a semiempirical (SE) model. An SEGT is any geophysical object that is at least semitransparent to radar illumination (clouds, rain, snowfall in the atmosphere, thick snow cover of the ground). The existing SE model does not take into account the statistical properties of the SEGT's media. To improve the SE model, a so-called ldquoslicerdquo approach is applied. In this approach, the particles located close to the wavefront of the radar illumination are assumed to produce backscatter that is mainly coherent. This method allows the contribution of the microphysical parameters of the scattering media to the volume component of the radar cross section to be described more comprehensively than the SE model based on the incoherent approach. It is shown that the slice concept results in the original SE model in the particular case when the particle number fluctuation within the slices pertains to the Poisson law. [J453]

## "Target Detection in Single- and Multiple-View Through-the-Wall Radar Imaging"

A detector of targets behind walls and in enclosed structures is presented. The detector is applied to through-the-wall radar images obtained by wideband delay and sum beamforming. We consider the detection problem using single- and multiple-view imaging. The statistics of noise, clutter, and target images are examined and formulated using sample scenes. The effects of wall parameter errors on the image statistics are shown. An iterative detection scheme, which adapts itself to the image statistics, is presented. The proposed detection schemes are evaluated using real data. [J454]

## "A Comparison of the Impact of QuikScat and WindSat Wind Vector Products on Met Office Analyses and Forecasts"

Several studies have demonstrated that retrievals of wind vectors from the WindSat polarimetric radiometer are of sufficient quality to be considered for assimilation in operational numerical weather prediction models. In this paper, WindSat data are used in a state-of-the-art global meteorological analysis and forecasting system. Each wind vector contains a directional ambiguity and so is assimilated in a similar way to that of scatterometer data. The forecast impact of using analyses containing information from WindSat data was investigated for a period during August and September of 2005, when a large number of tropical cyclones were present. Forecast errors were reduced in the surface pressure fields, and the average improvement across the forecast range was found to be 1.0%. This is comparable to the improvement of 1.1% found in the same fields when winds were assimilated from the QuikScat scatterometer. The impact on tropical cyclone tracks in the forecasts was also studied. The scatterometer improved (reduced) the track errors markedly by 25% in the analyses. When impacts across the forecast range out to five days were also included, the improvement was found to be 8%. In contrast, the assimilation of WindSat data improved the analysis track errors by 7%, although this figure was found to be 10% across the complete forecast range. [J455]

## "Focusing Spaceborne/Airborne Hybrid Bistatic SAR Data Using Wavenumber-Domain Algorithm"

This paper focuses on the bistatic synthetic aperture radar (SAR) data processing in a spaceborne/airborne hybrid bistatic configuration. Due to the extreme differences in platform velocities and slant ranges, the airborne system operates in the inverse sliding-spotlight mode, while the spaceborne system works in the sliding-spotlight mode to achieve a tradeoff between azimuth scene size and azimuth resolution. In this extreme bistatic configuration, our original bistatic formula shows a limitation of accurately describing the bistatic point-target reference spectrum, owing to the assumption of equal contributions of transmitter and receiver to the total Doppler spectrum. We extend our previous formula using the weighting operation where the weighting factor is the ratio of the azimuth time-bandwidth product (TBP) of the platform to the total azimuth TBP. In this paper, the bistatic-deformation and azimuth-dependent range-cell-migration terms were removed with phase multiplications performed blockwise in range-azimuth subsections. The remaining quasi-monostatic term shows the characteristic of the conventional monostatic SAR besides an additional azimuth-scaling term. For the monostatic characteristic, any precision monostatic SAR processing algorithms can handle. In this paper, we prefer the wavenumber-domain algorithm (also known as Omega-K), since it can accurately correct the range dependence of the range-azimuth coupling, as well as the azimuth-frequency dependence. For the azimuth-scaling term, an inverse scaled Fourier transformation is performed to correct it. Finally, a hybrid spaceborne/airborne simulation experiment is conducted to validate the proposed processing procedure. [J456]

## "Special Issue on Remote Sensing of Building Interior"

The 15 papers in this special issue focus on remote sensing of building interior and can be categorized into: 1) system design and instrumentation; 2) advanced imaging techniques for elimination of glint from large flat wall structures; 3) radar polarimetry; 4) passive microwave radiometry; 5) advanced forward models based on high-frequency methods as well as full-wave solutions based on finite-difference time-domain technique for large-scale problems; and 6) detection and identification techniques of behind the wall stationary and moving concealed and unconcealed targets. [J457]

## "The Two-Scale BPM Scattering Model for Sea Biogenic Slicks Contrast"

Sea oil slick observation by means of synthetic aperture radar is still a scientific and operational challenge. In this paper, the sea surface scattering with and without biogenic slicks is analyzed by using the two-scale Boundary Perturbation Method scattering model. The surface slick is supposed to modify both the full-range sea surface spectrum and the slope probability density function by means of the Marangoni damping and by a reduced friction velocity. In this paper, the full-range Universite Catholique de Louvain sea surface spectrum is considered. A new contrast model, which overcomes the drawbacks of the contrast model based on the untilted Small Perturbation Method scattering model, is presented and illustrated in some L- and C-band biogenic slick cases. [J458]

## "Comparison of SAR-Based Snow-Covered Area Estimation Methods for the Boreal Forest Zone"

Spaceborne synthetic aperture radar data have been utilized for regional-scale snow-covered area (SCA) monitoring for several years. Different methods have been developed and demonstrated for different geographical regions. A method utilizing a single reference image for SCA estimation has been shown to function well on mountainous and nonforested regions. For the boreal forest zone, a method using two reference images and a forest compensation procedure has been previously utilized. The single-reference-image method is evaluated here for the boreal forest zone, and its performance is compared with the Helsinki University of Technology (TKK) SCA method that is specifically developed for boreal forest regions. The SCA evaluations are carried out using Radarsat-1 data for the snow-melt seasons of 2004-2007. The SCA estimation accuracies for the radar-based methods are determined using optical satellite-based SCA data as reference. The results show that SCA estimation using a single reference image is usable for the boreal forest zone, although the accuracy is significantly weaker than that of the TKK-developed boreal forest-specific SCA method. The best accuracy obtained shows a root-mean-square error (rmse) of 0.176 for the single-reference-image method and an rmse of 0.123 for the TKK SCA method. [J459]

## "Through-the-Wall Imaging Using Differential SAR"

An algorithm for imaging of targets behind walls is proposed to reduce the wall reflection and enhance the signal-to-clutter ratio. The image formation is based on differential synthetic-aperture-radar image formation employing a continuous-wave radar system. In this approach, instead of using individual backscattered signals, the image is formed by employing the difference signals obtained by subtracting two successive signals along the track. This way, specular reflections are totally eliminated without the need for the knowledge of the wall parameters. This also affects the point target response which is corrected by an integration process. By using backscattered fields from small trihedral corner reflectors behind a poured concrete wall, measured over a frequency band of 1-2.5 GHz, the proposed method is demonstrated. [J460]

## "Cloud and Rain Effects on AltiKa/SARAL Ka-Band Radar Altimeter-Part II: Definition of a Rain/Cloud Flag"

The main instrument of the French-Indian AltiKa/SARAL mission scheduled for launch in 2010 is the Ka-band AltiKa altimeter. The high attenuation due to atmospheric water (liquid or vapor) at this frequency band is the major drawback of the use of Ka-band. In part I of this paper, the impact of rain/clouds on Ka-band data and on the accuracy of the estimates of the geophysical parameters has been analyzed and quantified using an analytical model of waveform. Waveform distortion and errors on the geophysical parameters can be significant particularly for small dense clouds and rain cells. It is thus necessary to flag the data potentially affected by rain and clouds. The use of a single channel for AltiKa prevents the use of the classical dual-frequency rain flag used for Topex or Jason altimeters, and requires the definition of a new flag based on the altimeter signal alone. Past studies showed that clouds and rain are characterized by sharp coherent along-track fluctuations of the off-nadir angle estimates. The new flagging algorithm is based on the analysis of the variations of this parameter by the Matching Pursuit (MP) algorithm. MP allows the decomposition of a signal into a few salient features or atoms chosen from a dictionary of elementary functions. The dictionary is here defined by the wavelet decomposition of

the signal. The method has been tested on an ensemble of AltiKa passes simulated for cloudy, rainy, and cloud/rain-free situations. The false alarm rate is almost nil while the detection performances are better than 90% at a range error of 5 cm and significant wave height error of 20 cm. The flag can easily be adapted to other altimeters' data and has been used to flag several Jason-1 passes. The comparison to the operational dual-frequency flag shows that the MP flag performs better in detecting range errors and waveforms distortion, while its performances are inferior in detecting samples attenuated by rain. [J461]

## "Cloud and Rain Effects on AltiKa/SARAL Ka-Band Radar Altimeter-Part I: Modeling and Mean Annual Data Availability"

The AltiKa project, developed by the French Centre National d'Etudes Spatiales, is based on a wideband Ka-band altimeter (35.75 GHz). The technical characteristic of the instrument will offer higher performance both in terms of spatial and vertical resolutions that will lead to the improved observation of ice, coastal areas, inland waters, and wave height. An Indian Space Research Organization satellite, called Satellite with ARgos and AltiKa, will embark the AltiKa altimeter. The launch is scheduled at the end of 2010. The major drawback of Ka-band use is the attenuation of the radar signal by atmospheric liquid water. Clouds and rain effects will thus be a strong constraining factor, because the altimeter link budget imposes an attenuation of less than 3 dB. The impact of rain and clouds on Ka-band altimeter data is analyzed and quantified using an analytical model that computes AltiKa waveforms in the presence of rain or clouds. The results are then used to quantify the waveform attenuation and distortion, as well as the error induced on the altimeter geophysical parameter estimates. Because of the nonlinearity of attenuation relations, the impact of clouds/rain depends more on the cloud/rain variability within the altimeter footprint than on the mean characteristics, which makes correction using coincident rain or cloud data difficult. Small rain cell and small dense clouds can thus strongly distort the waveforms and lead to erroneous geophysical parameter estimates. The probability of 20 Hz and 1-s averaged data loss are computed from the model results and from cloud and rain climatologies. On a global scale, about 3.5% of the 20-Hz data will be lost because of rain and clouds and 2.5% of the 1-s averaged data. However, the probability strongly varies over the global ocean and can exceed 10% in the Tropics. [J462]

## "Optimizing Information From the Jason-2 Altimeter"

A radar altimeter's normalized backscatter, sigma0, is used in many oceanographic applications to infer values of wind speed, wind stress, rain rate, and the presence of biogenic slicks. The waveform retracker used to estimate the key geophysical variables for the altimeters on the Jason-1 and Jason-2 satellites shows increased small-scale variability since the problem is ill-conditioned. A simple empirical adjustment to sigma0improves the separability between various parameters and also improves the along-track profiles of sigma0. This leads to the following: 1) more realistic wind fields; 2) better discrimination of rain events; and 3) improved comparison between the Jason-1 and Jason-2 altimeters during their tandem mission. [J463]

## "Polarimetric Dual-Baseline InSAR Building Height Estimation at L-Band"

This letter generalizes a multibaseline interferometric synthetic aperture radar (InSAR) signal model to the polarimetric scenario. Based on this formulation, two high-performance spectral analysis techniques are adapted to process multibaseline Pol-InSAR observations. These new methods enhance the height estimation of scatterers by calculating optimal polarization combinations and allow the determination of their physical characteristics. Applying the proposed algorithms to urban environments, the building layover problem is analyzed by means of polarimetric dual-baseline InSAR measurements: the ground and building height are estimated. The techniques are validated using dual-baseline Pol-InSAR data acquired by DLR's Experimental SAR (E-SAR) system over Dresden city. [J464]

## "Characterizing L-Band Scattering of Paddy Rice in Southeast China With Radiative Transfer Model and Multitemporal ALOS/PALSAR Imagery"

Rice is a major food supply in southeast China. With increased population and urbanization, reliable rice mapping is critical in this region. Because of frequent cloud cover and precipitation during the rice-growing season, it is difficult to conduct large-area rice monitoring with optical remote sensing techniques. L-band synthetic aperture radar (SAR), with its all-weather day and night imaging and canopy penetration capabilities, provides a unique alternative. In this study, a first-order radiative transfer model was developed to simulate L-band scattering properties of paddy rice. Three Advanced Land Observing Satellite (ALOS)/Phased-Array-Type L-band Synthetic Aperture Radar (PALSAR) images in dual-polarization mode (HH and HV) acquired in early tillering (June 28, 2007), tillering (August 13, 2007), and heading (September 28, 2007) stages were processed to test the temporal variation of rice backscatter. It was found that plant height and leaf mass amount were the two major structural parameters that contributed to rice backscatter in PALSAR images. The variation of the

simulated HH backscatter matched with PALSAR observations in sample fields, although the simulated backscatter coefficients were around 3 dB lower than image-extracted values. Leaf volume scattering and leaf-ground double bounce were found as the two major scattering components in L-band HH polarization and increased with leaf layer height and density. This paper demonstrated that L-band HH backscatter was more sensitive to rice's structural variation than the VV backscatter and may therefore be more useful in rice mapping and modeling studies. [J465]

## "Spaceborne Spotlight SAR Interferometry With TerraSAR-X"

Recently, synthetic aperture radar (SAR) data with 1-m resolution acquired by satellites in spotlight mode became available to the public. In this paper, we elucidate the differences between interferometric processing of strip map and of spotlight SAR data, and we outline adequate algorithms for key processing steps such as azimuth Doppler filtering. We further present first TerraSAR-X spotlight interferograms, together with an evaluation of the paraeters that are critical for interferometry. Our results indicate a very good geometric accuracy, stability, and phase fidelity of the TerraSAR-X sensor and its products. From the interferograms, we are able to determine the heights of larger buildings and millimeter-scale structural deformation in several examples. The high detail level of imaged buildings and the good temporal phase coherence of urban areas in X-band make spotlight interferometry an exciting processing technique that enables new applications such as surveying individual buildings. [J466]

## "Human Activity Classification Based on Micro-Doppler Signatures Using a Support Vector Machine"

The feasibility of classifying different human activities based on micro-Doppler signatures is investigated. Measured data of 12 human subjects performing seven different activities are collected using a Doppler radar. The seven activities include running, walking, walking while holding a stick, crawling, boxing while moving forward, boxing while standing in place, and sitting still. Six features are extracted from the Doppler spectrogram. A support vector machine (SVM) is then trained using the measurement features to classify the activities. A multiclass classification is implemented using a decision-tree structure. Optimal parameters for the SVM are found through a fourfold cross-validation. The resulting classification accuracy is found to be more than 90%. The potentials of classifying human activities over extended time duration, through wall, and at oblique angles with respect to the radar are also investigated and discussed. [J467]

## "Automatic Analysis of GPR Images: A Pattern-Recognition Approach"

In this paper, we propose a novel pattern-recognition system to identify and classify buried objects from ground-penetrating radar (GPR) imagery. The entire process is subdivided into four steps. After a preprocessing step, the GPR image is thresholded to put under light the regions containing potential objects. The third step of the system consists of automatically detecting the objects in the obtained binary image by means of a search of linear/hyperbolic patterns formulated within a genetic optimization framework. In the genetic optimizer, each chromosome models the apex position and the curvature associated with the candidate pattern, while the fitness function expresses the Hamming distance between that pattern and the binary image content. Finally, in the fourth step, the problem of the recognition of the material type of the identified objects is approached as a classification issue, which is solved by means of an opportune feature-extraction strategy and a support vector machine classifier. To illustrate the performances of the proposed system, we conducted a thorough experimental study based on GPR images generated by a GPR simulator based on the finite-difference time-domain method so as to construct different acquisition scenarios by varying the number of buried objects, their position, their size, their shape, and their material type. In general, the obtained experimental results show that the proposed system exhibits promising performances both in terms of object detection and material recognition. [J468]

## "Through-the-Wall SAR Attributed Scattering Center Feature Estimation"

We consider characterization of building interior structure from two-pass interferometric circular synthetic aperture radar data. We model returns from complex building structures as the sum of the responses from scattering primitives-plates, dihedrals, and trihedrals-observed through transfer functions that characterize both the transmission through and reflection from dielectric surfaces. Maximum-likelihood estimates for the location of primitive features and wall propagation/reflection parameters are obtained through a two-stage detection-and-estimation algorithm. We employ a sparse reconstruction algorithm to detect primitive signatures in the presence of wall effects and refine our estimates using a nonlinear minimization of local cost functions. We show that using simplified wall and primitive models, we can extract geometrically relevant features which can be combined to reveal 3-D floorplan estimates of buildings. Examples illustrate the effectiveness of the feature extraction

approach. [J469]

## "Intercomparison of Ground-Based Radar and Satellite Cloud-Top Height Retrievals for Overcast Single-Layered Cloud Fields"

The objective of this paper is to assess the accuracy of the Semi-Analytical CloUd Retrieval Algorithm (SACURA) that retrieves cloud-top heights (CTHs) using hyperspectral SCanning Imaging Absorption spectroMeter for Atmospheric CHartographY (SCIAMACHY) onboard Environmental Satellite measurements for overcast single-layer cloud fields. Intercomparisons with ground-based 35-GHz millimeter wave cloud radar CTHs were performed for 14 dates during 2003-2007 at the U.S. Atmospheric Radiation Measurement (ARM) program Southern Great Plains site (36.6deg N, 97.5deg W). In addition, for some of these dates, European Space Agency MEdium Resolution Imaging Spectrometer (MERIS) and the NASA-TERRA Moderate Resolution Imaging Spectroradiometer (MODIS) cloud-top pressure retrievals were also collected, transformed into CTHs using nearby ARM radiosonde profiles, and compared with the SACURA SCIAMACHY and radar retrievals. The accuracy of the SACURA-SCIAMACHY CTH retrievals is better than 0.34 km for low-level clouds and 2.22 km for high-level clouds with an underestimate in CTH on average for all clouds. The average bias in SCIAMACHY CTHs was about 0.07 km for low clouds and about 0.5 km for high-level clouds. Both MODIS and MERIS slightly overestimated the CTHs of low-level clouds by 300 m, with an uncertainty better than 1 km. However, although MODIS accuracy for high-level clouds is close to SCIAMACHY, MERIS CTHs were significantly underestimated for these fairly optically thick cases. [J470]

## "Separation of Ground and Low Vegetation Signatures in LiDAR Measurements of Salt-Marsh Environments"

Light detection and ranging (LiDAR) has been shown to have a great potential in the accurate characterization of forest systems; however, its application to salt-marsh environments is challenging because the characteristic short vegetation does not give rise to detectable differences between first and last LiDAR returns. Furthermore, the lack of precisely identifiable references (e.g., buildings, roads, etc.) in marsh areas makes the registration and bias correction of the LiDAR data much more difficult than in conventional urban- or forested-area applications. In this paper, we introduce reliable methods to remove random and systematic errors and to register raw data, as well as a new procedure, to determine the optimal filter window size to separate ground and canopy returns. A limited amount of field observations is used to determine the size of the filtering window which produces the minimally biased estimates of the digital terrain model (DTM). The digital surface model (DSM, representing the canopy top) is then obtained in a similar manner, and the digital vegetation model (DVM, representing the vegetation height) is computed as the difference between the DSM and the DTM. We apply this procedure to a study marsh within the Venice Lagoon, Italy, and obtain a high-accuracy DTM. The error (z_LiDAR-z_field) is 2.2 cm, with a standard deviation of 6.4 cm. The comparison of the estimated DVM with field observations shows an underestimation of the height of the canopy top (17.7 cm, on average). The height of the lowest canopy elements (e.g., basal leaves), however, is significantly correlated to the LiDAR-derived DVM, showing that this contains useful information on the canopy structure. [J471]

## "Development and Implementation of a Real-Time See-Through-Wall Radar System Based on FPGA"

This paper presents the development of a low-cost real-time ultrawideband (UWB) see-through-wall (STW) imaging radar system. The designs of the microwave front end, the UWB data acquisition, and the system integration are discussed in detail. As for the most challenging task, the UWB data acquisition, we introduce a custom low-cost module based on commercial field-programmable gate array (FPGA) boards and low-speed analog-to-digital converters. The introduced module does not require a custom implementation of high-speed wideband mixed-signal circuitry but only depends on the FPGA firmware design, which favors a rapid system prototyping. The data acquisition module accomplishes a 100-ps equivalent-time sampling resolution at 100-Msamples/s real-time rate, while the developed STW system provides a 2-D real-time view of motion with a 1.5-ms speed behind walls. The system allows for an easy reconfiguration to support multiple operating frequency ranges, pulse sampling resolutions, and array deployments, thus providing a tremendous experimental flexibility. Our studies indicate that utilizing available technologies and off-the-shelf components could produce a practical stand-alone STW system at reasonable design effort and cost, which will lead to a better understanding of the challenging problems associated with STW technology. [J472]

## "Phenomenological Vessel Scattering Study Based on Simulated Inverse SAR Imagery"

This paper presents a study on the origin of the dominating scattering mechanisms observed in polarimetric synthetic aperture radar (SAR) images of ships. The study has been made by using numerical simulations, which

have been carried out with a radar cross section (RCS) prediction tool (GRaphical Electromagnetic COmputing) and a SAR simulator. Extensive series of simulations has been run for realistic 3-D geometrical models of ships with various sizes. Different radar parameters, aspect angles, and sea surface states have been considered in the scenario. Data analysis with coherent target decompositions has indicated characteristic polarimetric signatures for particular ships within a specific range of viewing angles. This happens at highly oblique incidences where the responses appear to be less sensitive to changes in the operating frequency and bearing angles. Under such conditions, ship scattering can be schematized by the distribution of a set of guide scatterers with high RCS. Their positions and polarimetric characteristics are quantitatively summarized in a new feature vector, which has been proposed to be the basis for classification algorithms. Key ideas about this vector are presented at the end of this paper, jointly with some examples related to three different ships. Recent publications have shown that they can be successfully cast within a new unsupervised vessel classification scheme. [J473]

## "Polarization Symmetric Scatterer Metric Space"

The coherent polarization scattering matrix decomposition presented in Cameron et al. brought attention to the importance of Symmetric Scatterer Space, the space of scattering matrices corresponding to symmetric scatterers. Each symmetric scatterer scattering matrix can be associated with a complex number z, the scatterer-type parameter, where |z| les 1. A distance measure, d(z1, z2), was defined on Symmetric Scatterer Space providing a means of comparing scattering matrices. It will be demonstrated that Symmetric Scatterer Space is a metric space with metric d(z1, z2). A new mapping of the Unit Disc representation of Symmetric Scatterer Space to a sphere is also presented along with a metric on the sphere, ds(thetas1, phi1; thetas2, phi2), that is equivalent to the metric d(z1, z2) on the Unit Disc. [J474]

## "Windowed Fourier Transform for Noise Reduction of SAR Interferograms"

In this letter, since these methods are able to process signals locally, two spatial frequency analyses including windowed Fourier transform and wavelet transform are used to reduce synthetic aperture radar interferometric phase noise. [J475]

## "Estimation of Surface Roughness Parameter in Intertidal Mudflat Using Airborne Polarimetric SAR Data"

The coastal zones of the Korean peninsula are well known for their large tide ranges and vast expanse of intertidal flats. In this paper, methods of extracting the roughness of the scattering surface of intertidal mudflats from polarimetric synthetic aperture radar (SAR) data have been investigated. The L-band NASA/Jet Propulsion Laboratories airborne SAR data, which were acquired in the intertidal zone during PACRIM-II Korea campaign, were used to estimate the roughness of intertidal mudflats. Surface roughness can be utilized as a useful parameter to monitor the fishery activities in intertidal flats as well as the changes in textural characteristics of surface sediments. In order to retrieve roughness parameters, such as the rms height and the correlation length, of intertidal mudflats, three types of roughness inversion algorithms, based on the Integral Equation Method (IEM), semiempirical, and extended-Bragg models, have been investigated and developed. The inversion algorithms based on the IEM and semiempirical models can be applied to the dual-polarized SAR, while the extended-Bragg model-based inversion approach is also applicable to the fully polarimetric SAR observations. Results indicate the fully polarimetric approach is more pertinent to monitor geophysical parameters from space than the dual polarimetric approach, even if it is possible to reduce the number of unknown surface variables in the specific case of inversion problems. [J476]

## "Foreword to the Special Issue on Retrieval of Bio- and Geophysical Parameters From SAR Data for Land Applications"

This IEEE Transactions on Geoscience and Remote Sensing (TGRS) special issue is dedicated to the advances in synthetic aperture radar (SAR) techniques and applications presented at the 5th International Symposium on Retrieval of Bio- and Geophysical Parameters from SAR Data for Land Applications (BioGeoSAR), which was organized by Consiglio Nazionale delle Ricerche, with active support from the European Space Agency, and held in Bari, Italy, on September 25-28, 2007. The purpose of the symposium has been to provide a forum for researchers to review current trends in the field of retrieval of quantitative information from SAR data and to present and discuss new ideas and new research directions. The BioGeoSAR symposia are usually held every three years in Europe with worldwide participation. [J477]

## "Variability of Passive Microwave Radiometric Signatures at Different Spatial Resolutions and Its Implication for Rainfall Estimation"

Analysis of precipitation radar (PR) and Tropical Rainfall Measuring Mission (TRMM) microwave imager (TMI) data collected from the TRMM satellite shows that rainfall inhomogeneity, as represented by the coefficient of variation (CV), depends on a spatial scale, i.e., the CV appears to be nearly constant at all rain rates within the field of view (FOV) of the TMI 37-GHz channel, while it decreases with rain rate at lower spatial resolutions, such as the FOV sizes of the low-frequency TMI channels (10.7 and 19.4 GHz). It is known that the brightness temperature (Tb) for a low-frequency channel decreases with increasing rainfall inhomogeneity for a given rain rate. As such, more inhomogeneous rainfall at low rain rates leads to a lower Tbcompared with that of a FOV with homogeneous rainfall; however, less inhomogeneous rainfall at high rain rates tends to produce a Tbsimilar to that of homogeneous rainfalls. These results indicate that the observed radiometric signatures of low-frequency channels at low spatial resolutions are characterized by a larger response range and smaller variability than those at a higher spatial resolution. Based on the observational characteristics of the TMI and PR data sets, we performed synthetic retrievals of rainfalls, employing a Bayesian retrieval methodology at different retrieval resolutions corresponding to the FOV sizes of the TMI channels at 10.7, 19.4, and 37 GHz. Comparisons of the rainfalls retrieved at the different resolutions and their temporal and regional averages show that the systematic bias resulting from the rainfall inhomogeneity is smaller in the lower resolution data than in their higher resolution counterparts. We note that such low-resolution rainfall retrievals are not expected to describe the instantaneous features of rain fields; however, they could be useful for climatological estimates at large temporal and spatial scales. [J478]

## "Optimum Polarizations for Discrimination of a Foliage-Camouflaged Target, Using Genetic Algorithms"

Many realizations of foliage around a hard target are run to obtain the statistical variations of foliage and target responses. This is accomplished by using a hybrid target-foliage model, developed for the investigation of the scattering behavior of metallic targets embedded inside a forest canopy. This model is based on the coherent scattering theory of wave propagation through the foliage and an iterative physical optics approximation of scattering from the target. The model is capable of accounting for the first-order near-field interactions between the hard target and the foliage. Fully polarimetric simulation results of a foliage-camouflaged metallic target having complex geometry are generated at 2 GHz, and a polarization synthesis optimization method for improving signal-to-clutter ratio is carried out by applying genetic algorithms. [J479]

## "Through-the-Wall Surveillance With Millimeter-Wave LFMCW Radars"

The use of millimeter-wave radars allows a weight and size reduction of circuits and antennas, which is an important characteristic for Through-the-Wall Surveillance (TWS) applications. Furthermore, when using the millimeter-wave band, a large amount of bandwidth can be easily transmitted, given that the relative bandwidth is smaller. This leads to a high range resolution that allows for the discrimination of several targets that are very close in range, e.g., inside a room. The azimuth resolution is also improved due to the availability in this band of directive antennas with small dimensions. This paper studies the feasibility of using a millimeter-wave linear frequency-modulated continuous-wave radar in a TWS application. A TWS experiment in a real scenario has been done to demonstrate the validity of the theoretical analysis. [J480]

## "A Numerical Study of the Retrieval of Sea Surface Height Profiles From Low Grazing Angle Radar Data"

A numerical study of the retrieval of sea surface height profiles from low grazing angle radar observations is described. The study is based on a numerical method for electromagnetic scattering from 1-D rough sea profiles, combined with the ldquoimproved linear representationrdquo of Creamer for simulating weakly nonlinear sea surface hydrodynamics. Numerical computations are performed for frequencies from 2975 to 3025 MHz so that simulated radar pulse returns are achieved. The geometry utilized models a radar with an antenna height of 14 m, observing the sea surface at ranges from 520 to 1720 m. The low grazing angles of this configuration produce significant shadowing of the sea surface, and standard analytical theories of sea scattering are not directly applicable. Three approaches for retrieving sea height profile information are compared. The first method uses a statistical relationship between the surface height and the computed radar cross sections versus range (an incoherent measurement). A second method uses the phase difference between scattering measurements in two vertically separated antennas (ldquovertical interferometry) in the retrieval. The final technique retrieves height profiles from variations in the apparent Doppler frequency (coherent measurements) versus range and requires that time-stepped simulations be performed. The relative advantages and disadvantages of each of the three approaches are examined and discussed. [J481]

## "Defining a Sea Ice Flag for Envisat Altimetry Mission"

This letter presents the development of a sea ice flag algorithm for the Envisat altimetry mission to detect sea ice corrupted sea surface height data within quality control processing. The algorithm takes advantage of having both passive and active microwave sensors on the same platform with coregistered measurements. Its performances have been evaluated based on collocations between the along-track Envisat data with reference maps built from combination of daily grids of sea ice concentration from SSM/I sensors and backscatter cross section from SeaWinds scatterometer on QuikSCAT satellite. [J482]

## "On the Use of Auxiliary Receive Channels for Clutter Mitigation With Phased Array Weather Radars"

Phased array radars (PARs) are attractive in weather surveillance primarily because of their capability to electronically steer. When combined with the recently developed beam multiplexing (BMX) technique, these radars can obtain very rapid update scans that are useful in monitoring severe weather. A consequence is that the small number of contiguous samples of the time series obtained can be a challenge for temporal/spectral filters used for clutter mitigation. As a result, the accurate extraction of weather signals can become the limiting performance barrier for PARs that employ BMX in clutter-dominated scattering fields. By exploiting the spatial correlation of the auxiliary channel signals, the effect of clutter contamination can be reduced in these conditions. In this paper, three spatial filtering techniques that used low-gain auxiliary receive channels are presented. The effect of clutter mitigation was studied using numerical simulations of a tornadic environment for changes in signal-to-noise ratio, clutter-to-signal ratio, number of time series samples, varying clutter spectral widths, and maximum weight constraints. Since such data are not currently available from a horizontally pointed phased array weather radar, experimental validation was applied to an existing data set from the turbulent eddy profiler, which is a vertically pointed PAR. Although preliminary, the results show promise for clutter mitigation with extremely short nonuniform sampling. [J483]

## "Brightness-Temperature Retrieval Methods in Synthetic Aperture Radiometers"

Brightness-temperature retrieval techniques for synthetic aperture radiometers are reviewed. Three different approaches to combine measured visibility and antenna temperatures, along with instrument characterization data, into a general equation to invert are presented. Discretization and windowing techniques are briefly discussed, and formulas for reciprocal grids using rectangular and hexagonal samplings are given. Two known techniques are used to invert the equation, namely, inverse Fourier transform and G-matrix pseudoinverse. The proposed preprocessing approaches combined with these two inversion methods are implemented with real data measured by an airborne Y-shaped interferometric radiometer over land and water, and are compared. The images indicate that best results are obtained when inverting an incremental visibility obtained after substracting a term that includes the individual antenna temperatures, the physical temperatures of the receivers, and a flat-target response directly measured from cold-sky looks. [J484]

## "Installation of a Doppler Radar Monitoring System at Merapi Volcano, Indonesia"

Merapi Volcano, Indonesia, is one of the most active dome building volcanoes worldwide. Instabilities at the growing dome cause rockfalls and hot block and ash flows, which can reach run-out distances of several kilometers. Therefore, Merapi has been monitored extensively for many years. However, direct visual observation of the dome is often impossible due to cloud coverage of the summit. In October 2001, a first prototype Doppler radar system was installed to overcome this shortcoming. The system is able to penetrate clouds and observe material movements at the dome, giving valuable information about dynamic processes in the dome area. The system also allows detection of rainfall in several distance intervals. For precise positioning of the beam, the system was equipped with an electromechanical mounting in 2003. A charge-coupled device (CCD) camera attached to the radar mirror documents the radar beam position and provides visual observation of the dome. Recorded data, camera images, and status information are telemetered to the Merapi Volcano Observatory, where they can be processed and interpreted. Status information is also sent via short message service via a global system for mobile communications (GSM) modem. By processing the Doppler radar data, we are able to discriminate between three different types of instability events: sliding dome material, dome material gravitationally breaking off the dome, and explosive outbursts of dome material due to expansion of volcanic gas. In order to independently verify our observations, we compared rockfall events detected by the radar system to seismic recordings and found a good correlation. [J485]

## "Measurement of Ionospheric Faraday Rotation in Simulated and Real Spaceborne SAR Data"

The influence of the atmosphere on a frequency-modulated electromagnetic wave traversing the ionosphere is becoming increasingly important for recent and upcoming low-frequency and wide-bandwidth spaceborne synthetic aperture radar (SAR) systems. The ionized ionosphere induces Faraday rotation (FR) at these

frequencies that affects radar polarimetry and causes signal path delays resulting in a reduced range resolution. The work at hand introduces a simulation model of SAR signals passing through the atmosphere, including both frequency-dependent FR and path delays. Based on simulation results from this model [proven with real Advanced Land Observing Satellite Phased Array L-band Synthetic Aperture Radar (PALSAR) data], estimation of FR in quad-polarized SAR data using the given approach is shown for raw, range-compressed, and focused radar images. Path delays and signal chirp bandwidth effects are considered. Investigations discuss the suitability of raw and compressed data versus combination of total electron content maps with the Earth's magnetic field for FR estimation and deduced from a large number of analyzed PALSAR data sets. [J486]

## "Implementation of SDR Digital Beamformer for Microsatellite SAR"

The hardware reconfiguration feature of a software-defined radio (SDR) architecture can support multiple modes of a digital beamformer (DBF) striving for compactness and efficient processing power, which are important issues for microsatellite synthetic aperture radar (SAR) systems. In this letter, based on the SDR architecture, a DBF system, consisting of multiple beam, direction-of-arrival (DOA) estimation, and null-steering operation modes, is realized using a field-programmable gate array (FPGA) processor. Since the hardware reconfiguration has to be processed with minimal delay, the FPGA hardware must be of modularized design. Different modes can share the common module during mode switching. Experimental results verify the performance of DOA, null steering, and mode switching. The processing time of each DBF mode is less than the cross-range pulse repetition interval of the microsatellite SAR system. [J487]

## "Suitability and Limitations of ENVISAT ASAR for Monitoring Small Reservoirs in a Semiarid Area"

In semiarid regions, thousands of small reservoirs provide the rural population with water, but their storage volumes and hydrological impact are largely unknown. This paper analyzes the suitability of weather-independent radar satellite images for monitoring small reservoir surfaces. The surface areas of three reservoirs were extracted from 21 of 22 ENVISAT Advanced Synthetic Aperture Radar scenes, acquired bimonthly from June 2005 to August 2006. The reservoir surface areas were determined with a quasi-manual classification approach, as stringent classification rules often failed due to the spatial and temporal variability of the backscatter from the water. The land-water contrast is critical for the detection of water bodies. Additionally, wind has a significant impact on the classification results and affects the water surface and the backscattered radar signal (Bragg scattering) above a wind speed threshold of 2.6 mmiddots-1. The analysis of 15 months of wind speed data shows that, on 96% of the days, wind speeds were below the Bragg scattering criterion at the time of night time acquisitions, as opposed to 50% during the morning acquisition time. Night time acquisitions are strongly advisable over day time acquisitions due to lower wind interference. Over the year, radar images are most affected by wind during the onset of the rainy season (May and June). We conclude that radar and optical systems are complimentary. Radar is suitable during the rainy season but is affected by wind and lack of vegetation context during the dry season. [J488]

## "Surface-Based Polarimetric C-Band Microwave Scatterometer Measurements of Snow During a Chinook Event"

This paper presents a case study of C-band backscatter observations of snow during a Chinook event. A surface-based C-band polarimetric data set collected in February 2006 is used to contrast the polarimetric response to sampled conditions of bare frozen ground, cold snow-covered ground, and snow during a Chinook event. Chinook activity is inherently spatially and temporally variable across the region in winter and produces considerable spatial variability of snow-cover physical properties associated with snow-water-equivalent (SWE) estimates. A temporal analysis of polarimetric backscatter sensed during a Chinook-induced ablation event on February 27, 2006 is used to describe the associated changes in snow conditions and scattering mechanisms. Analysis reveals that the polarimetric surface-based C-band scatterometer data respond to changes in snow parameters associated with the specific ground and snow conditions and to the temporal Chinook ablation event. Use of the copolarizations, cross-polarization, depolarization ratio, copolarization ratio, complex copolarization correlation coefficient, and the copolarized phase difference information show promise in describing changes in snow physical parameters, differing ground and snow conditions, and transitional ablation events, based on differing scattering mechanisms. This paper infers that an increase in volume scattering and fluctuations in surface scattering during the Chinook ablation event may be associated with specific physical changes such as density, crystal structure, and permittivity caused by wind speed. This paper has implications for remotely sensed estimations of snow-covered area (SCA) and SWE. Association of SCA and SWE with backscatter coefficients is not explicit in this paper; however, changes in SWE and snow properties are inferentially linked to changes in backscatter. [J489]

## "An Adaptive and Fast CFAR Algorithm Based on Automatic Censoring for Target Detection in

## High-Resolution SAR Images"

An adaptive and fast constant false alarm rate (CFAR) algorithm based on automatic censoring (AC) is proposed for target detection in high-resolution synthetic aperture radar (SAR) images. First, an adaptive global threshold is selected to obtain an index matrix which labels whether each pixel of the image is a potential target pixel or not. Second, by using the index matrix, the clutter environment can be determined adaptively to prescreen the clutter pixels in the sliding window used for detecting. The G0distribution, which can model multilook SAR images within an extensive range of degree of homogeneity, is adopted as the statistical model of clutter in this paper. With the introduction of AC, the proposed algorithm gains good CFAR detection performance for homogeneous regions, clutter edge, and multitarget situations. Meanwhile, the corresponding fast algorithm greatly reduces the computational load. Finally, target clustering is implemented to obtain more accurate target regions. According to the theoretical performance analysis and the experiment results of typical real SAR images, the proposed algorithm is shown to be of good performance and strong practicability. [J490]

## "Analysis of Eccentered Dipole Antenna for Borehole Radar"

A dipole antenna in a borehole may be placed away from the center of the borehole, and this eccentricity produces additional complicated electromagnetic fields, which may influence borehole radar signals. In this paper, we analyze an eccentric dipole antenna in a borehole for borehole radars. Our approach is an extended version of the pseudoanalytical formulation that was previously applied for analyzing an induction logging tool and a dielectric logging tool. The proposed equations are suitable for modeling the finite dipole antenna, utilizing a method-of-moments. The eccentricity of the radar sonde has two consequences. First, it modifies the antenna characteristics such as its impedance, and second, it changes the electromagnetic field inside the borehole, owing to the change of the structure of the cylindrical layers. These two changes are evaluated by the proposed algorithm and two types of experiments. The first one is a measurement of the input impedance of a monopole antenna which is in cylindrical layers on a ground plane in air. The second one is about the transmission between two antennas, one of which is eccentered in cylindrical layers. This experiment was done in granite at a field test site and on a ground plane in air. In the field experiments, we controlled the position of the radar sonde in a borehole and made the antenna eccentered artificially. We found that a 4- cm displacement resulted in changes of 4 dB in amplitude and 4 ns in time delay. Comparing the experimental and calculated data obtained by the present method shows the validity of the proposed analytical formulation. [J491]

## "Cassini Radar Data: Estimation of Titan's Lake Features by Means of a Bayesian Inversion Algorithm"

The analysis derived from the Cassini SAR imagery reflects the complex Titan's surface morphology with a wide range of backscattering coefficients and peculiar features such as periodic structures and lakelike features, which were observed on July 22, 2006, when polar areas were first imaged, and are considered good candidates to be filled with liquid hydrocarbons. In this paper, the modeling description of lakes is addressed by means of a double-layer model which considers an upper liquid-hydrocarbon layer and a lower layer compatible with the radar response of the neighboring areas. This model is introduced into a Bayesian framework for the purpose of inferring the likely ranges of some parameters and, in particular, of the optical thickness of the hypothesized liquid-hydrocarbon layer and of the wind speed. The main idea is to use the information contained in the parameter probability density function, which describes how probability is distributed among the different values of parameters according to the various scenarios considered. The analysis carried out on lakes and surrounding areas on flybys T16 and T19 determines optical thickness values from 0.2 to 6. For T25 flyby, the inferred values of optical thickness indicate that a limit value of optical thickness may be 9. Considering that, beyond these values, the signal from the bottom layer is completely attenuated, information on the wind speed on the upper layer can be inferred. The found mean values of wind speed are around 0.2-0.3 m/s according to different hypotheses on the upper layer dielectric constant. [J492]

## "Enhanced SAR-Based Snow-Covered Area Estimation Method for Boreal Forest Zone"

In this paper, an enhanced method for fractional snow-covered area (SCA) estimation for the boreal forest zone is presented. The new approach, based on utilizing weather station data alongside with spaceborne synthetic aperture radar (SAR) imagery, leads to a significantly improved estimation accuracy. While the Helsinki University of Technology (TKK) SAR-based SCA estimation method serves as a basic tool in the SCA estimation, the ground-based weather station observations are employed to still strengthen its performance at the nearly melt-off or totally melt-off conditions. The method is still improved by a new reference image selection process, leading to more accurate results and an easier adaptivity to new areas. The SCA estimation accuracy of the new enhanced method is compared with optical satellite-based SCA data. Evaluation of the method is carried out using Radarsat wide-swath data for the snow-melt seasons of 2004-2006. The results show a significant increase in accuracy when the enhanced SCA method is applied. Correlation between the radar-

based and optical comparison data increases from 0.914 to 0.947 and root-mean-square error improves from 0.151 to 0.123 with the new method. Traditionally, the TKK method has provided SCA estimates for Finnish third-order subdrainage basins. In this paper, the method is adapted to produce SCA estimates also in 5 times 5 km spatial resolution. The analyses for the 5 times 5 km method indicate poorer estimation accuracy than the nominal drainage-basin-based method. [J493]

## "Estimation of the Surface Velocity Field of the Aletsch Glacier Using Multibaseline Airborne SAR Interferometry"

This paper presents a methodology to process airborne interferometric synthetic aperture radar (SAR) data to measure surface velocity fields (SVFs) of temperate glaciers, and applies it to data acquired over the Aletsch glacier. The first part of this paper deals with the main limitation in airborne interferometric SAR to retrieve reliable interferometric products, namely, the existence of the so-called residual motion errors-inaccuracies on the order of a few centimeters in the navigation system. An extended multisquint approach is proposed for their estimation in the case of nonstationary scenes. The second part of this paper expounds an efficient methodology to derive SVFs with airborne systems, where the line-of-sight displacement is estimated using differential interferometry and the along-track component by estimating the azimuth coregistration offsets. The necessary steps to finally obtain the 3-D SVF are also presented, as well as the possibility of combining different acquisition geometries. Airborne interferometric SAR data acquired by the Experimental SAR system of the German aerospace center over the Aletsch glacier, located in the Swiss Alps, are used to evaluate the performance of the proposed approach. The motion of the corner reflectors deployed in the scene is retrieved with an accuracy between 1 and 5 cm/day using L-band data. [J494]

## "Analysis by Wavelet Frames of Spatial Statistics in SAR Data for Characterizing Structural Properties of Forests"

Spatial statistics (texture) in SAR backscatter data of forested areas bears information on structural and geometric properties that could be useful in mapping forest extent, species type, and stages of regeneration or degradation. Based on a previously published theoretical approach in deriving texture measures from SAR data using wavelet frames, experiments are reported that aim to characterize, from a purely observational point of view, wavelet texture measures' sensitivity with respect to target structural properties and SAR configurations. Suitable analytical tools are introduced to represent dependences in the combined space-scale-polarization domain through signatures that condense information in graphical form. Moreover, class separability, afforded by wavelet texture measures in a supervised classification setting and based on the Fischer linear discriminant analysis, is considered. This paper focuses on two structurally different forest types (tropical rain forest in the Central Africa Congo Floodplain and mixed-species wooded savanna in Queensland, Australia) and uses data from orbital radars, particularly from the Japanese Advanced Land Observing Satellite Phased Arrayed L-band Synthetic Aperture Radar. The analysis indicated that textural information from spatial statistics can provide, in some cases, better class separability in forest mapping with respect to one-point statistics, although spatial resolution in texture products is reduced. However, dependences of texture measures on the polarization state are detected, particularly in forests where a greater diversity of scattering mechanisms occurs. [J495]

## "On the Reduction of the Systematic Error in Imaging Radiometry by Aperture Synthesis: A New Approach for the SMOS Space Mission"

The Soil Moisture and Ocean Salinity (SMOS) mission is a European Space Agency project aimed at global monitoring of surface SMOS from radiometric L-band observations. This letter is concerned with the reduction of the systematic error (or bias) in the reconstruction of radiometric brightness temperature maps from SMOS interferometric measurements. A recent and efficient method has been proposed for reducing this error. However, a residual bias still persists. A new approach for reducing this bias down to residual values less than 0.1 K is presented here and illustrated with numerical simulations. [J496]

## "Optimum Data Vector Approach to Multibaseline SAR Interferometry Phase Unwrapping"

Phase unwrapping is a key problem not only in all quantitative applications of synthetic aperture radar (SAR) interferometry but also in other fields. In this letter, a new phase unwrapping approach is investigated. Our study is based on the model of the optimum data vector. In order to autocoregister the SAR images, the proposed method takes advantage of the multibaseline optimal weighted joint data vector by extracting all the coherence information available in the neighboring pixels. Moreover, the method employs the projection of the joint signal subspace onto the corresponding noise subspace to estimate the unwrapped interferometric phases (or the terrain heights). The proposed method can accurately determine the dimensions of the noise subspace and provide the robust unwrapped interferometric phases even in the presence of the large image coregistration

errors. Moreover, the multibaseline processing idea is a combination of data optimization, image coregistration, interferogram filtering, and phase unwrapping. [J497]

## "Exploiting SAR and VHR Optical Images to Quantify Damage Caused by the 2003 Bam Earthquake"

Using satellite sensors to detect urban damage and other surface changes due to earthquakes is gaining increasing interest. Optical images at different resolutions and radar images represent useful tools for this application, particularly when more frequent revisit times will be available with the implementation of new missions and future possible constellations of satellites. Very high resolution (VHR) images (on the order of 1 m or less) may provide information at the scale of a single building, whereas images at resolutions on the order of tens of meters may give indications of damage levels at a district scale. Both types of information may be extremely important if provided with sufficient timeliness to rescue teams. The earthquake that hit the city of Bam, Iran, has been taken as a test case, where QuickBird VHR optical images and advanced synthetic aperture radar data were available both before and after the event. Methods to process these data in order to detect damage and to extract features used to estimate damage levels are investigated in this paper, pointing out the significant potential of these satellite data and their possible synergy. [J498]

## "Hierarchical Feature-Based Classification Approach for Fast and User-Interactive SAR Image Interpretation"

The framework of this paper is focused on semiautomatic fast recognition of areas of interest for fast and user-interactive synthetic aperture radar (SAR) image interpretation for which only a unique intensity SAR image is available. The goal is to label regions into classes significant to a given application in an image, as rapidly as possible. A semiautomated ldquoroughrdquo classification is proposed. It defines the information extraction as a two-level procedure. The technique is based on a first partition image into homogeneous regions using the approach proposed by Galland Then, discrimination characteristics are determined in each homogeneous region. This allows one to automatically obtain a first segmentation of the image into semantic regions of interest. Finally, this segmentation can be easily modified by a user in a limited computational time. At this level, they are considered as ldquoobjects,rdquo to identify which typical class of ground it can be attached to. Among a large set of tested measures, we have selected the most pertinent ones for the considered SAR images. In fact, we will see that to obtain an accurate measures estimation, measures need to be estimated inside a neighborhood as homogeneously as possible. This can be achieved with a reasonable confidence in the proposed approach due to the homogeneity properties of the segmentation technique applied. In this paper, we focus on linear structures, urban structures, agricultural parcels, and forest areas extraction in SAR images. [J499]

## "DEM Generation Combining SAR Polarimetry and Shape-From-Shading Techniques"

Estimation of the polarization orientation angle shifts induced by terrain azimuth slope variations is a recently developed application in radar polarimetry. In general, without any prior knowledge on the terrain, two polarimetric SAR (POLSAR) flight passes are required to derive terrain slopes in perpendicular directions for digital elevation model (DEM) generation. Moreover, we note that SAR intensity is a strong indicator of the range component of the terrain slopes. In this letter, we developed a method for DEM generation requiring only one POLSAR flight pass, by combining orientation angle estimation and a shape-from-shading technique. In particular, when limited POLSAR data are available, this POLSAR technique provides an alternative way for DEM generation. National Aeronautics and Space Administration Jet Propulsion Laboratory (NASA/JPL) AIRSAR L-band POLSAR data over Camp Roberts, California, is used to demonstrate the results of the method proposed in this letter, and a DEM derived from simultaneously measured C-band interferometric SAR from NASA/JPL topographic SAR instrument is selected as the comparative ground truth to validate the effectiveness of this single POLSAR method. Analyses and discussions are also included in this letter. [J500]

## "A Novel Approach to Range Doppler SAR Processing Based on Legendre Orthogonal Polynomials"

The range Doppler algorithm (RDA) is based on Taylor series expansion for the transfer function (TF) phase component, resulting in increasing phase error as the range frequency or the squint angle increases. We introduce Legendre orthogonal polynomials into synthetic aperture radar data processing steps to replace Taylor series expansion used in approximating the TF phase. A novel range Doppler imaging approach based on Legendre expansion is addressed with an extended RDA as example, and the analytical expressions of the new phase multiplication factors are then derived. The simulation results show that the proposed method provides better focusing performance than the conventional RDA in the same squint case and is more suitable for the large squint mode while there is negligible increment of computation load. [J501]

## "A Support-Vector-Machine-Based Approach to RF Sensor Spectral Signature Classifications"

In this paper, a support vector machine (SVM) classifier was designed to identify tornado vortices based on their characteristics that were determined from the Doppler spectra and eigenvalues that were calculated from the data that were collected in the vicinity of these vortices. To collect these data, weather surveillance radar (WSR-88D) was employed, which is locally operated by the National Severe Storms Laboratory (NSSL) on the north campus of the University of Oklahoma, Norman. This particular radar, which is devoted to experimental research rather than operational weather forecasting, has the unique capability of recording massive volumes of in-phase (I) and quadrature (Q) data over many hours. As such, the received radar echo power and Doppler shift information can be determined from these I and Q complex-valued data, which provides a rich environment for evaluating our new postprocessing algorithms. At the current time, most radar systems, including North America's national network of weather radar systems, process these I and Q data in real time to produce environmental measurements known as ldquospectral moments,rdquo which are the first three statistical moments of the data. These three moments (the reflectivity, the radial velocity, and the spectrum width) are then provided to scientists or forecasters, and the abundance of I and Q data is not preserved to save computer resources. One of the aims of this paper is to show how additional information about the atmosphere can be garnered from the I and Q data. To assist this mission, an SVM-based classifier evades the pitfalls of the traditional statistical learning algorithms, such as neural networks, by setting up a convex optimization problem with a single global minimum. In addition, through the use of kernels and a nonlinear mapping to higher dimensional spaces, the SVM classifier is able to effectively handle nonlinear classification problems. The idea behind this transformation is to facilitate the-- separability of classes by taking the input vectors to a higher dimensional space. The SVM classifier has the added advantage of reducing overfitting by constructing a maximum margin to separate hyperplanes in a higher dimensional feature space to ensure a small generalization error bound. Finally, our practical results are in positive agreement with our theoretical predictions. [J502]

## "CMP Antenna Array GPR and Signal-to-Clutter Ratio Improvement"

Ground-penetrating radar (GPR) is recognized as a promising sensor for detecting buried landmines. In this case, the GPR antenna(s) must be elevated above the ground. However, this requirement results in heavy surface clutter. It is therefore necessary to overcome the effect. A commonly used procedure of time gating and background averaging cannot suit to small shallow nonmetallic landmine beneath a rough ground surface. In this letter, we proposed techniques to enhance the target signal through common midpoint (CMP) antenna array and data processing techniques, including velocity spectrum and CMP multifold stacking. The method has been tested using experiment data over a rough ground under which small plastic antipersonnel landmines is shallowly buried. The result shows the signal-to-clutter ratio was dramatically improved. [J503]

## "Singular Unit Restoration in Interferograms Based on Complex-Valued Markov Random Field Model for Phase Unwrapping"

In generating a digital elevation map from an interferogram obtained by interferometric synthetic aperture radar, the filtering process is as important as the phase unwrapping process. Before unwrapping, we usually have to restore the data image by reducing so-called singular points (SPs) by filtering process without destroying or smearing delicate fringes. Previously, an effective SP restoration method was proposed based on the complex-valued Markov random field (CMRF) model. However, there is still room for improvement in the definition of SPs and in the formulation of CMRF parameter estimation. In this letter, we propose a novel scheme by introducing a new concept, namely, the ldquosingular unit.rdquo We also estimate CMRF parameters locally as a weighted sum by taking the distance and SP numbers in sample sites into account. By using this restoration method, we demonstrate a high-performance removal of SPs. We also find that delicate landscape features, which are often lost in conventional filtering, are preserved appropriately. We confirm the quality in higher signal-to-noise ratios obtained against actual height data. [J504]

## "Performance of Stereoradargrammetric Methods Applied to Spaceborne Monostatic-Bistatic Synthetic Aperture Radar"

This paper aims to investigate the performance of stereoradargrammetric methods applied to spaceborne monostatic-bistatic synthetic aperture radar (SAR) data for digital elevation model (DEM) generation. Stereoradargrammetric techniques for robust DEM generation were successfully experienced on monostatic repeat-pass SIR-A, SIR-B, SIR-C/X-SAR, ERS1/2, JERS-1, and Radarsat data. However, novel configurations achievable by modern spacecraft flying in formation will allow for the attainment of very large baselines between the antennas in a single-pass bistatic geometry so that the height determination accuracy can benefit from both stereo effect and simultaneous acquisition. Five models for relief reconstruction by monostatic-bistatic SAR stereoradargrammetry are presented, and an error budget is assessed for each of them. Results of the sensitivity

analysis exhibit metric accuracy, and therefore, the technique could be applied for height reconstruction as a methodology complementary to SAR interferometry. [J505]

## "Omega-k Algorithm for Airborne Spatial Invariant Bistatic Spotlight SAR Imaging"

Bistatic spotlight synthetic aperture radar (SAR) which uses a separated transmitter and receiver has been studied intensively due to its flexibility. To reconstruct the image for the bistatic SAR in the parallel track configuration, where the transmitter and the receiver have equal velocity, we modify the omega-k algorithm. Specifically, using the extended Taylor approximation (ETA), we convert the parallel track configuration into the single track configuration. Then, using the principle of the stationary phase, we propose an analytical method to increase the image quality of bistatic SAR systems. [J506]

## "Improved Sigma Filter for Speckle Filtering of SAR Imagery"

The Lee sigma filter was developed in 1983 based on the simple concept of two-sigma probability, and it was reasonably effective in speckle filtering. However, deficiencies were discovered in producing biased estimation and in blurring and depressing strong reflected targets. The advancement of synthetic aperture radar (SAR) technology with high-resolution data of large dimensions demands better and efficient speckle filtering algorithms. In this paper, we extend and improve the Lee sigma filter by eliminating these deficiencies. The bias problem is solved by redefining the sigma range based on the speckle probability density functions. To mitigate the problems of blurring and depressing strong reflective scatterers, a target signature preservation technique is developed. In addition, we incorporate the minimum-mean-square-error estimator for adaptive speckle reduction. Simulated SAR data are used to quantitatively evaluate the characteristics of this improved sigma filter and to validate its effectiveness. The proposed algorithm is applied to spaceborne and airborne SAR data to demonstrate its overall speckle filtering characteristics as compared with other algorithms. This improved sigma filter remains simple in concept and is computationally efficient but without the deficiencies of the original Lee sigma filter. [J507]

## "Radiometric Calibration of LIDAR Intensity With Commercially Available Reference Targets"

We present a new approach for radiometric calibration of light detection and ranging (LIDAR) intensity data and demonstrate an application of this method to natural targets. The method is based on 1) using commercially available sand and gravel as reference targets and 2) the calibration of these reference targets in the laboratory conditions to know their backscatter properties. We have investigated the target properties crucial for accurate and consistent reflectance calibration and present a set of ideal targets easily available for calibration purposes. The first results from LIDAR-based brightness measurement of grass and sand show that the gravel-based calibration approach works in practice, is cost effective, and produces statistically meaningful results: Comparison of results from two separate airborne laser scanning campaigns shows that the relative calibration produces repeatable reflectance values. [J508]

## "DEM Reconstruction Accuracy in Multichannel SAR Interferometry"

Interferometric synthetic aperture radar (InSAR) systems allow the estimation of the height profile of the Earth surface. When the height profile of the observed scene is characterized by high slopes or exhibits strong height discontinuities, the height reconstruction obtained from a single interferogram is ambiguous, since the solution of the estimation problem is not unique. To solve this ambiguity and restore the solution uniqueness, multiple interferograms, obtained with different baselines and/or with different frequencies, have to be used (multichannel InSAR). The height profile can then be estimated from multiple interferograms using maximum likelihood (ML) estimation techniques or by means of maximum aposteriori(MAP) estimation techniques, which take into account the relation between adjacent pixels. In this paper, the height estimation accuracy achievable with a given multibaseline interferometric configuration and using the aforementioned estimation techniques in terms of Cramer-Rao lower bound for the ML and of error lower bound for the MAP, is analyzed and discussed. It is shown that the MAP technique outperforms the ML one and that its attainable accuracy is not sensitive to the baselines choice, while mainly depends on the ground slopes. [J509]

## "Four-Dimensional SAR Imaging for Height Estimation and Monitoring of Single and Double Scatterers"

The superposition of contributions from different stable targets within the same pixel is a phenomenon that may impair the imaging and monitoring of ground scatterers via the multipass synthetic aperture radar (SAR) interferometry technique. Three-dimensional SAR imaging, also known as SAR tomography, uses multiple views to profile the scattering power at different heights. This technique has been shown to be capable of separating interfering target responses on real data. Differential SAR tomography has been recently proposed as a

technique that extends the potentialities of SAR tomography to the target deformation monitoring. It performs a 4-D space-velocity imaging that enables not only separating interfering targets in elevation but also distinguishing their single slow deformation velocities. This work addresses for the first time the application of 4-D SAR imaging to real data to determine the height and mean deformation velocity of single scatterers and double-scattering mechanisms interfering at high resolution in the same pixel. It also discusses the postprocessing steps required to identify the presence of stable single and double scatterers after elevation-velocity focusing. Moreover, it proposes a technique for the extraction of time series from interfering targets to measure possible nonlinear temporal deformations. [J510]

## "Effects of Birefringence Within Ice Sheets on Obliquely Propagating Radio Waves"

In this paper, effects of birefringence on radio waves obliquely propagating though polar ice sheets are examined to facilitate interpretations of bistatic and side-looking radar data. A formalism applicable for arbitrary radar configurations is developed to predict the returned power from within and beneath the ice sheets that have arbitrary alignments of ice crystals (ice fabrics). We applied this formalism to a range of ice fabrics found in ice cores and assessed the effects of birefringence in terms of ray-path configurations, ice fabrics, and radar frequency. Predicted frequency dependence of the bed return power replicates prominent features observed at Greenland NGRIP ice-core site. Results show that birefringence in ice of 1 km or more thickness with strong (weak) fabric can reduce the power returned from the bed 2 dB or more at frequencies higher than 200 MHz (20 MHz) as compared to isotropic ice. This suggests that quantitative interpretation of the power returned from the bed requires careful assessment of birefringence almost everywhere over the ice sheets. Application of this formalism also suggests a radar-frequency range usable for attenuation measurements, possible effects of fabric on synthetic aperture radar processing, and a feasibility of remote sensing of ice fabric. [J511]

## "Comparison of Compact Polarimetric Synthetic Aperture Radar Modes"

Compact polarimetry is a technique that allows construction of pseudo quad-pol information from dual-polarization synthetic aperture radar (SAR) systems. Compact polarimetry showed promise of being able to reduce the complexity, cost, mass, and data rate of a SAR system while attempting to maintain many capabilities of a fully polarimetric system. In this paper, we study different transmit/receive configurations to determine which polarimetric configurations allow for superior reconstruction of the fully polarimetric data. We discuss modifications of the original reconstruction algorithm proposed by Souyris, which show potential to better reconstruct fully polarimetric data. [J512]

## "LMMSE 3-D SAR Focusing"

Three-dimensional synthetic aperture radar (SAR) imaging, a technique also known as SAR tomography, uses multiple views to extend the capability of SAR systems to 3-D imaging by achieving a profiling of the scattering power at different heights. Multiple views are obtained with the current satellite technology via successive passes of a single antenna SAR sensor over the same scene, but next-generation sensor formations are foreseen to acquire multistatic data. Conventional processing, such as the beamforming, or singular values decomposition inversion is based on geometrical derivations and, hence, assumes the accurate phase calibration and the absence of target decorrelation. This paper analyzes the effects of phase miscalibration due to residual uncompensated atmospheric contribution and temporal decorrelation and proposes a 3-D imaging technique based on a linear minimum mean square error approach. The resulting algorithm extends the possibilities of the conventional processing by carrying out an integration of data that accounts for the aprioridata correlation properties. Hence, it allows handling of the presence of additional stochastic contributions such as: temporal coherence losses and atmospheric phase miscalibration. Moreover, with reference to future bistatic and multistatic systems, it permits an improved coherent integration of data acquired by simultaneous antenna in repeated passes. [J513]

## "Snowpack Characterization in Mountainous Regions Using C-Band SAR Data and a Meteorological Model"

This paper presents a method to characterize snow cover in mountainous regions using dual-polarization C-band synthetic aperture radar (SAR) data. It is demonstrated that an accurate modeling of the liquid water distribution inside the snowpack, using a multilayer meteorological snow model, is required to characterize snow with precision. A multilayer-snow electromagnetic (EM) backscattering model is developed based on the vector radiative transfer, the strong fluctuation theory, and physical parameters supplied by the meteorological model. However, the limited resolution of the meteorological snow model is insufficient for predicting a refined EM backscattering at a massif scale. An adequate spatial reorganization of these snow profiles, based on a comparison between simulated and measured dual-polarization SAR data, leads to a better estimation of some

snowpack parameters. In particular, the monitoring of snow liquid water content is presented improving the capacity of wet snow mapping as compared to a classical SAR-based method. This methodology shows good capacities both for qualitative and quantitative snow assessments, opening the way for a new operational method. [J514]

## "Wheat Crop Mapping by Using ASAR AP Data"

The purpose of this paper is to assess the use of C-band HH/VV backscatter ratio for mapping winter wheat. This paper analyzes two temporal series of images acquired in 2006 and 2007 by the Advanced Synthetic Aperture Radar (ASAR) system in alternating polarization (AP) mode, over an agricultural site located in southern Italy. Results on test data show that classification accuracies between 75% and 80% can be achieved by using a single ASAR image, acquired during the peak of the wheat-growing season. To achieve accuracies close to 90%, a spatial averaging at field scale is necessary. [J515]

## "Monitoring of the Rice Cropping System in the Mekong Delta Using ENVISAT/ASAR Dual Polarization Data"

The rice cropping system in Asia is undergoing major changes to cope with increasing demography and changing climate, making rice monitoring a critical issue. Past studies have demonstrated the use of C-band synthetic aperture radar (SAR) data to map rice areas. The methods were based on the temporal change of intensity backscattering coefficient of vertically or horizontally co-polarized data (VV or HH). In this paper, we assess the use of the HH/VV polarization ratio derived from Advanced SAR (ASAR) data from ENVISAT data for the production of rice paddy maps. The approach is based on past knowledge on the polarization behavior of rice canopy, i.e., VV backscattering is much lower than HH during a large part of the rice season, due to the attenuation of the wave by the vertical structure of the plants. The methodology is developed for the Mekong Delta, Vietnam, where a complex cropping pattern is found (one to three crops of rice per year). The approach includes a statistical analysis of the HH/VV distributions of rice and non-rice classes at different dates. The analysis results confirm that HH/VV can be used as classifier and point out the need for relevant speckle filtering prior to classification. A classification method is developed and applied to single- and multidate data sets. The methods are tested at one district of the province of An Giang and extended to the whole province. Comparisons of the mapping results to geographic-information-system land-use data and official agricultural statistics show very good agreement. The method will be further applied to the entire Mekong Delta. [J516]

## "Application of Target Decomposition Theorems Over Snow-Covered Forested Areas"

This paper compares two well-known polarimetric decomposition theorems, Cloude-Pottier and Freeman-Durden, applied to L- and C-band Airborne Polarimetric Synthetic Aperture Radar (AIRSAR-POLSAR) data acquired during the Cold-Land Processes Field Experiments. Three field campaigns were carried out in February 2002, March 2002, and March 2003 over a snow-covered open terrain, a sparse coniferous forest, and a dense coniferous forest. The analysis evaluates the ability of the two target decomposition methods for the identification and understanding of the main scattering mechanisms. [J517]

## "Estimation of the Minimum Number of Tracks for SAR Tomography"

Synthetic aperture radar tomography (SARTom) is the natural extension of SAR interferometry to solve for multiple phase centers within a resolution cell and obtain the 3-D representation of a scene. This paper deals with the determination of the minimum number of tracks required to perform SARTom. Through the prolate spheroidal wave functions, the number of equivalent targets of a volumetric source is derived, and from it, the minimum number of observations required to apply subspace superresolution methods is computed. The minimum tomographic aperture length is also investigated. The results are validated on real data acquired in L-band by the experimental SAR system of the German Aerospace Center. [J518]

## "Profiling the Rough Surface by Migration"

It is often advantageous to estimate the ground surface topography from radar returns. However, the popular method, searching for the brightest pixel in the ground-penetrating radar profile, cannot achieve accurate surface topography in the sharp variable surface case because of the effects of diffraction waves. In this letter, we propose a method to solve the problem and improve the accuracy of surface topography. A migration technique is introduced to refocus the diffraction waves before searching for the brightest pixel. Experimental data have been used to display the effects of diffraction waves and test the method. The result shows that the method can dramatically estimate accurate surface topography even in the sharp variable surface area. [J519]

## "An Analysis of Texture Measures in PCA-Based Unsupervised Classification of SAR Images"

In single-band single-polarized SAR images, intensity and texture are the information source available for unsupervised land cover classification. Every textural feature measure identifies texture patterns by different approaches. For efficient land cover classification, textural measures have to be chosen suitably. Therefore, in this letter, the role of various intensity and textural measures is analyzed for their discriminative ability for unsupervised SAR image classification into various land cover types like water, urban, and vegetation areas. To make the algorithm adaptable, these textural features are fused using principal component analysis (PCA), and principal components are used for classification purposes. To highlight the effectiveness of PCA, the difference between PCA- and non-PCA-based classifications is also analyzed. Analysis of the role of texture measures for unsupervised classification of real-world SAR data with application of PCA is presented in this letter. The analysis of how every individual feature measure contributes for classification process is presented, and then, textural measures for a feature set are chosen according to their role in improving classification accuracy. By analysis, it is observed that the feature set comprising mean, variance, wavelet components, semivariogram, lacunarity, and weighted rank fill ratio provides good classification accuracy of up to 90.4% than by using individual textural measures, and this increased accuracy justifies the complexity involved in the process. [J520]

## "3-D Radargrammetric Modeling of RADARSAT-2 Ultrafine Mode: Preliminary Results of the Geometric Calibration"

The geometry and the accuracy of the 3-D cartographic localization of RADARSAT-2 images are being evaluated as part of the Canadian Space Agency's Science and Operational Applications Research program. In a first step, the Toutin's 3-D physical model, previously developed for RADARSAT-1, was adapted to RADARSAT-2 sensor and applied to two ultrafine mode images (U2 and U25) acquired over an area in Beauport, Quebec. Both the 3-D modeling computed with only 12 ground control points and its geometric localization were evaluated with different check data: 1) independent check points; 2) the two quasi-epipolar images; 3) the two orthoimages; and 4) 1-m accurate orthophotos. All four results and validations are in agreement and confirm that the 3-D geometric localization and restitution accuracy are 1 m in planimetry and 2 m in elevation. The checked data error being included in these evaluations and the relative error computed from the quasi-epipolar comparison provided a high level of confidence that the precision of Toutin's 3-D radargrammetric model is better than 0.25 m. [J521]

## "Short-Range Clutter Suppression for Airborne Radar by Utilizing Prefiltering in Elevation"

Space-time adaptive processing (STAP) techniques have achieved good performance when applied to side-looking airborne radar (SLAR) where the ground clutter is relatively stationary, but due to severe range dependence, the performance is not so good in non-SLAR particularly when the pulse repetition frequency is high enough to induce range ambiguity. Because the short-range clutter Doppler for non-SLAR varies rapidly with range while the long-range clutter Doppler varies gently, at the presence of range ambiguity, the clutter in different ambiguous ranges does not coincide. The clutter range dependence mitigation for the case of range ambiguity is the major problem that this letter intends to solve. A subarray synthesis algorithm with prefiltering in elevation is presented. By this technique, the ambiguous short-range clutter is eliminated before STAP; therefore, the clutter range dependence is alleviated, and then, the STAP performance will be improved greatly. [J522]

## "C-Band Scatterometer Measurements of Multiyear Sea Ice Before Fall Freeze-Up in the Canadian Arctic"

Backscatter signatures of multiyear sea ice (MYI) during the late summer and early fall season before the fall freeze-up in the Canadian Arctic archipelago (CAA) have been obtained through the use of a ship-based polarimetric scatterometer. The device operates in C-band, and measurements were conducted in swaths from incidence angles of 20 deg-60deg. Three characteristic sites on MYI floes were investigated in the high Arctic and the central Arctic regions. Insitusnow and sea-ice thermophysical data were collected at each site in conjunction with local scatterometer measurements. The thermophysical data were subsequently analyzed using dielectric modeling techniques and coupled with the backscattering measurements (sigmadeg). Observed backscatter values and ratios were found to be in agreement with literature data, with volumetric scattering as the dominant scattering mechanism. [J523]

## "Interferometry by Deconvolution of Multicomponent Multioffset GPR Data"

Interferometric techniques are now well known to retrieve data between two receivers by the cross correlation of the data recorded by these receivers. Cross-correlation methods for interferometry rely mostly on the assumption that the medium is loss free and that the sources are all around the receivers. A recently developed method

introduced interferometry by deconvolution that is insensitive to loss mechanisms by principle and requires sources only on one side of the receivers. In this paper, we develop such method for ground-penetrating radar, illustrate the concept, and discuss implications for practical applications with numerical examples. [J524]

## "Using ENVISAT ASAR Global Mode Data for Surface Soil Moisture Retrieval Over Oklahoma, USA"

The Advanced Synthetic Aperture Radar (ASAR) onboard of the satellite ENVISAT can be operated in global monitoring (GM) mode. ASAR GM mode has delivered the first global multiyear C-band backscatter data set in HH polarization at a spatial resolution of 1 km. This paper investigates if ASAR GM can be used for retrieving soil moisture using a change detection approach over large regions. A method previously developed for the European Remote Sensing (ERS) scatterometer is adapted for use with ASAR GM and tested over Oklahoma, USA. The ASAR-GM-derived relative soil moisture index is compared to 50-km ERS soil moisture data and pointlike insitumeasurements from the Oklahoma MESONET. Even though the scale gap from ASAR GM to the insitumeasurements is less pronounced than in the case of the ERS scatterometer, the correlation for ASAR against the insitumeasurements is, in general, somewhat weaker than for the ERS scatterometer. The analysis suggests that this is mainly due to the much higher noise level of ASAR GM compared to the ERS scatterometer. Therefore, some spatial averaging to 3-10 km is recommended to reduce the noise of the ASAR GM soil moisture images. Nevertheless, the study demonstrates that ASAR GM allows resolving spatial details in the soil moisture patterns not observable in the ERS scatterometer measurements while still retaining the basic capability of the ERS scatterometer to capture temporal trends over large areas. [J525]

## "Using Altimetry Waveform Data and Ancillary Information From SRTM, Landsat, and MODIS to Retrieve River Characteristics"

In this paper, spaceborne radar altimeters are shown to have the potential for monitoring the height of large rivers with accuracies of approximately 1 m. However, the need for a better height accuracy and the observations of smaller continental basins have led to studies on how to improve and extend the use of nadir-altimeter data. Conventional retracking techniques over land are limited to the examination of altimeter waveforms on a case-by-case basis. Due to the arbitrary geometry which may be present at altimeter river crossings, this approach may be limited to large rivers, which approximate ocean crossings. To overcome this limitation, we introduce a waveform-fitting method which uses the entire set of waveforms associated with a water crossing, rather than individual waveforms. By using ancillary data, such as digital elevation model (obtained from Shuttle Radar Topography Mission and Gtopo30) and classification maps (obtained from Landsat and MODIS), it is possible to recast the retracking problems as a maximum-likelihood-estimation problem. Theoretical power returns based on the a priori knowledge of the observed scenes are generated, resulting in a parametric library of waveform histories, which is then used to constrain the estimation. For demonstration, we concentrate on the river Meuse in northern western Europe and on the river Lena in Russia. The Meuse has important social impact, since it has flooded in the past and better real-time predictions of its changing stage may improve flood-forecasting skill. Furthermore, it presents a challenge to conventional nadir-altimeter waveform retracking. We will present both theoretical performance results and demonstrate the feasibility based on real altimeter data. [J526]

## "Radar image processing with clusters of computers"

Some radar image processing algorithms such as shape-from-shading are particularly compute-intensive and time-consuming. If, in addition, a data set to be processed is large, then it may make sense to perform the processing of images on multiple workstations or parallel processing systems. We have implemented shape-from-shading, stereo matching, resampling, gridding, and visualization of terrain models in such a manner that they execute either on parallel machines or on clusters of workstations. We were motivated by the large image data set from NASA's Magellan mission to planet Venus, but received additional inspiration from the European Union's Center for Earth Observation program (CEO) and Austria's MISSION initiative for distributed processing of remote sensing images on remote workstations, using publicly-accessible algorithms. We developed a multi-processor approach that we denote as CDIP for Concurrent and Distributed Image Processing. The speedup for image processing tasks increases nearly linearly with the number of processors, be they on a parallel machine or arranged in a cluster of distributed workstations. Our approach adds benefits for users of complex image processing algorithms: the efforts for code porting and code maintenance are reduced and the necessity for specialized parallel processing hardware is eliminated. [J527]

## "Observation of Sea-Ice Thickness Using ENVISAT Data From LЬtzow-Holm Bay, East Antarctica"

To investigate the suitability of synthetic aperture radar (SAR) polarization data to estimate the sea-ice thickness

in early summer in Lutzow-Holm Bay, Antarctica, we compared insituice thicknesses with the corresponding backscattering co-efficient for each polarization and the VV-to-HH backscattering ratio. The VV-to-HH backscattering ratio was derived from data acquired by ENVISAT Advanced SAR (ASAR). This ratio is related to the near-surface dielectric constant of the sea ice, which is, in turn, related to the developing process of ice and, thus, its thickness via changes in the near-surface sea-ice salinity. The sea ice encountered in the study area is close first-year pack ice and fast ice. For these old and relatively rough sea-ice types, the VV-to-HH backscattering ratio can be expected to depend on salinity-driven changes in the near-surface dielectric constant rather than changes of the surface roughness. We applied the empirical relationships between the ice thickness and the VV-to-HH backscattering ratio with the linear and logarithm fits to ASAR data. The linear fit gave the reliable result, with an rms error being 0.08 m and a correlation coefficient being 0.91, when compared to insitufast-ice thickness. [J528]

## "Waveform-Diversity-Based Millimeter-Wave UAV SAR Remote Sensing"

To integrate a synthetic aperture radar (SAR) into an operational unmanned airborne vehicle (UAV), it should be as small as possible to meet stringent limitations of size, weight, and power consumption. It appears that the novel combination of millimeter-wave frequency-modulated continuous-wave (FMCW) technology and SAR techniques can provide an optimal solution. However, some efficient techniques should be applied to resolve range/Doppler ambiguities in FMCW UAV SAR systems. As such, a technique of waveform-diversity-based millimeter-wave UAV SAR imaging is presented in this paper. Along with the described system concept and signal model, the performance of the diversified waveforms evaluated by their cross correlations is detailed. As the conventional stop-and-go approximation is not valid for FMCW SAR, a modified wavenumber-domain algorithm with a consideration of continuous antenna motion during transmission and reception is derived. This imaging algorithm is validated with computer simulations. Furthermore, one parallel direct-digital-synthesizer-driven phase-locked-loop synthesizer with adaptive nonlinearity compensation, which has been validated by the experimental results, is proposed to obtain a millimeter-wave FMCW signal with fine frequency linearity. [J529]

## "DEM Reconstruction in Layover Areas From SAR and Auxiliary Input Data"

In this letter, a methodology to overcome the layover problem and obtain the 3-D reconstruction of urban areas will be discussed. Interferometric synthetic aperture radar (SAR) (InSAR) systems allow the estimation of height profiles of the Earth surface, but in the case of urban scenarios, estimation becomes a hard task due to the presence of SAR geometrical distortions, with layover above all. First, the layover signal in InSAR images is investigated; then, a procedure to specifically manage layover areas is presented. The proposed method consists of introducing an auxiliary data exploitation, optical data or SAR shadowing, in the maximum a posteriori statistical estimation technique to improve the digital elevation model reconstruction, particularly on phase discontinuities. We test the method on simulated data, showing its effectiveness. [J530]

## "An Assessment of a Ka-Band Radar Interferometer Mission Accuracy Over Eurasian Rivers"

The Water Elevation Recovery satellite mission is dedicated to the determination of land surface water extent, elevation, and slope using a Ka-band radar interferometer (KaRIn) as its primary instrument. Determining these parameters to the accuracy desired for hydrologic applications is challenging. The scientific objectives of the mission have been set up to 10 cm for the height budget and 10 murad (1 cm/1 km) for the slope budget. In this paper, we implement a Virtual Mission simulation and use it to examine the measurement performances for three case studies in Europe: a relatively small river such as the Meuse in Northern Western Europe, the Lena river in Russia, one of the major Siberian rivers, and Lake Leman in Western Europe. We simulate KaRIn data with the associated instrument and geophysical error sources and implement ground processing techniques to go from the original raw data to science data. We examine the impact of external errors in detail and implement calibration techniques that rely on the use of ancillary topographic data, such as the Shuttle Radar Topography Mission digital elevation model (DEM). We find that the impact of external errors can be reduced to a few centimeters. The random error budget can also be reduced below 10 cm by means of appropriate processing. The scientific requirements of the mission are shown to be met for all cases. [J531]

## "Using Multilook Averaging for Coherently Modeled Scattering From a Pine Tree at L-Band"

In this letter, we study scattering from a scots pine tree by using a realistic cylinder model of the tree and the coherent electric field scattering model. We study the directional variability of bistatic and monostatic scattering at L-band and show that, due to large variations in results, some averaging technique should be used to describe and interpret the model output efficiently. We propose that the needed averaging can be done by multilooking and that multilook data could be easily generated by rotating the tree model randomly around its vertical axis. We show that the resulting scattering data obey generally the multidimensional Gaussian

distribution or the more general K-distribution, in a way similar to synthetic aperture radar (SAR) image pixels, and can therefore be represented by a single averaged covariance matrix. The trunk-ground reflection to the backscattering direction adds to the model output non-Gaussian behavior, which can be treated as texture. Covariance matrix formalism allows us to use descriptors which are commonly used to analyze SAR images, like target entropy and alpha angle. The method helps interpretation and comparison between the model output and SAR image. [J532]

## "Radix- Resolution-Fusion for LASAR via Orthogonal Complement Decomposition"

This letter concerns the resolution-fusion method for linear array 3-D imaging SAR (LASAR). Limited by the length of the linear array, the cross-track resolution of LASAR is often lower than that in the along-track direction. To overcome this disadvantage, we assume that there are two LASAR systems whose trajectories are orthogonal to each other. Thus, we obtain a row low-resolution image and a column low-resolution image of the same scene. Using the orthogonal complement decomposition technique, we fuse the two images into one quasi-high-resolution image. Moreover, we find that the fusion distortion is unavoidable and contains the high-frequency component in both row and column directions. The information loss ratio is (N- 1)2/N2(Ndenotes the ratio of low resolution to high resolution). For a smooth image, the energy loss ratio is near to zero. With the increase of the noise energy, the energy loss ratio increases correspondingly. When the noise submerges the image completely, the energy loss ratio converges to the information loss ratio. [J533]

## "Local Degrees of Freedom of Airborne Array Radar Clutter for STAP"

In this letter, the local degree-of-freedom (LDOF) theorem for reduced-dimension space-time adaptive processing (STAP) methods is presented, and a rigorous proof is provided. LDOF is more valuable for practical STAP methods than conventional full degrees of freedom. The effectiveness of the LDOF theorem is verified, and the influences of some operations in practice on the LDOF are analyzed by simulations. [J534]

## "Polarimetric Differential SAR Interferometry: First Results With Ground-Based Measurements"

The Remote Sensing Laboratory of the Universitat Politecnica de Catalunya carried out a one-year measuring campaign in the village of Sallent, northeastern Spain, using a polarimetric ground-based synthetic aperture radar (SAR) sensor. The objective was to study the subsidence phenomenon induced by the salt mining activity conducted in this area up to the middle of the last century. Zero-Baseline polarimetric SAR (PolSAR) data were gathered at X-band in nine different days, from June 2006 to March 2007. In this letter, the problem of extracting subsidence information from fully PolSAR acquisitions for the retrieval of high-quality deformation maps is addressed. After compensating for the atmospheric artifacts caused by troposphere changes, the linear component of the deformation process is estimated separately for each polarization channel with the Coherent Pixels Technique (CPT). Afterward, a novel polarimetric approach mixing the differential-phase information of each polarization channel is proposed. The results obtained in the two cases are quantitatively compared, and the advantages provided by the polarimetric acquisitions are finally stressed. [J535]

## "Unambiguous Reconstruction and High-Resolution Imaging for Multiple-Channel SAR and Airborne Experiment Results"

Azimuth ambiguity occurs in synthetic aperture radar (SAR) systems due to the well-known constraint of minimum antenna area, particularly at high resolutions and wide swaths. A space time domain method can be utilized to remove this ambiguity if the multiple-channel data are available. In this letter, a modified approach is presented to determine the filter weight vectors. This approach was successfully applied to the real data, which were collected by an experimental airborne multiple-channel SAR system. The channel imbalance and the error in antenna phase center position are analyzed in detail. [J536]

## "A Wind and Rain Backscatter Model Derived From AMSR and SeaWinds Data"

The SeaWinds scatterometer was originally designed to measure wind vectors over the ocean by exploiting the relationship between wind-induced surface roughening and the normalized radar backscatter cross section. Rain can degrade scatterometer wind estimation; however, the simultaneous wind/rain (SWR) algorithm was developed to enable SeaWinds to simultaneously retrieve wind and rain rate data. This algorithm is based on colocating data from the Precipitation Radar on the Tropical Rainfall Measuring Mission and SeaWinds on QuikSCAT. This paper develops a new wind and rain radar backscatter model for SWR using colocated data from the Advanced Microwave Scanning Radiometer (AMSR) and SeaWinds aboard the Advanced Earth Observing Satellite II. This paper accounts for rain height in the model in order to calculate surface rain rate from the integrated rain rate. The performance of SWR using the new wind/rain model is measured by comparison of wind vectors and rain rates to the previous SWR algorithm, AMSR rain rates, and National Center

for Environmental Prediction numerical weather prediction winds. The new SWR algorithm produces more accurate rain estimates and improved winds, and detects rain with a low false alarm rate. [J537]

## "Chirp-Scaling Algorithm for Bistatic SAR Data in the Constant-Offset Configuration"

This paper discusses the processing method for bistatic SAR data in the constant-offset configuration. The constant-offset configuration is also known as the azimuth stationary or invariant configuration where transmitter and receiver follow each other, moving on identical velocity vector. In this paper, the proposed processing method for bistatic SAR data is based on Loffeld's bistatic formula that consists of two terms, i.e., the quasi-monostatic (QM) term and bistatic-deformation (BD) term. Our basic idea is to linearize the aforementioned two terms and then incorporate the BD term into the QM term to obtain an analogous monostatic spectrum. Based on the new spectrum, any efficient 2-D frequency or range-Doppler domain processor can easily be employed to process the bistatic data, where the Doppler phase parameters of the processor need to be adjusted. In this paper, we concentrate on the application of chirp-scaling-algorithm (CSA) processor. In addition, a bistatic-motion error model is developed where the position deviations of the two platforms are simplified as the bistatic slant-range displacement in the zero Doppler plane. Using this model, the monostatic motion-compensation technique is applied and integrated into CSA to compensate the trajectory deviations of transmitter and receiver. Finally, real and simulated data are used to validate the proposed processing method. [J538]

## "RONSARD Radar: Implementation of Dual Polarization on a C-Band Doppler Weather Radar"

The French C-band meteorological Doppler radar Recherche sur les Orages et Nuages par un Systeme Associe de Radars Doppler (RONSARD) was recently equipped with dual polarization. This modification required, on the one hand, an additional receiver and, on the other hand, a new design for the antenna geometry in order to decrease strongly the sidelobe level. This new radar configuration allows us to choose between two complementary modes: (1) the previous single-polarization mode, still preserved with fast Fourier transform calculations of the first three momentums of the Doppler spectrum, i.e., horizontal (H) reflectivity, radial wind velocity, and wind velocity variance calculated both in precipitation areas and clear air areas (depending on the gate), and (2) the dual-polarization mode with pulse pair processing of H and vertical reflectivities and velocities, differential phase shift, and coherence coefficient. Moreover, both modes work over contiguous gates along each direction, allowing fine radial range resolution. Thanks to the flexibility between these two modes, the RONSARD radar becomes a new major facility aimed at studying the dynamics-microphysics interactions within precipitation and their environment. [J539]

## "The GPS Contribution to the Error Budget of Surface Elevations Derived From Airborne LIDAR"

When using airborne LIDAR to produce digital elevation models, the global positioning system (GPS) positioning of the LIDAR instrument is often the limiting factor, with accuracies typically quoted as being 10-30 cm. However, a comprehensive analysis of the accuracy and precision of GPS positioning of aircraft over large temporal and spatial scales is lacking from the literature. Here, an assessment is made of the likely GPS contribution to the airborne LIDAR measurement error budget by analyzing more than 500 days of continuous GPS data over a range of baseline lengths (3-960 km) and elevation differences (400-2000 m). Height errors corresponding to the 95th percentile are <0.15 m when using algorithms commonly applied in commercial software over 3-km baselines. These errors increase to 0.25 m at 45 km and <0.5 m at 250 km. At aircraft altitudes, relative heights are shown to be potentially biased by additional errors approaching 0.2 m, partly due to unmodeled tropospheric zenith total delay (ZTD). The application of advanced algorithms, including parameterization of the residual ZTD, gives error budgets that are largely constant despite baseline length and elevation differences. In this case, height errors corresponding to the 95th percentile are <0.22 m out to 960 km, and similar levels are shown for one randomly chosen day over a 2300-km baseline. [J540]

## "Space-Surface Bistatic SAR Image Formation Algorithms"

This paper presents algorithms designed for a subclass of bistatic synthetic aperture radar (BSAR) called space-surface BSAR (SS-BSAR). Two SS-BSAR configurations are considered. The first one assumes a stationary, spaceborne transmitter and a moving airborne receiver. The second case is the generalized SS-BSAR configuration, where the transmitter is nonstationary. The transmitter and receiver have essentially different flight paths and velocities. For each configuration under investigation, the characteristics of the corresponding SS-BSAR received signal are examined first. Then, each proposed algorithm is derived analytically, and verified via simulation. [J541]

## "Spaceborne Bistatic SAR Processing Using the EETF4 Algorithm"

In this letter, the fourth-order extended exact transfer function (EETF4) is adapted for spaceborne bistatic

synthetic aperture radar (SAR) processing. The problems with high squint and large bistatic Doppler centroid variations are analyzed, and it is shown that if both transmitter and receiver are highly squinted in the same direction, then it may be demanding to achieve perfect quality of the point targets. It is shown that if both transmitter and receiver have high squint in opposite directions with small Doppler centroid variations, then the SAR image can be processed very precisely. [J542]

## "Glacier Velocity Monitoring by Maximum Likelihood Texture Tracking"

The performance of a tracking algorithm considering remotely sensed data strongly depends on a correct statistical description of the data, i.e., its noise model. The objective of this paper is to introduce a new intensity tracking algorithm for synthetic aperture radar (SAR) data, considering its multiplicative speckle/noise model. The proposed tracking algorithm is discussed regarding the measurement of glacier velocities. Glacier monitoring exhibits complex spatial and temporal dynamics including snowfall, melting, and ice flows at a variety of spatial and temporal scales. Due to these complex characteristics, most traditional methods based on SAR suffer from speckle decorrelation that results in a low signal-to-noise ratio. The proposed tracking technique improves the accuracy of the classical intensity tracking technique by making use of the temporal speckle structure. Even though a new intensity-based matching algorithm is proposed, particularly for incoherent data sets, the analysis of the proposed technique was also performed for correlated data sets. As it is demonstrated, the velocity monitoring can be continuously performed by using the maximum likelihood (ML) texture tracking without any assumption concerning the correlation of the data set. The ML texture tracking approach was tested on ENVISAT-ASAR data acquired during summer 2004 over the Inyltshik glacier in Kyrgyzstan, representing one of the largest alpine glacier systems of the world. It will be demonstrated that the proposed technique is capable of robustly and precisely detecting the surface velocity field and velocity changes in time. [J543]

## "TerraSAR-X Precise Trajectory Estimation and Quality Assessment"

Since the launch of TerraSAR-X on June 15, 2007, the required precise orbit products have been provided by the German Space Operations Center to support operational spaceborne synthetic aperture radar (SAR) and interferometric SAR image processing. The TerraSAR-X precise trajectory is reconstructed solely based on the Global Positioning System (GPS) measurements from a geodetic-grade dual-frequency Integrated Geodetic and Occultation Receiver (IGOR) onboard the spacecraft. The GPS-based precise orbit determination (POD) strategy used in the estimation of the precise TerraSAR-X orbit and its performance will be fully described in this paper. Five-month statistics from the internal and external orbit assessment indicate a root-mean-squared 3-D orbit accuracy of better than 10 and 20 cm for the precise science orbit and precise rapid orbit (PRO) products, respectively. The POD performance of the backup single-frequency MosaicGNSS receiver to support operational PRO product generation in case of IGOR tracking failure or interruptions is described as well. [J544]

## "Robust ISAR Range Alignment via Minimizing the Entropy of the Average Range Profile"

In this letter, a novel global approach to range alignment for inverse synthetic aperture radar (ISAR) image formation is presented. The algorithm is based on the minimization of the entropy of the average range profile (ARP), and the processing chain is capable of exploiting the efficiency of the fast Fourier transform. With respect to the existing global methods, the new one requires no exhaustive search operation and eliminates the necessity of the parametric model for the relative offset among the range profiles. The derivation of the algorithm indicates that the presented methodology is essentially an iterative solution to a set of simultaneous equations, and its robustness is also ensured by the iterative structure. Some alternative criteria, such as the maximum contrast of the ARP, can be introduced into the algorithm with a minor change in the entropy-based method. The convergence and robustness of the presented algorithm have been validated by experimental ISAR data. [J545]

## "Measurements of Faraday Rotation Using Polarimetric PALSAR Images"

For spaceborne synthetic aperture radar (SAR) systems operating at L-band frequencies or lower, the ionosphere may have a significant impact on the SAR images. The largest effect at L-band is caused by Faraday rotation (FR). Several studies have modeled the effect of FR and/or devised models to measure and correct FR. With the launch of the fully polarimetric L-band system Phased Array-type L-band SAR (PALSAR), it has become possible to test both models and measurement techniques on real SAR data. In this letter, the quality of calibrated polarimetric PALSAR data is assessed, and FR is measured. It is found that residual crosstalk and channel imbalance are small in the PALSAR data. Two methods are used to measure FR, the first using in-scene distributed targets and the second using large trihedrals. The two methods show very good agreement. The measurements are compared with values of the total electron content using a linear model. It is found that the model and measurements are in good agreement, with a root-mean-square error of 0.3degor 15% of the mean FR angle. [J546]

## "Data Flow and Workflow Organization-The Data Management for the TerraSAR-X Payload Ground Segment"

The payload ground segment (PGS) for the recently launched German radar satellite, TerraSAR-X, performs the operational data management of the acquired satellite data. This comprises well-known functions such as reception, systematic and on-demand processing, archiving and cataloguing, ordering, and dissemination of digital Earth-observation products. In addition, it comprises new functions like large-scale multimode acquisition ordering by users, integration with a commercial service segment, and new interfaces and workflows within the complete ground segment. The TerraSAR-X PGS is based on the Data Information and Management System (DIMS), the multimission data-handling infrastructure of the German Remote Sensing Data Center (DFD) at the German Aerospace Center. The development and integration of the new functions and complex workflows for TerraSAR-X were achieved and successfully tested on time. After the support of commissioning phase for five months, the system is now operational. As an intended side effect, the PGS for TerraSAR-X is, in several aspects, a pattern being reused for upcoming future missions, thus substantially reducing overall developmental costs. This paper investigates features of the TerraSAR-X PGS that enable the reuse in a multimission environment. It summarizes the achieved enhancements and extensions of DIMS to support the TerraSAR-X mission. Special emphasis is placed on the implementation of the request workflow initiated by user orders and the corresponding data flow within the distributed DFD multimission facility. [J547]

## "Optimization of Soil Hydraulic Model Parameters Using Synthetic Aperture Radar Data: An Integrated Multidisciplinary Approach"

It is widely recognized that synthetic aperture radar (SAR) data are a very valuable source of information for the modeling of the interactions between the land surface and the atmosphere. During the last couple of decades, most of the research on the use of SAR data in hydrologic applications has been focused on the retrieval of land and biogeophysical parameters (e.g., soil moisture contents). One relatively unexplored issue consists of the optimization of soil hydraulic model parameters, such as, for example, hydraulic conductivity values, through remote sensing. This is due to the fact that no direct relationships between the remote-sensing observations, more specifically radar backscatter values, and the parameter values can be derived. However, land surface models can provide these relationships. The objective of this paper is to retrieve a number of soil physical model parameters through a combination of remote sensing and land surface modeling. Spatially distributed and multitemporal SAR-based soil moisture maps are the basis of the study. The surface soil moisture values are used in a parameter estimation procedure based on the extended Kalman filter equations. In fact, the land surface model is, thus, used to determine the relationship between the soil physical parameters and the remote-sensing data. An analysis is then performed, relating the retrieved soil parameters to the soil texture data available over the study area. The results of the study show that there is a potential to retrieve soil physical model parameters through a combination of land surface modeling and remote sensing. [J548]

## "Detecting and Downscaling Wet Areas on Boreal Landscapes"

This letter presents an approach to classify wet areas from European Remote Sensing 2 (ERS-2) synthetic aperture radar (SAR)-, Landsat Thematic Mapper (TM)-, and Light Detection and Ranging (LiDAR)-derived terrain data and downscale the result from the coarse resolution of satellite images to finer resolutions needed for land managers. Using discrete wavelet transform (DWT) and support vector machines (SVM), the algorithm finds multiple relationships between the radar, optical, and terrain data and wet areas at different spatial scales. Decomposing and reconstructing processes are performed using a 2-D DWT (2D-DWT) and inverse 2D-DWT respectively. The underlying relationships between radar, optical, and terrain data and wet areas are learned by training an SVM at the coarse resolution of the wet-area map. The SVM is then applied on the predictors at a finer resolution to produce wet-area detailing images, which are needed to reconstruct a finer resolution wet-area map. The algorithm is applied to a boreal landscape in northern Alberta, Canada, characterized by many wet-area features including ephemeral and permanent streams and wetlands. [J549]

## "Quantifying Bird Density During Migratory Stopover Using Weather Surveillance Radar"

Increasingly, data from weather surveillance radars are being used by biologists investigating the ecology and behavior of birds, insects, and bats in the aerosphere. Unfortunately, these radars quantify echoes caused by layered biological targets such as migrating birds in a manner that introduces bias in radar measures. We investigated the performance of a bias-adjustment algorithm that adjusts radar measures for vertical variation of reflectivity, nonstandard beam refraction, and spatial displacement of radar targets. We evaluated the efficacies of four variations of this algorithm by their ability to increase correspondence between radar reflectivity measured at two weather radar sites and the ground density of migrating birds measured during two autumn seasons and two spring seasons among 24 hardwood forest sites along the northern coast of the Gulf of Mexico. The

algorithm integrated close-range reflectivity data from the five lowest elevation angle sweeps to derive high-resolution vertical profiles of reflectivity (VPRs) that closely corresponded to the observed vertical target density profiles based on a vertically oriented portable radar. The radar reflectivity of birds aloft near the onset of migratory flight was positively correlated with the bird density on the ground. All four radar data adjustment schemes that we tested produced significant improvement in the accuracy of bird density estimates relative to unadjusted radar data. In general, adjusting reflectivity based solely on the VPRs derived using observed refractive conditions yielded the most accurate radar-based estimates of bird density. [J550]

## "Orbit Accuracy Requirement for ABYSS: The Space Station Radar Altimeter to Map Global Bathymetry"

The Altimetric Bathymetry from Surface Slopes (ABYSS), which is the proposed science payload on the International Space Station (ISS), is a Johns Hopkins University Applied Physics Laboratory-developed flight-proved delay-Doppler phase-monopulse radar altimeter capable of measuring ocean surface slope in the 6-200-km half-wavelength frequency band range with an accuracy of 0.5 mu rad, with autonomous gimbal control to compensate for the ISS structural motions. This measurement allows an improved mapping of the global bathymetry, enabling a wide range of scientific research works and applications. The nonrepeat ISS orbital ground track is ideal for ABYSS. This letter describes a simulation study on the effects of the Earth's gravity field and other errors, including thermal bending of the ISS, on the orbit determination of the altimeter instrument antenna phase center location, fulfilling the science objectives of ABYSS. Our study concluded that the error due to mean gravity field is no longer limiting due primarily to the recent Gravity Recovery and Climate Experiment gravity modeling and that the ABYSS/ISS radial orbit slope error budget in the presence of various force and measurement model errors is estimated at the 0.2-mu rad root-sum-squared (RSS) level, which satisfies the ABYSS orbit accuracy science requirement to provide an improved mapping of global bathymetry. [J551]

## "A New Numerical Method for Calculating Extrema of Received Power for Polarimetric SAR"

A numerical method called cross-step iteration is proposed to calculate the maximal/minimal received power for polarized imagery based on a target's Kennaugh matrix. This method is much more efficient than the systematic method, which searches for the extrema of received power by varying the polarization ellipse angles of receiving and transmitting polarizations. It is also more advantageous than the Schuler method, which has been adopted by the PolSARPro package, because the cross-step iteration method requires less computation time and can derive both the maximal and minimal received powers, whereas the Schuler method is designed to work out only the maximal received power. The analytical model of received-power optimization indicates that the first eigenvalue of the Kennaugh matrix is the supremum of the maximal received power. The difference between these two parameters reflects the depolarization effect of the target's backscattering, which might be useful for target discrimination. [J552]

## "PALSAR Radiometric and Geometric Calibration"

This paper summarizes the results obtained from geometric and radiometric calibrations of the Phased-Array L-Band Synthetic Aperture Radar (PALSAR) on the Advanced Land Observing Satellite, which has been in space for three years. All of the imaging modes of the PALSAR, i.e., single, dual, and full polarimetric strip modes and scanning synthetic aperture radar (SCANSAR), were calibrated and validated using a total of 572 calibration points collected worldwide and distributed targets selected primarily from the Amazon forest. Through raw-data characterization, antenna-pattern estimation using the distributed target data, and polarimetric calibration using the Faraday rotation-free area in the Amazon, we performed the PALSAR radiometric and geometric calibrations and confirmed that the geometric accuracy of the strip mode is 9.7-m root mean square (rms), the geometric accuracy of SCANSAR is 70 m, and the radiometric accuracy is 0.76 dB from a corner-reflector analysis and 0.22 dB from the Amazon data analysis (standard deviation). Polarimetric calibration was successful, resulting in a VV/HH amplitude balance of 1.013 (0.0561 dB) with a standard deviation of 0.062 and a phase balance of 0.612deg with a standard deviation of 2.66deg . [J553]

## "Efficient SAR Raw Data Generation for Anisotropic Urban Scenes Based on Inverse Processing"

This letter describes efficient synthetic aperture radar raw data generation in the wavenumber domain using inverse processing. An exact form based on an inverse Omega-k algorithm and an approximate form based on an inverse Chirp Scaling algorithm are described, and examples are presented for a point scatterer. A methodology to incorporate the anisotropic behavior of an urban scene in a reflectivity map is also presented and demonstrated by means of a subaperture analysis. [J554]

## "An Inversion Method for Extraction of Wind Speed From High-Frequency Ground-Wave Radar

## Oceanic Backscatter"

A new approach to extracting sea surface wind speed from high-frequency radar Doppler spectra is presented. Based on certain appropriate approximations associated with the Doppler region close to the first-order (Bragg) peaks, the second-order radar cross section equation is differentiated. Once Doppler shifts due to ocean currents are removed from the data, an expression that relates the wind speed to the frequency position of the second-order peak is derived. The method is applied to simulated noisy data as well as to field data obtained from a Seasonde (a product of CODAR Oceans Sensors) in Breezy Point, NY. In the latter case, the retrieved wind speeds are then compared to ground truth data measured by an anemometer from a National Oceanic and Atmospheric Administration weather station located in the vicinity of the illuminated patch of ocean. Subject to certain constraints as detailed in the manuscript, the algorithm shows significant promise. [J555]

## "Scale-Dependent Surface Roughness Behavior and Its Impact on Empirical Models for Radar Backscatter"

One goal of radar remote sensing is the extraction of terrain statistics and surface dielectric properties from backscatter data for some range of wavelengths, incidence angles, and polarizations. This paper addresses empirical approaches used to estimate terrain properties from radar data over a wider range of roughness than permitted by analytical models. Many empirical models assume, at least implicitly, that roughness parameters like rms height or correlation length are independent of the horizontal length scale over which they are measured, in contrast to recent surveys of natural terrain, which show that self-affine, or power-law scaling, between horizontal scale and roughness statistics is very common. The rms slope at the horizontal scale of the illuminating wavelength s(lambda) is directly related to the variogram or structure function of a self-affine surface, can be readily obtained from field-measured topography, and, when used in an empirical model, avoids the need for arbitrary wavelength-dependent terms. To facilitate comparison with earlier approaches, an expression that links the rms height at some profile length with the rms (Allan) deviation at an equivalent horizontal sampling interval is obtained from numerical simulations. An empirical model for polarimetric scattering as a function of s(lambda) at 35deg-60deg incidence from smooth to rugged lava surfaces is derived and compared with earlier models for backscatter from modestly rough soil surfaces. The asymptotic behavior of polarization ratios for the lava flows suggests that the depolarization of linear-polarized illuminating signals occurs as a first-order process, likely through single scattering by rock edges or other discontinuities, rather than as the solely multiple-scattering effect predicted by some analytical models. Efforts to fully understand radar scattering from geological surfaces need to incorporate wavelength-scale roughness, perhaps through computational simulat--ions. [J556]

## "An Optimization Procedure of the Lagrange Multiplier Method for Polarimetric Power Optimization"

The Lagrange multiplier method is one of the basic optimization procedures to find the optimum polarizations for the incoherent scattering case. This letter proves for the first time that a fixed relationship exists between the optimum polarization and the Lagrange multiplier. Then, an optimization procedure is proposed to simplify the computational complexity of the Lagrange multiplier method. To speed up the convergence of the proposed procedure, the minimum search intervals are discussed and given theoretically. A numerical example is shown to demonstrate the effectiveness of the proposed procedure. [J557]

## "Ship Detection Using Polarization Cross-Entropy"

In this letter, polarization cross-entropy is introduced based on the eigendecomposition of the polarimetric coherence matrix. Then, the new parameter is employed for ship detection. From experimental results, it is derived that the distribution of the polarization cross-entropy in ocean regions can be well approximated by a generalized exponential distribution. Then, a constant-false-alarm-rate ship-detection method is proposed based on the distribution of the polarization cross-entropy. Using experimental results, the authors demonstrate the effectiveness of the new method in ship detection. [J558]

## "Inference of Spatial Scaling Properties of Rainfall: Impact of Radar Rainfall Estimation Uncertainties"

The existence of relationships able to connect quantities across different spatio-temporal scales represents an attractive way of describing and characterizing the high spatial and temporal variability of the rainfall process. Several studies investigated the scaling properties of spatial rainfall, and in most of the cases, these analyses were performed using radar-based estimates of rainfall, which are notoriously affected by systematic and random uncertainties. The impact of these errors on the estimated scaling properties of spatial rainfall still remains an open question. By using an empirically based radar rainfall error model, the authors explore this issue by generating ensembles of probable true rainfall fields, conditioned on radar rainfall maps. Fifteen rainfall events over Oklahoma are analyzed, and it is shown how the presence of radar rainfall errors results in biased

estimates of the scaling properties of rainfall. [J559]

## "An Optimized Algorithm for InSAR Phase Unwrapping Based on Particle Filtering, Matrix Pencil, and Region-Growing Techniques"

This letter presents a new phase unwrapping algorithm for synthetic aperture radar interferometry which combines a particle filter, a matrix-pencil (MP) local slope estimator, and an optimized region-growing technique. The advantages of the new method rely on the following contributions: The MP estimator provides better resolution to the local slope estimation, the particle filter enables simultaneous unwrapping and filtering without a prioristatistics constraints, and the implemented region-growing technique adds diversity of unwrapping paths and ensures an optimum solution. Results introduced in this letter illustrate the main aspects of the new approach. [J560]

## "L-Band Radar Estimation of Forest Attenuation for Active/Passive Soil Moisture Inversion"

In the radiometric sensing of soil moisture through a forest canopy, knowledge of canopy attenuation is required. Active sensors have the potential of providing this information since the backscatter signals are more sensitive to forest structure. In this paper, a new radar technique is presented for estimating canopy attenuation. The technique employs details found in a transient solution where the canopy (volume-scattering) and the tree-ground (double-interaction) effects appear at different times in the return signal. The influence that these effects have on the expected time-domain response of a forest stand is characterized through numerical simulations. A coherent forest scattering model, based on a Monte Carlo simulation, is developed to calculate the transient response from distributed scatterers over a rough surface. The forest transient-response model for linear copolarized cases is validated with the microwave deciduous tree data acquired by the Combined Radar/Radiometer (ComRAD) system. The attenuation algorithm is applicable when the forest height is sufficient to separate the components of the radar backscatter transient response. The frequency correlation functions of double-interaction and volume-scattering returns are normalized after being separated in the time domain. This ratio simply provides a physically based system of equations with reduced parameterizations for the forest canopy. Finally, the technique is used with ComRAD L-band stepped-frequency data to evaluate its performance under various physical conditions. [J561]

## "Airborne Ku-Band Polarimetric Radar Remote Sensing of Terrestrial Snow Cover"

Characteristics of the Ku-band polarimetric scatterometer (POLSCAT) data acquired from five sets of aircraft flights in the winter months of 2006-2008 for the second Cold Land Processes Experiment (CLPX-II) in Colorado are described in this paper. The data showed the response of the Ku-band radar echoes to snowpack changes for various types of background vegetation in the study site in north central Colorado. We observed about 0.15-0.5-dB increases in backscatter for every 1 cm of snow-water-equivalent (SWE) accumulation for areas with short vegetation (sagebrush and pasture). The region with the smaller amount of biomass, signified by the backscatter in November, seemed to have the stronger backscatter response to SWE in decibels. The data also showed the impact of surface hoar growth and freeze/thaw cycles, which created large snow-grain sizes, ice crust layers, and ice lenses and consequently increased the radar signals by a few decibels. The copolarized HH/VV backscatter ratio seems to indicate double-bounce scattering between the ground surface and snow or vegetation. The cross-polarized backscatter [vertical-horizontal (VH)] showed not only the influence of vegetation but also the strong response to snow accumulation. The observed HV/VV ratio suggests the importance of multiple scattering or nonspherical scattering geometry of snow grain in the dense-media radiative transfer scattering model. Comparison of the POLSCAT and QuikSCAT data was made and confirmed the effects of mixed terrain covers in the coarse-resolution QuikSCAT data. [J562]

## "LIDAR Observations of Aerosol Properties Over Tropical Urban Region-A Case Study During a Low-Pressure System Over Bay of Bengal"

Variations in aerosol properties and ground-reaching solar irradiance over a tropical urban environment in Hyderabad, India, associated with a low-pressure system during December 3-10, 2008, over Bay of Bengal (BoB) were analyzed. Considerable variations in aerosol properties and ground-reaching solar irradiance due to changes in wind velocity and direction associated with the low-pressure system formed over southeast BoB were observed. Terra/Aqua Moderate Resolution Imaging Spectroradiometer AOD550variations showed trends matching with ground observations. Nighttime Light Detection and Ranging (LIDAR) observations suggested considerable reduction in atmospheric particulate matter (PM) loading under the influence of low-pressure system. Results of the study have implications for monitoring urban air quality as synoptic weather systems are capable of modifying the atmospheric PM loading. [J563]

## "Multiscale Change Detection in Multitemporal Satellite Images"

In this letter, we propose a novel technique for unsupervised change detection in multitemporal satellite images. The difference image which is computed from multitemporal images acquired on the same geographical area at two different time instances is decomposed using S-levels undecimated discrete wavelet transform (UDWT). For each pixel in the difference image, a multiscale feature vector is extracted using the subbands of the UDWT decomposition and the difference image itself. The final change detection map is achieved by clustering the multiscale feature vectors using k-means algorithm into two disjoint classes: changed and unchanged. Experimental results confirm the efficacy of the proposed approach on both optical and synthetic aperture radar images. [J564]

## "Nondestructive Sensor Using Microwaves From Laser Plasma by Subnanosecond Laser Pulses"

Conventional ground-penetrating radar (GPR) requires large-aperture antennas or long-span measurements to survey a remote location precisely. We propose a laser-driven GPR (LGPR) as a new detection method. LGPR uses microwaves from laser-produced plasmas as remote transmitters and can survey a remote location using a compact instrument. We performed numerical simulations to investigate the radiation mechanism of microwaves from laser plasmas and confirmed the pulsewidth of the laser suitable for LGPR. Experiments with subnanosecond pulse lasers clarified the feasibility and detection performance of LGPR. [J565]

## "Comparison of the ASI Ice Concentration Algorithm With Landsat-7 ETM+ and SAR Imagery"

Continuous monitoring of sea ice and its changes is mainly done by passive microwave sensors on satellites. One frequently used technique of retrieving sea-ice concentrations is the Arctic Radiation and Turbulence Interaction STudy Sea Ice (ASI) algorithm, which uses the near-90-GHz channels, here those of the Advanced Microwave Scanning Radiometer-Earth Observing System to calculate sea-ice concentrations. The ASI ice concentrations are compared with ice concentrations derived from the following: 1) the multispectral imager Enhanced Thematic Mapper Plus operating on Landsat and 2) from Envisat and Radarsat SAR images. In this paper, we focus on marginal ice zones, as the ice concentrations in those regions are in general observed with higher errors. First-year ice (bias: -1%-0% and rms error: 1%-4%) and young ice (bias: -4%-0% and rms error: 3%-9%) are fairly well recognized with little underestimation of ASI ice concentrations with respect to Landsat ice concentrations. New ice is identified with less accuracy by the ASI algorithm (bias: -16%-9% and rms error: 18.3%-26.2%). Averaged over all ice types, the bias ranges between -8.4% and 4.5%, and the rms error ranges between 2.0% and 17.4%. Discrepancies mainly occur in polynya areas (underestimation by ASI) and along the ice edge (overestimation by ASI). The results of the ASI-SAR comparison yield contrasting results. ASI underestimates the ice concentrations near the ice edge but overestimates them in some interior areas (bias: -2.9%-2.5% and rms error: 16.9%-20.1%). The discrepancies between both comparisons may be due to the different interaction mechanisms of the different sensor types, particularly with the newly formed ice. [J566]

## "MST Radar Signal Processing Using Wavelet-Based Denoising"

Atmospheric signal processing is of interest to many scientists, where there is scope for the development of new and efficient tools for cleaning the spectrum, detection, and estimation of parameters like zonal (U), meridional (V), wind speed (W), etc. This letter deals with a signal processing technique for the estimation of the aforementioned parameters, based on the wavelets, by analyzing the mesosphere-stratosphere-troposphere radar data that are backscattered from the atmosphere at high altitudes and severe weather conditions with low signal-to-noise ratio. The proposed algorithm is self-consistent in detecting wind speeds up to a height of 18 km, in contrast to the existing method which estimates the Doppler manually and fails at higher altitudes. The results have been validated using the Global Positioning System sonde data. [J567]

## "Multi Scat-A Helicopter-Based Scatterometer for Snow-Cover and Sea-Ice Investigations"

A helicopter-based Doppler scatterometer (Multi3Scat) is described. It allows simultaneous measurements of the surface radar backscatter at five different frequencies at co- and cross-polarization at incidence angles of 20deg-65degfrom an altitude of 30-300 m. Video and infrared (IR) cameras simultaneously sense the surface in the scatterometers' footprint. The Multi 3Scat is calibrated using measurements carried out over corner reflectors. The stability of the Multi3Scat's signal is found to be, on average, better than 0.5 dB. Typical signal-to-noise-ratio values for sigma-0 range between 10 and 20 dB for cross-polarization and between 15 and 25 dB for copolarization over snow and ice surfaces. The potential of the Multi3Scat to acquire multifrequency multipolarization radar backscatter data and coincident video and IR temperature observations at different incidence angles over remote terrain such as the Arctic Ocean or the Alps is demonstrated. [J568]

## "Depolarization ratio measurement using single photomultiplier tube in micropulse lidar"

The conventional dual polarization micropulse lidar uses two separate photomultiplier tubes (PMT) to detect both the copolarized and cross-polarized beam. The prominent sources of error in the depolarization ratio measurement are mismatch in PMT, improper selection of discriminator threshold and unequal PMT high voltage. In the present work a technique for the measurement of lidar depolarization ratio using only one PMT sensor has been developed. The same PMT detects both copolarized and cross-polarized lidar backscatter. A stepper motor is used along with the mirrors to bring both the received polarization signals over the PMT window. Application of the same PMT minimizes the error caused in the depolarization ratio measurement due to error in photon counting of an individual channel. The design description of this technique along with the preliminary results depicting its functionality has been mentioned in this article. [J569]

## "Comparison of balloon-carried atmospheric motion sensors with Doppler lidar turbulence measurements"

Magnetic sensors have been added to a standard weather balloon radiosonde package to detect motion in turbulent air. These measure the terrestrial magnetic field and return data over the standard uhf radio telemetry. Variability in the magnetic sensor data is caused by motion of the instrument package. A series of radiosonde ascents carrying these sensors has been made near a Doppler lidar measuring atmospheric properties. Lidar-retrieved quantities include vertical velocity (w)profile and its standard deviation (sigma w). sigma wdetermined over 1 h is compared with the radiosonde motion variability at the same heights. Vertical motion in the radiosonde is found to be robustly increased when sigma w  0.75m s-1and is linearly proportional to sigma w. [J570]

## "Aerosol Lidar Intercomparison in the Framework of SPALINET-The Spanish Lidar Network: Methodology and Results"

A group of eight Spanish lidars was formed in order to extend the European Aerosol Research Lidar Network-Advanced Sustainable Observation System (EARLINET-ASOS) project. This study presents intercomparisons at the hardware and software levels. Results of the system intercomparisons are based on range-square-corrected signals in cases where the lidars viewed the same atmospheres. Comparisons were also made for aerosol backscatter coefficients at 1064 nm (2 systems) and 532 nm (all systems), and for extinction coefficients at 532 nm (2 systems). In total, three field campaigns were carried out between 2006 and 2007. Comparisons were limited to the highest layer found before the free troposphere, i.e., either the atmospheric boundary layer or the aerosol layer just above it. Some groups did not pass the quality assurance criterion on the first attempt. Following modification and improvement to these systems, all systems met the quality criterion. The backscatter algorithm intercomparison consisted of processing lidar signal profiles simulated for two types of atmospheric conditions. Three stages with increasing knowledge of the input parameters were considered. The results showed that all algorithms work well when all inputs are known. They also showed the necessity to perform, when possible, additional measurements to attain better estimation of the lidar ratio, which is the most critical unknown in the elastic lidar inversion. [J571]

## "Improved Correction of Beam Mismatch of the Precipitation Radar After Orbit Boost of the TRMM Satellite"

One effort in developing the Tropical Rainfall Measuring Mission (TRMM) precipitation radar (PR) data processing algorithm is to correct the PR received power for mismatched-beam data after the orbit is boosted. The current standard algorithm employs a beam-mismatch correction algorithm based on the rain-echo radar equation (Takahashi's method). However, there remains a need for improving the estimated power of the mismatched-pulse echo returned from the Earth's surface and weak rain because the echo is represented with the surface-echo radar equation and the noise-power level. The error in Takahashi's method causes a negative bias (around 1 dB) in the PR received power near the main lobe clutter. This paper formulates an improved estimate of the mismatched pulse based on the rain-echo radar equation and the surface-echo radar equation for a flat-Earth surface. The improved estimate is then evaluated numerically and experimentally with the actual data obtained by TRMM/PR for observations over the ocean. The consistency of TRMM/PR data sets between preboost and postboost was improved by eliminating the negative bias (around 1 dB) in the PR received power. The mean rain rate near the surface-echo range increases by 10%, and the angle-bin asymmetry of the mean rainfall rate, which is present in the postboost data corrected by Takahashi's method, is resolved. [J572]

## "An Adaptive Noise-Filtering Algorithm for AVIRIS Data With Implications for Classification Accuracy"

This paper describes a new algorithm used to adaptively filter a remote-sensing data set based on signal-to-

noise ratios (SNRs) once the maximum noise fraction has been applied. This algorithm uses Hermite splines to calculate the approximate area underneath the SNR curve as a function of band number, and that area is used to place bands into ldquobinsrdquo with other bands having similar SNRs. A median filter with a variable-sized kernel is then applied to each band, with the same size kernel used for each band in a particular bin. The proposed adaptive filters are applied to a hyperspectral image generated by the airborne visible/infrared imaging spectrometer sensor, and results are given for the identification of three different pine species located within the study area. The adaptive-filtering scheme improves image quality as shown by estimated SNRs. Classification accuracies of three pine species improved by more than 10% in the study area as compared to that achieved by the same discriminant method without adaptive spatial filtering. [J573]

## "Spatial Filtering for Wall-Clutter Mitigation in Through-the-Wall Radar Imaging"

Radio-frequency imaging of targets behind walls is of value in several civilian and defense applications. Wall reflections are often stronger than target reflections, and they tend to persist over a long duration of time. Therefore, weak and close by targets behind walls become obscured and invisible in the image. In this paper, we apply spatial filters across the antenna array to remove, or at least significantly mitigate, the spatial zero-frequency and low-frequency components which correspond to wall reflections. Unmasking the behind-the-wall targets via the application of spatial filters recognizes the fact that the wall electromagnetic (EM) responses do not significantly differ when viewed by the different antennas along the axis of a real or synthesized array aperture which is parallel to the wall. The proposed approach is tested with experimental data using solid wall, multilayered wall, and cinder block wall. It is shown that the wall reflections can be effectively reduced by spatial preprocessing prior to beamforming, producing similar imaging results to those achieved when a background scene without the target is available. [J574]

## "3-D Radargrammetric Modeling of RADARSAT-2 Ultrafine Mode: Preliminary Results of the Geometric Calibration"

The geometry and the accuracy of the 3-D cartographic localization of RADARSAT-2 images are being evaluated as part of the Canadian Space Agency's Science and Operational Applications Research program. In a first step, the Toutin's 3-D physical model, previously developed for RADARSAT-1, was adapted to RADARSAT-2 sensor and applied to two ultrafine mode images (U2 and U25) acquired over an area in Beauport, Quebec. Both the 3-D modeling computed with only 12 ground control points and its geometric localization were evaluated with different check data: (1) independent check points; (2) the two quasi-epipolar images; (3) the two orthoimages; and (4) 1-m accurate orthophotos. All four results and validations are in agreement and confirm that the 3-D geometric localization and restitution accuracy are 1 m in planimetry and 2 m in elevation. The checked data error being included in these evaluations and the relative error computed from the quasi-epipolar comparison provided a high level of confidence that the precision of Toutin's 3-D radargrammetric model is better than 0.25 m. [J575]

## "Performance of Discrete-Fourier-Transform-Based Velocity Estimators for a Wind-Sensing Coherent Doppler Lidar System in the Kolmogorov Turbulence Regime"

The performance of discrete-Fourier-transform (DFT)-based velocity estimators for wind-sensing coherent Doppler lidar systems in the Kolmogorov turbulence regime is summarized using Monte Carlo simulations. Furthermore, a signal model, a simulation procedure, velocity estimators, and simulation conditions are explained. The relationships between signal-to-noise ratio, line-of-sight velocity estimation precision, and signal detection probability are simulated and summarized. In addition to the basic DFT estimator, signal matching estimators which utilize DFT are studied. The performances in the Kolmogorov turbulence regime and those in the Gaussian autocovariance signal model are compared. The performances are compared for wavelength regions of 1.5, 2, and 10 mum. [J576]

## "A Change Detection Algorithm for Retrieving High-Resolution Soil Moisture From SMAP Radar and Radiometer Observations"

A change detection algorithm has been developed in order to obtain high-resolution soil moisture estimates from future Soil Moisture Active and Passive (SMAP) L-band radar and radiometer observations. The approach combines the relatively noisy 3-km radar backscatter coefficients and the more accurate 36-km radiometer brightness temperature into an optimal 10-km product. In preparation for the SMAP mission, an observation system simulation experiment (OSSE) and field experimental campaigns using the Passive and Active L- and S-band Airborne Sensor (PALS) have been conducted. We use the PALS airborne observations and OSSE data to test the algorithm and develop an error budget table. When applied to four-month OSSE data, the change detection method is shown to perform better than direct inversion of the radiometer brightness temperatures

alone, improving the root mean square error by 2% volumetric soil moisture content. The main assumptions of the algorithm are verified using PALS data from the soil moisture experiments held during June-July 2002 (Soil Moisture Experiment 2002) in Iowa. The algorithm error budget is estimated and shown to meet SMAP science requirements. [J577]

## "Forest Biophysical Parameter Estimation Using L- and P-Band Polarimetric SAR Data"

L- and P-band airborne polarimetric synthetic aperture radar (SAR) data acquired by the RAMSES system over different height maritime pine (Pinus Pinaster Ait.) stands of the Nezer forest (Landes, France) have been evaluated for forest biophysical parameter estimation. A pseudolinear correlation has been brought to evidence at P-band between polarimetric anisotropy and mean tree height, which is also linked to other biophysical parameters in the Nezer forest, meaning that SAR polarimetry constitutes a promising tool for forest parameter retrieval at low frequency. The spatial conditions have been evaluated through the quantification of the impact of signal-to-noise ratio diminution and resolution degradation on the forest height inversion. It has been shown that the inversion accuracy remains acceptable for N Esigma0, representing the noise level of the SAR image, which is lower than -15 dB, and for spatial resolution increasing up to 15 m. [J578]

## "Modeling and Simulation of SAR Image Texture"

The characteristics of synthetic aperture radar (SAR) image texture may be related to the properties of underlying elemental scene scatterers through established models based on the properties of a backscattering coefficient (in this paper, we use and unnormalized coefficient s) of these scatterers. In this paper, we generate raw SAR data by simulating the statistical characteristics of elemental scene scatterers such as the order of the gamma distribution, the form and length of their spatial correlation, and their spatial density. This simulation is carried out using a SAR signal simulation system called cSAR. We describe a particular set of methods to simulate image texture used in cSAR, and provide a detailed analysis of simulated sand of the speckle and texture characteristics of simulated images. We found that the distribution of swas strongly affected by the order, density, and correlation length of the underlying scatterers. We found that the simulated SAR images were consistently K-distributed as expected. The estimated image order was a strong function of the scattering properties and that the estimated image order is a relatively weak descriptor of image texture when used on its own. The correspondence between the observed image autocorrelation function (ACF) and the theoretical models of Oliver is excellent, and we could estimate the scatterer correlation length by fitting the Oliver model to the observed ACF. We combined the estimated image order and correlation length and found potential for using these two image texture descriptors in classification and segmentation algorithms. [J579]

## "The EnviSat RA-2 Instrument Design and Tracking Performance"

The EnviSat satellite embarks an innovative radar altimeter, the RA-2 which represents a new generation of radar altimeters compared to previous instruments such as the European Remote Sensing Satellite (ERS) altimeters and The Ocean Topography Experiment/Poseidon. This is due to its integration of many new features. In particular, the RA-2 is the first satellite altimeter to incorporate autonomous resolution selection and a model-free tracker. The behavior of the instrument in orbit is controlled by onboard algorithms which determine the instrument logic, and a list of onboard parameters which control when switches in resolution occur. This logic and the choice of these parameters have a strong influence on the tracking performance. This paper describes the operation of the RA-2 onboard tracker and the resolution selection logic. We provide a detailed description of the algorithm and its configuration parameters after optimization during the EnviSat Commissioning Phase. Finally, we show the tracking performance, in particular compared to the ones of the ERS-2 altimeter, over different types of surfaces. [J580]

## "An Accurate Strategy for 3-D Ground-Based SAR Imaging"

In this letter, an analytical description of the 2-D and 3-D imaging of ground-based synthetic aperture radar data is given. The ability of the 3-D imaging to separate targets along the elevation direction will also be shown, thus allowing their complete localization in space. The validation of the proposed method is done by exploiting simulated data. [J581]

## "Relationship Between PALSAR Backscatter and Surface-Roughness Parameters From Iron Laterites in CarajЂs, Amazon Region"

The objective of this investigation was to evaluate the influence of micro- and macrotopography on PALSAR fine-beam dual backscattering in the characterization of iron laterites in Carajas Province, Amazon Region. The moderate linear correlation between sigma0and surface roughness indicated that, only for L-HH polarization, sigma0was modulated by the morphology of the geological surfaces. [J582]

## "Assessment of Atmospheric Propagation Effects in SAR Images"

TerraSAR-X, the first civil German synthetic aperture radar (SAR) satellite, was successfully launched on June 15, 2007. After 4.5 days, the first processed image was obtained. The overall quality of the image was outstanding; however, suspicious features could be identified which showed precipitation-related signatures. These rain-cell signatures are thoroughly investigated, and the physical background of the related propagation effects is provided. In addition, rain-cell signatures from former missions like SIR-C/X and the Shuttle Radar Topography Mission are provided for comparison. During the commissioning phase of TerraSAR-X, a total of 12 000 scenes were investigated for potential propagation effects, and about 100 scenes revealed atmospheric effects to a visible extent. Some of the particularly interesting events were selected and are discussed in greater detail. An interesting case of data acquisition over New York will be presented, which shows typical rain-cell signatures, and the SAR image will be compared with weather-radar data acquired nearly simultaneously (within the same minute). By comparing the images, it can be clearly seen that reflectivities in the weather-radar image of 50 dBZ may cause visible artifacts in SAR images. Furthermore, in this paper, we discuss the influence of the atmosphere (troposphere) on the external calibration of TerraSAR-X. By acquiring simultaneous weather-radar data over the test site and the SAR acquisition, it was possible to flag affected SAR images and to exclude them from the procedure to derive the absolute calibration constant. Thus, it was possible to decrease the 1 sigma uncertainty of the absolute calibration factor by 0.15 dB. [J583]

## "Hybrid GPU-Based Single- and Double-Bounce SAR Simulation"

In this paper, a new hybrid graphics-processing-unit (GPU)-based real-time synthetic aperture radar (SAR) simulation system is presented. Previous real-time SAR simulators only supported single-bounce simulation in real time. The new hybrid system uses the rasterization approach for real-time single-bounce simulation and a new image-based GPU ray-tracing approach for monostatic SAR double-bounce simulation. This approach provides fast simulation results even while simulating complex and extended scenes. The simulation results are compared to a high-resolution airborne SAR image, and the limitations of the approach are discussed. [J584]

## "Operational Large-Area Forest Monitoring in Siberia Using ALOS PALSAR Summer Intensities and Winter Coherence"

Focusing on Siberia, the feasibility of using Advanced Land Observing Satellite Phased Arrayed L-band Synthetic Aperture Radar (PALSAR) summer-intensity and winter-coherence images for large-area forest monitoring was investigated. Fine beam dual horizontal/horizontal and horizontal/vertical (polarization) intensity strip images were acquired during the summer of 2007. The processing consisted of radiometric calibration, orthorectification, and topographic normalization. The coherence was estimated from interferometric pairs with 46-day repeat-pass intervals. The pairs were acquired during the winters of 2006/2007 and 2007/2008. During both winters, suitable weather conditions that allow for low temporal decorrelation had been reported. By using PALSAR intensities and winter-coherence data, areas of forest and nonforest were separated. By combining both data types, a minimal overlap of the class signatures was observed, even though the analysis was conducted at the pixel level and no speckle filter was applied. The study concludes that the operational delineation of forest cover using PALSAR data is feasible. By applying a segmentation-based classification, an accuracy of 93% was obtained. [J585]

## "Microwave Subsurface Imaging Using Direct Finite-Difference Frequency-Domain-Based Inversion"

We have developed a new algorithm for electromagnetic inverse scattering problems in inhomogeneous media using finite-difference frequency-domain (FDFD) forward modeling, referred to as the FDFD-based inversion method. The key issue of this method is to build a linear expression for the inverse problem from an FDFD forward model by using Born approximation to neglect mutual coupling between scattered pixels and to then solve for the inverse coefficient matrix. An important advantage of this matrix-based method is that there is no need to specify a Green's function. As such, this inverse scattering algorithm is easily implemented and is robust to the heterogeneity in the background. We test the algorithm with a microwave subsurface object detection application using cross-well radar. The new method is compared with conventional inversion using Green's function-based Born approximation. Numerical experiments are presented for a 2-D borehole geometry for buried object detection in uniform soil and in multilayered soil backgrounds. [J586]

## "Combined Passive and Active Microwave Observations of Soil Moisture During CLASIC"

An important research direction in advancing higher spatial resolution and better accuracy in soil moisture

remote sensing is the integration of active and passive microwave observations. In an effort to address this objective, an airborne instrument, the passive/active L-band sensor (PALS), was flown over two watersheds as part of the cloud and land surface interaction campaign (CLASIC) conducted in Oklahoma in 2007. Eleven flights were conducted over each watershed during the field campaign. Extensive ground observations (soil moisture, soil temperature, and vegetation) were made concurrent with the PALS measurements. Extremely wet conditions were encountered. As expected from previous research, the radiometer-based retrievals were better than the radar retrievals. The standard error of estimates (SEEs) of the retrieved soil moisture using only the PALS radiometer data were 0.048 m3/m3for Fort Cobb (FC) and 0.067 m3/m3for the Little Washita (LW) watershed. These errors were higher than typically observed, which is likely the result of the unusually high soil moisture and standing water conditions. The radar-only-based retrieval SEEs were 0.092 m3/m3for FC and 0.079 m3/m3for LW. Radar retrievals in the FC domain were particularly poor due to the high vegetation water content of the agricultural fields. These results indicate the potential for estimating soil moisture for low-vegetation water content domains from radar observations using a simple vegetation model. Results also showed the compatibility between passive and active microwave observations and the potential for combining the two approaches. [J587]

## "Arctic sea ice mapping with satellite radars"

The drastic reduction of Arctic sea ice in recent years demands ice monitoring over various spatial and temporal scales. Sea ice backscatter signatures from field measurements and from model analyses are obtained at L-band and C-band frequencies. Based on these signatures, capabilities for Arctic sea ice mapping are determined for current and future satellite active microwave sensors including synthetic aperture radars (SAR) and scatterometers. This study includes L-band and C-band radars such as the ERS (European Remote Sensing), Envisat (Environmental Satellite), RADARSAT-1 and 2, ALOS (Advanced Land Observing Satellite), and DESDnyl (Deformation, Ecosystem Structure, and Dynamics of Ice). SARs with resolutions from 10 to 100 m, and the SMAP (Soil Moisture Active-Passive) scatterometer with resolutions from 1 to 10 km. [J588]

## "Phased Array Radar Polarimetry for Weather Sensing: A Theoretical Formulation for Bias Corrections"

It is becoming widely accepted that radar polarimetry provides accurate and informative weather measurements, while phased-array technology can shorten data updating time. In this paper, a theory of phased array radar (PAR) polarimetry is developed to establish the relation between electric fields at the antenna of the PAR and the fields in a resolution volume filled with hydrometeors. It is shown that polarimetric measurements with an electronically steered beam can cause measurement biases that are comparable to or even larger than the intrinsic polarimetric characteristics of hydrometeors. However, these biases are correctable if the transmitted electric fields are known. A correction to the measured scattering matrix that removes biases in meteorological variables is derived. The challenges and opportunities for weather sensing with a polarimetric PAR are discussed. [J589]

## "GPS-Based Time & Phase Synchronization Processing for Distributed SAR"

Distributed synthetic aperture radar (DiSAR), including bi- and multistatic SAR, operates with distinct transmitting and receiving antennas that are mounted on separate platforms. Spatial separation has several operational advantages, such as reduced vulnerability in military applications and increased radar cross section (RCS); which may increase the capability, reliability, and flexibility of future aerospace remote sensing missions. However, in this configuration, there is no cancellation of reference oscillator phase noise as in monostatic cases. There are additional technical problems associated with temporal synchronization of the transmit and receive systems. Therefore, highly accurate time and phase synchronization must be provided. Little work on these challenges has been reported. This paper presents a Global Positioning System (GPS)-based technique for achieving successful time and phase synchronization for DiSAR. This technique offers high-frequency stability. More importantly, residual time synchronization errors may be compensated for with a high-precision range alignment method, and residual phase synchronization errors may be compensated for with a subaperture autofocus algorithm. [J590]

## "Space-borne technology and inversion techniques for radar"

This presents recent progress of the state-of-the-art of space-borne radar technology in case of either earth-orbiting or planetary-orbiting satellites and space probes, respectively. In addition to that, recent progress is also discussed concerning specific inversion techniques to evaluate radar measurements; i.e., the art of deriving the relevant physical quantities to be determined such as terrain and depth profiles for planetary surface and/or subsurface structures ((3D)-profiles) from radar data measured depending on signal frequency, aspect angle, polarization, etc., as a function of time. [J591]

## "The PALSAR Polarimetric Mode for Sea Oil Slick Observation"

A study on sea oil slick observation by means of L-band polarimetric synthetic aperture radar (SAR) data is accomplished. It is based on different sea surface scattering mechanism expected with and without surface slicks. Polarimetric measurements are processed by means of a simple and very effective filtering technique which is electromagnetically based on the Mueller scattering matrix. Moreover, some polarimetric features, evaluated on both slick-free and slick-covered sea surfaces, are analyzed for confirming the filter output. Experiments are accomplished on the polarimetric SAR data acquired by the Phased Array-type L-band Synthetic Aperture Radar (PALSAR) sensor, mounted on board of the Advanced Land Observing Satellite (ALOS), and are relevant to oil slick, due to a tank accident, and look-alikes. Results demonstrate for the first time that L-band polarimetric SAR measurements are useful for oil slick observation purposes and witness the capability of the ALOS PALSAR data for such application. [J592]

## "A New Method for Correcting ScanSAR Scalloping Using Forests and Inter-SCAN Banding Employing Dynamic Filtering"

The Scanning Synthetic Aperture Radar (ScanSAR) is very useful for Earth observation because of its wider imaging swath and shorter revisit time. However, ScanSAR is sometimes affected by the following three artifacts: (1) scalloping, which often appears as repeating weak azimuth stripes at both edges of the focused burst image; (2) azimuth ambiguity (i.e., a form of ghosting that appears over the adjacent uniform area when the pulse repetition frequency is below the Doppler bandwidth); and (3) radiometric discontinuity (i.e., banding) between two adjacent scans. This paper proposes three methods to correct these artifacts, which are, specifically, the proposal for scalloping correction using Amazon Rainforest data, band limitation, and the correction for the inter SCAN banding using the dynamic gain correction algorithm. Several corrected sample data sets of the Phased-Array L-band SAR onboard the Advanced Land-Observing Satellite are presented to demonstrate the validity of the proposed methods. [J593]

## "Estimation of Soil Moisture and Faraday Rotation From Bare Surfaces Using Compact Polarimetry"

The potential of compact polarimetry (CP) mode at longer wavelengths in a space environment for surface parameter estimation is investigated. CP consists of transmitting a single polarization while receiving two polarizations. At longer wavelengths, one of the main challenges associated with CP from space is Faraday rotation (FR) estimation and correction. In this paper, an estimation procedure for FR is presented, which relies on the scattering properties of bare surfaces. The selection of the bare surfaces is based on a new parameter, the conformity coefficient computed from CP measurements. This parameter is shown to be FR invariant. Once estimated, the FR can be corrected over the whole image. A simple approximation to sigmaHHoand sigmaVVobased on CP measurements over bare soil surfaces is presented, from which soil moisture can be estimated using the 1995 Dubois algorithm. The results obtained using CP are shown to be in good agreement with those obtained from the standard Dubois algorithm using fully polarimetric data. This implies that, for soil moisture, CP can be used instead of HH and VV dual-polarized measurements. [J594]

## "Foreword to the Special Issue on Calibration and Validation of ALOS Sensors (PALSAR, AVNIR-2, and PRISM) and Their Use for Bio- and Geophysical Parameter Retrievals"

The 17 papers in this special issue focus on the calibration and validation of ALOS sensors and their use for bio- and geophysical parameter retrievals. [J595]

## "Polarimetric PALSAR Calibration"

Polarimetric Phased-Array-type L-band Synthetic Aperture Radar (PALSAR) system parameters are assessed using data sets collected over several calibration sites. The data collected over the Amazonian rain forest help validate the hypothesis that Faraday rotation is zero near the equator. The analysis of the Amazonian forest data and the response of the corner reflectors deployed there during the PALSAR acquisitions lead to the conclusion that the antenna is highly isolated (better than -35 dB). These results are confirmed using the data collected over calibration sites located in Sweden and Canada. The 5-m-height corner reflector deployed at the Remningstorp (Sweden) calibration site by Chalmers University of Technology provides accurate measurement of antenna parameters and detection of a (2deg -3deg) Faraday rotation during day-time acquisitions, whereas no Faraday rotation was noted during night-time acquisitions. Small Faraday rotation angles (2deg-3deg) have been measured using acquisitions over the DLR Oberpfaffenhofen and the Ottawa calibration sites. The presence of small but still significant Faraday rotation (2deg-3deg) induces a corner reflector return at the cross-polarization HV and VH that should not be interpreted as the actual antenna crosstalk. These results show that the PALSAR

antenna is highly isolated (better than -35 dB), and diagonal antenna distortion matrices (with zero crosstalk terms) can be used for accurate calibration of PALSAR polarimetric data. [J596]

## "The German satellite mission TerraSAR-X"

TerraSAR-X is Germany's first national remote sensing satellite being implemented in a public-private partnership between the German Aerospace Centre (DLR) and EATS Astrium GmbH. TerraSAR-X was launched on June 15, 2007 and will supply high-quality radar data for purposes of scientific observation of the Earth for a period of at least five years. At the same time, it is designed to satisfy the steadily growing demand of the private sector for remote sensing data in the commercial market. [J597]

## "A Dual-Polarized Planar-Array Antenna for S-Band and X-Band Airborne Applications"

A new dual-frequency dual-polarized array antenna for airborne applications is presented in this paper. Two planar arrays with thin substrates (R/T Duroid 5880 substrate, with epsivr= 2.2 and a thickness of 0.13 mm) are integrated to provide simultaneous operation at S band (3 GHz) and X band (10 GHz). Each 3 GHz antenna element is a large rectangular ring-resonator antenna, and has a 9.5 dBi gain that is about 3 dB higher than the gain of an ordinary ring antenna. The 10 GHz antenna elements are circular patches. They are combined to form the array with a gain of 18.3 dBi, using a series-fed structure to save the space of the feeding line network. The ultra-thin array can be easily placed on an aircraft's fuselage, due to its lightweight and conformal structure. It will be useful for wireless communication, radar, remote sensing, and surveillance applications. [J598]

## "Collision Sensing by Stereo Vision and Radar Sensor Fusion"

To take advantage of both stereo cameras and radar, this paper proposes a fusion approach to accurately estimate the location, size, pose, and motion information of a threat vehicle with respect to a host one from observations that are obtained by both sensors. To do that, we first fit the contour of a threat vehicle from stereo depth information and find the closest point on the contour from the vision sensor. Then, the fused closest point is obtained by fusing radar observations and the vision closest point. Next, by translating the fitted contour to the fused closest point, the fused contour is obtained. Finally, the fused contour is tracked by using rigid body constraints to estimate the location, size, pose, and motion of the threat vehicle. Experimental results from both synthetic data and real-world road test data demonstrate the success of the proposed algorithm. [J599]

## "Satellite Retrievals of Arctic and Equatorial Rain and Snowfall Rates Using Millimeter Wavelengths"

A new global precipitation retrieval algorithm for the millimeter-wave Advanced Microwave Sounding Unit is presented that also retrieves Arctic precipitation rates over surface snow and ice. This algorithm improves upon its predecessor by excluding some surface-sensitive channels and by reducing the number of principal components (PCs) used to represent those that remain. The training sets were also modified to better represent cold regions. The algorithm still incorporates conversion of brightness temperatures to nadir, spatial filtering to better detect pixels scattering near 54 GHz, PC filtering of surface effects, and use of separate neural networks trained with the fifth-generation National Center for Atmospheric Research/Penn State Mesoscale Model (MM5) for land and sea, where warm and cold ocean are now treated differently. The validity of the snowfall detections is supported by nearly coincident CloudSat radar observations, and the physics of the model is largely validated by the reasonable agreement in annual precipitation obtained for 231 globally distributed rain gauges, including many at latitudes where snowfall dominates. Observed annual global precipitation statistics are also presented to permit comparisons with other algorithms and sensors. [J600]

## "Verification of Polarimetric Calibration Method Including Faraday Rotation Compensation Using PALSAR Data"

The spaceborne Phased Array L-band Synthetic Aperture Radar (PALSAR) needs polarimetric calibration in order for PALSAR data to be utilized for various applications such as geophysical analysis. In case of a PALSAR system using L-band, the Faraday rotation (FR) effect, which rotates the polarization plane of radio waves, becomes a problem when full-polarimetric observation data are used, such as target classification using polarization synthesis. Therefore, we need to estimate and remove both antenna distortion matrices and the FR effect. In this paper, we propose a polarimetric calibration method taking both channel imbalance and crosstalk of receiving and transmitting antennas and FR effect into consideration using two reference reflectors, namely, polarization preserving reflector and polarization rotating one. Then, we apply our calibration method to PALSAR data and derive antenna distortion matrices and FR angle simultaneously. Our calibration results show that the estimated antenna distortion matrices are almost equal to the calibration results from the Japan Aerospace

Exploration Agency and that the estimated FR angle has a reasonable value. [J601]

## "Employing a Method on SAR and Optical Images for Forest Biomass Estimation"

In this paper, we develop a novel method for forest biomass estimation. The intensity values of Advanced Land Observation Satellite-Advanced Visible and Near Infrared Radiometer type 2 and PRISM images and the texture features of the Japanese Earth Resources Satellite 1 image are used in a multilayer perceptron neural network (MLPNN) that relates them to the forest variable measurements on the ground. A proposed speckle noise model is also applied for modeling and reducing the speckle noise in the synthetic aperture radar (SAR) image. Reducing the speckle would improve the discrimination among different land use types and would make the textual classifiers more efficient in SAR images. Ideally, filters will reduce the speckle without loss of information. In the process of the forest biomass estimation, the filters should preserve the backscattering coefficient values and edges between different areas. We investigate both quantitative and qualitative criteria in speckle reduction and texture preservation to evaluate the performance of the proposed filter in the forest biomass estimation. We will also show that the biomass estimation accuracy is significantly improved in an MLPNN when the radar and the optical data are used in combination compared to estimating the biomass by using a single datum only. The root-mean-square error (rmse) value is decreased when the proposed method is used (rmse= 2.175 ton) compared with that of the classic method (rmse= 5.34 ton). [J602]

## "Calibration of Polarimetric PALSAR Imagery Affected by Faraday Rotation Using Polarization Orientation"

For spaceborne polarimetric synthetic aperture radar (SAR), it is important to ensure the removal of both polarimetric system distortion and the effect of Faraday rotation. This paper proposes a new calibration method to derive the system distortion using polarization orientation (PO) induced in built-up areas and applies to Phased-Array-Type L-Band SAR (PALSAR) calibration. Faraday rotation is corrected by the circular-polarization-based method from the distortion matrix (DM)-calibrated data. The derived DMs do not coincide with those by the Japan Aerospace Exploration Agency (JAXA), but our calibration results compare well to JAXA's results in PO angles and calibrator's responses. The two results satisfy polarimetric calibration requirements, and the cross-polarized isolation improves by more than 5 dB after Faraday rotation correction following DM calibration-even in the case of small Faraday rotation (-2deg to -0.5deg). The proposed method is robust to noise and is useful when using an area of mixed polarimetric response for calibration. This method is also applicable to a large crosstalk system and the case of large Faraday rotation. [J603]

## "Linear and adaptive spaceborne threedimensional SAR tomography: a comparison on real data"

Three-dimensional (3-D) synthetic aperture radar (SAR) imaging is a recent technique, based on coherent SAR data combination, and aims to obtain a full 3-D analysis in space. It is a multibaseline extension of the SAR interferometry concept and offers new options for the analysis and monitoring of ground scenes by means of the capability of separating the scattering phenomena along the height dimension. In this work, the authors summarise and extend the results obtained by processing real ERS satellite urban data characterised by a long time span of acquisition and non-uniformly spaced satellite passes, comparing the performance in height focusing obtained with a singular value decomposition (SVD)-based method and adaptive beamforming. [J604]

## "Comparative Study on the Performance of Multiparameter SAR Data for Operational Urban Areas Extraction Using Textural Features"

The advent of a new generation of synthetic aperture radar (SAR) satellites, such as Advanced SAR/Environmental Satellite (C-band), Phased Array Type L-band Synthetic Aperture Radar/Advanced Land Observing Satellite (L-band), and TerraSAR-X (X-band), offers advanced potentials for the detection of urban tissue. In this letter, we analyze and compare the performance of multiple types of SAR images in terms of band frequency, polarization, incidence angle, and spatial resolution for the purpose of operational urban areas delineation. As a reference for comparison, we use a proven method for extracting textural features based on a Gaussian Markov Random Field (GMRF) model. The results of urban areas delineation are quantitatively analyzed allowing performing intrasensor and intersensors comparisons. Sensitivity of the GMRF model with respect to texture window size and to spatial resolutions of SAR images is also investigated. Intrasensor comparison shows that polarization and incidence angle play a significant role in the potential of the GMRF model for the extraction of urban areas from SAR images. Intersensors comparison evidences the better performances of X-band images, acquired at 1-m spatial resolution, when resampled to resolutions of 5 and 10 m. [J605]

## "Azimuth Phase Center Adaptation on Transmit for High-Resolution Wide-Swath SAR Imaging"

Synthetic aperture radar (SAR) systems with multiple receive channels allow for high-resolution wide-swath imaging thus overcoming a fundamental limitation of conventional single-aperture SAR. By using multiple apertures in azimuth, additional samples are received for each transmitted pulse. This allows for a reduced pulse repetition frequency (PRF) thereby enabling a wider swath. However, a nonoptimum PRF is associated with a nonuniform sample spacing in azimuth and needs to be compensated by a multichannel reconstruction algorithm. For strong deviations from the optimum PRF, the inverse character of such an algorithm might result in a degraded performance. This can be overcome by an innovative advanced transmit antenna architecture which allows for a pulse-to-pulse shift of the phase center. Such an antenna enables the adaptive adjustment of the system's phase center positions to the respective PRF, thereby ensuring constant performance over a clearly extended PRF range. In particular, in combination with conventional multichannel processing strategies, this technique represents the next step toward a fully active multiple-input multiple-output (MIMO) SAR and has a great potential for future systems. [J606]

## "Estimating Spatiotemporal Ground Deformation With Improved Persistent-Scatterer Radar Interferometry"

Synthetic aperture radar interferometry has been applied widely in recent years to ground deformation monitoring although difficulties are often encountered when applying the technology, among which the spatial and temporal decorrelation and atmospheric artifacts are the most prominent. The persistent-scatterer interferometric synthetic aperture radar (PS-InSAR) technique has overcome some of the difficulties by focusing only on the temporally coherent radar targets in a time series of synthetic aperture radar (SAR) images. This paper presents an improved PS-InSAR technique by introducing PS-neighborhood networking and empirical mode decomposition (EMD) approaches in the PS-InSAR solution. Linear deformation rates and topographic errors are estimated based on a least squares method, while the nonlinear deformation and atmospheric signals are computed by singular value decomposition and the EMD method. An area in Phoenix, AZ, is used as a test site to determine its historical subsidence with 39 C-band SAR images acquired by European Remote Sensing 1 and 2 satellites from 1992 to 2000. [J607]

## "Generalized Frequency-Domain SAR Processing"

The range-Doppler algorithm and the chirp-scaling algorithm (CSA) process synthetic aperture radar (SAR) data with approximations to ideal SAR processing. These approximations are invalid for data from systems with wide beamwidths, large bandwidths, and/or low center frequencies. While simple and efficient, these frequency-domain methods are thus limited by the SAR parameters. This paper explores these limits and proposes a generalized chirp-scaling approach for extending the utility of frequency-domain processing. We demonstrate how different order approximations of the SAR signal in the 2-D frequency domain affect image focusing for varying SAR parameters. From these results, a guideline is set forth, which suggests the required order of approximation terms for proper focusing. A proposed generalized frequency-domain processing approach is derived. This method is an efficient arbitrary-order CSA that processes the data using the appropriate number of approximation terms. The new method is demonstrated using simulated data. [J608]

## "Signatures of ALOS PALSAR L-Band Backscatter in Swedish Forest"

The Phased Array type L-band Synthetic Aperture Radar onboard the Advanced Land Observing Satellite has, since its launch, been acquiring an extensive data set of images over two forest test sites in Sweden. The sites of Remningstorp (Lat. 58deg30' N, Long. 13deg40' E) in the south and Krycklan (Lat. 64deg14' N, Long. 19deg50' E) in the north of Sweden are characterized by hemiboreal and boreal forests, respectively. In this paper, we have investigated the signatures of standwise backscatter measurements from forests with different growth stages in relation to polarization, environmental conditions, image viewing geometry, and spatial resolution. The HV backscatter presented stronger sensitivity to the forest growth stage than the HH and VV backscatter. Under unfrozen conditions, the dynamic range of fine-beam data acquired at 34.3deg was 8-9 dB for the HV polarization and 6-7 dB for the HH polarization. At 21.5deg, in the polarimetric mode, the dynamic range was 6, 7, and 9 dB at VV, HH, and HV polarizations, respectively. Regardless of the specific polarization, the backscatter was temporally consistent under unfrozen conditions, with a small increase of backscatter in regrowing young forest for wet conditions. Under thawing and frozen conditions, repeated measurements were available only for the HH backscatter at 34.3deg. For thawing conditions, the backscatter level was similar to the unfrozen conditions even though the signatures differed depending on temperature dynamics, snow-cover properties, and precipitation. Under frozen conditions, the signatures varied depending on temperature. For images acquired when the temperature was well below the freezing point, the backscatter was low, and the dynamic range was small (2-4 dB); nonetheless, the measurements were consistent. Images acquired when temperature was close to the freezing point presented a behavior similar to unfrozen conditions. The sensitivity of the backscatter to the image viewing geometry for d--ifferent growth stages was studied for data acquired

under dry unfrozen conditions. The backscatter difference increased for increasing look angle because of the increase in volume scattering and the decrease of ground-surface backscatter. The largest difference was observed at 41.5deg with 2.5-4-dB difference for the HH and 4-5-dB difference for the HV case. Loss of spatial resolution (20-50 m) did not have any effect on the backscatter signatures in Krycklan, whereas in Remningstorp, the smallest stands were affected. [J609]

## "Analysis of the Main Scattering Mechanisms in Forested Areas: An Integral Representation Approach for Monostatic Radar Configurations"

In this paper, a coherent forest scattering model based on the electric-field integral representation is developed. This model gives the scattered field by the forest, resulting from the interaction of an electromagnetic plane wave with its main elements (trunks, branches, and plane ground) in a frequency range of 100 to 400 MHz. The Method of Moments is used to solve the electric-field integral equation. In our treatment, there are three possible scattering mechanisms that contribute to the scattered field defined as follows: 1) single-; 2) double-; and 3) triple-bounce scattering mechanisms. The internal fields inside the tree trunks and branches are calculated by considering all of the multiple-scattering interactions within the forest. Our model is then constructed by coherently summing the three scattering mechanisms previously given. We can also obtain an approximate result by ignoring some or all of the multiple-scattering interactions in the calculation of internal fields inside the trees. The aim of this paper is, first, to determine the relative contribution of each scattering mechanism to the total scattered field, followed by the relative contribution of tree-trunk and branch scattering responses to the total scattering field, and, finally, the multiple-scattering interaction effects on the total backscattered field. [J610]

## "Joint Regularization of Phase and Amplitude of InSAR Data: Application to 3-D Reconstruction"

Interferometric synthetic aperture radar (SAR) images suffer from a strong noise, and their regularization is often a prerequisite for successful use of their information. Independently of the unwrapping problem, interferometric phase denoising is a difficult task due to shadows and discontinuities. In this paper, we propose to jointly filter phase and amplitude data in a Markovian framework. The regularization term is expressed by the minimization of the total variation and may combine different information (phase, amplitude, optical data). First, a fast and approximate optimization algorithm for vectorial data is briefly presented. Then, two applications are described. The first one is a direct application of this algorithm for 3-D reconstruction in urban areas with very high resolution images. The second one is an adaptation of this framework to the fusion of SAR and optical data. Results on aerial SAR images are presented. [J611]

## "Design of Compact UWB Planar Monopole Antennas for Cross-Hole Radar Application"

Printed rectangular antennas with a relatively small width (less than 60 cm) have been specifically designed to serve in a cross-hole radar for soil characterization in the frequency band [0.5; 1.5] GHz. Antenna geometries, including coplanar waveguide or microstrip line feed lines, have been optimized to show a low S11 when inserted in an air-filled borehole surrounded by a high dielectric soil supposed to be wet in a practical situation. [J612]

## "Automatic Target Recognition by Means of Polarimetric ISAR Images and Neural Networks"

Inverse synthetic aperture radar (ISAR) images are often used for classifying and recognizing targets. Moreover, the use of fully polarimetric ISAR (Pol-ISAR) images enhances classification capabilities. In this paper, the authors propose a novel automatic target recognition (ATR) technique based on the use of fully Pol-ISAR images and neural networks (NNs). In order to reduce the amount of data processed by the classifier, the brightest scattering centers are first extracted by means of the Pol-CLEAN technique, and then, their scattering matrices are decomposed using Cameron's decomposition. A classifier based on the use of multilayer perceptron NN that makes use of the features extracted from the Pol-ISAR images is then implemented. A proof-of-concept test is performed on real data acquired during a controlled experiment in an anechoic chamber. [J613]

## "Assessment of Heart Rate Variability and Respiratory Sinus Arrhythmia via Doppler Radar"

An investigation of heart rate variability (HRV) and respiratory sinus arrhythmia (RSA) indices using data obtained from Doppler radar cardiopulmonary remote sensing is presented in this paper. High accuracy in extracting the HRV and RSA indices was achieved using a direct-conversion quadrature radar system with linear demodulation method. This method was validated using data obtained from 12 human subjects in seated and supine positions. For supine position measurements, all standard deviation of normal beat-to-beat interval indices from Doppler radar and electrocardiogram reference differed less than plusmn9 ms of each other, while all the root mean square of differences of successive normal beat-to-beat interval indices differed less than plusmn76 ms. The measurements from subjects in seated and supine positions with normal RSA demonstrated

that the results from radar correlated well with both respiratory piezoresistor chest belts. Higher level of HRV and RSA was detected in seated position, as expected. [J614]

## "Support Vector Machine for Multifrequency SAR Polarimetric Data Classification"

The objective of this paper is twofold: first, to assess the potential of radar data for tropical vegetation cartography and, second, to evaluate the contribution of different polarimetric indicators that can be derived from a fully polarimetric data set. Because of its ability to take numerous and heterogeneous parameters into account, such as the various polarimetric indicators under consideration, a support vector machine (SVM) algorithm is used in the classification step. The contribution of the different polarimetric indicators is estimated through a greedy forward and backward method. Results have been assessed with AIRSAR polarimetric data polarimetric data acquired over a dense tropical environment. The results are compared to those obtained with the standard Wishart approach, for single frequency and multifrequency bands. It is shown that, when radar data do not satisfy the Wishart distribution, the SVM algorithm performs much better than the Wishart approach, when applied to an optimized set of polarimetric indicators. [J615]

## "The Application of the Principle of Chirp Scaling in Processing Stepped Chirps in Spotlight SAR"

A new approach to process stepped chirps in spotlight synthetic aperture radar is presented in this letter, which is based on exploiting the principle of chirp scaling (PCS). In particular, PCS is integrated into the polar format algorithm (PFA), obtaining a more efficient solution compared with the existing polar interpolation technique. The main contribution of this letter is the implementation of azimuth scaling, in which the bandwidth synthesis is embedded. The algorithm is developed dedicatedly for dealing with stepped chirps. The signal processing flow is investigated in detail, in which no interpolations but only fast Fourier transform and complex multiplications are involved. Point-target simulation has validated the new approach and indicated that it is more efficient than the classic interpolation-based one. The achieved computational gain measured in execution time is around 25%-30%. [J616]

## "Algebraic Synthesis of Forest Scenarios From Multibaseline PolInSAR Data"

In this paper, a new methodology is proposed for the analysis of forested areas basing on multipolarimetric multibaseline synthetic aperture radar (SAR) surveys. Such a methodology is based on three hypotheses: 1) statistical uncorrelation of the different scattering mechanisms (SMs), such as ground, volume, and ground-trunk scattering; 2) independence of volumetric and temporal coherence losses of each SM on the choice of the polarimetric channel; and 3) invariance (up to a scale factor) of the average polarimetric signature of each SM with respect to the choice of the track. Under these hypotheses, the data covariance matrix can be expressed as a Sum of Kronecker Products, after which it follows that K SMs are uniquely identified by K (K-1) real numbers. This result provides the basis to perform SM separation by employing not only model-based approaches, generally retained in literature but also model-free and hybrid approaches, while yielding the best Least Square solution given the hypothesis of K SMs. It will be shown that this approach to SM separation is consistent with the inversion procedures usually exploited in single-baseline polarimetric SAR interferometry. Experimental validation of this methodology is provided on the basis of the P-band data set relative to the forest site of Remningstorp, Sweden, acquired by German Aerospace Center's E-SAR airborne system in the framework of the European Space Agency campaign BioSAR. [J617]

## "DEM Error Retrieval by Analyzing Time Series of Differential Interferograms"

Two-pass differential synthetic aperture radar interferometry processing have been successfully used by the scientific community to derive velocity fields. Nevertheless, a precise digital elevation model (DEM) is necessary to remove the topographic component from the interferograms. This letter presents a novel method to detect and retrieve DEM errors by analyzing time series of differential interferograms. The principle of the method is based on the comparison of fringe patterns with the perpendicular baseline. First, a mathematical description of the algorithm is exposed. Then, the algorithm is applied on a series of four one-day European Remote Sensing 1 and 2 satellite (ERS-1/2) interferograms. [J618]

## "Feature Enhancement of Stripmap-Mode SAR Images Based on an Optimization Scheme"

Based on a nonquadratic-optimization method originally proposed for spotlight-mode SAR image reconstruction, a modification for stripmap-mode SAR images is presented in this letter. This is done by mathematically reformulating the projection kernel and numerically putting it into a form that is suitable for optimization. The performance was evaluated by measures of the target contrast and 3-dB beamwidth using Radarsat-1 data. Results were analyzed and compared with those using minimum-variance and multiple-signal-classification methods. Results demonstrate that the target's features are effectively enhanced and that the dominant

scattering centers are well separated using the proposed method. In addition, the image fuzziness is greatly reduced, and the image fidelity is well preserved. The effectiveness of the modification is thus validated. [J619]

## "The Contribution of ALOS PALSAR Multipolarization and Polarimetric Data to Crop Classification"

Mapping and monitoring changes in the distribution of cropland provide information that aids sustainable approaches to agriculture and supports early warning of threats to global and regional food security. This paper tested the capability of Phased Array type L-band Synthetic Aperture Radar (SAR) (PALSAR) multipolarization and polarimetric data for crop classification. L-band results were compared with those achieved with a C-band SAR data set (ASAR and RADARSAT-1), an integrated C- and L-band data set, and a multitemporal optical data set. Using all L-band linear polarizations, corn, soybeans, cereals, and hay-pasture were classified to an overall accuracy of 70%. A more temporally rich C-band data set provided an accuracy of 80%. Larger biomass crops were well classified using the PALSAR data. C-band data were needed to accurately classify low biomass crops. With a multifrequency data set, an overall accuracy of 88.7% was reached, and many individual crops were classified to accuracies better than 90%. These results were competitive with the overall accuracy achieved using three Landsat images (88.0%). L-band parameters derived from three decomposition approaches (Cloude-Pottier, Freeman-Durden, and Krogager) produced superior crop classification accuracies relative to those achieved using the linear polarizations. Using the Krogager decomposition parameters from all three PALSAR acquisitions, an overall accuracy of 77.2% was achieved. The results reported in this paper emphasize the value of polarimetric, as well as multifrequency SAR, data for crop classification. With such a diverse capability, a SAR-only approach to crop classification becomes increasingly viable. [J620]

## "Quantifying Surface Reflectivity for Spaceborne Lidar via Two Independent Methods"

Spaceborne differential absorption lidar has been proposed for accurate measurements of atmospheric CO2(and surface properties). Lidar instruments typically observe the highest possible surface reflectance due to observing in the retroreflection direction (the so-called ldquohotspotrdquo) where viewed shadow is minimized. The range of observed reflectance will determine instrument dimensions and signal-to-noise ratio, but it is difficult to predict this range globally apriori. Two complementary methods are presented for estimating lidar reflectivity over a range of vegetated surface types. The first method simulates the expected response of a lidar instrument from multiangle multispectral reflectance data. The second method uses detailed 3-D vegetation structural models and Monte Carlo ray tracing to simulate the lidar signal. The simulations are used to validate the first method and assess the impact of possible instrument configurations. Both methods agree well and are robust to error in observations, with predicted lidar reflectivity (at 1570 and 2050 nm here) typically between 10% and 33% higher relative to off-nadir reflectance and ranging from 0.02 to ~ 0.7. We use the 3-D simulations to show that the impact of shifted on-off lidar pulses is not likely to be significant for accuracy of retrieved CO2, and we demonstrate that the 3-D simulation method is a flexible and powerful way of prototyping future spaceborne lidar missions. [J621]

## "Unsupervised Change Detection From Multichannel SAR Data by Markovian Data Fusion"

In applications related to environmental monitoring and disaster management, multichannel synthetic aperture radar (SAR) data present a great potential, owing both to their insensitivity to atmospheric and Sun-illumination conditions and to the improved discrimination capability they may provide as compared with single-channel SAR. However, exploiting this potential requires accurate and automatic techniques to generate change maps from (multichannel) SAR images acquired over the same geographic region in different polarizations or at different frequencies at different times. In this paper, a contextual unsupervised change-detection technique (based on a data-fusion approach) is proposed for two-date multichannel SAR images. Each SAR channel is modeled as a distinct information source, and a Markovian approach to data fusion is adopted. A Markov random field model is introduced that combines together the information conveyed by each SAR channel and the spatial contextual information concerning the correlation among neighboring pixels and formulated by using ldquoenergy functions.rdquo In order to address the task of the estimation of the model parameters, the expectation-maximization algorithm is combined with the recently proposed ldquomethod of log-cumulants.rdquo The proposed technique was experimentally validated with semisimulated multipolarization and multifrequency data and with real SIR-C/XSAR images. [J622]

## "Motion Compensation for UAV SAR Based on Raw Radar Data"

Unmanned aerial vehicle (UAV) synthetic aperture radar (SAR) is very important for battlefield awareness. For SAR systems mounted on a UAV, the motion errors can be considerably high due to atmospheric turbulence and aircraft properties, such as its small size, which makes motion compensation (MOCO) in UAV SAR more urgent than other SAR systems. In this paper, based on 3-D motion error analysis, a novel 3-D MOCO method is

proposed. The main idea is to extract necessary motion parameters, i.e., forward velocity and displacement in line-of-sight direction, from radar raw data, based on an instantaneous Doppler rate estimate. Experimental results show that the proposed method is suitable for low- or medium-altitude UAV SAR systems equipped with a low-accuracy inertial navigation system. [J623]

## "A Spatially Adjusted Elevation Model in Dronning Maud Land, Antarctica, Based on Differential SAR Interferometry"

In this paper, a new digital elevation model (DEM) is derived for the ice sheet in western Dronning Maud Land, Antarctica. It is based on differential interferometric synthetic aperture radar (SAR) from the European Remote Sensing 1/2 (ERS-1/2) satellites, in combination with ICESat's Geoscience Laser Altimeter System (GLAS). A DEM mosaic is compiled out of 116 scenes from the ERS-1 ice phase in 1994 and the ERS-1/2 tandem mission between 1996 and 1997 with the GLAS data acquired in 2003 that served as ground control. Using three different SAR processors, uncertainties in phase stability and baseline model, resulting in height errors of up to 20 m, are exemplified. Atmospheric influences at the same order of magnitude are demonstrated, and corresponding scenes are excluded. For validation of the DEM mosaic, covering an area of about 130 000 km2on a 50-m grid, independent ICESat heights (2004-2007), ground-based kinematic GPS (2005), and airborne laser scanner data (ALS, 2007) are used. Excluding small areas with low phase coherence, the DEM differs in mean and standard deviation by 0.5 + /-10.1, 1.1 + /-6.4, and 3.1 +/-4.0 m from ICESat, GPS, and ALS, respectively. The excluded data points may deviate by more than 50 m. In order to suppress the spatially variable noise below a 5-m threshold, 18% of the DEM area is selectively averaged to a final product at varying horizontal spatial resolution. Apart from mountainous areas, the new DEM outperforms other currently available DEMs and may serve as a benchmark for future elevation models such as from the TanDEM-X mission to spatially monitor ice sheet elevation. [J624]

## "Separation Between Water and Land in SAR Images Using Region-Based Level Sets"

This letter presents a method for the separation between land and water in synthetic aperture radar (SAR) amplitude images. The proposed technique uses region-based level sets and adopts a mixture of lognormal densities as the probabilistic model for the pixel intensities in both water and land classes. The expectation-maximization algorithm is used to estimate the probability density functions for each class. Experimental results with real SAR images of riverbeds, flood extent areas, and shorelines demonstrate the good performance of the proposed algorithm compared with state-of-the-art approaches. [J625]

## "Improved Understanding of Soil Surface Roughness Parameterization for L-Band Passive Microwave Soil Moisture Retrieval"

Surface roughness parameterization plays an important role in soil moisture retrieval from passive microwave observations. This letter investigates the parameterization of surface roughness in the retrieval algorithm adopted by the Soil Moisture and Ocean Salinity mission, making use of experimental airborne and ground data from the National Airborne Field Experiment held in Australia in 2005. The surface roughness parameter is retrieved from high-resolution (60 m) airborne data in different soil moisture conditions, using the ground soil moisture as input of the model. The effect of surface roughness on the emitted signal is found to change with the soil moisture conditions with a law different from that proposed in previous studies. The magnitude of this change is found to be related to soil textural properties: in clay soils, the effect of surface roughness is higher in intermediate wetness conditions (0.2-0.3 v/v) and decreases on both the dry and wet ends. Consequently, this letter calls for a rethink of surface roughness parameterization in microwave emission modeling. [J626]

## "A New Coherency Formalism for Change Detection and Phenomenology in SAR Imagery: A Field Approach"

Optimal utilization of complex synthetic aperture radar imagery for coherent change detection (CCD) is achieved by maximizing the amount of information extracted from the coherent correlation of images. Conventional techniques cannot fully exploit the coherent information due to limited application of few products or indicators, e.g., correlation factor and phase maps. Also, considering the lack of a systematic formulation of change observables and their nature, unsupervised change detection or classification is not feasible. To address this, an analytic framework is established by taking advantage of the analogy to partially polarized electromagnetic fields to introduce vectors and observables that can establish a complete change space. Decomposition of the coherent correlation or change characteristics into this basis set can provide a better understanding of the associated change phenomenology. [J627]

## "Bistatic SAR Data Focusing Using an Omega-K Algorithm Based on Method of Series Reversion"

This paper deals with an omega-K algorithm for focusing bistatic synthetic aperture radar (SAR) data. The key of the proposed algorithm is the derivation of a frequency mapping function by using Neo's method of series reversion. The registration of the focused image onto the ground plane is discussed in detail, which is based on a conclusion that the targets whose instantaneous Doppler frequencies at zero azimuth time are the same as that of the reference target at zero azimuth time will all be focused at the reference target's azimuth position in the focused image. The range invariance region size, which the proposed algorithm can process, is also determined in this paper. The proposed algorithm can handle extreme bistatic configurations with wide apertures and large squint angles. The effectiveness of the proposed algorithm is confirmed by simulation results. Although developed for the azimuth-invariant case, the proposed algorithm can be readily extended to the azimuth-variant case, as long as we divide the SAR data into blocks in the azimuth direction so that each block of SAR data can be assumed quasi-stationary in the azimuth direction. [J628]

## "An Improvement of the Performance of Multiple-Aperture SAR Interferometry (MAI)"

Multiple-aperture synthetic aperture radar (SAR) interferometry (MAI) enables the measurement of along-track surface deformations by means of split-beam SAR processing. This paper examines the effects of flat-Earth and topographic phases on the MAI phase and derives formulas to correct them. Detailed MAI processing steps are introduced and discussed with particular consideration given to coherence improvement, as well as to computational efficiency. Forward- and backward-looking MAI pairs have different perpendicular baselines, which play a key role in phase distortion; consequently, an orbital deviation of only a few centimeters could result in a significant flat-Earth phase. A second-order polynomial model was used to estimate the perpendicular baseline difference. European Remote Sensing 2 satellite SAR data sets of the Hector Mine earthquake event in 1999 were used for performance evaluation. The proposed processing with the flat-Earth and topographic phase corrections achieved precision of along-track deformation ranging from 10.2 to 13.1 cm. Two coseismic pairs were compared and the standard deviation of the difference between the two independent measurements was 7.0 cm, with a mean difference of -0.24 cm. Thus, the measurement accuracy of MAI was improved using flat-Earth correction and coherence enhancement. [J629]

## "A Waveform Model for Near-Nadir Radar Altimetry Applied to the Cassini Mission to Titan"

The radar altimeter of the Cassini mission to Titan operates in a transition region between pulse- and beam-limited conditions. Due to the specific observation geometry, low values of mispointing angle have been found to significantly affect altimeter impulse response (IR). This involves a nonconventional formulation of the system response which is the main goal of this paper. An analytical model of the average return power waveform, valid for near-nadir altimetry measurements, has been developed in order to cope with the particular operating conditions of Cassini mission. The model used to approximate the altimeter waveform is based on the same general assumptions of the classical Brown's model (1977) but exploits a flat surface response approximation by Prony's methods. Both theoretical considerations and simulated data have been taken into account to support the accuracy of the proposed model. To infer the main geophysical parameters describing surface topography from altimetry data, a parametric estimation procedure has been used. The maximum likelihood estimator procedure has been chosen since, in principle, it can assure optimal performance as a consequence of the analytical model we used to describe the system IR. Performances of the implemented method have been numerically evaluated through simulation of data received by CASSINI in high-resolution altimeter mode. [J630]

## "A Hybrid Conditional Random Field for Estimating the Underlying Ground Surface From Airborne LiDAR Data"

Recent advances in airborne light detection and ranging (LiDAR) technology allow rapid and inexpensive generation of digital surface models (DSMs), 3-D point clouds of buildings, vegetations, cars, and natural terrain features over large regions. However, in many applications, such as flood modeling and landslide prediction, digital terrain models (DTMs), the topography of the bare-Earth surface, are needed. This paper introduces a novel machine learning approach to automatically extract DTMs from their corresponding DSMs. We first classify each point as being either ground or nonground, using supervised learning techniques applied to a variety of features. For the points which are classified as ground, we use the LiDAR measurements as an estimate of the surface height, but, for the nonground points, we have to interpolate between nearby values, which we do using a Gaussian random field. Since our model contains both discrete and continuous latent variables, and is a discriminative (rather than generative) probabilistic model, we call it a hybridconditionalrandomfield. We show that a Maximum aPosterioriestimate of the surface height can be efficiently estimated by using a variant of the Expectation Maximization algorithm. Experiments demonstrate that the accuracy of this learning-based approach outperforms the previous best systems, based on manually tuned heuristics. [J631]

## "Conditioning Stochastic Rainfall Replicates on Remote Sensing Data"

Temporally and spatially variable rainfall replicates are frequently required in hydrologic applications of ensemble forecasting and data assimilation. Ensemble methods can be expected to work better when the rainfall replicates more closely resemble observed storms. In particular, the replicates should capture the intermittency and variability that are dominant features of rainfall events. In this paper, we present a new probabilistic procedure for generating realistic rainfall replicates that are constrained by (or conditioned on) remote sensing measurements. The procedure uses remotely sensed cloud top temperatures to identify potentially rainy regions. The cloud top temperatures are obtained from visible/infrared instruments in geostationary orbit. A multipoint geostatistical algorithm generates areas of nonzero rain (rain clusters) within each cloudy region. This algorithm relies on statistics derived from ground-based weather radar [National Operational Weather Radar (NOWRAD)] data. A truncated multiplicative cascade generates rain rates within each rain cluster. A computational experiment based on summer 2004 data from the Central U.S. indicates that the rainfall replicates simulated by the procedure are visually and statistically similar to individual NOWRAD images and to a large ensemble of NOWRAD images collected throughout the summer simulation period. [J632]

## "A New Range Finder Based on a Four-Port Junction"

The design and performance of a prototype range finder based on a four-port junction are presented. The four-port junction is used as a precision phase detector. The system proposed presents advantages such as compact size, low cost, low consumption, and low computational time. The principle of operation, the sensor and the results are described in this paper. [J633]

## "Effectiveness of 2-D and 2.5-D FDTD Ground-Penetrating Radar Modeling for Bridge-Deck Deterioration Evaluated by 3-D FDTD"

Computational modeling effectively analyzes the wave propagation and associated interaction within heterogeneous reinforced concrete bridge decks, providing valuable information for sensor selection and placement. It provides a good basis for the implementation of the inverse problem in defect detection and the reconstruction of subsurface properties, which is beneficial for defect diagnosis. The objective of this study is to evaluate the effectiveness of lower order models in the evaluation of bridge-deck subsurfaces modeled as layered media. The two lower order models considered are a 2-D model and a 2.5-D model that uses the 2-D geometry with a compressed coordinate system to capture wave behavior outside the cross-sectional plane. Both the 2- and 2.5-D models are compared to the results obtained from a full 3-D model. A filter that maps the 3-D excitation signal appropriately for 2- and 2.5-D simulations is presented. The 2.5-D model differs from the 2-D model in that it is capable of capturing 3-D wave behavior interacting with a 2-D geometry. The 2.5-D matches results from the corresponding 3-D model when there is no variation in the third dimension. Computational models for air-launched ground-penetrating radar with 1-GHz central frequency and bandwidth for the detection of bridge-deck delamination are implemented in 2-, 2.5-, and 3-D using FDTD simulations. In all cases, the defect is identifiable in the results. Thus, it is found that in layered media (such as bridge decks) 2- and 2.5-D models are good approximations for modeling bridge-deck deterioration, each with an order of magnitude reduction in computational time. [J634]

## "An Examination of the Validity of the Mean Raindrop-Shape Model for Dual-Polarization Radar Rainfall Retrievals"

Information about the shape of raindrops is critical for the retrieval of rainfall rate from dual-polarization radar measurements. As described in the literature, the relation describing drop oblateness as a function of its equivolumetric diameter is nonlinear. There are several relations that express the shape-size dependence as a nonlinear fourth-order polynomial that has five coefficients or 5 DOF. While these are important for studying raindrop shape, it is not clear that they are needed to estimate an integral quantity such as rainfall rate. This paper examines the validity of using a simple equivalent linear shape-size model based on the principle of the mean-value theorem for estimating rain from dual-polarization radar measurements. Assuming Rayleigh-Gans scattering for spheroids to describe raindrop scattering and drop oblateness described by a linear relation between axis ratio and equivolumetric diameter, a general self-consistency equation relating reflectivity factor, differential reflectivity, specific differential phase shift, and slope of the shape-size relation is obtained for each radar operating frequency. In this 4-D space, relations for estimating rainfall rate without requiring an assumption of a specific drop-shape model from polarimetric radar measurements were obtained. To study all the implications arising from electromagnetic and microphysical aspects, reconstructed rain and radar measurement profiles obtained from real radar observations were used to test the performance of the proposed rain estimation procedure. The performance is compared with algorithms derived assuming specific a priori fixed drop-shape-size relations expressed by a fourth-order polynomial. Results show that, in general, the proposed rain algorithms perform better or at least equal to the algorithms derived assuming a priori fixed shape-size models,

demonstrating that the prevailing model directly derived from data is suitable for rainfall retrieval purposes. [J635]

## "The Utility of Spaceborne Radar to Render Flood Inundation Maps Based on Multialgorithm Ensembles"

On December 12, 2006, both the European Remote Sensing Satellite 2 and Environmental Satellite recorded a high-magnitude flood event on the River Dee in Wales (U.K.) only 28 min apart. This unique opportunity enables the creation of a very rare but extremely useful observed data set for flood inundation studies. For flood management purposes, hydrodynamic models are often run after an event but with field data gauged during the event to approximate both flood area and depth. As an adequate aprioridefinition of model parameters is difficult, they tend to be run with multiple parameter sets to generate a likelihood of inundation map. However, as field observations of events are often very scarce, these output maps cannot be validated with field-observed probabilities. This paper illustrates how this unique set of spaceborne radar images can be used in combination with five widely used image processing techniques to generate an event-specific inundation map that expresses a degree of belief that a given pixel is possibly flooded. It is expected that the value of this multialgorithm ensemble-based map opens up new ways to evaluate the performance of hydrodynamic models, as it contains information which has, to the authors' knowledge, not previously been available. [J636]

## "Retrieval of Cloud Optical Properties From Multiple Infrared Hyperspectral Measurements: A Methodology Based on a Line-by-Line Multiple-Scattering Code"

A methodology to retrieve cloud optical properties using high spectral resolution (HSR) infrared (IR) measurements is presented. This new method has the ability to easily adapt to multiple instruments and viewing angles. The retrieval uses a line-by-line multiple-scattering simulation and HSR IR measurements to retrieve spectrally resolved cloud optical depths (ODs). The spectral ODs are compared to a precomputed OD database generated from an ensemble of cloud particle-size distributions and precomputed single-scattering and single-particle optical properties for a variety of ice-crystal habits. Cloud microphysics are retrieved by finding the closest fit to the database. Results are independent of first-guess optical property assumptions on size and habit. The retrieval method has been applied to aircraft, satellite, and uplooking HSR measurements with results evaluated against coincident HSR lidar and radar measurements. Analysis of retrieval errors produced by assumptions and uncertainties in the atmospheric state demonstrates different sensitivities to atmospheric parameters when uplooking or downlooking data are analyzed. For both viewing geometries, the retrieval is most sensitive to the uncertainties in the assumed cloud boundaries. It is also found that nonuniform vertical distribution of cloud OD can result in significant biases in the IR retrieved cloud ODs. [J637]

## "Radar Response of Firn Exposed to Seasonal Percolation, Validation Using Cores and FDTD Modeling"

We use ground-penetrating radars (GPRs), firn cores, and electromagnetic finite-difference time-domain (FDTD) numerical modeling to characterize the GPR response to a frozen high-arctic firn pack. As a result of extensive summertime percolation, the firn pack comprises a high fraction of ice layers, lenses, and vertical glands. We show that the GPR response on the firn pack mainly depends on the following: (1) the thickness of the ice layers; (2) the distance between layers; (3) the layer roughness; and (4) the presence or absence of elliptical ice lenses. Using 3-D FDTD modeling, we show that the GPR is not sensitive to typical ice glands, which implies that the GPR underestimates firn heterogeneity, such that firn stratigraphy in percolation and wet-snow zones could be incorrectly interpreted as being better preserved than it actually is. We find that thin ice layers (< 0.05 m) or multiple thin ice layers give a strong response. Thicker ice layers typically give a weaker backscatter per unit area, mainly due to the lack of interference of the reflections from the upper and lower interfaces, but are, due to their continuity, easily trackable. Ice layers with a thickness comparable to the GPR wavelength give 180deg phase-shifted upper and lower reflections and are, in general, separated by a band of low GPR response, due to the lack of permittivity contrast within the ice layers. Despite the ice lenses' relatively short horizontal correlation length, as inferred from cores, bands of high-amplitude clutter caused by these features can be traced over several kilometers in GPR profiles. [J638]

## "Sea Surface Manifestation of Along-Tidal-Channel Underwater Ridges Imaged by SAR"

A group of submerged ocean bottom sand ridges in the Bohai Sea, China, are shown in RADARSAT-1 and ENVISAT synthetic aperture radar (SAR) images. The sand ridges appear as fingerlike quasi-linear features in the SAR images. Examining the detailed local bathymetry chart, we find that these features coincide with the satellite images. The heights of the sand ridges are less than 10 m, and the water depth is between 10 and 30 m. The spacing of the sand ridges is about 10 km, and the length of the sand ridges is about 20 km. The same sand ridges are also visible on a Moderate Resolution Imaging Spectroradiometer (MODIS) true-color image.

The semidiurnal and diurnal tidal currents in this area are almost parallel to the major axis of these sand ridges. These observations cannot be explained using the existing 1-D SAR imaging model, which is not applicable to sand ridges parallel to the tidal current. In this paper, we consider the shallow-water current bathymetry in a 2-D space. An analytical ocean model was applied to demonstrate the temporal variations of the current divergence and convergence that are induced by the along-sand-ridge-direction current and ridge interaction. A radar simulation model is used to simulate the variation of normalized radar cross section (NRCS) induced by the ocean surface current. The simulated NRCS variation is similar to that extracted from the calibrated SAR image. Simulation results also show that the NRCS variation becomes negligible when the ocean current is set to about half of the maximum tidal current. [J639]

## "An L-Band Ocean Geophysical Model Function Derived From PALSAR"

This paper examines L-band normalized radar cross section (NRCS) dependence on ocean surface wind. More than 90 000 match-ups, each consisting of the L-band HH NRCS, incidence angles, wind speeds, and wind directions, were collected from the Phased-Array L-Band Synthetic Aperture Radar (PALSAR) and scatterometer wind vectors. Based on the match-ups, the L-band HH NRCS dependence on incidence angle and wind vector is modeled for 0-20-m/s wind speeds and 17deg-43deg incidence angles. The derived relation indicates that the wind sensitivity of the L-band NRCS is less than that of the C-band at moderate winds and large incidence angles, whereas comparable at stronger winds ((>10 m/s) and small incidence angles. The upwind-crosswind difference is amplified in the 10-15-m/s range followed by an almost zero amplitude from 4 to 8 m/s, which represents a clear phase shift with the C-band VV and Ku-band HH models. Wind speeds are then estimated from the match-ups, based on the derived model function. A comparison with the reference scatterometer winds reveals a 0.05-m/s bias and a 1.85-m/s root mean square error, where crosswind data give rise to large errors due to low wind sensitivity at wind speeds of around 10 m/s, particularly at large incidence angles. The L-band NRCS behavior in strong winds (>20 m/s), at which the C-band is saturated, was not determined in the current model due to the limited number of the match-ups. [J640]

## "Space-Based Motion Estimators-Evaluation With the First RADARSAT-2 MODEX Data"

Synthetic aperture radar (SAR)-based motion estimation algorithms, which have been developed and validated for airborne SAR data, are now being extended to the RADARSAT-2 Moving Object Detection Experiment (MODEX). Several modifications of the classical along-track interferometry (ATI) approach are considered. Some of the first MODEX results are presented, demonstrating the estimation of target position and velocity from a commercial satellite using ATI methods. [J641]

## "Study of Hypersaline Deposits and Analysis of Their Signature in Airborne and Spaceborne SAR Data: Example of Death Valley, California"

Field measurements of dielectric properties of hypersaline deposits were realized over an arid site located in Death Valley, CA. The dielectric constant of salt and water mixtures is usually high but can show large variations, depending on the considered salt. We confirmed values observed on the field with laboratory measurements and used these results to model both the amplitude and phase behaviors of the synthetic aperture radar (SAR) signal at C- and L-bands. Our analytical simulations allow reproducing specific copolar signatures observed in both Airborne SAR (AIRSAR) and Spaceborne Imaging Radar (SIR-C) data, corresponding to the saltpan of the Cottonball Basin. More precisely, the main objective of the present paper is to understand the influence of soil salinity as a function of soil moisture on the dielectric constant of soils and then on the backscattering coefficients recorded by airborne and spaceborne SAR systems. We also propose the copolarized backscattering ratio and phase difference as indicators of moistened and salt-affected soils. More precisely, we show that these copolar indicators should allow monitoring of the seasonal variations of the dielectric properties of saline deposits at both C- and L-bands. Because of the frequency dependence of the ionic conductivity, we also show that L-band SAR systems should be efficient tools for detecting both soil moisture and salinity, while C-band SAR systems are more suitable for the monitoring of soil moisture only. Through the study of terrestrial evaporitic environments by means of spaceborne SAR systems, our results could also be of great interest for defining future planetary missions, particularly for the exploration of Mars. [J642]

## "Injection Heights of Biomass Burning Debris Estimated From WSR-88D Radar Observations"

Understanding the vertical distribution of aerosols is critical to accurately determining their effects on air quality. Since current tools for obtaining this information have limited spatial and temporal coverage, we explore the use of Doppler radar data for obtaining the injection heights of biomass burning debris (BBD) produced from large fires in southern Georgia during Spring 2007. Due to their submicrometer sizes, the smoke aerosols are not detected by the radar. Therefore, we use BBD as a possible surrogate for aerosol height since smoke aerosols

are often collocated with the debris. Using 32 h of Weather Surveillance Radar-1988 Doppler (WSR-88D) radar data from Jacksonville, FL, between May 23 and 25, 2007, the injection heights of BBD (D ~ 1mm) are calculated. Our analysis indicates that the maximum injection height is ~5 km for the strongest fire, with a mean injection height of 3 plusmn 1.0 km. Maximum injection heights are present between 1800 and 0000 UTC, during the late afternoon periods when both the intensity of the fire (based on radar information) and the convective mixing are greatest. The injection heights estimated from this approach represent the first step at providing inputs for future air-quality forecasting applications within numerical simulations, particularly ones that require diurnal information. [J643]

## "Detection of Single Scatterers in Multidimensional SAR Imaging"

Multidimensional synthetic aperture radar (SAR) imaging is a technique based on coherent SAR data combination for space (full 3-D) and space deformation-velocity (4-D) analysis. It is an extension of the concepts of SAR interferometry and differential interferometry SAR and offers new options for the analysis and monitoring of ground scenes. In this paper, we consider the problem of detecting single scatterers for localization and monitoring issues. To this end, we resort to a constant false alarm rate (CFAR) detection scheme which can be synthesized according to three different design criteria: generalized likelihood ratio test, Rao test, and Wald test. At the analysis stage, the performance of the aforementioned detector is compared to that of a previously proposed CFAR scheme, based on the multi-interferogram complex coherence and widely used in persistent scatterer interferometry. The analysis is conducted both on simulated and on real SAR data, acquired by ERS-1/2 satellites. Finally, Cramer-Rao lower bounds for the estimation of the scatterer elevation and velocity are provided. [J644]

## "An Improved Soil Moisture Retrieval Algorithm for ERS and METOP Scatterometer Observations"

The scatterometers onboard the European Remote Sensing satellites (ERS-1 & ERS-2) and the METeorological OPerational satellite (METOP) have been shown to be useful for surface soil moisture retrieval using the so-called TU-Wien change detection method. This paper presents an improved soil moisture retrieval algorithm based on the existing TU-Wien method but with new parameterization as well as a series of modifications. The new algorithm, WAter Retrieval Package 5 (WARP5), copes with some limitations identified in the earlier method WARP4 and provides the possibility of migrating soil moisture retrieval from ERS-SCAT to METOP-ASCAT data. The WARP5 algorithm results in a more robust and spatially uniform soil moisture product, thanks to its new processing elements, including a method for the correction of azimuthal anisotropy of backscatter, a comprehensive noise model, and new techniques for calculation of the model parameters. Cross-comparisons of WARP4 and WARP5 data sets with the Oklahoma Mesonet insituobservations and also with European Centre of Medium Range Weather Forecast (ECMWF) ReAnalysis (ERA-Interim) global modeled data show that the new algorithm has a better performance and effectively corrects retrieval errors in certain areas. [J645]

## "Ultrawideband (UWB) Radar Imaging of Building Interior: Measurements and Predictions"

In this paper, we explore using the ultrawideband radar technology for sensing through-the-wall imaging. We conducted a field experiment with our in-house designed impulse-based radar, in which a stripmap synthetic aperture radar (SAR) geometry was employed in mapping an abandoned army barrack building with a large footprint area. The images obtained from two sides of the building were combined in order to obtain the full building layout, including the interior structure. Computer simulations performed with Xpatch, a physical optics-based ray tracing code, are used to explain some phenomena observed in the measured SAR images. [J646]

## "Unsupervised Synthetic Aperture Radar Image Segmentation Using Fisher Distributions"

A new and fast unsupervised technique for segmentation of high-resolution synthetic aperture radar (SAR) images into homogeneous regions is proposed. This technique is based on Fisher probability density functions (pdfs) of the intensity fluctuations and on an image model that consists of a patchwork of homogeneous regions with polygonal boundaries. The segmentation is obtained by minimizing the stochastic complexity of the image. Different strategies for the pdf parameter estimation are analyzed, and a fast and robust technique is proposed. Finally, the relevance of the proposed approach is demonstrated on high-resolution SAR images. [J647]

## "Monitoring Sugarcane Growth Using ENVISAT ASAR Data"

The objective of this paper is to investigate potential of satellite C-band synthetic aperture radar (SAR) radar in monitoring sugarcane growth in southern China. This paper proposes a method to map sugarcane growing area and retrieve sugarcane leaf area index (LAI) in different growth stages using ENVISAT Advanced SAR (ASAR) alternating polarization HH/HV data. The temporal response of ASAR alternating polarization HH/HV data to sugarcane fields and sugarcane LAI was first analyzed in the study area. The analysis shows that sugarcane

fields have increasing temporal radar response trend with sugarcane growth and ratio of ASAR HV to HH data has a better correlation with the increase of sugarcane LAI. A theoretical radiative transfer model was adopted to interpret the trend. Based on the temporal variation of the radar response of sugarcane fields, a method for mapping sugarcane planting area was developed using ASAR HH and HV polarization data at two acquisition dates with a certain classification accuracy. The empirical models were also established to estimate LAI of sugarcane using the HV/HH polarization ratio. The results suggest that C-band ASAR data appear promising in the development of an operational system for monitoring sugarcane growth in southern China. [J648]

## "Simulation of ASIRAS Altimeter Echoes for Snow-Covered First-Year Sea Ice"

We have developed a simulator for the European Space Agency's Airborne SAR/Interferometric Radar Altimeter System (ASIRAS) altimeter echoes from snow-covered first-year sea ice. The simulated echoes are used to investigate how measurements are affected by the snow and ice characteristics. Our simulations show that when the snow cover is dry, the echo from the upper ice surface typically dominates. The simulated echoes prove to be very sensitive to the presence of liquid water in snow and the small-scale roughness of the ice surface. The accurate estimation of the ice freeboard is likely possible only under dry snow conditions and when the snow load is known. The ASIRAS simulator concept can also be used for the CryoSat altimeter. [J649]

## "Alternatives to Target Entropy and Alpha Angle in SAR Polarimetry"

The purpose of this paper is to discuss two polarimetric parameters which are widely used in synthetic aperture radar (SAR) polarimetry, namely, target entropy and alpha angle. We propose alternative parameters based on our analysis on how they are connected to covariance matrix similarity invariants and how they can be physically interpreted in optical polarimetry. The proposed alternatives can be computed by a fairly simple algorithm and even by the use of software without complex mathematics abilities. As an example, a NASA/Jet Propulsion Laboratory Airborne SAR L-band image of the San Francisco Bay is used to compare the proposed parameter schemes with the original entropy and alpha. A coherent rationale for these alternative parameters is formulated in order to provide insight to polarimetric parameter interpretation. [J650]

## "Data Compression for Multilook Polarimetric SAR Data"

This letter attempts to address the problem on the emergence of negative eigenvalues in the coherency matrix after the compressing of multilook polarimetric synthetic aperture radar (SAR) data. A new nine-parameter expression for the eigenvalue decomposition of the coherency matrix is introduced, and a new compression algorithm is proposed for multilook polarimetric data with this expression. By comparing it with the NASA/Jet Propulsion Laboratory's Airborne SAR compression algorithm, the authors analyze the new algorithm's compression accuracy, signal-to-noise ratio, and the ability to preserve the data's polarimetric property. For polarimetric SAR data, it is important to preserve the polarimetric property of a target. The proposed algorithm has this ability which is illustrated by the comparison of the polarimetric signatures. Finally, the effectiveness of the proposed methods is demonstrated by using the experimental SAR data. [J651]

## "Integrating LiDAR Intensity and Elevation Data for Terrain Characterization in a Forested Area"

Separating ground from nonground laser returns from airborne light detection and ranging (LiDAR) data is a key step in creating digital terrain models (DTMs). In this letter, bare-earth and forested surfaces are classified from LiDAR intensity data in a data set from central Idaho, U.S. Next, a Gaussian fitting (GF) method is applied to determine ground elevations from LiDAR elevation data according to the land-cover information. In comparison to ground-based reference data, the GF method generated an accurate DTM in this study area. Overall, the DTM underestimated the ground observations by approximately 31 cm. A combination of LiDAR intensity and elevation data may be effectively used to develop DTMs in similar terrain of relatively simple land-cover classes. [J652]

## "On-Ground Characterization of the SMOS Payload"

The on-ground characterization of the synthetic aperture radiometer onboard the Soil Moisture and Ocean Salinity mission is described. Characterization includes basic functionality, internal calibration, thermal cycling, response to point and flat sources, self-radio-frequency interference, and others. The description of the different tests performed as well as the detailed results are provided. The results show that the instrument is very stable and has all gains and offsets consistent with the ones obtained at subsystem level. On the other hand, the phase of the visibility has a larger variation with temperature than expected, a small signal leakage from the local oscillators is present, and a small interference from the X-band transmitter during short periods of time has been detected. The implementation of internal-calibration procedures, along with the accurate thermal characterization performed, have been used to produce highly accurate brightness-temperature values well within specifications. [J653]

## "Use of a Frequency-Hopping Radar for Imaging and Motion Detection Through Walls"

A small frequency-agile radar has been developed and configured into different systems for performing imaging of static and dynamic targets through common building materials. Radar operating parameters are defined through software control, allowing radar system operations to be tailored to operational needs. Field testing has shown the radar's ability to detect stationary individuals concealed behind concrete walls at significant ranges. [J654]

## "Experiments and Algorithms to Detect Snow Avalanche Victims Using Airborne Ground-Penetrating Radar"

Snow avalanche victims have only a good chance to survive when they are located within a short time. This requires an active beacon for them to wear or a very rapid deployment of a search-and-rescue team with dogs. Customary ground-penetrating radar (GPR) instruments used on the snow surface are not able to reduce fatality numbers because they are slow to search a field. A potential alternative could be an airborne search using radar. An airborne radar search is technologically challenging because a very large data stream has to be processed and visualized in real time, and the interaction of the electromagnetic waves with snow, subsurface, and objects must be understood. We studied a two-step algorithm to locate avalanche victims in real time. The algorithm was validated using realistic test arrangements and conditions using an aerial tramway. The distance dependence of the reflection energy with increased flight heights, the coherence between the use of more antennas and the detectable range, and the reflection images of different avalanche victims were measured. The algorithm detected an object for each investigated case, where the reflection energy of the scans was higher than for the scans of pure snow. Airborne GPR has a large potential to become a rapid search method in dry snow avalanches. However, a fully operational version still requires substantial improvements in hardware and software. [J655]

## "Antenna Mask Design for SAR Performance Optimization"

In this letter, an effective technique for synthetic aperture radar (SAR) antenna mask design is presented for optimizing the system performance of an active phased array SAR. The SAR antenna radiation pattern has an important effect on the system performance. Therefore, the authors derived the quantitative equations for the SAR antenna mainlobe and sidelobe mask design on the basis of the system performance measures such as the range-to-ambiguity ratio (RAR), the noise-equivalent sigma zero (NESZ), and the radiometric accuracy. The antenna mask template should be designed to minimize the ambiguous signals reflected from the antenna sidelobes and maximize the system sensitivity, i.e., the NESZ, determined by the antenna mainlobe. The simple iterative method such as random-mutation hill climbing was utilized to successfully assign the sidelobe level at each ambiguous area using the derived equations. Finally, the antenna patterns were synthesized with reference to the optimized antenna mask templates using the particle swarm optimization, and the swath width, RAR, and NESZ performances were evaluated in order to confirm the effectiveness of the proposed technique. [J656]

## "Achieving Higher Resolution ISAR Imaging With Limited Pulses via Compressed Sampling"

Recent theory of compressed sampling (CS) suggests that exact recovery of an unknown sparse signal with overwhelming probability can be achieved from very limited number of samples. In this letter, we adapt this idea and present a framework of high-resolution inverse synthetic aperture radar imaging with limited measured data. During the framework, we mathematically convert the imaging into a problem of signal reconstruction with orthogonal basis; hence, a conceptive upper bound of the cross-range resolution is presented based on the CS theory. Real data results show that the CS imaging approach outperforms the conventional range-Doppler one in resolution. [J657]

## "An Extended Nonlinear Chirp-Scaling Algorithm for Focusing Large-Baseline Azimuth-Invariant Bistatic SAR Data"

For an azimuth-invariant bistatic synthetic aperture radar (BiSAR), not only is the secondary range compression dependent on range, but also the range-cell migration in the range-Doppler domain is nonlinearly dependent on range. To get a better focusing performance, the two range-dependent factors must be taken into account in an imaging algorithm. In this letter, a nonlinear chirp-scaling algorithm is extended for focusing the BiSAR data under a large baseline and a wide range swath. This algorithm leads to more effective processing with computational efficiency, and no interpolation is required. [J658]

## "Selecting Suitable Coherent Processing Time Window Lengths for Ground-Based ISAR Imaging

## of Cooperative Sea Vessels"

Inverse synthetic aperture radar (ISAR) imaging of sea vessels is a challenging task because their 3-D rotational motion over the coherent processing interval (CPI) often leads to blurred images. The selection of the duration of the CPI, also known as the coherent processing time window length (CPTWL), is critical because it should be short enough to limit the blurring caused by the 3-D rotational motion and long enough to ensure that the desired cross-range resolution is obtained. This paper proposes an algorithm, referred to as the motion-aided CPTWL selector (MACS) algorithm, which selects suitable CPTWLs for ISAR imaging of cooperative sea vessels. The suggested CPTWLs may be used to obtain motion-compensated ISAR images that have the desired medium cross-range resolution and limited blurring due to 3-D rotational motion. The proposed algorithm is applied to measured motion data of three different classes of sea vessels: a yacht, a fishing trawler, and a survey vessel. Results show that longer CPTWLs are needed for larger vessels in order to obtain ISAR images with the desired cross-range resolution. The effectiveness of the CPTWLs, suggested by the MACS algorithm, is shown using measured radar data. The suggested CPTWLs may also be used to select an effective initial CPTWL for Martorella/Berizzi's optimum imaging selection algorithm when it is applied to measured radar data of small vessels. Lastly, the proposed technique offers significant computational savings for radar cross section measurement applications where a few high-quality ISAR images are desired from long radar recordings. [J659]

## "Cross-Range Scaling for ISAR Based on Image Rotation Correlation"

For better understanding of the imaging result provided by inverse synthetic aperture radar (ISAR), it is more desirable to present it from the conventional range-Doppler domain to the homogeneous range-cross-range domain. To accomplish the process of cross-range scaling, the rotating velocity (RV) of the target should be estimated first. For a uniformly planar rotating object, a novel method based on a concept of rotation correlation is proposed to obtain the RV in this letter, and neither prominent scattering centers nor phase coefficient extraction is required. Furthermore, a three-step fast-Fourier-transform-based convolution interpolation scheme is proposed to realize the above correlation, which makes the proposed method more efficient for implementation. Finally, experimental results with both simulated and real ISAR data are provided to demonstrate the effectiveness of the proposed method for different targets. [J660]

## "Improving the Intercalibration of Values for the Jason-1 and Jason-2 Altimeters"

The normalized backscatter from a radar altimeter sigma0is a measure of the surface roughness at scales of a few radar wavelengths; over the ocean, this is used to infer wind speed. Long-term studies of wind speed rely on consistent measurements within an altimetric mission and good intercalibration between missions. For the Jason-1 and Jason-2 altimeters, the derivation of sigma0from the full waveform data is known to be sensitive to the recovered value for psi2, a term encompassing both mispointing and inhomogeneities within the altimetric footprint. The six months of data from the Jason-1/2 tandem mission reveal that different sigma0corrections are needed for these two causes of nonzero psi2values. With these corrections implemented, the rms difference of Ku-band sigma0values for Jason-1 and Jason-2 drops from 0.15 to 0.05 dB, with the bias between the two showing a clear trend with wind speed; Jason-1 being 0.04 dB greater in high winds but 0.19 dB greater in low winds. No clear change in offset is noted during the six months of overlapping data. Implementation of this correction will improve consistency of Jason-1 sigma0values and may impact on orbit-fitting procedures. [J661]

## "Polarimetric SAR Internal Calibration Scheme Based on T/R Module Orthogonal Phase Coding"

Two important aspects of internal calibration of polarimetric synthetic aperture radar (SAR) are discussed, i.e., individual transmit/receive module (TRM) calibration and system gain calibration. The system has a general structure utilizing a phased array antenna composed of dual-channel TRMs. TRM gain and phase calibration is carried out using orthogonal phase coding (OPC). The signal of the individual TRM is phase-encoded according to a set of orthogonal codes to be separated from the composite calibration signal. OPC uses 1 bit of a digital phase-shifter for encoding, without the need for additional encoding hardware. Performance of the method is examined. Calibration results are developed both theoretically and through simulation in case of TRM amplifier or phase-shifter failure. Zero-padding is used to eliminate calibration error of the first TRM. A crosstalk model is proposed to investigate the effect of imperfect isolation between the two polarization channels of each TRM, and a way to reduce this error is also given. At last, system path gain variation is measured utilizing the internal calibration loop. The OPC method has an accuracy of 0.2 dB for gain and better than 2deg for phase, with 10-dB signal-to-noise ratio and perfect isolation between the two polarization channels. The error due to imperfect isolation is usually small and can be ignored. The simple way to detect TRM malfunction is verified through simulation, and it is also in accordance with TerraSAR-X in-orbit calibration outcomes. The proposed OPC method is shown to be an effective way of internally calibrating TRMs of a phased array antenna. [J662]

## "Electromagnetic Scattering From Objects Above a Rough Surface Using the Method of Moments With Half-Space Green's Function"

An efficient approach is proposed to analyze the electromagnetic scattering from objects above a 2-D perfectly electric conducting rough surface. A half-space Green's function with the rough-surface interface is first derived from the Kirchhoff approximation (KA). The method of moments is then applied to analyze the scattering problem of 3-D arbitrarily shaped objects above the rough surface. Since only the objects need to be discretized, the computational time and memory requirement are greatly reduced. The radar cross sections of typical objects above the rough surface have been computed using the proposed method. Numerical results show that the proposed method has good accuracy in the valid range of KA. [J663]

## "Design of a Wideband Antenna for a Narrow Borehole Radar Using FDTD Modeling"

For the design of a narrow wideband antenna (with diameter less than 3 cm) to serve in a borehole radar in the band [0.5,1.5] GHz for moisture content measurements, we have considered five different geometries. These geometries have been modeled using the finite-difference time-domain approach. The frequency- and time-domain responses have been analyzed in detail in the transmission configuration in the presence of a dielectric soil. We present radargrams for the multiple offset gather configuration. This study will help to define the best antenna geometry for the present application. [J664]

## "BRDF Analysis of Savanna Vegetation and Salt-Pan Samples"

In this paper, laboratory-based bidirectional reflectance distribution function (BRDF) analysis of vegetation leaves, soil, and leaf-litter samples is presented. The leaf litter and soil samples, numbered 1 and 2, were obtained from a site located in the savanna biome of South Africa (Skukuza: 25.0deg S, 31.5deg E). A third soil sample, number 3, was obtained from Etosha Pan, Namibia (19.20deg S, 15.93deg E, altitude of 1100 m). In addition, BRDF of local fresh and dry leaves from tulip polar tree (Liriodendron tulipifera) and black locust tree (Robinia pseudoacacia) were studied. It is shown how the BRDF depends on the incident and scatter angles, sample size (i.e., crushed versus whole leaf), soil samples fraction size, sample status (i.e., fresh versus dry leaves), vegetation species (i.e., poplar versus locust), and the vegetation's biochemical composition. As a demonstration of the application of the results of this paper, airborne BRDF measurements acquired with NASA's Cloud Absorption Radiometer over the same general site where the soil and leaf-litter samples were obtained are compared to the laboratory results. Good agreement between laboratory and airborne-measured BRDF is reported. [J665]

## "Layover Solution in SAR Imaging: A Statistical Approach"

In this letter, a statistical-based approach to recover layover solution in synthetic aperture radar (SAR) images is proposed. The aim of this letter is to develop a methodology in order to separate different scattering contributions collapsed in a single SAR image pixel. After a brief discussion about layover, the proposed model is presented, followed by a discussion about achievable performances using Cramer-Rao lower bounds. In the final part of this letter, the performances of a maximum likelihood estimator are evaluated in a simulated data scenario, showing the effectiveness of the method. [J666]

## "Mine Classification With Imbalanced Data"

In many remote-sensing classification problems, the number of targets (e.g., mines) present is very small compared with the number of clutter objects. Traditional classification approaches usually ignore this class imbalance, causing performance to suffer accordingly. In contrast, the recently developed infinitely imbalanced logistic regression (IILR) algorithm explicitly addresses class imbalance in its formulation. We describe this algorithm and give the details necessary to employ it for remote-sensing data sets that are characterized by class imbalance. The method is applied to the problem of mine classification on three real measured data sets. Specifically, classification performance using the IILR algorithm is shown to exceed that of a standard logistic regression approach on two land-mine data sets collected with a ground-penetrating radar and on one underwater-mine data set collected with a sidescan sonar. [J667]

## "Phase of Target Scattering for Wetland Characterization Using Polarimetric C-Band SAR"

Wetlands continue to be under threat, and there is a major need for mapping and monitoring wetlands for better management and protection of these sensitive areas. Only a few studies have been published on wetland characterization using polarimetric synthetic aperture radars (SARs). The most successful results have been obtained using the phase difference between HH and VV polarizations, phiHH- phiVV, which has shown promise for separating flooded wetland classes. Recently, we have introduced a new decomposition, the Touzi

decomposition, which describes target scattering type in terms of a complex entity, the symmetric scattering type. Huynen's target helicity is used to assess the symmetric nature of target scattering. In this paper, the new complex-scattering-type parameters, the magnitude alphasand phase Phialphas, are investigated for wetland characterization. The use of the dominant-scattering-type phase Phialphasmakes it possible to discriminate shrub bogs from poor (sedge or shrub) fens. These two classes cannot be separated using phiHH- phiVV, or the radiometric scattering information provided by alphas, the Cloude alpha, the entropy H, and the multipolarization HH-HV-VV channels. phialphas, which cannot detect deep (45 cm below the peat surface) water flow in a bog, is more sensitive to the shallower (10-20-cm) fen beneath water, and this makes possible the separation of poor fens from shrub bogs. Phialphasalso permits the discrimination of conifer-dominated treed bog from upland deciduous forest under leafy conditions. Target helicity information is exploited to introduce a new parameter, the target asymmetry. The latter is shown very promising for detection of forest changes between leafy and no-leaf conditions. The analysis of low-entropy marsh scattering showed that both the scattering-type magnitude and phas--e alphasand Phialphas, respectively, as well as the maximum polarization intensity of the dominant scattering m, are needed for a better understanding of marsh complex scattering mechanisms. The unique information provided by the new roll-invariant decomposition parameters are demonstrated using repeat-pass Convair-580 polarimetric C-band SAR data collected in June and October 1995 over the RAMSAR Mer Bleue wetland site near Ottawa (Canada). [J668]

## "Multichannel Phase Unwrapping With Graph Cuts"

Markovian approaches have proven to be effective for solving the multichannel phase-unwrapping (PU) problem, particularly when dealing with noisy data and big discontinuities. This letter presents a Markovian approach to solve the PU problem based on a new apriorimodel, the total variation, and graph-cut-based optimization algorithms. The proposed method turns out to be fast, simple, and robust. Moreover, compared with other approaches, the proposed algorithm is able to unwrap and restore the solution at the same time, without any additional filtering. A set of experimental results on both simulated and real data illustrates the effectiveness of our approach. [J669]

## "Comments on "Modified Hough Transform for Searching Radar Detection""

This correspondence points out an important error of calculating the detection probability in a recent paper by Jiankui et al. (2008). The authors make a mistake in the analysis of the distribution of the detector statistic. Therefore, the calculation of the detection probability is wrong. In this correspondence, a new detection probability is calculated. [J670]

## "Digital Beamforming on Receive: Techniques and Optimization Strategies for High-Resolution Wide-Swath SAR Imaging"

Synthetic Aperture Radar (SAR) is a well-proven imaging technique for remote sensing of the Earth. However, conventional SAR systems are not capable of fulfilling the increasing demands for improved spatial resolution and wider swath coverage. To overcome these inherent limitations, several innovative techniques have been suggested which employ multiple receive-apertures to gather additional information along the synthetic aperture. These digital beamforming (DBF) on receive techniques are reviewed with particular emphasis on the multi-aperture signal processing in azimuth and a multi-aperture reconstruction algorithm is presented that allows for the unambiguous recovery of the Doppler spectrum. The impact of Doppler aliasing is investigated and an analytic expression for the residual azimuth ambiguities is derived. Further, the influence of the processing on the signal-to-noise ratio (SNR) is analyzed, resulting in a pulse repetition frequency (PRF) dependent factor describing the SNR scaling of the multi-aperture beamforming network. The focus is then turned to a complete high-resolution wide-swath SAR system design example which demonstrates the intricate connection between multi-aperture azimuth processing and the system architecture. In this regard, alternative processing approaches are compared with the multi-aperture reconstruction algorithm. In a next step, optimization strategies are discussed as pattern tapering, prebeamshaping-on-receive, and modified processing algorithms. In this context, the analytic expressions for both the residual ambiguities and the SNR scaling factor are generalized to cascaded beamforming networks. The suggested techniques can moreover be extended in many ways. Examples discussed are a combination with ScanSAR burst mode operation and the transfer to multistatic sparse array configurations. [J671]

## "Estimation of the Equivalent Number of Looks in Polarimetric Synthetic Aperture Radar Imagery"

This paper addresses estimation of the equivalent number of looks (ENL), an important parameter in statistical modeling of multilook synthetic aperture radar (SAR) images. Two new ENL estimators are discovered by looking at certain moments of the multilook polarimetric covariance matrix, which is commonly used to represent

multilook polarimetric SAR (PolSAR) data, and assuming that the covariance matrix is complex Wishart distributed. First, a second-order trace moment provides a polarimetric extension of the ENL definition and also a matrix-variate version of the conventional ENL estimator. The second estimator is obtained from the log-determinant matrix moment and is also shown to be the maximum likelihood estimator under the Wishart model. It proves to have much lower variance than any other known ENL estimator, whether applied to single-polarization or PolSAR data. Moreover, this estimator is less affected by texture and thus provides more accurate results than other estimators should the assumption of Gaussian statistics for the complex scattering coefficients be violated. These are the first known estimators to use the full covariance matrix as input, rather than individual intensity channels, and therefore to utilize all the statistical information available. We finally demonstrate how an ENL estimate can be computed automatically from the empirical density of small sample estimates calculated over a whole scene. We show that this method is more robust than procedures where the estimate is calculated in a manually selected region of interest. [J672]

## "Raw signal processing of stripmap bistatic synthetic aperture radar"

Under the translational invariant (TI) configuration of stripmap imaging bistatic synthetic aperture radar (BISAR), the frequency domain expression of signal model is developed. Two forms, with an approximation of extracting the range dependence and an accurate iterative solution, as well as their respective focusing methods, that is the approximated solution method and the iterative solution method are presented here. The range-Doppler method is extended to the TI configuration of BISAR. Imaging simulation of the point targets and comparison with the bistatic backprojection method shows the feasibility of these methods as well as their merits and demerits. [J673]

## "A Low-Power and Small-Size HF Backscatter Radar for Ionospheric Sensing"

A new high-frequency backscatter radar (Wuhan Ionospheric Oblique Backscattering Sounding System) for ionospheric sensing and study has been developed. With the new system design, oblique backscatter sounding and oblique sounding can be achieved in this radar just through simply loading appropriate software. Furthermore, due to alternate transmission and reception in equal interval, this radar can detect the ionospheric state in the range of a few thousand kilometers and achieve the largest gain of applied pseudorandom sequences. In addition, this radar usually obtains 27-dB gain from phase coded pulse compression and 21-dB gain from coherent spectral integration using pseudorandom code, pulse compression, and coherent spectral integration techniques. This radar also exploits merits of Peripheral component interconnect eXtensions for Instruments (PXI) bus technology and is designed as a modular and compact PXI-based system. Details of system design, sounding timing, and signal-processing algorithm are described. Except for the antenna systems and power amplifier, this radar's dimension is 177.8 times 431.8 times 457.2 mm. With this radar, the oblique backscatter ionogram and Dopplerionogram can be clearly obtained in the range of a few thousand kilometers with 100-W power. The oblique ionogram for propagation over a distance of several kilometers can also be clearly acquired at the time of oblique backscatter sounding. The initial observations obtained with this radar are included to demonstrate its performance. [J674]

## "Estimating Spatiotemporal Ground Deformation With Improved Permanent-Scatterer Radar Interferometry"

Synthetic aperture radar interferometry has been applied widely in recent years to ground deformation monitoring although difficulties are often encountered when applying the technology, among which the spatial and temporal decorrelation and atmospheric artifacts are the most prominent. The permanent-scatterer interferometric synthetic aperture radar (PS-InSAR) technique has overcome some of the difficulties by focusing only on the temporally coherent radar targets in a time series of synthetic aperture radar (SAR) images. This paper presents an improved PS-InSAR technique by introducing PS-neighborhood networking and empirical mode decomposition (EMD) approaches in the PS-InSAR solution. Linear deformation rates and topographic errors are estimated based on a least squares method, while the nonlinear deformation and atmospheric signals are computed by singular value decomposition and the EMD method. An area in Phoenix, AZ, is used as a test site to determine its historical subsidence with 39 C-band SAR images acquired by European Remote Sensing 1 and 2 satellites from 1992 to 2000. [J675]

## "Large-Area Soil Moisture Estimation Using Multi-Incidence-Angle RADARSAT-1 SAR Data"

The sensitivity of synthetic aperture radar (SAR) backscatter to soil moisture has been adequately established. However, monitoring of soil moisture over large agricultural areas is still difficult because SAR backscatter is also sensitive to other target properties like surface roughness, crop cover, and soil texture (soil type), along with its strong sensitivity to soil moisture. Hence, to develop a methodology for large-area soil moisture estimation using

SAR, it is necessary to incorporate the effects of surface roughness, crop cover, and soil texture in the soil moisture retrieval model. In this paper, a methodology for soil moisture estimation over a large area is developed using a pair of low- and high-incidence-angle RADARSAT-1 SAR data over parts of Agra, Mathura, and Bharatpur districts, India, during March 1999. The methodology requires acquisition of synthetic aperture radar data at low and high incidence angles, such that the soil moisture changes are negligible between the two acquisitions. In order to demonstrate the applicability of the developed methodology, the same was validated over a different area (parts of Saharanpur and Haridwar districts, India) during March 2005. Both test sites provided the variety of agricultural heterogeneity required for development and validation of the methodology for large-area soil moisture estimation. The proposed methodology offers an approach to incorporate the effects of surface roughness, crop cover, and soil texture in the soil moisture retrieval model from the space platform, without making any assumptions on the distributions of these parameters or without knowing the actual values of these parameters on ground. [J676]

## "Autobinomial Model for SAR Image Despeckling and Information Extraction"

This paper presents a model-based despeckling (MBD) of synthetic aperture radar (SAR) images using Bayesian analysis. The SAR image is despeckled using first-order Bayesian inference. The novelty in this paper is an autobinomial model (ABM), which models a priorprobability density function (pdf); meanwhile, the likelihoodpdf is modeled as a gamma distribution. Analytically, a solution for a maximum aposterioriestimate using an autobinomial prior cannot be computed; therefore, an approximation is introduced using differential. The best ABM for approximating the texture parameters in SAR images is found by using second-order Bayesian inference. The edges in the SAR images are detected using region borders, which have statistically different properties. Coefficient of variation is used to distinguish between homogeneous and heterogeneous areas. The experimental results show that the proposed method preserves the textural features and removes noise significantly in the homogeneous and heterogeneous regions. The proposed despeckling method is good regarding objective measures for synthetic images and better despeckles the real SAR images, when compared with the state-of-the-art MBD methods. [J677]

## "Performance analysis of interrupted sparse HFSWR waveform coded with successive fast Fourier transforms"

A successive Fourier transform technique is applied to efficiently generate an interrupted sparse waveform for a monostatic high-frequency surface wave radar. With few iterations a good stop to passband ratio is reached, and it is show that, when using an optimised envelope, a better average and a lower standard deviation are obtained in terms of minimal contrast ratio than in the case of a simple train of pulses. [J678]

## "Transmission Through Layered Media With Rough Boundaries: First-Order Perturbative Solution"

We investigate analytically the fully polarimetric electromagnetic wave propagation through a 3-D layered structure. In the framework of the first-order limit of the perturbation theory, a transmission model for a layered structure with an arbitrary number of rough interfaces is developed and an elegant closed-form solution is obtained. The final expressions, in terms of generalized reflection/transmission coefficients, provide parametrically a direct characterization of the scattering properties of the layered structure in terms of the structure's (geometric and electromagnetic) parameters. In addition, we point out the complementary character of the obtained scattering solution with respect to the existing one. Finally, we demonstrate that our solution satisfies the reciprocity principle. [J679]

## "Integration of InSAR Time-Series Analysis and Water-Vapor Correction for Mapping Postseismic Motion After the 2003 Bam (Iran) Earthquake"

Atmospheric water-vapor effects represent a major limitation of interferometric synthetic aperture radar (InSAR) techniques, including InSAR time-series (TS) approaches (e.g., persistent or permanent scatterers and small-baseline subset). For the first time, this paper demonstrates the use of InSAR TS with precipitable water-vapor (InSAR TS + PWV) correction model for deformation mapping. We use MEdium Resolution Imaging Spectrometer (MERIS) near-infrafred (NIR) water-vapor data for InSAR atmospheric correction when they are available. For the dates when the NIR data are blocked by clouds, an atmospheric phase screen (APS) model has been developed to estimate atmospheric effects using partially water-vapor-corrected interferograms. Cross validation reveals that the estimated APS agreed with MERIS-derived line-of-sight path delays with a small standard deviation (0.3-0.5 cm) and a high correlation coefficient (0.84-0.98). This paper shows that a better TS of postseismic motion after the 2003 Bam (Iran) earthquake is achievable after reduction of water-vapor effects using the InSAR TS + PWV technique with coincident MERIS NIR water-vapor data. [J680]

## "A Feasibility Assessment for Low-Cost InSAR Formation-Flying Microsatellites"

Multistatic interferometric synthetic aperture radar (InSAR) is a promising potential payload for a small satellite constellation. CanX-4 and CanX-5 are a pair of formation-flying nanosatellites launching in 2009; once formation flight has been demonstrated, a future multistatic InSAR constellation of low-cost microsatellites can exploit subcentimeter intersatellite baseline knowledge, with digital elevation map height errors on the order of 1 m in the flat-terrain case. This paper evaluates the feasibility of such a mission, using case studies of commonly proposed configurations: the Interferometric Cartwheel, the Cross-Track Pendulum, and the Cartwheel-Pendulum (Car-Pe) configuration. In each case, several SAR transmitters are considered: L-, C-, and X-band transmitters with parameters mirroring existing ldquolargerdquo satellite SAR missions, and a theoretical X-band microsatellite transmitter. The available interferometric baselines, ground coverage, and image resolutions are evaluated in each scenario. The X-band ldquomicrordquo transmitter is feasible, but the low transmit power severely limits the ground coverage. The X-band ldquolargerdquo transmitter provides the largest ground coverage and the highest resolution along with the X-band ldquomicrordquo option. The resolutions are wavelength dependent and remain relatively constant among the configurations. The operating areas of the pendulum demonstrate the largest degree of overlap, while the longer along-track baselines of the cartwheel result in a smaller overlap. Both two-receiver (pendulum and cartwheel) configurations demonstrate baseline characteristics that may be optimal for different applications, while the three-receiver Car-Pe demonstrates the advantages of both the pendulum and cartwheel. [J681]

## "Ensemble Kalman filter"

Meteorological models are used to predict the weather, study atmospheric processes, and provide input to decision makers on the consequences of increased greenhouse gas emissions to the Earth's climate. Predictions of future atmospheric states are accomplished as an initial value or marching problem, where the initial atmospheric state is specified and the variables are advanced in time using numerical techniques. The challenge of data assimilation in meteorology is to estimate, based on a set of limited observations of varying types, the complete three-dimensional atmospheric state at a given time to provide an initial value for a meteorological model. [J682]

## "A Closed-Form Expression Relating Classification Accuracy to SAR System Calibration Uncertainty"

The choice of synthetic aperture radar (SAR) system design parameters such as radiometric calibration uncertainty and noise-equivalent sigma zero has a significant impact on applications exploiting SAR image data. However, methods for quantitatively translating the impact of system and mission parameter choices into the application context are lacking. This letter addresses this subject and derives a closed-form algebraic expression for translating radiometric biases due to calibration uncertainties-an important SAR engineering specification-into estimates of classification uncertainties for the restricted case of two homogeneous classes characterized by different backscatter intensity levels. The expression is exploited within this letter to estimate the potential impact of radiometric uncertainty on SAR-derived thematic maps. The results indicate that classification results based on the joint use of data from future SAR constellations in particular may be significantly degraded due to calibration uncertainties. [J683]

## "Longshore Surface Currents Measured by Doppler Radar and Video PIV Techniques"

Mean longshore surface currents within the surf zone were measured using two remote sensing techniques: microwave Doppler radar and optical video. Doppler radar relies on small-scale surface roughness that scatters the incident electromagnetic radiation so that velocities are obtained from the Doppler shift of the backscattered radiation. Video relies on texture and contrast of scattered sunlight from the sea surface, and velocity estimates are determined using particle imaging velocimetry (PIV). This paper compares video PIV and Doppler radar surface velocities over a 1-km alongshore by 0.5-km cross-shore area in the surf zone of a natural beach. The two surface velocity estimates are strongly correlated (R2ges 0.79) over much of the surf zone. Estimates differ at the outer edge of the surf where strong breaking is prevalent, with radar-estimated velocities as much as 50% below the video estimates. The radar and PIV velocities at particular locations in the surf zone track each other well over a 6-h period, showing strong modulations in the mean alongshore flow occurring on 10-20-min time intervals. In one case, both systems observe a strong eddy-like mean flow pattern over a 200-m section of coastline, with the mean alongshore current changing direction at about the mid surf zone. The good spatial and temporal agreement between the two remote measurement techniques, which rely on very different mechanisms, suggests that both are reasonably approximating the true mean longshore surface velocity. [J684]

## "Sparse Two-Dimensional Phase Unwrapping Using Regular Grid Methods"

Phase unwrapping is usually defined as the reconstruction of a function sampled on a spatial grid given its value modulo 2pi. Phase unwrapping is a key step in image reconstruction in many imaging techniques including interferometric synthetic aperture radar (InSAR). In recent years, many new methods have been developed to exploit the presence of coherent or persistent scattering points for extracting deformation signatures in regions where conventional InSAR fails. These techniques often yield measurements that are only poorly sampled spatially, yet these sparse data must still be unwrapped if we are to be able to extract useful geophysical information. The conventional well-sampled 2-D phase unwrapping problem based on phase residues is fairly well understood and many novel techniques involving geometry and network flow concepts have been implemented successfully to date. For sparse data, residues may be computed over the Delaunay triangulation of the data points, but published algorithms meet with limited success when the sparse data are unwrapped. The advantages of modern unwrapping methods applicable to well-sampled data are often lost when sparse data are analyzed. In this letter, we show that a nearest neighbor interpolation scheme allows powerful and existing 2-D solvers to be applied to sparse data. We present results using both simulated and real data sets to illustrate our method. [J685]

## "SAR Image Regularization With Fast Approximate Discrete Minimization"

Synthetic aperture radar (SAR) images, like other coherent imaging modalities, suffer from speckle noise. The presence of this noise makes the automatic interpretation of images a challenging task and noise reduction is often a prerequisite for successful use of classical image processing algorithms. Numerous approaches have been proposed to filter speckle noise. Markov random field (MRF) modelization provides a convenient way to express both data fidelity constraints and desirable properties of the filtered image. In this context, total variation minimization has been extensively used to constrain the oscillations in the regularized image while preserving its edges. Speckle noise follows heavy-tailed distributions, and the MRF formulation leads to a minimization problem involving nonconvex log-likelihood terms. Such a minimization can be performed efficiently by computing minimum cuts on weighted graphs. Due to memory constraints, exact minimization, although theoretically possible, is not achievable on large images required by remote sensing applications. The computational burden of the state-of-the-art algorithm for approximate minimization (namely the alpha -expansion) is too heavy specially when considering joint regularization of several images. We show that a satisfying solution can be reached, in few iterations, by performing a graph-cut-based combinatorial exploration of large trial moves. This algorithm is applied to joint regularization of the amplitude and interferometric phase in urban area SAR images. [J686]

## "Terrain: Slope Influence on QuikSCAT Backscatter"

Soil moisture (SM) is an important variable in determining streamflow, agricultural productivity, weather, and climate. An effective way to map SM over large areas on a regular basis is by using active microwave observations. This paper examines the influence of topography on radar backscatter measurements for a range of vegetation conditions and on the development of a normalization technique for the correction of topography-induced variability. Radar backscatter observations derived from the QuikSCAT sensor were analyzed to investigate the effect of sloping terrain over the North American Monsoon Experiment region that is characterized by heterogeneous surface conditions and complex topographic terrain. A digital elevation model, along with local incidence angle and slope, was used to investigate the backscatter dependence on topography variation for eight main vegetation classes. Pearson product-moment correlation (R) analysis showed strong backscatter dependence on the local incidence angle caused by changes in slope. The overall average reduction in variances after correction for August 2004 depended on vegetation type and ranged between -16% to -42% and -18% to -37% for horizontal and vertical polarizations, respectively. The corrected sigma-0 was also evaluated using insituSM observations obtained during the Soil Moisture Experiment 2004 field campaign. The computed percent change in Rbetween sigma-0 and SM demonstrated significant improvement after correction when using vertically observed sigma-0. The standard errors of estimate for these two vegetation classes were lowered by about 12% and 5%, respectively, after applying the proposed topographic normalization technique to the QuikSCAT observations. [J687]

## "Lake Level Variations Monitored With Satellite Altimetry Waveform Retracking"

Over lake shores, altimetric waveforms are generally contaminated by lands, rough lake surfaces, and lag effects of the altimeter's automatic gain control. To improve altimeter ranging accuracy and in turn to get better surface height measurement, contaminated waveforms should be retracked against geophysical corrections. In this paper, an improved threshold retracker (ITR) is developed to retrack waveforms over lakes. ITR considers not only the physical characteristics of the reflecting surface, but also the stochastic feature of waveform, and two new retrackers, the N-Beta function model, and the N-5-Beta function model, are also put forward to develop the waveform retracking program of this study. TOPEX/POSEIDON waveforms over Hulun Lake in the North

China are retracked to monitor the temporal lake level variations. A comparison with the in situhydrological data indicates ITR is very efficient to monitor the lake level variations with the retracked altimetric data. The result of our study shows accurate seasonal level variations and the descending trend of Hulun Lake. [J688]

## "GPR Response From Buried Pipes: Measurement on Field Site and Tomographic Reconstructions"

The identification of the physical nature of an object or target causing a ground-penetrating radar (GPR) anomaly, as well as the estimation of a target's dimensions and geometry, is rather challenging. To improve target identification, basic studies are still required, and they can be addressed primarily using a laboratory- or field-based physical model. The field model (test site) is usually expensive and difficult to build, but it provides data for controlled target properties and geometry from a natural environment that are essential for testing processing techniques. In this paper, we present the results from a field experiment where GPR data were collected on plastic and metallic pipes. The main objective is the comparison of the classical migration technique with a microwave tomography approach for reconstructing the geometrical target properties. The use of the microwave tomography approach will allow us to obtain more focused and stable images of the buried objects compared to the ones obtained using classical migration techniques. [J689]

## "Coherence-Improving Algorithm for Image Pairs of Bistatic SARs With Nonparallel Trajectories"

Ground moving target indication (GMTI) is one of the most important applications in a general bistatic synthetic aperture radar (SAR) system, where the transmitter and receiver move along nonparallel trajectories with different velocities. In order to improve the capability of clutter cancellation in bistatic SAR/GMTI processing, the coherence between two echoes collected by two receivers is investigated, and the full-coherence conditions are derived. A new coherence-improving algorithm for general bistatic SAR complex image pairs is proposed, which can be realized in the following steps: 2-D range azimuth prefiltering processing, relative geometric deformation correction, and image registration. An approximate implementation of 2-D prefiltering and the corresponding prefilter parameter analysis are also given. Last, two numerical experiment results are given to demonstrate the effectiveness of the proposed algorithm. [J690]

## "Noise Reduction in Interferograms Using the Wavelet Packet Transform and Wiener Filtering"

A novel noise reduction scheme for synthetic aperture radar (SAR) interferograms based on the wavelet packet transform (WPT) and the Wiener filter is introduced in this letter. First, by employing the WPT in the spatial frequency domain, the real and imaginary parts of the complex noisy interferogram are decomposed, respectively, and the wavelet coefficients are obtained. Then, for these coefficients, Wiener filtering is adopted to remove noise. This scheme can filter noise adaptively according to the local noise level, without requiring any a priori information. By using a simulated noisy interferogram and two ENVISAT advanced synthetic aperture radar C-band interferograms, the performance of this scheme, in terms of noise reduction and fringes preservation, is reported and compared with other filter algorithms. The experimental results demonstrate the effectiveness of the proposed scheme. [J691]

## "An Error Prediction Framework for Interferometric SAR Data"

Three of the major error sources in interferometric synthetic aperture radar measurements of terrain elevation and displacement are baseline errors, atmospheric path length errors, and phase unwrapping errors. In many processing schemes, these errors are calibrated out by using ground control points (GCPs) (or an external digital elevation model). In this paper, a simple framework for the prediction of error standard deviation is outlined and investigated. Inputs are GCP position, aprioriGCP accuracy, baseline calibration method along with a closed-form model for the covariance of atmospheric path length disturbances, and a model for phase unwrapping errors. The procedure can be implemented as a stand-alone add-on to standard interferometric processors. It is validated by using a set of single-frame interferograms acquired over Rome, Italy, and a double difference data set over Flevoland, The Netherlands. [J692]

## "An Artificial-Neural-Network-Based Integrated Regional Model for Rain Retrieval Over Land and Ocean"

An integrated regional model is proposed for rain-rate retrievals over land/ocean from the brightness temperature (Tb) values of the Tropical Rainfall Measuring Mission (TRMM) Microwave Imager (TMI). The polarization-corrected temperature calculated from the 85.5-GHz channels is also considered as one of the inputs along with the nine channel Tb values. This model is applicable over the region between and . For this purpose, an artificial neural network is utilized. The collocated precipitation radar (PR) near-surface rain rates as given by a 2A25

data product is considered as a target value. The methodology consists of the separation of land and ocean pixels, the separation of stratiform and convective pixels over land/ocean, and the selection of important features (inputs) for the multilayer perceptron network by the feature selection technique for each group. For the separation of land/ocean pixels, the Tb values of the 10.65-GHz vertical channel are utilized. The values are utilized to separate the stratiform and convective pixels both over land and ocean. The rain retrieval from the developed model is validated with TRMM PR. Overall result shows the better agreement of the model-retrieved rain rate with the PR observation compared to the TMI (2A12) rain rate particularly over land. The rain retrieved from the developed model is further validated with Doppler weather radar. A reasonably good agreement is observed between these two estimations. [J693]

## "POLSAR Image Analysis of Wetlands Using a Modified Four-Component Scattering Power Decomposition"

It is important to monitor environmental changes of the Earth's cover by remotely sensed data. This paper analyzes seasonal changes of a wetland by a modified polarimetric four-component scattering power decomposition method. The data sets analyzed here are L- and X-band fully polarimetric synthetic aperture radar (POLSAR) data, which have been acquired by the NICT/JAXA airborne polarimetric and interferometric synthetic aperture radar system in 2004. Since there existed a deficiency in the currently adopted decomposition schemes in that negative powers appear in a few pixels in the image analysis, we modified the approach taking into account physical conditions. It is shown by the modified scheme that the seasonal changes and features of the vegetation near Sakata Lagoon in Niigata, Japan, are observed clearly, demonstrating the utility of POLSAR image analysis for wetland assessments in general. [J694]

## "Quantifying the Size of a Lidar Footprint: A Set of Generalized Equations"

Light detection and ranging (lidar) technologies provide a practical solution to 3D terrain mapping through laser ranging and scanning technologies. A lidar footprint, which is the critical parameter describing the size of a laser sampling area, varies with the scanning geometry and the local topography encountered. Integrating the effects of the scanning geometry and terrain orientations, this letter analyzes the intersection geometry of a laser beam and the terrain and develops a set of rigorous generalized footprint equations on inclined terrain for both across-track and Palmer scanning systems. [J695]

## "Data correction for visualisation and classification of sidescan SONAR imagery"

Of all the remote sensing modalities available for underwater applications, acoustic methods, covering frequency ranges from a few Hz to several MHz, are by far the most flexible and widely used. The authors propose a method for preprocessing sidescan sonar data for visualisation, detection and classification purposes. Sidescan imagery is highly sensor specific and is typically affected by factors that have either a range dependency or an angular dependency. Each of these is altered in a different way given variations in sensor altitude over the seabed. Working from the physics and geometry of the sonar process, the proposed method estimates separate correction factors for range and angular dependencies directly from the image data. Once calculated, these factors can be applied over large data sets to provide radiometric correction over the entire survey area. Simpler image processing algorithms are more effective because the image statistics are improved with more stable means and variances across the sonar swath. The method requires a good bottom detection algorithm for estimation of sensor altitude at each transmission time and incorporates a resampling scheme for the calculation and application of the angular-dependency correction factors. Results showing improved classification performance for two large area surveys are presented. The method proposed provides a more complete solution than previously reported resampling schemes and offers significant improvements in terms of accuracy, robustness, usability and execution times. [J696]

## "Impact of Biannual Rossby Waves on the Indian Ocean Dipole"

TOPEX/Poseidon sea surface height anomalies during 1993-2002 are decomposed using 2-D finite impulse response filters which showed biannual Rossby waves (BRWs) in the equatorial Indian Ocean (peak at 1.5degS) and in the southern tropical Indian Ocean (peak at 10.5degS) during Indian Ocean dipole (IOD) years. Anomalous downwelling BRWs in the equatorial Indian Ocean triggered by the wind stress curl-induced Ekman pumping near the eastern boundary started propagating westward from the eastern boundary in July/August 1993 and 1996, i.e., more than one year prior to the formation of the IOD events of 1994 and 1997 respectively. These strong downwelling signals reach the western equatorial Indian Ocean during the peak dipole time. [J697]

## "Overview of the TECSAR Satellite Hardware and Mosaic Mode"

TECSAR satellite is part of a spaceborne synthetic-aperture-radar (SAR) satellite technology demonstration

program. The purpose of this program is to develop and evaluate the technologies required to achieve high-resolution images combined with large-area coverage. These requirements can be fulfilled by designing a satellite with multimode operation. The TECSAR satellite is developed by the MBT Space Division, Israel Aerospace Industries, acting as a prime contractor, which develops the satellite bus, and by ELTA Systems Ltd., which develops the SAR payload. This paper reviews the TECSAR radar system design, which enables to perform a variety of operational modes. It also describes the unique hardware components: deployable parabolic mesh antenna, multitube transmitter, and data-link transmission unit. The unique mosaic mode is presented. It is shown that this mode is the spot version of the scan mode. [J698]

## "Using the Existing Spectral Clutter Filter With the Nonuniformly Spaced Time Series Data in Weather Radar"

The National Weather Service (NWS) has a network of weather surveillance Doppler radars, WSR-88D, that is routinely upgraded to reflect current technological and engineering advances. During the last decade, the staggered pulse repetition time (SPRT) was proposed to mitigate range/velocity ambiguity in WSR-88D; however, it could not be used at lowest elevation tilts due to the inability to filter ground clutter from the nonuniformly spaced time series. A complicated spectral procedure was developed to address this issue, but the procedure was derived for a specific set of data acquisition parameters and used a lookup table to provide a value for the clutter spectrum width. Attempts to use SPRT with different sets of acquisition parameters always led to the degradation of filtering. It is proposed here that the clutter spectrum width be estimated by using Gaussian model adaptive processing (GMAP) that is currently used by NWS for uniformly sampled time series. GMAP is an adaptive ground clutter filter that performs an iterative fit of a Gaussian curve to the spectral coefficients identified as being due to ground clutter. GMAP cannot be used directly with the SPRT spectrum because of multiple clutter replicas that are due to staggered nonuniform sampling. However, the elements of GMAP can be exploited and used in the SPRT procedure. This letter presents how the elements of GMAP can be used with the SPRT data to provide successful clutter filtering at lowest elevation tilts. [J699]

## "On the Design and Evaluation of Multiobjective Single-Channel SAR Image Segmentation Algorithms"

Multiobjective segmentation algorithms are based on an objective function, consisting of two or more terms, that is minimized by using an optimization algorithm. The objective terms represent differing segmentation objectives, the most popular of which are statistical likelihood of pixel values and smoothness of segment boundaries. Many assumptions are built into the objective function, and we present a case study based on the algorithm of Stewart to demonstrate the importance of analyzing algorithm characteristics to test the validity of hidden assumptions. We develop a set of simulated test images and a novel segmentation performance metric for use with simulated data. An innovative aspect of the Stewart algorithm (SA) is the probability of false alarm (PFA) model used to weight the objective terms. This is intended to dynamically balance the terms as the algorithm progresses. The PFA model is only valid for false edges, and we have shown that the number of selected true edges increases as segmentation evolves, making the theoretical weight model increasingly invalid. In addition, we found problems with several other algorithm assumptions. We tested algorithm performance against a fixed-weight version. We found that the performance of the SA was worse than a fixed-weight version. Thus, while the two-term objective function algorithm does deliver reasonable performance for multilook data, the fixed-weight version gives better performance. While these results hold only for simulated data, we believe that the experimental results indicate the need for a more powerful approach to multiobjective synthetic aperture radar segmentation. [J700]

## "Some Aspects of Improving the Frequency Scaling Algorithm for Dechirped SAR Data Processing"

The frequency scaling algorithm (FSA) was proposed to process the synthetic aperture radar (SAR) data acquired via the dechirp-on-receive approach. Some aspects of improving the FSA are investigated in this paper, based on which an extended FSA (EFSA) is presented. The general purpose of the EFSA is to reduce the effect of range spectrum shift of the intermediate processing results, which occurs during the scaling operation in the FSA, so as to achieve a more effective utilization of the processed bandwidth. The EFSA is implemented through time shifting the scaling and the inverse scaling functions used in the FSA and also the adjustment of the scaling factor. The derivation of the EFSA is detailed in this paper. Point target simulation in squinted imaging geometry indicates that the presented algorithm is more suitable for large-squint applications. [J701]

## "Conditional Copulas for Change Detection in Heterogeneous Remote Sensing Images"

A new preprocessing technique is presented in this paper to automatically highlight changes in multitemporal strongly heterogeneous remotely sensed images. The proposed technique is devoted to the case where the two

acquisitions, before and after a given event, are significantly different, due, for instance, to different sensors, acquisition modalities, or climatic conditions. In a previous study, it was proven that the local statistics of the images acquired at the two dates could be used to extract a relevant change indicator. Nevertheless, this measure is valid when the two observations have been derived from similar acquisitions. When the acquisition modalities differ, local statistics tend to be too different from one image to the other one to be relevant in highlighting the ground evolution without mixing with the changes at ground. The technique proposed in this paper to overcome this limitation is based on the assumption that some dependence indeed exists between the two images in unchanged areas. This dependence is modeled by quantile regression applied according to the copula theory and used to perform an estimation of the local statistics that would have been observed if the acquisition conditions of the first image had been similar to the ones of the second image. The method yields an estimate of the local statistics of the first image through the point of view of the second one. Then, usual Kullback-Leibler-based comparisons of those statistics are applied to define a change measure, which may be analyzed (e.g., by thresholding) in order to detect changes. Experimental results are shown to validate the proposed method by using a pair of Synthetic Aperture Radar (SAR) images onboard European Remote Sensing (ERS) Satellite images and a pair of optical-SAR images (from the High Resolution Visible (HRV) sensor onboard Satellite Pour l'Observation de la Terre (SPOT) satellite and from ERS-SAR) acquired before and after a flood. [J702]

## "Data-Level Fusion of Multilook Inverse Synthetic Aperture Radar Images"

Although techniques for resolution enhancement in single-aspect radar imaging have made rapid progress in recent years, it does not necessarily imply that such enhanced images will improve target identification or recognition. However, when multiple looks of the same target from different aspects are obtained, the available knowledge increases, allowing more useful target information to be extracted. Physics-based image fusion techniques can be developed by processing the raw data collected from multiple inverse synthetic aperture radar sensors, even if these individual images are at different resolutions. We derive an appropriate data fusion rule to generate a composite image containing enhanced target shape characteristics for improved target recognition. The rule maps multiple data sets collected by multiple radars with different system parameters on to the same spatial-frequency space. The composite image can be reconstructed using the inverse 2-D Fourier transform over the separated multiple integration areas. An algorithm called the Matrix Fourier Transform is proposed to realize such a complicated integral. This algorithm can be regarded as an exact interpolation such that there is no information loss caused by data fusion. The rotation centers need to be carefully selected to properly register the multiple images before performing the fusion. A comparison of the image attribute rating curve between the fused image and the spatially averaged images quantifies the improvement in the detected target features. The technique shows considerable improvement over a simple spatial averaging algorithm and thereby enhances target recognition. [J703]

## "Polarimetric Characterization of Bistatic Coherent Mechanisms"

This paper proposes a generalization of the Huynen theory to bistatic radar configurations for which the scattering matrices can no longer be assumed symmetrical. A set of parameters characterizing the physical mechanisms is extracted from the disoriented bistatic Kennaugh matrix. The distribution of amplitude between the parameters of the disoriented Kennaugh matrix is studied. [J704]

## "Neuroinspired Architecture for Robust Classifier Fusion of Multisensor Imagery"

Two new algorithms for robust and fault-tolerant classifier combination are presented. The attractor dynamics (AD) algorithm models some properties of sensory integration in the central nervous system and is based on the application of the dynamical systems for classifier fusion. The classifier masking (CM) algorithm is a nonneural version of the AD algorithm based on finding intersecting classifier intervals. Both of the proposed algorithms employ the idea of consensus among individual classifiers. The individual classifiers have been trained using resampled feature sets. They fuse the information from advanced synthetic aperture radar, medium resolution imaging spectrometer, and advanced along track scanning radiometer envisat satellite sensors for the improved sea ice classification. The results of our experiments show that training and combing the individual classifier outputs in a multiple classifier system significantly improve the robustness and the fault tolerance of the classification system as compared to the single classifier combining all sources of information. The robustness of the single classifier has been largely reduced in cases of single sensor failures (87.9 % in normal conditions versus 64.8% and 66.1% for two artificially corrupted data sets), whereas the CM algorithm is more tolerant to the sensor and preprocessing errors (86.4% in normal conditions versus 78.9% and 73.6% for two artificially corrupted data sets). The performance of the CM algorithm is superior to those of the simple multiple classifier combination strategies based on classifier averaging and majority voting (78.9% versus 70.9% and 69.5%, respectively) because the AD and CM algorithms are able to discard the corrupted classifier outputs based on

classifier agreement and, in fact, represent hybrid approaches combining the properties of classifier averaging and classifier selection methods. [J705]

## "Classifying Multilevel Imagery From SAR and Optical Sensors by Decision Fusion"

A strategy for the joint classification of multiple segmentation levels from multisensor imagery is introduced by using synthetic aperture radar and optical data. At first, the two data sets are separately segmented, creating independent aggregation levels at different scales. Each individual level from the two sensors is then preclassified by a support vector machine (SVM). The original outputs of each SVM, i.e., images showing the distances of the pixels to the hyperplane fitted by the SVM, are used in a decision fusion to determine the final classes. The fusion strategy is based on the application of an additional classifier, which is applied on the preclassification results. Both a second SVM and random forests (RF) were tested for the decision fusion. The results are compared with SVM and RF applied to the full data set without preclassification. Both the integration of multilevel information and the use of multisensor imagery increase the overall accuracy. It is shown that the classification of multilevel-multisource data sets with SVM and RF is feasible and does not require a definition of ideal aggregation levels. The proposed decision fusion approach that applies RF to the preclassification outperforms all other approaches. [J706]

## "An Investigation of Using the Spectral Characteristics From Ground Penetrating Radar for Landmine/Clutter Discrimination"

Ground penetrating radar (GPR)-based discrimination of landmines from clutter is known to be challenging due to the wide variability of possible clutter (e.g., rocks, roots, and general soil heterogeneity). This paper discusses the use of GPR frequency-domain spectral features to improve the detection of weak-scattering plastic mines and to reduce the number of false alarms resulting from clutter. The motivation for this approach comes from the fact that landmine targets and clutter objects often have different shapes and/or composition, yielding different energy density spectrum (EDS) that may be exploited for their discrimination (this information is also present in time-domain data, but in the frequency domain we can remove a phase if desired and can reveal better spatial characteristics and therefore often achieve greater robustness). This paper first applies the finite-difference time-domain (FDTD) modeling technique to establish the theoretical foundation. The method to generate EDS from GPR measurements is then described. The consistency of the frequency-domain features is examined through two different GPRs that have different spatial sampling rates and frequency bandwidths. Experimental results from several test sites, based on GPR data collected over buried mines and emplaced buried clutter objects, corroborate the theoretical development and the effectiveness of the proposed spectral feature to increase the accuracy of landmine detection and discrimination. [J707]

## "Calibration and Validation of DMSP SSMIS Lower Atmospheric Sounding Channels"

The Special Sensor Microwave Imager Sounder (SSMIS), a new type of conically scanning microwave sounder, was launched by the Defense Meteorological Satellite Program in October 2003. Performance of the instrument and retrieval software was characterized in an extensive calibration/validation campaign. This paper describes results based on comparisons between SSMIS Lower Atmospheric Sounding (LAS) channel measurements and radiative transfer calculations based on conventional synoptic radiosondes, numerical weather prediction models, and special observations campaigns including dedicated lidar measurements and scientific radiosonde and dropsonde measurements. Retrieved lower atmospheric profiles were also directly compared with these data sources. Two significant sources of bias were identified. The emissivity of the primary reflector contributes to measured brightness temperatures, and the warm load calibration source is susceptible to uncompensated solar heating. Otherwise, it was determined that LAS channels are locally stable and accurately track atmospheric changes. Polarization of some channels was found to differ from the design. Several approaches were identified to mitigate sources of bias. [J708]

## "Urban Mapping Using Coarse SAR and Optical Data: Outcome of the 2007 GRSS Data Fusion Contest"

The 2007 data fusion contest that was organized by the IEEE Geoscience and Remote Sensing Data Fusion Technical Committee was dealing with the extraction of a land use/land cover maps in and around an urban area, exploiting multitemporal and multisource coarse-resolution data sets. In particular, synthetic aperture radar and optical data from satellite sensors were considered. Excellent indicators for mapping accuracy were obtained by the top teams. The best algorithm is based on a neural classification enhanced by preprocessing and postprocessing steps. [J709]

## "Extinction Behavior of Soil at 26.5 to 110 GHz"

Soil electromagnetic properties at the microwave frequencies have been extensively documented in the literature. However, similar information at the higher millimeter frequencies is not available. A laboratory experiment was conducted to investigate the extinction behavior of wet and dry soil at millimeter wavelengths (26.5-110 GHz). For dry soil, the extinction coefficient increased from 0.02 to 0.6 cm-1as the frequency increased from 26.5 to 110 GHz. The presence of even a small amount of water in the soil (5% by weight) reduced the penetration of millimeter wave signals into soil by a factor of ten. [J710]

## "Estimation of Radial Velocity of Moving Targets by Along-Track Interferometric SAR Systems"

Along-track interferometric synthetic aperture radar (AT-InSAR) can be used to estimate the radial velocity of ground moving targets, starting from interferometric phase measures. The estimation obtained from a single-phase interferogram suffers from ambiguities. To solve these problems, multichannel AT-InSAR systems are required. In this letter, we analyze the radial velocity maximum-likelihood estimation accuracy with respect to AT-InSAR system parameters, such as velocity values and different clutter and thermal noise levels. We consider two different models for the target response: a deterministic model and a zero-mean Gaussian model. The presented results show that AT-InSAR systems exhibit better estimation accuracies for low-velocity values (slow targets). [J711]

## "Fusion of Hyperspectral and LIDAR Remote Sensing Data for Classification of Complex Forest Areas"

In this paper, we propose an analysis on the joint effect of hyperspectral and light detection and ranging (LIDAR) data for the classification of complex forest areas. In greater detail, we present: 1) an advanced system for the joint use of hyperspectral and LIDAR data in complex classification problems; 2) an investigation on the effectiveness of the very promising support vector machines (SVMs) and Gaussian maximum likelihood with leave-one-out-covariance algorithm classifiers for the analysis of complex forest scenarios characterized from a high number of species in a multisource framework; and 3) an analysis on the effectiveness of different LIDAR returns and channels (elevation and intensity) for increasing the classification accuracy obtained with hyperspectral images, particularly in relation to the discrimination of very similar classes. Several experiments carried out on a complex forest area in Italy provide interesting conclusions on the effectiveness and potentialities of the joint use of hyperspectral and LIDAR data and on the accuracy of the different classification techniques analyzed in the proposed system. In particular, the elevation channel of the first LIDAR return was very effective for the separation of species with similar spectral signatures but different mean heights, and the SVM classifier proved to be very robust and accurate in the exploitation of the considered multisource data. [J712]

## "A New Algorithm for Wind-Vector Retrieval From Scatterometers"

A new efficient algorithm for retrieving wind-vector solutions from scatterometers is developed based on a criterion of minimum normalized standard deviation (NSD) of wind speed derived from backscatter measurements using a geophysical model function (GMF). Its performance has been evaluated through simulations using QSCAT-1 GMF and the QuikSCAT observational geometry. The present algorithm, named the NSD algorithm, is found to be computationally more efficient (two to three times) besides being at par with the maximum-likelihood estimator (MLE) algorithm in terms of retrieval skill, retrieval errors, and distribution of solutions, on the basis of simulations as well as comparison of limited QuikSCAT-data-derived winds with National Centers for Environmental Prediction and European Centre for Medium-Range Weather Forecasts model winds. Simulation results and analysis of sample QuikSCAT data are presented. [J713]

## "A New Look at the Bistatic-to-Monostatic Conversion for Tandem SAR Image Formation"

The bistatic synthetic aperture radar (SAR) data, which are converted into equivalent monostatic data by proper preprocessing, can be processed by standard monostatic focusing algorithms. The dip moveout (DMO) approach, which is derived from seismic data processing, converts the bistatic data into equivalent monostatic data by a short time-domain Rocca's smile operator. A 2D exact point-target (PT) reference spectrum is derived in this letter for the tandem bistatic configuration. The geometry-based bistatic formulation is shown to be actually equivalent to Rocca's smile operator, although they are derived from the pure SAR and geophysics points of view, respectively. Moreover, the new PT spectrum can be extended to deal with azimuth-invariant bistatic SAR data. Interpretations on the equivalent monostatic range wavenumber are presented in this letter, which help understand the conversion from the radar signal processing viewpoint. [J714]

## "How Does Multiple Scattering Affect the Spaceborne W-Band Radar Measurements at Ranges

## Close to and Crossing the Sea-Surface Range?"

A radar simulator capable of treating multiple-breakscattering effects has been upgraded to include the interaction with a Kirchoff surface, which realistically reproduces the effect of water surfaces. Multiple-scattering effects explain in a straightforward way some peculiar features of the first images delivered by the 94-GHz cloud-profiling radar onboard the CloudSat, overpassing precipitating systems. The reflectivity profiles without the usual peaks at surface range are found to be distinctive signatures of strong multiple scattering. Moreover, multiple scattering is responsible for producing long signal tails at apparent ranges far below the surface with a strong sensitivity on the microphysical assumptions of the icy segment of the cloud. The estimates of multiple-scattering enhancement at surface and close to the surface range and the saturation levels for simplified precipitating profiles for both CloudSat and EarthCARE configurations are provided. [J715]

## "Analysis of Ground-Based SAR Data With Diverse Temporal Baselines"

In this paper, the algorithms developed for satellite synthetic aperture radar (SAR) interferometry were adapted to the ground-based SAR (GB-SAR) configuration and used for detecting the displacements of an alpine landslide which have occurred over many years. Indeed GB-SAR interferometry is based on the same principles as satellite SAR techniques but benefits from the GB-SAR's versatility and capability of gathering many images per day. In monitoring applications of landslides moving only few centimeters per year, as the case here reported, the GB-SAR sensor is installed at repeated intervals several months apart over the observation period. Although the revisiting time is very similar to the satellite one, for each survey, lasting two or three days, more than ten images are available. They are analyzed separately and in combination with images from other surveys for coherent pixel selection. Interferograms are formed by cross-combining images from different surveys. Finally, the evolution of the deformation across the surveys is retrieved in a least square sense without any assumptions on its regularity. The used GB-SAR technique is described in detail in this paper, and the results obtained with regard to a landslide in the Italian Alps that has been monitored over a period of about three years are discussed. [J716]

## "Refocusing Through Building Walls Using Synthetic Aperture Radar"

Through-wall imaging/sensing using a synthetic aperture array technique is studied by employing ultrawideband antennas and for wide incidence angles. The propagation through building walls, such as brick and poured concrete in response to point sources near the walls, is simulated by using high-frequency methods. Reciprocity is used to find the responses of point targets behind walls, which are then used to simulate the synthetic aperture radar (SAR) imaging through the walls. The effect of building walls on the target-image distortions is investigated by simulations and measurements. It is shown that by using the idea of match filtering, the effect of the wall can be compensated for, and the point target response can be reconstructed, provided that the wall parameters are known. An optimization method based on minimization of squared error in the SAR image domain within an area confined within the expected point-spread function is used to estimate the wall parameters and sharpen the image simultaneously. A controlled experiment within the laboratory environment is performed to verify the methods presented. It is shown that for an ultrawideband system operating over a frequency band of 1-3 GHz, highly distorted images of two point targets in close proximity of each other behind a wall can be resolved after refocusing. A dual-frequency synthetic method is also presented that can improve the cross-range resolution of the refocused image. [J717]

## "Retrieval of Snow and Rain From Combined X- and W-Band Airborne Radar Measurements"

Two independent airborne dual-wavelength techniques, based on nadir measurements of radar reflectivity factors and Doppler velocities, respectively, are investigated with respect to their capability of estimating microphysical properties of hydrometeors. The data used to investigate the methods are taken from the ER-2 Doppler radar (X-band) and cloud radar system (W-band) airborne Doppler radars during the Cirrus Regional Study of Tropical Anvils and Cirrus Layers-Florida Area Cirrus Experiment campaign in 2002. Validity is assessed by the degree to which the methods produce consistent retrievals of the microphysics. For deriving snow parameters, the reflectivity-based technique has a clear advantage over the Doppler-velocity-based approach because of the large dynamic range in the dual- frequency ratio (DFR) with respect to the median diameter D0and the fact that the difference in mean Doppler velocity at the two frequencies, i.e., the differential Doppler velocity (DDV), in snow is small relative to the measurement errors and is often not uniquely related to D0. The DFR and DDV can also be used to independently derive D0in rain. At W-band, the DFR-based algorithms are highly sensitive to attenuation from rain, cloud water, and water vapor. Thus, the retrieval algorithms depend on various assumptions regarding these components, whereas the DDV-based approach is unaffected by attenuation. In view of the difficulties and ambiguities associated with the attenuation correction at W-band, the DDV approach in rain is more straightforward and potentially more accurate than the DFR method. [J718]

## "Multisensor Data Product Fusion for Aerosol Research"

Combining data sets from multiple satellite sensors is a powerful method for studying Earth-atmosphere problems. By fusing data, we can utilize the strengths of the individual sensors that may not be otherwise possible. In this paper, we provide the framework for combining level 2 data products, using data from three sensors aboard the National Aeronautics and Space Administration (NASA)'s Terra satellite. These data include top-of-the-atmosphere (TOA) radiative energy fluxes obtained from the Clouds and the Earth's Radiant Energy System (CERES), aerosol optical thickness from the multispectral Moderate Resolution Imaging Spectroradiometer (MODIS), and aerosol properties from the Multi-angle Imaging SpectroRadiometer (MISR). The CERES Single Scanner Footprint (SSF) contains the pixel level CERES TOA fluxes and the level 2 MODIS aerosol data. We specifically focus upon fusing the CERES SSF with the MISR aerosol products. Although this project was undertaken specifically to address aerosol research, the methods employed for fusing data products can be used for other problems requiring synergistic data sets. We present selected case studies over different aerosol regimes and indicate that multisensor information provides value-added information for aerosol research that is not available from a single sensor. [J719]

## "Possibilistic Versus Belief Function Fusion for Antipersonnel Mine Detection"

Two approaches for combining humanitarian mine detection sensors are presented-one based on belief functions and the other one based on possibility theory. The approaches are described in parallel. First, different measures are extracted from the sensor data. Mass functions and possibility distributions are then derived from the measures based on prior information. After that, the combination of masses and the combination of possibility degrees are performed in two steps, on a separate sensor level and between the sensors. Combination operators are chosen to account for different characteristics of the sensors. The selection of the decision rules is discussed for both approaches. The proposed approaches are illustrated on a set of real mines and nondangerous objects, and promising results have been obtained. [J720]

## "Ground Moving Target Indication Using an InSAR System With a Hybrid Baseline"

In this letter, a two-channel airborne experimental interferometric synthetic aperture radar (InSAR) designed for terrain height estimation is exploited to acquire the ability of ground moving target indication (GMTI). Due to the hybrid baseline of this system, the interferometric phase changes with the target motion as well as the terrain height. The fluctuation of the interferometric phase worsens the performance of the clutter suppression and the radial velocity estimation. In order to resolve this problem, a GMTI method with three steps is proposed. After two steps are used to eliminate the local flat-Earth phase and the cross-track interferometric phase of the scene, respectively, an adaptive filtering method is used to suppress the stationary clutter with the benefit of calibrating the sensor responses. A conventional constant false alarm rate detector is then used to indicate the moving targets. The validity of the proposed method is demonstrated with real data collected using an experimental airborne InSAR system. [J721]

## "Fiber lasers: A future technology for lasers in space"

The constraints of operation in space have largely precluded the use of conventional solid-state laser systems for applications including remote sensing, communication relays, and active laser radars. A new technology, fiber lasers, may offer all of the needed features at an affordable price. An appealing aspect of the fiber laser is that it does not need a rigid optical bench. Only the output end of the fiber need be held in rigid reference to the optical tracking system. Design, fabrication, and testing of the laser resonator is generally the most expensive and longest lead part of the effort for conventional solid-state lasers. Advances in fiber optic technology and devices mean that the "fiber laser" need not be a simple device but may be a complex system employing sophisticated technology, such as wavelength selective Bragg reflectors and nonlinear optical frequency shifters. Three companies have obtained single-mode outputs of 35-40 watts single mode at 1.03-1.1 mu. [J722]

## "Interactive Dynamic Range Reduction for SAR Images"

The visualization of synthetic aperture radar (SAR) data involves the mapping from high dynamic range amplitude values to gray values of a lower dynamic range display device. This dynamic range reduction process controls the amount of information in the displayed result and is therefore an important part of each SAR visualization system. Interactive systems provide the user with immediate feedback on the changes of the reduction method and its parameters. In this letter, we examine different dynamic range reduction techniques known from the tone mapping of optical images. The techniques are analyzed, regarding their applicability to SAR data, and incorporated into our interactive visualization framework based on programmable graphics hardware. [J723]

## "Fisher Distribution for Texture Modeling of Polarimetric SAR Data"

The multilook polarimetric synthetic aperture radar (PolSAR) covariance matrix is generally modeled by a complex Wishart distribution. For textured areas, the product model is used, and the texture component is modeled by a Gamma distribution. In many cases, the assumption of Gamma-distributed texture is not appropriate. The Fisher distribution does not have this limitation and can represent a large set of texture distributions. As an example, we examine its advantage for an urban area. From a Fisher-distributed texture component, we derive the distribution of the complex covariance matrix for multilook PolSAR data. The obtained distribution is expressed in terms of the KummerU confluent hypergeometric function of the second kind. Those distributions are related to the Mellin transform and second-kind statistics (Log-statistics). The new KummerU-based distribution should provide in many cases a better representation of textured areas than the classic Kdistribution. Finally, we show that the new model can discriminate regions with different texture distribution in a segmentation experiment with synthetic textured PolSAR images. [J724]

## "A Bistatic Point Target Reference Spectrum for General Bistatic SAR Processing"

A bistatic point target reference spectrum (BPTRS) based on Loffeld's bistatic formula (LBF) is derived in this letter. For LBF, the same contributions of the transmitter and receiver to the total azimuth modulation are assumed. This assumption results in the failure of LBF in the extreme configuration (i.e., spaceborne/airborne configuration). For general bistatic configurations, the azimuth modulations are unequal for the transmitter and receiver due to the different slant ranges and velocities. Therefore, the azimuth time-bandwidth products (TBPs) from the transmitter and receiver are different; in some cases (e.g., spaceborne/airborne case), one of them might be very small, which might even result in a serious error of the principle of stationary phase. This letter uses TBP to weight the azimuth phase modulation contributions of the transmitter and receiver to the common azimuth spectrum to approximately obtain the point of stationary phase of the total azimuth phase history. Simulations show that the proposed BPTRS can work well for spaceborne/airborne configurations. [J725]

## "Validation of the Submetric Accuracy of Vertical Positioning of PSs in C-Band"

The permanent scatterers (PSs) technique is an operational tool in the context of spaceborne synthetic aperture radar interferometry for monitoring the displacement of radar targets with millimetric accuracy. Recently, the target localization capability of the PS technique has been subject of study, and the possibility of generating digital elevation models (DEMs) and digital terrain models (DTMs) by means of the height of a sparse set of points has been evaluated. In this letter, for the first time, the PS height estimate has been validated by exploiting about 250,000 spot heights at street level derived from photogrammetric techniques in the urban area around Milan, Italy. The very high correlation between the two independent measurements confirms the theoretical submetric accuracy of vertical positioning. A multitrack PS DTM has then been generated and compared to the spot heights together with the corresponding Shuttle Radar Topography Mission (SRTM) DEM, showing the very high improvement given by the PS technique to the freely available topographic data. The results have been obtained by processing about 300 European Space Agency (ESA) European Remote Sensing (ERS) satellite and Envisat images acquired from two descending tracks and an ascending one over Milan. [J726]

## "Least Squares-Based Filter for Remote SensingImage Noise Reduction"

The Vondrak filter is a unique technique for smoothing data. The filter aims to achieve a balance between the fidelity and the smoothness of the filtered results. It can therefore preserve the original attributes of the observational data while, at the same time, smooth out the noise. We reformulate the 1-D Vondrak filter that has been widely used in data processing in fields such as astronomy and geophysics and then extend it into two dimensions. The method of conjugate gradients is used to solve the least squares optimization problem. The proposed 2-D filter is a powerful tool for enhancing the quality of various geoscience and remote sensing data such as satellite images. Various tests with simulated and real synthetic aperture radar interferograms show that the new filter is very effective in removing the noise. [J727]

## "A New Approach for Simultaneous Range Measurement and Doppler Estimation"

To circumvent the dilemma of range and Doppler ambiguity in the conventional pulsed Doppler radars, a stepped time interval pulse train (STIPT) scheme is proposed in this letter. The STIPT approach eliminates range and Doppler ambiguities by setting the pulse interval difference appropriately. The range sidelobes are removed through a modified aperiodic correlation algorithm. Furthermore, the fast Fourier transform can be used in the Doppler processing. Consequently, the newly proposed approach can be applied to the conventional pulsed radar systems. [J728]

## "Limitations in the Hydrologic Applications of C-Band SRTM DEMs in Low-Relief Settings"

The shuttle radar topography mission (SRTM) data represent a major breakthrough in terms of providing accurate and consistent elevation data on a worldwide basis. These data are being used in many scientific applications, hydrology in particular. This letter examines the feasibility of using SRTM data for hydrologic characterizations, particularly in a region of low relief exemplified by the Otter Tail basin in Minnesota. The Version 2 SRTM data product provides a useful starting place for estimating the stage for larger lakes. Indications for Minnesota are that these estimates are accurate to several meters but are biased toward underestimation. Over land, the inherent noise in the data makes watershed boundary and stream network extraction problematic. We found large errors in estimated basin shape and area, and in the geometry of extracted stream networks, as compared to more traditional U.S. Geological Survey data products. [J729]

## "Spectral Clustering Ensemble Applied to SAR Image Segmentation"

Spectral clustering (SC) has been used with success in the field of computer vision for data clustering. In this paper, a new algorithm named SC ensemble (SCE) is proposed for the segmentation of synthetic aperture radar (SAR) images. The gray-level cooccurrence matrix-based statistic features and the energy features from the undecimated wavelet decomposition extracted for each pixel being the input, our algorithm performs segmentation by combining multiple SC results as opposed to using outcomes of a single clustering process in the existing literature. The random subspace, random scaling parameter, and Nystrom approximation for component SC are applied to construct the SCE. This technique provides necessary diversity as well as high quality of component learners for an efficient ensemble. It also overcomes the shortcomings faced by the SC, such as the selection of scaling parameter, and the instability resulted from the Nystrom approximation method in image segmentation. Experimental results show that the proposed method is effective for SAR image segmentation and insensitive to the scaling parameter. [J730]

## "A Two-Dimensional Spectrum Model for General Bistatic SAR"

This paper derives a 2-D spectrum model for general bistatic synthetic aperture radar (SAR). By introducing some new parameters such as equivalent monostatic parameters, bistatic factor, and weighted-equivalent range, the 2-D spectrum of general bistatic SAR can be expressed in the form of monostatic SAR even when the transmitter and receiver move along unparallel trajectories with different velocities. The result formulates bistatic SAR into an equivalent monostatic SAR model and would be useful for developing efficient bistatic SAR algorithms in frequency-domain or hybrid-domain processing. Simulation results are given to validate the performance of the model. For special bistatic SAR configurations, the model can be simplified. Compared to other similar models, the proposed model is clearer and much more concise. [J731]

## "Determination of Bathymetric and Current Maps by the Method DiSC Based on the Analysis of Nautical X-Band Radar Image Sequences of the Sea Surface (November 2007)"

Morphodynamic processes in coastal areas are affected by tidal currents and sea state. The continuous observation of near coastal areas is important in order to monitor dangerous current-regime and bathymetry changes. Therefore, there is an urgent need for remote sensing techniques delivering the important hydrographic parameters with a high spatial resolution. Dispersive surface classificator (DiSC) is a newly developed method based on the analysis of nautical X-band radar image sequences of sea surface waves to determine spatial maps of hydrographic parameters, e.g., spatial maps of the bathymetry and the ocean current field. The method DiSC is described and is illustrated by the presentation of results based on a dataset acquired with a ground-based X-band radar installation mounted on the Island of Sylt in the German Bight. The calculated bathymetric maps are verified by multibeam echo sounder observations. [J732]

## "Through-Wall Tracking of Human Movers Using Joint Doppler and Array Processing"

In this letter, a radar combining Doppler processing and spatial beamforming is presented for tracking humans through walls. Multiple targets are tracked by resolving the targets in the Doppler and bearing space. To overcome the high sidelobes associated with an array of limited size, the CLEAN and RELAX algorithms are implemented, and their performances are compared with standard beamforming. The radar is tested in indoor line-of-sight and through-wall scenarios for multiple loudspeakers and human subjects. [J733]

## "Radar Revisited (review of "Radar Handbook, 3rd ed." by Merrill Skolnik) [JBook Reviews]"

This is the third edition of an established handbook, edited by one of the most-recognized names in the field of radar technology. The volume is a compilation of 26 chapters, authored by individuals with a thorough command of, and incredible credentials in, the topics of their chapters. Most chapters have a large number of figures (up to

several dozen) and extensive bibliographies. Chapters range from fairly quantitative and mathematical ones to cursory and descriptive ones. Some sections of the handbook represent a concise and readable summary of the state-of-the-art of knowledge on their topics; others are a sketchy collection of remarks for which it is difficult to identify the benefits to be derived by the reader. There is little coordination between chapters where similar topics may be discussed, and a lack of any cross-referencing. There are also weaknesses in the index, as well. While the older, classical radar topics receive much attention, the book overlooks newer areas such as coverage of automotive radars. This volume will appeal to the generalists with interest in the conventional radar subjects, and to others as a starting point for locating sources with more detailed information. [J734]

## "Potential Effects of the Ionosphere on Space-Based SAR Imaging"

There has been a considerable interest in the use of lower frequency (VHF/UHF) space-based synthetic aperture radar (SAR) for realizing the foliage and ground penetration. The phase perturbation, signal distortion and imaging resolution degradation by the ionosphere will be particularly severe, however the model is not yet well established and still needs to be further studied. In this paper, on the basis of possible improvements for the model proposed by Ishimaru and others, potential ionospheric effects on SAR imaging are evaluated. First, for analyzing azimuthal resolution, we apply the fourth moment recently obtained in general case of strong fluctuation regimes, which is expected to give results for wider conditions. The Gaussian approximation was used in the previous model; however it is only valid in the fully saturated regimes. Second, for analyzing image shift and distortion, besides group delay, the higher-order dispersion is considered. Third, for discussing range resolution degraded due to pulse broadening, besides the dispersion, the multiple scattering of ionospheric turbulence is studied. Fourth, the Faraday rotation effect is analyzed. Numerical simulations are shown using ionospheric turbulence spectrum and TEC inferred from the International Reference Ionosphere (IRI) and satellite beacon observations. [J735]

## "Squint Spotlight SAR Raw Signal Simulation in the Frequency Domain Using Optical Principles"

Synthetic aperture radar (SAR) distributed target scene raw signal simulation is an important tool for the study and test of SAR systems and processing algorithms, mission planning, and inversion algorithm design. In this paper, the squint spotlight SAR scene model is evaluated to achieve spotlight SAR raw signals in the 2-D frequency domain and the precision of the model is analyzed. It is known that the range migration phenomenon in the time domain is explained as the coupling between the range and azimuth in the 2-D frequency domain. To realize the coupling relation in the 2-D frequency, interpolation may be needed. However, interpolation is a time-consuming manipulation. For efficiency, some signal processing methods are employed to couple the range and azimuth frequencies. Those tricks are derived from some optical principles, which give us some novel thoughts. Therefore, the efficiency of the simulator is highly improved, which facilitates its application to the verification and test of the real-time processor. [J736]

## "Sea Ice Deformation State From Synthetic Aperture Radar Imagery-Part II: Effects of Spatial Resolution and Noise Level"

C- and L-band airborne synthetic aperture radar (SAR) imagery acquired at like- and cross-polarizations over sea ice under winter conditions is examined with the objective to study the discrimination between level ice and ice deformation features. High-resolution low-noise data were analyzed in the first paper. In this second paper, the main topics are the effects of spatial resolution and signal-to-noise ratio. Airborne high-resolution SAR scenes are used to generate a sequence of images with increasingly coarser spatial resolution from 5 to 25 m, keeping the number of looks constant. The signal-to-noise ratio is varied between typical noise levels for airborne imagery and satellite data. Areal fraction of deformed ice and average deformation distance are determined for each image product. At L-band, the retrieved values of the areal fraction get larger as the image resolution is degraded. The areal fraction at C-band remains constant. The retrieved average distance between deformation features increases both at C- and L-bands as the image resolution gets coarser. The influence of noise becomes noticeable if its level is equal or larger than the average intensity backscattered from the level ice. The retrieval of deformation parameters using simulated images that resemble ERS-2 SAR, Envisat ASAR, and ALOS PALSAR data products is discussed. Basic differences between real and simulated ERS-2 SAR images are analyzed. [J737]

## "Spatial and Temporal Scaling Behavior of Surface Shortwave Downward Radiation Based on MODIS and In Situ Measurements"

In this letter, a new Moderate Resolution Imaging Spectroradiometer (MODIS)-based 5-km surface shortwave downward (SWD) radiation data set is used to examine the spatial scaling behavior of the surface radiative fluxes. In situ measurements of SWD radiation at time scales from 5 to 55 min from the Oklahoma MesoNet and

the Baseline Surface Radiation Network sites over the U.S. are employed to examine the temporal scaling behavior of surface downward radiation and to evaluate the estimates based on MODIS observations from both Terra and Aqua platforms. Analysis reveals that the surface SWD radiation derived from MODIS Terra is in better agreement with ground observations than those from MODIS Aqua. Spatial scaling behavior is investigated based on the MODIS-derived SWD radiation at scales varying from 5 to 100 km. The root mean square difference and the mean standard deviation are found to be highly correlated with the scale exhibiting a strong log-linear relationship. This is a first study on the scaling behavior for surface SWD. Such information is expected to provide linkage between different satellite-based radiation data sets including those derived from geostationary satellites usually of coarser spatial resolutions. [J738]

## "An Omega-K Algorithm With Phase Error Compensation for Bistatic SAR of a Translational Invariant Case"

This paper first shows the 3D property of bistatic synthetic aperture radar (BiSAR) geometry, which clarifies that the algorithms for bistatic SAR should be deduced in 3D space. It then models the bistatic echo according to the 3D geometry and obtains the signal spectrum in the wavenumber domain. Based on the spectrum, the formula for the wavenumber-domain interpolation of the omega-K algorithm is deduced, and the residual phase is obtained. Then, the impacts of the residual phase, including position displacement, range, and azimuth defocusing, and a constant phase for each pixel, are explicated. Finally, the simulating results exhibited at the end of this paper validate the correctness of the analysis and the feasibility of the algorithm. [J739]

## "Characteristics of TRMM/PR System Noise and Their Application to the Rain Detection Algorithm"

This study investigates the characteristics of system noise sampled by the Precipitation Radar (PR) onboard the Tropical Rainfall Measuring Mission satellite. First, we examine the long-term trend in system noise. The result shows that the system noise level was quite stable for a long time period except for a few sudden change events. The averaged system noise shows a periodic change that relates to the temperature of the PR. This change corresponds to the changes in the solar beta angle, and the amplitude of the fluctuation is about 0.15 dB. The contribution of surface emission from the ocean to the system noise is also examined by averaging the system noise data under a no-rain condition over a long period (e.g., one month) to remove the effect of the temperature fluctuation related to the solar beta angle. The resulting amplitude is less than 0.1 dB, and the spatial distribution almost corresponds to the pattern of the sea surface temperature. These results confirm that the system noise of the PR is quite stable, indicating that the fluctuation of the sampled system noise is caused mainly by the fading effect. The characteristics of the system noise of three rain categories-ldquorain certain,rdquo ldquorain possible,rdquo and ldquono-rainrdquo-are examined by taking a histogram. Because the PRpsilas system noise is supposed to be stable, broadening the system noise level of about 2.5 dB almost corresponds to the fading effect. The histograms of rain-certain and of no-rain show a similar shape with a difference of a few tenths of decibels. The higher noise levels in rain-certain conditions are caused by the emission from raindrops. In contrast, the rain-possible histogram shows a widespread and skewed shape. It can be explained by saying that the rain-possible pixels are obtained when the sampled noise level is made accidentally small by the fading effect. Therefore, a fixed noise level threshold is introduced to the rain/no-rain classification for a more rel--iable rain-possible classification. The result shows that the rain area increases by about 15%, and the amount of rainfall increases by about 1% by adding reliable rain-possible pixels to the current standard product. [J740]

## "Quantifying Bird Migration by a High-Resolution Weather Radar"

We propose a bird detection and count algorithm designed to work with radar maps of plan-position-indicator type. The spatial arrangement of birds is modeled according to the Poisson distribution. It is possible to handle a nonuniform target distribution both on the vertical and horizontal planes. The method is applied to measurements carried out by an S-band Doppler weather radar located on the south side of the Alps. Quantitative estimates are given for the distribution of bird volume density with height, the cumulative density (integrated over height), and, finally, the daily migration traffic rate of nocturnal migrants over an area of about 2000 km2. [J741]

## "Phase-Offset Estimation in Multichannel SAR Interferometry"

Multichannel interferometric synthetic aperture radar (InSAR) systems allow the estimation of the height profile of the Earth's surface, exploiting the availability of multiple radar acquisitions, obtained via different baselines/frequencies. Statistical approaches, in particular maximum aposterioritechnique and Markov random-field image models, can be exploited for such estimation problem, which proved to be effective. However, despite the particular solution method used, the problem with multichannel interferometry is that interferograms can be affected from the presence of undetermined phase offsets, which makes it difficult to get correct height

estimation in any case. In this letter, we present a procedure to estimate these phase offsets using statistical estimation; we test the procedure on both simulated and real data. For the latter, we show how an optimal estimation of the phase offsets can be used to improve the resolution of an available Shuttle Radar Topography Mission digital elevation model. The obtained results prove the effectiveness of the method and assess the overall quality of the height estimation procedure. [J742]

## "The Pyramids of Gizeh Seen by TerraSAR-X-A Prime Example for Unexpected Scattering Mechanisms in SAR"

Multiple scattering may render synthetic aperture radar (SAR) image interpretation difficult, particularly when it comes to imaging of man-made structures. In medium-resolution SAR images, contributions from different scattering mechanisms can only be distinguished for large objects and under favorable conditions, like bridges over calm water. Since the launches of TerraSAR-X and COSMO-SkyMed, high-resolution SAR imagery is readily available from every spot on the Earth, and multiple scattering image features will be increasingly found in many of these data. Some of the first TerraSAR-X images show the pyramids of Gizeh in a seemingly unexpected geometry. Instead of being geometrically distorted, the near-range faces of the pyramids look like ground projected. This letter explains this image puzzle by a mixture of two scattering effects. The theory is confirmed by an interferometric evaluation. The discussed image artifact can be seen as representative for many other multiple-scattering SAR imaging scenarios in high-resolution images. This letter also demonstrates once again that the interpretation of complex scattering configurations benefits from interferometric information. [J743]

## "SBAS-DInSAR Analysis of Very Extended Areas: First Results on a 60 000- Test Site"

We present the results of the first experiment to survey the temporal evolution of the deformation affecting very large areas using the small baseline subset (SBAS) differential synthetic aperture radar interferometry (DInSAR) algorithm. In particular, we have analyzed a set of 264 descending European Remote Sensing (ERS) SAR data frames from 1992 to 2000; these data are relevant to an area in central Nevada (U.S.) that extends for about 600times100 km. The starting point of our study has been the generation of an appropriate set of small baseline multilook interferograms computed from long SAR image strips, which were obtained by jointly focusing six contiguous raw data frames. Following their generation, the selected interferograms, which are computed on a spatial grid of 160times160 m, have been inverted via the SBAS technique to retrieve, for each coherent pixel, the displacement time series and the corresponding mean deformation velocity. The presented results are, to our knowledge, the first ones with such an extended multitemporal SAR data set, and they demonstrate the effectiveness of the approach to analyze the deformation of the investigated zone. [J744]

## "Physical Optics Curved-Boundary Dielectric Plate Scattering Formulas for an Accurate and Efficient Electromagnetic Characterization of a Class of Natural Targets"

Closed-form representations of the physical optics (PO) field scattered in the far zone by plane penetrable dielectric angular sectors of arbitrary opening angle featuring a conical-section boundary are derived in terms of incomplete cylindrical functions (ICFs). The proposed expressions, possibly in combination with PO formulas for the scattering from polygonal plates, allow one to evaluate the scattering from flat dielectric plates with both convex and concave curved edges in a very efficient manner and constitute a useful tool to improve the accuracy of the geometrical characterization of a class of natural scatterers. In order to check the correctness and computational effectiveness of the proposed scattered-field solutions, comparisons with results obtained by accurate completely numerical PO calculations are provided. Simulation data by the method of moments are also presented to assess the applicability of the PO approximation to the considered sample scattering geometries. [J745]

## "Traffic Surveillance System Based on a High-Resolution Radar"

Traffic surveillance is an important civilian application of radars. The current high-resolution radars give new opportunities so that the traffic application may be redefined. In this paper, a traffic scenario with a high-resolution radar is presented. A range-bin alignment method, the Global Range Alignment, which comes from the focusing techniques in inverse synthetic aperture radar, is applied to obtain further capabilities than the usual velocity measurement: distinction between vehicle types via length estimation and adequate management in situations with simultaneous targets. Preliminary results from a real scenario using a high-resolution linear frequency-modulated continuous-wave millimeter-wave radar are shown. [J746]

## "Three-Dimensional ISAR Imaging Using a Two-Dimensional Sparse Antenna Array"

Conventional antenna array 3-D inverse synthetic aperture radar (ISAR) imaging method does imaging by first

carrying out ISAR imaging for all the different antennas and then using array direction of arrival (DOA) estimation on every scatterer to get the position of that scatterer. The aperture formed by the target's motion is used to separate the scatterers, and the antenna array aperture is used for position measurement. In this letter, a 3-D imaging method based on a combination of sparse array beamforming and ISAR imaging is proposed, where 3-D images are formed by space-time match filtering. The estimation of the target's rotation parameters is also given. Simulation results have shown the effectiveness of the proposed methods. [J747]

## "Improvement of Image Segmentation Accuracy Based on Multiscale Optimization Procedure"

This letter proposes an optimization approach that enhances the quality of image segmentation using the software Definiens Developer. The procedure aims at the minimization of over- and undersegmentations in order to attain more accurate segmentation results. The optimization iteratively combines a sequence of multiscale segmentation, feature-based classification, and classification-based object refinement. The developed method has been applied to various remotely sensed data and is compared to the results achieved with the established segmentation procedures provided by the Definiens Developer software. The quantitative assessment of segmentation accuracy based on reference objects is derived from an aerial image, and a high-resolution synthetic aperture radar scene shows an improvement of 20%-40% in object accuracy by applying the proposed procedure. [J748]

## "Classification of Ground Clutter and Anomalous Propagation Using Dual-Polarization Weather Radar"

This paper presents the results of a study designed to classify weather radar clutter echoes obtained from ground-based dual-polarization weather radar systems. The clutter signals are due to ground clutter, sea clutter, and anomalous propagation echoes, which represent sources of error in quantitative radar rainfall estimation. Fuzzy and Bayes classifiers are evaluated as an alternative approach to traditional polarimetric-based methods. Both systems were trained and validated by using C-band dual- polarization radar measurements, and a novel technique is proposed to calculate the texture function to mitigate against the edge effects at the boundaries of precipitation regions. A methodology is presented to extract the membership functions and conditional probability density functions to train the classifiers. The critical success index indicates that the Bayes classifier has, on average, a slightly better performance than the fuzzy classifiers. However, when optimal weighting was applied, the fuzzy classifier gave one of the best performances. The classifiers are sufficiently robust to be used when only single-polarization radar measurements are available. [J749]

## "Distributed sensing based on intelligent sensor networks"

Network centric approach to complex systems has been attracting a lot of attention in the recent past. With specific applications in space, military and other information enterprises, such an approach is capable of yielding autonomy at the system level. This article describes a distributed approach to information processing in sensor networks. The network architecture entails a hierarchy of capabilities, information and control, where nodes in the network are thoroughly or partially autonomous. The network also consists of slave nodes dedicated to sensing and gathering information. Individual nodes are expected to possess resources for networking and computing and presume autonomy through multi functional modules for sensory processing and situation assessment. Data association, registration and fusion are formulated into a joint process, and an expectation maximization (EM) approach is developed to solve the three problems simultaneously. A fuzzy cognitive map (FCM) is proposed to perform situation assessment, while a genetic algorithm (GA) is applied for learning, to identify an optimal structure. The distributed architecture is applied to coastal surveillance with simulations on the west coast of Canada. [J750]

## "Phase-Based Clutter Identification in Spectra of Weather Radar Signals"

A novel method for suppression of ground clutter (GC) in weather radar is presented. The novel identification scheme is entirely phase based, unlike power-based schemes that are generally used. GC contributions to the Doppler spectrum are identified from the differential phase between complex spectral coefficients of two spectra estimated for odd- and even-indexed half-sequences of the original time series. Phase values near zero are used as indicators of clutter contributions for Doppler bins close to zero velocity. Indicated Doppler bins are notched from the original spectrum, and the moments are then obtained. The identification scheme is motivated by spectra of an electronically steered phased array of the National Weather Radar Testbed (NWRT) and requires a sufficient number of pulses/samples for spectral analyses. However, the method can be used with a mechanically steered antenna with an appropriate adjustment compensating smearing due to antenna rotation. The method was tested on several NWRT data sets obtained in clear air and in precipitation. One example of clutter-filtered power in precipitation is shown here. There is no baseline for comparison, as the NWRT does not

have clutter filtering at the present time. Nonetheless, for a comparison of power- and phase-based identification schemes, a power-based clutter filter similar to the one used by the National Weather Service on the network of mechanically steerable Weather Surveillance Doppler radars WSR-88Ds is implemented on NWRT and used as a preliminary baseline for comparison. [J751]

## "Focusing Azimuth-Invariant Bistatic SAR Data With Chirp Scaling"

This letter presents a bistatic chirp scaling algorithm to processing the azimuth-invariant bistatic synthetic aperture radar data. Two methods are used to derive the different parts of the range-Doppler expression of the point target. Compared with the method relying on the two-order expansion of the bistatic range model, the new algorithm can give the close-form azimuth modulation. Through the introduction of the fractional Fourier transform into the range processing, the resolutions are enhanced further. [J752]

## "Effect of Salinity on the Dielectric Properties of Geological Materials: Implication for Soil Moisture Detection by Means of Radar Remote Sensing"

We consider the exploitation of dielectric properties of saline deposits for the detection and mapping of moisture in arid regions on both Earth and Mars. We present simulated and experimental study in order to assess the effect of salinity on the complex permittivity of geological materials and, therefore, on the radar backscattering coefficient in the [1-7 GHz] frequency range. Laboratory measurements are performed on sand/sodium chloride aqueous mixtures using a vectorial network analyzer coupled to an open-ended coaxial dielectric probe. We aim at calibrating and validating semiempirical dielectric mixing models. In particular, we evaluated the dependence of the real and imaginary parts of complex permittivity on the microwave frequency, water content, and salinity. Our results confirm that if the real part is mainly affected by the moisture content, the imaginary part is more sensitive to salinity. In addition to the classic formulas of mixing models, the ionic-conductivity losses, which are due to mobile ions in the saline solution, are taken into account in order to better assess the effect of salinity on the dielectric properties of mixtures. Dielectric mixing models are then used as input parameters for the simulation of the radar backscattering coefficients by means of an analytical model: the integral equation model. Simulation results show that salinity should have a significant impact on the radar backscattering recorded in synthetic aperture radar data in terms of the magnitude of the backscattering coefficient. Moreover, our results suggest that VV polarization provides a greater sensitivity to salinity than HH polarization. [J753]

## "Radar Handbook, 3rd Edition (M.I. Skolnik, Ed; 2008) [JBook Review]"

Thirty eight radar experts contribute to this edition, which includes six completely new chapters on the following topics: ground penetrating radar; remote sensing with radar on satellites; multifunctional radar systems for fighter aircraft (MFAR); digital signal processing for radar; civil marine radar; and propagation. Each chapter contains references, ranging from 10 to 197, with a median of 71. The index runs 18 pages printed in double columns, but is not necessarily complete. Some topics, such as MIMO radar and long range radars to track satellites and ballistic missiles, will have to wait for a 4th edition. This text is the most authoritative, broadest, and deepest single volume on radar. The emphasis is on real world performance and real hardware that has been tested and works successfully in the real world, and the physics relevant to radar systems, as well as radar system engineering cost tradeoffs. [J754]

## "Interference Cancellation for High-Frequency Surface Wave Radar"

The performance of high-frequency surface wave radar (HFSWR) is known to suffer from external environmental interference and noise, such as cochannel radio-frequency interference from other radiating source, ionospheric clutter, lightning impulsive noise, etc. This paper experimentally evaluates the interference cancellation performance of various adaptive beamforming schemes with respect to the aforementioned three types of interferences in an attempt to find the most promising adaptive cancellation scheme in practical HFSWR environment. [J755]

## "Potential for Surface Parameter Estimation Using Compact Polarimetric SAR"

The retrieval of soil surface parameters using a dual-polarization synthetic aperture radar operating in a compact polarimetric mode is examined. It is shown that by employing a two-component model of surface polarimetric coherency, soil surface parameter retrieval is possible directly from measurements without the need for any additional assumptions. Model surface parameters inverted by using the full polarimetric coherency matrix may be recovered equally well from a compact polarimetric coherency matrix. [J756]

## "Response to “Corrections to ‘Calibration of Linearly Polarized Polarimetric SAR Data Subject to

## Faraday Rotation'" [Jorig. paper Aug 04 1617-1624]"

Provides a response to the corrections submitted (vol. 46, no. 4, p. 1278, Apr 08) to the original article. [J757]

## "A Method for Soil Moisture Estimation in Western Africa Based on the ERS Scatterometer"

The analysis of feedback phenomena, which occur between continental surfaces and the atmosphere, is one of the keys to an improved understanding of African monsoon dynamics. For this reason, the monitoring of surface parameters, particularly soil moisture, is very important. This paper presents a new methodology for the estimation of surface soil moisture over Western Africa based on the data provided by the European Remote Sensing wind scatterometer instrument, in which an empirical model is used to estimate volumetric soil moisture. This approach takes into account the effects of vegetation and soil roughness in the soil moisture estimation process. The proposed estimations have been validated using different methods, and a good degree of coherence has been observed between satellite estimations and ground truth measurements over the Banizambou site in Niger. Moisture and rainfall estimations for the same site are shown to be strongly correlated. Comparison with the multimodel analysis product provided by the Global Soil Wetness Project, Phase 2, indicates that their estimations are well correlated, although land surface models provide slightly overestimated levels of soil moisture. [J758]

## "Soil Moisture Retrieval From Remotely Sensed Data: Neural Network Approach Versus Bayesian Method"

Neural network (NN) approaches and statistical methods, based on a Bayesian procedure, are applied and compared in soil moisture (SM) retrieval from remotely sensed data. The principles and the practical implementations of Bayesian procedures and NNs are briefly discussed in terms of the advantages and disadvantages of each. Experimental tests are carried out by using the same set of training and test data for each method. The methodologies have been applied to two sets of data to retrieve SM from bare soils and to verify their accuracy. One data set contains scatterometer and radiometer data acquired on a variety of agricultural fields in different polarizations, frequencies, and incidence angles. The other is made up of five experiments carried out with a C-band scatterometer on rough and smooth soils at different polarizations and incidence angles. There are significant similarities in the performance of each method; they both retrieve the same features and trends in the analyzed data sets. Algorithm performances change according to SM level and data configuration. The main difficulties are found in retrieving low SM values, and in this case, the error on estimates is reduced when the data with two polarizations or two incidence angles are inserted in the inversion procedure. One major difference between the methodologies is that the NN performance improves, with respect to the Bayesian method, when more inputs are presented as two polarizations or two incidence angles in the training phase. [J759]

## "Modeling of the Bistatic Electromagnetic Scattering From Sea Surfaces Covered in Oil for Microwave Applications"

This paper describes the influence of oil pollution over sea surfaces on the height spectrum and the height autocorrelation function of rough surfaces. An oil slick damps the capillarity waves of the surface height spectrum and reduces the root mean square slope of the surface. These modified functions then have an influence on the radar cross section (RCS) from contaminated sea surfaces. The bistatic RCS of the contaminated sea surface is then presented by comparison with a clean sea: results from a benchmark numerical model are presented and compared with a new semiempirical model using the geometric optics approximation and then the first-order smallslope approximation. [J760]

## "Three-Dimensional ISAR Imaging Based on Antenna Array"

In this paper, a 3D inverse synthetic aperture radar (ISAR) imaging method based on an antenna array configuration is proposed. The performance of conventional interferometric ISAR imaging system using three antennas is poor, as the positions of scatterers, which have the same range-Doppler value and projected onto the ISAR plane as a synthesis scatterer, cannot be correctly estimated. However, by using two antenna arrays perpendicular to each other, the system's ability to separate these scatterers can be improved. The criterion for the selection of a range unit that contains an isolated scatterer in the 2-D array domain for doing motion compensation is discussed. If there is no range unit which contains only an isolated scatterer, then radial and cross-range motion compensation has to be carried out by motion parameter estimation. Two cross-range motion parameters measurement algorithms, one based on array processing of the range profile and another based on correlation of ISAR images of different antennas, are proposed. The coordinates registration problem for the scatterers of a synthesis scatterer is also discussed. Simulation results have shown the effectiveness of the proposed methods. [J761]

## "Processing of Azimuth-Invariant Bistatic SAR Data Using the Range Doppler Algorithm"

This paper discusses bistatic synthetic aperture radar processing (complex image formation) using the Range Doppler Algorithm. The key step is to use an analytical form of the signal spectrum derived by the method of series reversion. The spectrum is used for secondary range compression (SRC), range cell migration correction, and azimuth compression. The algorithm is able to focus the azimuth-invariant bistatic configuration where the transmitter and receiver platforms are moving in parallel tracks with identical velocities. Moreover, the algorithm is able to handle reasonably high squints and wide apertures because SRC can be performed in the 2-D frequency domain. [J762]

## "Phase Unwrapping for SAR Interferometry-A Data Fusion Approach by Kalman Filtering"

This paper considers the problem of unwrapping the phase image obtained from a noisy interferometric synthetic aperture radar (InSAR) image. The implicit nonlinearity of the problem is reflected, as well as the drawbacks of this nonlinearity on the performance of phase unwrapping approaches. Some general concepts concerning basic estimation techniques are shortly reviewed. On this background, a Kalman filter-based data fusion approach to unwrap and simultaneously filter the phases of InSAR images is developed. The data fusion concept exploits phase information extracted from the complex interferogram rather than from the phase image and fuses that information with phase slope information extracted from the power spectral density of the interferogram. [J763]

## "Using C-Band Synthetic Aperture Radar Data to Monitor Forested Wetland Hydrology in Maryland's Coastal Plain, USA"

Hydrology (i.e., inundation and soil moisture) is the most important abiotic factor controlling wetland function and extent, and scientists predict that wetland hydrology can be significantly altered over relatively short timescales due to climate change and anthropogenic impact. Whereas broadscale hydrology is difficult to monitor in forested wetlands with ground-based and optical remote sensing methods, C-band synthetic aperture radar (SAR) systems have the potential to improve the capability to monitor forested wetland hydrology. In this study, we examined the use of Environmental Satellite Advanced SAR (C-HH and C-VV) data for monitoring levels of inundation and soil moisture throughout the year in a typical Mid-Atlantic floodplain and some of the main limitations inherent to C-band data (i.e., polarization and plant phenology) in this environment. The relationships between the backscatter coefficient and inundation, soil moisture, tree basal area, tree height, and forest canopy closure were examined. Significant differences in C-HH were found between forested areas of varying hydrology (0%-60% area inundated) throughout the year and in C-VV during the leaf-off season. As expected, C-HH SAR backscatter was better correlated with inundation and soil moisture than was C-VV SAR backscatter, and the correlations between both polarizations of backscatter and hydrology were stronger during the leaf-off season (C-HH leaf-off, leaf-on ; C-VV leaf-off, leaf-on ; all significant at level). Based on our findings, we concluded that the C-HH data are useful for monitoring hydrology beneath forest canopies throughout the year, whereas the C-VV data can be used during the leaf-off season. Our findings support previous studies that concluded that C-band imagery can be used to monitor forested wetland hydrology in large floodplains that are fully inundated. However, this study used detailed in situ measurements and demonstrated that C-band SAR data can also be used to monitor-forested wetland hydrology in smaller partially inundated floodplains, which are more common in the Mid-Atlantic. [J764]

## "High-Resolution Three-Dimensional Radar Imaging for Rapidly Spinning Targets"

A 3-D inverse synthetic aperture radar imaging method for rapidly spinning targets, i.e., a generalized Radon transform (GRT)-CLEAN algorithm, is proposed in this paper. The signal model is first changed into an equivalent high-speed turntable model after the compensation of the translational motion. Second, based on the relationship between the range profile variation of the spinning targets and the scatterers' positions, the GRT is utilized to estimate the scatterers' positions. Finally, combining the GRT with the modified CLEAN approach, the parameters of each scatterer and, thus, the 3-D image of the targets can be obtained. In addition to the development of the GRT-CLEAN algorithm, the estimation and compensation of the linear translational motion error in the imaging process is also considered in this paper. Good images yielded confirm the effectiveness of the GRT-CLEAN algorithm in the simulations. [J765]

## "X-Band Airborne Differential Interferometry: Results of the OrbiSAR Campaign Over the Perugia Area"

Differential synthetic aperture radar interferometry (DInSAR) is a remote sensing technique that allows monitoring ground deformation with accuracy of the order of fractions of the radiated wavelength, by means of proper combination and processing of repeat-pass data. In contrast to the satellite case, application of such a

technique to airborne data is not, today, a well-established task. Several airborne campaigns, involving mainly C/L-band data, have been planned in the last years to exploit the potentialities of these more flexible platforms for deformation monitoring. In this paper, we show the results of an airborne DInSAR X-band experiment carried out over the Perugia area (center of Italy) by using the OrbiSAR system. We discuss the processing chain applied to the acquired data, which allows achieving a satisfactory compromise between accuracy and efficiency. Eleven repeated passes were carried out in two days; two corner reflectors were located on the ground in a hilly region. One corner reflector was vertically moved between the two days to evaluate the system detection capability. Moreover, we carry out an analysis of all possible differential interferograms for a region 2 4 km wide. [J766]

## "Analysis and Synthesis of Raindrop Size Distribution Time Series From Disdrometer Data"

Hydrometeorological and radio propagation applications can benefit from the capability to model the time evolution of raindrop size distribution (RSD). A new stochastic vector autoregressive semi-Markov model is proposed to randomly synthesize (generate) the temporal series of the three driving parameters of a normalized gamma RSD. Rainfall intermittence is reproduced through a discrete semi-Markov process, modeled from disdrometer measurements using two-state analytical statistics of rain and dry period duration. The overall model is set up by means of a large set of disdrometer measurements, collected from 2003 to 2005 at Chilbolton, U.K. The driving parameters of the retrieved RSD are estimated using three approaches: the Gamma moment method and the 1D and 3D maximum-likelihood methods. Interestingly, these methodologies lead to quite different results, particularly when one is interested in evaluating RSD higher order moments such as the rain rate. The accuracy of the proposed RSD time-series generation technique is evaluated against available disdrometer measurements, providing excellent statistical scores. [J767]

## "Matching-Pursuit-Based Analysis of Moving Objects in Polarimetric SAR Images"

This letter deals with the analysis of moving and nonstationary objects in already focused synthetic aperture radar (SAR) images. A method based on the matching pursuit (MP) algorithm is proposed to decompose the SAR signal into a set of atoms. A model of a moving object response with frequency- and angle-dependent reflectivity is introduced to design the MP atoms. Each selected atom is associated to a scatterer of the scene and is parameterized by relevant physical descriptors, leading to a multidimensional model of the object. The efficiency of this technique is demonstrated in terms of SAR response refocusing and physical parameter map derivation, using a polarimetric SAR image of a moving object lying in a natural background. [J768]

## "High-Resolution SAR Interferometry: Estimation of Local Frequencies in the Context of Alpine Glaciers"

Synthetic aperture radar (SAR) interferometric data offer the opportunity to measure temperate glacier surface topography and displacement. The increase of the resolution provided by the most recent SAR systems has some critical implications. For instance, a reliable estimate of the phase gradient can only be achieved by using interferogram local frequencies. In this paper, an original two-step method for estimating local frequencies is proposed. The 2-D phase signal is considered to have two deterministic components corresponding to low-resolution (LR) fringes and high-resolution (HR) patterns due to the local microrelief, respectively. The first step of the proposed algorithm consists in the LR phase flattening. In the second step, the local HR frequencies are estimated from the phase 2-D autocorrelation function computed on adaptive neighborhoods. This neighborhood is the set of connected pixels belonging to the same HR spatial feature and respecting the ldquolocal stationarityrdquo hypothesis. Results with both simulated TerraSAR-X interferograms and real airborne E-SAR images are presented to illustrate the potential of the proposed method. [J769]

## "Evaluation of a Near-Field Monostatic-to-Bistatic Equivalence Theorem"

This paper presents the results of an investigation to quantitatively determine the limits of Falconer's monostatic-to-bistatic equivalence theorem (MBET). Falconer developed two extensions to Kell's MBET: one that is applicable to near-zone data and one that is valid in both the near- and far-zone regions. This paper encompassed collecting and analyzing both monostatic and bistatic radar cross-section data for perfect electrically conducting objects. Specifically, the authors analyzed the effects of varying the transmission frequency, scattering object complexity, and receiver bistatic angle. Objects ranged in geometric complexity from simple canonical objects to multifaceted shapes that produce multiple reflections. Empirical data collected in the far zone were compared with the analytical predictions produced by a commercially available method-of-moment (MoM) code. The code was run at X-band through K-band frequencies for a comparison with the measured data. The empirical bistatic data were then compared with the estimate produced by the MBET to ascertain the region in which the MBET approximation is applicable. Finally, the MoM code was used to produce near-field

scattering predictions to facilitate the evaluation of Falconer's near-field MBET. It is shown that the complexity of the scatterer restricts the region of validity for the MBET, where shadowing and multipath interactions prevail. The disparity between the MBET accuracies for the different test objects used clearly illustrates this point. [J770]

## "Stokes Antenna Temperatures"

The growing importance of polarimetric radiometers has led to the need for a detailed theory for Stokes antenna temperatures. In this paper, we provide a full Stokes vector formulation of an antenna temperature that accounts for the entire antenna pattern, which includes polarization mixing in the main-beam and sidelobe effects. To derive the Stokes antenna temperatures, we follow the conventional methods in the Earth remote sensing literature while relying on a coherency algebra approach from radio astronomy. Connections and parallels to the conventional approaches are noted along the way. We also introduce generalizations of beam efficiency and cross polarization for use with polarimetric radiometers. These provide important metrics in the design of future systems. [J771]

## "Brightness Measurements and Calibration With Airborne and Terrestrial Laser Scanners"

Brightness measurement with an airborne or terrestrial laser scanner is a new concept since the intensity information recorded by the laser scanner detectors has, thus far, not been used or implemented in surface brightness studies. This is partly due to the calibration problems and the lack of information on the behavior of laser light in the observation geometry where laser scanners operate. In addition, the 3-D position information has, thus far, been sufficient for surface modeling. We present a new type of empirical calibration scheme for laser scanner intensity developed with a terrestrial laser scanner in laboratory and field conditions using brightness targets and a calibrated reference panel. We compare the results with those obtained from airborne laser scanner flight campaigns using the same set of brightness targets. It turns out that the relative calibration of laser scanner intensity is possible using a calibrated grayscale but requires background information of the targets and the conditions in which the measurements are carried out. We also discuss the feasibility and uses of a laser-scanner-based intensity measurement in general. [J772]

## "Rice Mapping and Monitoring Using ENVISAT ASAR Data"

Radar remote sensing technology has become an important method for stable and long-time rice monitoring for its capability to operate in all weather conditions. In this letter, ENVISAT advanced synthetic aperture radar (ASAR) alternative-polarization VV/HH data were used for rice monitoring in the Xinghua rice experiment site in the middle of Jiangsu Province. First, a threshold classification method was developed for mapping rice growth area according to the different characteristic of backscatter coefficients between paddy rice and other land surface objects. Then, relational models were built for retrieving rice growth parameters from ASAR images based on correlation analysis between backscatter coefficients and field measurements. Meanwhile, an optical multispectral image was used as ancillary data for rice parameters retrieval. As expected, the retrieved rice growth parameters were consistent with those of field measurements. [J773]

## "Authors' Reply to Comments by Takuya Sakamoto, Shouhei Kidera, and Toru Sato on “Seabed Algorithm and Comments on ‘Modeling and Migration of 2-D Georadar Data: A Stationary Phase Approach’”"

This article addresses the comments of Sakamato et al. on Greenhalgh et al.'s "Modeling and migration of 2-D georadar data: A stationary phase approach". Here, Greenhalgh et al. emphasizes the comprehensiveness of their approach over Sakamato et al.'s SEABED algorithm. [J774]

## "Efficient SAR Raw Data Generation Including Low Squint Angles and Platform Instabilities"

The performance of high-resolution synthetic aperture radar (SAR) systems under degrading conditions such as uncontrolled platform motion can only be analyzed and evaluated by modeling the whole imaging system through simulation. A major scientific problem, however, is the generation of spotlight mode SAR raw data because of the need for high numerical and modeling accuracy, and restricted computer time and space. Taking into account a squinted geometry and platform instabilities, the common generation of raw data in the time domain becomes time inefficient. This letter proposes a raw data generator with which the spotlight mode raw data set of an extended scene can be simulated and which combines the precision obtainable when working in the time domain with the efficiency of work in the frequency domain. The generated raw data are processed and analyzed to quantify the quality of the proposed simulation tool. [J775]

## "Detection of Breathing and Heartbeat Through Snow Using a Microwave Transceiver"

The potential of a continuous-wave microwave transceiver as a tool for detecting breathing and heartbeat of people buried in snow has been experimentally evaluated. The breathing has been clearly detected through a 1.8-m-thick snow barrier as well as through the 1.2-m-thick roof of an igloo dugout to simulate the experimental conditions of a human being trapped under an avalanche. [J776]

## "Multibaseline Polarimetric SAR Interferometry Coherence Optimization"

This letter analyzes different approaches for polarimetric optimization of multibaseline (MB) interferometric coherences. Two general methods are developed to simultaneously optimize coherences for more than two data sets. The first method provides every data set with a distinct dominant scattering mechanism (SM). The second optimization method is constrained to use equal SMs at all data sets. As the experimental results indicate, MB coherence optimization does improve the accuracy in the estimation of dominant SMs and the associated interferometric phases. Both methods are evaluated on real data acquired by the German Aerospace Agency (DLR)'s enhanced synthetic aperture radar sensor (ESAR) at L-band. [J777]

## "Classifiers and Confidence Estimation for Oil Spill Detection in ENVISAT ASAR Images"

An improved classification approach is proposed for automatic oil spill detection in synthetic aperture radar images. The performance of statistical classifiers and support vector machines is compared. Regularized statistical classifiers prove to perform the best on this problem. To allow the user to tune the system with respect to the tradeoff between the number of true positive alarms and the number of false positives, an automatic confidence estimator has been developed. Combining the regularized classifier with confidence estimation leads to acceptable performance. [J778]

## "On the Use of CloudSat and MODIS Data for Estimating Hurricane Intensity"

This letter presents preliminary results concerning the use of new observations from the A-Train Constellation for testing a new technique of remotely sensing hurricane intensity from space based on modeling a hurricane as a balanced, convectively neutral vortex. The key observational requirements are simultaneous, accurate measurements of cloud-top height, cloudtop temperature, and cloud profiling information across the center of the storm, although there are ways to bypass the need for cloud-top temperature. In this letter, the Moderate Resolution Imaging Spectroradiometer onboard Aqua provides an estimation of the cloud-top temperature, and the near-simultaneous CloudSat observations provide the essential cloud-top height and cloud profiling information. Initial results indicate that the new technique is a promising method for estimating storm intensity when compared post facto to the best track database. Potential uncertainties and room for further refinement of the technique are discussed. [J779]

## "Basic Slant Range-Doppler Modeling of Moving Scatterers for SAR Applications"

A fundamental spectral domain model for moving point and distribution of scatterers is presented. The approach is accurate as the spherical phase front is rigorously treated throughout the Doppler analysis. Due to the analytic nature of the model in the range-Doppler plain, large squint-angle operations (e.g., SpotSAR) can be characterized. Furthermore, motion characteristics can be extracted in the subaperture level to better reflect the general motion (e.g., nonuniform). The range-Doppler model can serve as a tool for polarimetric and multichannel analysis. [J780]

## "Measurement of the Wind Vector Over Sea by an Airborne Radar Altimeter Using an Antenna Characterized by Different Beamwidth in the Vertical and Horizontal Planes"

In this letter, a possibility of recovering the wind vector over sea using an airborne radar altimeter in a short-pulse scatterometer mode is discussed. The nadir-looking wide-beam antenna, with the modified beam shape forming an ellipse footprint, is assumed for the purpose of analysis. Simultaneous range Doppler discrimination techniques are also used and a measuring algorithm of the sea-surface wind speed and direction is proposed. [J781]

## "Bistatic Spotlight SAR Processing Using the Frequency-Scaling Algorithm"

This letter derives the bistatic point target spectrum for the translational invariant case. Based on the derived spectrum and the linear approximation of the bistatic range cell migration factor, a bistatic frequency-scaling algorithm (FSA) is proposed for spotlight synthetic aperture radar data processing. This algorithm leads to a very precise and efficient processing since it performs the focusing in the frequency domain and no interpolation is required in the whole processing chain. In addition, it is shown that the case considered in the monostatic FSA is a specialization of the more general one considered in this letter. Finally, simulation results are provided to

illustrate the validity of the presented approach. [J782]

## "Supervised Classification and Estimation of Hydrometeors From C-Band Dual-Polarized Radars: A Bayesian Approach"

In this paper, a Bayesian statistical approach for supervised classification and estimation of hydrometeors, using a C-band polarimetric radar, is presented and discussed. The Bayesian Radar Algorithm for Hydrometeor Classification at C-band (BRAHCC) is supervised by a backscattering microphysical model, aimed at representing ten different hydrometeor classes in water, ice, and mixed phase. The expected error budget is evaluated by means of contingency tables on the basis of C-band radar noisy and attenuated synthetic data. Its accuracy is better than that obtained from a previously developed fuzzy logic C-band classification algorithm. As a second step of the overall retrieval algorithm, a multivariate regression is adopted to derive water content statistical estimators, exploiting simulated polarimetric radar data for each hydrometeor class. The BRAHCC methodology is then applied to a convective hail event, observed by two C-band dual-polarized radars in a network configuration. The hydrometeor classification along the line of sight, connecting the two C-band radars, is performed using the BRAHCC applied to path-attenuation-corrected data. Qualitative results are consistent with those derived from the fuzzy logic algorithm. Hydrometeor water content temporal evolution is tracked along the radar line of sight. Hail vertical occurrence is derived and compared with an empirical hail detection index applied along the radar connection line during the whole event. [J783]

## "Vegetation Mapping for Landmine Detection Using Long-Wave Hyperspectral Imagery"

We develop a vegetation mapping method using long-wave hyperspectral imagery and apply it to landmine detection. The novel aspect of the method is that it makes use of emissivity skewness. The main purpose of vegetation detection for mine detection is to minimize false alarms. Vegetation, such as round bushes, may be mistaken as mines by mine detection algorithms, particularly in synthetic aperture radar (SAR) imagery. We employ an unsupervised vegetation detection algorithm that exploits statistics of emissivity spectra of vegetation in the long-wave infrared spectrum for identification. This information is incorporated into a Choquet integral-based fusion structure, which fuses detector outputs from hyperspectral imagery and SAR imagery. Vegetation mapping is shown to improve mine detection results over a variety of images and fusion models. [J784]

## "Afterpulsing Effects in Free-Running InGaAsP Single-Photon Avalanche Diodes"

We demonstrate large-area (80 mum diameter) InP-based single-photon avalanche diodes for Geiger-mode operation at 1.06 mum with dark count rates of ~1000 Hz at high detection efficiencies of 30% at 237 K, as well as simulations of dark count rate and detection efficiency that provide good agreement with measured data. Experimental results obtained using free-running operation illustrate the strong impact of afterpulsing effects for short (~200 ns) hold-off times. We present an analysis of these free-running results that quantifies the contribution of afterpulsing to the total count rate. [J785]

## "Multidimensional Waveform Encoding: A New Digital Beamforming Technique for Synthetic Aperture Radar Remote Sensing"

This paper introduces the innovative concept of multidimensional waveform encoding for spaceborne synthetic aperture radar (SAR). The combination of this technique with digital beamforming on receive enables a new generation of SAR systems with improved performance and flexible imaging capabilities. Examples are high-resolution wide-swath radar imaging with compact antennas, enhanced sensitivity for applications like alongtrack interferometry and moving object indication, and the implementation of hybrid SAR imaging modes that are well suited to satisfy hitherto incompatible user requirements. Implementation-specific issues are discussed and performance examples demonstrate the potential of the new technique for different remote sensing applications. [J786]

## "Pine Forest Height Inversion Using Single-Pass X-Band PolInSAR Data"

A sparse pine forest is investigated at X-band on a single-pass polarimetric synthetic aperture radar interferometry (PolInSAR) data set using HH and HV channels. These first preliminary results show that the associated phase centers present a significant vertical separation (about 6 m) allowed by penetration through gaps in the canopy. Forest parameter inversion using the random volume over ground (RVoG) model is evaluated and adapted at this frequency. The forest height can be retrieved accurately by supposing a high mean extinction coefficient (around 1.6 (dB/m). The penetration depth is estimated to be around 4 m, based on the forest height ground measurements. Finally, a time-frequency analysis using a sublook decomposition is performed to increase the vertical separation of the polarimetric phase centers. As a consequence, RVoG-

inversion performance is improved, and a penetration depth that is in better accordance with a previous work (of the order of 2 m) is found. This paper has shown that the height inversion of a pine forest was possible using PolInSAR X-band data and that the performance was more dependent on the forest density than at lower frequencies. [J787]

## "Atmospheric Artifact Compensation in Ground-Based DInSAR Applications"

In this letter, a coherence-based technique for atmospheric artifact removal in ground-based (GB) zero-baseline synthetic aperture radar (SAR) acquisitions is proposed. For this purpose, polarimetric measurements acquired using the GB-SAR sensor developed at the Universitat Politecnica de Catalunya are employed. The heterogeneous environment of Collserola Park in the outskirts of Barcelona, Spain, was selected as the test area. Data sets were acquired at X-band during one week in June 2005. The effects of the atmosphere variations between successive zero-baseline SAR polarimetric acquisitions are treated here in detail. The need to compensate for the resulting phase-difference errors when retrieving interferometric information is put forward. A compensation technique is then proposed and evaluated using the control points placed inside the observed scene. [J788]

## "Improving Coherence of Complex Image Pairs Obtained by Along-Track Bistatic SARs Using Range-Azimuth Prefiltering"

An along-track interferometric synthetic aperture radar (SAR) can be used for ground moving target indication (GMTI) by comparing two SAR images obtained at different observation times. Different geometries of the two observations bring the decorrelation noise, which will degrade the detection performance. For bistatic SARs, the decorrelation theory is quite different from that for monostatic ones. This paper deals with the coherence between two complex SAR images formed by two along-track bistatic SARs with different baseline lengths. Using the single scattering model, the coherence between the two echoes collected by the two receivers is investigated, and the full-coherence conditions are derived. Then, a new method based on range-azimuth prefiltering is proposed to improve the coherence of complex image pairs. As the precise prefiltering is complicated, its three approximate implementations are given. The effects of prefiltering on SAR images are also analyzed. Finally, simulation results validate the effectiveness of the proposed method. [J789]

## "Model-Associated Forest Parameter Retrieval Using VHF SAR Data at the Individual Tree Level"

A simple statistical extension at the individual tree level for an earlier-developed very high frequency forest backscatter model is proposed. This extended model treats trunk volumes as random quantities. A concept of random forest reflection coefficient is also introduced to characterize radar returns from individual trees. Based on the extended model, a set of algorithms for estimating the mean trunk (stem) volume from synthetic aperture radar data at the individual tree level is developed assuming that the areal tree density is known. The algorithms are specified for different scenarios related to a prioriinformation on parameters of statistical distributions for the trunk volume and fluctuations of the forest reflection coefficient. An approximate lower bound on the standard deviation in the unbiased estimation of the mean trunk (stem) volume is proposed. This bound can be readily obtained by means of computer simulation for any specified statistical distribution for the trunk volume and fluctuations of the forest reflection coefficient. Performance analysis for the proposed algorithms is numerically performed by means of Monte Carlo simulation for a variety of scenarios. This analysis has shown that the algorithms provide nearly unbiased and efficient estimates, and the proposed lower bound is a very accurate approximation. The results of the study have demonstrated that the approach and methods developed in this paper suggest promising solutions in accurate forest parameter retrieval. [J790]

## "Effects of Background Removal in Linear Inverse Scattering"

This paper deals with the effect of the background removal procedure on ground-penetrating radar data in the framework of a Born-based inverse-scattering solution approach for a scalar 2-D geometry. The theoretical investigation is performed by resorting to diffraction tomography reasoning, and then it is numerically confirmed thanks to the singular value decomposition of the operator that connects the unknown contrast function to the scattered field data achieved under background removal. Numerical and experimental tests are presented. [J791]

## "A New Adaptive Multiresolution Noise-Filtering Approach for SAR Interferometric Phase Images"

This letter presents a novel adaptive multiresolution technique to estimate the local fringe frequency in synthetic aperture radar (SAR) interferometric phase images. According to the coherent summation principle, the size and the shape of the interferogram spatial resolution for local frequency estimation are adapted pixel by pixel to track the topographic changes and optimize the space-frequency resolution. We show that, comparing conventional filters with the processing window of a fixed size (such as 7 times 7) and shape (such as a square), the

proposed approach avoids the loss of phase fringes and provides a more accurate representation of the scene topography. In this letter, we present a method to eliminate invalid frequency estimation. A fast frequency estimation approach modified from the method proposed by Trouve et al. is also shown. Finally, both simulated data and actual SAR data are utilized to illustrate the effectiveness of the proposed method. [J792]

## "Receiver Operating Characteristic Curve Confidence Intervals and Regions"

Many researchers have presented results showing the empirical performance of target detection algorithms using hyperspectral or synthetic aperture radar imagery. In nearly all cases, these probabilities of detection and false alarm are presented as precise values as opposed to their true nature as estimates of random values. In this letter, we provide analytical tools and examples of computing confidence intervals and regions around these estimates commonly presented as points on receiver operating characteristic (ROC) curves. It is suggested that these tools be adopted by researchers when presenting their results to provide their audience with a quantitative metric for proper interpretation of empirically estimated ROC curves. [J793]

## "Estimation of the Temporal Evolution of the Deformation Using Airborne Differential SAR Interferometry"

This paper presents airborne differential synthetic aperture radar (SAR) interferometry results using a stack of 14 images, which were acquired by the Experimental SAR system of the German Aerospace Center (DLR) during a time span of 2.5 h. An advanced differential technique is used to retrieve the error in the digital elevation model and the temporal evolution of the deformation for every coherent pixel in the image. The two main limitations in airborne SAR processing are analyzed, namely, the existence of residual motion errors (RMEs) (inaccuracies in the navigation system on the order of 1-5 cm) and the accommodation of the topography and the aperture dependence on motion errors during the processing. The coupling between them is also addressed, showing that the estimation of the differential RME, i.e., baseline error, can be biased when using techniques based on the coregistration between interferometric looks. The SAR focusing chain to process the data is also presented together with the modifications in the differential interferometry processor to deal with the remaining baseline error. The detected motion of a corner reflector and the measured deformation in several agricultural fields allows one to validate the proposed techniques. [J794]

## "Processing of Envisat Alternating Polarization Data for Vessel Detection"

The alternating polarization (AP)-mode data from Envisat/Advanced Synthetic Aperture Radar (ASAR) can simultaneously generate two well-georegistered images in different polarizations, including VV/HH, HH/HV, and VV/VH combinations. This additional polarimetric information between channels is helpful for enhancing the accuracy of vessel detection. In this letter, different processing methods of AP single-look complex (APS) and precision (APP) data for vessel detection are investigated. For APS data, we propose a dual-polarization whitening fusion filter to combine dual-channel data and present its superiority to other traditional detectors. For APP data, based on the distinct polarimetric properties of each polarization, we utilize different fusion methods for different polarization combinations, including a wavelets-based method for VV/HH and a simple product fusion method for the other two pairs including the cross-polarization channel (HV or VH). Finally, in the experiments, we use real Envisat AP data sets to verify the method, and the results of our proposed processing strategy indicate that it cannot only suppress the speckle and the sea clutter but also improve the vessel detection performance. [J795]

## "Sea Surface Current-Wave-Wind Interactions Measured by Coastal Ground Wave HF Radars"

The performance and operational feasibility of the high-frequency Wellen Radar Doppler radar have been demonstrated in a region dominated by strong tidal currents during the SURveillance LITtorale OPerationnelle experiment in Brittany (France). Local weather-oceanic phenomena (current-wave-wind interactions) were measured for the first time by temporal-spatial analyses of the sea surface current measurements, sea surface current spatial gradient, and significant wave heights under conditions of spring tides and current mainly in the wind direction. The results, showing a variation of wave height with the tidal cycle, are presented in this letter. [J796]

## "A Tunable Closed-Form Model for the Structure Function of Tropospheric Delay"

Several interferometric synthetic aperture radar applications could benefit from the availability of a closed-form model for the second-order statistics of atmospheric delay. Due to the variability of the latter, it would also be desirable for the model to be tunable to some acquisition-specific information, describing the atmospheric state. In this letter, a closed-form expression for the zenith delay structure function of tropospheric propagation delay is

derived from a two-regime power spectral density function reported in the literature. The power at a specific spatial frequency is used as a free model parameter, which may be tuned to available measurements or, in the absence of these, to atmospheric statistics. The latter approach is used to compare the derived model with previously published results. [J797]

## "Radar Polarization Orientation Shifts in Built-Up Areas"

Polarization orientation angle shifts can be seen not only in rugged terrain areas but also in urban areas. The latter is explained by backscatter from a wall of a building or house, which is equivalent to a tilted ground-surface patch. From the scattering model of built-up areas, the polarization orientation angle shift in the built-up areas is given as, where is the wall or street orientation angle, and is the radar incidence angle. Japan Aerospace Exploration Agency Pi-SAR L-band polarimetric data of Gifu, Japan, show a good agreement with the theory. The phase difference between VH and HH polarizations is used to demonstrate the contribution of double-bounce scattering ground-wall and wall-ground over a wide range of wall orientation angles. [J798]

## "Three-Dimensional Stereo Reconstruction of Buildings Using Polarimetric SAR Images Acquired in Opposite Directions"

Polarimetric synthetic aperture radar (SAR) images describe objects via polarization synthesis and present much richer information than monopolarized SAR images. Furthermore, multidirectional flights of polarimetric SAR can see 3-D stereo objects in different angles. The height and the location of the 3-D objects can be retrieved from the polarimetric SAR images in multidirectional flights. This letter presents a tractable approach for the reconstruction of 3-D stereo buildings from two airborne PI-SAR images taken from opposite directions (at X-band with a spatial resolution of 1.5 m). [J799]

## "The Effect of Conduction on VHF Radar Images Shot in Water-Filled Boreholes"

A downhole digital memory-logging pulsed borehole radar transceiver operating in the 10-125-MHz band was run repeatedly down two 1.25-km-deep, uncased, water-filled 60-mm boreholes in the Northern Limb of the Bushveld Complex, South Africa. Suspended on an insulating cord, it mapped a steep fault in the Main Zone from a range of 75 m down through its intersection with the borehole. Lowered on a wire rope, the transceiver launched guided ~75 m/mus first-order transverse magnetic pulses which shuttled axially between the radar and the bedding planes. Decoupled from the wire by 2 m of insulating cord, it yielded a profile in which radar reflections and guided bedding plane echoes superimposed. As the radar descended through the mineralized, stratified Platreef, traces were found to be imprinted with voltage level shifts that showed, with Laterolog-comparable resolution, the conductivity profile of the Platreef. [J800]

## "Simultaneous Least Squares Adjustment of Multiframe Velocities Derived From Interferometric and Speckle-Tracking Methods"

This letter extends the simultaneous least squares adjustment method to the calibration and merging of velocity measurements, which are obtained by applying interferometric and speckle-tracking methods to multiple frames of repeat-pass interferometric synthetic aperture radar (InSAR) data. The underlying observation equations have been derived for velocity control points and tie points. By exploiting a set of tie points, individual frames within a strip or a block can be correlated with each other, and the parameters of calibration models for all individual frames can be simultaneously determined. With Radarsat InSAR data over the Recovery Glacier, Antarctica, we demonstrate that our simultaneous least squares adjustment method has effectively removed velocity discontinuities between adjacent frames and greatly reduced the velocity-control-point requirement. [J801]

## "Predicted Effects of Nonuniform Beam Filling on GPM Radar Data"

The global precipitation measurement mission (GPM) will carry the first dual-frequency spaceborne radar (DPR) for rainfall observation. We use dual-frequency airborne radar data to simulate observations at GPM DPR resolution and frequencies and to investigate errors due to nonuniform beam filling effects. Errors at Ku-band are similar to those found in previous studies. Errors in the Ka-band path-integrated attenuation and near-surface reflectivity are larger than at Ku-band. Errors in rain-top reflectivity, where attenuation is neglected, are smaller at Ka-band than at Ku-band because the Ka-band Z-R relation is closer to being linear. [J802]

## "The Hybrid CramЙr-Rao Bound on Broadside DOA Estimation of Extended Sources in Presence of Array Errors"

In this correspondence we derive explicit expressions for the hybrid Cramer-Rao lower bound (HCRB) on the estimation accuracy of signal direction of arrival (DOA) from data collected by randomly perturbed arrays. The

presence of a wavefront spatial decorrelation, which is modeled as a multiplicative correlated noise, has also been taken into account in the data model, since it is typical in those applications involving extended sources. In particular, we consider perturbations in sensor positions. Existing approaches to DOA HCRB calculation do not consider the presence of multiplicative noise and are referred to the assumption of small perturbations only, still not being worked out explicitly. Here, we assume that the impinging wavefronts are coming from broadside or more generally from a narrow DOA sector, allowing the explicit derivation of the HCRB for any variance of the sensor positioning errors in the line-of-sight direction. This scenario corresponds to the typical operative condition of remote sensing systems such as synthetic aperture radar (SAR) multibaseline interferometers, for which a few HCRB sample curves are reported. [J803]

## "Autofocus for ISAR Imaging Using Higher Order Statistics"

Autofocus is imperative for inverse synthetic aperture radar (ISAR) imaging. In this letter, a new approach for ISAR autofocus is developed by using fourth-order statistics properties of the radarpsilas return signal. After the ISAR signal model is established, the approach is described. The results of processing real data confirm the effectiveness of the proposed approach and show its capability for suppressing noise. The developed approach has a numerical stability and a smaller computational load compared with the maximum image contrast and the minimum image entropy methods. [J804]

## "Analytic Search Method for Interferometric SAR Image Registration"

We propose an analytic search method for interferometric synthetic aperture radar (InSAR) image registration. An analytic cost function is established, and the subpixel offsets associated with the maximum of the cost function are continuously searched by direction-alternate optimization methods along vertical and horizontal directions. We establish a novel dual-quartic analytic cost function for extraction of subpixel offsets from a corresponding pixel pair established by pixel-level registration. A robust optimization method that is called biiteration algorithm for searching the maximum point of the dual-quartic cost function is developed to solve the subpixel offsets. Since the dual-quartic cost function is quartic if one of two parameters is fixed, one of two substeps including in each iterative step of the efficient biiterative method is to find the solution by the secant method. The performances of the proposed method are shown by using simulated and real data and compared with those of representative existing registration method. [J805]

## "Accuracy of the -Distribution Regression Model for Forest Biomass Estimation by High-Resolution Polarimetric SAR: Comparison of Model Estimation and Field Data"

In our previous regression model for estimating forest biomass, it was shown that non-Gaussian amplitude fluctuations in high-resolution polarimetric synthetic aperture radar (SAR) data of coniferous forests can accurately be described by the -distribution and that the order parameter of the -distribution can be useful in estimating the tree biomass of coniferous forests from L-band cross-polarization amplitude images in a wider range than the conventional method using the radar cross section alone. The result was based on the analysis of the ldquoground-truthrdquo biomass data of 19 forest stands and airborne polarimetric interferometric SAR L-band data over the Tomakomai forests in Hokkaido, Japan. From this relation, an empirical regression model was developed to estimate forest biomass from SAR data. In this paper, we report the results on further analyses of this regression model. The validity of the -distribution is first reconfirmed using the Akaike information criterion, followed by the description on the accuracy of the model. To examine model accuracy, we carried out further field measurements on 22 forest stands in 2005, and the ground survey was made in 2006 to find out the causes of several anomalous data. Based on a comparison of the model-based biomass and the ground-truth data, the accuracy of the model was found to be approximately 86%. The regression model was then updated for practical application in estimating the biomass of the Hokkaido forests by including the ground-truth data of all 41 forest stands. [J806]

## "Validating Mixed-Phase Cloud Optical Depth Retrieved From Infrared Observations With High Spectral Resolution Lidar"

Single-layer mixed-phase clouds are prevalent in the Arctic atmosphere. The properties of mixed-phase clouds, including the optical depth of both the liquid and ice components, can be retrieved from spectrally resolved infrared radiance observations that are made in both the 8-13-mum and 17-24-mum windows. The accuracy of the retrieved properties from this algorithm has been established in single-phase clouds (i.e., clouds that contain only liquid or only ice) but not in mixed-phase clouds. A polarization-sensitive high spectral resolution lidar (HSRL) was deployed to the Atmospheric Radiation Measurement Program's Barrow, Alaska site during the fall of 2004. The HSRL measures optical depth directly, and the phase can be discriminated using the depolarization ratio measured by the lidar. Comparisons of the infrared retrieved optical depths with the optical depths directly

observed by the lidar in clouds that consist of supercooled liquid layers precipitating ice are in good agreement, with the slope and correlation being 1.055 and 0.65 for the ice portion of the mixed-phase cloud and 0.954 and 0.82 for the liquid portion. [J807]

## "Three-Dimensional Attributes of Clear-Air Scatterers Observed With the Polarimetric Weather Radar"

In this letter, we present a spectral technique for observation and analysis of scatterers' polarimetric attributes. This technique allows one to visualize the scatterers' spectral signatures as a function of azimuth, Doppler velocity, and polarimetric variable at the same time. Such visualization can be used to evaluate the participants of the detected motions, to understand what constitutes the polarimetric averages, and to provide resources for establishing intrinsic polarimetric values (functions) for different types of scatterers, which are necessary for the scatterers' classification algorithms. We demonstrate this technique on a clear-air case observed with the S-band polarimetric research radar in Norman, OK, on September 7, 2004. We discuss the preference for spectral density of backscatter differential phase versus other polarimetric spectral densities for the observations of clear air. The proposed visualization technique is not limited to observations of echoes in clear air and invites study of intrinsic properties for other types of scatterers. [J808]

## "Equivalence Between Cameron's Unit Disc and PoincarЙ's Sphere for Symmetric Scattering Characterization and Classification"

Scattering type classification represents a significant step toward target classification. Both the surface of Poincare's sphere and Cameron's unit disc have been used separately to represent symmetric scattering matrices and to define classification methods. In this letter, the equivalence of using the surface of Poincare's sphere and Cameron's unit disc in terms of characterization and classification of symmetric scattering types is demonstrated mathematically. [J809]

## "The Effect of the Bistatic Scattering Angle on the High-Frequency Radar Cross Sections of the Ocean Surface"

High-frequency (HF) bistatic Doppler cross sections of the ocean surface are examined with respect to their dependency on the bistatic angle. Previously derived results which incorporate a pulsed dipole source and two orders of scatter are considered. It is trivially seen that the first-order result has a linear dependence on the cosine of the bistatic angle. The second-order echo accounts for a double scatter of incident radiation from first-order surface waves-the so-called electromagnetic term-and a single scatter from a second-order ocean wave. The latter, generally referred to as the second-order hydrodynamic term because it originates from coupling between first-order ocean waves, predominates the Doppler continuum in most regions of interest. The analysis presented here verifies that in addition to a cosine-dependent reduction in cross section magnitude with increasing bistatic angle, both components of the second-order scatter tend to zero under the condition of near-forward scatter for bistatic HF radar operation. Of course, this imposes practical limitations on the region over which a bistatically configured HF radar system may be used to remotely sense ocean surface parameters. [J810]

## "Three-Dimensional Wideband Beamforming for Imaging Through a Single Wall"

Through-the-wall imaging and urban sensing is an emerging area of research and development. The incorporation of the effects of signal propagation through wall material in producing an indoor image is important for reliable through-the-wall mission operations. We have previously analyzed wall effects, such as refraction and change in propagation speed, and designed a wideband beamformer for 2D imaging using line arrays. In this letter, we extend the analysis to 3D imaging via delay-and-sum beamforming in the presence of a single uniform wall. The third dimension provides valuable information on target heights that can be used for enhancing target discrimination/identification. Supporting simulation results are provided. [J811]

## "Using a Grid-Based Filter to Solve InSAR Phase Unwrapping"

This letter presents a phase-unwrapping (PU) algorithm for synthetic aperture radar interferometry based on a grid-based filter. The proposed PU algorithm, which is based on state-space techniques, simultaneously performs noise filtering and PU. The formulation of this technique provides independence from noise statistics and is not constrained by the nonlinearity of the problem. Results obtained with synthetic data show a significant improvement with respect to other conventional PU algorithms in some situations. [J812]

## "On the Disaggregation of Passive Microwave Soil Moisture Data Using A Priori Knowledge of

## Temporally Persistent Soil Moisture Fields"

Water and energy fluxes at the interface between the land surface and atmosphere are affected by the surface water content of the soil, which is highly variable in space and time. The sensitivity of active and passive microwave remote sensing data to surface soil moisture content has been investigated in numerous studies. Recent satellite mission concepts as, for example, the soil moisture and ocean salinity (SMOS) mission, are dedicated to provide global soil moisture information with a temporal frequency of a few days to capture the high temporal dynamics of surface soil moisture. SMOS soil moisture products are expected to have geometric resolutions on the order of 40 km. Mesoscale flood forecasting or water balance models typically operate at much higher spatial resolutions on the order of 1 km. It seems therefore essential to develop appropriate disaggregation schemes to benefit from the high temporal frequency of the SMOS data for hydrological applications as well as, for example, local numerical weather prediction models that are operated at a resolution of a few kilometers. This paper investigates the potential of using prior information on spatially persistent soil moisture fields to disaggregate SMOS scale soil moisture products. The approach is based on a ten-year soil moisture climatology for a mesoscale hydrological catchment, situated in southern Germany, which was generated using a state-of-the-art land-surface process model. The performance of the disaggregation algorithm is verified by comparison of disaggregated soil moisture fields with another ten-year period. To investigate the potential of the suggested disaggregation method for SMOS soil moisture products, a ten-year synthetic brightness temperature data set is generated at the 1-km scale. soil moisture is then retrieved from the aggregated brightness temperature data at the SMOS type scale of 40 km and then disaggregated using the suggested approach. The results are compared against reference--soil moisture at the 1-km scale. Uncertainties in the retrieval of the SMOS soil moisture products are explicitly considered, and the uncertainties of the disaggregated fields are quantified. The developed method shows a generally good performance for large parts of the test site, where soil moisture can be disaggregated with an accuracy that is better than the 4 vol.% benchmark of the SMOS mission. As the suggested method shows high sensitivity to biased soil moisture retrievals, uncertainties of the SMOS soil moisture products will directly reflect on the absolute accuracy of the disaggregated soil moisture fields, resulting in a much worse performance under noisy conditions. Nevertheless, the resulting soil moisture distributions show that it is feasible to derive relative soil moisture distributions in these cases. [J813]

## "Signal Processing Issues for the Exploitation of Pulse-to-Pulse Encoding SAR Transponders"

Synthetic aperture radar signal processing issues related to the exploitation of a pulse-to-pulse encoding transponder using pseudorandom codes discussed analytically. Namely the focusing algorithm, the code synchronization procedure and the properties of the code induced gain against non-encoding point scatterers and distributed ones. A time-domain processing algorithm and a code synchronization procedure are proposed and validated on simulated data and on a European Remote Sensing Satellite-2 data set containing prototypes of such a device. The interaction of the transponder signal with terrain backscattering is analyzed by deriving parameters that are useful for performance assessment. These are related to the relevant parameters in radiometric calibration, interferometric applications, and tagging. [J814]

## "Suppression of Clutter Residue in Weather Radar Reveals Birds' Corridors Over Urban Area"

An adaptive spectral technique for ground clutter and noise suppression in weather radar echoes is presented. This technique detects weak echoes that are masked by the residuals from ground clutter. The technique is demonstrated on two clear air cases observed with Doppler weather radar. After adaptive suppression of ground clutter and its residue, features appear over the Oklahoma City urban area where otherwise none could be seen. These are interpreted as birds' corridors between two lakes and along a river. [J815]

## "Sea-Surface Current Features Observed by Doppler Radar"

A coherent X-band radar was operated from the shore to measure velocities at the sea surface. The test site at a tidal inlet (Lister Tief) in the German Bight lay protected from swell and long wind waves. A vertical-vertical antenna was used to obtain the backscattered radar signal caused by Bragg scattering. To cover a sector of the circle, the antenna was rotated in 1Dstroksteps. At each step, the data acquisition was performed to obtain a time series of the backscattered radar signal. The maximum range is 1905 m with a range resolution of 7.5 m and an azimuthal resolution of 3.5diam. Maps of the averaged backscattered radar power and radial Doppler velocities are obtained. The radar backscatter maps show the modulation of the radar cross section due to changes in the surface roughness. The radar Doppler velocity maps show the modulations of the surface scatterer speed. The maps show many features, for example, the impact of subsurface sand waves, eddies, current shears, slicks, ship wakes, atmospheric effects, and small-scale current changes behind sheet pile walls. As the radar backscatter is caused by short wind waves, the wind influence on the Doppler signal was calculated for a first attempt to obtain true current motions. The results were compared with in situ current measurements.

By subsequently measuring the surfaces current from two radar positions and performing the wind correction, the current vector fields are assessed. [J816]

## "A Stationary Wavelet-Domain Wiener Filter for Correlated Speckle"

In this paper, we develop a Wiener-type speckle filter that operates in the stationary wavelet domain. We denote it as the stationarywavelet-domainWiener(SWW) speckle filter. We assume that both the speckle-free image and the speckle contribution have spatial correlations and utilize well-established models for the power density spectrum of the radar cross section to estimate the autospectra that define the filter. It turns out that the filter is independent of the wavelet-domain scale level, i.e., the filter is the same at all scale levels. The SWW filter works on nonoverlapping blocks in the wavelet domain, which are obtained by a quadtree algorithm. Due to the dyadic support of the wavelet coefficients, a natural smoothing is carried out on the boundaries between neighboring blocks, and no visual boundary effects can be observed. The SWW filter is unbiased and shows good performance in despeckling synthetic aperture radar (SAR) images. It smooths homogeneous areas while preserving textured areas and point scatterers. In contrast to most other speckle filters, the SWW filter requires the SAR data to be given in single-look complex form. [J817]

## "A Method to Extend the Estimation Range of the Existing Time-Domain Doppler Centroid Estimators"

In this letter, we use the summation-by-parts formula as a simple tool to extend the estimation range of a certain class of the already existing correlation-based Doppler centroid estimators. The resulting estimators are as robust as the original ones but cover a much larger estimation range of about 50% of the pulse-repetition frequency. Two examples with simulations are provided to demonstrate the benefits of the proposal. [J818]

## "Multilayered 3D LiDAR Image Construction Using Spatial Models in a Bayesian Framework"

Standard 3D imaging systems process only a single return at each pixel from an assumed single opaque surface. However, there are situations when the laser return consists of multiple peaks due to the footprint of the beam impinging on a target with surfaces distributed in depth or with semitransparent surfaces. If all these returns are processed, a more informative multilayered 3D image is created. We propose a unified theory of pixel processing for Lidar data using a Bayesian approach that incorporates spatial constraints through a Markov Random Field with a Potts prior model. This allows us to model uncertainty about the underlying spatial process. To palliate some inherent deficiencies of this prior model, we also introduce two proposal distributions, one based on spatial mode jumping and the other on a spatial birth/death process. The different parameters of the several returns are estimated using reversible-jump Markov chain Monte Carlo (RJMCMC) techniques in combination with an adaptive strategy of delayed rejection to improve the estimates of the parameters. [J819]

## "Assessment of Radar Signal Attenuation Caused by the Melting Hydrometeor Layer"

Attenuation of radar signals by melting hydrometeors is studied using modeling approaches and comparisons of simulated and observed results. In spite that the melting layer in precipitating systems is usually relatively thin ( ~ 500 m), this attenuation can be substantial at X-band frequencies for low elevation angles and at millimeter-wavelength frequencies that are used by the U.S. Department of Energy's Atmospheric Radiation Measurement Program and CloudSat radars operating at vertical/nadir incidence. Melting layer attenuation is stronger than the attenuation in the resultant rain at comparable path lengths and needs to be accounted for in remote sensing methods that use radar reflectivity measurements for retrieving cloud and precipitation parameters if the radar beam penetrates this layer. The choice of the mixing rule for calculating dielectric constants of melting hydrometeors determines, to a significant degree, the magnitude of the modeled attenuation values. A relatively simple Wiener mixing rule provides results that are consistent with melting layer reflectivity enhancements and attenuation estimates from the X-band radar observations. The total melting layer attenuation Ais related to the resultant rain rate Rin an approximately linear manner at X- and Kalpha-band frequencies, whereas at W-band, the melting layer attenuation increase with rain rate is slower due to strong non-Rayleigh scattering effects. Typical A-Rrelations are suggested, and the variability of these relations is discussed. This paper is mostly concerned with precipitating systems associated with snowflakes that are unrimed or only slightly rimed above the freezing level, as indicated by relatively low values of vertical Doppler velocities. [J820]

## "Using SAR Images to Detect Ships From Sea Clutter"

An innovative constant false alarm rate (CFAR) algorithm was studied for ship detection using synthetic aperture radar (SAR) images of the sea. Two advances were achieved. An alpha-stable distribution rather than a traditional Weibull or -distribution was used to model the distribution of sea clutter. The distribution of sea clutter in a SAR image was typically heterogeneous, caused mainly by variable wind and current conditions. Image

segmentation was carried out to improve the homogeneity of the distribution in each subimage or region. In comparison with ship detection using the CFAR algorithms based on the Weibull or K -distribution, our algorithm detected the most number of ships with the smallest number of false alarms. [J821]

## "Corrections to “Calibration of Linearly Polarized Polarimetric SAR Data Subject to Faraday Rotation” [JAug 04 1617-1624]"

In the above titled paper (ibid., vol. 42, no. 8, pp. 1617-1624, Aug 04), Equation (15) has an error. Corrections are presented here. [J822]

## "Genetic SVM Approach to Semisupervised Multitemporal Classification"

The updating of classification maps, as new image acquisitions are obtained, raises the problem of ground-truth information (training samples) updating. In this context, semisupervised multitemporal classification represents an interesting though still not well consolidated approach to tackle this issue. In this letter, we propose a novel methodological solution based on this approach. Its underlying idea is to update the ground-truth information through an automatic estimation process, which exploits archived ground-truth information as well as basic indications from the user about allowed/forbidden class transitions from an acquisition date to another. This updating problem is formulated by means of the support vector machine classification approach and a constrained multiobjective optimization genetic algorithm. Experimental results on a multitemporal data set consisting of two multisensor (Landsat-5 Thematic Mapper and European Remote Sensing satellite synthetic aperture radar) images are reported and discussed. [J823]

## "Brightness Temperature Map Reconstruction from Dual-Polarimetric Visibilities in Synthetic Aperture Imaging Radiometry"

Synthetic aperture imaging radiometers are powerful sensors for high-resolution observations of the Earth at low microwave frequencies. Within this context, the European Space Agency is currently developing the soil moisture and ocean salinity (SMOS) mission devoted to the monitoring of SMOS at global scale from L-band spaceborne radiometric observations obtained with a 2-D interferometer. This paper is concerned with the reconstruction of radiometric brightness temperature maps from interferometric measurements. More exactly, it extends the concept of ldquoband-limited resolving matrixrdquo to the case of the processing of dual-polarimetric data. [J824]

## "Comparison of Processing Algorithms for a Delay/Doppler Altimeter"

The use of a radar altimeter is to measure the height of the reflecting surface when the instrument passes overhead. A delay/Doppler altimeter (DDA) reduces the along-track resolution cell using correlation of pulses within burst, as in a synthetic aperture radar, with the net effect of synthesizing an array with a narrower lobe. The processing of DDA data therefore implies the correction of the phase delay of pulses, which is said to be Dopplerbeamsharpeningsince it can be reduced to a DFT in the along-track direction. The noise term on Doppler echoes is decreased by incoherent summing of contributions of different bursts. Summation of these contributions requires that pointing of each beam is directed toward a given output grid of samples on ground, and this can be a nontrivial task, depending on the topography profile. In this letter, a comparison between different beam sharpening algorithms is presented: Two of them are similar in their basic idea even if with different implementations; the third one can be considered as reference since no approximations are needed in principle, but is computationally inefficient. What results is that the first couple can be considered basically equivalent in terms of precision and computational efficiency, with little differences at the change of the environmental conditions. Results based on simulated data of simple and complex scenarios are presented as support of the reasoning. [J825]

## "Validation of Envisat Rain Detection and Rain Rate Estimates by Comparing With TRMM Data"

This letter provides validation results on both Envisat altimeter rain detection flag and rain rate estimates. This assessment was performed based on 18-month collocated data sets between Envisat with two sensor measurements from the Tropical Rainfall Measuring Mission, i.e., the microwave imager and the precipitation radar. Along with the comparison between closest sensor measurements with strict spatial and temporal criteria, discussion is also provided on environmental context insight when interpreting comparison results based on collocated data. [J826]

## "Some Reflections on Bistatic SAR of Forward-Looking Configuration"

Forward-looking imaging has many potential applications, but it is impossible with the usual monostatic synthetic aperture radar (SAR) principle. Through the bistatic SAR configuration, forward-looking imaging can be realized

for one of the bistatic platforms. This letter designs a bistatic configuration with a stationary transmitter and a forward-looking airborne receiver. It then analyzes the 2-D resolution and finds out which geometric parameter affects the imaging ability mostly. Besides, it gives out the signal formulation in the frequency domain and shows its imaging characteristics. Then, an imaging method is chosen for this special configuration, and the simulation results are exhibited, which validate the correctness of the analysis and prove the 2-D imaging ability of forward-looking bistatic SAR. [J827]

## "Comparison of Microwave and Infrared Land Surface Temperature Products Over the NAFE'06 Research Sites"

Two different remotely sensed land surface temperature (Ts) products are compared with insituobservations from the National Airborne Field Experiment research site in the western part of the Murrumbidgee catchment, Australia. The remotely sensed Tsproducts are retrieved from the following: 1) Ka-band passive microwave (MW) observations using several of space-based MW radiometers and 2) thermal infrared observations from the Moderate Resolution Imaging Spectroradiometer (MODIS) on two satellite platforms. Both methods show similar accuracy when compared to ground observations, although the dynamic range and mean differ significantly. However, a direct comparison of the two products at the same overpass time reveals a strikingly constant relation, with a standard error of ~ 4 K. The results of this study indicate that a merged Tsproduct of both MODIS and MW observations is feasible and would decrease the amount of data gaps and increase the sampling frequency for this region to 12 observations a day. [J828]

## "Multiple-Component Scattering Model for Polarimetric SAR Image Decomposition"

A multiple-component scattering model (MCSM) is proposed to decompose polarimetric synthetic aperture radar (PolSAR) images. The MCSM extends a three-component scattering model, which describes single-bounce, double-bounce, volume, helix, and wire scattering as elementary scattering mechanisms in the analysis of PolSAR images. It can be found that double-bounce, helix, and wire scattering are predominant in urban areas. These elementary scattering mechanisms correspond to the asymmetric reflection condition that the copolar and cross-polar correlations are not close to zero. The MCSM is demonstrated with a German Aerospace Center (DLR) Experimental Synthetic Aperture Radar (ESAR) L-band full-polarized image of the Oberpfaffenhofen Test Site Area (DE), Germany, which was obtained on September 30, 2000. The result of this decomposition confirmed that the proposed model is effective for analysis of buildings in urban areas. [J829]

## "Region-Based Classification of Polarimetric SAR Images Using Wishart MRF"

The scattering measurements of individual pixels in polarimetric SAR images are affected by speckle; hence, the performance of classification approaches, taking individual pixels as elements, would be damaged. By introducing the spatial relation between adjacent pixels, a novel classification method, taking regions as elements, is proposed using a Markov random field (MRF). In this method, an image is oversegmented into a large amount of rectangular regions first. Then, to use fully the statistical aprioriknowledge of the data and the spatial relation of neighboring pixels, a Wishart MRF model, combining the Wishart distribution with the MRF, is proposed, and an iterative conditional mode algorithm is adopted to adjust oversegmentation results so that the shapes of all regions match the ground truth better. Finally, a Wishart-based maximum likelihood, based on regions, is used to obtain a classification map. Real polarimetric images are used in experiments. Compared with the other three frequently used methods, higher accuracy is observed, and classification maps are in better agreement with the initial ground maps, using the proposed method. [J830]

## "Estimation of Ship Radial Speed by Adaptive Processing of RADARSAT-1 Fine Mode Data"

This letter describes a new method for estimating the radial component of a ship's velocity using single-channel synthetic aperture radar data acquired by RADARSAT-1. Unlike previous methods, this approach is applicable in the absence of any visible wakes. Experimental results confirm the robustness of the proposed algorithm. [J831]

## "Quaternion-Based Transformation for Extraction of Image-Generating Doppler for ISAR"

Inverse synthetic aperture radar (ISAR) is an imaging technique that is dependent on an object's rotational motion over a coherent processing interval. Maritime vessels and aircraft possess 3-D rotational motion, whereas it is only their ISAR contributing motion that is useful to the ISAR imaging process; the contributing motion consists of the Doppler generating axis and the effective angle of rotation. This letter presents a quaternion-based transformation that converts measured attitude and position data into an object's Doppler generating axis and effective angular rotation rate. This transformation is significant since it isolates the component of the motion that directly influences the ISAR image. It provides an alternative approach that can be used to understand the causes of blurring of most ISAR images of sea vessels as well to identify good imaging intervals for applications

such as cooperative ISAR for radar cross section measurement purposes. [J832]

## "Study on Spaceborne/Airborne Hybrid Bistatic SAR Image Formation in Frequency Domain"

To better understand the fundamental of the spaceborne/airborne hybrid bistatic SAR (SA-BSAR) image formation, the range cell migration (RCM) of the SA-BSAR is studied in the range-Doppler domain, where the RCM in SA-BSAR can be explicitly expressed in close form. Through the analysis of RCM relationship with target's azimuth and range position, we can find that, because of the system platforms' velocity difference along the azimuth direction, the RCM in SA-BSAR is 2D space variant. Therefore, the fundamental of frequency-domain image formation in SA-BSAR is to process the 2D space-variant RCM correction (RCMC) for nonreferent targets besides the bulk RCMC operation in the frequency domain. Furthermore, appropriate solutions in the frequency domain to remove the RCM in SA-BSAR are proposed and verified with five-point-target simulation. [J833]

## "Modified Hough Transform for Searching Radar Detection"

In this letter, we propose a modified Hough transform (HT) algorithm for radar detection by shifting the parameter space cells as well as exploiting the phase information of signal. The proposed modified HT brings (1) significant improvement of radar target detection at low signal-to-noise ratios and (2) complexity reduction of HT implementation in radar detection applications compared to the conventional HT-based methods. Simulation results are presented showing the performance gain obtained by the proposed modified HT over the conventional methods. [J834]

## "An Imaging HF GPR Using Stationary Antennas: Experimental Validation Over the Antarctic Ice Sheet"

Terrestrial And Planetary Imaging Radar (TAPIR) is an innovative high-frequency ground-penetrating radar (GPR) developed in the frame of the Martian NetLander mission to probe the subsurface down to kilometric depths. Unlike most GPRs, TAPIR is able to image underground reflectors with stationary antennas. In this paper, after a brief presentation of the instrument, we describe the method developed to interpret data collected during the RAdar of NEtlander in Terre Ade acutelie (RANETA) field survey in Antarctica. This method consists of retrieving the direction of arrival of each detected echo through the measurement of five components of the electromagnetic field (the three magnetic components and the horizontal components of the electric field). Thus, both the range and the direction of each individual reflection or diffraction due to the ice-bedrock interface are resolved. We validated this method on finite-difference time-domain numerically simulated data for different subsurface configurations before applying it to RANETA observations. In particular, the irregular topography of the bedrock in two sounding sites was revealed. We discuss the accuracy of our results. [J835]

## "GPS Reflections for Sea Surface Wind Speed Measurement"

In this letter, Global Positioning System (GPS) reflections for sea surface wind speed measurement are explored. The reflected signal correlation power is employed to retrieve the sea surface wind speed with a certain degree of accuracy. The GPS coarse-acquisition code autocorrelation sidelobe is studied and considered in the reflected signal model. This technique proves to be valid for the correlation power calculation. It is expected that this technique could further be studied for spaceborne applications with high dynamics. [J836]

## "SAR Image Segmentation Based on Level Set With Stationary Global Minimum"

In this letter, we propose a new level-set-based energy functional for the purpose of synthetic aperture radar (SAR) image segmentation into Gamma homogeneous regions. The segmentation of SAR images is a difficult problem due to the presence of speckles, which can be modeled as strong multiplicative noise. Our proposed energy functional is designed to get a stationary global minimum. As a result, the level set function that evolves by the Euler-Lagrange equation of the energy functional has a unique stationary convergence state. Moreover, it is easy to set a termination criterion on the curve evolution via a level set by using our energy functional. The experimental results on both synthetic and real SAR images demonstrate the effectiveness of our method. [J837]

## "Three-Dimensional LiDAR Data Classifying to Extract Road Point in Urban Area"

The Light Detection and Ranging (LiDAR) system is one of the best ways to accurately and effectively gather 3-D terrain information. However, it is complicated to process the LiDAR cloud data due to its irregularity and large number of collected data points. This letter proposes a novel method to automatically extract urban road network from 3-D LiDAR data. This method uses height and reflectance of LiDAR data, and clustered road point information. Geometric information of general roads is also applied to correctly extract road points group. The

proposed method has been tested on various urban areas which contain complicated road networks. The results demonstrate that the integration of height, reflectance, and geometric information of roads is a crucial factor that distinguishes the proposed method in its ability to reliably and correctly classify road points. [J838]

## "A Novel Algorithm for Estimating the Rotation Angle in ISAR Imaging"

A novel algorithm for estimating the rotation angle in inverse synthetic aperture radar imaging by generally considering the received signals as cubic phase signals is presented. The rotation angle is determined by the coefficients of the cubic phase signals, and the results of real data demonstrate the validity of the algorithm. [J839]

## "The Polar Format Imaging Algorithm Based on Double Chirp-Z Transforms"

Spotlight mode offers finer azimuth resolution than that achievable in stripmap mode using the same physical antenna. The most popular spotlight synthetic aperture radar (SAR) reconstruction method is the classic polar format algorithm (PFA). However, PFA needs to perform range and azimuth interpolation operations during SAR imaging, which, in turn, affect the imaging precision and the computation efficiency. In this letter, we present a novel polar format algorithm, which may avoid interpolation operations by double chirp-Z transform. In this letter, we also analyze the nondefocus and the nondistortion constraints and discuss the along-track acceleration constraint for the PFA as well. [J840]

## "Land Cover Characteristics of Airborne LiDAR Intensity Data: A Case Study"

Airborne light detection and ranging (LiDAR) systems provide precise geometric information over the surface of the Earth, as well as radiometric information. studies on LiDAR have primarily focused on topographic mapping and urban 3-D modeling. The radiometric characteristics of backscattered laser intensity are meanwhile not yet clearly understood. Recently, the interest in the radiometric properties of LiDAR has been rapidly expanding, and several works have performed the normalization or correction of laser intensity data. However, the effect of radiometric correction is still unclear, and a suitable radiometric correction method has yet to be proposed. This letter investigated the radiometric properties of LiDAR intensity data as a prerequisite procedure for the practical use of intensity. On the basis of a comparison with the surface reflectance measured by a portable spectroradiometer, it was found that the LiDAR intensity of vegetation was unusual. For land cover types other than vegetation, it was observed that range distance was the dominant factor of the intensity of LiDAR. Therefore, this letter suggests that the correction of LiDAR intensity in terms of range is effective to the land cover types except vegetation. [J841]

## "Multiple-Mode Selection of Walled-LTSA Array Elements for High-Resolution Imaging to Visualize Antipersonnel Plastic Landmines"

We propose a resolution improvement technique for a high-density array of walled linearly tapered slot antennas (LTSAs) in ground-penetrating radar imaging. In the system, we use the walled-LTSA array in a near-field measurement configuration and select various pairs of transmitter and receiver antennas out of the array elements. We prepare four selection modes so that we can practically enhance the imaging resolution. We remove the direct-coupling effect and compensate the path-length fluctuation caused by element individuality and element selection. Experiments demonstrate that the technique realizes higher resolution image acquisition to yield a clearer segmentation of antipersonnel plastic landmines in combination with adaptive image processing, based on complex-amplitude texture, even on a wet laterite soil condition. [J842]

## "On the Superresolution of Microwave Scanning Radiometer Measurements"

Microwave radiometer measurements are exploited to extract important geophysical information. Although it is beneficial to merge different frequency channels, it requires extra effort to refer all measurements to a common spatial resolution. Therefore, the capability to enhance the spatial resolution of a single channel is of special interest. In this study, a new numerical procedure to get superresolution microwave scanning radiometer measurements is presented. The approach is physically based on the occurrence of multiple partially correlated measurements. Mathematically, the approach is equivalent to a linear inversion problem, and its solution is pursued by means of a superresolution numerical procedure based on the Tikhonov regularization method. A set of numerical examples illustrates the results of the study in which hypothetical scanning microwave radiometer sensor configuration and reference test cases have been considered. [J843]

## "Assessment of Recent Short-Term Water-Level Fluctuations in Caspian Sea Using Topex/Poseidon"

The Caspian Sea (CS) has long been the focus of an interest due to its large water-level fluctuations. The primary factors of the CS water-level variations have usually been deemed to changes in climatic parameters. The climate-induced changes particularly in precipitation over the Volga River catchment and evaporation over CS mainly affect the CS level (CSL). We constructed extended and refined TOPEX/Poseidon time series to compute temporal mean water-level fluctuations from December 1992 to August 2005 over CS using the new gravity recovery and climate experiment orbits data, new sea state bias model, and TOPEX microwave radiometer drift correction. Four distinct phases in water-level variations are observed: a significant water-level rise between 1993 and mid-1995 followed by an abrupt decline from mid-1995 to summer 1997, then relatively modest decrease until mid-2002 and rise from summer 2002 onward. The analysis of water budget parameters favors the recent understanding that Volga River discharge in conjunction with evaporation over CS are the two main components controlling water-level fluctuations of CS. Volga River discharge positively correlates with CS water-level rise and drop from 1993 to 1997 and in 1999, respectively. Evaporation should dominate over the Volga River runoff and primarily controls CSL fluctuations after 1997 through 2003. Additionally, we find that anthropogenic factors are insufficient to affect water-level oscillations except for reservoir development or demolition, and water-level changes during 13-year time series are temporary variations. [J844]

## "Averaging and Formulation Impact on GB-SAR Topographic Mapping"

A novel processor for the generation of a digital terrain model (DTM) using ground-based synthetic aperture radar (GB-SAR) imagery is presented. The performance of the processor has been assessed using the archive of C-band GB-SAR images available at the Joint Research Centre from the Sion Valley (CH) test site, from which a high-resolution ground-truth DTM is available. In order to reduce the standard deviation of the differences between the two DTMs, several techniques have been applied: interferogram averaging, phase referencing, and differential path calibration. In addition, different formulations have been reviewed, and its impact has been quantified in the DTM accuracy obtained. Results show that the standard deviation of the differences between the ground-truth DTM and that of the C-band GB-SAR can be reduced from the 5 m that was previously reported down to 3 m with the new processor. [J845]

## "Sifting Through the Jungle of Sensor Standards"

The domain of sensors is still a wild jungle in which nothing is quite standardized. To fix this, we need a device standard to characterize physical and electrical features and constraints, describe necessary data processing and message parsing procedures, and, more importantly, enable automatic device integration into the world of computers we already have. This paper highlights five standards, some of which are labeled "device," "sensor," or "transducer," but all of them are equally capable of describing devices. If sensors are considered as simple or primitive devices, it follows that all five standards are also capable of describing sensors. No distinction between sensors and devices are done here. [J846]

## "Theory and Application of Motion Compensation for LFM-CW SAR"

Small low-cost high-resolution synthetic aperture radar (SAR) systems are made possible by using a linear frequency-modulated continuous-wave (LFM-CW) signal. SAR processing assumes that the sensor is moving in a straight line at a constant speed, but in actuality, an unmanned aerial vehicle (UAV) or airplane will often significantly deviate from this ideal. This nonideal motion can seriously degrade the SAR image quality. In a continuous-wave system, this motion happens during the radar pulse, which means that existing motion compensation techniques that approximate the position as constant over a pulse are limited for LFM-CW SAR. Small aircraft and UAVs are particularly susceptible to atmospheric turbulence, making the need for motion compensation even greater for SARs operating on these platforms. In this paper, the LFM-CW SAR signal model is presented, and processing algorithms are discussed. The effects of nonideal motion on the SAR signal are derived, and new methods for motion correction are developed, which correct for motion during the pulse. These new motion correction algorithms are verified with simulated data and with actual data collected using the Brigham Young University muSAR system. [J847]

## "A Physical Full-Resolution SAR Ship Detection Filter"

Synthetic aperture radar (SAR) ship detection is an important application in the context of environment and security monitoring. It allows monitoring traffic, fisheries, and associating ships with oil discharge over wide areas with high spatial resolution almost independently from weather conditions and both day and night time. Since full-resolution SAR images are heavily affected by the presence of speckle, ship detection algorithms generally employ speckle reduced SAR images at the expense of a degradation of the spatial resolution. A new physical approach, which considers ships as dominant scatterers and, therefore, responsible for a strong and coherent backscattered signal, is here proposed. Based on this rationale, a new simple and very effective filtering

technique, which is able to process full-resolution SAR images, has been conceived and implemented. Experiments, accomplished over C-band European Remote Sensing satellite (ERS) 1/2 single-look complex SAR images, show the effectiveness of the proposed approach. [J848]

## "Angular and Radiometric Resolution of Y-Shaped Nonuniform Synthetic Aperture Radiometers for Earth Observation"

MIRAS is the single payload of the European Space Agency's Soil Moisture and Ocean Salinity (SMOS) satellite mission, and it will be the first synthetic aperture radiometer for Earth observation from space. It consists of an array of 69 antennas uniformly spaced along three arms forming a Y-shaped antenna array. This work analyzes the angular resolution improvement, and the radiometric performance degradation when the spacing between antennas is geometrically increased. [J849]

## "Conditioning Water Stages From Satellite Imagery on Uncertain Data Points"

Observed spatially distributed water stages with uncertainty are of considerable importance for flood modeling and management purposes but are difficult to collect in the field during a flood event. Synthetic aperture radar (SAR) remote sensing offers an inviting alternative to provide this kind of data. A straightforward technique to derive water stages from a single SAR flood image is to extract heights from a digital elevation model at the flood boundaries. Schumann et al. have presented a regression modeling approach as an improvement to this simple technique. However, regression modeling associated with their model may restrict output to mapping purposes rather than extend it to integration with other data or models. This letter introduces an inviting alternative that conducts statistical analysis on river cross-sectional data points, thereby allowing uncertainty assessment of remote-sensing-derived water stages without any regression modeling constraint. This renders remote-sensing data fit for, e.g., flood inundation model evaluation with uncertainty in observations and data assimilation studies, where (linear) ldquotransformation,rdquo i.e., modeling, to observed data should be minimal. [J850]

## "Doppler Keystone Transform: An Approach Suitable for Parallel Implementation of SAR Moving Target Imaging"

In this letter, a synthetic aperture radar (SAR) data reformatting approach named Doppler keystone transform (DKT) is proposed to correct the range migration of a moving target. By using the DKT, the SAR imaging program, i.e., the 2-D matched filtering, can be transformed into separate 1-D operations along range or azimuth direction, and therefore, the DKT is suitable for the parallel implementation of SAR imaging of the moving target. Our simulations show that by combining the DKT and the Doppler phase compensation methods, the moving target can be well imaged in high signal-clutter-ratio case. [J851]

## "Level Set Method for SAR Image Coregistration"

In this letter, a novel approach for the coregistration of synthetic aperture radar (SAR) images is proposed based on the level set method. The features of regions are detected by segmenting the images, and the images are coregistered by matching the detected features. The energy functional of level sets is formulated with respect to detecting and matching features. The coregistration is achieved by minimizing the energy functional. Compared with the conventional tie-patch method, the results on a series of simulated experiments and real SAR data demonstrate the feasibility of the proposed approach. [J852]

## "Using Multibaseline InSAR to Recover Layovered Terrain Considering Wideband Array Problem"

This letter deals with the problems of retrieving height and synthetic aperture radar (SAR) reflectivity of layovered terrain using multibaseline SAR interferometry (InSAR). In particular, we focus on the wideband array problem caused by practically large InSAR arrays and high-resolution SAR images, i.e., the problem of signal envelope misalignment, which is neglected in the work by Gini We propose two methods to eliminate or mitigate the effect of envelope misalignment, one called the aligning method and the other called the joint range cell processing method. In the aligning method, we align each signal envelope for each searched height of the layovered components (i.e., ground resolution cells with different altitudes) during searching procedure. The joint range cell processing method jointly processes the neighboring cells in range to estimate the parameters of layovered components so that the effect of the envelope misalignment can be mitigated. Theoretical analysis and computer simulation results show that both methods have the ability to provide accurate estimation of the heights and radar reflectivities of multiple layovered resolution cells in the presence of large envelope misalignments. [J853]

## "Ground Moving Target Indication With Tandem Satellite Constellations"

Ground moving target indication (GMTI) from space by existing dual-channel radar systems such as TerraSAR-X and RADARSAT-2 has been shown to perform only insufficiently with respect to the relocation error of targets to their true ground position. Only two parallel receiver channels are too little to suppress the severe ground clutter and to estimate the target's parameters. Although this deficiency may partly be alleviated through antenna aperture switching, the resulting positioning accuracy is still not adequate for effective traffic monitoring purposes. Satisfactory results are only achievable with extended apertures, primarily with satellite constellations. This letter presents a statistical analysis of the performance of different concepts for cooperating back-to-back flying satellite systems. Particularly in anticipation of TanDEM-X, which will form the first operational GMTI-capable coherent synthetic aperture radar constellation after its launch in 2009. [J854]

## "Image-Quality Focusing of Rotating SAR Targets"

Synthetic aperture radar (SAR) is a popular tool for long-range imaging of stationary ground objects. Moving targets in the imaged scene will have a mismatch to the matched filter in the image formation process, thus degrading target image quality. In this letter, the impact of uncompensated target rotation in SAR imagery is studied. An efficient algorithm for image-quality-based target rotation correction is proposed. [J855]

## "On the Mueller Scattering Matrix for SAR Sea Oil Slick Observation"

In this letter, a fully polarimetric electromagnetic model for sea surface Mueller matrix is exploited to characterize the scattering from oil and biogenic slicks, under low-to-moderate wind conditions. The model predicts a completely different scattering mechanism for oil-covered and oil-free sea surface, while biogenic slicks are indistinguishable from sea surface in terms of polarimetric scattering. Following this theoretical rationale, a simple and very effective filtering technique is proposed for synthetic aperture radar (SAR) sea oil slick observation. Experiments, accomplished over C-band multilook complex SIR-C/X-SAR data, show the effectiveness of the proposed model and the capabilities of the filter to both observe oil slicks and distinguish them from biogenic look-alikes. [J856]

## "3-D SAR Tomography: The Multibaseline Sector Interpolation Approach"

Multibaseline (MB) synthetic aperture radar (SAR) tomography is a promising mode of SAR interferometry, allowing full 3-D imaging of volumetric and layover scatterers in place of a single elevation estimation capability for each SAR cell However, Fourier-based MB SAR tomography is generally affected by unsatisfactory imaging quality due to a typically low number of baselines with irregular distribution. In this paper, we improve the basic elevation focusing technique by reconstructing a set of uniform baselines data exploiting in the interpolation step the ancillary information about the extension of a height sector which contains all the scatterers. This aprioriinformation can be derived from the knowledge of the kind of the observed scenario (e.g., forest or urban). To demonstrate the concept, an imaging enhancement analysis is carried out by simulation. [J857]

## "Improved Space-Based Moving Target Indication via Alternate Transmission and Receiver Switching"

Ground moving target indication (GMTI) by space-based radar systems requires special antenna and data acquisition concepts to overcome the problem of discriminating target signals from clutter returns. Owing to the high satellite speed, the clutter contains a broad mixture of radial velocities within the antenna beam, leading to a large Doppler spread. Effective clutter suppression can solely be achieved by multiple aperture or phase center antennas. For space-based systems, however, the number of receiver channels connected to subapertures is very limited due to their weight, volume, and high data rates (current systems such as TerraSAR-X and RADARSAT-2 possess only two). This classical along-track interferometry architecture, in which the antenna is split into two halves, achieves only suboptimum GMTI performance. This paper presents and statistically analyzes an innovative approach to create additional independent phase centers to improve the GMTI performance considerably. The extra degrees of freedom are created by cyclical phase and amplitude switchings of the transmit/receive modules for transmitter and receiver between pulses, hence trading Doppler bandwidth for extra spatial diversity. In the first part of this paper, different strategies of spatial-temporal diversity are introduced and analyzed for realistic system parameters with respect to ambiguities and detection performance. The second part is concerned with the elaborate theoretical analysis of the relocation improvement for the spatial diversity approach. [J858]

## "Model-Based Polarimetric SAR Speckle Filter"

In this paper, a new framework to filter speckle noise in polarimetric synthetic aperture radar (PolSAR) data is presented. The proposed filter, named the model-based PolSAR (MBPolSAR) filter, is based on exploiting the multiplicative-additive speckle noise model for multidimensional SAR data. The entries of the sample covariance

matrix are processed according to this multiplicative-additive speckle noise model as a function of the complex correlation coefficient. Hence, the covariance matrix elements are processed differently. This filtering scheme improves the reduction of speckle noise and ameliorates the estimation of the polarimetric information. The filtering performances of the MBPolSAR approach are first tested quantitatively by means of simulated PolSAR data. In a second stage, they are evaluated by means of experimental SAR data acquired by the Deutsches Zentrum fu umlr Luft-und Raumfahrt. [J859]

## "Efficient FFT-Accelerated Approach to Invariant Optical-LIDAR Registration"

This paper presents a fast Fourier transform (FFT)-accelerated approach designed to handle many of the difficulties associated with the registration of optical and light detection and ranging (LIDAR) images. The proposed algorithm utilizes an exhaustive region correspondence search technique to determine the correspondence between regions of interest from the optical image with the LIDAR image over all translations for various rotations. The computational cost associated with exhaustive search is greatly reduced by exploiting the FFT. The substantial differences in intensity mappings between optical and LIDAR images are addressed through local feature mapping transformation optimization. Geometric distortions in the underlying images are dealt with through a geometric transformation estimation process that handles various transformations such as translation, rotation, scaling, shear, and perspective transformations. To account for mismatches caused by factors such as severe contrast differences, the proposed algorithm attempts to prune such outliers using the random sample consensus technique to improve registration accuracy. The proposed algorithm has been tested using various optical and LIDAR images and evaluated based on its registration accuracy. The results indicate that the proposed algorithm is suitable for the multimodal invariant registration of optical and LIDAR images. [J860]

## "Observing and Modeling Multifrequency Scattering of Maize During the Whole Growth Cycle"

The objective of this paper is to carry out a systematic investigation about the sensitivity of radar to maize crop growth and soil moisture by considering a wide range of frequencies and angles and all linear polarizations. We show the results of a correlation study carried out on the data collected on a maize field at Suberg, in the Swiss region named Central Plain, by the multifrequency RAdio ScAtteroMeter (RASAM). This agricultural field was monitored over a long period of time at a wide range of frequencies and observation angles so that the correlation between the backscattering and crop height and the biomass and soil moisture was studied under several plant and observation conditions. Moreover, we describe some recent refinements applied to the vegetation scattering model developed at Tor Vergata University, Rome, Italy, and we evaluate the accuracy of extended comparisons between model outputs and RASAM signatures. The Tor Vergata model is finally applied to give a theoretical basis to the experimental correlation findings. [J861]

## "Particle Filtering Based Approach for Landmine Detection Using Ground Penetrating Radar"

In this paper, we present an online stochastic approach for landmine detection based on ground penetrating radar (GPR) signals using sequential Monte Carlo (SMC) methods. The processing applies to the two-dimensional B-scans or radargrams of 3-D GPR data measurements. The proposed state-space model is essentially derived from that of Zoubir etal., which relies on the Kalman filtering approach and a test statistic for landmine detection. In this paper, we propose the use of reversible jump Markov chain Monte Carlo in association with the SMC methods to enhance the efficiency and robustness of landmine detection. The proposed method, while exploring all possible model spaces, only expends expensive computations on those spaces that are more relevant. Computer simulations on real GPR measurements demonstrate the superior performance of the SMC method with our modified model. The proposed algorithm also considerably outperforms the Kalman filtering approach, and it is less sensitive to the common parameters used in both methods, as well as those specific to it. [J862]

## "Imaging of Micromotion Targets With Rotating Parts Based on Empirical-Mode Decomposition"

For micromotion targets with rotating parts, the inverse synthetic-aperture-radar image of the main body may be shadowed by the micro-Doppler. To solve this problem, this paper proposes an imaging algorithm based on the complex-valued empirical-mode decomposition. First, the radar echoes are decomposed into a series of complex-valued intrinsic-mode functions (IMFs). Then, the IMFs from the rotating parts and those from the main body are separated according to the characteristics of their zero-crossings. Finally, the well-focused imaging of the main body via traditional imaging algorithm and the accurate parameter estimation of the rotating part can be obtained. Both the imaging results for the simulated and measured data are given to verify the validity of the proposed algorithm. [J863]

## "On the Exploitation of Target Statistics for SAR Interferometry Applications"

This paper focuses on multiimage synthetic aperture radar interferometry (InSAR) in the presence of distributed scatterers, paying particular attention to the role of target decorrelation in the estimation process. This phenomenon is accounted for by splitting the analysis into two steps. In the first step, we estimate the interferometric phases from the data, whereas in the second step, we use these phases to retrieve the physical parameters of interest, such as line-of-sight (LOS) displacement and residual topography. In both steps, we make the hypothesis that target statistics are at least approximately known. This approach is suited both to derive the performances of InSAR with different decorrelation models and for providing an actual estimate of LOS motion and topography. Results achieved from Monte Carlo simulations and a set of repeated pass ENVISAT images are shown. [J864]

## "Ocean Surface Currents From AVHRR Imagery: Comparison With Land-Based HF Radar Measurements"

We focus on inverting the surface temperature (or heat) equation to obtain the surface velocity field in the coastal ocean and compare the results with those from the maximum cross correlation (MCC) technique and with the insituvelocity fields measured by the Rutgers University Coastal Ocean Dynamics Radar (CODAR). When compared with CODAR fields, velocities from the heat equation and MCC have comparable accuracies, but the heat equation technique better resolves the finer scale flow features. We use the results to directly calculate the surface divergence and vorticity. This is possible because we convert the traditionally underdetermined heat inversion problem to an overdetermined one without constraining the velocity field with divergence, vorticity, or energy statements. Because no aprioriassumptions are made about the vorticity, it can be calculated directly from the velocity results. The derived vorticity field has typical open-ocean magnitudes ( ~ 5 times 10-5/s) and exhibits several structures (a warm core ring, Gulf Stream filament, and a diverging flow) consistent with the types of flows required to kinematically deform the sea surface temperature patterns into the observed configurations. [J865]

## "Squint LFMCW SAR Data Processing Using Doppler-Centroid-Dependent Frequency Scaling Algorithm"

A linear frequency-modulated continuous-wave (LFMCW) synthetic aperture radar (SAR) is a highly miniaturized SAR that is suitable for use on a small unmanned aerial vehicle. In squint stripmap mode, the LFMCW SAR image quality is degraded by the presence of nonlinearities in the transmitted signal, combined with the large bandwidth introduced by the frequency scaling in the nonlinear frequency scaling (NLFS) algorithm. This paper proposes an extension of the NLFS algorithm called the Doppler-centroid-dependent frequency scaling algorithm. The algorithm introduces a new Doppler-centroid-dependent scaling factor to decrease the introduced bandwidth, effectively removing the range frequency aliasing, without extra computational load. Nonlinearity correction is performed at the same time as range cell migration correction. The validity of the proposed algorithm is demonstrated with point target simulation results. [J866]

## "A GB-SAR Processor for Snow Avalanche Identification"

An algorithm for the automatic detection and classification of snow avalanches has been developed and assessed through the archive of synthetic aperture radar (SAR) images acquired during six winter campaigns with a ground-based linear SAR. The scheme, based on the following classic steps: 1) detection; 2) features extraction; and 3) object classification, is fully described in this paper, representing the first attempt to implement a semiautomatic near-real-time operational snow avalanche monitoring tool by SAR. Detection of possible avalanche events is performed by the combined application of thresholding and morphological filters to the differential coherence of consecutive images. Classification of events likely to be snow avalanches is based on statistics extracted from the whole image and features associated to the single regions. Tests have been conducted over more than 60 000 images. Results show a drastic reduction on the images to manually supervise (2.2%). With a 9% false-negative rate and 60% accuracy over the 2.2% of images to examine, the processor represents an interesting support tool for the daily operations of avalanche risk assessment in a commercial ski resort. [J867]

## "Feature Extraction and Discriminator Design for Landmine Detection on Double-Hump Signature in Ultrawideband SAR"

An air- or vehicleborne ultrawideband synthetic aperture radar (UWB SAR) has ground penetrating capability, which provides a sufficient approach to detect landmines over wide areas from a safe standoff distance. In this paper, a support vector machine (SVM) with hypersphere classification boundary, which is referred to as HyperSphere-SVM (HS-SVM), using a hidden Markov model (HMM) kernel on the feature vector extracted by a

postfilter-based method is proposed for landmine detection. The postfilter-based method can extract the feature containing not only the amplitude but also the amplitude varying information of the double-hump signature of metallic and plastic landmines. Compared with simple kernels, e.g., the Gaussian kernel, the HMM kernel employs the state-transition information in the extracted feature into the discrimination procedure and, thus, can improve detection performance. The proposed postfilter-based feature extraction method and the HMM kernel HS-SVM are verified on the field data collected by a UWB SAR system in different scenarios. [J868]

## "LABVIEW graphical user interface for precision multichannel alignment of Raman lidar at Jet Propulsion Laboratory, Table Mountain Facility"

The Jet Propulsion Laboratory operates lidar systems at Table Mountain Facility (TMF), California (34.4°N, 117.7°W) and Mauna Loa Observatory, Hawaii (19.5°N, 155.6°W) under the framework of the Network for the Detection of Atmospheric Composition Change. To complement these systems a new Raman lidar has been developed at TMF with particular attention given to optimizing water vapor profile measurements up to the tropopause and lower stratosphere. The lidar has been designed for accuracies of 5% up to 12 km in the free troposphere and a detection capability of 5ppmv. One important feature of the lidar is a precision alignment system using range resolved data from eight Licel transient recorders, allowing fully configurable alignment via a LABVIEW/C++ graphical user interface (GUI). This allows the lidar to be aligned on any channel while simultaneously displaying signals from other channels at configurable altitude/bin combinations. The general lidar instrumental setup and the details of the alignment control system, data acquisition, and GUI alignment software are described. Preliminary validation results using radiosonde and lidar intercomparisons are briefly presented. [J869]

## "Effect of standing stubble on radar backscatter from harvested rice fields"

The radar backscatter from standing rice stubble in a harvested rice field is computed numerically using the method of moments with the equivalence principle and impedance sheet theory. The radar backscatter from a bare surface is also computed based on an empirical model, and combined with the numerical results from the standing rice stubble. Based on the analyses of the radar backscatter for various conditions of standing stubble, it is found that the effect of the standing stubble in a typical harvested rice field is negligible when the water content of the stubble is less than about 40%. [J870]

## "Snow Facies Over Ice Sheets Derived From Envisat Active and Passive Observations"

This paper aims to separate different snow regions over the terrestrial ice sheets based on their measured microwave signatures. It takes advantage of coregistered data from passive and active sensors on the Environmental Satellite (Envisat) to directly derive a snow facies indicator in a point-by-point basis. This paper represents the first attempt of this kind in exploiting nadir-viewing and dual-frequency data from both altimeter and radiometer sensors. The approach is based on a clustering method. Such representation of the data by means of fewer clusters necessarily loses fine details but achieves simplification in geographical representation and eases the description of the condition of the ice sheets in 2004. Our approach broadens the description of the snow pack by taking into account characteristics such as surface roughness, grain size, stratification, and snowmelt effects, whereas the latter has often solely been considered in most previous work. Such partition of the ice sheets might help to better understand relationships between microwave signatures and snow morphology. It could also be useful for estimating elevation uncertainty in altimeter data, which, in turn, is essential to correctly interpret the significance of the rates of elevation change in a changing climate and to convert elevation change to snow mass change. [J871]

## "Comparing Scatterometric and Radiometric Simulations With Geophysical Model Functions to Tune a Sea Wave Spectrum Model"

A unified approach to simulate both microwave radiometric and scatterometric observations over a sea surface based on the two-scale electromagnetic scattering model has been implemented. The simulations have been compared with empirically derived geophysical model functions (GMFs) for the purpose of tuning the electromagnetic forward model and the embedded sea surface characterization and wave spectrum. The comparison has concerned a large number of wind speeds, frequencies, and observation angles for both the passive and active cases. Two widely adopted literature spectra have been used as benchmarks. A new expression for the hydrodynamic modulation function has been developed too. The proposed new spectrum has allowed us to reproduce both the passive and active GMFs' behaviors fairly well, generally improving the agreement yielded by literature models, particularly for scatterometric simulations. [J872]

## "Surface-Tracing-Based LASAR 3-D Imaging Method via Multiresolution Approximation"

This paper concerns the surface-tracing-based (STB) linear-array synthetic-aperture-radar (LASAR) 3-D imaging technique. The basic idea of this technique is to consider the 3-D SAR imaging problem as tracing a surface in the low height-resolution level. The STB 3-D imaging technique first initiates a low-resolution digital elevation map (DEM) using 3-D backprojection (BP) algorithm, predicts a higher resolution DEM from the known elevation using multivariate-interpolation technique, searches from the predicted elevation and obtains a higher resolution DEM, then repeats the prediction and searching recursively and obtains the fine-resolution DEM finally. By converting the 3-D LASAR imaging problem to a 2-D surface-tracing problem, the STB 3-D imaging technique can reduce the computational complexity by one order. The computational cost of STB 3-D imaging technique is analyzed, and we find out that the computational cost of STB 3-D LASAR imaging technique is determined by the surface prediction error and the fluctuation of ground. In particular, for normal distribution, when one of the earlier two factors is small, the computational cost is proportional to the other factor approximately. Finally, a new STB 3-D BP algorithm that implements the surface-prediction operation via multiresolution-approximation (MRA) technique (named as MRA 3-D BP algorithm) is presented. By operating the interpolation in frequency domain, the computational cost of MRA algorithm for sparse LASAR is near to that of RD algorithm for full-element LASAR. [J873]

## "Estimation of Urban Green Volume Based on Single-Pulse LiDAR Data"

Estimating urban green volume is getting more and more important within the frame of an ecologically orientated city planning and environmentally sustainable development. The first and the last pulse of airborne Light Detection and Ranging (LiDAR) data provide the basis for the estimation of green volume, but these optimal data are not always available, particularly for urban areas. That is why this paper deals with the question whether LiDAR data (last pulse only) that have not been taken during the vegetation period allow a sufficient estimation of the green volume. This paper sets up on previous results where LiDAR data have been compared to photogrammetrically determined vegetation height measurements. The subtraction of the laser-based Digital Terrain Model and Digital Surface Model in vegetated areas leads to a vast underestimation of green volume of up to 85%, which is mainly due to the standing deciduous trees with an underestimation of 90%. Starting from the existence of different laser response characteristics of various vegetation types, the relative point density and the normalized height of classified nonground points were analyzed in depth. The results show a good separation of different vegetation types. Furthermore, a pragmatic approach of reconstruction of the underestimated vegetation (mainly deciduous trees) is carried out by generating cylinders for the classified nonground points to compensate the volume loss. The point density of nonground points and the normalized height of the laser responses were used to regulate the adaptive cylinder construction based on fuzzy logic techniques. Using reference data, the accuracy could be estimated. In spite of the suboptimal LiDAR data, this paper leads to a sufficiently exact and efficient estimation of green volume compared to the costly conventional methods like field investigations. The method makes a contribution in the field of data improvement and is applicable to similar LiDAR data of other areas. [J874]

## "CloudSat's Cloud Profiling Radar After Two Years in Orbit: Performance, Calibration, and Processing"

The Cloud Profiling Radar, the sole science instrument of the CloudSat Mission, is a 94-GHz nadir-looking radar that measures the power backscattered by hydrometeors (clouds and precipitation) as a function of distance from the radar. This instrument has been acquiring global time series of vertical cloud structures since June 2, 2006. In this paper, an overview of the radar performance and status, to date, is provided together with a description of the basic data products and the surface clutter rejection algorithm introduced for the Release 04 data product release. [J875]

## "Characterizing Bidimensional Roughness of Agricultural Soil Surfaces for SAR Modeling"

In the description of agricultural soil roughness, the hypothesis of surface isotropy is currently admitted, and linear measurements are often used to characterize the soil roughness considered as a single-scale process. However, multiscale roughness is frequently observed, and tillage practices created oriented roughness. This paper presents a new technique to measure precisely the bidimensional soil roughness. Digital elevation model derived using photogrammetric technique reproduces the millimeter-scale height variations of three different soil surfaces (ploughed, smoothed, and row structured field) over about 8 m2. A single surface measurement is sufficient to accurately measure the soil roughness parameters. Geostatistic parameterization allows the measurement of the roughness anisotropy. For smooth surface, a two-scale roughness is observed. Anisotropy is observed in the larger scale roughness. The proposed method allows the computation of the bidimensional correlation function, which is required by the integral equation method model for the simulation of the SAR signal over anisotropic soil surfaces. [J876]

## "Algorithm to Retrieve Aerosol Optical Properties From High-Spectral-Resolution Lidar and Polarization Mie-Scattering Lidar Measurements"

We developed an algorithm to estimate the vertical profiles of extinction coefficients at 532 nm for three aerosol types that are water-soluble, soot, and dust particles, using the extinction and backscattering coefficients at 532 nm for total aerosols derived from high-spectral-resolution lidar (HSRL) measurements and the receiving signal at 1064 nm and total depolarization ratio at 532 nm measured with Mie scattering lidar (MSL). The mode radii, standard deviations, and refractive indexes for each aerosol component are prescribed by the optical properties of aerosols and clouds database; the optical properties for each aerosol component are computed from Mie theory on the assumption that their particles are spherical and homogeneous, except for dust. To consider the effect of nonsphericity, the dust lidar ratio at 532 nm is assumed to be 50 sr, the value that is reported for Asian dust from the other observational studies. We performed sensitivity study on retrieval errors. The errors in extinction coefficient for each aerosol component were smaller than 30% and 60% when the measurement errors were plusmn5% and plusmn 10%. We demonstrated the ability of the algorithm by applying to the HSRL + MSL data measured at Tsukuba, Japan. Plumes consisting of water-soluble aerosols, soot, dust, or their mixture were retrieved; these results were consistent with simulation with a global aerosol transport model. Introducing the dust lidar ratio significantly improved a correlation between the retrieved dust concentration and the aerosol depolarization ratio at 532 nm derived from HSRL + MSL than the use of spherical dust optical model in the retrieval. [J877]

## "A C-Band Scatterometer Simultaneous Wind/Rain Retrieval Method"

Using collocated ERS scatterometer (ESCAT), Tropical Rainfall Measuring Mission (TRMM) Precipitation Radar (PR), and European Centre for Medium-Range Weather Forecasts (ECMWF) data, the effects of rain on ESCAT wind-only retrieval are evaluated. Additional scattering from rain causes estimated wind speeds to appear higher than expected. Selected directions of the rain-corrupted wind vectors are biased toward along-track directions under conditions of heavy rain, which is regardless of the true wind direction. Rain becomes more significant for data acquired at a high incidence angle. To compensate for rain-induced backscatter, a simultaneous wind/rain retrieval (SWRR) method, which simultaneously retrieves wind velocity and surface rain rate from ESCAT measurements with an incidence angle >40deg, is developed by using a C-band wind/rain backscatter model. The performance of SWRR under typical wind/rain conditions is evaluated through simulation and validation with collocated TRMM PR and ECMWF data sets. SWRR is shown to significantly improve wind velocity estimates, and the SWRR estimated surface rain rate has relatively high accuracy in moderate to heavy rain cases. Although SWRR-retrieved rain is somewhat biased, it can be corrected. We note that for ESCAT, about 1.5% of all the collocated measurements is affected by significant rain. [J878]

## "Doppler Ambiguity Resolving in Compressed Azimuth Time and Range Frequency Domain"

For high-quality synthetic aperture radar (SAR) processing, Doppler centroid ambiguity resolving is an essential procedure. A novel method for the resolution of Doppler ambiguity is presented which exploits the fact that, in the compressed azimuth time and range frequency domain, all targets span the same range frequency bandwidth and exhibit the same slope which is just proportional to the Doppler ambiguity number. The slope is removed by interpolation so that a simplified Radon transform can be applied. The use of entropy to find the maximum concentration of the Radon-transformed image can improve the robustness of the method. The proposed method directly gives a reliable estimate of the Doppler ambiguity number and is not affected by the azimuth partially covered targets. Experimental results show that the proposed method works well in medium- to high-contrast scenes. [J879]

## "Multiapproach System Based on Fusion of Multispectral Images for Land-Cover Classification"

Satellite image classification is usually marked by several types of imperfection such as uncertainty, imprecision, and ignorance. Data fusion of additional sensors tries to overcome the types of imperfection by using probability, possibility, and evidence theories. Our approach will lead to improve classification accuracy of satellite images by choosing the optimum theory for a particular image context and proposing a theoretical framework based on a multiagent system and case-based reasoning. We validate our approach trough a set of optical images from the satellite Satellite Positioning and Tracking 4 and radar images from the European Remote Sensing satellite 2, and we show that the overall accuracy is considerably increased from 83% for maximum-likelihood classification applied to multispectral imagery to 94% with the proposed approach. [J880]

## "Interpretation of Multisensor Remote Sensing Images: Multiapproach Fusion of Uncertain Information"

Land cover interpretation using multisensor remote sensing images is an important task that allows the extraction of information that is useful for several applications. However, satellite images are usually characterized by several types of imperfection, such as uncertainty, imprecision, and ignorance. Using additional sensors can help improve the image interpretation process and decrease the associated imperfections. Fusion methods such as the probability, possibility, and evidence methods can be used to combine information coming from these sensors. An extensive literature has accumulated during the last decade to resolve the issue of choosing the best fusion method, particularly for satellite images. In this paper, we present a semiautomatic approach based on case-based reasoning (CBR) and rule-based reasoning, allowing intelligent fusion method retrieval. This approach takes into account the advantage of data stored in the case base, allowing a more efficient processing and a decrease in image imperfections. The proposed approach incorporates three modules. The first is a learning module based on evaluating three fusion methods (probability, possibility, and evidence) applied to the given satellite images. The second looks for the best fusion method using CBR. The last is devoted to the fusion of multisensor images using the method retrieved by CBR. We validate our approach on a set of optical images coming from the Satellite Pour l'Observation de la Terre 4 and radar images coming from European Remote Sensing Satellite 2 (ERS-2) representing a central Tunisian region. [J881]

## "Infrared Thermography for Buried Landmine Detection: Inverse Problem Setting"

This paper deals with an inverse problem arising in infrared (IR) thermography for buried landmine detection. It is aimed at using a thermal model and measured IR images to detect the presence of buried objects and characterize them in terms of thermal and geometrical properties. The inverse problem is mathematically stated as an optimization one using the well-known least-square approach. The main difficulty in solving this problem comes from the fact that it is severely ill posed due to lack of information in measured data. A two-step algorithm is proposed for solving it. The performance of the algorithm is illustrated using some simulated and real experimental data. The sensitivity of the proposed algorithm to various factors is analyzed. A data processing chain including anomaly detection and characterization is also introduced and discussed. [J882]

## "Scatterometer-Derived Soil Moisture Calibrated for Soil Texture With a One-Dimensional Water-Flow Model"

Current global satellite scatterometer-based soil moisture retrieval algorithms do not take soil characteristics into account. In this paper, the characteristic time length of the soil water index has been calibrated for ten sampling frequencies and for different soil conductivity associated with 12 soil texture classes. The calibration experiment was independently performed from satellite observations. The reference soil moisture data set was created with a 1-D water-flow model and by making use of precipitation measurements. The soil water index was simulated by applying the algorithm to the modeled soil moisture of the upper few centimeters. The resulting optimized characteristic time lengths Tincrease with longer sampling periods. For instance, a Tof 7 days was found for sandy soil when a sampling period of 1 day was applied, whereas an optimized T-value of 18 days was found for a sampling period of 10 days. A maximum rmse improvement of 0.5% vol. can be expected when using the calibrated T-values instead of T= 20. The soil water index and the differentiated T-values were applied to European Remote Sensing (ERS) satellite scatterometer data and were validated against insitusoil moisture measurements. The results obtained using calibrated T-values and T= 20 did not differ ( r= 0.39, rmse = 5.4% vol.) and can be explained by the averaged sampling period of 4-5 days. The soil water index obtained with current operational microwave sensors [Advanced Wind Scatterometer (ASCAT) and Advanced Microwave Scanning Radiometer-Earth Observation System] and future sensors (Soil Moisture and Ocean Salinity and Soil Moisture Active Passive) should benefit from soil texture differentiation, as they can record on a daily basis either individually or synergistically using several sensors. The proposed differentiated characteristic time length enables the continuation of the soil water index of sen--sors with varying sampling periods (e.g., ERS-ASCAT). [J883]

## "Parametric Velocity Synthetic Aperture Radar: Multilook Processing and Its Applications"

Based on a parametric model and some optimum methods, it has been previously proved that parametric velocity synthetic aperture radar (VSAR) may improve the performances of moving target detection and parameter estimation simultaneously. In this paper, multilook processing is studied for parametric VSAR. At first, statistical signal models are established for azimuth multilook processing (AMLP) and range multilook processing (RMLP), respectively. By combining the multiple AMLP sublook pixel vectors, it is shown that the clutter parameter estimation accuracy can be further improved via the maximum-likelihood estimation methods. Meanwhile, based on the adaptive implementation for the optimum processing of VSAR, RMLP can be used to improve slowly moving target detection performance via the noncoherent integration of multiple range sublooks. Furthermore, it is shown that the Doppler frequencies of moving targets vary linearly with different range sublooks due to the different carrier frequencies of sublooks. Therefore, based on a proposed novel two-step multilook diversity (TS-

MLD) estimator for RMLP, the "azimuth location ambiguity" of VSAR can be well resolved via least squares linear regression, without configuration change of the conventional VSAR. Also, the estimation accuracy of target's unambiguous Doppler frequency, as well as target's azimuth location, is derived for the proposed TS-MLD method. Finally, numerical experiments and scene simulations are provided to demonstrate the effectiveness of the proposed multilook-based methods. [J884]

## "Sea-Surface Polarization Ratio From Envisat ASAR AP Data"

The polarization ratio (VV/HH) of normalized radar cross section over ocean surface is processed from Envisat Advanced Synthetic Aperture Radar (ASAR) alternating polarization (AP) data and compared with existing electromagnetic (EM) scattering models. The processing of the AP data is based on Level0 (raw data) product that enables us to accurately compute the contribution from additive noise separately from each burst. This is important in estimating the correct polarization ratio, particularly at higher incidence angles where the relative contribution from noise becomes severe. A recently published EM scattering model, general curvature method (GCM), is extended here to incorporate scattering from breaking waves. The performance of this model with and without breaking waves is compared with AP data and with other models for the polarization ratio. The extended GCM model is furthermore used to assess the performance of wind speed retrieval in HH polarization. The inclusion of wave breaking in the GCM model reduces the polarization ratio standard deviation from 0.64 to 0.50 and the bias from -0.34 to 0.16, as compared to the measured ASAR AP polarization ratio. The best semiempirical model from literature gives 0.51 and 0.63 for the standard deviation and bias, respectively. The difference in performance is shown to be caused by the wind speed dependence not accounted for in the semiempirical model. Validation of the new polarization ratio model in combination with C-band Model Function (CMOD) for wind speed retrieval at HH polarization shows similar performance as at VV polarization. We conclude that the GCM polarization ratio model incorporating wave-breaking effects is found to reproduce well polarization ratio measurements (ASAR AP) versus wind vector and incidence angle. [J885]

## "High-Resolution and Real-Time Three-Dimensional Imaging Algorithm With Envelopes of Spheres for UWB Radars"

Ultrawideband pulse radars have a great potential for high-range resolution in near field imaging and can be used for noncontact measuring in precision or specular products such as reflector antennas and aircraft fuselages. We have already proposed a high-speed 3-D imaging algorithm, SEABED, which is based on a reversible transform, which is the boundary scattering transform, between the received signals and the target shape. However, the estimated image with SEABED is unstable with random noise because it utilizes a derivative of the received data. In this paper, we propose a robust 3-D imaging algorithm with an envelope of spheres that completely resolves the instability due to derivative operations. Moreover, to enhance the resolution of estimated images, this method is combined with a direct waveform compensation method that does not sacrifice high-speed calculation. Numerical simulations and an experiment confirm that the proposed method can realize fast, robust, and high-resolution 3-D imaging for arbitrary targets. [J886]

## "Phase Synchronization and Doppler Centroid Estimation in Fixed Receiver Bistatic SAR Systems"

This paper discusses temporal and phase synchronization in bistatic synthetic aperture radar (SAR) systems that use orbital sensors as coherent sources of opportunity and receivers at a fixed location. The discussion is particularized to SAR Bistatic Receiver for INterferometric Applications (SABRINA), a ground-based bistatic receiver that uses ENVISAT and ERS-2 as transmitters. Transmitter-receiver synchronization is hindered by the presence of independent reference oscillators at the transmit and receive end and by the lack of a common time frame. Phase synchronization and pulse alignment are achieved using a dedicated channel that receives a clean signal directly from the satellite. How to align the acquired data with the satellite orbit and how to estimate the Doppler centroid (DC) are studied. It is shown that in the bistatic configuration considered, the receiver provides an implicit control point which limits the negative impact of a DC misestimation on the resulting images. An algorithm to achieve this temporal alignment using the apparent phase history of the received pulses is proposed. Finally, this algorithm is validated through Monte Carlo simulations and experimental data acquired by SABRINA. [J887]

## "Forest Height Inversion Using High-Resolution P-Band Pol-InSAR Data"

In this paper, a high-resolution P-band Pol-InSAR data set acquired by the airborne RAMSES system over pine forest stands of different height is investigated. A significant penetration depth in all the polarimetric channels and a wide range of polarimetric phase center heights are observed, attesting of an interaction of the radar waves with different forest structural elements. The main objective of this paper concerns forest height inversion at P-band. First, forest-modeling assumptions are evaluated using aprioriinformation, such as ground-level and

forest height measurements. The full extend of the forest height is shown to be responsible of the volume decorrelation, and a significant orientation effect is clearly identified over the highest stands. As a consequence, the Oriented Volume over Ground model (OVoG) is determined to be the most appropriated model for the forest height inversion. At P-band, the ground contribution is present in all the polarimetric channels due to the important penetration at this frequency. To overcome this difficulty, a time-frequency optimization method based on sublook decomposition is developed to separate the pure ground and canopy contributions, allowing forest height estimation with OVoG with an rms error on the order of 2 m. In the last section of this paper, a sensitivity analysis of the inversion with respect to two important system parameters, the signal-to-noise ratio and the resolution, is presented, leading to a discussion on the inversion robustness in spaceborne conditions, where these system parameters are the most deteriorated as compared to airborne configurations. [J888]

## "Accuracy and Resolution of ALOS Interferometry: Vector Deformation Maps of the Father's Day Intrusion at Kilauea"

We assess the spatial resolution and phase noise of interferograms made from L-band Advanced Land Observing Satellite (ALOS) synthetic-aperture-radar (SAR) data and compare these results with corresponding C-band measurements from European Space Agency Remote Sensing Satellite (ERS). Based on cross-spectral analysis of phase gradients, we find that the spatial resolution of ALOS interferograms is 1.3times better than ERS interferograms. The phase noise of ALOS (i.e., line-of-sight precision in the 100-5000-m wavelength band) is 1.6times worse than ERS (3.3 mm versus 2.1 mm). In both cases, the largest source of error is tropospheric phase delay. Vector deformation maps associated with the June 17, 2007 (Father's day) intrusion along the east rift zone of the Kilauea Volcano were recovered using just four ALOS SAR images from two look directions. Comparisons with deformation vectors from 19 continuous GPS sites show rms line-of-site precision of 14 mm and rms azimuth precision (flight direction) of 71 mm. This azimuth precision is at least 4times better than the corresponding measurements made at C-band. Phase coherence is high even in heavily vegetated areas in agreement with previous results. This improved coherence combined with similar or better accuracy and resolution suggests that L-band ALOS will outperform C-band ERS in the recovery of slow crustal deformation. [J889]

## "A Numerical Method for Studying Modulation Effects in Radar Observations of the Sea Surface"

A numerical method for performing detailed investigations of modulation effects in sea backscattering is presented. The method is based on a combination of numerical hydrodynamic and electromagnetic codes as well as repeated simulations as the spectral content of the sea surface is varied. The results obtained can be useful in separating ldquotiltrdquo and hydrodynamic modulations in computed sea backscattering cross sections, and help to provide some insight into the need for ldquothree-scalerdquo modeling of sea surface returns. Sample results are presented to illustrate the basic process. [J890]

## "Inversion of Spaceborne X-Band Synthetic Aperture Radar Measurements for Precipitation Remote Sensing Over Land"

Several spaceborne X-band synthetic aperture radar (X-SAR) systems were launched in 2007, and more will be launched in the current decade. These sensors may significantly augment the sensors that comprise the global precipitation mission (GPM) constellation. X-SAR rainfall measurements may be beneficial particularly over land where rainfall is difficult to measure by means of satellite microwave radiometers. Inversion techniques to quantitatively derive precipitation fields over land at high spatial resolution are developed and illustrated in this paper. These inversion algorithms are the model-oriented statistical (MOS) methodology and the Volterra integral equation (VIE) approach. Simplified rain-cloud models are used to train and test the inversion algorithms by evaluating the expected error budget. Two case studies, using data obtained from measurements of SIR-C/X-SAR in 1994 over Bangladesh and the Amazon, are introduced, and retrieved precipitation maps are discussed. Even though no validation of the precipitation estimates was possible, the obtained results are encouraging, showing physically consistent retrieved structures and patterns. [J891]

## "From Glacier Facies to SAR Backscatter Zones via GPR"

We present a comparison between data acquired with frequency-modulated ground-penetrating radar (GPR) and satellite synthetic aperture radar (SAR). Both radars are polarimetric and operate at a center frequency of 5.3 GHz. The field site is the polythermal glacier Kongsvegen, Svalbard. Along glacier GPR profiles cover the ablation area and the accumulation area, where the latter consists of superimposed ice (SI) and firn. The glacier facies are clearly identifiable on the GPR profiles, although we show that the copolarized response is better for distinguishing different ice zones, whereas the SI-firn boundary is most obvious in the cross-polarized response. A calibrated backscatter coefficient is calculated for the GPR data and compared with the SAR backscatter

coefficient. The SAR zones are in very good agreement with the GPR-derived glacier facies. We show that, in the ablation area, the SAR response is dominated by backscatter from the previous summer surface. In the SI and firn areas, it is dominated by sources below the previous summer surface. [J892]

## "A Physical-Optics Model for Double-Bounce Scattering From Tree Stems Standing on an Undulating Ground Surface"

In this paper, a model for prediction of radar backscatter from coniferous forests in the VHF and UHF band is proposed. The model includes the double-bounce scattering originating from vertical stems standing on an undulating ground surface and is based on a physical-optics approach. The model can be used to assess the importance of ground topography in synthetic aperture radar (SAR) imagery of forests, and it is applicable to SAR systems using horizontally transmit and receive polarization (HH). The model was validated against data from the airborne SAR systems CARABAS-II and LORA. Precision measurements of ground topography and forest characterization at a single tree level were used as model input to simulate SAR images. The simulated images were compared to radar data in the frequency bands 22-82 and 225- 470 MHz, and it was found that the model could predict much of the variation in backscatter observed in images (R2= 0.44 and 0.65 at best, for the lower and higher frequency band, respectively), which should be compared to R2= 0.1 if the same model, but assuming a flat ground, was used. The results thus indicate that ground topography must be considered when predicting the variations in backscatter in the SAR images studied. The model did, however, fail to predict the absolute values of the backscattered intensity. The reason for the discrepancy is believed to be the value chosen for stem dielectric constant and unmodeled effects due to wave attenuation, tilting stems, and small-scale surface roughness. [J893]

## "Bispectral analysis of atmospheric radar signals"

The bispectral analysis techniques have been applied on signals received from the back-scattered signals by the MST radar. The results of this analysis are compared with that of the conventional power spectral analysis using the fast Fourier transform (FFT) technique. Our results showed that there is a significant advantage in using the bispectral technique over the conventional FFT technique. This study focuses on the importance of bispectral analysis in applications to atmospheric signals. [J894]

## "Fiber lasers: A future space technology [Jsame article as "Fiber lasers: A future technology for lasers in space", ibid, vol. 23, n. 4, pp. 25-30, 08]"

The constraints of operation in space have largely precluded the use of conventional solid-state laser systems for applications including remote sensing, communication relays, and active laser radars. A new technology, fiber lasers, may offer all of the needed features at an affordable price. An appealing aspect of the fiber laser is that it does not need a rigid optical bench. Only the output end of the fiber need be held in rigid reference to the optical tracking system. Design, fabrication, and testing of the laser resonator is generally the most expensive and longest lead part of the effort for conventional solid-state lasers. Advances in Fiber Optic technology and devices mean that the "fiber laser" need not be a simple device but may be a complex system employing sophisticated technology such as wavelength selective Bragg reflectors and nonlinear optical frequency shifters. Three companies have recently obtained single-mode outputs of 3540 watts single mode at 1.03-1.1 microns. [J895]

## "Refractivity Retrieval Using the Phased-Array Radar: First Results and Potential for Multimission Operation"

In this paper, an investigation of the potential of rapid refractivity retrieval is presented. The retrieval technique utilizes radar phase measurements of ground clutter to derive near-surface refractivity, which has been commonly used as a proxy for humidity, given its close relation to vapor pressure. Surface humidity is an important meteorological parameter and has been known to play an important role in convective initiation. In this paper, the refractivity retrieval technique is exploited by using smaller numbers of samples for phase calculation, which is a fundamental process in refractivity retrieval. The impetus for this paper is to explore the possibility of rapid refractivity retrieval by exploiting the rapid beam-steering capability of a phased-array radar. Using the National Weather Radar Testbed in Norman, OK, a 64-pulse per radial raw-data set was collected for conventional refractivity processing. Then, subsets of the 64 samples were extracted to emulate shorter dwell periods and the corresponding more rapid experiments. The test cases that were considered are 2, 4, 8, 16, and 32 samples. Refractivity fields retrieved using smaller numbers of samples are compared against the reference field, which was obtained using the entire 64-sample data set. It will be shown that, statistically, significant refractivity fields can be obtained from as short as a two-sample dwell. [J896]

## "A Comparison of Point Target Spectra Derived for Bistatic SAR Processing"

The existence of a double hyperbola in the bistatic range equation makes it difficult to find an exact analytical solution for the 2D point target spectrum. Several approximate solutions for the spectrum have been derived and used to focus bistatic synthetic aperture radar data. In this paper, we establish the relationship between three independently derived bistatic point target spectra. The first spectrum is Loffeld's bistatic formula, which consists of a quasi-monostatic and a bistatic phase term. The second spectrum makes use of Rocca's smile operator, which transforms bistatic data in a defined configuration to a monostatic equivalent. The third spectrum is derived using a power series-called the method of series reversion (MSR). The MSR spectrum is the most general among the three. This paper shows that this spectrum can be reduced to the same formulation as the former two when certain conditions are met. In addition, a new approximate spectrum is derived using a Taylor series expansion about the two stationary phase points of the transmitter and receiver. We also give an alternative geometrical proof of the relationship between Rocca's smile operator and Loffeld's bistatic deformation term. The accuracies of the point target spectra are demonstrated using simulations of an X-band bistatic airborne radar with a fixed baseline. [J897]

## "Mapping the Shallow Water Seabed Habitat With the SHOALS"

The scanning hydrographic operational airborne light detection and ranging (LiDAR) Survey (SHOALS) consists of a bathymetric LiDAR system that provides high-precision measurements of water depth. Although the acquisition is focused on depth accuracy, the return signal, i.e., waveform, contains other relevant information because of integration signatures from the water surface, the water column, and the seabed. This paper highlights the benthic characterization in extracting statistical parameters derived from the bottom backscatter and classifying them. In implementing a specific unsupervised classification, it is significantly proven that the signals derived from habitat, described as statistically homogeneous throughout ground-truth analysis, are similar within an intrahabitat view, whereas they are different between themselves. [J898]

## "Parametric Velocity Synthetic Aperture Radar:Signal Modeling and Optimal Methods"

Velocity synthetic aperture radar (VSAR) is equipped with a linear array to receive the echoes from a radar illuminating area via multiple channels, each of which can reconstruct a reflectivity image for the same stationary scene. Based on analysis of pixel vector sampled among multi-images, VSAR may effectively suppress the strong ground clutter and improve moving target detection and location. In this paper, different Doppler-distributed properties are derived for the moving target and clutter, respectively. Then, we propose a novel parametric statistical model for VSAR by dividing the pixel vector into three components, namely, target, clutter, and noise. Furthermore, a method of adaptive implementation of optimal processing (AIOP-VSAR) is presented for moving target detection. It is shown that the optimum detection performance may be obtained via AIOP-VSAR, particularly for the slowly moving target in an inhomogeneous clutter environment. Also, the Cramer-Rao bounds (CRBs) are derived for the estimation of unknown model parameters, as well as the azimuth locations of moving targets, and the maximum-likelihood methods are proposed to reach these CRBs. Based on the proposed target detection and parameter estimation methods, we present a complete parametric flowchart for VSAR. It is demonstrated that the proposed flowchart may effectively mitigate the "azimuth location ambiguity" of VSAR and has the super-resolution ability to resolve "velocity layover" for multiple targets. Finally, some detailed numerical experiments and scene simulations are provided to show the effectiveness of the proposed methods. [J899]

## "Monitoring Urban Land Cover in Rome, Italy, and Its Changes by Single-Polarization Multitemporal SAR Images"

This study contributes an assessment of the potential of single-polarization decametric synthetic aperture radar (SAR) images in classifying land cover within and around large urban areas and in monitoring their changes. The decision task is performed on a pixel basis and is carried out by supervised neural network algorithms fed by radar image features including backscattering intensity, coherence and textural parameters. Two configurations are considered: a short-term classification and change detection scheme intended for providing information in near-real time and a long-term scheme aimed at observing the urban changes at year time scales. We use a pair of interferometric images for the short-term case, while the long-term exercise utilizes two interferometric pairs and a fifth single acquisition. The images are acquired by the ERS SAR in late winter, spring and early summer over 836 square kilometers including Rome, Italy, and its surroundings. The accuracy of the short-term algorithm in discriminating seven types of surface is higher than 86%, while the accuracy of the long-term algorithm is beyond 88%. The many changes undergone by Rome from 1994 to 1999 have been identified by the postclassification comparison change detection procedure. The pixel-by-pixel analysis of the results has been carried out for a 160 square kilometers test area, obtaining a correct detection above 82% (less than 18%

missed alarms and 0.3% false alarms). [J900]

## "Urban RF multipath mitigation"

Sensing in urban environments is of growing interest to the surveillance community, as is observation of targets with micro-Doppler features-elements of the target structure with independent range-Doppler behaviour about some target centroid. Multipath effects unique in character to urban sensing can conceal important features in the range-Doppler response of a target with micro-Doppler behaviour. The range-Doppler smearing because of multipath is analysed, and this analysis serves as the basis for a prominent point multipath mitigation algorithm. The effectiveness of this technique is evaluated with simulated micro-Doppler data with artificial multipath effects. [J901]

## "Electromagnetic Coherent Tomography Array Imaging in Random Scattering Media"

Imaging through discrete random media is an important problem in several applications such as medicine, remote sensing, and security. Discrete random media create scattering which deteriorates the quality of the image and there have been several efforts to mitigate the problem. We propose an array processing method called coherence tomography array (CTA) whose algorithm is derived from that of optical coherence tomography. We use the Monte Carlo method to simulate the imaging scenarios in random scattering media. The results show that CTA can be used to alleviate the clutter effects from discrete random scatterers. [J902]

## "Synergetic Use of Radar and Optical Satellite Images to Support Severe Storm Prediction for Offshore Wind Farming"

In this paper, we show how satellite images taken by space-borne radar sensors can be used to determine mesoscale high-resolution wind fields in synergy with cloud parameters from optical data and, thus, help in the task of maintenance and planning offshore wind farms. The aim of this paper is to use synthetic aperture radar (SAR) and medium resolution imaging spectrometer (MERIS) onboard the environmental satellite (ENVISAT) in synergy to analyze severe weather systems, in particular, to describe the spatial evolution of the atmospheric boundary layer processes involved in cold air outbreaks. We investigated the fine-scale structure of a severe weather case on November 1, 2006 over the North Sea using satellite data. The satellite data are compared with numerical model results of the German Weather Service ldquoLokal Modellrdquo (LM) and the high-resolution limited area model (HIRLAM). LM and HIRLAM show differences in mesoscale turbulent behavior and coastal shadowing. Maximum wind speeds of up to 25 m/s are measured by SAR and are confirmed by the models. Significant differences are observed in the location of the maxima. High-resolution ENVISAT ASAR measurements provide very detailed information on small-scale atmospheric features, which seem to not be captured well by the analyzed numerical models, in particular, in coastal areas. Meteosat second generation (MSG) is used to determine the movement of cloud patterns. Cloud patterns seen in the optical data and radar cross-section modulation give a consistent dynamical picture of the atmospheric processes. The relevance for offshore wind farming is discussed. [J903]

## "Regional Mapping of the Offshore Wind Resource: Towards a Significant Contribution From Space-Borne Synthetic Aperture Radars"

This paper reviews and discusses the benefits of synthetic aperture radar (SAR) satellite imagery for regional mapping of the offshore wind resources, mostly in comparison to the more standard approach of numerical mesoscale and/or microscale models. Remote sensing measurements can be used as a complementary approach to numerical models, as well as a semi-autonomous approach to assess offshore and coastal wind resources using such methods as the newly developed strategic sampling. An important benefit of using SAR satellite data is to validate numerical model results, and possibly to provide surface wind data to pilot numerical models in coastal regions where observations are scarce. A relatively small sample of SAR scenes can already indicates the best wind sites for offshore wind farms that should be investigated for further analysis. Finally, future challenges facing remote sensing to support the wind energy fields, including new satellites and methodology improvements for the SAR technique, are reviewed. [J904]

## "Measurements of Wind and Turbulence Profiles With Scanning Doppler Lidar for Wind Energy Applications"

High-quality profiles of mean and turbulent statistics of the wind field upstream of a wind farm can be produced using a scanning Doppler lidar. Careful corrections for the spatial filtering of the wind field by the lidar pulse produce turbulence estimates equivalent to point sensors but with the added advantage of a larger sampling volume to increase the statistical accuracy of the estimates. For a well-designed lidar system, this permits

accurate estimates of the key turbulent statistics over various subdomains and with sufficiently short observation times to monitor rapid changes in conditions. These features may be ideally suited for optimal operation of wind farms and also for improved resource assessment of potential sites. [J905]

## "Reply to “Comments on `Statistics of the Degree of Polarization'""

For comment paper see L. Tao, ibid., p.3085-3086, (2008). For original paper see V. Santalla del Rio et. al., ibid., vol.54, no.7, p.2173-2175, (2006). The author claims that the sample estimator of the degree of polarization is not its maximum likelihood estimator (MLE) based on several wrong statements. First the author argues: "since the different Stokes parameters are not independent and the degree of polarization and Stokes parameters have no relation of one to one, the sample estimator is no longer a MLE". Finally, the author concludes that the estimator he obtained is the MLE because its bias is lower than the bias of the sample estimator. It is false that the MLE is the minimum bias estimator. [J906]

## "Spatial Indexes for the Extraction of Formal and Informal Human Settlements From High-Resolution SAR Images"

In this paper, a novel procedure for extracting human settlement extent in high-resolution SAR images, based on local autocorrelation and morphological processing, is presented. The algorithm is based on two steps. Hints for human settlements by information fusion based on local indexes of spatial autocorrelation are the outputs of the first step. A morphological chain builds on top of them the final settlements' borders. Examples from very different areas, i.e., the Darfur region in Sudan and the Lombardy region in Italy, stress the robustness of the procedure as well as its effectiveness. [J907]

## "Beam Sharpening of Delay/Doppler Altimeter Data Through Chirp Zeta Transform"

The main goal of a satellite radar altimeter is to measure the height of the reflecting surface scanned by the passage of the instrument overhead. A delay/Doppler altimeter reduces the along-track footprint size by exploiting the coherence of the emitted pulses to synthetize a narrower antenna. Doppler beam formation is then a straightforward procedure that implies application of the discrete Fourier transform to time-domain bursts. Speckle and thermal noise on Doppler echoes are usually reduced using multilooking, i.e., summing incoherent contributions coming from different bursts. The summation of Doppler beams requires precise pointing toward output sample locations, particularly when highly variable topography is effective. However, the procedure of steering after beam sharpening needs a step of interpolation. In this paper, a Doppler beam sharpening and direction toward the sample position are presented which make use of the Chirp Zeta Transform to join the two operations together. This method must be compared with the existing ones to show that a little can be sacrificed to precision for computational gain. To support the discussion, experimental results will be compared with a precise-and so of reference-direct 2-D correlation algorithm over puntiform targets and more complex scenarios. [J908]

## "Whitening Dual-Polarized Weather Radar Signals With a Hermitian Transformation"

Oversampling weather radar signals in range and then whitening these signals has been shown to improve the accuracy of spectral moments. For dual-polarized radar, the polarimetric variables depend upon information gleaned from the cross correlation of the different received signals. Theoretical improvements to the polarimetric variables have been provided to date, but experimental evidence of improvements through whitening has been limited. This paper provides an analysis of the effects of whitening on the estimated cross correlation along with experimental results of whitening applied to polarimetric variables. Different whitening transformations based solely on covariance matrix inversions will be shown to affect the copolar correlation of the whitened data. A Hermitian symmetric whitening transformation will be shown to produce better estimates of polarimetric variables obtained from whitened data than the original whitening transformation defined for use with range oversampling. [J909]

## "The Detection of Buried Pipes From Time-of-Flight Radar Data"

Ultrawideband radar is commonly used in the frequency range of 50-500 MHz to detect buried pipes at a depth of about 1-2 m depending on the soil characteristics. The typical feature used to locate the pipes is the hyperbolic pattern of the time of flight generated by a linear scan of the antenna above the surface. When the pipes are close together, the hyperbolas overlap, and a straightforward least squares fit is not possible. The Hough transform provides one possible solution. This paper extends the Hough transform by introducing a weighting factor depending on the differentials of the unknown parameters with respect to the experimental errors, namely, the probe position error and the time-of-flight error. This enables optimally placed sets of data pairs to be given greater weight than "ill-conditioned" sets, as for example when all data pairs lie near one end

of the arc. The result is a decrease in the background amplitude with respect to the maximum of the peaks in the Hough accumulator space. It is shown that this improvement persists even when many arcs are present. A mathematical analysis with analytical results is given for the case of four unknowns: pipe radius R, pipe center position (Y, Z), and soil propagation velocity V. The results are presented through simulations introducing controlled uncertainties in the probe position, the time of flight, and its bin size. The simulations demonstrate the correlations that occur between the radius, depth, and velocity for given experimental uncertainties. [J910]

## "Soil Moisture Retrieval During a Corn Growth Cycle Using L-Band (1.6 GHz) Radar Observations"

This paper reports on the retrieval of soil moisture from dual-polarized L-band (1.6 GHz) radar observations acquired at view angles of 15deg, 35deg, and 55deg, which were collected during a field campaign covering a corn growth cycle in 2002. The applied soil moisture retrieval algorithm includes a surface roughness and vegetation correction and could potentially be implemented as an operational global soil moisture retrieval algorithm. The surface roughness parameterization is obtained through inversion of the Integral Equation Method (IEM) from dual-polarized (HH and VV) radar observations acquired under nearly bare soil conditions. The vegetation correction is based on the relationship found between the ratio of modeled bare soil scattering contribution and observed backscatter coefficient (sigmasoil/sigmaobs) and vegetation water content (W). Validation of the retrieval algorithm against ground measurements shows that the top 5-cm soil moisture can be estimated with an accuracy between 0.033 and 0.064 cm3ldr cm-3, depending on the view angle and polarization. [J911]

## "Imaging Simulation of Bistatic Synthetic Aperture Radar and Its Polarimetric Analysis"

Employing the 3-D mapping and projection algorithm (MPA), an imaging simulation of bistatic synthetic aperture radar (BISAR) observation over a complex scenario is developed. Based on the explicit expression of the point target response of stripmap BISAR imaging, raw data are efficiently generated from the scattering map precalculated by MPA. Some examples of BISAR image simulation are studied. The polarimetric characteristics of a BISAR image are then discussed. It is found that some typical polarimetric parameters such as Cloude's alpha, beta and gamma and might become unable to describe the scattering mechanism under bistatic observation. A transform of unified bistatic polar bases for a BISAR image is proposed. The parameters alpha, beta and gamma and are modified to retain the property of orientation independence in the bistatic circumstance. Analysis of simulated images shows that the redefined alpha, beta and gamma and after the unified bistatic polar bases transform well describe different scattering mechanisms in BISAR imaging. It provides a primary tool for BISAR image interpretation and terrain classification. [J912]

## "Relating Microwave Modulation to Microbreaking Observed in Infrared Imagery"

Microwave modulation by swell waves and its relation to microbreaking waves were investigated in an ocean experiment. Simultaneous collocated microwave and infrared (IR) measurements of wind waves and swell on the ocean were made. The normalized radar cross section sigma0and the skin temperature Tskinwere both modulated by the swell, but with differing phases. In general, sigma0maxima occurred on the front face, whereas Tskinmaxima occurred on the rear face of the swell. Infrared imagery has shown that swell-induced microbreaking occurred at or near the swell crest and that the resulting warm wakes occurred on the rear face of the wave. When tilt and range modulations are taken into account, the location of microbreaking also accounts for the maximum of sigma0occurring on the front face of the swell. Thus, microbreaking waves generated near the crest of low-amplitude swell can produce microwave and IR signatures with the observed phase. The relationship between microwave and IR signals was further emphasized by comparing microwave Doppler spectra with simultaneous IR and visible images of the sea surface from the same location. When small and microscale breaking waves were present, Doppler spectra exhibited characteristics that are similar to those from whitecaps, having peaks with large Doppler offsets and polarization ratios near unity. When no microbreakers were present, Doppler offsets and polarization ratios were much smaller in accordance with a composite surface scattering theory. [J913]

## "AMTA Corner"

{no data available} [J914]

## "A Consistent Metric for Performance Evaluation of Multi-Object Filters"

The concept of a miss-distance, or error, between a reference quantity and its estimated/controlled value, plays a fundamental role in any filtering/control problem. Yet there is no satisfactory notion of a miss-distance in the well-established field of multi-object filtering. In this paper, we outline the inconsistencies of existing metrics in the context of multi-object miss-distances for performance evaluation. We then propose a new mathematically

and intuitively consistent metric that addresses the drawbacks of current multi-object performance evaluation metrics. [J915]

## "Wavelet Contribution to Remote Sensing of the Sea and Target Detection for a High-Frequency Surface Wave Radar"

High-frequency waves (3-30 MHz) interact with the sea surface. Thus, a high-frequency surface wave radar (HFSWR) is well suited to perform remote sensing of the sea. The HFSWR coverage range is not limited by the radio horizon: it is possible to keep watch over the sea up to a few hundred kilometers from the coastline. Oceanographic parameters (i.e., wave height, surface current velocity, wind direction, and wind velocity) are derived from the so-called sea spectrum. Moreover, the HFSWR can be used for maritime surveillance of the Exclusive Economic Zone. In that case, the sea spectrum is an unwanted signal because it can mask targets. Sea spectrum extraction is an important issue for HFSWR signal processing since it is a key point for the remote sensing accuracy and the target detection features. In this letter, we show how wavelets may be applied to improve the remote sensing of oceanographic parameters and the target detection using wavelet-based sea clutter extraction. The results obtained using real data with opportune targets validate our approach. [J916]

## "Sikkim's Teesta River fog, mist and dust particle monitoring using monostatic LiDAR"

Fog, mist, and atmospheric dust particles, having the dimension of one micrometer or less, play an important role in the deterioration of visibility, as well as in causing local warming in the atmosphere. With an attempt to reduce the deterioration, a scientific approach has to be taken to determine their origins. A monostatic LIDAR may be one of the best instruments for such work. The authors are tempted to develop such a LIDAR for fog, mist, and dust particle monitoring over River Teesta at Sikkim. LIDAR is an acronym for Light Detection And Ranging. What can we do with LIDAR? Measure distance, measure speed, measure rotation, measure chemical composition and concentration, and measure cross-sections of the targets. The digital technique is always utilized for its development which results in better security, lower power consumption, higher power efficiency, higher reliability, lower transmitter power, lower multipath effect, higher interference suppression as compared to an analog system. The commercial systems like disdometer, rain radar, mobile robot, etc., utilizing LIDAR principles are operational in different parts of the world. The authors are highly motivated for such LIDAR development and their development effort follows. [J917]

## "Focusing Bistatic SAR Data Using the Nonlinear Chirp Scaling Algorithm"

Bistatic synthetic aperture radar data are more challenging to process than the common monostatic counterparts because the flight geometry is more complicated and the data are usually nonstationary. Whereas time-domain algorithms can handle general bistatic cases, they are very inefficient; therefore, frequency-domain methods are preferred. Several frequency-domain monostatic algorithms have been modified to handle a limited number of bistatic cases, but a general algorithm is sought, which can handle cases such as nonequal platform velocities, nonparallel flight tracks, and high squints. In this paper, we modify the nonlinear chirp scaling (NLCS) algorithm to handle a general case of bistatic data. The key is to use a linear range cell migration correction to reduce the range-azimuth coupling, an NLCS to precondition the data for azimuth compression, and a series expansion to obtain an accurate form of the signal spectrum. The azimuth nonstationarity is handled through the use of invariance regions. Simulations have shown that the modified NLCS algorithm can handle data with more complicated bistatic geometries than the previous algorithms. [J918]

## "Segmentation-Based MAP Despeckling of SAR Images in the Undecimated Wavelet Domain"

In this paper, a novel despeckling algorithm based on undecimated wavelet decomposition and maximum aposterioriestimation is proposed. Such a method represents an improvement with respect to the filter presented by the authors, and it is based on the same conjecture that the probability density functions (pdfs) of the wavelet coefficients follow a generalized Gaussian (GG) distribution. However, the approach introduced here presents two major novelties: 1) theoretically exact expressions for the estimation of the GG parameters are derived: such expressions do not require further assumptions other than the multiplicative model with uncorrelated speckle, and hold also in the case of a strongly correlated reflectivity; 2) a model for the classification of the wavelet coefficients according to their texture energy is introduced. This model allows us to classify the wavelet coefficients into classes having different degrees of heterogeneity, so that adhocestimation approaches can be devised for the different sets of coefficients. Three different implementations, characterized by different approaches for incorporating into the filtering procedure the information deriving from the segmentation of the wavelet coefficients, are proposed. Experimental results, carried out on both artificially speckled images and true synthetic aperture radar images, demonstrate that the proposed filtering approach outperforms the previous filters, irrespective of the features of the underlying reflectivity. [J919]

## "Information Theory-Based Approach for Contrast Analysis in Polarimetric and/or Interferometric SAR Images"

We propose a new approach for evaluating the contribution of the different channels of polarimetric and interferometric synthetic aperture radar (PolInSAR) images. For that purpose, we demonstrate that the Bhattacharyya distance between the probability density functions of neighboring regions in the image provides an efficient scalar contrast measure. We show that the analysis of this contrast measure allows one to precisely characterize the contribution of each channel for different system configurations, including intensity, polarimetric, and interferometric images. We illustrate this approach using a real synthetic aperture radar image to compare several polarimetric system architectures. Since PolInSAR imaging configurations can correspond to complex and expensive systems, the proposed method can be helpful in system imaging optimization. [J920]

## "Radarsat-1 and ERS InSAR Analysis Over Southeastern Coastal Louisiana: Implications for Mapping Water-Level Changes Beneath Swamp Forests"

Detailed analysis of C-band European Remote Sensing 1 and 2 (ERS-1/ERS-2) and Radarsat-1 interferometric synthetic aperture radar (InSAR) imagery was conducted to study water-level changes of coastal wetlands of southeastern Louisiana. Radar backscattering and InSAR coherence suggest that the dominant radar backscattering mechanism for swamp forest and saline marsh is double-bounce backscattering, implying that InSAR images can be used to estimate water-level changes with unprecedented spatial details. On the one hand, InSAR images suggest that water-level changes over the study site can be dynamic and spatially heterogeneous and cannot be represented by readings from sparsely distributed gauge stations. On the other hand, InSAR phase measurements are disconnected by structures and other barriers and require absolute water-level measurements from gauge stations or other sources to convert InSAR phase values to absolute water-level changes. [J921]

## "A Multistatic GNSS Synthetic Aperture Radar for Surface Characterization"

Bistatic global navigation satellite system (GNSS) radar has received increased attention in recent years within both the radar and GNSS communities. In this paper, the traditional bistatic GNSS radar and bistatic synthetic aperture radar (SAR) concepts are fused into a more generic multistatic GNSS SAR system for surface characterization. This is done by using the range and Doppler processing techniques on signals transmitted by multiple satellites to determine the angular dependence of the surface reflectivity. The method has also been tested experimentally, and the results are presented. [J922]

## "A Refined GTD Ray System for an Embedded Object and Its Polarimetric Behavior"

A refined ray system based on the geometrical theory of diffraction (GTD) for an object embedded in soil for a monostatic transmitter-receiver alignment is presented. Apart from the investigation of the ldquoclassicalrdquo reflections from the target, creeping waves are also taken into account, and their formalism is presented. The objective of such a ray set is to better understand the different scattering mechanisms, which are presented in the complex scattering framework. In electromagnetic modeling based on GTD, the complex shape of a target is replaced by simpler canonical objects, e.g., facets, cones, wedges, spheres, or cylinders. Here, a cylinder is located in parallel and closely to the plane interface of two dielectric half-spaces. The example of air-soil is taken into account. The numerical results obtained for various directions of incidence are employed to describe the polarimetric characteristics of the diffracted field from grazing to perpendicular incidence to the surface. By representing the diffracted GTD field on the Poincare sphere, the location on the sphere has a one-to-one relationship to the dielectric properties of the soil. The relation can be employed to extract information as the soil moisture. [J923]

## "Side-Face Effect of a Dielectric Strip on Its Optical Properties"

Light scattering by horizontally oriented platelike particles under normal incidence, such as ice plates or tree leaves under spaceborne lidar or radar waves, needs to be investigated for remote sensing of cirrus clouds or vegetation canopies. The solutions from the conventional geometrical ray tracing method for the scattering of electromagnetic waves by these particles are quite inaccurate because of the singularity problem that is inherent to this method. The scattering properties of large horizontally oriented platelike particles are usually approximated by using physical optics or electromagnetic wave theory while ignoring the side-face effect of the plates. In this paper, to examine the effect of side faces on light scattering by platelike particles, a 2-D finite-difference time-domain technique is applied to calculate light scattering by horizontally oriented ice and leaf strips under normal or quasi-normal incidence. It is found that for moderate-sized strips, the side faces of the particles scatter a significant amount of energy, resulting in strong maxima in the scattering phase function at certain scattering

angles. By ignoring the effect of side faces, the scattering phase functions derived from electromagnetic wave theory have significant errors for small or moderate-sized strips. However, the ratio of the amount of energy scattered by the side faces to the total scattered energy decreases with the increase of strip width. When the size parameter of the strip is in the limit of geometric optics, the side-face effect is reduced to a negligible amount. However, even in this case, the polarization degrees from the approximation solutions of physical optics or electromagnetic wave theory ignoring the side-face effect still have large errors. [J924]

## "Design and Calibration of a Large Open-Ended Coaxial Probe for the Measurement of the Dielectric Properties of Concrete"

The subject of this paper is the design and calibration of an open-ended coaxial probe for the nondestructive measurement of the dielectric properties of concrete. Measurements are made between 100-900 MHz, frequencies which are often used in geophysics and civil engineering for ground penetrating radar inspection. The probe is calibrated using measurements on saline solutions in conjunction with three different mathematical techniques for comparative study. Measurements of mortar and concrete specimens having different water/cement ratios were made in order to observe the standard deviations due to their heterogeneous nature. Similar to the case of relatively homogeneous rock specimens (limestone and granite), the standard deviation for heterogeneous concrete samples do not exceed 5%. In addition, the effect of the concrete's porosity on its dielectric properties was clearly observed: measured permittivity between 4-4.5 at 900 MHz for porous concrete, and between 6.5-7.5 at 900 MHz for dense concrete. [J925]

## "Statistical Characterization and Modeling of Raindrop Spectra Time Series for Different Climatological Regions"

A large data set of raindrop size distribution (RSD) measurements collected with the Joss-Waldvogel disdrometer (JWD) and the 2-D video disdrometer (2DVD) in the U.K., Greece, Japan, and the U.S. are analyzed and modeled. This work extends a previous effort devoted to the exploitation of U.K. data and the design of a stochastic procedure to randomly generate synthetic RSD intermittent time series. This study seeks to: (1) explore the differences of RSD-derived moments for distinct hydroclimate regions, ranging from tropics to subtropics and mid and northern latitudes; (2) compare the governing parameters of the normalized gamma RSD for both stratiform and convective events and perform a sensitivity analysis by using different best fitting techniques; (3) exploit the time-correlation structure of the estimated RSD parameters as the input of a vector autoregressive stationary model used to simulate time series (or horizontal profiles) of RSDs and, consequently, its moments as the rain rate and concentration; and (4) characterize the distribution of the inter-rain duration and rain duration to design a semi-Markov chain to represent the intermittency feature of the rainfall process in a climatological framework. This climatological analysis and the related stochastic RSD generation model may find useful applications within both hydrometeorology and radio propagation. [J926]

## "Estimation of Hurricane Winds From SeaWinds at Ultrahigh Resolution"

Although the SeaWinds scatterometer was not specifically designed to observe tropical cyclones, new high-resolution wind products resolve much of the horizontal structure of these storms. However, these higher resolution products (2.5 km) are inherently noisier than the standard 25-km near-surface wind products. These noise levels combined with rain contamination complicate high-resolution wind estimation-particularly in tropical cyclones. Fortunately, tropical cyclones have structures that can be exploited by using a wind field model. This paper develops a new procedure for hurricane wind field estimation from the SeaWinds instrument at ultrahigh resolution. A simplified hurricane model is developed to provide prior information to be used in maximum aposterioriprobability estimation of ocean winds. Using the hurricane model ameliorates the effects of rain and noise and provides useful hurricane parameters such as the eye center location. The model also improves ambiguity selection. The new method reduces the variability of the wind speed and direction estimates, although high wind speeds still tend to be underestimated. The method also greatly improves wind direction estimates in hurricanes-even in rain-contaminated portions of the storm. [J927]

## "A Comparison of Algorithms for Retrieving Soil Moisture from ENVISAT/ASAR Images"

In this paper, we present an intercomparison of algorithms for retrieving soil moisture content (SMC) from ENVIronmental SATtellite (ENVISAT)/Advanced Synthetic Aperture Radar images. The algorithms taken into consideration were a feedforward artificial neural network (ANN) with two hidden layers, a statistical approach based on Bayes' theorem, and an iterative algorithm based on the nelder-mead direct-search method. The comparison was carried out by using both simulated and experimental data. Simulated data were obtained by means of the integral equation model (IEM). Experimental data were collected in an agricultural area in Northern Italy during 2003-2005; they included backscattering coefficient at HH and HV polarizations and at an incidence

angle of thetas = 23deg, as well as detailed ground truth measurements of SMC, surface roughness, and vegetation parameters. HH-polarized data were related to SMC, whereas the information of the cross-polarized channel was used to correct the backscatter for the effects of surface roughness. A comparison of the algorithms with experimental data showed that all the tested approaches produced SMC values that are very close to the measured ones. However, the predictions of the ANN were slightly more suitable than the other methods for generating maps in reasonable time. The production of moisture maps carried out at different dates using this algorithm pointed out the feasibility of separating up to six levels of spatial/temporal variations of SMC in the range of 10%-35%. [J928]

## "Additional Corrections to “Unconstrained Inversion of Waveheight Spectra From SAR Image” [JFeb 02 261-270]"

Lyzenga's paper ("Unconstrained inversion of waveheight spectra from SAR images" IEEE Trans. Geosci. Remote Sens., vol. 40, no. 2, pp. 261-270, Feb. 2002) after being corrected (ibid., vol. 40, no. 3, p. 729, Mar. 2002) has still a few remaining errors. This paper presents the additional corrections. [J929]

## "Evaluation and Bias Removal of Multilook Effect on Entropy/Alpha/Anisotropy in Polarimetric SAR Decomposition"

Entropy, alpha, and anisotropy (H/alpha/A) of the polarimetric target decomposition have been an effective and popular tool for polarimetric synthetic aperture radar (SAR) image analysis and for a geophysical parameter estimation. However, multilook processing can severely affect the values of these parameters. In this paper, a Monte Carlo simulation is used to evaluate and remove the bias generated by the multilook effect on these parameters for various media composed of grassland, forest, and urban returns. Due to insufficient averaging, entropy is underestimated, and anisotropy is overestimated. We also found that the bias in the alpha angle can be either underestimated or overestimated depending on scattering mechanisms. Based on simulation results, efficient bias removal procedures have been developed. In particular, the entropy bias can be precisely corrected, and the amount of correction is independent of the radar frequency and SAR systems. Data from L-band Advanced Land Observing Satellite/phased array type L-band SAR, German Aerospace Research Center (DLR)/enhanced SAR, Jet Propulsion Laboratory (JPL)/airborne SAR, and X-band polarimetric and interferometric SAR are used for demonstration in this paper. [J930]

## "Glacier Volume Changes Using ASTER Satellite Stereo and ICESat GLAS Laser Altimetry. A Test Study on EdgeШуа, Eastern Svalbard"

Currently, one of the major methodological gaps in the observation of glaciers from space is the measurement of volume changes of mountain glaciers and ice caps. In this paper, we present a case study of comparing a digital elevation model derived from Advanced Spaceborne Thermal Emission and Reflection Radiometer (ASTER) satellite optical stereo, elevation data derived from Ice, Cloud, and land Elevation Satellite Geoscience Laser Altimeter System (GLAS) laser altimetry, and contour lines from a topographic map from the 1970s. For two ice caps in Eastern Svalbard, Kvalpyntfonna and Digerfonna, we obtain an overall elevation change of -0.55 or -0.61 m/year between 1970 and 2002 (ASTER) or GLAS (2006), respectively. From comparison of different methods and from different quality checks, we estimate the error of this numbers to be on the order of 5%. This paper demonstrates that and on how long-term glacier volume changes can be observed from space over a large number of ice caps and glaciers. [J931]

## "Prediction, Detection, and Correction of Faraday Rotation in Full-Polarimetric L-Band SAR Data"

With the synthetic aperture radar (SAR) sensor PALSAR onboard the Advanced Land Observing Satellite, a new full-polarimetric spaceborne L-band SAR instrument has been launched into orbit. At L-band, Faraday rotation (FR) can reach significant values, degrading the quality of the received SAR data. One-way rotations exceeding 25 degare likely to happen during the lifetime of PALSAR, which will significantly reduce the accuracy of geophysical parameter recovery if uncorrected. Therefore, the estimation and correction of FR effects is a prerequisite for data quality and continuity. In this paper, methods for estimating FR are presented and analyzed. The first unambiguous detection of FR in SAR data is presented. A set of real data examples indicates the quality and sensitivity of FR estimation from PALSAR data, allowing the measurement of FR with high precision in areas where such measurements were previously inaccessible. In examples, we present the detection of kilometer-scale ionospheric disturbances, a spatial scale that is not detectable by ground-based GPS measurements. An FR prediction method is presented and validated. Approaches to correct for the estimated FR effects are applied, and their effectiveness is tested on real data. [J932]

## "Correction of the Sea State Impact in the L-Band Brightness Temperature by Means of Delay-

## Doppler Maps of Global Navigation Satellite Signals Reflected Over the Sea Surface"

This paper presents an efficient procedure based on 2-D convolutions to obtain delay-Doppler maps (DDMs) of Global Navigation Satellite Signals reflected (GNSS-R) over the sea surface and collected by a spaceborne receiver. Two DDM-derived observables (area and volume) are proposed to link the sea-state-induced brightness temperature to the measured normalized DDM. Finally, the requirements to use Global Positioning System reflectometry to accurately correct for the sea state impact on the L-band brightness temperature (quantization levels, decimation, truncation, and noise impact) are analyzed in view of its implementation in the Passive Advanced Unit instrument of the Spanish Earth Observation Satellite (SeoSAT/INGENIO) project. [J933]

## "Radar Bistatic Configurations for Soil Moisture Retrieval: A Simulation Study"

The possible contribution of bistatic radar measurements for bare soil moisture retrieval is investigated in this paper. A simulation study based on well-established electromagnetic models of rough surface scattering (both coherent and incoherent components) has been accomplished for this purpose. The retrieval accuracy has been evaluated by using both the Cramer-Rao lower bound and the error variance of a linear regression estimator, thus considering slightly different assumptions on retrieval conditions. Both methods have allowed us to identify the optimal system configurations in terms of observation directions, polarizations, and frequency. This identification has been carried out for single-polarization and multipolarization receivers and for the case in which bistatic measurements are complemented by monostatic ones, which are expected to be available through already-existing spaceborne synthetic aperture radars. The optimal systems have first been singled out by considering a Gaussian autocorrelation function (ACF) and a constant value of correlation length. Successively, the simulations for an exponential ACF and a variable correlation length have been analyzed, demonstrating that the results substantially remain the same. The comparison between the soil moisture estimation accuracy yielded by the optimal configurations and that provided by the standard monostatic radar has shown that a significant improvement in the quality of retrieval can be achieved by complementing bistatic and monostatic measurements. [J934]

## "Land Use and Land Cover Mapping in the Brazilian Amazon Using Polarimetric Airborne P-Band SAR Data"

In September 2000, an airborne synthetic aperture radar (SAR) mission acquired unprecedented full polarimetric P-band data over the Tapajos National Forest (Para State), which is an area in the Brazilian Amazon which has been continuously monitored in the last three decades. Eight land use/cover classes were identified, namely, primary forest, regeneration older than 25 years, regeneration between 12 and 25 years, regeneration between 6 and 12 years, regeneration younger than six years, crops/pasture, bare soil, and floodplain (FP). The objective of this paper is to analyze the potential of full polarimetric P-band data in distinguishing different land use/cover classes with a minimum established Kappa value of 75%, using the latest development on SAR statistical characterization. The iterated conditional mode (ICM) contextual classifier was applied to amplitude, intensity images, biomass index, and some polarimetric parameters (entropy, alpha angle, and anisotropy) extracted from the polarimetric P-band data. As the accuracy obtained for eight classes was not acceptable, another two sets, with five and four classes, were formed by the combination of the previous ones. They were defined by confusion matrix analysis and by the graphical analysis of average backscatter values, entropy, [alpha] angle, and anisotropy images and by the H/alpha plans of the land use samples. The classification accuracy with four classes (three levels of biomass plus FP) was then considered acceptable with a Kappa value of 76.81%, using the ICM classification with the adequate bivariate distribution for the HV and VV channels. [J935]

## "Imaging Small PEC Spheres by a Linear Approach"

The problem of localizing small inhomogeneities from the knowledge of their scattered field is dealt with. In particular, the case of small perfect electric conducting spheres is of concern, with the scattered field data collected under multistatic/multifrequency/single-view or multistatic/single-frequency/multiview far zone configurations. The multiple scattering between the spheres is neglected, and their locations are represented as the supports of the Dirac delta functions. This allows one to cast the problem as the inversion of a linear integral operator, with the delta functions being the unknowns of the problem. The inversion of this linear integral operator is achieved by means of the truncated singular value decomposition. The performance of the linear inversion algorithm against the model error (i.e., for situations where the multiple scattering is not negligible) is investigated by numerical simulations. Furthermore, the effect of noise is also analyzed by corrupting the data by an uncorrelated additive white Gaussian process. [J936]

## "A-Train Data Depot: Bringing Atmospheric Measurements Together"

This paper describes the satellite data processing and services that constitute current functionalities of the A-

Train Data Depot. We first provide a brief introduction to the original geometrical intricacies of the platforms and instruments of the A-Train constellation and then proceed with a description of our A-Train collocation-processing algorithm that provides subsets that facilitate synergistic use of the various instruments. Finally, we present some sample image products from our web-based Giovanni tool which allows users to display, compare, and download coregistered A-Train-related data. [J937]

## "A Kirchhoff-Based Shape Reconstruction Algorithm for the Multimonostatic Configuration: The Realistic Case of Buried Pipes"

A shape reconstruction algorithm is formulated for the multimonostatic configuration and the 2-D geometry. The imaging algorithm is based on the Kirchhoff approximation, works in the frequency domain, and exploits the singular value decomposition tool to achieve a stable solution. The effectiveness of the reconstruction algorithm is shown by processing synthetic data in the time domain generated via a finite-difference time-domain code. A performance analysis of the solution algorithm is addressed with varying host medium and measurement configurations, also by processing synthetic data for a 3-D geometry. Finally, an experimental validation of the technique is performed due to data collected by a time-domain ground-penetrating radar for buried pipe detection and localization. [J938]

## "Calibration Method for Fully Polarimetric Microwave Radiometers Using the Correlated Noise Calibration Standard"

In this paper, a new and improved L-band version of the correlated noise calibration standard (CNCS) has been developed to aid in the characterization of polarimetric microwave radiometers. The CNCS generates a series of known polarimetric test signals using a two-channel commercial arbitrary waveform generator (AWG) and a pair of frequency-upconversion modules. When it is inserted in place of the antenna used by a radiometer-under-test (RUT), it can fully characterize the polarimetric response of the receiver portion of the RUT. Both hardware and software improvements have been made over a previous version of the CNCS. The frequency upconverters now include integral warm and cold calibration-reference targets to automatically compensate for small drifts in AWG output-signal strength. The procedure used to calibrate the RUT has been generalized to correct for nonideal characteristics of the CNCS itself. Moreover, the effects on the derived polarimetric gain matrix of impedance mismatches between the RUT, and either the CNCS or the antenna have been determined. Details of the CNCS improvements are presented. The results of an experimental demonstration of its use and of a series of validation tests of its performance are also presented. [J939]

## "An Improved NLCS Algorithm With Capability Analysis for One-Stationary BiSAR"

This paper deals with the imaging problem of one-stationary bistatic SAR (BiSAR) with large bistatic angle. An improved nonlinear chirp scaling (NLCS) algorithm is proposed for this BiSAR. The main work here includes three aspects. First, a range chirp scaling function for correcting the differential range cell migration correction is derived. Then, the azimuth perturbation is generated by local fit method, which makes the NLCS algorithm suitable for the large bistatic angle case. Furthermore, the negative effects introduced by the perturbation (including phase error and locality error) are discussed, and some compensation methods are proposed to enhance the capability of the algorithm. The simulating results exhibited at the end of this paper validate the correctness of the analysis and the feasibility of the algorithm. [J940]

## "Measurements of the Effect of Rain-Induced Sea Surface Roughness on the QuikSCAT Scatterometer Radar Cross Section"

Radar measurements of the sea surface, with satellite scatterometers that operate at Ku-band, are affected by the presence of rain through modification of the sea surface roughness by rain impacts. This is in addition to wind driven roughness, atmospheric scattering, and attenuation that affect the measured normalized radar cross section (NRCS). This paper presents a case study of the increase of the total radar cross section, averaged across surface illuminated areas (individual footprints) of the SeaWinds scatterometer (on QuikSCAT) caused by rain striking the sea surface. This effort combines satellite-based Ku-band data with high-resolution 3-D volumetric rain measurements, from simultaneous collocated Next Generation Weather Radar data. The results to be presented were acquired during a significant rain event in the Gulf of Mexico, to the east of Corpus Christi, and just south of Houston, TX, in May 2005. The results of this paper show dependence on wind speed, rainrate, and polarization. They agree with numerous surface-based studies (single point measurements), using ocean platforms and wind-wave tanks, whose data were collected under similar conditions. For example, at rainrates less than 10 mm/hr, the relative change in surface roughness is seen to decrease as the wind magnitude increases from 5 to 7 m/s. Another consistent observation is that the vertical polarization NRCS shows less sensitivity to rainrate than does horizontal. [J941]

## "An Approach for Solving Rank-Deficient Systems That Enable Atmospheric Path Delay and Water Vapor Content Estimation"

This paper develops mathematical techniques and makes use of interferometric synthetic aperture radar (InSAR) for improving the quality of digital elevation models derived from SAR images and providing accurate estimations of atmospheric path and absolute phase delays and water vapor content estimation. The problem of solving parameters such as atmospheric path delay, height, and unwrapping errors is to be described in a mathematical form that uses QR factorization techniques for solving rank-deficient systems. A new approach for the solution of rank-deficient systems with few independent equations is proposed. In the new approach, the bounds are considered known and provided by the eigenvalues. New eigenvalues are added inside the bounds. During the implementation, attention is given not to exceed the bounds of the reorganized matrix. This approach is the first time that is used for phase parameterization in terms of height, tropospheric delay, and phase unwrapping errors. Expanding the approach was also studied for absolute phase delay and water vapor content estimation. The investigation and the implementation of the approach make use of ENVISAT images. The validation of results was implemented through GPS and meteorological measurements. [J942]

## "Principle and Methods on Bistatic SAR Signal Processing via Time Correlation"

In this paper, we discuss the mapping between the 3-D scene space and the bistatic synthetic aperture radar (SAR) image space and show that when the direction of the angular velocity of the bistatic SAR remains constant, the process of bistatic SAR imaging can be approximately modeled as a perspective operator from the 3-D scene space to the 2-D image space, and the perspective line is perpendicular to the plane determined by the composition direction of the T/R line of sight and the composition direction of the angular velocity of the T/R platform. Then, we show that the 2-D point spread function of the bistatic SAR is determined not only by the range and ldquoazimuthrdquo resolutions but also by the geometry of the bistatic SAR and the bases of the SAR image space, and the concept ldquoambiguity regionrdquo is introduced to describe the ambiguity problem in the 3-D scene space. Then, the range-Doppler algorithm is discussed, and a new translational-variant bistatic SAR imaging method is proposed, which uses the scaled inverse fast Fourier transform (IFFT) technique to eliminate the translational-variant feature of the SAR space resolution. The space truncation error of this new algorithm is discussed to analyze the depth of focus of the scaled IFFT bistatic SAR imaging algorithms, and we find that the upper bounce of the space truncation error is proportional to the square of the distance from the scatterer to the T/R platforms. Last, the effects of motion measurement errors are discussed in detail, and, through theoretical analysis and numerical experiments, we show that the absolute position measurement error, the baseline measurement error, the perpendicular (vertical) component of the absolute velocity measurement error (AVME), and the perpendicular component of the relative velocity measurement error (RVME) cause SAR image shifting in the image space mainly, and the parallel component of the AVME and the parallel component of the RVME cause the SAR image to s--everely defocus. [J943]

## "Evaluation of Underwater Rainfall Measurements During the Ionian Sea Rainfall Experiment"

Rainfall on the sea surface generates a loud and distinctive sound underwater. This sound propagates downward and attenuates, producing an effective listening area or an equivalent ldquo catchmentbasinrdquo for a listening device that is a function of depth and frequency. Acoustical measurements of rainfall are reported from four passive aquatic listeners (PALs) at 60-, 200-, 1000-, and 2000-m depths from a mooring in the Ionian Sea off the southwestern coast of Greece (37N, 21.5E) from January to April 2004. These measurements are compared to colocated high-resolution X-band dual-polarization (XPOL) radar rainfall measurements. The XPOL radar reports the spatial distribution of rainfall variability over the listening areas of the PALs. Four quality-controlled rainfall events, including drizzle, squall line, and heavy rainfall, are presented in this study. The radar rainfall is spatially averaged over the mooring and compared with the four different acoustic measurements at different depths. To understand the issue of spatial averaging, quantitative comparisons are presented, showing a high correlation between the acoustic measurements and the area-averaged radar estimates at corresponding resolutions. [J944]

## "Feature Extraction and Visualization of Bridges Over Water From High-Resolution InSAR Data and One Orthophoto"

Modern airborne SAR sensor systems provide geometric resolution in the order well below half a meter. By SAR interferometry from pairs of such images, DEM of the same grid size can be obtained. In data of this kind, many features of urban objects become visible, which were beyond the scope of radar remote sensing only a few years ago. However, because of the side-looking SAR sensor principle, layover and occlusion issues inevitably arise in undulated terrain or urban areas. Therefore, SAR data are difficult to interpret even for senior human interpreters. Furthermore, the quality of the InSAR DEM may vary significantly depending on the local

topography. In order to support interpretation, SAR data are often analyzed using additional complementary information provided by maps or other remote sensing imagery. In this paper, object feature extraction and visualization from high-resolution InSAR data and one orthophoto is discussed for the example of a scene containing several bridges over water. Bridges are key elements of man-made infrastructure. Monitoring of these important connecting parts of the traffic network is vital for applications such as disaster management or in the context of political crisis, for instance, to evacuate inhabitants and to deliver goods and equipment. Aims of the approach are to derive key features of the bridge's geometry from the complementary data sources, to determine the water level, smooth the noisy InSAR DEM data, especially at water surfaces, and, finally, to generate an improved 3-D visualization of the scene by overlapping the optical image on the InSAR DEM. [J945]

## "A Contrast-Based Algorithm For Synthetic Range-Profile Motion Compensation"

In stepped-frequency radar, target motions produce range-profile distortions. Range shift, signal-to-noise ratio loss, and symmetric spreading are produced by target radial velocity, whereas target radial acceleration is mainly responsible for asymmetric smearing. Acceleration-distortion effects are usually negligible when a high Pulse Repetition Frequency (PRF) is used, although this is not the case for low-PRF radars. In this paper, a new motion-compensation technique based on contrast optimization is proposed. The innovative contributions of this paper are as follows: (1) A theoretical analysis of the distortions produced by target motions on the reconstruction of synthetic aperture radar is provided; (2) the proposed technique compensates both phase terms, which are due to target radial velocity and acceleration; therefore, synthetic range profiles can be focused by processing low-PRF radar returns; (3) a new cost function for the synthetic range profiles (namely, contrast) is defined and used for motion compensation; (4) the proposed technique can be applied to any kind of stepped-frequency waveforms; and (5) an estimation error analysis is performed, first theoretically and then by means of both simulations and real data. [J946]

## "Evaluation of X-Band Polarimetric-Radar Estimates of Drop-Size Distributions From Coincident S-Band Polarimetric Estimates and Measured Raindrop Spectra"

Recent research has demonstrated the value of polarimetric measurements for the correction of rain-path attenuation at X-band radar frequency and the estimation of rain parameters including drop-size distributions (DSD). The issue this paper is concerned with is to what degree uncertainties in attenuation correction can affect the estimation of DSD. Since attenuation-correction uncertainty enhances with rain path, our hypothesis is that DSD retrieval uncertainty at X-band may deteriorate with range. In this paper, we evaluate the relative accuracy of X-band DSD retrieval against DSD estimates from S-band radar observations and insitudisdrometer spectra. We present comparisons of various techniques for estimating DSD model parameters from attenuation-corrected X-band dual-polarization radar data. Coincident X-band polarimetric-radar (XPOL) and S-band polarimetric-radar dual-polarized radar measurements from the International H2O Project experiment as well as coincident XPOL (MP-X) measurements over disdrometer during a typhoon storm case in Japan are used to assess the accuracy of the different DSD retrieval algorithms applied to X-band radar measurements. [J947]

## "A Wavelet-Based Technique for Sea Wind Extraction from SAR Images"

We present the follow-up of our previously published work, where we described a wavelet-based method to characterize the sea surface backscatter structures in Synthetic Aperture Radar (SAR) images. The method relies on the ability of the 2-D continuous wavelet technique to detect the spatial structure of the Marine Atmospheric Boundary Layer (MABL) and to isolate wind-related cells and features. The analysis of the cells' geometry, molded by the radiometric characteristics of the sea surface, permits the identification of the wind direction inside the cells, due to the along-wind asymmetry of backscatter structures, and thus the computation of the wind speed through standard algorithms. Twenty-one SAR images (ERS-2 and Envisat ASAR Wide Swath) over the Mediterranean Sea have been analyzed, and the results are compared with satellite wind fields. The images cover a range of meteorological conditions from low to moderate winds. Comparison of the SAR-derived wind fields with those provided by satellite scatterometers indicates a good score of success (roughly 70%-80%). The developed methodology, once tested over an adequate number of images to derive statistically reliable results, could be routinely used to enrich SAR images with the wind field as well as to characterize the MABL in terms of size, distribution, and shape of the backscatter cells. [J948]

## "Accuracy of Bathymetric Assessment by Locally Analyzing Radar Ocean Wave Imagery (February 2008)"

In this paper, the error source in assessing the bathymetry by a recently presented method, the dispersive surface classificator, is discussed. This method is based on the analysis of X-band radar image sequences of sea-surface waves to determine spatial maps of hydrographic parameters. To implement this objective, the

radar-deduced bathymetry is validating by multibeam echosounder data. The accuracy of the method is high in homogeneous areas and reduced at the areas of bathymetric gradient and lower but comparable with multibeam echosounder data, under the assumption of the spatial resolution. The identification of systematic correlation of the absolute value of the error with the slope is significant and insignificant with the actual depth itself. The spatial correlation of the error illustrates that the direction of the wave field influences the neighboring grid cell in the same direction. The application of the method during crucial weather conditions is the main advantage and permits the accurate operational nearshore monitoring for several applications. [J949]

## "Model-Based Interpretation of High-Resolution SAR Images of Buildings"

High-resolution (HR) synthetic aperture radar (SAR) images of urban areas reveal a large variety of details that, although potentially bringing a lot of information, are often very difficult to interpret. Until now, most of the research activity in this field has been devoted to the attempt to retrieve geometric information on buildings in terms of their positions and sizes, by using simplified geometrical models. However, this approach does not allow us to fully exploit the large amount of information present in HR SAR images. In order to improve information retrieval from such images, and, hence, their interpretation, in this paper, we propose to employ a more refined model that accounts for both geometrical (including fine details) and electromagnetic properties of the building. A meaningful case study is presented to show that the main features appearing on the SAR image of a building can be interpreted by using our geometric and electromagnetic model. In addition, a first example of retrieval of the complex dielectric constant of building materials from a SAR image is presented. [J950]

## "Remote Sensing Observation Used in Offshore Wind Energy"

Remote sensing observations used in offshore wind energy are described in three parts: ground-based techniques and applications, airborne techniques and applications, and satellite-based techniques and applications. Ground-based remote sensing of winds is relevant, in particular, for new large wind turbines where meteorological masts do not enable observations across the rotor-plane, i.e., at 100 to 200 m above ground level. Light detection and ranging (LiDAR) and sound detection and ranging (SoDAR) offer capabilities to observe winds at high heights. Airborne synthetic aperture radar (SAR) used for ocean wind mapping provides the basis for detailed offshore wind farm wake studies and is highly useful for development of new wind retrieval algorithms from C-, L-, and X-band data. Satellite observations from SAR and scatterometer are used in offshore wind resource estimation. SAR has the advantage of covering the coastal zone where most offshore wind farms are located. The number of samples from scatterometer is relatively high and the scatterometer-based estimate on wind resources appears to agree well with coastal offshore meteorological observations in the North Sea. Finally, passive microwave ocean winds have been used to index the potential offshore wind power production, and the results compare well with observed power production (mainly land-based) covering nearly two decades for the Danish area. [J951]

## "Classification With a Non-Gaussian Model for PolSAR Data"

In this paper, we present a generalized Wishart classifier derived from a non-Gaussian model for polarimetric synthetic aperture radar (PolSAR) data. Our starting point is to demonstrate that the scale mixture of Gaussian (SMoG) distribution model is suitable for modeling PolSAR data. We show that the distribution of the sample covariance matrix for the SMoG model is given as a generalization of the Wishart distribution and present this expression in integral form. We then derive the closed-form solution for one particular SMoG distribution, which is known as the multivariate K-distribution. Based on this new distribution for the sample covariance matrix, termed as the K-Wishart distribution, we propose a Bayesian classification scheme, which can be used in both supervised and unsupervised modes. To demonstrate the effect of including non-Gaussianity, we present a detailed comparison with the standard Wishart classifier using airborne EMISAR data. [J952]

## "Impact of Sun Glint on Salinity Remote Sensing: An Example With the Aquarius Radiometer"

The Aquarius/SAC-D mission will employ three L-band (1.41 GHz) radiometers dedicated to the remote sensing of sea surface salinity. The radiation from the Sun reflected at the ocean surface toward the radiometer is an important source of interference for retrieving salinity; in fact, the mission will be in a dawn/dusk Sun-synchronous orbit with the beams oriented toward the night side of the orbit in order to limit this signal. In this paper, the effect of ocean surface roughness on the reflected radiation is examined. The reflected Sun radiation can be separated into two components: (1) a quasi-specular component and (2) a scattered component, due largely to small-scale roughness. We show that the first component has a large brightness temperature but, in the Aquarius geometry, is located far from the antenna boresight. The scattered component has relatively small brightness temperature but can extend to the antenna boresight where the gain is maximum. This can occur at high latitude near the summer solstice when the antenna footprint is not in shadow and can cause significant

contamination. While the calculations have been done for the specific geometry of the Aquarius instrument, the conclusions drawn regarding the effect of roughness on the reflected solar radiation are characteristic of remote sensing at L-band. [J953]

## "The Compact Polarimetry Alternative for Spaceborne SAR at Low Frequency"

In spaceborne synthetic aperture radar (SAR), a single-polarization on-transmit offers twice the swath width compared to full polarization. This is linked to SAR system design issues, and, without getting into the technical details deserving by themselves a full paper, we can just mention the swath characteristics of ALOS PALSAR (the Advanced Land Observing Satellite, Phased Array L-Band Synthetic Aperture Radar), reducing from 70 km for the dual-pol mode to 30 km for the full polarization mode. The reduced coverage in the full polarization mode has a harmful impact on the revisit time, which is always a major drive for the Earth-observing community. The options chosen up to now for dual-pol system designs (or single-polarization on-transmit) rely on a linear polarization on-transmit [either horizontal (H) or vertical (V)], with two orthogonal polarizations on-receive. Souyris and Raney in earlier papers proposed more pertinent alternatives for the selection of the transmit polarization leading to a better characterization of the scattering mechanisms. In this paper, the analysis is pursued in more depth by including the effect of the ionosphere on the wave propagation and extending the applications to polarimetric interferometry SAR (PolInSAR). A compact mode is developed where the transmit polarization is circular, whereas the only constraint on the two receiving polarizations is independence. Indeed, the choice of the polarizations of the two receive channels does not matter, as any polarization on-receive can be synthesized from these two measurements. This is, however, not the case for the unique transmit polarization. At a low frequency, where the ionosphere has a significant effect, the circular transmit polarization is the only sensible option, as it provides an effective constant polarization as seen by the scattering surface. This is an essential condition for a meaningful multitemporal analysis. Both the polarimetric SAR applications and the PolInSAR appl--ications in the context of this compact polarimetry (CP) mode are explored. A pseudocovariance matrix can be reconstructed following Souyris' proposed approach for distributed targets and is shown to be very similar to the full polarimetric (FP) covariance matrix. The reconstruction of the cross-polarized Sigma0 is shown to be reliable and to have very low sensitivity to Faraday rotation. A PolInSAR vegetation height inversion for P-band is presented and applied to the CP data with a level of performance that is similar to the one derived from FP (a 1.2-m root-mean-square height error on the ONERA Airborne radar (RAMSES) data over the Landes Forest). A procedure is developed to correct for the ionospheric effects for the PolInSAR acquisition in the FP or CP mode and is assessed on the data simulated from an airborne acquisition. The results demonstrate that the technique is efficient and robust. The calibration of CP data is identified as an important challenge to be solved, and some clues are provided to address the problem. [J954]

## "Measurement and Characterization of Entropy and Degree of Polarization of Weather Radar Targets"

To date, few polarimetric weather radars have exhibited the capability to measure full scattering matrices. In contrast, in the synthetic aperture radar (SAR) community, considerable experience has been gained in dealing with complete scattering matrices and their statistical behavior. This paper aims to place weather radar parameters in a wider context in order to exploit more general concepts like target decomposition theorems and polarization basis transformations. Entropy, which is a fully polarimetric variable derived from the Cloude-Pottier decomposition, and the degree of polarization, which is derived from Wolf's coherence matrix, are the subject of this paper. The theoretical analysis carried out in the first part is checked against fully polarimetric data from POLDIRAD, which is the german aerospace center research weather radar. The entropy and the degree of polarization are compared with the copolar correlation coefficient in order to understand whether they can add value to radar meteorological investigations. Because the degree of polarization is available to conventional dual-polarization coherent systems, it is important to assess its potential for operational use. [J955]

## "Radar Imaging of Urban Areas by Means of Very High-Resolution SAR and Interferometric SAR"

In remote-sensing applications, the monitoring of urban areas by means of synthetic aperture radar (SAR) sensors has grown into a valuable and indispensable tool. Although SAR imaging with a spatial resolution down to 1 m is widespread, a resolution as fine as 10 cm and below is offered only by very few SAR sensors worldwide. In this paper, the potential of very high-resolution radar imaging of urban areas by means of SAR and interferometric imaging will be demonstrated and discussed. Results of urban SAR imaging down to subdecimeter resolution will be shown. Even though the immanent layover situation in urban areas is an obstacle to simple image understanding, a remedy can be found by using interferometric SAR imaging. Interferometric results based on very high-resolution SAR images acquired over urban areas, partially with a severe layover situation, will be presented. The corresponding data was acquired with the phased array multifunctional imaging radar (PAMIR), the X-band demonstrator of the Research Institute for High Frequency

Physics and Radar Techniques (FHR), Forschungsgesellschaft fur Angewandte Naturwissenschaften (FGAN), Wachtberg, Germany. It can be stated that high-resolution interferometric SAR will be an important basis for upcoming radar-based urban analysis. [J956]

## "Wide-Area Traffic Monitoring With the SAR/GMTI System PAMIR"

This paper presents a wide area traffic monitoring experiment under real conditions, using the scan-MTI mode of the airborne radar sensor PAMIR. This flexible GMTI (Ground Moving Target Indication) mode was designed in order to rapidly monitor wide areas for moving targets. The scan operation enables the detection of targets from different aspect angles with a high revisit rate. The parameters (e.g., radial velocity, signal-to-noise ratio, and positioning accuracy) of the detected vehicles are investigated and compared to the expected theoretical GMTI performance. It will be shown that the scan-MTI mode is particularly adapted to perform an efficient wide-area traffic monitoring. [J957]

## "An Autofocus Approach for Residual Motion Errors With Application to Airborne Repeat-Pass SAR Interferometry"

Airborne repeat-pass SAR systems are very sensible to subwavelength deviations from the reference track. To enable repeat-pass interferometry, a high-precision navigation system is needed. Due to the limit of accuracy of such systems, deviations in the order of centimeters remain between the real track and the processed one, causing mainly undesirable phase undulations and misregistration in the interferograms, referred to as residual motion errors. Up to now, only interferometric approaches, as multisquint, are used to compensate for such residual errors. In this paper, we present for the first time the use of the autofocus technique for residual motion errors in the repeat-pass interferometric context. A very robust autofocus technique has to be used to cope with the demands of the repeat-pass applications. We propose a new robust autofocus algorithm based on the weighted least squares phase estimation and the phase curvature autofocus (PCA) extended to the range-dependent case. We call this new algorithm weighted PCA. Different from multisquint, the autofocus approach has the advantage of being able to estimate motion deviations independently, leading to better focused data and correct impulse-response positioning. As a consequence, better coherence and interferometric-phase accuracy are achieved. Repeat-pass interferometry based only on image processing gains in robustness and reliability, since its performance does not deteriorate with time decorrelation and no assumptions need to be made on the interferometric phase. Repeat-pass data of the E-SAR system of the German Aerospace Center (DLR) are used to demonstrate the performance of the proposed approach. [J958]

## "Investigating Attenuation, Scattering Phase Center, and Total Height Using Simulated Interferometric SAR Images of Forested Areas"

The objective of this paper is to examine the link between the attenuation coefficients and the interferometric phase center heights, for several frequencies from P- to L-band, and to study the extent to which it depends on the canopy architecture and description. This paper relies on the use of a coherent and full polarimetric scattering model, which simulates the fields backscattered by a forested area. In the first part, we study the behavior with a frequency of the interferometric phase center heights, and in the second part, we focus on the attenuation coefficients. Then, we compare the behaviors of these two quantities, and we propose to empirically derive a relation between these two quantities and the mean forest height. Finally, we investigate if a change in the initial forest or radar configuration has an impact on the determination of this relation. [J959]

## "Retrieving Optical Depths and Lidar Ratios for Transparent Layers Above Opaque Water Clouds From CALIPSO Lidar Measurements"

For measurements that are made by the CALIPSO lidar, the layer-integrated attenuated backscatter of opaque water clouds gamma'water,Ocan be accurately estimated for those cases for which there is no overlying aerosol or cloud layer. When transparent overlying layers of clouds or aerosols are present, the layer-integrated attenuated backscatter that is measured for the water cloud is reduced by a factor that is equal to the two-way transmittance of the upper layer. Because the layer-integrated depolarization ratio can be used to obtain an independent estimate of gamma'water,O, we can subsequently derive both the optical depth and an estimate of the layer-averaged lidar ratio of the overlying layer. [J960]

## "Geocoding of Synthetic Aperture Radar Images Using Digital Vector Maps"

In this letter, a possible approach to automate synthetic aperture radar (SAR) geocoding (or to automatically refine the existing one) is presented. The procedure is based on edge detection, where ground control lines obtained from digital vector maps are located in the SAR images. In geocoding, affine, projective, and rigorous

SAR sensor transformation models can be used. According to the experiments, the procedure seems to be accurate and reliable as long as the initial values of the geocoding transformation model are accurate enough. The procedure copes well with displacements of about ten pixels on SAR images, but good results have been obtained in cases of even larger displacements. According to the well-defined checkpoints, the resulting geocoding accuracies for test images were around a few pixels. When the rigorous SAR sensor model was used, the accuracies were less than two pixels in most cases. [J961]

## "Singularity-Spreading Phase Unwrapping"

How to process phase singular points (SPs), or residues, is a difficult problem in a 2-D phase-unwrapping process to generate digital elevation maps (DEMs). Although the minimum-cost network-flow method is an effective and widely used technique, some problems still remain. That is, the method often generates spikes in high SP-density areas and long clifflike artifacts for isolated SPs. It also takes a long time to unwrap phase data that contain many SPs. In this paper, we propose a new unwrapping method, namely, singularity-spreading phase unwrapping (SSPU), which solves these problems. In this method, we spread the singularity at SPs around to make the closely located positive and negative SPs combine gently with each other or make the isolated SPs fade away. Experiments demonstrate that the spreading process compensates the distortion in phase values in the vicinities of SPs appropriately for landscape reconstruction. The SSPU generates high-quality DEMs with smaller calculation costs than the conventional method. Besides the simple SSPU, we also present weighted SSPU where we utilize amplitude information to improve the performance further. In addition, we discuss the relationship between landscape characteristics and SSPU performance. [J962]

## "High-Resolution Spaceborne SAR Focusing by SVD-Stolt"

In spaceborne synthetic aperture radars (SARs), the orbit curvature may prevent the use of the processor, causing artifacts that depend on both the extent of the orbit arc and the slant range interval. A viable solution has been derived by extending the singular value decomposition-Stolt approach that was proposed for geophysical applications to microwave SAR. The resulting processor has the same simple scheme as the approach but a different (numerical) computation of both the reference and the Stolt interpolation. [J963]

## "Comparison of Raindrop Size Distribution Estimates From X-Band and S-Band Polarimetric Observations"

This letter evaluates the consistency of rainfall drop size distribution (DSD) parameters that were estimated from attenuation-corrected X-band dual-polarization (XPOL) radar measurements with estimates from a colocated S-band dual-polarization radar (S-Pol). The DSD retrieval technique uses reflectivity and differential reflectivity, and a constrained relationship to estimate the three parameters of a ldquonormalizedrdquo gamma distribution model. The more definitive S-Pol DSD parameter estimates are used as a reference to assess the performance of the corresponding XPOL estimates for different rain-path attenuation values. Results show that XPOL attenuation-corrected profiles can provide rainfall DSD estimations that are consistent to an S-band dual-polarization radar, even in cases of moderate to high rain-path attenuation. [J964]

## "Impact of Uncertainty in the Drop Size Distribution on Oceanic Rainfall Retrievals From Passive Microwave Observations"

The variability of the drop size distribution (DSD) is one of the factors that must be considered in understanding the uncertainties in the retrieval of oceanic precipitation from passive microwave observations. Here, we have used observations from the Precipitation Radar on the Tropical Rainfall Measuring Mission spacecraft to infer the relationship between the DSD and the rain rate and the variability in this relationship. The impact on passive microwave rain rate retrievals varies with frequency and rain rate. The total uncertainty for a given pixel can be slightly larger than 10% at the low end (ca. 10 GHz) of frequencies commonly used for this purpose and smaller at higher frequencies (up to 37 GHz). Since the error is not totally random, averaging many pixels, as in a monthly rainfall total, should roughly halve this uncertainty. The uncertainty may be lower at rain rates less than about 30 mm/h, but the lack of sensitivity of the surface reference technique to low rain rates makes it impossible to tell from the present data set. [J965]

## "Short-Pulse Electromagnetic Scattering by Buried Perfectly Conducting Cylinders"

In this letter, the electromagnetic scattering problem of a short-pulse plane wave by a finite set of buried perfectly conducting circular cylinders is addressed in the time domain. The described procedure is applicable for arbitrary polarization and for any cylinder size and configuration in both near- and far-field regions. The solution is performed through an angular-spectrum representation of the scattered field. A parametric analysis on the

effects of the various geometrical parameters is reported, and numerical results are presented. [J966]

## "Motion Analysis in SAR Images of Unfocused Objects Using Time-Frequency Methods"

Synthetic aperture radar (SAR) image formation processing assumes that the scene is stationary, and to focus an object, one coherently sums a large number of independent returns. Any target motion introduces phases that distort and/or translate the target's image. Target motion produces a smear primarily in the azimuth direction of the SAR image. Time-frequency (TF) modeling is used to analyze and correct the residual phase distortions. An interactive focusing algorithm based on TF modeling demonstrates how to correct the phase and to rapidly focus the mover. This is demonstrated on two watercraft observed in a SAR image. Then, two time-frequency representations (TFRs) are applied to estimate the motion parameters of the movers or refocus them or both. The first is the short-time Fourier transform, from which a velocity profile is constructed based on the length of the smear. The second TFR is the time-frequency distribution series, which is a robust derivative of the Wigner-Ville distribution that works well in this SAR environment. The smear is a modulated chirp, from which a velocity profile is plotted and the phase corrections are integrated to focus the movers. The relationship between these two methods is discussed. Both methods show good agreement on the example. [J967]

## "A Beginner's Guide to Interferometric SAR Concepts and Signal Processing [JAESS Tutorial IV]"

Interferometric synthetic aperture radar (IFSAR, also abbreviated as InSAR) employs pairs of high resolution SAR images to generate high quality terrain elevation maps using phase interferometry methods. IFSAR provides an all-weather, day/night capability to generate measurements of terrain elevation on a dense grid of sample points with accuracies of ones of meters. Both spaceborne and airborne IFSAR systems are in use. In this paper we present a tutorial introduction to the concepts, techniques, and applications of IFSAR. After a brief introduction to digital elevation models (DEMs) and digital terrain elevation data (DTED), the fundamental IFSAR equation relating interferometric phase measurements to terrain elevation is derived from simple geometric considerations. The central section of the paper describes the major algorithmic steps required to form an IFSAR terrain map. Finally, variations of IFSAR for mapping terrain elevation or reflectivity changes are briefly described. A Web site at users.ece.gatech.edu/~mrichard/AESSJFSAR.htm provides access to color versions of many of the IFSAR images included in this paper. [J968]

## "A Rapid and Automatic MRF-Based Clustering Method for SAR Images"

This letter presents a precise and rapid clustering method for synthetic aperture radar (SAR) images by embedding a Markov random field (MRF) model in the clustering space and using graph cuts (GCs) to search the optimal clusters for the data. The proposed method is optimal in the sense of maximum a posteriori (MAP). It automatically works in a two-loop way: an outer loop and an inner loop. The outer loop determines the cluster number using a pseudolikelihood information criterion based on MRF modeling, and the inner loop is designed in a ldquohardrdquo membership expectation-maximization (EM) style: in the E step, with fixed parameters, the optimal data clusters are rapidly searched under the criterion of MAP by the GC; and in the M step, the parameters are estimated using current data clusters as ldquohardrdquo membership obtained in the E step. The two steps are iterated until the inner loop converges. Experiments on both simulated and real SAR images test the performance of the algorithm. [J969]

## "Single Range Matching Filtering for Space Debris Radar Imaging"

In the recent literature, only single-range Doppler interferometry (SRDI) has been considered for radar imaging of space debris with dimensions smaller than the radar range resolution. Considering the typical trajectories and dynamics of space debris, a single-range matching filtering (SDMF) approach is proposed in this letter. SDMF permits obtaining a 2-D image of space debris by using range unit cross-range echo data and by matched filtering the signals with different turning radii. The analysis and simulations show that, compared with SRDI, the proposed approach has less computational load and better images, particularly, for targets with smaller size. [J970]

## "Sea-Ice Deformation State From Synthetic Aperture Radar Imagery-Part I: Comparison of C- and L-Band and Different Polarization"

In this paper, we present a quantitative comparison of L- and C-band airborne synthetic aperture radar imagery acquired at like- and cross-polarizations over deformed sea ice under winter conditions. The parameters characterizing the deformation state of the ice are determined at both radar bands and at different polarizations. The separation of deformed and level ice is based on a target detection technique. The threshold is set such that image pixels with intensities equal to or larger than the highest 2% of the level-ice intensity distribution are classified as deformed ice, independent of the radar configuration and ice conditions. Optical imagery of

sufficient quality for comparison is available only in a very few cases. To characterize the deformation state, the areal fraction of deformation features and the average distance between these features are evaluated. The values obtained for both parameters are very sensitive to the radar frequency. Aeral fractions are larger, and average distances are smaller at L-band than at C-band because of the much higher intensity contrast between the deformed and level ice at L-band. The differences between polarizations at one radar band are smaller but not always negligible. In comparison to optical images, it was observed that deformed-ice areas can be distinguished from level ice over their whole length and extension at L-band, whereas at C-band, often, only prominent parts are visible. [J971]

## "Least Squares Estimation of Doppler and Polarimetric Parameters for Weather Targets"

Doppler and polarimetric parameters have shown to be of great utility in weather radar applications. Different measurement schemes have been proposed and implemented to obtain Doppler and polarimetric information of the sensed weather target. To date, none of these methods is capable of providing all polarimetric and Doppler parameters of interest for the whole range of temporal correlation conditions. To obtain all parameters, some of the systems require to assume different hypotheses about the Doppler or polarimetric characteristics of the targets. Failure of the assumed hypotheses leads to unacceptable bias and loss of performance of the estimated parameters. Other methods reach a tradeoff, reducing either the number of polarimetric parameters to be estimated or the maximum measurable range of Doppler parameters. With respect to polarimetric parameter estimation, it has already been shown that alternate transmission of three different polarizations improves polarimetric parameter estimation through decoupling of temporal and polarimetric effects. In this paper, this measurement system is generalized by means of a new data processing algorithm and a least squares estimation to provide joint estimates of all Doppler and polarimetric parameters for all temporal correlation conditions. No hypotheses are required. In fact, this method provides minimum variance unbiased linear estimates of all elements of the polarimetric covariance matrix. It also allows Doppler parameter estimation within their corresponding maximum measurable ranges, which are determined by the radar base pulse repetition frequency. The performance of Doppler parameter estimates is comparable to that reached by nonpolarimetric systems. Implementation of the method requires transmitting three known polarizations. Moreover, phase shifts between them should be either known or measured. [J972]

## "A Novel Clutter Suppression Algorithm for Landmine Detection With GPR"

In this paper, we propose a new algorithm for the enhancement of plastic-cased antipersonnel mine detection using a video-impulse ground-penetrating radar (GPR). The algorithm is implemented as a nonlinear signal processor, which searches for the presence of a reference waveform in a 1D GPR echo return. The reference waveform represents a class of targets within a certain environment. The processor marks the presence of all responses similar to the reference waveform with a sharp mono-cycle. Simultaneously, responses with different waveforms, which presumably correspond to clutter, are suppressed. The reference waveform and other algorithm parameters are determined from training data sets acquired in a controlled environment. After training, the algorithm can be successfully applied at sites where soil, targets, and measurement scenarios are similar but not identical to those of the training site. The processor is integrated into an automated data processing and mine detection scheme as an additional clutter suppression step. The scheme consists of clutter suppression, synthetic aperture radar focusing, construction of a confidence map, and automated detection in it. The suggested algorithm is tested on experimental data, and its performance is compared against schemes where clutter suppression is organized by means of background removal and the cross correlation with a reference wavelet. The performance comparison is done in terms of receiver operating characteristic curves. It has been found that the suggested algorithm reduces the false alarm rate in about two and a half times in comparison to the cross-correlation-based clutter suppression. [J973]

## "An Interacting Multiple-Model-Based Abrupt Change Detector for Ground-Penetrating Radar"

In this letter, we propose an interacting multiple-model (IMM)-based abrupt change detector for ground-penetrating radar (GPR) applications. Ground clutter varies with surface roughness, soil nature, as well as depth of the soil layer, necessitating a multiple-model approach. The IMM is first trained for a chosen number of models and then used to characterize the GPR data. The IMM predictor segments the entire GPR data into regions of identical models and then identifies targets by detecting abrupt changes in model parameters. The number of models is determined using the minimum prediction error criterion. The prediction performance of the IMM predictor is theoretically analyzed, and its detection performance is also evaluated through an receiver operating characteristics analysis to illustrate the improved performance of the proposed detector. [J974]

## "Radar Signatures of a Passenger Car"

Upcoming new synthetic aperture radar (SAR) satellites such as TerraSAR-X and Radarsat-2 offer high spatial image resolution and dual receive antenna capabilities, which open new opportunities for worldwide traffic monitoring applications. If the radar cross section (RCS) of the vehicles is strong enough, they can be detected in the SAR data, and their speed can be measured. For system performance prediction and algorithm development, it is therefore indispensable to know the RCS of typical passenger cars. The geometry parameters that have to be considered are the radar look direction, incidence angle, and vehicle orientation. In this letter, the radar signatures of nonmoving or parking cars are presented. They are measured experimentally from airborne experimental SAR (E-SAR) data, which have been collected during flight campaigns in 2005 and 2006 with multiple overflights at different aircraft headings. The radar signatures could be measured for the whole range of aspect angles from 0 to 180 and with high angular resolution due to the large synthetic aperture length of the E-SAR radar sensor. The analysis for one type of passenger car and particular incidence angles showed that the largest radar cross-sectional values and, thus, the greatest chance of detection of the vehicles appear when the car is seen from the front, back, and side. Radar cross-sectional values for slanted views are much lower and are therefore less suitable for car detection. The measurements have been performed in the -band (9.6 GHz) with VV-polarization, and at incidence angles of 41.5deg and 42.5deg. The derived radar signature profile can also be used for the verification of radar cross-sectional simulation studies. [J975]

## "DEM by Ground-Based SAR Interferometry"

In this letter, a ground-based synthetic aperture radar (SAR) interferometer was used to generate digital elevation maps (DEMs) of the illuminated area. With respect to other ground-based data processing techniques, here, the effect of the propagation through the atmosphere is considered. An algorithm similar to multipass satellite SAR techniques was developed in accordance with the phase model used in the ground-based interferometry. Many images taken from different viewing angles were collected and combined to form different interferograms at a test site in Austria. Results from this technique have been compared with an existing geographic model of the test area. [J976]

## "Texture-Preserving Despeckling of SAR Images Using Evidence Framework"

In this letter, a texture-preserving despeckling algorithm for synthetic aperture radar images using an evidence framework is proposed. The salient aspects of this approach are given as follows. (1) The maximum a posteriori estimate can be guaranteed to converge to the optima by selecting the Gaussian distribution and Gaussian Markov random field model as the likelihood function and prior model, respectively. (2) MacKay's evidence framework can automatically sustain the balance between speckle reduction and texture preservation. (3) We use the Jeffreys prior to perform the second-level inference of the evidence framework. Experimental results are given to demonstrate the validity of the proposed despeckling method. [J977]

## "Effect of Long Waves on Ku-Band Ocean Radar Backscatter at Low Incidence Angles Using TRMM and Altimeter Data"

This letter uses a large ocean satellite data set to document relationships between Ku-band radar backscatter (sigmao) of the sea surface, near-surface wind speed (U), and ocean wave height (SWH). The observations come from satellite crossovers of the Tropical Rainfall Mapping Mission (TRMM) Precipitation Radar (PR) and two satellite altimeters, namely: 1) Jason-1 and 2) ENVISAT. At these nodes, we obtain TRMM clear-air normalized radar cross-section data along with coincident altimeter-derived significant wave height. Wind speed estimates come from the European Centre for Medium-Range Weather Forecast. TRMM PR is the first satellite to measure low incidence Ku-band ocean backscatter at a continuum of incidence angles from 0deg to 18deg. This letter utilizes these global ocean data to assess hypotheses developed in past theoretical and field studies. [J978]

## "Signal Representation and the Nonlinear Property of Phase Images"

This letter proposes a representation of pixel value in a phase image as a complex number, which implies that the phase image is a nonlinear field. Consequently, conventional linear filtering will not properly work. Local statistics filters (LSFs) are chosen as a special case of the signal-processing algorithm to show the significance of signal representation to filtering performance. First, relationships among various LSFs, namely, ordinary LSF, speckle LSF, and phasor LSF, are discussed. We found that they are related to each other, whose general form is a complex-valued LSF (CV-LSF). It is also realized that directional windowing for the CV-LSF is actually not required, which indicates that the complex-valued formulation (representation and algorithm) is the most suitable one for phase image filtering. We demonstrate that the linear filtering to a simulated complex-valued image and an actual interferometric synthetic aperture radar image will start to fail when the window size is subsequently enlarged due to the nonlinear nature of the phase image. [J979]

## "Effects of Forest Biomass and Stand Consolidation on P-Band Backscatter"

In previous studies, P-band synthetic aperture radar (SAR) has shown potential for biomass retrieval in forests. However, while measurements show a general agreement that backscatter increases with increasing biomass, different studies show that the backscatter from stands of similar biomass can significantly vary depending on forest structure, hence making biomass retrieval more challenging. In this letter, we show that, while biomass may be the single most important parameter determining the backscatter from a forest, the number density of trees has also a major impact. This can be explained using simple arguments, leading us to propose the use of the biomass-consolidation index to describe P-band HV-polarized backscatter. This is supported by electromagnetic-modeling studies and by a few measurements from boreal forest made with the AIRSAR system over the BOREAS test site in Canada. [J980]

## "An Ocean Surface Wind Vector Model Function for a Spaceborne Microwave Radiometer"

Surface wind vector measurements over the oceans are vital for scientists and forecasters to understand the Earth's global weather and climate. In the last two decades, operational measurements of global ocean wind speeds were obtained from passive microwave radiometers (Special Sensor Microwave/ Imagers); and over this period, full ocean surface wind vector data were obtained from several National Aeronautics and Space Administration and European Space Agency scatterometry missions. However, since SeaSat-A in 1978, there have not been other combined active and passive wind measurements on the same satellite until the launch of Japan Aerospace Exploration Agency's Advanced Earth Observing Satellite-II in 2002. This mission provided a unique data set of coincident measurements between the SeaWinds scatterometer and the Advanced Microwave Scanning Radiometer (AMSR). The AMSR instrument measured linearly polarized brightness temperatures (TB) over the ocean. Although these measurements contained wind direction information, the overlying atmospheric influence obscured this signal and made wind direction retrievals not feasible. However, for radiometer channels between 10 and 37 GHz, a certain linear combination of vertical and horizontal brightness temperatures causes the atmospheric dependence to cancel and surface parameters such as wind speed and direction and sea surface temperature to dominate the resulting signal. In this paper, an empirical relationship between AMSR TB's (specifically A .TBV- TBH) and surface wind vectors (inferred from SeaWinds' retrievals) is established for three microwave frequencies: 10, 18, and 37 GHz. This newly developed wind vector model function for microwave radiometers can serve as a basis for wind vector retrievals either separately or in combination with active scatterometer measurements. [J981]

## "Global Analysis of Envisat RA-2 Burst Mode Echo Sequences"

The Envisat RA-2 burst echoes are being gathered throughout the mission; however, these data are only now being made generally available by the European space agency. Considerable work has been necessary to turn these engineering-level data into a useable altimeter product. This paper documents the processing steps undertaken to generate usable data and presents the first extensive analysis of this unique dataset, using over 75 000 burst sequences with a global distribution. The results show that the burst echo data from Envisat are of extremely low noise, which is particularly evident over non-ocean surfaces, and contain a wealth of detailed information from both land and ocean surfaces. Examples illustrate the complexity of surface response from targets such as inland water and rough terrain. These unique data clearly have the potential to inform future instrument design as well as to improve the understanding of existing altimeter datasets. [J982]

## "Image-Driven Data Mining for Image Content Segmentation, Classification, and Attribution"

Image-driven data mining methods are described for image content segmentation, classification, and attribution, where each pixel location of an image-under-analysis is the center point of a pixel-block query that returns an estimated class label. Feature attribute estimates may also be mined when sufficient attribute strata exist in the data warehouse. Novel methods are presented for pixel-block mining, pattern similarity scoring, class label assignments, and attribute mining. These methods are based on a direct sum tree structure called a sigma-tree that is utilized with near-neighbor similarity scoring. The sigma-tree structure provides a solution to the challenge of high computation/memory costs of pixel-block similarity searching. The sigma-trees are integrated into warehouse subsystems that provide referential capability into feature attribute data, resulting in a foundation for data mining called Source Optimized, Labeled, DIgital Expanded Representations (SOLDIER). The variable depth "bit-plane" data representations produced by sigma-tree path selections provide an approach to image content segmentation, and provide a structure for formulation of Bayesian classification with data-adaptive Parzen classifiers with variably sized windows. Preliminary methods and results for postprocessing of mined feature-thematic layers for higher level scene understanding are also presented. Sample results are shown with synthetic aperture radar images and with high-resolution pan-sharpened satellite images of the Payagala, Sri Lanka area before the site was devastated by the 2004 Asian Tsunami. [J983]

## "Correlation Properties of Signals Backscattered From Fractal Profiles"

A successful mathematical description of natural landscapes relies upon a class of random processes known as fractional Brownian motions (fBms), which may exhibit correlation with long-range dependence (LRD). In remote sensing applications, the sensor observes a certain real scene Band records data Ifor successive signal processing tasks. Assuming that B is modeled as an fBm, does the recorded signal Ipreserve the LRD character of B? More in general, can we relate the Hurst coefficient (an index of LRD) of the real scene to that of the recorded data? We address the problem in a simplified setup in which the data are related to (the slope of) the original scene through a zero-memory mapping. A mathematical framework is presented in which the above questions can be answered in the asymptotic regime of infinite data size. The effect of the finite sample size is also investigated. The mathematical model is also validated by real data, which are collected by a synthetic aperture radar that is mounted onboard of ERS-1/2 satellites. [J984]

## "Paddy Fields as Electrically Dense Media: Theoretical Modeling and Measurement Comparisons"

Early models for paddy fields consist of a single-layered medium in which coherent effects within clusters of leaves are considered but multiple volume scattering is not. In this paper, the paddy canopy is modeled as a multilayered dense discrete random medium consisting of cylindrical and needle-shaped scatterers. Consideration is given to the coherent and near-field effects of the closely spaced scatterers through the Dense Medium Phase and Amplitude Correction Theory and Fresnel corrections, respectively, in the phase matrix. Then, this dense medium phase matrix is applied in the radiative transfer equations and solved up to the second order to consider double-volume scattering. Ground truth measurements of paddy fields were acquired at Sungai Burung, Selangor, Malaysia, for an entire season from the early vegetative stage of the plants to their reproductive stage. Measured parameters are used in the theoretical model to calculate the backscattering coefficients of paddy fields. Theoretical analysis of the simulation results shows in particular that second-order effects are important for cross-polarized backscatter data and that coherent effects need to be considered at lower frequencies. However, the use of needles to represent paddy leaves tends to underestimate the HH-polarized backscattering coefficients especially at the latter stages of plant growth, i.e., when the leaves are broader. The results are also used for comparisons with the backscattering coefficients obtained from RADARSAT images as well as that of earlier models to test the validity of the dense medium model with promising results. [J985]

## "Ultrawideband Radar Measurements of Thickness of Snow Over Sea Ice"

An accurate knowledge of snow thickness and its variability over sea ice is crucial in determining the overall polar heat and freshwater budget, which influences the global climate. Recently, algorithms have been developed to extract snow thicknesses from satellite passive microwave data. However, validation of these data over the large footprint of the passive microwave sensor has been a challenge. The only method used thus far has been with meter sticks during ship cruises. To address this problem, we developed an ultrawideband frequency-modulated continuous-wave radar to measure the snow thickness over sea ice. We synthesized a very linear chirp signal by using a phase-locked loop with a digitally generated chirp signal as a reference to obtain a fine-range resolution. The radar operates over the frequency range from 2-8 GHz. We made snow-thickness measurements over the Antarctic sea ice by operating the radar from a sled in September and October 2003. We performed radar measurements over 11 stations with varying snow thicknesses between 4 and 85 cm. We observed an excellent agreement between radar estimates of snow thickness with physical measurements, achieving a correlation coefficient of 0.95 and a vertical resolution of about 3 cm. Comparison of simulated radar waveforms using a simple transmission line model with the measurements confirms our expectations that echoes from snow-covered sea ice are dominated by reflections from air-snow and snow-ice interfaces. [J986]

## "Full-Waveform Inversion of Crosshole Radar Data Based on 2-D Finite-Difference Time-Domain Solutions of Maxwell's Equations"

Crosshole radar techniques are important tools for a wide range of geoscientific and engineering investigations. Unfortunately, the resolution of crosshole radar images may be limited by inadequacies of the ray tomographic methods that are commonly used in inverting the data. Since ray methods are based on high-frequency approximations and only account for a small fraction of the information contained in the radar traces, they are restricted to resolving relatively large-scale features. As a consequence, the true potential of crosshole radar techniques has yet to be realized. To address this issue, we introduce a full-waveform inversion scheme that is based on a finite-difference time-domain solution of Maxwell's equations. We benchmark our new scheme on synthetic crosshole data generated from suites of increasingly complex models. The full-waveform tomographic images accurately reconstruct the following: (1) the locations, sizes, and electrical properties of isolated subwavelength objects embedded in homogeneous media; (2) the locations and sizes of adjacent subwavelength

objects embedded in homogeneous media; (3) abrupt media boundaries and average and stochastic electrical property variations of heterogeneous layered models; and (4) the locations, sizes, and electrical conductivities of water-filled tunnels and closely spaced subwavelength pipes embedded in heterogeneous layered models. The new scheme is shown to be remarkably robust to the presence of uncorrelated noise in the radar data. Several limitations of the full-waveform tomographic inversion are also identified. For typical crosshole acquisition geometries and parameters, small resistive bodies and small closely spaced dielectric objects may be difficult to resolve. Furthermore, electrical property contrasts may be underestimated. Nevertheless, the full-waveform inversions usually provide substantially better results than those supplied by traditional ray methods. [J987]

## "Scale Model Experimental Validation and Calibration of the Half-Space Green's Function Born Approximation Model Applied to Cross-Well Radar Sensing"

Efficient forward models that describe the physical nature of the geophysical problem are desired for subsurface sensing and reconstruction of a contrasting contaminant pool volume. An analytical model to approximate sensing with radar is developed and implemented in the frequency domain in terms of the half-space lossy dyadic Green's function. The Born approximation is employed as a linear forward model, which will eventually be used for tomographic inversion for object detection. The forward model is compared with measurements generated by a cross-well radar (CWR) experiment in a controlled soil test tank using broadband borehole antennas. Soil parameter (dielectric constant and loss tangent) variance with frequency is represented by a quadratic polynomial. Calibration for soil parameters is performed via CWR data using an iterative nonlinear parameterized inversion technique. With the appropriate calibration, good agreement is obtained with wideband experimental measurements for several different borehole antenna placements, confirming the accuracy of the model. [J988]

## "A Large-Scale Systematic Evaluation of Algorithms Using Ground-Penetrating Radar for Landmine Detection and Discrimination"

A variety of algorithms for the detection of landmines and discrimination between landmines and clutter objects have been presented. We discuss four quite different approaches in using data collected by a vehicle-mounted ground-penetrating radar sensor to detect landmines and distinguish them from clutter objects. One uses edge features in a hidden Markov model; the second uses geometric features in a feed-forward order-weighted average network; the third employs spectral features as its basis; and the fourth clusters edge histograms. We present the results of a large-scale cross-validation evaluation that uses a diverse set of data collected over 41 807.57 m2of ground, including 1593 mine encounters. Finally, we discuss the results of that ranking and what one can conclude concerning the performance of these four algorithms in various settings. [J989]

## "Fundamental and Higher Mode Inversion of Dispersed GPR Waves Propagating in an Ice Layer"

Dispersion of ground-penetrating radar (GPR) waves can occur when they are trapped in a layer. In this paper, we analyze the modal propagation of GPR pulses through a layer of ice that is overlying water. Dispersed transverse electric (TE) waves that are trapped in the waveguide have larger amplitudes than the critically refracted waves that travel through air, whereas the transverse magnetic (TM) critically refracted waves traveling through air are more dominant than the trapped dispersed TM waves. This can be explained by the leaky waveguide behavior of the ice layer. The reflection coefficients for the waves incident on the ice-water interface show that the TM modes are more leaky than the TE modes. Still, clear dispersion is observed in both cases, which depends on the permittivity and thickness of the ice. Similar to inversion of dispersed Rayleigh waves, these parameters can be estimated by calculating phase-velocity spectra, picking dispersion curves, and inverting the dispersion curves using a combined local and global minimization procedure. Synthetic data show several higher order modes of which separate and combined inversions return the input modeling parameters accurately. Experimental data acquired on a frozen lake show strong dispersion for the TE and TM modes. The phase-velocity spectra of the field data show three TE and four TM modes of which separate and combined inversion of different modes return similar values for the ice thickness and known permittivity of ice. Due to the more leaky behavior of the TM modes, the TE inversion is better constrained and more suitable for inversion. [J990]

## "Instructions for AP-S and URSI Authors"

{no data available} [J991]

## "SAR Remote Sensing Analysis of the Sea Surface by Polynomial Filtering [JApplications Corner]"

Synthetic aperture radar (SAR) allows the observation of the sea surface over large areas regardless of weather

conditions. In what follows we discuss a digital signal processing (DSP) formalism that makes use of polynomial filters such as Volterra models to extract the geophysical information from SAR images and to model several nonlinear transfer functions. Polynomial filters allow the extension of algorithms derived for the linear case to the nonlinear case. First, we will briefly discuss the types and sources of nonlinearities in SAR mapping of the ocean surface. Next, we will summarize the main characteristics of the Volterra filters and apply them to the understanding of hydrodynamic nonlinearities and instrumental nonlinearities. Then, we will combine their Volterra models to model the complete mapping process. Although we have only focused on the particular example of Volterra filters here, nonlinear autoregressive moving average (NARMA) models can also been applied to extract geophysical information from a nonlinear marine feature signature. [J992]

## "Real-Time Tree-Foliage Surface Estimation Using a Ground Laser Scanner"

The optimization of most pesticide and fertilizer applications is based on overall grove conditions. In this paper, we propose a measurement system to estimate the foliage surface of a tree crop. The system is based on a ground laser scanner that estimates the volume of the trees and then extrapolates their leaf area using simple and fast algorithms to allow true real-time operation. Tests with pear trees demonstrated that the relation between the volume and the foliage can be interpreted as linear with a coefficient of correlation (R) of 0.81, and the foliage surface can be estimated from this volume with an average error less than 6%. [J993]

## "Linear Fusion of Image Sets for Display"

Many remote-sensing applications produce large sets of images, such as hyperspectral images or time-indexed image sequences. We explore methods to display such image sets by linearly projecting them onto basis functions designed for the red, green, and blue (RGB) primaries of a standard tristimulus display, for the human visual system, and for the signal-to-noise ratio of the dataset, creating a single color image. Projecting the data onto three basis functions reduces the information but allows each datapoint to be rendered by a single color. Principal components analysis is perhaps the most commonly used linear projection method, but it is data adaptive and, thus, yields inconsistent visualizations that may be difficult to interpret. Instead, we focus on designing fixed basis functions based on optimizing criteria in the perceptual colorspace CIELab and the standardized device colorspace sRGB. This approach yields visualizations with rich meaning that users can readily extract. Example visualizations are shown for passive radar video and Airborne Visible/Infrared Imaging Spectrometer hyperspectral imagery. Additionally, we show how probabilistic classification information can be layered on top of the visualization to create a customized nonlinear representation of an image set. [J994]

## "Use of Enhanced-Resolution QuikSCAT/SeaWinds Data for Operational Ice Services and Climate Research: Sea Ice Edge, Type, Concentration, and Drift"

Enhanced-resolution QuikSCAT/SeaWinds (QSer) data recently entered the daily ice chart operation of the national ice services. Algorithms have been developed to extract four important sea ice parameters from this data over the whole Arctic: sea ice edge, type, concentration, and drift. This paper will summarize the different algorithms with a more detailed presentation of the sea ice concentration (IC) algorithm that has not been previously published. The sea ice edge can be detected to IC as low as 10%. Sea ice types can be roughly separated by a single threshold of 12 dB in the horizontal polarization. The IC algorithm gives reasonable qualitative results, separating into three classes: high, medium, and low ICs. It resolves even some characteristic ice features in the marginal ice zone and dynamic areas like the Fram Strait. However, it is very empirical and quantitatively not reliable. Sea ice drift can be determined with an accuracy of about 2.6 cm/s for a 48-h drift. Operating since 1999, QS is an important global data set for climate research, and two crucial applications how these sea ice products can be used for climate research are presented: the seasonal evolution of the sea ice cover and the export of sea ice volume through Fram Strait. [J995]

## "Classifying Multifrequency Fully Polarimetric Imagery With Multiple Sources of Statistical Evidence and Contextual Information"

This paper presents the use of a new distribution for fully polarimetric image classification. Several classification strategies are compared in order to assess the importance of a careful statistical modeling of the data and the complementary nature of the information provided by different frequencies. Spatial context, which is relevant in order to obtain good results with noisy data, is described by means of the multiclass Potts model, and an iterated conditional modes classification algorithm that employs pseudolikelihood is proposed. The data are described using multivariate Gaussian laws and fully multilook polarimetric distributions arising from the multiplicative model. L-band, C-band, and both bands are used to assess the influence of dimensionality on the classification. Contextual and pointwise maximum-likelihood classifications are compared using real data. Results show that both context and number of frequencies contribute for better classification products, and that, a careful

statistical description of the data leads to improved results. [J996]

## "SEABED Algorithm and Comments on “Modeling and Migration of 2-D Georadar Data: A Stationary Phase Approach”"

An imaging algorithm with a transform between the real and data spaces was proposed by Greenhalgh and Marescot for georadar data in 2006. This technique utilizes a reversible transform between the real space (X, Z = F(X)) and the data space (x, z = f(x)). The inverse transform is equivalent to the imaging method that is proposed by Li et al. (2005) if an antenna interval is short. This method was applied to preprocessing for breast cancer detection in 2005. These transforms were originally proposed by Sakamoto and Sato (2004) for an imaging with ultrawideband radar systems. By utilizing these transforms, a high-speed imaging algorithm, which is called as SEABED algorithm, was developed, which was extended to compensate for the phase rotation at caustic points, which was also described by Greenhalgh and Marescot. In addition, the SEABED algorithm was extended to apply to noisy data, 3D systems, experimental data, and bistatic radars. Note that the transform is fundamentally sensitive to noise because it includes derivative operations. A new algorithm was developed by extending the SEABED algorithm to avoid the derivative operations, which is stable and has a high resolution even for noisy data. The reversible transform in is now simultaneously and independently studied by some research groups because it is the sole solution for the imaging with wave fields. In addition, the transform has a variety of applications because it can be applied to electromagnetic waves, sonic and ultrasonic waves, seismic waves, and other waves. [J997]

## "Modeling Interferogram Stacks"

Synthetic aperture radar interferometry is limited by temporal and geometrical decorrelation. Permanent scatterers (PSs) are helpful to overcome these problems, but their density in agricultural and out-of-town areas is not always sufficient. The forthcoming availability of satellite platforms with thinner orbital tubes and shorter revisit times will enhance the use of interferogram stacks, which are usable for distributed and progressively decorrelating targets, like those found in agricultural areas. To estimate the possibilities of the interferogram stack technique, a Markovian model for the temporal decorrelation is considered. ERS-1 data measured in C-band over Rome with a three-day repeat cycle are used to identify the parameters for this model, namely, the decorrelation time (estimated as 40 days) and the short-term coherence (estimated as 0.6). In the hypothesis of small deviations from a model of the motion, the optimal weights to be used to combine a sequence of interferograms taken at intervals that are shorter than the decorrelation time are calculated in the cases of progressive and sinusoidal ground motion. The dispersion of the optimal estimate of the motion is then determined. This model is extended to frequencies other than C-band. These evaluations are compared with the known results obtained for PSs. As an example, the case of a time interval between the takes of T = 12 days is considered. With N consecutive images, interferogram stack results are equivalent to PSs if the pixel count in the window used to smooth the interferograms grows with N2. [J998]

## "Inferring Vegetation Water Content From C- and L-Band SAR Images"

This paper addresses the capability of synthetic aperture radar and optical images in combination with theoretical models to detect the vegetation water content (VWC) at field level. In this paper, a retrieval algorithm for the estimation of VWC from AirSAR acquired on vegetated fields during the SMEX'02 experiment is addressed. The aforementioned campaign has been chosen because, along with sensor observations, extensive ground truth measurements were acquired. The retrieval procedure, which is based on a Bayesian approach, has been initially developed for soil moisture extraction. It consists of two modules: one is pertinent to bare soils and the other one has been modified for vegetated fields. The last one uses the synergy with optical images to correct for the contribution of VWC. The VWC, a variable in the inversion procedure, as well as soil moisture can be estimated. The results indicate a good correlation with both ground measurements and VWC calculated from Landsat images through the use of normalized difference water index (NDWI). Furthermore, in the inversion procedure, the introduction of the dependence on roughness improves the estimates. This indicates that, even for dense vegetation, the contribution from bare soil greatly influences the radar signal. Three main levels of VWC are discriminated in the inversion procedure: values below 1 kg/m2, values between 1 and 3 kg/m2, and values greater than 3 kg/m2. [J999]

## "Along-Track Focusing of Airborne Radar Sounding Data From West Antarctica for Improving Basal Reflection Analysis and Layer Detection"

This paper presents focused synthetic aperture radar (SAR) processing of airborne radar sounding data acquired with the High-Capability Radar Sounder system at 60 MHz. The motivation is to improve basal reflection analysis for water detection and to improve layer detection and tracking. The processing and reflection analyses

are applied to data from Kamb Ice Stream, West Antarctica. The SAR processor correlates the radar data with reference echoes from subsurface point targets. The references are 1-D responses limited by the pulse nadir footprint or 2-D responses that include echo tails. Unfocused SAR and incoherent integration are included for comparison. Echoes are accurately preserved from along-track slopes up to about 0.5deg for unfocused SAR, 3deg for 1-D correlations, and 10deg for 2-D correlations. The noise/clutter levels increase from unfocused SAR to 1-D and 2-D correlations, but additional gain compensates at the basal interface. The basal echo signal-to-noise ratio improvement is typically about 5 dB, and up to 10 dB for 2-D correlations in rough regions. The increased noise degrades the clarity of internal layers in the 2-D correlations, but detection of layers with slopes greater than 3deg is improved. Reflection coefficients are computed for basal water detection, and the results are compared for the different processing methods. There is a significant increase in the detected water from unfocused SAR to 1-D correlations, indicating that substantial basal water exists on moderately sloped interfaces. Very little additional water is detected from the 2-D correlations. The results from incoherent integration are close to the focused SAR results, but the noise/clutter levels are much greater. [J1000]

## "Atmospheric Components Determination From Ground-Level Measurements During the Spectra Barax Campaigns (SPARC) Field Campaigns"

The surface processes and ecosystem changes through response analysis (SPECTRA) Barrax campaigns were validation campaigns developed in the framework of the SPECTRA mission in order to verify that the geophysical data products provided by satellite imagery are consistent with the measurements made by independent means. Two campaigns took place in Barrax, Spain, during the summers of 2003 and 2004. This paper presents the results of the characterization of the atmospheric composition from solar radiation, radiosoundings, and lidar measurements. Several potentially interesting situations involving atmospheric layers with different types of aerosols and water content are discussed. The presence of a residual layer capping the mixing layer during some days of the 2003 campaign and the arrival of a dust-rich air mass from the Sahara on the last two days of the 2004 campaign provide some relevant aerosol vertical profiles to test atmospheric correction algorithms. The study of the effects of these atmospheric situations on radiative transfer calculations is required in the development and validation of advanced atmospheric correction codes for the new generation of Earth observation systems. [J1001]

## "The Influence of Antenna Pattern on Faraday Rotation in Remote Sensing at L-Band"

The influence of the pattern of the receive antenna on measured Faraday rotation is examined in the context of passive remote sensing of soil moisture and ocean salinity at L-band. Faraday rotation is an important consideration for radiometers on future missions in space, such as SMOS and Aquarius. Using the radiometer on Aquarius as an example, it is shown that, while I = Tv + Th is independent of Faraday rotation to first order, it has rotation dependence when realistic antenna patterns are included in the analysis. In addition, it is shown that using the third Stokes parameter to measure the rotation angle can yield a result that is biased by as much as 1deg by purely geometrical issues that are associated with the finite width of the main beam. [J1002]

## "A System for the Measurement of the Amazon"

The System for the Vigilance of the Amazon (SIVAM) is a $1.4 billion dollar project of Brazil aimed at the development and deployment of a high-technology system-of-systems to perform monitoring, protection, and control of the land, air, and water resources of the Brazilian Amazon region. The primary challenge of the SIVAM project is to perform remote sensing and communications over a vast and undeveloped land area. The SIVAM network meets this challenge through an extensive network of Air Traffic Control/Surveillance Radars, Environmental Sensors, Communications Systems, Airborne Sensor Systems, and Coordination Centers. Now fully operational, the SIVAM system is the world's largest fully integrated remote monitoring system of the environment and provides critical information on a timely basis to the Brazilian government, law enforcement agencies, and to commercial, educational, and research groups. [J1003]

## "Approach of Adaptive Synchronization for Bistatic SAR Real-Time Imaging"

The use of a novel synchronization link to compensate time, phase, and spatial synchronization errors is proposed, aiming at the development of a practical synchronization technique for bistatic synthetic aperture radar (BiSAR) real-time imaging. With the proposed technique, an amplitude-modulated signal emitting from the transmitter is received by a passive receiver and divided into two channels. One is passed through an envelope detector and then used to trigger the sampling clock, and the second is used to achieve spatial synchronization and phase synchronization. Finally, the residual time synchronization errors are compensated with a proposed high-precision range realignment method, and the residual phase synchronization errors are compensated with autofocus algorithms. This technique allows a passive receiver, which is teamed with an illuminator at a safe

standoff distance, to receive the data reflected from potentially hostile areas of interest. Thus, this configuration, making real-time imaging possible, has a particular value in military applications. Simulation results show that successful adaptive synchronization for BiSAR real-time imaging is possible by using this dedicated synchronization link. [J1004]

## "Polarimetric Analysis of Bistatic SAR Images From Polar Decomposition: A Quaternion Approach"

This paper focuses on polar decomposition, which is based on the quaternion formalism, in single-look and multilook synthetic aperture radar polarimetry. Polar decomposition is used to decompose a bistatic or monostatic polarimetric scattering matrix into a product of a Hermitian matrix (boost) and a unitary matrix (rotation). After an overview of polar decomposition principle and quaternion properties, coherent (single-look complex) and incoherent (multilook) polar decompositions are discussed. In single-look polar decomposition, we introduce the boost parameter and the rotation parameter with the purpose of classifying scattering mechanisms of different natures. New relationships between these geometrical parameters and the scattering matrix elements are obtained. We also briefly reexamine the standard coherent polarimetric target decomposition algorithms in the light of quaternions. Next, an original use of polar decomposition for incoherent polarimetric imaging is proposed, which leads to the definition of the multilook boost parameter and of the degree of polarization dispersion. Subsequently, a new approach is presented, which consists in decomposing the scattering matrix into boost and rotation components before vectorization, then in averaging to generate boost and rotation coherency matrices separately. This leads to new inferred parameters: the boost and rotation entropies, and the concurrent dominant scattering mechanisms. The link between these new parameters and standard polarimetric invariants from the Cloude and Pottier decomposition is discussed. Eventually, the multilook extension of polar decomposition may allow this to be applied to the classification of remote sensing data. In this framework, a set of five parameters reducing to four in the monostatic case can be considered. [J1005]

## "Initial Images of the Synthetic Aperture Radiometer 2D-STAR"

Initial results are presented for the new synthetic aperture radiometer, 2D-STAR, which is a dual-polarized L-band radiometer that employs aperture synthesis in two dimensions. This airborne instrument is the natural evolution of the Electronically Scanned Thinned Array Radiometer, which employs aperture synthesis only in the across-track dimension, and represents a further step in the development of aperture synthesis for remote sensing applications. 2D-STAR was successfully tested in June 2003 and, then, participated in the SMEX03 and SMEX04 soil moisture experiments. A description of the instrument and initial results in the form of first images and a preliminary comparison with changes in soil moisture during SMEX03 are presented here. [J1006]

## "Improving River Flood Extent Delineation From Synthetic Aperture Radar Using Airborne Laser Altimetry"

Flood extent maps that are derived from synthetic aperture radar (SAR) images provide spatially distributed data for validating hydraulic models of river flood flow. The accuracy of such maps is reduced by a number of factors, including variation in backscatter from the different land cover types that are adjacent to the flood, changes in returns from the water surface that are caused by different meteorological conditions, and the presence of emergent vegetation. This paper describes how improved accuracy can be achieved by modifying an existing flood extent delineation algorithm to use airborne laser altimetry [light detection and ranging (lidar)] as well as SAR data. The lidar data provide an additional constraint that water line heights should vary smoothly along the flooded reach. The method was tested on a SAR image of a flood for which contemporaneous aerial photography existed, together with lidar data of the un flooded reach. The water line heights of the SAR flood extent that was conditioned on both SAR and lidar data matched the corresponding heights from the aerial photograph water line significantly more closely than those from the SAR flood extent that was conditioned only on SAR data. For water line heights in areas of low slope and vegetation, the root-mean-square error on the height differences reduced from 221.1 cm for the latter case to 55.5 cm for the former. [J1007]

## "Foreword to the Special Issue on Pattern Recognition in Remote Sensing"

The papers in this special section are devoted to pattern recognition in remote sensing applications. [J1008]

## "Spatially Nonstationary Anisotropic Texture Analysis in SAR Images"

This paper deals with spatial analysis of texture in synthetic aperture radar (SAR) images. A new parametric model for local two-point statistics of the image is introduced, in order to characterize the spatially nonstationary and anisotropic behavior of the image. The texture is first modeled by a nonstationary Gaussian process resulting from the convolution of a Gaussian white noise with a field of anisotropic Gaussian kernel with spatially varying parameters. Hence, under the hypothesis of locally stationary signal, the analytic expression of the local

autocovariance is derived. It is then explained how to simulate nonstationary K-distributed random fields by combining the new model with an already existing simulation method. A method for parameter estimation is then introduced. This method, based on the statistical product model, first corrects the speckle contribution to the local autocovariance and estimates the parameters of the model by analyzing the shape of the autocovariance. The algorithm is then evaluated over simulated and experimental data. Stationary simulations permit to show that, for a sufficient sample size, the estimator is unbiased. A test over a nonstationary simulation proves the ability of the algorithm to capture the spatial fluctuations of the texture. Finally, the method is applied to the experimental SAR data, and it is shown that a large amount of spatial information may be retrieved from the data. [J1009]

## "A Multiple Conditional Random Fields Ensemble Model for Urban Area Detection in Remote Sensing Optical Images"

With complex building composition and imaging condition, urban areas show versatile characteristics in remote sensing optical images. It demonstrates that multiple features should be utilized to characterize urban areas. On the other hand, since levels of development in neighboring areas are not statistically independent, the features of each urban area site depend on those of neighboring sites. In this paper, we present a multiple conditional random fields (CRFs) ensemble model to incorporate multiple features and learn their contextual information. This model involves two aspects: one is to use a CRF as the base classifier to automatically generate a set of CRFs by changing input features, and the other is to integrate the set of CRFs by defining a conditional distribution. The model has some distinct merits: each CRF component models a kind of feature, so that the ensemble model can learn different aspects of training data. Moreover, it lets the ensemble model search in a wide solution space. The ensemble model can also avoid the well-known overfitting problem of a single CRF, i.e., the many features may cause the redundancy of irrelevant information and result in counter-effect. Experiments on a wide range of images show that our ensemble model produces higher detection accuracy than single CRF and is also competitive with recent results in urban area detection. [J1010]

## "SAR Sea-Ice Image Analysis Based on Iterative Region Growing Using Semantics"

Synthetic aperture radar (SAR) has been intensively used for sea-ice monitoring in polar regions. A computer-assisted analysis of SAR sea-ice imagery is extremely difficult due to numerous imaging parameters and environmental factors. This paper presents a system which, with some limited information provided, is able to perform an automated segmentation and classification for the SAR sea-ice imagery. In the system, both the segmentation and classification processes are based on a Markov random-field theory and are formulated in a joint manner under the Bayesian framework. Solutions to the formulation are obtained by a region-growing technique which keeps refining the segmentation and producing semantic class labels at the same time in an iterative manner. The algorithm is a general-segmentation approach named iterative region growing using semantics, which, in this paper, is dedicated to the problem of classifying the operational SAR sea-ice imagery provided by the Canadian Ice Service (CIS). The classified image results have been validated by the CIS personnel, and the resulting classifications are quite successful using the same algorithm applied to diverse data sets. [J1011]

## "Multiscale Isotropic Matched Filtering for Individual Tree Detection in LiDAR Images"

This paper addresses the issue of automated tree detection in remote-sensing imagery, particularly in the case of light detection and ranging (LiDAR) height data. The proposed method consists of multiscale isotropic matched filtering using a nonlinear image operator optimized for object detection and recognition. The method provides a robust scale- and orientation-invariant localization of the objects of interest. The local maxima of the matched-filtering operator are located at the potential centers of the objects of interest such as the trees. The tree verification stage consists of feature extraction at the candidate tree locations and comparison with the feature reference values. Experimental examples of the application of this matched-filtering method to LiDAR images of dense forest stands and sparsely distributed trees in residential areas are provided. [J1012]

## "A New Application for PolSAR Imagery in the Field of Moving Target Indication/Ship Detection"

Recent analysis of a polarimetric synthetic aperture radar (PolSAR) velocity experiment has shown that azimuth ambiguities can provide useful information for the detection of moving targets with an across-track velocity component in PolSAR images using cross-polarization clutter cancellation. This paper examines this phenomenon using theoretical analysis and simulations and illustrates its application with experimental results. It is shown that, for reciprocal scatterers, the phase difference between HV and VH images is zero, whereas for HV and VH ambiguities, the phase difference is pi. For land applications, clutter cancellation is essential for the detection of moving targets in PolSAR images. For maritime applications, it can be used to distinguish images

from ambiguities. However, it is important to note that the underlying physical reasons for the performance of clutter cancellation are entirely different from ground moving target indication along-track interferometric SAR. It is also shown that cross-pol clutter cancellation is related to filtering of a double-rate-sampled single-channel SAR signal. [J1013]

## "TanDEM-X: A Satellite Formation for High-Resolution SAR Interferometry"

TanDEM-X (TerraSAR-X add-on for digital elevation measurements) is an innovative spaceborne radar interferometer that is based on two TerraSAR-X radar satellites flying in close formation. The primary objective of the TanDEM-X mission is the generation of a consistent global digital elevation model (DEM) with an unprecedented accuracy, which is equaling or surpassing the HRTI-3 specification. Beyond that, TanDEM-X provides a highly reconfigurable platform for the demonstration of new radar imaging techniques and applications. This paper gives a detailed overview of the TanDEM-X mission concept which is based on the systematic combination of several innovative technologies. The key elements are the bistatic data acquisition employing an innovative phase synchronization link, a novel satellite formation flying concept allowing for the collection of bistatic data with short along-track baselines, as well as the use of new interferometric modes for system verification and DEM calibration. The interferometric performance is analyzed in detail, taking into account the peculiarities of the bistatic operation. Based on this analysis, an optimized DEM data acquisition plan is derived which employs the combination of multiple data takes with different baselines. Finally, a collection of instructive examples illustrates the capabilities of TanDEM-X for the development and demonstration of new remote sensing applications. [J1014]

## "A Self-Initializing PolInSAR Classifier Using Interferometric Phase Differences"

This paper describes an unsupervised classifier for polarimetric interferometric synthetic aperture radar (PolInSAR) data. Expectation maximization is used to estimate class parameters that maximize the likelihood of observations in an input data set for a given number of classes. Polarimetric information, in the form of coherency matrices, and interferometric information, in the form of complex coherences, are taken into account. Differences in interferometric phase across different polarization states are explicitly modeled to make the classifier sensitive to the vertical structure of the scene under observation, and the distribution over such phase differences is introduced. The classifier is self-initializing, in that it does not rely on decompositions or thresholds. Classification results obtained for real polarimetric interferometric data are presented and discussed. [J1015]

## "Polarimetric and Interferometric SAR Image Partition Into Statistically Homogeneous Regions Based on the Minimization of the Stochastic Complexity"

In this paper, we show that polarimetric and interferometric SAR (PolInSAR) images can be efficiently partitioned into homogeneous regions with a statistical technique based on minimization of a parameter-free criterion. This technique consists of finding a polygonal partition of the image that minimizes the stochastic complexity, assuming that the image is made of a tessellation of statistically homogeneous regions. The obtained results demonstrate that a global partition in statistically homogeneous regions of PolInSAR images can provide better results than a partition based on a single characteristic such as polarimetry or interferometry only. [J1016]

## "Signal Processing for FMCW SAR"

The combination of frequency-modulated continuous-wave (FMCW) technology and synthetic aperture radar (SAR) techniques leads to lightweight cost-effective imaging sensors of high resolution. One limiting factor to the use of FMCW sensors is the well-known presence of nonlinearities in the transmitted signal. This results in contrast- and range-resolution degradation, particularly when the system is intended for high-resolution long-range applications, as it is the case for SAR. This paper presents a novel processing solution, which solves the nonlinearity problem for the whole range profile. Additionally, the conventional stop-and-go approximation used in pulse-radar algorithms is not valid in FMCW SAR applications under certain circumstances. Therefore, the motion within the sweep needs to be taken into account. Analytical development of the FMCW SAR signal model, starting from the deramped signal and without using the stop-and-go approximation, is presented in this paper. The model is then applied to stripmap, spotlight, and single-transmitter/multiple-receiver digital-beamforming SAR operational mode. The proposed algorithms are verified by processing real FMCW SAR data collected with the demonstrator system built at the Delft University of Technology. [J1017]

## "Supervised Fuzzy-Logic Classification of Hydrometeors Using C-Band Weather Radars"

A model-based fuzzy-logic method for hydrometeor classification using C-band polarimetric radar data is presented and discussed. Membership functions of the fuzzy-logic algorithm are designed for best fitting simulated radar signatures at C-band. Such signatures are derived for ten supervised hydrometeor classes by

means of a fully polarimetric radar scattering model. The Fuzzy-logic Radar Algorithm for Hydrometeor Classification at C-band (FRAHCC) is designed to use a relatively small set of polarimetric observables, i.e., copolar reflectivity and differential reflectivity, but a version of the algorithm based on the use of specific differential phase is also numerically tested and documented. The classification methodology is applied to volume data coming from a C-band two-radar network that is located in north Italy within the Po valley. Numerical and experimental results clearly show the improvements of hydrometeor classification, which were obtained by using FRAHCC with respect to the direct use of fuzzy-logic-based algorithms that are specifically tuned for S-band radar data. Moreover, the availability of two C-band rainfall observations of the same event allowed us to implement a path-integrated attenuation correction procedure, based on either a composite radar field approach or a network-constrained variational algorithm. The impact of these correction procedures on hydrometeor classification is qualitatively discussed within the considered case study. [J1018]

## "Percolation-Based Models for Ray-Optical Propagation in Stochastic Distributions of Scatterers With Random Shape"

This letter deals with ray propagation in stochastic distributions of discrete scatterers having random shapes. The propagation medium is described by means of a semi-infinite percolating lattice and two different propagation models are considered. The propagation depth inside the medium is analytically estimated in terms of the probability that a ray reaches a prescribed level before being reflected back in the above empty half-plane. A comparison with Monte Carlo-like experiments validate the proposed solutions. Applications are in wireless communications, remote sensing, and radar engineering. [J1019]

## "Instructions for AP-S and URSI Authors"

{no data available} [J1020]

## "Effect of Apodization on SAR Image Understanding"

This paper investigates the effect of apodization on the statistical properties of synthetic aperture radar (SAR) images and its impact on the capability of extracting information from homogeneous regions of apodized SAR images. The statistical model for the pixel complex amplitude of the apodized image is derived in terms of both probability density function and statistical moments. Knowledge of the statistical properties is then used to develop appropriate schemes for parameter estimation and supervised classification of homogeneous regions with different radar cross sections in apodized SAR images. The performance analysis shows that the new techniques (properly derived for the apodized case) provide information extraction capabilities only slightly worse than those provided by the conventional techniques applied to the nonapodized case. This allows us to conclude that the use of nonlinear apodization yields sidelobe level reduction and main lobe resolution preservation that can be traded with the small losses above. A full characterization of the estimation and classification performance of these new techniques shows that nonlinear apodization globally introduces a performance degradation comparable to a reduction of the number of looks of a factor of 1.455 for a homogeneous region. [J1021]

## "A Physically Consistent Speckle Model for Marine SLC SAR Images"

A new physically based speckle model for marine single-look complex (SLC) synthetic aperture radar (SAR) images is here presented and investigated. The model allows using full-resolution SAR images instead of multilook SAR images, in which, at the expense of a coarser spatial resolution, the speckle is mitigated. The model is based on the three-parameters generalized-K (GK) probability density function (pdf). GK pdf is a suitable physically-based speckle model for marine SAR images ensuring a continuous and physically consistent transition among different scattering scenarios. This speckle model embodies Rayleigh, K, and Rice scattering scenes which are typical of marine scenes. The use of the three parameters, related to the GK pdf ones, is able to highlight the presence of both low backscattering areas and areas in which a small dominant scatterer is present. This is operationally interesting in SAR oil spill detection procedures. [J1022]

## "Remote data sensing using SAR and harmonic reradiators"

In sensor networks distributed over large areas, communication by means of active transmitters on sensor nodes is inherently energy expensive and poses a significant bottleneck to achieve a long battery life. We propose modulated reradiation of radar illumination as a means to transmit information from a group of sensors to an airborne radar. This puts the communications energy burden on the radar transmitter rather than on the sensor nodes, thus increasing their battery lifetimes. To distinguish the sensor return from the clutter return, the modulation on the sensors is done by switching a nonlinear load on the sensor antenna and processing the

harmonic reradiation. We present techniques to transmit information from the sensors, which use stripmap mode synthetic aperture radar (SAR) ideas to decode the information and to simultaneously obtain a geographic map of the sensor locations. [J1023]

## "Editorial Electro-Magnetic Remote Sensing Defence Technology Centre (EMRS-DTC)"

First Page of the Article [J1024]

## "Refraction and Dispersion Effects Compensation for UWB SAR Subsurface Object Imaging"

It is a trend to use airborne or vehicle-borne ultrawideband synthetic aperture radar (UWB SAR) to quickly detect subsurface objects, i.e., landmines or minefields, over large areas from a safe standoff distance. The traditional image formations without considering the refraction and dispersion of electromagnetic wave will lead to locating error and defocusing for subsurface objects. In this paper, an efficient refraction and dispersion effects compensation method is proposed, which can be integrated with the traditional three-stage automatic target detection framework for detection of subsurface landmines. The compensation method can focus and correctly locate multiple objects buried in different soils with different depths over large areas, which satisfies the operating requirement of an airborne or vehicle-borne UWB SAR system. The proposed method is proved efficient for subsurface object imaging by the field data collected by a UWB SAR system. [J1025]

## "Wavelet-Based Despeckling of SAR Images Using Gauss-Markov Random Fields"

In this paper, a wavelet-based speckle-removing algorithm is represented and tested on synthetic aperture radar (SAR) images. The SAR image is first transformed using a dyadic wavelet transform. The noise in the wavelet-transformed image is modeled as an additive signal-dependent noise with Gaussian distribution. The distribution of a noise-free image in a wavelet domain is modeled as a generalized Gauss-Markov random field (GGMRF). An unsupervised stochastic model-based approach to image denoising is represented. If the observed area is homogeneous, the parameters of the Gaussian distribution and GGMRFs are estimated from incomplete data using mixtures of wavelet coefficients. An expectation-maximization algorithm is used to estimate the parameters of both noisy and noise-free images. The unknown parameters are estimated using image and noise models that are defined in the wavelet domain for heterogeneous areas. Different inter-and intrascale dependences of wavelet coefficients were used to estimate the unknown parameters. The represented wavelet-based method efficiently removes noise from SAR images. [J1026]

## "Focused 70-cm Wavelength Radar Mapping of the Moon"

We describe new 70-cm wavelength radar images of the lunar near-side and limb regions obtained via a synthetic-aperture-radar patch-focusing reduction technique. The data are obtained by transmitting a circularly polarized pulsed waveform from the Arecibo telescope in Puerto Rico and receiving the echo in both senses of circular polarization with the Robert C. Byrd Green Bank Telescope in West Virginia. The resultant images in both polarizations have a spatial resolution as fine as 320 m 450 m near the lunar limb. The patch-focusing technique is a computationally efficient method for compensating for range migration and Doppler (azimuth) smearing over long coherence times, i.e., 983 s, which is needed to achieve the required Doppler resolution. Three to nine looks are averaged for speckle reduction and to improve the signal-to-noise ratio. At this long wavelength, the radar signal penetrates up to several tens of meters into the dry lunar surface materials, thus revealing details of the bulk loss properties and decimeter-scale rock abundance not evident in multispectral and other remote-sensing data. Application of the new radar images to the analysis of basalt flow complexes in Mare Serenitatis shows that the long-wavelength radar data are sensitive to differences in both flow age and composition, and may be particularly useful for studies of smaller deposits that do not have robust crater statistics. The new 70-cm lunar radar data are archived at the National Aeronautics and Space Administration Planetary Data System. [J1027]

## "An Offset Linear-Array-Fed Ku /Ka Dual-Band Reflectarray for Planet Cloud/Precipitation Radar"

A Ku/Ka band dual-frequency offset array-fed microstrip reflectarray antenna using thin membranes has been developed. This antenna is a demonstration model for the next generation titan cloud precipitation radar and altimeter (TCPRA) and is intended to enhance the capability of the future cloud and precipitation remote sensing system for Earth and other planets. The reflectarray has a dimension of 0.5-m square and a flat aperture that emulates a cylindrical reflector antenna. Two sets of linear arrays with linearly polarized microstrip elements and having low cross polarization and low sidelobe levels (SLL) are placed along the focal line to illuminate the reflectarray. One set is for Ku-band, while the other is for Ka-band. Within each set, the wide-swath scanning capability of the antenna is provided by the two fixed-beam feed arrays with one for broadside beam and the other one for a 20deg tilted beam. The unique feature of this paper is that this is the first offset-fed reflectarray

that has ever been practically developed to emulate a cylindrical/parabolic type of reflector antenna. In addition, new dual-concentric-ring elements and ring-patch elements are uniquely applied here to achieve the desirable wide phase variation characteristics. Tests of feed arrays and the reflectarray in the anechoic chamber of Texas A&M University result in good pattern performance and the successful demonstration of beam scanning at both frequency bands. [J1028]

## "Current Measurements in Rivers by Spaceborne Along-Track InSAR"

The global monitoring of river discharges is a technologically challenging problem, with important applications in a variety of disciplines. Due to the limited availability and/or quality of river runoff data from many regions, an increasing use of remote sensing techniques is highly desirable. Altimeter specialists have already demonstrated water level retrievals in rivers from available data. The along-track interferometric synthetic aperture radar [along-track InSAR (ATI)] capabilities of state-of-the-art imaging radars on satellites such as the German TerraSAR-X, which was launched on June 15, 2007, also permit high-resolution line-of-sight surface current measurements. In this paper, we evaluate the potential of current measurements in rivers by spaceborne ATI on the basis of fundamental theoretical considerations, existing spaceborne InSAR data from the shuttle radar topography mission (SRTM), and simulated TerraSAR-X data. We show that an SRTM-derived line-of-sight surface current field in the Elbe river, Germany, agrees well with numerical hydrodynamic model results. The data quality is sufficient to resolve characteristic lateral variations of the currents in the river around a pronounced main flow channel. Assuming that the flow direction is usually aligned with the river bed, even a quasi-2D total surface current field can be derived. Simulations indicate that TerraSAR-X was even better suited for current measurements in rivers. Depending on width, surface roughness, and relative flow direction of a river, current estimates with an accuracy better than 0.1 m/s were possible with an effective spatial resolution of a few hundred meters to kilometers. [J1029]

## "Urban-Target Recognition by Means of Repeated Spaceborne SAR Images"

The relative low resolution (~25 m times 5 m on the ground) of spaceborne C-band synthetic aperture radar (SAR) data as acquired, for example, by European Space Agency sensors ERS and Envisat, can be significantly increased (up to submeter precisions) by processing coherently long series of images. Moreover, by analyzing the amplitude of the radar signal and by exploiting polarization diversity, the main radar characteristics of urban targets can be estimated, and a system for automatic recognition of a set of scattering structures can be developed. In this paper, we study the variation of the amplitude of the received radar signal as a function of the acquisition geometry [normal baseline and Doppler centroid (DC)] to retrieve the extension of the targets in range and azimuth. The dependence of the radar amplitude on temperature at the time of acquisition has been discovered to be very useful to identify extended resonating targets. Dihedrals are discriminated from specular or trihedral reflectors through the phase of Envisat alternating polarization (AP) acquisitions. By means of all gathered radar measurements, the bases for the development of a system for the automatic recognition of six main typologies of urban SAR targets (ground-level and elevated backscatterers, simple and resonating dihedrals, poles and trihedrals) have been laid. Radar data are then combined with in situ surveys and aerial photos, allowing a first assessment of the methodology in urban area. [J1030]

## "Analysis of Polarization Orientation Angle Shifts by Artificial Structures"

In this paper, the polarization orientation angle shifts induced by artificial structures were analyzed and attempted to combine target orientation information which characterizes an urban area with the polarization orientation angle information extracted by the circular-polarization method. In order to illustrate the characteristic of the polarization orientation angle shifts represented in an urban area, the X-band polarimetric synthetic aperture radar (SAR) datasets of Sendai City acquired by Pi-SAR were used. This paper is based on Kimura's idea that the variation of the polarization orientation angle shifts depends on the artificial structures, particularly for the target rotation angle. We found that the polarization orientation angle shift is also affected by the relative relationship between the target rotation angle and the flight direction. From these results, it is possible to estimate the target rotation angle via computation of the polarization orientation angle shift from polarimetric SAR data. [J1031]

## "Statistical CLEAN Technique for ISAR Imaging"

Inverse synthetic aperture radar (ISAR) images are frequently used in target classification and recognition applications. Some classifiers often require features that can be more easily obtained by extracting scattering centers from ISAR data rather than by reconstructing ISAR images. An available method for scattering center extraction, namely, the CLEAN technique, was proposed in a recent paper by Yang et al. In this paper, an improvement of this CLEAN technique is proposed that introduces a new method for detecting scattering

centers. The proposed technique is based on a Gaussianity test, and its effectiveness is first theoretically proven and then tested on real data. Moreover, a comparison with the technique proposed by Yang et al. is shown. [J1032]

## "Single-Pass Polarimetric SAR Interferometry for Vessel Classification"

This paper presents a novel method for vessel classification based on single-pass polarimetric synthetic aperture radar (SAR) interferometry. It has been developed according to recent ship scattering studies that show that the polarimetric response of many types of vessels can be described by trihedral- and dihedral-like mechanisms. The adopted methodology is quite simple. The input interferometric data are decomposed in terms of the Pauli basis, and hence, one height image is derived for each simple mechanism. Then, the local maxima of these images are isolated, and a 3-D map of scatters is generated. The correlation of this map with the scattering distribution expected for a set of reference ships provides the final classification decision. The performance of the proposed method has been tested with the orbital SAR simulator developed at Universitat Politecnica de Catalunya. Different vessel models have been processed with a sensor configuration similar to the incoming TanDEM-X system. The analysis of diverse vessel bearings, vessel speeds, and sea states shows that the map of scatters matches reasonably the geometry of ships allowing a correct identification even for adverse environmental conditions. [J1033]

## "Bistatic Radar Imaging of the Marine Environment-Part I: Theoretical Background"

We describe in detail the theoretical and practical implementation aspects of a simulation for marine radars which can, in particular, be used in multistatic configurations. Since the simulator is intended to deliver pseudoraw signals, it can be used later as a tool to benchmark and improve postprocessing algorithms such as bistatic synthetic aperture radar focusing algorithms and ship wake detection algorithms. The work is divided into two parts. This paper reviews and recalls theoretical prerequisites necessary in implementing such a simulator. Included are the full derivation of the bistatic radar equation from the transmitter to the receiver, accounting also for the transmit-receive time, a description of the sea state phenomenology, a review of the theory of electromagnetic scattering from the sea surface, and the presentation and validation of the method used in the simulation. A companion paper discusses the practical implementation aspects of the simulator as well as an analysis of our results. [J1034]

## "Bistatic Radar Imaging of the Marine Environment-Part II: Simulation and Results Analysis"

We present a bistatic, polarimetric, and real aperture marine radar simulator (MaRS) producing pseudoraw radar signals. The simulation takes the main elements of the environment into account (sea temperature, salinity, and wind speed). Realistic sea surfaces are generated using a two-scale model on a semideterministic basis to incorporate the presence of ship wakes. Then, the radar acquisition chain (antennas, modulation, and polarization) is modeled, as well as the movements of the sensors, on which uncertainties can be introduced, and ship wakes. The pseudoraw temporal signals delivered by MaRS are further processed using, for instance, bistatic synthetic aperture beamforming. The scene itself represents the sea surface as well as ship wakes. The main points covered here are the scene discretization, the ship wake modeling, and the computational cost aspects. We also present images simulated in various monostatic and bistatic configurations and discuss the results. This paper follows its companion paper, where much of the theory used here is recalled and developed in detail. a bistatic, polarimetric, and real aperture marine radar simulator (MaRS) producing pseudoraw radar signals. The simulation takes the main elements of the environment into account (sea temperature, salinity, and wind speed). Realistic sea surfaces are generated using a two-scale model on a semideterministic basis to incorporate the presence of ship wakes. Then, the radar acquisition chain (antennas, modulation, and polarization) is modeled, as well as the movements of the sensors, on which uncertainties can be introduced, and ship wakes. The pseudoraw temporal signals delivered by MaRS are further processed using, for instance, bistatic synthetic aperture beamforming. The scene itself represents the sea surface as well as ship wakes. The main points covered here are the scene discretization, the ship wake modeling, and the computational cost aspects. We also present images simulated in various--monostatic and bistatic configurations and discuss the results. This paper follows its companion paper, where much of the theory used here is recalled and developed in detail. [J1035]

## "Fusion of Support Vector Machines for Classification of Multisensor Data"

The classification of multisensor data sets, consisting of multitemporal synthetic aperture radar data and optical imagery, is addressed. The concept is based on the decision fusion of different outputs. Each data source is treated separately and classified by a support vector machine (SVM). Instead of fusing the final classification outputs (i.e., land cover classes), the original outputs of each SVM discriminant function are used in the

subsequent fusion process. This fusion is performed by another SVM, which is trained on the a priori outputs. In addition, two voting schemes are applied to create the final classification results. The results are compared with well-known parametric and nonparametric classifier methods, i.e., decision trees, the maximum-likelihood classifier, and classifier ensembles. The proposed SVM-based fusion approach outperforms all other approaches and significantly improves the results of a single SVM, which is trained on the whole multisensor data set. [J1036]

## "Building Recognition From Multi-Aspect High-Resolution InSAR Data in Urban Areas"

The improved ground resolution of state-of-the-art synthetic aperture radar (SAR) sensors suggests utilizing SAR data for the analysis of urban areas. The appearance of buildings in SAR or interferometric SAR (InSAR) data is characterized by the consequences of the inherent oblique scene illumination, such as layover, occlusion by radar shadow, and multipath signal propagation. Therefore, particularly in dense built-up areas, building reconstruction is often impossible from a single SAR or InSAR measurement alone. But, the reconstruction quality can be significantly improved by a combined analysis of multi-aspect data. In this paper, two approaches are proposed to detect and reconstruct buildings of different size from multi-aspect high-resolution InSAR data sets. Both approaches focus on the recognition of buildings supported by knowledge-based analysis considering the mentioned SAR-specific effects observed in urban areas. Building features are extracted independently for each direction from the magnitude and phase information of the interferometric data. Initial primitives are segmented and afterward projected from slant-range into the world coordinate system. From the fused set of primitives of both flight directions, building hypotheses are generated. The first approach exploits the frequently observed lines of bright double-bounce scattering, which are used for building reconstruction in residential districts. In the case of larger buildings, such as industrial halls, often additional features of roof and facade elements are visible. Therefore, in a second approach, extended buildings are extracted by grouping primitives of different kinds. The two approaches are demonstrated in an urban environment for an InSAR data set, which has spatial resolution of about 30 cm and was taken from two orthogonal flight directions. [J1037]

## "Surface-Based Polarimetric C-Band Scatterometer for Field Measurements of Sea Ice"

A portable surface-based polarimetric C-band scatterometer for field deployment over sea ice is presented. The scatterometer system, its calibration, signal processing, and near-field correction are described. The near-field correction is shown to be effective for both linear polarized and polarimetric backscatter. Field methods for the scatterometer are described. Sample linear polarized and polarimetric backscatter results are presented for snow-covered first-year sea ice (FYI), multiyear hummock ice, and rough melt pond water on FYI. The magnitude of backscatter signature variability due to system effects is presented, providing the necessary basis for quantitative analysis of field data. [J1038]

## "Ultrawideband Synthetic Aperture Radar Landmine Detection"

In this paper, we consider landmine detection using ultrawideband synthetic aperture radar, where the two main challenges are feature extraction and discriminator design. The space-wavenumber processing is proposed to retrieve the frequency-and aspect-angle-dependent scattering features of suspected objects. In order to reduce the dimensionality of the input feature vector for a discriminator, the sequential forward floating selection method is used to choose efficient features. Based on the obtained feature vector, a fuzzy hypersphere support vector machine is designed to deal with the problem of detecting landmines in an unconstrained environment. The experimental results show that the proposed method can achieve a significant improvement in detection performance for antitank mines. [J1039]

## "Target Detection and Texture Segmentation in Polarimetric SAR Images Using a Wavelet Frame: Theoretical Aspects"

Theoretical aspects of a technique for target detection and texture segmentation in synthetic aperture radar (SAR) imagery using a wavelet frame are presented. Texture measures consist of multiscale local estimates of the following: 1) normalized second moment of the backscattered intensity and 2) variance of the wavelet-frame coefficients. This work is an extension of a method proposed in the image-processing literature. Novel issues, which are considered in the passage to radar imagery, are the influence of speckle on texture measures afforded by the wavelet frame and their dependence on polarization states (polarimetric texture). Regarding speckle, estimators that decouple the influence of speckle over texture are introduced and characterized by their expected value and variance. The response of the wavelet frame to discontinuities, which is an important issue in target detection problems, is addressed in terms of signal-to-speckle-noise ratio. The notion of polarimetric texture is revisited, providing a theoretical model that explains the dependences of texture measures on the polarization states. For one-point statistics, such model calls for a mixture of diverse polarimetric scattering

mechanisms within the texture estimator support. For two-point statistics, the difference in spatial correlation properties among the polarimetric channels is called into play. To analyze these effects in polarimetric SAR data, a novel tool is introduced that is called the Wavelet Polarimetric Signature. The tool encapsulates, in graphical form, the dependence on scale and polarization state of the texture measure afforded by the wavelet frame. The theory exposed here underpins a method that has been proven successful and computationally attractive in a selected number of SAR thematic applications. It also sets the stage for the exploitation of novel target detection and textural segmentation capabilities based on polarimetric diversity. [J1040]

## "ScanSAR-to-Stripmap Mode Interferometry Processing Using ENVISAT/ASAR Data"

Interferometric synthetic aperture radar (InSAR) images of geophysical events such as preeruptive volcano deformation or interseismic strain accumulation are often limited by phase distortions from the superimposed atmospheric signature. Additionally, the approximate monthly repeat cycle of many radar satellites cannot accurately capture rapidly time-varying processes. The Scanning Synthetic Aperture Radar (ScanSAR) mode of the ENVISAT/ASAR instrument permits more frequent revisits of a given area, potentially overcoming both of these limitations. In particular, stripmap mode-to-ScanSAR images provide a denser time series of interferograms than is possible with conventional stripmap-to-stripmap mode InSAR. We present images of ENVISAT/ASAR data acquired over Hawaii in which data acquired roughly weekly in ScanSAR mode are combined with ENVISAT/ASAR conventional stripmap mode data to form interferograms at a much denser temporal spacing. The burst nature of ScanSAR data requires a new processing method to form the interferograms. We use traditional matched filtering for the range compression. For the azimuth processing, we compute the stripmap mode data on the ScanSAR sampling grid using a variation, consisting of different reference functions, of Lanari's modified SPECAN algorithm that is itself an adaptation of the chirp z-transform to readjust the azimuth pulse spacing. The resulting interferograms faithfully reflect the phase of conventional interferograms, but exhibit fewer looks and coarser resolution than those produced by fully stripmap mode data. For many problems, temporal density of the deformation observations is paramount, and the time series analysis and temporal averaging that were made possible using ScanSAR interferograms far outweigh the loss in looks and resolution. [J1041]

## "Hybrid-Polarity SAR Architecture"

A synthetic aperture radar (SAR) often is constrained to transmit only one polarization. Within this constraint, two aggressive measurement objectives are 1) full characterization and exploitation of the backscattered field, and 2) invariance to geometrical orientations of features in the scene. Full characterization implies coherent dual-polarization to support the four Stokes parameters. These are rotationally invariant with respect backscatterer orientation if and only if the transmission is circularly polarized. Given that the data products are the Stokes parameters, the receivers can use any orthogonal polarization basis. A SAR in hybrid-polarity architecture (CL-pol) transmits circular polarization and receives two orthogonal mutually coherent linear polarizations, which is one manifestation of compact polarimetry. The resulting radar is relatively simple to implement, and has unique self-calibration features and low susceptibility to noise and cross-channel errors. It is the architecture of choice for two lunar radars scheduled for launch in 2008. Data from a CL-pol SAR yield to decomposition strategies such as the m-delta method introduced in this paper. [J1042]

## "Processing of Bistatic SAR Data From Quasi-Stationary Configurations"

Standard synthetic aperture radar (SAR) processing algorithms use analytically derived transfer functions in the 2D frequency and range/Doppler domains. These rely on the assumption of hyperbolic range histories of monostatic SARs with straight flight paths. For bistatic SARs, the range histories are no longer hyperbolic, and simple analytic transforms do not exist. This paper offers two solutions for bistatic SAR data processing under the restriction of quasi-stationarity, i.e., sufficiently equal velocity vectors of transmitter and receiver. 1) Moderately bistatic configurations can be handled satisfactorily by using hyperbolic range functions with a modified velocity parameter, which is a solution already well known for the accommodation of curved orbits in the monostatic case. This "equivalent velocity" approach is shown to be of surprising range of validity even for pronounced bistatic situations. It is not to be confused with the "equivalent monostatic flight path" approximation, which is shown to be inapplicable for any practical case. 2) With increasing separation of transmitter and receiver, the equivalent velocity approximation deteriorates. To cope with extreme bistatic configurations, a general approach named "NuSAR" is proposed, where the involved transfer functions are replaced by numerically computed ones. This paper describes how the transfer functions are computed from the given orbits and the shape of the Earth surface. In any of these two cases, the bistatic SAR data can be processed by standard SAR processors; only the conventional transfer functions need to be replaced. Neither are there time-domain prefocusing or post focusing steps required nor complicated mathematical expansions involved. The presented algorithms are also applicable to very high resolution wide-swath (or squinted) SARs on curved orbits.

[J1043]

## "DEM Control in Arctic Alaska With ICESat Laser Altimetry"

Use of Ice, Cloud, and land Elevation Satellite (ICESat) laser altimetry is demonstrated for control of a digital elevation model (DEM) that is synthesized from repeat-pass ERS-1 and 2 synthetic aperture radar (SAR) imagery using interferomet-ric SAR (InSAR). Our study area is 15 650 km2of the Barrow, AK coastal plain adjacent to the Arctic Ocean; a vast expanse of tundra, lakes, and arctic wetlands of such low relief as to be nearly devoid of terrain features. The accuracy of the ICESat-derived elevation measurements is assessed by comparison with differential global positioning system (DGPS) data acquired along ICESat ground tracks. The ICESat-derived elevations have a mean accuracy, relative to the DGPS elevations, of -0.01 plusmn 0.18 m. ICESat-derived elevations on the Arctic coastal plain provide an excellent source for DEM control. We employ the ICESat-derived ground control points (GCPs) in two distinct InSAR processing steps: 1) selected points are used to perform baseline refinements, which improves the ERS-1 and 2 interfero-grams and 2) the ICESat-derived GCP position data (latitude, longitude, elevation) are then used as control in mosaicking multiple InSAR-derived DEMs. The resulting ICESat-controlled DEM has a mean accuracy of -1.11plusmn 6.3 m relative to an independent standard, which is a commercial airborne InSAR-derived DEM having 0.5 m rms accuracy. This easily meets DTED-2 standards and suggests that DEMs derived using only ICESat altimetry for ground control would meet similar standards in other regions of low relief. [J1044]

## "Results of a Space-Surface Bistatic SAR Image Formation Algorithm"

This paper reports progress in the development of an image formation algorithm suitable for stripmap space-surface bistatic synthetic aperture radar. A description of the proposed algorithm, which is a modification of the standard range-Doppler algorithm, is provided for the case when the transmitter and the receiver have parallel flight paths and unequal velocities. Both simulation and initial experimental results are presented to verify our analysis. [J1045]

## "Focusing Parallel Bistatic SAR Data Using the Analytic Transfer Function in the Wavenumber Domain"

In recent years, bistatic synthetic aperture radar (BiSAR) has attracted the attention of many radar researchers. It is well known that the slant range history of BiSAR is the sum of two square-rooted terms, which correspond to the transmitting and receiving slant ranges, respectively. For a point target in the SAR scene, it is quite difficult, if not impossible, to obtain an analytic formula to describe the target echo data in the 2-D frequency domain without any approximation by using the conventional stationary phase method, which makes it very difficult to develop fast-focusing algorithms for BiSAR. In this paper, based on the concept of an instantaneous Doppler wavenumber and by defining a new variable called half quasi-bistatic angle, an analytic formula of the point target response in the spectral domain is developed for BiSAR with parallel trajectory (referred to as parallel BiSAR for simplicity). Relying on a first-order Taylor expansion of the above formula with respect to the parameter called the sum of closest distances on the swath center, a bistatic range migration algorithm is proposed for any azimuth-shift-invariant BiSAR data processing. Simulation results have confirmed the effectiveness of the proposed novel approach. [J1046]

## "Foreword to the Special Issue on Synthetic Aperture Radar (SAR) Technologies and Techniques"

{no data available} [J1047]

## "An Unsupervised Segmentation With an Adaptive Number of Clusters Using the SPAN/H/α/A Space and the Complex Wishart Clustering for Fully Polarimetric SAR Data Analysis"

In this paper, an unsupervised segmentation is proposed for fully polarimetric synthetic aperture radar (SAR) data analysis. The backscattering power SPANcombined with H/alpha/Ais used to obtain the initial cluster centers. We use the Wishart test statistic to perform an agglomerative hierarchical clustering to obtain the segmentation results with different numbers of clusters. The appropriate number of clusters is automatically estimated using the data log-likelihood (Lm), and the resulting images with the estimated number of clusters are the final segmentation results. The experiments show that the SPANhas additional information that is not contained in H/alpha/A, and this information could be useful for the initialization. The number of clusters seems to be a crucial point for the segmentation, which will affect the segmentation performance. It is also shown that the data log-likelihood has the potential ability to reveal the inner structure of fully polarimetric SAR data. [J1048]

## "Retrieving 3-D Topography by Using a Single-Antenna Squint-Mode Airborne SAR"

In this paper, a novel method is proposed for retrieving 3-D topography of the ground surface by using a single-antenna squint-mode airborne synthetic aperture radar (SAR). The main idea of the method is based on the fact that the spatial 3-D location of a target can be found as the intersection of the range sphere, the Doppler cone, and the elevation plane of the antenna pattern. An accurate estimation of the Doppler centroid for each resolution cell is required to realize this method. Experimental results obtained with a Ku-band airborne SAR are presented. The method calls for using a precise calibrated attitude determination unit. [J1049]

## "ALOS PALSAR: A Pathfinder Mission for Global-Scale Monitoring of the Environment"

The Advanced Land Observing Satellite (ALOS) is Japan's new-generation Earth Observation satellite, launched in January 2006 by the Japan Aerospace Exploration Agency. ALOS carries two optical instruments (Panchromatic Remote-sensing Instrument for Stereo Mapping and Advanced Visible and Near-Infrared Radiometer type 2) and, to maintain Japan's commitment to spaceborne L-band Synthetic Aperture Radar (SAR), the Phased Array L-band SAR (PALSAR). The successor to the SAR onboard the Japanese Earth Resources Satellite (1992-1998), the PALSAR instrument provides enhanced sensor characteristics, including full polarimetry, variable off-nadir viewing, and ScanSAR operations, as well as significantly improved radiometric and geometric performance. As important as the technical improvements and the reason PALSAR here is referred to as a pathfinder mission for global environmental monitoring is the systematic data-acquisition strategy which has been implemented for ALOS. With a priority second only to emergency observations, the PALSAR observation strategy has been designed to provide consistent, wall-to-wall observations at fine resolution of all land areas on the Earth on a repetitive basis, in a manner which has earlier been conceived only for coarse- and medium-resolution instruments. [J1050]

## "Model Limitations and Parameter-Estimation Methods for Agricultural Applications of Polarimetric SAR Interferometry"

Application of polarimetric synthetic aperture radar interferometry to the retrieval of geophysical parameters from vegetated scenes is based on simple direct models of such scenes. The first part of this paper presents an analysis of the correspondence between these simple models, namely, the random volume over ground and the oriented volume over ground (OVoG), and experimental data from samples of two agricultural crops (maize and rice) acquired in controlled conditions. Although an overall agreement between model and data is clear, some discrepancies have been found as a consequence of two assumptions in the model formulation: vertical homogeneity of the vegetation volume and absence of multiple scattering effects inside the volume. This paper presents the shape and location of the visible region of the experimental coherences on the complex plane and compares it with the feasible region predicted by the model. This comparison has also pointed out the low sensitivity of the direct model to extinction coefficients. In the second part, two different strategies for a complete inversion (i.e., estimation of all model parameters) of the OVoG model are proposed and compared, using the same data set. The first one is based on a combination of geometrical and numerical approaches (genetic algorithms) and the second one on a dual-baseline configuration. In all cases, ground topography is accurately estimated, with a maximum error of 10 cm. Vegetation height estimates are accurate up to 30 cm, with some bands and baseline configurations providing errors below 15 cm. However, results obtained for the extinction coefficients are not stable with frequency and exhibit high variability. [J1051]

## "Analysis and Focusing of Bistatic Airborne SAR Data"

Bistatic synthetic aperture radar (SAR) processing requires precise knowledge about geometrical parameters of the flown bistatic constellation, whereas estimation of these parameters is even more important than in the monostatic case. As it is impossible to separate the individual semimonostatic parameters from the bistatic raw data, the searched parameters are derived from the tracks of the moving platforms. For this reason, global positioning system (GPS) and inertial navigation system (INS) position and velocity data of transmitter and receiver are combined in an optimal way by a Kalman filter approach. As a consequence of model-based interpolation, we can easily determine varying parameters like Doppler centroid frequency, azimuth velocity, and the bistatic parameters a2and a0referring to the illuminated scene at each time instant. Accurately determined position and velocity of the transmitter and receiver enable a first-order bistatic motion compensation (MC), which is also described in this paper. In verifying our approach, GPS/INS tracks and raw data of a bistatic airborne SAR experiment flown in 2003 were used, where the data were provided by Forschungsgesellschaft fu umlr Angewandte Naturwissenschaften e.V., Wachtberg, Germany. The focusing was done by a scaled inverse Fourier transformation processor for nearly parallel trajectories for transmitter and receiver. This paper focuses on analyzing the trajectories and antenna beams of bistatic missions to obtain accurate processing parameters and MC functions. [J1052]

## "Extreme Compression of Weather Radar Data"

A method for achieving extreme levels of compression of high-volume weather radar data is presented. Weather reflectivity contours, as per National Weather Service or custom thresholds, are processed by tracing their departure from a smoothed version to obtain the local extrema which serve as control points. The control points, which are transmitted in relative coordinates for further compression, are interpolated using a second-degree B-spline to retrieve the contours. The encoding-decoding method is capable of capturing the random undulations inherent in weather contours. It is shown that over two orders of magnitude of compression is possible without perceptible loss of meteorological information. Multiple enhancements to the basic method are quantitatively studied and compared with the existing methods for radar data compression. [J1053]

## "Power Optimization for Polarimetric Bistatic Random Mechanisms"

The aim of this paper is to investigate the optimal polarizations (i.e., emitted and received polarizations for which the received power is maximum or minimum) in the general case of random mechanisms observed by a bistatic full-polarimetric radar. We are particularly interested in the methods leading to analytical solution as far as this is possible. It is the reason why the Kennaugh matrix is taken as the starting point of the optimizations. The optimal polarizations corresponding to the monostatic and bistatic deterministic cases are found again as particular cases. [J1054]

## "Evaluation of a New Airborne Microwave Remote Sensing Radiometer by Measuring the Salinity Gradients Across the Shelf of the Great Barrier Reef Lagoon"

Over the last ten years, some operational airborne remote sensing systems have become available for mapping surface salinity over large areas in near real time. A new dual-polarized Polarimetric L-band Multibeam Radiometer (PLMR) has been developed to improve accuracy and precision when compared with previous instrument generations. This paper reports on the first field evaluation of the performance of the PLMR by measuring salinity gradients in the central Great Barrier Reef. Before calibration, the raw salinity values of the PLMR and conductivity-temperature-depth (CTD) differed by 3-6 psu. The calibration, which uses in situ salinity data to remove long-term drifts in the PLMR as well as environmental effects such as surface roughness and radiation from the sky and atmosphere, was carried out by equating the means of the PLMR and CTD salinity data over a subsection of the transect, after which 85% of the salinity values between the PLMR and CTD are within 0.1 psu along the complete transect. From offshore to inshore across the shelf, the PLMR shows an average cross-shelf salinity increase of about 0.4 psu and a decrease of 2 psu over the inshore 20 km at -19deg S (around Townsville) and -18deg S (around Lucinda), respectively. The average cross-shelf salinity increase was 0.3 psu for the offshore 100 km over all transects. These results are consistent with the in situ CTD results. This survey shows that PLMR provided an effective method of rapidly measuring the surface salinity in near real time when a calibration could be made. [J1055]

## "A Novel Direction-Finding Algorithm for Directional Borehole Radar"

A directional borehole radar system has been developed for the purpose of 3-D imaging of subsurface targets in a single-hole measurement. The radar system is equipped with a uniform circular array consisting of four dipole antennas as a receiver in order to realize azimuth bearing sensitivity. We propose a new direction-finding (DF) algorithm that is suitable for directional borehole radar measurement, and we apply this algorithm to actual field measurement data. This algorithm is based on the Adcock DF antenna principle where the complex time series (analytic signal) expression, the optimization, and the filtering procedure are incorporated to provide more accurate estimation. The algorithm was first verified in a transmission measurement in boreholes with a cross-hole configuration (15 m apart from each other) by estimating a direction of the incident wave from a transmitter to the receiver. Finally, the algorithm was applied to single-hole measurement data to demonstrate the ability to detect the 3-D location of a subsurface tunnel which was located 5.5 m from the borehole. The result showed fairly good agreement with the actual location of the tunnel, i.e., to an azimuth estimation error of within 10deg. [J1056]

## "Reconstruction From Antenna-Transformed Radar Data Using a Time-Domain Reconstruction Method"

This paper discusses the reconstruction of the subsurface from radar data using a time-domain reconstruction method. Before the reconstruction is conducted, data preprocessing is carried out. The preprocessing transforms measured data transmitted and received by 3-D dipole antennas into equivalent data excited and received by 3-D ideal electric dipoles and, then, into equivalent data excited and received by 2-D ideal electric dipoles. Distributions of permittivity, conductivity, and permeability are reconstructed from the preprocessed data by a 2-D forward-backward time-stepping waveform inverse scattering technique. Two 2-D examples of permittivity and conductivity reconstruction from synthetic noisy and field borehole radar data are demonstrated to show the

effectiveness of the proposed method [J1057]

## "Matching radar and satellite images for ship trajectory estimation using the Hausdorff distance"

A novel technique to obtain position, velocity and radar biases estimates of a ship is described by matching ship-borne radar images to geo-referenced satellite images. The matching is performed through the minimisation of the averaged partial Hausdorff distances between data points in each image. The minimisation rapidly yields robust geographical latitude and longitude position measurements, as well as ship heading and radar biases. The accuracy of the measurements is improved by feeding them into a Kalman filter that also allows estimates of the ship's velocity to be obtained. The method provides an alternative effective position sensor for GPS denied environments, which may also be employed for automatic radar calibration of bearing and range biases or for indoor autonomous mobile robot navigation [J1058]

## "Shift–Scale Complex Correlation for Wide-Angle Coherent Cross-Track SAR Stereo Processing"

Automated synthetic aperture radar (SAR) stereo correspondence becomes increasingly difficult when imaging high-relief terrain utilizing large stereo crossing-angle geometries because high-relief SAR image features can undergo significant spatial distortions, causing a failure of traditional correlation matching. This paper presents eight coherent spotlight-mode cross-track stereo pairs with stereo crossing angles averaging 93.7deg collected over a terrain with slopes greater than 20deg. These stereo pairs suffer from terrain-induced distortions, resulting in a decrease in complex correlation (coherence) when utilizing scanning-window correlation calculations. The search to maximize complex correlation is changed from a shift-only (disparity) search to a shift-and-scale search using the downhill simplex method. This approach is tested against complex imagery with simulated distortions and then employed on the eight wide-angle stereo collects. The resulting digital terrain maps (DTMs) are compared to ground truth. Using a shift-and-scale correlation approach to estimate disparity, the relative height errors decrease, and the number of reliable DTM posts increase [J1059]

## "Oil Spill Detection in Radarsat and Envisat SAR Images"

We present algorithms for automatic detection of oil spills in synthetic aperture radar (SAR) images. The algorithms consist of three main parts, namely: 1) detection of dark spots; 2) feature extraction from the dark spot candidates; and 3) classification of dark spots as oil spills or look-alikes. The algorithms have been trained on a large number of Radarsat and Envisat Advanced Synthetic Aperture Radar (ASAR) images. The performance of the algorithm is compared to manual and semiautomatic approaches in a benchmark study using 59 Radarsat and Envisat images. The algorithms can be considered to be a good alternative to manual inspection when large ocean areas are to be inspected [J1060]

## "Frequency Subband Processing and Feature Analysis of Forward-Looking Ground-Penetrating Radar Signals for Land-Mine Detection"

There has been significant amount of study on the use of ground-penetrating radar (GPR) for land-mine detection. This paper presents our analysis of GPR data collected at a U.S. Army test site using a new approach based on frequency subband processing. In this approach, from the radar data that have over 2.5 GHz of bandwidth, we compute separate radar images using the one wide (2 GHz) and four narrow (0.6 GHz) frequency subbands. The results indicate that signals for different frequency subbands are significantly different and give very different performance in land-mine detection. In addition, we also examine a number of features extracted from the GPR data, including magnitude and local-contrast features, ratio between copolarization and cross-polarization signals, and features obtained using polarimetric decomposition. Feature selection procedures are employed to find subsets of features that improve detection performance when combined. Results of land-mine detection, including performance on blind test lanes, are presented [J1061]

## "Binary Weighted Averaging of an Ensemble of Coherently Collected Image Frames"

Recent interest in the collection of remote laser radar imagery has motivated novel systems that process temporally contiguous frames of collected imagery to produce an average image that reduces laser speckle, increases image SNR, decreases the deleterious effects of atmospheric distortion, and enhances image detail. This research seeks an algorithm based on Bayesian estimation theory to select those frames from an ensemble that increases spatial resolution compared to simple unweighted averaging of all frames. The resulting binary weighted motion-compensated frame average is compared to the unweighted average using simulated and experimental data collected from a fielded laser vision system. Image resolution is significantly enhanced as quantified by the estimation of the atmospheric seeing parameter through which the average image was formed [J1062]

## "A Multiscale Curvature Algorithm for Classifying Discrete Return LiDAR in Forested Environments"

One prerequisite to the use of light detection and ranging (LiDAR) across disciplines is differentiating ground from nonground returns. The objective was to automatically and objectively classify points within unclassified LiDAR point clouds, with few model parameters and minimal postprocessing. Presented is an automated method for classifying LiDAR returns as ground or nonground in forested environments occurring in complex terrains. Multiscale curvature classification (MCC) is an iterative multiscale algorithm for classifying LiDAR returns that exceed positive surface curvature thresholds, resulting in all the LiDAR measurements being classified as ground or nonground. The MCC algorithm yields a solution of classified returns that support bare-earth surface interpolation at a resolution commensurate with the sampling frequency of the LiDAR survey. Errors in classified ground returns were assessed using 204 independent validation points consisting of 165 field plot global positioning system locations and 39 National Oceanic and Atmospheric Administration-National Geodetic Survey monuments. Jackknife validation and Monte Carlo simulation were used to assess the quality and error of a bare-earth digital elevation model interpolated from the classified returns. A local indicator of spatial association statistic was used to test for commission errors in the classified ground returns. Results demonstrate that the MCC model minimizes commission errors while retaining a high proportion of ground returns and provides high confidence in the derived ground surface [J1063]

## "Snow-Covered Area Estimation Using Satellite Radar Wide-Swath Images"

Satellite radar-based remote sensing of snow cover during the snow-melt season has been widely studied for different geographical regions, such as mountainous, open, and forested areas. However, a single method has not been found to function well on all regions. The investigations on boreal forest zone have allowed the Helsinki University of Technology (TKK) to develop a snow-covered area (SCA) method that is feasible using spatially limited European Remote Sensing-1/2 Satellite data. This paper investigates the use of wide-swath radar data for boreal forest SCA estimation for the first time. The TKK SCA method is adapted here for HH-polarization Radarsat data. The predominant aspect originated by the use of wide-swath synthetic aperture radar (SAR) data is the large variation in the radar incidence angle. The effect of incidence angle variation on SCA estimation is characterized in this paper. The foundation for operational implementation of the TKK SCA method is also established by an error propagation analysis presented in this paper. The error propagation analysis is compared with accuracy characteristics acquired between SAR and optical SCA evaluation. The performance of forest compensation, which is a key element of the TKK method, was analyzed for the wide-swath radar data. Furthermore, the correlation between the topography and the SCA estimation accuracy was examined in this paper. This paper lays the foundation for operational SCA estimation on boreal forest zone using wide-swath SAR data [J1064]

## "Impact of Multiresolution Active and Passive Microwave Measurements on Soil Moisture Estimation Using the Ensemble Kalman Smoother"

An observing system simulation experiment is developed to test tradeoffs in resolution and accuracy for soil moisture estimation using active and passive L-band remote sensing. Concepts for combined radar and radiometer missions include designs that will provide multiresolution measurements. In this paper, the scientific impacts of instrument performance are analyzed to determine the measurement requirements for the mission concept. The ensemble Kalman smoother (EnKS) is used to merge these multiresolution observations with modeled soil moisture from a land surface model to estimate surface and subsurface soil moisture at 6-km resolution. The model used for assimilation is different from that used to generate "truth." Consequently, this experiment simulates how data assimilation performs in real applications when the model is not a perfect representation of reality. The EnKS is an extension of the ensemble Kalman filter (EnKF) in which observations are used to update states at previous times. Previous work demonstrated that it provides a computationally inexpensive means to improve the results from the EnKF, and that the limited memory in soil moisture can be exploited by employing it as a fixed lag smoother. Here, it is shown that the EnKS can be used in large problems with spatially distributed state vectors and spatially distributed multiresolution observations. The EnKS-based data assimilation framework is used to study the synergy between passive and active observations that have different resolutions and measurement error distributions. The extent to which the design parameters of the EnKS vary depending on the combination of observations assimilated is investigated [J1065]

## "On the Reduction of the Reconstruction Bias in Synthetic Aperture Imaging Radiometry (Corrected) "

Synthetic aperture imaging radiometers (SAIRs) are powerful instruments for high-resolution observation of planetary surfaces at low microwave frequencies. This paper is concerned with the reconstruction of radiometric brightness temperature maps from SAIR interferometric measurements. Even in the absence of modeling errors

and radiometric noise, a systematic error, or bias, has been observed in the reconstructed maps. The origin of this bias is analyzed and an efficient solution is proposed for reducing it. The core reconstruction procedure is not changed, and no additional measurements are needed. Throughout the scientific rationale, particular emphasis is laid on numerical simulations carried out for the Soil Moisture and Ocean Salinity space mission, a project led by the European Space Agency and devoted to the remote sensing of soil moisture and ocean salinity from a low-orbit platform [J1066]

## "Analysis of Random Step Frequency Radar and Comparison With Experiments"

Linear stepped frequency radar is used in wide-band radar applications, such as airborne synthetic aperture radar (SAR), turntable inverse SAR, and ground penetration radar. The frequency is stepped linearly with a constant frequency change, and range cells are formed by fast Fourier transform processing. The covered bandwidth defines the range resolution, and the length of the frequency step restricts the nonambiguous range interval. A random choice of the transmitted frequencies suppresses the range ambiguity, improves covert detection, and reduces the signal interference between adjacent sensors. As a result of the random modulation, however, a noise component is added to the range/Doppler sidelobes. In this paper, relationships of random step frequency radar are compared with frequency-modulated continuous wave noise radar and the statistical characteristics of the ambiguity function and the sidelobe noise floor are analyzed. Algorithms are investigated, which reduce the sidelobes and the noise-floor contribution from strong dominating reflectors in the scene. Theoretical predictions are compared with Monte Carlo simulations and experimental data [J1067]

## "Effective Solution of 3-D Scattering Problems via Series Expansions: Applicability and a New Hybrid Scheme"

Accurate and reliable evaluation of the electromagnetic field scattered by dielectric objects is a canonical problem in the electromagnetic community. In the framework of integral equation formulations, iterative techniques, and in particular conjugate gradient (CG) schemes, are widely used. However, when the number of parameters grows, CG techniques may become too demanding from a computational point of view. In this paper, we show that many forward scattering problems can be conveniently solved by means of very simple series expansions, which allow a lower computational complexity and memory storage with respect to other iterative schemes. In particular, we consider three different series expansions, namely: 1) the traditional Born series; 2) the contrast source-extended Born series, which is recently introduced by rewriting the traditional source-type integral equations; and 3) a new series, which is a hybridization of the previous ones. Theoretical conditions for the applicability of the series expansions are discussed, and practical tools to foresee that a problem can be solved by means of these simple iterative schemes are provided. Numerical examples are reported for the sake of comparison and to assess performance [J1068]

## "Statistical Analysis of High-Resolution SAR Ground Clutter Data"

This paper deals with the problem of modeling high-resolution synthetic aperture radar clutter data from different vegetated areas. We analyzed moving and stationary target recognition (MSTAR) data sets focusing on histograms, moments, and covariance of clutter amplitude, texture, and speckle. The most celebrated statistical models are tested on real data of grass field or wood and trees to validate the goodness of fit of the compound Gaussian model in different scenarios. The results demonstrate that for grass fields, the compound Gaussian model provides a good data fitting. This is not the case for woods images where the speckle is not more Gaussian distributed. Covariance analysis and concluding remarks complete this paper [J1069]

## "Spheroidal Mode Approach for the Characterization of Metallic Objects Using Electromagnetic Induction"

We propose a spheroidal mode approach to characterize the electromagnetic induction (EMI) response of buried objects, assumed to be much more conductive than their environment. Both the excitation and the response are formulated as the linear superpositions of basic spheroidal modes. The scattering coefficients characterize objects, regardless of their geometrical complexity and material inhomogeneity, due to the orthogonality of the spheroidal modes. The ill-conditioning encountered in retrieving the scattering coefficients is dealt with by mode truncation and Tikhonov regularization. The approach is tested for both simulated and measured data, and the retrieval results show encouragingly that only few excitation and response modes effectively represent the EMI response of the objects. The proposed approach is therefore promising in the detection and classification of buried objects [J1070]

## "Iterative robust filtering for ground target tracking"

Robust filtering for state-space estimation has been studied. The application domain emphasises air-to-ground target tracking with remote sensing devices such as radar. An analysis indicates that in this application, target model uncertainties predominantly exist in the observation model and target input process noise model. For this reason, the development of a filter with robustness towards these two types of uncertainties has been the focus of the authors. A challenge to the design is that the uncertainties are highly non-stationary with the result that predefined bounds on uncertainties generally cannot provide the required filtering accuracy. Therefore, a successful robust filter for such applications must include a mechanism to predict instant bounds on certainties and, to this end, an iterative robust filter is developed on the basis of least squares optimisation criteria. Compared with existing robust filters, the novelty of this new filtering is to predict the worst-case uncertainty so that tight bounds on the involved uncertainties can be applied and the state estimates can be obtained more accurately. [J1071]

## "On the Reduction of the Reconstruction Bias in Synthetic Aperture Imaging Radiometry"

Synthetic aperture imaging radiometers (SAIRs) are powerful instruments for high-resolution observation of planetary surfaces at low microwave frequencies. This paper is concerned with the reconstruction of radiometric brightness temperature maps from SAIR interferometric measurements. Even in the absence of modeling errors and radiometric noise, a systematic error, or bias, has been observed in the reconstructed maps. The origin of this bias is analyzed and an efficient solution is proposed for reducing it. The core reconstruction procedure is not changed, and no additional measurements are needed. Throughout the scientific rationale, particular emphasis is laid on numerical simulations carried out for the Soil Moisture and Ocean Salinity space mission, a project led by the European Space Agency and devoted to the remote sensing of soil moisture and ocean salinity from a low-orbit platform [J1072]

## "A Joint Image Coregistration, Phase Noise Suppression, and Phase Unwrapping Method Based on Subspace Projection for Multibaseline InSAR Systems"

As is well known, image coregistration, interferometric phase noise suppression, and phase unwrapping are three key processing procedures of synthetic aperture radar interferometry (InSAR). The three procedures are cascaded in the conventional processing flow of InSAR. Unlike the conventional processing flow, in this paper we propose a joint processing idea to carry out image coregistration, interferometric phase noise filtering, and phase unwrapping simultaneously based on subspace projection for multibaseline InSAR systems. The joint processing method can perform the fine coregistration of all SAR images implicitly by extracting the correlation information in the neighboring pixel sets, suppress the phase noise by utilizing the orthogonality of the signal subspace and the corresponding noise subspace, and optimally estimate the unwrapped interferometric phases (or the terrain heights) by combining the pixel coherence and the baseline diversity of a multibaseline InSAR system. Simulated results are presented to verify the effectiveness of the joint processing method [J1073]

## "Capabilities of Dual-Frequency Millimeter Wave SAR With Monopulse Processing for Ground Moving Target Indication"

Ground moving target indication (GMTI) for synthetic aperture radar (SAR) provides information on nonstatic objects in radar imagery of a static ground scene. An efficient approach for GMTI is the use of multichannel SAR systems for a space- and time-variant analysis of moving targets. This allows the indication, correction of position displacement, and estimation of radial velocity components of moving targets in a SAR image. All three steps are possible due to a determinable Doppler frequency shift in the radar signal caused by radial target movement. This paper focuses on the millimeter wave (mmW) SAR system MEMPHIS with multichannel amplitude-comparison monopulse data acquisition and the ability to use carrier frequencies of 35 and 94 GHz simultaneously, making it a dual-frequency SAR. This paper includes mmW-specific SAR GMTI considerations, an adaptive algorithm to collect velocity and position information on moving targets with mmW monopulse radar, and a discussion on GMTI blind speed elimination and target velocity ambiguity resolving by dual-frequency SAR. To determine the capabilities of both, system and algorithm, three large-scale experiments with MEMPHIS in different environments are presented [J1074]

## "A New Technique for Forecasting Surface Wind Field From Scatterometer Observations: A Case Study for the Arabian Sea"

The possibility of predicting ocean-surface wind field a few days ahead from satellite scatterometer observations in the Arabian Sea has been explored in this paper. The prediction technique is based on a combination of empirical orthogonal function (EOF) analysis and genetic algorithm (GA). The space-time distributed satellite data (zonal or meridional wind field) have been decomposed into a set of spatial eigenmodes ranked by their temporal variance. The associated temporal amplitude functions have been used by the GA for carrying out

forecasts with lead times varying from one to five days. The GA finds the analytical equations that best describe the behavior of the different temporal amplitude functions in the EOF decomposition. Later, the predicted wind field has been generated as a linear combination of the dominant spatial modes weighted by the corresponding predicted amplitudes. The technique has been tested using independent validation data sets. It has been further tested by comparing the forecast fields with buoy data. The performance of GA is comparable to that of persistence forecast for the first two days of forecast, while it is better than that of persistence for three- to five-day-ahead forecasts [J1075]

## "A C-Band Wind/Rain Backscatter Model"

With the confirmed evidence of rain surface perturbation in recent studies, the rain effects on C-band scatterometer measurements are reevaluated. By using colocated Tropical Rainfall Measuring Mission Precipitation Radar, ESCAT on European Remote Sensing Satellites, and European Centre for Medium-Range Weather Forecasts data, we evaluate the sensitivity of C-band sigmadeg to rain. We develop a low-order wind/rain backscatter model with inputs of surface rain rate, incidence angle, wind speed, wind direction, and azimuth angle. We demonstrate that the wind/rain backscatter model is accurate enough for describing the total backscatter in raining areas with relatively low variance. We also show that the rain surface perturbation is a dominating factor of the rain-induced backscatter. Using three distinct regimes, we show under what conditions the wind, rain, and both wind and rain can be retrieved from the measurements. We find that the effect of rain has a more significant impact on the measurements at high incidence angles than at low incidence angles [J1076]

## "Bistatic Linear Antenna Array SAR for Moving Target Detection, Location, and Imaging With Two Passive Airborne Radars"

In this paper, we propose a bistatic linear array synthetic aperture radar (BLA-SAR) system for moving target detection, location, and imaging. In the BLA-SAR system, a geostationary satellite is used as a transmitter, and two airborne linear array radars are used as passive receivers, where the transmitted waveforms from the geostationary satellite may have two different carrier frequencies, two linear array antennas on two different airplanes may be equipped with different spacings, or two airplanes may fly with two different velocities. It is shown that, using the BLA-SAR, not only the stationary clutter can be suppressed but also locations of both slow and fast moving targets can be accurately estimated. Furthermore, an effective BLA-SAR algorithm of moving target imaging is also proposed. Lastly, some numerical experiments are given to demonstrate the effectiveness of the BLA-SAR [J1077]

## "Filtering Soil Surface and Antenna Effects From GPR Data to Enhance Landmine Detection"

The detection of antipersonnel landmines using ground-penetrating radar (GPR) is particularly hindered by the predominant soil surface and antenna reflections. In this paper, we propose a novel approach to filter out these effects from 2-D off-ground monostatic GPR data by adapting and combining the radar antenna subsurface model of Lambot with phase-shift migration. First, the antenna multiple reflections originating from the antenna itself and from the interaction between the antenna and the ground are removed using linear transfer functions. Second, a simulated Green's function accounting for the surface reflection is subtracted. The Green's function is derived from the estimated soil surface dielectric permittivity using full-wave inversion of the radar signal for a measurement taken in a local landmine-free area. Third, off-ground phase-shift migration is performed on the 2-D data to filter the effect of the antenna radiation pattern. We validate the approach in laboratory conditions for four differently detectable landmines embedded in a sandy soil. Compared to traditional background subtraction, this new filtering method permits a better differentiation of the landmine and estimation of its depth and geometrical properties. This is particularly beneficial for the detection of landmines in low-contrast conditions [J1078]

## "Feature-Independent Aperture Evaluator for the Curvilinear SAR"

Curvilinear synthetic aperture radar (SAR), as a more practicable 3-D SAR imaging system, utilizes parametric target feature estimates extracted from the received data to reconstruct the target image. The reconstructed image quality is then impacted by the estimation accuracy of the features. In this letter, through discussing the correlation between the system parameters and the estimation performance of the curvilinear SAR, a conclusion can be drawn on how the overall location accuracy of a target is determined by the correlation between the azimuth and elevation coordinates of the flight path, compactly characterizing the curvilinear aperture. Consequently, a new index, determined only with the aperture parameters, is proposed as an aperture evaluator, which is referred to as the feature-independent aperture evaluator (FAE). FAE can be used for guiding the operational aperture design [J1079]

## "Quartic-Phase Algorithm for Highly Squinted SAR Data Processing"

In this letter, an algorithm based on a quartic-phase model is discussed for processing highly squinted synthetic aperture radar (SAR) data from a large range swath. In the algorithm, a precise quartic-phase model is adopted to describe a range-dependent property of the SAR signal; a constant factor and a secondary scaling process are introduced to make the algorithm easy to be utilized compared with traditional nonlinear chirp scaling algorithms. The novel algorithm can process SAR data under a squint angle above 50deg and achieve a focus depth over 60 km [J1080]

## "Tree Detection in Urban Regions Using Aerial Lidar and Image Data"

In this letter, we present an approach to detecting trees in registered aerial image and range data obtained via lidar. The motivation for this problem comes from automated 3-D city modeling, in which such data are used to generate the models. Representing the trees in these models is problematic because the data are usually too sparsely sampled in tree regions to create an accurate 3-D model of the trees. Furthermore, including the tree data points interferes with the polygonization step of the building roof top models. Therefore, it is advantageous to detect and remove points that represent trees in both lidar and aerial imagery. In this letter, we propose a two-step method for tree detection consisting of segmentation followed by classification. The segmentation is done using a simple region-growing algorithm using weighted features from aerial image and lidar, such as height, texture map, height variation, and normal vector estimates. The weights for the features are determined using a learning method on random walks. The classification is done using the weighted support vector machines, allowing us to control the misclassification rate. The overall problem is formulated as a binary detection problem, and the results presented as receiver operating characteristic curves are shown to validate our approach [J1081]

## "Unsupervised Change Detection From Multichannel SAR Images"

Multichannel synthetic aperture radar (SAR) data present a good potential for environmental monitoring and disaster management, owing both to their insensitivity to atmospheric and sun-illumination conditions, and to the improved discrimination capability they may provide as compared to single-channel SAR. However, this requires accurate and possibly automatic techniques to generate change maps from multichannel SAR images acquired from the same geographic area at different times. In this letter, an automatic unsupervised contextual change-detection method is proposed for two-date multichannel SAR images, by integrating a SAR-specific extension of the Fisher transform with a variant of the expectation-maximization algorithm and with Markov random fields. The method is validated by experiments on SIR-C/XSAR data [J1082]

## "SABRINA: A SAR Bistatic Receiver for Interferometric Applications"

This letter discusses the implementation of SABRINA, Synthetic Aperture radar Bistatic Receiver for Interferometric Applications. The ground resolution of a fixed-receiver bistatic system is studied, showing that it is comparable to that of a monostatic system. Due to the short distance from target to receiver, large sensitivity is obtained. The noncooperative nature of the bistatic system forces a conservative data-acquisition strategy based on continuously sampling the scattered signal during a temporal window around the predicted satellite overpass time. Also, to be able to synchronize the system in time and in frequency, sampling of a direct signal obtained through an antenna pointed at the satellite is required. Besides the signal processing required to phase-lock the received signal, the bistatic synthetic aperture radar processing needs to take into account the azimuth-dependent phase history. First focused images obtained with the SABRINA-ENVISAT combination are discussed [J1083]

## "A Segment-Based Speckle Filter Using Multisensoral Remote Sensing Imagery"

In the proposed approach, the well-known enhanced Lee filter is modified to allow the integration of feature outlines-previously extracted from segmented optical images. The filter is applied to several ENVISAT ASAR images that cover urban, agricultural, and forest areas during different plant phenological stages. The performance of this segment-based speckle filter is compared to those of other filters using ratio images, visual interpretation, and statistical indexes. The approach reduces the loss of radiometry and spatial information. It performs comparable to more complex methods and outperforms common techniques [J1084]

## "Submillimeter Accuracy of InSAR Time Series: Experimental Validation"

This paper presents the results of a blind experiment that is performed using two pairs of dihedral reflectors. The aim of the experiment was to demonstrate that interferometric synthetic aperture radar (InSAR) measurements can indeed allow a displacement time series estimation with submillimeter accuracy (both in horizontal and vertical directions), provided that the data are properly processed and the impact of in situas well as atmospheric

effects is minimized. One pair of dihedral reflectors was moved a few millimeters between SAR acquisitions, in the vertical and east-west (EW) directions, and the ground truth was compared with the InSAR data. The experiment was designed to allow a multiplatform and multigeometry analysis, i.e., each reflector was carefully pointed in order to be visible in both Envisat and Radarsat acquisitions. Moreover, two pairs of reflectors were used to allow the combination of data gathered along ascending and descending orbits. The standard deviation of the error is 0.75 mm in the vertical direction and 0.58 mm in the horizontal (EW) direction. GPS data were also collected during this experiment in order to cross-check the SAR results [J1085]

## "A New Statistical Similarity Measure for Change Detection in Multitemporal SAR Images and Its Extension to Multiscale Change Analysis"

In this paper, we present a new similarity measure for automatic change detection in multitemporal synthetic aperture radar images. This measure is based on the evolution of the local statistics of the image between two dates. The local statistics are estimated by using a cumulant-based series expansion, which approximates probability density functions in the neighborhood of each pixel in the image. The degree of evolution of the local statistics is measured using the Kullback-Leibler divergence. An analytical expression for this detector is given, allowing a simple computation which depends on the four first statistical moments of the pixels inside the analysis window only. The proposed change indicator is compared to the classical mean ratio detector and also to other model-based approaches. Tests on the simulated and real data show that our detector outperforms all the others. The fast computation of the proposed detector allows a multiscale approach in the change detection for operational use. The so-called multiscale change profile (MCP) is introduced to yield change information on a wide range of scales and to better characterize the appropriate scale. Two simple yet useful examples of applications show that the MCP allows the design of change indicators, which provide better results than a monoscale analysis [J1086]

## "Random Noise Radar/Sodar With Ultrawideband Waveforms"

Random noise waveforms with ultrawide bandwidth improve the range resolution and reduces the probability of intercept in radar/sodar. As a result of the nonperiodic waveform, the range ambiguity is removed as well. By transmitting a sine signal that is phase or frequency modulated by random noise, autocorrelation functions with improved side lobe suppression in range can be formed. There are great similarities in the signal-processing algorithms applied in noise radar and sodar. The much slower propagation velocity of sound compared to light reduces the signal bandwidth but increases the time of measurement, however. In both sodar and radar, the range resolution is determined by the wavelength band occupied by the transmitted waveform, while the velocity resolution is controlled by the ratio of wavelength and time of measurement. The slower sound velocity also enhances the range/Doppler ambiguity problem in sodar when periodic waveforms are applied. This ambiguity could be suppressed if nonperiodic waveforms are introduced, such as random noise. In this paper, fundamental similarities and differences on system level between sodar and radar are first discussed, and signal-processing algorithms applied in random noise radar/sodar are reviewed. In particular, the noise floor of the ambiguity function and its relationship to spectrum width and time of measurement are analyzed, including improved side lobe suppression using mismatched filtering. The signal-processing algorithms were tested on raw data from sodar measurements on moving targets, buildings, vegetation, and water surfaces. An adaptive filter algorithm for suppression of the increased noise floor from dominant reflectors was derived and successfully applied to both sodar and stepped frequency radar data [J1087]

## "Reduced-Dimensional Processing for Ground Moving Target Detection in Distributed Space-Based Radar"

With multisatellite radar systems, several additional features are achieved: multistatic observation, interferometry, ground moving target indication (GMTI). In this letter, a new reduced-dimensional method based on joint pixels sum-difference (Sigma-Delta) data for clutter rejection and GMTI is proposed. The reduced-dimensional joint pixels Sigma-Delta data are obtained by the orthogonal projection of the joint pixels data of different synthetic aperture radar (SAR) images generated by a multisatellite radar system. In the sense of statistic expectation, the joint pixels Sigma-Delta data contain the common and different information among SAR images. Then, the objective of clutter cancellation and GMTI can be achieved by adaptive processing. Simulation results demonstrate the effectiveness and robustness of the proposed method even with clutter fluctuation and image coregistration errors [J1088]

## "Coregistration Based on Three Parts of Two Complex Images and Contoured Windows for Synthetic Aperture Radar Interferometry"

The coregistration of complex image pairs is a very important step in synthetic aperture radar interferometry

(InSAR) data processing. This letter proposes a novel coregistration method that only needs three arbitrary parts of the two complex images instead of four parts in the existing coregistration methods. This method constitutes an integrated three-part method for InSAR data processing with our contoured-correlation-interferometry method for phase-image generation. Saving one part transmission makes a significant advantage when processing SAR images on satellites. Furthermore, we demonstrate that, by means of using fringe contoured windows instead of squared windows, the accuracy of the coregistration for both the three-part coregistration method and the existing methods can be improved considerably [J1089]

## "Observations of Snow Water Equivalent Change on Landfast First-Year Sea Ice in Winter Using Synthetic Aperture Radar Data"

In this paper, we examine the utility of synthetic aperture radar (SAR) backscatter data to detect a change in snow water equivalent (SWE) over landfast first-year sea ice during winter at relatively cold temperatures. We begin by reviewing the theoretical framework for linking microwave scattering from SAR to the thermodynamic and electrical properties of first-year sea ice. Previous research has demonstrated that for a given ice thickness and air-temperature change, a thick snow cover will result in a smaller change in the snow-ice interface temperature than will a thin snow cover. This small change in the interface temperature will result in a relatively small change in the brine volume at the interface and the resulting complex permittivity, thereby producing a relatively small change in scattering. A thin snow cover produces the opposite effect-a greater change in interface temperature, brine volume, permittivity, and scattering. This work is extended here to illustrate a variation of this effect over landfast first-year sea ice using in situ measurements of physical snow properties and RADARSAT-1 SAR imagery acquired during the winter of 1999 in the central Canadian Archipelago at cold (~-26degC) and moderately cold (~-14degC) snow-sea-ice interface temperatures. We utilize in situ data from five validation sites to demonstrate how the change in microwave scattering covaries and is inversely proportional with the change in the magnitude of SWE. These changes are shown to be detectable over both short (2 days) and longer (45 days) time durations [J1090]

## "Coherence Loci for a Homogeneous Volume Over a Double-Bounce Ground Return"

The formulation of the polarimetric interferometric coherences derived by simple homogeneous-volume-over-ground models is revisited for the case of ground returns dominated by the double-bounce terms. The differences between single-transmit (single-tx) and alternate-transmit modes of the interferometer are analyzed by inspecting the positions of the coherences on the complex plane. An additional volume-decorrelation term appears when the interferometer is operated in a single-tx mode, which adds complexity in the potential inversion of the model parameters. This effect is even more noticeable for the cross-polar channels in the oriented case, since the phase of the coherence with an infinite ground-to-volume ratio does not correspond to the topographic phase, as observed for the copolar channels [J1091]

## "Experimental Demonstration of the Corbella Equation for Aperture Synthesis Microwave Radiometry"

The fundamental equation of aperture synthesis microwave radiometry has been recently revised into a new so-called Corbella equation to include antenna coupling effects and the interferometry formulation into a single equation. This equation has been experimentally demonstrated for the first time with a full prototype of the Microwave Imaging Radiometer with Aperture Synthesis. Several tests have been carried out to demonstrate the new visibility equation with different targets. The test results show better agreement with simulations based on the Corbella equation than the old fundamental equation. An initial analysis of the influence of the antenna pattern characterization errors shows the importance of these errors in the final results according to the new formulation [J1092]

## "GEOSAT Follow-On Water Vapor Radiometer: Performance With a Shared Active/Passive Antenna"

The GEOSAT Follow-On mission marks the first time that an Earth-orbiting microwave radiometer and radar have shared the same antenna. The antenna design must simultaneously accommodate the radar's high-gain requirement and the high beam efficiency needed by the radiometer. Guaranteeing sufficiently high isolation between the radar transmitter and the radiometer receivers is also a critical part of the antenna design. The radiometer receiver includes a transmitter blanking circuit to further mitigate possible radar interference. Preflight and on-orbit tests of the antenna and radiometer receivers and an evaluation of end-to-end radiometric accuracy are presented. Together, they demonstrate that the shared-antenna approach can be implemented without compromising radiometric performance [J1093]

## "Combining Airborne Photographs and Spaceborne SAR Data to Monitor Temperate Glaciers: Potentials and Limits"

Monitoring temperate glacier activity has become more and more necessary for economical and security reasons and as an indicator of the local effects of global climate change. Remote sensing data provide useful information on such complex geophysical objects, but they require specific processing techniques to cope with the difficult context of moving and changing features in high-relief areas. This paper presents the first results of a project involving four laboratories developing and combining specific methods to extract information from optical and synthetic aperture radar (SAR) data. Two different information sources are processed, namely: 1) airborne photography and 2) spaceborne C-band SAR interferometry. The difficulties and limitations of their processing in the context of Alpine glaciers are discussed and illustrated on two glaciers located in the Mont-Blanc area. The results obtained by aerial triangulation techniques provide digital terrain models with an accuracy that is better than 30 cm, which is compatible with the computation of volume balance and useful for precise georeferencing and slope measurement updating. The results obtained by SAR differential interferometry using European Remote Sensing Satellite images show that it is possible to measure temperate glacier surface velocity fields from October to April in one-day interferograms with approximately 20-m ground sampling. This allows to derive ice surface strain rate fields required to model the glacier flow. These different measurements are complementary to results obtained during the summer from satellite optical data and ground measurements that are available only in few accessible points [J1094]

## "Attenuation and Differential Attenuation Correction of C-Band Radar Observations Using a Fully Self-Consistent Methodology"

A new methodology for correcting the reflectivity factor and differential reflectivity at C-band for rain attenuation is presented. Following a methodology already proposed for X-band, new algorithms are developed based on a full self-consistency condition, describing the interrelation between polarimetric measurements and attenuation along the rain medium. The performance of the algorithms for application to C-band dual-polarization radars is evaluated extensively using radar data collected by the Polar 55C in the Rome region (Italy). Quantitative evaluation of attenuation and differential attenuation estimates is conducted based on C-band dual-polarization observations generated from S-band radar measurements. Evaluation of the new full self-consistency algorithms shows a significant improvement in performance. A key result of this iterative technique is the capability to remove any systematic bias from attenuation and differential attenuation estimates that could arise from drop size distribution variability [J1095]

## "A Novel Technique for Noise Reduction in InSAR Images"

This letter proposes a new technique for noise reduction applied to synthetic aperture radar interferometry. This technique involves a nonlinear filter that separates the interferogram into two components: one containing the smooth (low frequency) part and the other containing the detail (high frequency) part. The smooth part is obtained using a combination of a median filter and a smoothing filter. The detail component is obtained by subtracting the smooth component from the original signal. This detail component is filtered to remove noise and then added to the smooth component to generate the final output. Both simulated and real data are used to evaluate the performance of the proposed technique under different conditions. The experimental results show that the proposed technique outperforms most commonly used interferometric phase filters [J1096]

## "Bathymetric Estimation Using MERIS Images in Coastal Sea Waters"

Bathymetric estimation using remote sensing images has previously been applied to high spatial resolution imagery such as CASI, Ikonos, or SPOT but not on medium spatial resolution images (i.e., MERIS). This choice can be justified when there is a need to map the bathymetry on large areas. In this letter, we present the results of the bathymetry estimation over a large known area, the Gulf of Lion (France), expanding over 270times180 km [J1097]

## "A Novel Method for Removal of Emitter Noise in SAR Images"

Traditionally, interfering emitter signatures have been removed through notched filtering in the range (fast-time) dimension. This works well when a narrowband emitter interferes with a wideband radar pulse; however, when the emitter and radar signal bandwidths are comparable, then this approach fails since the noise is distributed throughout the pulse and the image as well. In cases where the interfering signal is localized in the cross range, joint time-frequency methods can often focus this interference signal, thereby transforming the image. In this transformed image, the interferer is the foreground, and the desired synthetic aperture radar image is blurred and now the background. The focused compressed interferer can be analyzed and censored from the

transformed image. Back transformation restores the image with the interference removed. This technique has been fully automated and applied to an Electromagnetics Institute Synthetic Aperture Radar (EMISAR) image contaminated by a nonstationary emitter. The cleansed image is virtually free of the emitter interference [J1098]

## "Toward Hyperspectral Lidar: Measurement of Spectral Backscatter Intensity With a Supercontinuum Laser Source"

We have tested the use of a supercontinuum laser source in laser-based spectral backscatter measurement. The calibration and first results with the prototype instrument are presented with a discussion of improvements and applications in laser-based hyperspectral remote sensing and laboratory measurements. This technique enables the spectral study of the backscatter effects and the calibration and test measurements for the purpose of airborne laser measurement. We also explore the prospect of using a supercontinuum laser source in a broadband (hyperspectral) lidar [J1099]

## "Dependence of Waterline Mapping on Radar Frequency Used for SAR Images in Intertidal Areas"

Waterline detection in the intertidal areas was investigated through synthetic aperture radar (SAR) images and field measurements. Two valuable facts were found in this letter: 1) A discrepancy of waterlines between L- and P-band airborne SAR images was discovered and investigated through precise global positioning system measurements and the theory of the SAR imaging mechanism. In the intertidal areas having low slopes, the Bragg waves resonant with the radar signal can reside in different depths depending on the radar frequency, with the result that the boundary between water and land can be mapped differently in the respective SAR images. 2) Intertidal areas covered with a water film present low radar backscatter in SAR images, which can cause mislocation of waterlines [J1100]

## "A Fusion Scheme for Joint Retrieval of Urban Height Map and Classification From High-Resolution Interferometric SAR Images"

The retrieval of 3-D surface models of the Earth is a major issue of remote sensing. Some nice results have already been obtained at medium resolution with optical and radar imaging sensors. For instance, missions such as the Shuttle Radar Topography Mission (SRTM) or the SPOT HRS have provided accurate digital terrain models. The computation of a digital surface model (DSM) over urban areas is the new challenging issue. Since the recent improvements in radar image resolution, synthetic aperture radar (SAR) interferometry, which had already proved its efficiency at low resolution, has provided an accurate tool for urban 3-D monitoring. However, the complexity of urban areas and high-resolution SAR images prevents the straightforward computation of an accurate DSM. In this paper, an original high-level processing chain is proposed to solve this problem, and some results on real data are discussed. The processing chain includes three main steps, namely: (1) information extraction; (2) fusion; and (3) correction. Our main contribution addresses the merging step, where we aim at retrieving both a classification and a DSM while imposing minimal constraint on the building shapes. The joint derivation of height and class enables the introduction of more contextual information. As a consequence, more flexibility toward scene architecture is possible. First, the initial images (interferogram, amplitude, and coherence images) are converted into higher-level information mapping with different approaches (filtering, object recognition, or global classification). Second, these new images are merged into a Markovian framework to jointly retrieve an improved classification and a height map. Third, DSM and classification are improved by computing layover and shadow from the estimated DSM. Comparison between shadow/layover and classification allows some corrections. This paper mainly addresses the second step, while the two others are briefly explained and referred to already publis- hed papers. The results obtained on real images are compared to ground truth and indicate a very good accuracy in spite of limited image resolution. The major limit of DSM computation remains the initial spatial and altimetric resolutions that need to be made more precise [J1101]

## "Dual-Baseline Coherence Tomography"

In this letter, we consider a dual-baseline formulation of coherence tomography and show how practical application of the method is limited by numerical stability. To help reduce this, we propose a regularization technique based on a matrix singular value decomposition to stabilize the inversion. We then apply the new dual-baseline algorithm to ground-based radar data from the European Microwave Signature Laboratory. We consider a sample of maize plants and employ dual-baseline interferometric data to reconstruct vertical tomograms through the vegetation as a function of frequency. We use these reconstructions to interpret the primary scattering mechanisms and their polarization dependence [J1102]

## "On the Use of Multiantenna Radars for Spaceborne Doppler Precipitation Measurements"

We propose the use of multiantenna radars for precipitation measurement from moving platforms. The primary motivation is measurement of vertical motion from spaceborne radars. Preliminary analysis of the concept and application to a specific example indicate that such a system would be feasible [J1103]

## "Measuring Surface Roughness Height to Parameterize Radar Backscatter Models for Retrieval of Surface Soil Moisture"

Surface roughness is a crucial input for radar backscatter models. Roughness measurements of root mean-squared height (hrms) of the same surface can vary depending on the measuring instrument and how the data are processed. This letter addresses the error in hrms associated with instrument bias and instrument deployment issues such as number and length of measurement transects. It was found that at least 20 transect measurements, 3 m in length, for study sites ranging from 3.5 to 1225 m2in size were necessary to get a consistent hrmsmeasurement. Also, roughness heights of longer transect lengths were highly dependent on the method of detrending the transects. Finally, soil moisture was predicted by inverting the integral equation model using roughness heights taking into account instrument bias, number of measurements, and the detrending method. For common configurations of the Radarsat sensor and reasonable hrmsvalues, error associated with measurement of hrms generally exceeded plusmn20% of soil-moisture prediction [J1104]

## "Accurate Centerline Detection and Line Width Estimation of Thick Lines Using the Radon Transform"

Centerline detection and line width estimation are important for many computer vision applications, e.g., road network extraction from high resolution remotely sensed imagery. Radon transform-based linear feature detection has many advantages over other approaches: for example, its robustness in noisy images. However, it usually fails to detect the centerline of a thick line due to the peak selection problem. In this paper, several key issues that affect the centerline detection using the radon transform are investigated. A mean filter is proposed to locate the true peak in the radon image and a profile analysis technique is used to further refine the line parameters. The thetas-boundary problem of the radon transform is also discussed and the erroneous line parameters are corrected. Intensive experiments have shown that the proposed methodology is effective in finding the centerline and estimating the line width of thick lines [J1105]

## "Selection of Forest Stands for Stem Volume Retrieval From Stable ERS Tandem InSAR Observations"

Environmental factors influence the accuracy in stem volume retrieval using European Remote Sensing Satellite (ERS) tandem synthetic aperture radar (SAR) interferometry. Some forest stands are more sensitive than others to heterogeneity of environmental properties, forest properties, and noise. It is shown that the consistency of coherence observations between different image pairs or the consistency of the estimated stem volume can be used to sort forest stands according to increasing errors in stem volume estimates associated with varying forest properties. Fifteen ERS tandem pairs were used to determine the relative root mean square error (RMSE) of stem volume estimated from C-band SAR interferometry. The test site, Tuusula in Finland, contains 210 forest stands with stem volumes up to 539 m3/ha. RMSE varies between 17% and 63% depending on number and type of stands included in the retrieval accuracy analysis. The more homogeneous forest stands with larger area and higher stem volumes of spruce and pine are those with highest retrieval accuracy [J1106]

## "Terrain Moisture Classification Using GPS Surface-Reflected Signals"

In this letter, a novel method of land-surface classification using surface-reflected global positioning system (GPS) signals in combination with digital imagery is presented. Two GPS-derived classification features are merged with visible image data to create terrain moisture classes, defined here as visibly identifiable terrain or landcover classes containing a surface/soil moisture component. As compared to using surface imagery alone, classification accuracy is significantly improved for a number of visible classes when adding GPS-based signal features. Since the strength of the reflected GPS signal is proportional to the amount of moisture in the surface, the use of these GPS features provides information about the surface that is not obtainable using visible wavelengths alone. Application areas include hydrology, precision agriculture, and wetlands mapping [J1107]

## "Effect of Look Angle on the Accuracy Performance of Fixed-Baseline Interferometric SAR"

The effect of look angle on the accuracy performance of fixed-baseline interferometric synthetic aperture radar is studied. It is shown that there exists an optimal look angle that minimizes the variance of the surface height estimate for a resolution cell, and it depends upon the system as well as surface parameters. Numerical analysis confirming the existence of the optimal look angle is presented [J1108]

## "Synergistic Fusion of Interferometric and Speckle-Tracking Methods for Deriving Surface Velocity From Interferometric SAR Data"

This letter presents a technique to adjust and unify disconnected interferogram fringe regions for the derivation of accurate surface-velocity measurements. The interferogram from repeat-pass interferometric synthetic aperture radar data is often partitioned by shear margins of ice streams and other low-coherence zones into many small disconnected fringe regions. Although these isolated fringe regions can be unwrapped separately, the unwrapped phase for each region is referenced to a different seed point. Our technique exploits absolute range-offset measurements from the speckle-tracking method to bridge the isolated fringe regions in the interferogram. In this way, the unwrapped phases in these regions can be adjusted into consistent surface-displacement measurements with a common reference point. Using Radarsat interferometric data in Antarctica, we demonstrated that the synergetic fusion of the measurements from the interferometric and speckle-tracking methods can produce a highly accurate two-dimensional velocity field [J1109]

## "Feasibility of Retrieving Land-Surface Temperature From ASTER TIR Bands Using Two-Channel Algorithms: A Case Study of Agricultural Areas"

The Advanced Spaceborne Thermal Emission and Reflection Radiometer (ASTER) provides the user community with standard products of land-surface temperature (LST) and emissivity using the temperature and emissivity separation (TES) algorithm. This letter analyzes the feasibility of using two-channel (TC) algorithms for LST retrieval from ASTER data, which could be considered as an alternative or complementary procedure to the TES algorithm. TC algorithms have been developed for all the ASTER thermal infrared bands combinations, and they have been applied to six ASTER images acquired over an agricultural area of Spain in 2000, 2001, and 2004. LST values obtained with TC algorithms were compared with the TES product. In addition, the TC algorithms were tested using simulated data and ground-based measurements collected coincident with the ASTER acquisition in 2004. The results show that TC algorithms provide similar accuracies than the TES algorithm (~1.5 K), with the main advantage that the atmospheric correction is included in the algorithm itself [J1110]

## "Spatial Interpolation of Elevation Data With Variable Density: A New Methodology to Derive Quality DEMs"

A new methodology for spatial interpolation of elevation data with variable density is proposed. The method is based on two-step interpolation and data processing to minimize interpolation artifacts caused by variable data density. In the first step, the parameterization of the spline interpolation method is focused on areas with sparse data that need smoother interpolation. Then, the resulting surface in these areas is randomly sampled to densify the original data set. In the second step, the parameterization of the interpolation method is focused on areas with a required high level of detail. The final resulting surface contains the properties of surfaces optimized for different data densities and levels of detail [J1111]

## "Multiple-Scattering Formulation of Pulsed Beam Waves in Hydrometeors and Its Application to Millimeter-Wave Weather Radar"

This letter deals with the backscattering of millimeter pulsed beam waves from hydrometeors. A new approach is presented for a solution of time-dependent three-dimensional vector radiative transfer equation for the Stokes vectors to study the multiple-scattering effects of beam waves on radar echoes. General solutions for beam waves are derived in an integral form without any approximation. They are given in numerically tractable forms representing the scattering process in the space and time domain. Time-dependent second-order solutions for radar echoes of pulsed beam waves are straightforwardly obtained to predict multiple-scattering effects depending on the variation of an incident beam size. It is shown that the inhomogeneity of the radial direction of beam waves causes the mode coupling of waves between the azimuth directions in the scattering matrix, and that the mode coupling depends on the ratio of the incident beam size to the total mean free path length of the medium [J1112]

## "Integration of Ground-Penetrating Radar and Laser Position Sensors for Real-Time 3-D Data Fusion"

Full-resolution 3-D ground-penetrating radar (GPR) imaging of the near surface should be simple and efficient. Geoscientists, archeologists, and engineers need a tool capable of generating interpretable subsurface views at centimeter-to-meter resolution of field sites ranging from smooth parking lots to rugged terrain. The authors have integrated novel rotary laser positioning technology with GPR into such a 3-D imaging system. The laser positioning enables acquisition of centimeter accurate x, y, and z coordinates from multiple small detectors attached to moving GPR antennas. Positions streaming with 20 updates/s from each detector are fused in real

time with the GPR data. The authors developed software for automated data acquisition and real time 3-D GPR data quality control on slices at selected depths. Industry standard (SEGY) format data cubes and animations are generated within an hour after the last trace has been acquired. Such instant 3-D GPR can be used as an on-site imaging tool supporting field work, hypothesis testing, and optimized excavation and sample collection in the exploration of the static and dynamic nature of the shallow subsurface [J1113]

## "A GPS-Reflections Receiver That Computes Doppler/Delay Maps in Real Time"

This paper describes a new instrument that was specially designed and developed to gather Global Positioning System (GPS) signals after they have been reflected from suitable surfaces (sea, ice, and ground), for Earth remote sensing. The device has been called the GPS open-loop differential real-time receiver (GOLD-RTR). Its main and most innovative feature is its computation and storage, in real time, of complex-valued (I and Q) cross correlations (waveforms) between GPS L1-C/A signals-received directly and after reflection-and the corresponding models of these signals. Particularly, the GOLD-RTR schedules consecutive coherent integration time slots of 1 ms over which ten parallel correlation channels, with 64 lags each, work simultaneously and continuously with the input raw data sampled at 40 MHz. The total throughput is 10 000 waveforms per second, each waveform being 64 lags long. These real-time correlation resources can be flexibly distributed in several configurations according to the observational requirements, for instance: Doppler/delay maps or up to ten simultaneous reflected waveforms for ten different GPS satellites are examples of what can be done. The further processing of the real-time computed 1-ms waveforms in a flight campaign over the ocean, ice, or ground can be used to obtain geophysical parameters such as sea level and tides, sea surface mean-square slopes, ice roughness and thickness, soil moisture and biomass, or future applications. This paper covers the GOLD-RTR architecture and hardware, signal processing and data storage issues, machine-user interface, laboratory readiness tests, and waveform data samples from the first two jet aircraft campaigns at 9300 m over the sea [J1114]

## "Detection of Antipersonnel Mines by Using the Factorization Method on Multistatic Ground-Penetrating Radar Measurements"

The factorization method (FM) has been applied to measurement data from a multistatic ground-penetrating radar operating in close proximity to the ground, which was used in a measurement campaign on the Joint Research Centre mine test lane in Ispra, Italy. This paper is targeted toward a future hand-held demining system. The according space limits restrict an independent positioning of transmit and receive antennas. Hence, very small multistatic datasets are obtained, representing a difficult case for the reconstruction with the FM [J1115]

## "Verification of the Vertical Error in C-Band SRTM DEM Using ICESat and Landsat-7, Otter Tail County, MN"

The Shuttle Radar Topography Mission (SRTM) provided scientists with digital elevation data on a nearly global scale and with highly consistent accuracy. This paper compares elevation values of the C-band SRTM 30-m digital elevation model (DEM) with pointwise elevations from the Ice, Cloud, and land-Elevation Satellite (ICESat) laser altimetry for Otter Tail County, Minnesota. The accuracy of SRTM DEM is measured as a function of land covers and geomorphologic characteristics. The typical mean vertical difference between the SRTM DEM and ICESat elevations in this paper was determined in each classified land-use type and is approximately 1.5 m over bare ground, with the SRTM measuring lower elevations. Significant changes in the SRTM DEM uncertainties have been identified over different surface types classified from Landsat-7 imagery, e.g., bare ground, urban, and forested areas. Based on this result, the difference of the SRTM 30-m DEM and ICESat elevations has been removed from the DEM and made available for improved hydrological applications [J1116]

## "Subsurface Sensing of Buried Objects Under a Randomly Rough Surface Using Scattered Electromagnetic Field Data"

This paper proposes a new inverse method for microwave-based subsurface sensing of lossy dielectric objects embedded in a dispersive lossy ground with an unknown rough surface. An iterative inversion algorithm is employed to reconstruct the geometry and dielectric properties of the half-space ground as well as that of the buried object. B-splines are used to model the shape of the object as well as the height of the rough surface. In both cases, the control points for the spline function represent the unknowns to be recovered. A single-pole rational transfer function is used to capture the dispersive nature of the background. Here, the coefficients in the numerator and denominator are the unknowns. The approach presented in this paper is based on the state-of-the-art semianalytic mode matching forward model, which is a fast and efficient algorithm to determine the scattered electromagnetic fields. Numerical experiments involving two-dimensional geometries and TM incident

plane waves demonstrate the accuracy and reliability of this inverse method [J1117]

## "Estimating Snow Accumulation From InSAR Correlation Observations"

Snow accumulation in remote regions, such as Greenland and Antarctica, is a key factor for estimating the Earth's ice mass balance. In situdata are sparse; hence, they are useful to derive snow accumulation from remote sensing observations, such as microwave thermal emission and radar brightness. These data are usually interpreted using electromagnetic models in which volume scattering is the dominant mechanism. The main limitation of this approach is that microwave brightness is not well related to backscatter if the ice sheet is layered. Because larger grain size and thicker annual layers both increase radar image brightness, with the first corresponding to lower accumulation rate and the second to higher accumulation rate, models of radar brightness alone cannot accurately reflect accumulation. Consideration of correlation measurements can also resolve this ambiguity. We introduce an interferometric ice scattering model that relates the interferometric synthetic aperture radar correlation and radar brightness to both ice grain size and hoar layer spacing in the dry-snow zone of Greenland. We use this model and the European Remote Sensing satellite radar observations to derive several parameters related to snow accumulation rates in a small area in the dry-snow zone. These parameters show agreement with four in situcore accumulation rate measurements in this area, whereas models using only radar brightness data do not match the observed variation in accumulation rates [J1118]

## "A Two-Dimensional Bandwidth Extrapolation Technique for Polarimetric Synthetic Aperture Radar Images"

The resolution of a synthetic aperture radar (SAR) image, in range and azimuth, is determined by the transmitted bandwidth and the synthetic aperture length, respectively. Various superresolution techniques for improving resolution have been proposed, and we have proposed an algorithm that we call polarimetric bandwidth extrapolation (PBWE). To apply PBWE to a radar image, one needs to first apply PBWE in the range direction and then in the azimuth direction, or vice versa . In this paper, PBWE is further extended to the 2-D case. This extended case (2D-PBWE) utilizes a 2-D polarimetric linear prediction model and expands the spatial frequency bandwidth in range and azimuth directions simultaneously. The performance of the 2D-PBWE is shown through a simulated radar image and a real polarimetric SAR image [J1119]

## "Target Scattering Decomposition in Terms of Roll-Invariant Target Parameters"

The Kennaugh-Huynen scattering matrix con-diagonalization is projected into the Pauli basis to derive a new scattering vector model for the representation of coherent target scattering. This model permits a polarization basis invariant representation of coherent target scattering in terms of five independent target parameters, the magnitude and phase of the symmetric scattering type introduced in this paper, and the maximum polarization parameters (orientation, helicity, and maximum return). The new scattering vector model served for the assessment of the Cloude-Pottier incoherent target decomposition. Whereas the Cloude-Pottier scattering type alpha and entropy H are roll invariant, beta and the so-called target-phase parameters do depend on the target orientation angle for asymmetric scattering. The scattering vector model is then used as the basis for the development of new coherent and incoherent target decompositions in terms of unique and roll-invariant target parameters. It is shown that both the phase and magnitude of the symmetric scattering type should be used for an unambiguous description of symmetric target scattering. Target helicity is required for the assessment of the symmetry-asymmetry nature of target scattering. The symmetric scattering type phase is shown to be very promising for wetland classification in particular, using polarimetric Convair-580 synthetic aperture radar data collected over the Ramsar Mer Bleue wetland site to the east of Ottawa, Ontario, Canada [J1120]

## "Accurate Imaging of Multicomponent GPR Data Based on Exact Radiation Patterns"

Scalar migration algorithms developed for three-dimensional seismic data are commonly used for imaging ground-penetrating radar (GPR) data. Yet, radar is a vector phenomenon, such that the GPR amplitudes and phases depend on the antenna orientations and wave propagation paths. To address this issue, vector imaging algorithms that fully account for the vector characteristics of GPR data are required. All previously developed vector imaging algorithms are based on far-field approximations of radiation patterns. We demonstrate the limited applicability of these algorithms and introduce a computationally efficient practically exact-field method that accounts for the far-, intermediate-, and near-field contributions to the radiation patterns. To compute rapidly the required "exact" radiation patterns, inverse fast Fourier transforms are applied to their horizontal wavenumber-frequency domain formulations, balancing the tradeoff between accuracy and efficiency by an appropriate oversampling in the wavenumber-frequency domain, and taking advantage of vertical wavenumber phase shifting. We include the exact radiation patterns in a multicomponent vector imaging scheme that jointly images copolarized and cross-polarized data. This scheme is tested on synthetic and field data containing dipping planar

and near-planar structures. For both suites of data, high-quality multicomponent images with reflection amplitudes that are nearly independent of the antenna and reflector orientations are obtained [J1121]

## "Theoretical Evaluation of Several Possible Along-Track InSAR Modes of TerraSAR-X for Ocean Current Measurements"

The German satellite TerraSAR-X, scheduled for launch in late 2006, will permit high-resolution ocean current measurements by along-track interferometric SAR (along-track InSAR) in various experimental modes of operation, using different sections of its X-band SAR antenna array with a total length of 4.8 m as individual receive antennas. Depending on antenna and receive-chain settings, effective InSAR time lags of about 0.17 to 0.29 ms can be realized in combination with different noise levels, single-look resolutions, swath widths, and incidence angles. We give an overview of the characteristics of the possible InSAR modes and evaluate their suitability for current measurements on the basis of simulated data products. Our results indicate that the quality of interferometric stripmap data from TerraSAR-X will be clearly superior to the quality of the existing data acquired over the Dutch coast during the Shuttle Radar Topography Mission; accurate current retrievals can be expected at effective spatial resolutions on the order of 500 m. However, in modes using a multiplexed single receive chain, the effective swath width of stripmap data will be limited to only 15 km, while dual receive-chain operation offers a swath width of 30 km for stripmap data and promises a reasonable data quality even for ScanSAR data with a maximum swath width of 100 km. Finally, we consider fundamental relations between along-track baseline, instrument noise, and resulting InSAR phase noise to discuss the potential for current measuring performance improvements of TerraSAR-X follow-on satellites [J1122]

## "Investigation of Time–Frequency Features for GPR Landmine Discrimination"

Ground-penetrating radar (GPR) is capable to detect plastic antipersonnel landmines as well as other subsurface targets. In order to reduce false alarms, an option of automatic landmine discrimination from neutral minelike targets would be very useful. This paper presents a possibility for such discrimination and analyzes it experimentally. The authors investigate time-frequency features of an ultrawideband (UWB) target response for the discrimination between buried landmines and other objects. The discrimination method includes the extraction of an early-time target impulse response, its time-frequency transformation, and the extraction of time-frequency features based on a singular value decomposition of the transformed image. In order to take into account the changes in the UWB target signals, the experimental conditions are completely controlled to focus on the behavior of the target's response with respect to its depth and the horizontal position of the GPR above it. The dependence of the features on the GPR bandwidth is analyzed as well. The Mahalanobis distance is used as a criterion for optimal discrimination. The obtained results define the best features and conditions when the landmine discrimination is successful. For comparison, the discriminant power of the proposed features has been tested on a dataset, acquired during a field campaign in Angola [J1123]

## "Optimizing the Area Under a Receiver Operating Characteristic Curve With Application to Landmine Detection"

A common approach to training neural network classifiers in a supervised learning setting is to minimize the mean-square error (mse) between the network output for each labeled training sample and some desired output. In the context of landmine detection and discrimination, although the performance of an algorithm is correlated with the mse, it is ultimately evaluated by using receiver operating characteristic (ROC) curves. In general, the larger the area under the ROC curve (AUC), the better. We present a new method for maximizing the AUC. Desirable properties of the proposed algorithm are derived and discussed that differentiate it from previously proposed algorithms. A hypothesis test is used to compare the proposed algorithm to an existing algorithm. The false alarm rate achieved by the proposed algorithm is found to be less than that of the existing algorithm with 95% confidence [J1124]

## "Decision Fusion of Ground-Penetrating Radar and Metal Detector Algorithms—A Robust Approach"

Numerous detection algorithms, using various sensor modalities, have been developed for the detection of mines in cluttered and noisy backgrounds. The performance for each detection algorithm is typically reported in terms of the receiver operating characteristic (ROC), which is a plot of the probability of detection versus false alarm as a function of the threshold setting on the output decision variable of each algorithm. In this paper, we present multisensor decision-fusion algorithms that combine the local decisions of existing detection algorithms for different sensors. This offers an expedient, attractive, and much simpler alternative to the design of an algorithm that fuses multiple sensors at the data level, especially in cases of limited training data where it is difficult to make accurate estimates of multidimensional probability density functions. The goal of our multisensor decision-

fusion approach is to exploit the complimentary strengths of existing multisensor algorithms so as to achieve performance (ROC) that exceeds the performance of any sensor algorithm operating in isolation. Our approach to multisensor decision fusion is based on the optimal signal detection theory using the likelihood ratio. We consider the optimal fusion of local decisions for two sensors: a ground-penetrating radar and a metal detector. A new robust algorithm for decision fusion that addresses the problem in which the statistics of the training data are not likely to exactly match the statistics of the test data is presented. ROCs are presented and compared for field data [J1125]

## "Electromagnetic Scattering From Multilayer Rough Surfaces With Arbitrary Dielectric Profiles for Remote Sensing of Subsurface Soil Moisture"

Radar remote sensing of soil moisture content at low frequencies requires an accurate scattering model of realistic soils, which often involves multilayer rough surfaces and dielectric profiles. In this paper, a hybrid analytical/numerical solution to two-dimensional scattering from multilayer rough surfaces separated by arbitrary dielectric profiles based on the extended boundary condition method (EBCM) and scattering matrix technique is presented. The reflection and transmission matrices of rough interfaces are constructed using EBCM. The dielectric profiles are modeled as stacks of piecewise homogeneous dielectric thin layers, whose scattering matrices are computed by recursively cascading reflection and transmission matrices of individual dielectric interfaces. The interactions between the rough interfaces and stratified dielectric profiles are taken into account by applying the generalized scattering matrix technique. The scattering coefficients are obtained by combining the powers computed from the resulting Floquet modes of the overall system. The bistatic scattering coefficients are validated against existing analytical and numerical solutions. Field-collected soil moisture data are then used for numerical simulations to investigate the penetration capability at different frequencies and to address the potential of low-frequency radar systems in estimating deep soil moisture. In particular, soil moisture profiles during dry ground, wet ground, and wet subsurface layer conditions are examined. The results show that both backscattering coefficients and copolarized phase difference at low frequencies are sensitive to the roughness of subsurface interfaces and deep soil moisture. Also, much larger depth sensitivity can be achieved using copolarized phase difference than scattering coefficients [J1126]

## "Adding Sensitivity to the MLBF Doppler Centroid Estimator"

The multilook beat frequency (MLBF) algorithm is the Doppler centroid estimator most commonly used in practice to solve the Doppler ambiguity. However, it still makes errors, notably in medium- or low-contrast scenes. In this paper, we present two ways in which the estimation sensitivity of the MLBF algorithm can be improved. First, we give a more thorough frequency-domain explanation of how the MLBF algorithm works and explain how cross beating and range migration cause estimation difficulties. The first improvement to the algorithm replaces the fast Fourier transform (FFT)-based beat frequency estimator with a more accurate one that uses phase increments. It avoids the FFT limitations of resolution and quantization, especially when the signal is discontinuous in one range cell due to range cell migration or burst mode operation (ScanSAR). A second improvement uses range cell migration correction to straighten the target trajectories before the beat frequency estimator is applied. This has the effect of narrowing the bandwidth of the beat signal and reducing the effect of cross beating. Finally, experiments with RADARSAT-1 data are used to illustrate the improved estimation accuracy of the modified algorithm [J1127]

## "Depolarization, Scattering, and Attenuation of Circularly Polarized Radio Waves by Spherically Asymmetric Melting Ice Particles"

The eccentric spheres model and an extended Mie solution are used to formulate scattering of a plane, electromagnetic wave by a single melting ice particle as well as by a horizontal layer of such particles. The incident wave is left-hand circularly polarized, whereas the scattered wave, as a result of depolarization by the spherically asymmetric particles, comprises left-hand and right-hand circularly polarized components. The Stokes parameters of the scattered wave are calculated throughout the melting process. Furthermore, radar observables of backscattering and depolarization, as well as the specific attenuation, across the melting layer are calculated. The numerical application manifests how the internal spherical asymmetry of melting ice particles is imprinted on backscattering, forward scattering, and depolarization. Moreover, it is shown how each part of the melting layer contributes to the attenuation and depolarization of the radio waves crossing that layer [J1128]

## "On the Extension of Multidimensional Speckle Noise Model From Single-Look to Multilook SAR Imagery"

Speckle noise represents one of the major problems when synthetic aperture radar (SAR) data are considered. Despite the fact that speckle is caused by the scattering process itself, it must be considered as a noise source

due to the complexity of the scattering process. The presence of speckle makes data interpretation difficult, but it also affects the quantitative retrieval of physical parameters. In the case of one-dimensional SAR systems, speckle is completely determined by a multiplicative noise component. Nevertheless, for multidimensional SAR systems, speckle results from the combination of multiplicative and additive noise components. This model has been first developed for single-look data. The objective of this paper is to extend the single-look data model to define a multilook multidimensional speckle noise model. The asymptotic analysis of this extension, for a large number of averaged samples, is also considered to assess the model properties. Details and validation of the multilook multidimensional speckle noise model are provided both theoretically and by means of experimental SAR data acquired by the experimental synthetic aperture radar system, operated by the German Aerospace Center [J1129]

## "Application of DInSAR-GPS Optimization for Derivation of Fine-Scale Surface Motion Maps of Southern California"

A method based on random field theory and Gibbs-Markov random fields equivalency within Bayesian statistical framework is used to derive 3-D surface motion maps from sparse global positioning system (GPS) measurements and differential interferometric synthetic aperture radar (DInSAR) interferogram in the southern California region. The minimization of the Gibbs energy function is performed analytically, which is possible in the case when neighboring pixels are considered independent. The problem is well posed and the solution is unique and stable and not biased by the continuity condition. The technique produces a 3-D field containing estimates of surface motion on the spatial scale of the DInSAR image, over a given time period, complete with error estimates. Significant improvement in the accuracy of the vertical component and moderate improvement in the accuracy of the horizontal components of velocity are achieved in comparison with the GPS data alone. The method can be expanded to account for other available data sets, such as additional interferograms, lidar, or leveling data, in order to achieve even higher accuracy [J1130]

## "Geometrical Variations of Gain Patterns"

This paper studies the effect of the altitude and the elliptical nature of the Earth on projected antenna pattern functions (APFs). These variations can play a significant role in spatial filter algorithms, such as the Backus-Gilbert method. In this paper, a solution for projecting an APF from an arbitrary sensor and platform onto an elliptical Earth is presented. A general time integration of this projection is presented, which is important for dynamically generating the effective antenna pattern functions (EAPFs) in cases where the variations are nonnegligible. It is shown that the elliptical nature of the Earth provides a variation of order 1% in the area of the EAPF. These results suggest that approximating the Earth as a sphere is valid. It is also shown that elliptical orbits should consider the implication of the altitude variation before precomputing EAPFs [J1131]

## "Vibration and Rotation in Millimeter-Wave SAR"

Synthetic aperture radar (SAR) provides high-resolution images of static ground scenes, whereas processing of data containing ground object motion results in varying focusing effects. Special cases of such motion are vibration and rotation, which are closely related to each other. Their patterns may be distinctly recognizable in focused SAR intensity images as well as in a time-frequency analysis. Millimeter-wave (mmW) SAR is well suited to image vibration because its wavelength is close to typical vibration amplitudes. Through a thorough motion analysis in a standard SAR system model, we show the effects of rotation and vibration in mmW SAR theoretically and in simulated and real data [J1132]

## "SAR Polarimetry to Observe Oil Spills"

A study on sea oil spill observation by means of polarimetric synthetic aperture radar (SAR) data is accomplished. It is based on the use of a polarimetric constant false alarm rate filter to detect dark patches over SAR images. Then, the target decomposition theorem is exploited to distinguish oil spills and look-alikes. Experiments are conducted on polarimetric SAR data acquired during the SIR-C/X-SAR mission on October 1994. The data were processed and calibrated at the Jet Propulsion Laboratory, National Aeronautics and Space Administration. Results show that the new polarimetric approach is able to assist classification [J1133]

## "Systems Engineering Analysis of a TRMM PR-Like Rainfall Retrieval Algorithm"

Systems engineering constitutes a group of processes and methods to design and implement a system for optimal performance given limited time, technology, or resources. As with any system, it is important to understand which subcomponents are most important and which are less important so that appropriate resource allocations may be made. An example of a complex system is the Tropical Rainfall Measuring Mission (TRMM). Its subsystems include the satellite vehicle, the precipitation radar (PR), the ground validation system, and the

retrieval algorithms. Each of these subsystems contributes to the overall success of the mission. Sensitivity analysis (SA) is a method whereby the output response from a model can be linked back to the variability in the input parameters. This paper describes a method of performing SA on a TRMM PR-like (TL) rainfall retrieval algorithm (based on the TRMM 2A25 algorithm) to better describe how the uncertainty in the model output can be apportioned to the uncertainty in the input factors and gain greater understanding as to the relative importance of each factor. For example, assuming a model with several input factors, if one factor is found to be the dominating cause of model error, and the others contribute relatively little, then resources can be devoted to improving the accuracy of one factor, thereby improving the overall model accuracy. This paper is based on global SA using a variance decomposition technique. Analyses are done and results are presented for factor importance for cases over both ocean and land. Results for the simple TL algorithm considered in this paper show that at low rain rate, the a and b coefficients in the R=aZebrelationship contribute the greatest amount to the output variance. At higher rain rates, above about 8 mm/h, the error from Deltasigmadeg is the greatest contributor to error in algorithm output [J1134]

## "The Distribution and Classification of Bottom Crevasses From Radar Sounding of a Large Tabular Iceberg"

Bottom crevasses at the base of an iceberg or ice shelf are identified in radar sounding observations from their long echo tails. In November 2001, a radar sounding survey was conducted over iceberg B15A, which calved off from the Ross Ice Shelf, Antarctica, in March 2000. Pervasive basal cracking was observed, and the distribution of bottom crevasses along the flight lines is presented. The echo tails were quantitatively analyzed using a physically based model for backscattering from bottom crevasses. The identified crevasses are classified as either major water-filled crevasses or incipient/freezing crevasses, and estimates for crevasse heights are given [J1135]

## "A Technique for Jamming Bi- and Multistatic SAR Systems"

Bi- and multistatic synthetic aperture radars (SARs) can achieve reduced vulnerability in military systems, especially in directional responsive jamming, and avoid physical attack to radar platforms. In this letter, a technique for jamming bi- and multistatic SAR systems is proposed, which is implemented with a novel transponder. This technique is based on a delayed retransmission of the received radar signal toward the scene. Unlike conventional delayed jamming, here, the jammer's delay time is random in the whole range interval. Moreover, the jamming signal is not retransmitted to the receiver directly but to the areas with targets that need to be protected against being imaged by radar. By this, it is then possible to jam the radar echoes independent of the receiver location [J1136]

## "A Two-Dimensional Spectrum for Bistatic SAR Processing Using Series Reversion"

This letter derives the two-dimensional point target spectrum for an arbitrary bistatic synthetic aperture radar configuration. The method described makes use of series reversion, the method of stationary phase, and Fourier transform pairs to derive the point target spectrum. The accuracy of the spectrum is controlled by keeping enough terms in the two series expansions, and is verified with a point target simulation [J1137]

## "Efficient Calculation of Born Scattering for Fixed-Offset Ground-Penetrating Radar Surveys"

A formulation is presented for efficient calculation of linear electromagnetic scattering by buried penetrable objects, as involved in the analysis of fixed-offset ground-penetrating radar (GPR) systems. The actual radiation patterns of the GPR antennas are incorporated in the scattering calculation by using their plane-wave transmitting and receiving spectra [J1138]

## "Evaluation of Peak Current Polarity Retrieved by the ZEUS Long-Range Lightning Monitoring System"

This letter presents the first assessment of a newly developed polarity retrieval scheme augmenting a very low frequency (VLF) long-range lightning detection network (named ZEUS). The polarity scheme uses extremely low frequency (ELF) in conjunction with the VLF waveform. The measured ELF signal is compared with the simulated ELF signal to extract the polarity sign. This comparison also produces correlation coefficients that are used to assign four confidence index categories on the polarity sign. This letter presents polarity results for a period of ZEUS network operation from November 26 to December 15, 2004. Assessment of the polarity measurements is conducted through comparisons against the Brazilian lightning network Rede Integrada Nacional de Detecccedilatildeo de Descargas Atmosfeacutericas (RINDAT) that uses a well-established lightning location technology. Contingency test analysis shows that algorithm performance is consistent with the assigned

confidence level, e.g., at medium confidence level, the algorithm has a 5% bias, whereas at high level, perfect agreement is shown with RINDAT. Peak current strength was found not to influence the accuracy of the polarity retrieval [J1139]

## "An Adaptive Contoured Window Filter for Interferometric Synthetic Aperture Radar"

An adaptive contoured window filter is proposed to filter off the noise from phase images of interferometric synthetic aperture radar (InSAR) in this letter. The contoured windows can best satisfy the requirement that constrains the phase signal constant inside windows on which low-pass filtering can remove the noise well while the fringe phases are well preserved. The contoured windows are determined by tracing along the local fringe orientation. An algorithm for determining window sizes adaptive to the fringe density is also proposed. The theoretical analysis and experiments prove that the proposed filter can greatly remove decorrelation noise while preserving the fringe phase well, even for those fringes with strong curvatures for InSAR processing [J1140]

## "Analysis of the Backscattering Coefficient of Salt-Affected Soils Using Modeling and RADARSAT-1 SAR Data"

Salt significantly changes the backscattering coefficient of wet soil. This is easily observed on RADARSAT-1 synthetic aperture radar (SAR) images acquired over a salty depression located in the Egyptian desert. The aim of this paper is to use backscattering models to understand the behavior of the backscattering coefficient over salt-affected soils and to evaluate the possibility of monitoring the salt content. Simulations conducted over salt-affected soils show a lower sensitivity of these models to soil moisture compared to nonaffected soils. Besides, there is no model suitable to represent the variation of the backscattering coefficient due to changes in soil salinity. These results are discussed with regard to the magnitude of the two components of the dielectric constant (epsiv' and epsiv''). Based on a series of relationships, we propose a parametric formulation that allows us to determine the salinity acting on RADARSAT-1 SAR images without any use of backscattering models [J1141]

## "Precision and Accuracy of Satellite Radar and Laser Altimeter Data Over the Continental Ice Sheets"

The unprecedented accuracy of elevations retrieved from the Ice Cloud and Land Elevation Satellite (ICESat) laser altimeter is investigated and used to characterize the range errors in the Environmental Satellite (Envisat) and European Remote Sensing 2 Satellite (ERS-2) radar altimeters over the continental ice sheets. Cross-mission crossover analysis between time-coincident ERS-2-, Envisat-, and ICESat-retrieved elevations and comparisons to an ICESat-derived digital elevation map are used to quantify the radar elevation error budget as a function of surface slope and to investigate the effectiveness of a method to account for the radar altimeter slope-induced error. The precision and accuracy of the elevations retrieved from the ICESat Geoscience Laser Altimeter System and the European Space Agency radar altimeters on ERS-2 and Envisat are calculated over the Greenland and Antarctic ice sheets using a crossover analysis. As a result of this work, the laser precision is found to vary as a function of surface slope from 14 to 59 cm, and the radar precision varies from 59 cm to 3.7 m for ERS-2 and from 28 cm to 2.06 m for Envisat. Envisat elevation retrievals when compared with ICESat results over regions with less than 0.1deg surface slopes show a mean difference of 9plusmn5 cm for Greenland and -40plusmn98 cm over Antarctica. ERS-2 elevation retrievals over these same low surface slope regions differ from ICESat results by -56plusmn72 cm over Greenland and 1.12plusmn1.16 m over Antarctica. At higher surface slopes of 0.7deg to 0.8deg, the Envisat/ICESat differences increase to -2.27plusmn23 m over Greenland and to 0.05plusmn26 m over Antarctica [J1142]

## "Wind-Vector Estimation for RADARSAT-1 SAR Images: Validation of Wind-Direction Estimates Based Upon Geometry Diversity"

In this letter, a new wind-vector algorithm is presented that uses radar backscatter sigma0measurements at two adjacent subscenes of RADARSAT-1 synthetic aperture radar (SAR) images, with each subscene having slightly different geometry. Resultant wind vectors are validated using in situ buoy measurements and compared with wind vectors determined from a hybrid wind-retrieval model using wind directions determined by spectral analysis of wind-induced image streaks and observed by colocated QuikSCAT measurements. The hybrid wind-retrieval model consists of CMOD-IFR2 [applicable to C-band vertical-vertical (VV) polarization] and a C-band copolarization ratio according to Kirchhoff scattering. The new algorithm displays improved skill in wind-vector estimation for RADARSAT-1 SAR data when compared to conventional wind-retrieval methodology. In addition, unlike conventional methods, the present method is applicable to RADARSAT-1 images both with and without visible streaks. However, this method requires ancillary data such as buoy measurements to resolve the ambiguity in retrieved wind direction [J1143]

## "Eigensubspace-Based Filtering With Application in Narrow-Band Interference Suppression for SAR"

Synthetic aperture radar (SAR) has found wide applications in many areas, e.g., battlefield awareness. However, SAR is vulnerable to various kinds of interference, among which narrow-band interference (NBI) is commonly used. In this letter, an eigensubspace-based filtering approach is proposed for NBI suppression in SAR without using passive-sniff data as the reference signal. Moreover, the proposed method can deal with smart or interrupted NBI. Both simulation and experimental results are provided to illustrate the performance of the proposed approach [J1144]

## "A Keystone Transform Without Interpolation for SAR Ground Moving-Target Imaging"

Synthetic aperture radar (SAR) image formation for a ground moving target necessitates the compensation of the unknown target trajectory. The keystone transform has been employed to remove the linear component of the range migration for the moving target, where interpolation is required. In this letter, a realization of the keystone transform avoiding interpolation is presented. The kernel of this transform, i.e., the range-frequency-dependent azimuth time rescaling, is implemented using only complex multiplications and fast Fourier transforms based on the scaling principle, which has been successfully applied in the equalization of the space-variant range cell migration in SAR processing. In addition, the moving target is coarsely focused according to the SAR geometry and the platform velocity while exploiting the scaling principle. This preliminary focusing is helpful in the isolation of the moving target from ground clutter, so as to facilitate a more refined processing with respect to each mover. SAR raw data combined with simulated echoes of moving targets are utilized to validate the presented approach [J1145]

## "A Low-Power High-Resolution Broad-Band Radar Using a Pulse Compression Technique for Meteorological Application"

A new high-resolution Ku-band Doppler radar for meteorological applications has been developed. With the new system design, the radar can accurately measure the radar reflectivity factor with 4-m resolution over a range from 40 m to several kilometers for 100-mW power using a pulse compression technique. Details of the system design, signal processing algorithm, and data acquisition procedures are described. To demonstrate the accuracy of the system, the radar reflectivity measurements are compared with the Joss-Waldvogel disdrometer measurements, and fairly good agreement is shown. The ability of the system to capture the backscattered signal and Doppler spectrum from rain volume at low altitude with high resolution is demonstrated for both convective- and stratiform-type rain events. [J1146]

## "Knab Sampling Window for InSAR Data Interpolation"

Interferometric synthetic aperture radar processing requires interpolating a slave image onto a master one. Since the signals requiring interpolation are limited in both time and bandwidth, the Knab sampling window provides an almost optimal and viable interpolation kernel. Its performance in terms of coherence preservation and interferometric phase error as a function of the number of retained samples and oversampling factor are shown. [J1147]

## "Ocean Mixed-Layer Depth and Current Variation Estimated From Imagery of Surfactant Streaks"

The ability of high-resolution imaging systems to resolve small-scale structure on the ocean surface suggests the possibility of using characteristics of Langmuir circulation to map the surface mixed-layer depth and near-surface current. We illustrate this using synthetic aperture radar and infrared imagery that are collected across the edge of the Gulf Stream (GS), which reveals surfactant streaks, or ldquowindrows,rdquo that are induced by Langmuir circulation. Based on changes in the windrow spacing and orientation, the mixed layer is estimated to deepen from 7 to 12 m across the edge of the GS and the current to increase from about 1 to 2 m/s. These spatial changes compare reasonably well with independent data, suggesting that the approach is plausible. It may also be possible to extract additional environmental information from the windrows. [J1148]

## "Adjustment of Discrepancies Between LIDAR Data Strips Using Linear Features"

Despite the recent developments in light detection and ranging systems, discrepancies between strips on overlapping areas persist due to the systematic errors. This letter presents an algorithm that can be used to detect and adjust such discrepancies. To achieve this, extracting conjugate features from the strips is a prerequisite step. In this letter, linear features are chosen as conjugate features because they can be accurately extracted from man-made structures in urban area and more easily extracted than the point features. Based on

such a selection strategy, a simple and robust algorithm is proposed that is generally applicable for extracting such features. The algorithm includes methods that can be used to establish observation equations from similarity measurements of the extracted features. Then, several transformations are selected and used to adjust the strips. Following the transformation, the fitness of linear features is tested to determine whether the discrepancies have been resolved; the results are then evaluated statistically. The results demonstrate that the algorithm is effective in reducing the discrepancies between the strips. [J1149]

## "Monitoring of an Alpine Glacier by Means of Ground-Based SAR Interferometry"

Spaceborne differential synthetic aperture radar (SAR) interferometry has been proven to be a powerful tool in monitoring environmental phenomena and, in particular, in observing glaciers and retrieving information about their surface topography and dynamics. In the last decade, the use of this technique has been successfully extended from space to ground-based observations as a tool for monitoring, on a smaller scale, single landslides, unstable slopes, and more recently, areas covered by snow but not yet glaciers. In this letter, the results of an experimental activity carried out to evaluate the potential of ground-based microwave interferometry to estimate the velocity of an unstable area belonging to a glacier is reported. This experiment demonstrated the possibility of remotely monitoring surface displacements of the monitored glacier up to a distance of about 3 km even if, due to the lack of ground truths on the observed area, the data interpretation must be carefully worked out. [J1150]

## "On the Distribution of the Estimated Coherence"

The recent paper by Abdelfattah and Nicolas proposed a novel coherence magnitude estimator and studied its properties. Here, we derive simpler and more explicit expressions for four of the properties that were studied: 1) the probability density function; 2) moments; 3) Mellin transform; and 4) second-kind moments. We establish numerical efficiency of these expressions and provide simple Maple programs for inversion. We expect that the results presented here could enhance applicability of the new estimator. [J1151]

## "Efficient Interpolation of SAR Images for Coregistration in SAR Interferometry"

An efficient polynomial interpolation method is proposed to reduce the computational burden of the coregistration of synthetic aperture radar images in interferometric processing. The method can be viewed as an application of the Farrow interpolator technique and requires a series of 2-D fast Fourier transforms (FFTs). Mainly, it has two advantages relative to the usual coregistration procedure. First, it does not require to compute or store in memory any kernel sample. Second, it involves less floating-point operations than the conventional coregistration, with a clear advantage if the image needs to be oversampled. The efficiency of the method is based on the fact that the complexity of one 2-D FFT is much smaller than the complexity of one spatial convolution. These advantages are demonstrated by both analyzing the interpolation procedure itself and by defining an efficient code implementation. [J1152]

## "Feature Evolution for Classification of Remotely Sensed Data"

In a number of remote-sensing applications, it is critical to decrease the dimensionality of the input in order to reduce the complexity and, hence, the processing time and possibly improve classification accuracy. In this letter, the application of genetic algorithms as a means of feature selection is explored. A genetic algorithm is used to select a near-optimal subset of input dimensions using a feed-forward multilayer perceptron trained by backpropagation as the classifier. Feature and topology evolution are performed simultaneously based on actual classification results (wrapper approach). [J1153]

## "Comparison of Topography- and Aperture-Dependent Motion Compensation Algorithms for Airborne SAR"

This letter presents a comparison between three Fourier-based motion compensation (MoCo) algorithms for airborne synthetic aperture radar (SAR) systems. These algorithms circumvent the limitations of conventional MoCo, namely the assumption of a reference height and the beam-center approximation. All these approaches rely on the inherent time-frequency relation in SAR systems but exploit it differently, with the consequent differences in accuracy and computational burden. After a brief overview of the three approaches, the performance of each algorithm is analyzed with respect to azimuthal topography accommodation, angle accommodation, and maximum frequency of track deviations with which the algorithm can cope. Also, an analysis on the computational complexity is presented. Quantitative results are shown using real data acquired by the Experimental SAR system of the German Aerospace Center (DLR). [J1154]

## "On the Existence of Coverage and Integration Time Regimes in Bistatic SAR Configurations"

Bistatic synthetic aperture radar (SAR) is an extension of traditional monostatic SAR, which increases the flexibility in designing SAR missions. We describe a scheme for the computation of integration time and azimuth coverage of bistatic SARs based on space-time diagrams. A classification of bistatic SAR configurations is introduced in terms of size and velocity on the ground of antenna footprints. Bistatic SAR regimes are also identified. [J1155]

## "Height Estimation of Boreal Forest: Interferometric Model-Based Inversion at L- and X-Band Versus HUTSCAT Profiling Scatterometer"

In this letter, we present results from the FinSAR project, where the E-SAR and Helsinki University of Technology Scatterometer (HUTSCAT) instruments were operated together in order to validate tree-height retrieval algorithms for boreal forest. The campaign was carried out in Finland in fall 2003. The main instruments of the campaign were the E-SAR airborne radar (operating at L- and X-band) and the HUTSCAT helicopter-borne profiling scatterometer (operating at X- and C-band). We compare and discuss forest height obtained from the inversion quad-pol polarimetric interferometric synthetic aperture radar (SAR) data sets at L-band and forest height obtained from the inversion of single-pol X-band in SAR data with forest height estimates from HUTSCAT scatterometer data. Our results show that the forest height values, which are estimated by means of two different radar instruments, are in good agreement. The correlation between HUTSCAT and E-SAR height estimates ( at L-band and at X-band) underlines the good agreement between the results obtained by the two approaches. [J1156]

## "Selection of Pulse Repetition Frequency in High-Precision Oceanographic Radar Altimeters"

A readily computable formula to perform versatile analysis of the nonstationary pulse-to-pulse correlation properties of ocean altimeter returns is presented. Using this formula, the correlation coefficient and correlation interval depending on the reference time, sea state, and system parameters have been analyzed. The results have suggested that the pulse repetition frequency should adaptively be adjusted to the sea state to ensure precise altitude measurements. [J1157]

## "Automatic Reconstruction of Building Objects From Multiaspect Meter-Resolution SAR Images"

Reconstruction of 3-D objects from multiaspect high- resolution synthetic aperture radar (SAR) images is of great importance for SAR technology applications. In this paper, simple building objects are modeled as cuboids, and an approach for automatic reconstruction of 3-D building objects from multiaspect SAR images in meter resolution is developed. The edge detector of constant false alarm rate and a Hough transform technique for parallel line segment pairs are first employed to extract the parallelogram-like image of the building walls in SAR images. A set of probability density functions is presented to describe the object images and their multiaspect coherence. The maximum-likelihood estimation of an object is then derived from its multiaspect object images. A hybrid priority criterion is defined to evaluate the reliability of the reconstruction result. An automatic reconstruction algorithm is further developed to match object images of different aspects and, finally, to reconstruct the building objects. Besides, an iterative method is proposed for the coregistration of multiaspect building images. Four-aspect simulated images of a virtual scene and four-aspect Pi-SAR images over the campus of Tohoku University, Japan, are investigated. Reconstruction of building objects from their multiaspect images shows the fidelity of the whole process chain and the feasibility of 3-D objects automatic reconstruction from multiaspect SAR images. At last, a practical application that is based on spaceborne meter-resolution SAR is proposed. [J1158]

## "Comparison of Deep Underwater Measurements and Radar Observations of Rainfall"

Deep-water acoustical measurements of rainfall are compared to high-resolution ground radar observations for the first time. The measurements of underwater ambient sound were made from a subsurface mooring near Methoni, Greece, in 2004. The acoustical measurements were at 60-, 200-, 1000-, and 2000-m depths. Simultaneous ground-based polarimetric -band radar observations were made over the acoustic mooring. Comparisons show acoustic detection of rain events and storm structure that are in agreement with the radar observations. Results from a comparison between the underwater sound pressure level at different depths and the observed radar reflectivities are presented. [J1159]

## "Texture Features for Antitank Landmine Detection Using Ground Penetrating Radar"

In this paper, we consider the application of texture features for antitank landmine detection in ground-penetrating-radar data in the difficult scenario of very high clutter environments. In particular, we develop a

technique for 3-D texture feature extraction, and we compare the results for landmine/clutter discrimination using classifiers that are built on 3-D as well as on 2-D texture feature sets. Our results indicate performance improvements across several different challenging testing scenarios when using the relevance-vector-machine classifiers that are trained on our 3-D feature sets as compared to the performance using the 2-D texture feature sets. [J1160]

## "Reconstruction of DEMs From ERS-1/2 Tandem Data in Mountainous Area Facilitated by SRTM Data"

A new approach is presented in this paper to produce Digital Elevation Model (DEM) in mountainous areas with steep slope using ERS-1/2 tandem data. In order to reduce the impact of phase errors on the Interferometric Synthetic Aperture Radar (InSAR)-generated DEM, an external DEM such as that from Shuttle Radar Topography Mission (SRTM) is utilized in this approach. The proposed algorithm includes two steps: The first step is to model and remove phase trends with a linear regression analysis before converting phase to height; the second step is to filter unreliable height points before interpolating the DEM from the InSAR height map. The critical points are the following: 1) determining the one-to-one correspondence between the interferogram and the SRTM DEM before knowing the InSAR-derived elevation values and 2) estimating the elevation range of every pixel from SRTM DEM. To solve the first problem, an iteratively geocoding algorithm is performed. A DEM interpolation error model solves the second one. For InSAR data processing, the SRTM DEM is not only usable for modeling systematic phase errors but also for filtering gross height errors. The experiments in Zhangbei and the Three Gorges areas in China show that our approach has improved the accuracy of the resulting DEMs significantly without any ground control points. [J1161]

## "Maximum-Likelihood Retrieval of Modeled Convective Rainfall Patterns from Midlatitude C-Band Weather Radar Data"

A spatial characterization of the midlatitude meso- scale rain fields from C-band radar measurements is performed by means of a systematic analysis and modeling of convective rain-cell bidimensional shapes and spatial correlation. A large rainfall dataset that is derived from an operational C-band dual-polarized radar, which is placed in S. Pietro Capoflume near Bologna (Italy), has been collected and analyzed for this purpose. Different models of convective rainy horizontal structures are described and compared. Special attention is devoted to the consolidated unimodal models (or unimodal patterns) like Gaucell with a Gaussian rain-rate profile and Excell with an exponential rain-rate profile, and the hybrid models like Hycell and Dexcell based on a proper combination of the previous unimodal models. The new hybrid model Dexell, which is introduced here, is an extension of the Hycell model, which is previously proposed in literature. A pixel-by-pixel model numerical integration is carried out in order to perform a homogeneous comparison between the rain-cell model and the measured features such as peak, average, root mean square, gradient average, and gradient deviation of rain rate. A maximum-likelihood algorithm, which is expressed in terms of the principal component of the previous rain-cell features, is introduced to estimate rain-cell pattern parameters from the available radar data. A detailed sensitivity analysis, which is devoted to find the best behavior in terms of root-mean-square error and correlation coefficient between the modeled and measured rain-cell features, is finally carried out. [J1162]

## "A Discrete Wavelet Transform Approach to Multiresolution Complex SAR Image Generation"

We present a signal processing approach using discrete wavelet transform (DWT) for the generation of complex synthetic aperture radar (SAR) images at an arbitrary number of dyadic scales of resolution. The method is computationally efficient and is free from significant system-imposed limitations present in traditional subaperture-based multiresolution image formation. Problems due to aliasing associated with biorthogonal decomposition of the complex signals are addressed. The lifting scheme of DWT is adapted to handle complex signal approximations and employed to further enhance the computational efficiency. Multiresolution SAR images formed by the proposed method are presented. [J1163]

## "Continental-Scale Evaluation of Remotely Sensed Soil Moisture Products"

A new data assimilation-based approach for the continental-scale evaluation of remotely sensed surface soil moisture retrievals is applied to four separate soil moisture products over the contiguous U.S. The approach is based on quantifying the ability of a given soil moisture product to correct for known rainfall errors when sequentially assimilated into a simple water balance model. Analysis results provide new insight into the continental-scale performance of surface soil moisture retrieval algorithms based on satellite passive microwave, scatterometer, and thermal remote sensing observations. [J1164]

## "A Chirp Transform Algorithm for Processing Squint Mode FMCW SAR Data"

Frequency-modulated continuous-wave (FMCW) synthetic aperture radar (SAR) is a lightweight cost-effective high-resolution airborne imaging radar. In squint case, the frequency scaling algorithm, which is suitable for processing nonchirped raw data, cannot be used directly in FMCW SAR data processing because of low system sampling frequency. On the other hand, the continuous antenna motion of FMCW SAR can cause serious distortions in the reconstructed images. In this letter, an improved algorithm called the chirp transform algorithm is proposed. When the effects of the residual video phase are negligible, the algorithm uses a chirp transform to perform the time scaling operation to alleviate the sampling frequency problem. It requires only fast Fourier transforms and multiplications. The range cell migration introduced by the continuous motion is also compensated completely in range-Doppler domain. The algorithm performances are analyzed and are supported by point target simulation experiments. [J1165]

## "Cloud Optical Depth Retrievals From Solar Background "Signals" of Micropulse Lidars"

Pulsed lidars are commonly used to retrieve vertical distributions of cloud and aerosol layers. It is widely believed that lidar cloud retrievals (other than cloud base altitude) are limited to optically thin clouds. Here, we demonstrate that lidars can retrieve optical depths of thick clouds using solar background light as a signal, rather than (as now) merely a noise to be subtracted. Validations against other instruments show that retrieved cloud optical depths agree within 10%-15% for overcast stratus and broken clouds. In fact, for broken cloud situations, one can retrieve not only the aerosol properties in clear-sky periods using lidar signals, but also the optical depth of thick clouds in cloudy periods using solar background signals. This indicates that, in general, it may be possible to retrieve both aerosol and cloud properties using a single lidar. Thus, lidar observations have great untapped potential to study interactions between clouds and aerosols. [J1166]

## "Revised Landsat-5 Thematic Mapper Radiometric Calibration"

Effective April 2, 2007, the radiometric calibration of Landsat-5 (L5) Thematic Mapper (TM) data that are processed and distributed by the U.S. Geological Survey (USGS) Center for Earth Resources Observation and Science (EROS) will be updated. The lifetime gain model that was implemented on May 5, 2003, for the reflective bands (1-5, 7) will be replaced by a new lifetime radiometric-calibration curve that is derived from the instrument's response to pseudoinvariant desert sites and from cross calibration with the Landsat-7 (L7) Enhanced TM Plus (ETM+). Although this calibration update applies to all archived and future L5 TM data, the principal improvements in the calibration are for the data acquired during the first eight years of the mission (1984-1991), where the changes in the instrument-gain values are as much as 15%. The radiometric scaling coefficients for bands 1 and 2 for approximately the first eight years of the mission have also been changed. Users will need to apply these new coefficients to convert the calibrated data product digital numbers to radiance. The scaling coefficients for the other bands have not changed. [J1167]

## "Application of ENVISAT ASAR Data in Mapping Rice Crop Growth in Southern China"

This research letter presents preliminary results of mapping rice crop growth using ENVISAT advanced synthetic aperture radar (ASAR) alternating polarization HH/HV data. Four ASAR HH/HV images were collected in the early rice-growth cycle in the test site in 2006, and the temporal response of ASAR data to the rice field was analyzed. The height and biomass of rice were measured during acquisition of ASAR data, and empirical relationships were established between the backscattering coefficient and these two parameters. Based on the temporal variation of the radar response, a method for mapping a rice growth area was developed using the combination of ASAR HH and HV polarization data between two acquisition dates. The results confirm that C-band SAR data have great potential in the development of an operational system for monitoring rice crop growth in Southern China. [J1168]

## "Microwave Observatory of Subcanopy and Subsurface (MOSS): A Mission Concept for Global Deep Soil Moisture Observations"

The Microwave Observatory of Subcanopy and Subsurface (MOSS) is a mission concept for a spaceborne synthetic aperture radar (SAR) system that provides global observations of soil moisture under substantial vegetation cover (exceeding 20 kg/m2) and at useful depths (1-5 m). The concept was developed and a number of new required technologies were demonstrated through a National Aeronautics and Space Administration Earth Science Technology Office Instrument Incubator Program project. This very high frequency (VHF)/ultrahigh frequency (UHF) polarimetric SAR is designed to provide 7-10-day observations of soil moisture at 1-km resolution. The rapid repeat cycle mandates swath widths in the range of 300-400 km, which must be realized by a 30-m-long antenna. Conventional array implementations would result in a mass of more than 4000 kg, whereas with the technology proposed and demonstrated in this project, the total antenna mass is less than 500 kg. The antenna concept is a dual-stacked patch array feed illuminating a 30-m mesh reflector to synthesize the

long apertures and achieve the wide swath. The feed system prototype was fabricated and its performance demonstrated. Other major project components were: (1) system-level SAR and mission design; (2) demonstration of science data and products, using a tower-based VHF/UHF radar; (3) spacecraft and mesh reflector antenna mechanical design; (4) developing mitigation strategies for ionospheric effects; and (5) assessing frequency interference effects. Experimental science data were generated from the tower radar for soil moisture profiling in Arizona and for forest penetration in Oregon. The soil moisture products were demonstrated through an integrated inversion-processing algorithm. This paper summarizes the results from the MOSS project and demonstrates the feasibility of the spaceborne mission. [J1169]

## "Improving GPR Image Resolution in Lossy Ground Using Dispersive Migration"

As a compact wave packet travels through a dispersive medium, it becomes dilated and distorted. As a result, ground-penetrating radar (GPR) surveys over conductive and/or lossy soils often result in poor image resolution. A dispersive migration method is presented that combines an inverse dispersion filter with frequency-domain migration. The method requires a fully characterized GPR system including the antenna response, which is a function of the local soil properties for ground-coupled antennas. The GPR system response spectrum is used to stabilize the inverse dispersion filter. Dispersive migration restores attenuated spectral components when the signal-to-noise ratio is adequate. Applying the algorithm to simulated data shows that the improved spatial resolution is significant when data are acquired with a GPR system having 120 dB or more of dynamic range, and when the medium has a loss tangent of 0.3 or more. Results also show that dispersive migration provides no significant advantage over conventional migration when the loss tangent is less than 0.3, or when using a GPR system with a small dynamic range. [J1170]

## "Walled LTSA Array for Rapid, High Spatial Resolution, and Phase-Sensitive Imaging to Visualize Plastic Landmines"

We propose a walled linearly tapered slot antenna (LTSA) array to visualize plastic landmines. Previously, we reported an adaptive nonlinear visualization system based on a complex-valued self-organizing map (CSOM) that deals with complex amplitude texture in reflection images at multiple frequencies. The system distinguishes landmines from clutter by paying attention to textural features obtained by high spatial resolution and wideband reflection measurement. Because the system employed a mechanical scan of a pair of horn antennas, the measurement required a long time. An array antenna can reduce the time. The antenna element to be used there should therefore be compact and wideband. This paper reports the design and fabrication of a walled LTSA array visualization system. The antenna element has a 14 times 28 mm aperture size, and works at the 8-12 GHz frequency band. Because the structure is a simple combination of glass epoxy substrates and metal plates, we can easily fabricate low-cost and lightweight arrays. Electrical switches realize a high-speed scanning of 12 times 12 = 144 elements in total. We also report the results of a visualization experiment, in which plastic landmines are clearly visualized with the array in combination with the adaptive CSOM processing. Detection of landmines at frequencies of 10 GHz is only likely to be possible for targets buried a few centimeter deep or where the soil attenuation is very low. This might be a severe limitation of applicability of the method, as in field conditions soil attenuations of 10 dB or considerably more are commonly encountered, requiring the radar to operate at frequencies below 2-3 GHz. The best solution may be a multisensor system comprising these complementary high- and low-frequency radars. [J1171]

## "Thin-Pavement Thickness Estimation Using GPR With High-Resolution and Superresolution Methods"

In the field of civil engineering, sounding the top layer of carriageways, i.e., the pavement layer, is classically performed using standard ground-penetrating radar (GPR), whose resolution is bandwidth dependent. The layer thickness is deduced from both the time delays of backscattered echoes and the known dielectric constant of the medium. This paper focuses on superresolution and high-resolution techniques, which serve to improve the time resolution of GPR signals, and presents a parametric technique and five subspace methods, namely, estimation of signal parameters via rotational invariance techniques (ESPRIT), multiple-signal classification (MUSIC) algorithm, Min-Norm, and their polynomial versions root-MUSIC and root-Min-Norm. The performance of these algorithms will be compared in terms of resolution power as well as root-mean-square error on the estimated thickness. The paper also presents the results of computer tests and radar measurements in the far field. [J1172]

## "Wave Interferometry Applied to Borehole Radar: Virtual Multioffset Reflection Profiling"

Based on wave-interferometry principles, we describe a procedure to synthesize monostatic and multioffset borehole radar reflection data from cross-hole radar tomography data. The procedure is equivalent to placing

multiple transmitting sources in the receiving hole and conducting wide-angle reflection and refraction surveys. The procedure is illustrated using transmission and reflection data generated by numerical simulation of electromagnetic waves for a simple fracture model. The numerically simulated reflection data compare favorably with the reflection data synthesized using the wave-interferometry method. An experimental test of this procedure is also applied to a piece of field data from a pair of boreholes in crystalline igneous bedrock. The results demonstrate the potential of practical use of wave-interferometry methods for extracting reflection information from cross-hole radar tomography data. [J1173]

## "Unsupervised Classification of Scattering Mechanisms in Polarimetric SAR Data Using Fuzzy Logic in Entropy and Alpha Plane"

The eigenvalue-eigenvector-based approach for understanding the scattering mechanisms of polarimetric synthetic aperture radar (POLSAR) data leads to noisy classification results due to arbitrarily fixed zone boundaries in the H/alpha macr plane. In this paper, a new classification scheme that can address the inherent vagueness of class boundaries in the H/alpha macr plane was tested in order to improve the unsupervised classification of the microwave scattering mechanism by introducing concepts related to fuzzy sets. A 2-D fuzzy membership function was developed for the fuzzification of the 2-D H/alpha macr plane. The proposed fuzzy H/alpha macr classifier is composed of three steps: fuzzification of the H/alpha macr plane, iterative refinement of membership degrees using the c-means algorithm, and defuzzification for the final decision process. The performance of this new approach for the L-band NASA/Jet Propulsion Laboratory's Airborne SAR data obtained during the PACRIM-II experiment was shown to be consistently improved. This new classification technique can be applied to POLSAR data without any a priori information. The fuzzification of the zone boundaries can be further applied to the interpretation of the POLSAR data, e.g., multifrequency classification, retrieval of bio- and geophysical parameters, etc. In order to propose another implementation of the fuzzy boundary representation, we exploited the combination of the H/alpha macr state space and anisotropy information. [J1174]

## "GPR Without a Source: Cross-Correlation and Cross-Convolution Methods"

Several formulations exist for retrieving the Green's function from cross correlation of (passive) recordings at two locations. For media without losses, these known formulations retrieve Green's functions from sources on a closed boundary. Until recent, these formulations were only developed for acoustic waves in fluids and elastodynamic waves in solids. Now, Green's function representations for electromagnetic (EM) waves in matter exist and can be exploited for passive ground-penetrating radar (GPR) applications using transient or ambient noise sources, either natural or man-made. We derive general exact EM Green's function retrieval formulations based on cross correlations and cross convolutions of recorded wave fields. For practical applications, simplified forms are derived that directly apply to field recordings due to unknown uncorrelated noise or transient sources. Only naturally present sources are needed, which allows for all kinds of applications of ldquoGPR without a source.rdquo We illustrate the consequences of using the simplified forms for Green's function retrieval with 2-D numerical examples. We show that in dissipative media, the Green's function is most accurately retrieved using the cross-convolution method when the sources are located on a sufficiently irregular boundary. [J1175]

## "Localization of the Interfaces of a Slab Hidden Behind a Wall"

In this paper, a 1-D inverse-scattering problem laying within the framework of through-wall imaging is addressed. In particular, the problem of localizing the interfaces of a slab hidden behind an obstacle, another slab whose electromagnetic features and thickness are known, is considered. To this end, an approximate linear mathematical relationship between the scattered field and the unknown slab-interface positions is stated. Such an approximate relationship arises from neglecting the multiple-reflections between the two unknown slab's interfaces and between the slab and the obstacle. The unknown locations of the slab's interfaces are represented as the support of Dirac-delta functions, and the problem is cast as the inversion of a linear integral operator whose inversion is achieved by means of the Truncated-Singular-Value-Decomposition (TSVD) inversion scheme. The effect of the parameters of the obstacle on the inversion algorithm and the performances achievable by the solution approach are assessed by exploiting synthetic data. Furthermore, a comparison with the reconstructions obtained under the Born approximation and with the time-backscattered field is achieved. Finally, results obtained by employing experimental data collected owing to a stepped-frequency ground-penetrating radar system are also presented. [J1176]

## "A Novel Directional Borehole Radar System Using Optical Electric Field Sensors"

A directional borehole radar system using an array antenna connected to passive optical electric field sensors was developed and evaluated by laboratory and field experiments. This system uses a single dipole antenna for a transmitter and a four-dipole element circular array for a receiver. The received signals are transmitted through

optical fibers from optical electric field sensors. The receiver array measures the phase differences between four dipole antennas and estimates the azimuth direction of the incoming reflection wave. The accuracy of the phase measurement was first evaluated in a laboratory test and then tested in a field experiment. To compensate for the sensitivity differences among the sensors, we propose an in situcalibration technique. The dominant operating frequency of the system is 70 MHz. Subsequently, we used borehole radar for subsurface measurements in a vertical borehole in granite. Estimation of the azimuth orientations of subsurface fractures was successfully demonstrated. [J1177]

## "Accurate Determination of Underground GPR Wavefront and B-Scan Shape From Above-Ground Point Sources"

While the determination of the wavefront shape radiated by ground-penetrating radar (GPR) in contact with the ground is trivial, the refraction of rays at the ground surface from a point source in the air makes accurate determination of the transmitted wavefront challenging. Impulse GPRs usually have their emitters in air, transmitting waves through a quasi-planar interface into the soil. The waves radiated initially in air can be approximated as circular, but once they enter the soil half-space, they propagate with a wavefront shape that resembles a hyperbola. The exact shape is derived and shown to be well approximated by a hyperbola with specific parameters depending on the relative dielectric constant of the half-space epsiv' ( = n2), the height of the source h, and the propagation time from source to wavefront multiplied by the wave velocity in the half-space p. A correction formula is provided to reduce the error between the approximate hyperbola and the exact shape. In addition, an equation for the shape of the B-scan contour of a point scatterer is derived. [J1178]

## "Observations, Modeling, and Applications of ERS-ENVISAT Coherence Over Land Surfaces"

European Remote Sensing satellite (ERS) ENVISAT coherence is a new repeat-pass interferometric synthetic aperture radar product characterized by a very short repeat-pass interval between acquisitions (28min). In this paper, we investigate the properties of two 28-mins coherence images acquired over the regions of Paris, France, and Prague, Czech Republic, as well as a 35-day coherence image from Prague. Bare soils showed higher coherence compared to forests and urban areas. The range of coherence was larger for 28-min pairs, perpendicular baseline closer to 2km, and stable weather conditions between acquisitions. Coherence modeling shows that because of the long baseline: 1) significant surface decorrelation occurs when slopes are not accounted for in the common-band filtering and for variation of topography in the resolution cell and 2) volume decorrelation is significant. Temporal decorrelation seems to be relevant for vegetation even at the 28-min interval time scale. Observations and modeled coherence were found to be in good agreement. Land cover classification using coherence and backscatter has been tested for the Paris scene for mapping the four major classes. The classification accuracy was 86% when an edge-eroded version of the reference land cover map was used. It decreases to 68% when the full land cover map was used as reference because of local mismatches between the coherence image and the land cover map, and the reduced common band in range. The high coherence difference between forests and bare fields suggests the possibility to use the ERS-ENVISAT coherence for forest/nonforest mapping and estimation of biophysical properties of short vegetation. Coherence, decorrelation, ENVISAT Advanced Synthetic Aperture Radar (ASAR), European Remote Sensing satellite (ERS), land cover, synthetic aperture radar interferometry (InSAR). [J1179]

## "Measurement of Layer Thickness and Permittivity Using a New Multilayer Model From GPR Data"

The conventional method, i.e., the common middle point (CMP) method, has been used for many years for estimating the depth and permittivity of layered media from ground-penetrating radar (GPR) data. However, the CMP method results in noticeable errors in thickness and permittivity readings with the increase of antenna separation. To improve the measurement accuracy, a new mathematical model is presented, covering GPR measurement in one- and two-layer cases. In this model, we first check all the possible wave paths when the GPR signal propagates in the multilayer environment. We not only consider the effects from the air-ground interface but also introduce a ray-path-searching process in the GPR measurement using Fermat's shortest path law. The shortest path is then used in the process of GPR data inversion in order to calculate the depth and permittivity of each layer. Finally, we use the transmission-line matrix (TLM) method to simulate the propagation of a GPR signal in the multilayered formation. A time-sequence image that was produced by the finite-difference time-domain method has also been used to explain this presented model. By comparing the numerical simulation results with the measured results, it is found that the estimated layer thickness and permittivity by the new model agree well with the simulated results. It proves that the new model is more accurate and closer to the real measured situation. [J1180]

## "Consistency Analysis of Subsurface Fracture Characterization Using Different Polarimetry

## Techniques by a Borehole Radar"

We present a fully polarimetric borehole radar in conjunction with radar polarimetry, Pauli decomposition, and H-alpha decomposition techniques to carry out physical characterization of subsurface fractures. Further tests are needed to validate the applicability of radar polarimetry analysis for physical characterization of subsurface targets. Toward this goal, we present the implementation of two other decomposition techniques, namely: (1) the Durden-Freeman decomposition and (2) polarimetric anisotropy parameter methods, in the context of previous research and examine the consistency of results using various polarimetric decomposition techniques. While results from the radar polarimetry decomposition were found to depend greatly upon the kind of physical or mathematical models, these techniques seem to provide comparable performances in terms of fracture characterization and classification. [J1181]

## "High-Resolution Forecast Models of Water Vapor Over Mountains: Comparison With MERIS and Meteosat Data"

Propagation delay due to variable tropospheric water vapor (WV) is one of the most intractable problems for radar interferometry, particularly over mountains. The WV field can be simulated by an atmospheric model, and the difference between the two fields is used to correct the radar interferogram. Here, we report our use of the U.K. Met Office Unified Model in a nested mode to produce high-resolution forecast fields for the 3-km-high Mount Etna volcano. The simulated precipitable-water field is validated against that retrieved from the Medium-Resolution Imaging Spectrometer (MERIS) radiometer on the Envisat satellite, which has a resolution of 300 m. Two case studies, one from winter (November 24, 2004) and one from summer (June 25, 2005), show that the mismatch between the model and the MERIS fields ( rms = 1.1 and 1.6 mm, respectively) is small. One of the main potential sources of error in the models is the timing of the WV field simulation. We show that long-wavelength upper tropospheric troughs of low WV could be identified in both the model output and Meteosat WV imagery for the November 24, 2004 case and used to choose the best time of model output. [J1182]

## "Tornadic Time-Series Detection Using Eigen Analysis and a Machine Intelligence-Based Approach"

The research Weather Surveillance Radar-1988 Doppler locally operated by the National Severe Storms Laboratory in Norman, OK, has the unique capability of collecting massive volumes of Level I time-series data over many hours, which provides a rich environment for evaluating our new postprocessing algorithms. In this letter, an approach of identifying tornado vortices in Doppler spectra is proposed and investigated using eigen analysis, cluster estimation, and fuzzy logic technique. [J1183]

## "A New Algorithm for Sparse Aperture Interpolation"

A new algorithm for filling sparse aperture synthetic aperture radar (SAR)/inverse SAR (ISAR) data, which applies for widely gapped apertures, is proposed in this letter. An Estimating Signal Parameter via Rotational Invariance Techniques(ESPRIT)-based parametric approach is first used to estimate the power distribution with the sparse data. With the estimated power spectrum as prior information, by minimizing a weighted norm as a constraint, the full aperture data can be estimated. Although the algorithm is proposed for the sparse aperture interpolation in SAR/ISAR, it can be applied to other gapped data spectral estimation problems as well. Both numerical and experimental examples are provided to demonstrate the performance of the proposed algorithm. [J1184]

## "Polarimetric Calibration Using a Genetic Algorithm"

This letter presents a novel calibration approach to polarimetric synthetic aperture radar using distributed targets with known scattering characteristics. A genetic algorithm with complex-valued encoding is proposed to solve the overdetermined system of nonlinear equations associated with the polarimetric calibration problem. The proposed genetic algorithm is described in detail, and validation of the algorithm is performed by numerical simulations. [J1185]

## "Rain Retrieval Performance of a Dual-Frequency Precipitation Radar Technique With Differential-Attenuation Constraint"

Assessments on the performance of dual-frequency (13.6/35.5 GHz) Precipitation Radar (DPR) rain retrieval techniques are performed by means other than relying on the surface reference technique. A DPR inversion technique (DPR-IT) with an independent estimate of the differential attenuation, i.e., the difference of attenuation differences between two frequencies over a certain range, is introduced as an alternative to surface reference or iterative methods for resolving the path-integrated attenuation (PIA) information. Retrieval performance of the

proposed method is tested to some vertical rain profiles synthesized with arbitrarily defined and disdrometer-measured raindrop-size distribution data. Retrievals of two other DPR-IT-type methods, namely the DPR-IT with sets of preselected surface PIAs at two frequencies from wide ranges and the DPR-IT iterative algorithm, are also considered for the analysis. The comparison of the simulated results obtained from these three methods is presented and discussed. [J1186]

## "Fitting a Two-Component Scattering Model to Polarimetric SAR Data From Forests"

Two simple scattering mechanisms are fitted to polarimetric synthetic aperture radar (SAR) observations of forests. The mechanisms are canopy scatter from a reciprocal medium with azimuthal symmetry and a ground scatter term that can represent double-bounce scatter from a pair of orthogonal surfaces with different dielectric constants or Bragg scatter from a moderately rough surface, which is seen through a layer of vertically oriented scatterers. The model is shown to represent the behavior of polarimetric backscatter from a tropical forest and two temperate forest sites by applying it to data from the National Aeronautic and Space Agency/Jet Propulsion Laboratory's Airborne SAR (AIRSAR) system. Scattering contributions from the two basic scattering mechanisms are estimated for clusters of pixels in polarimetric SAR images. The solution involves the estimation of four parameters from four separate equations. This model fit approach is justified as a simplification of more complicated scattering models, which require many inputs to solve the forward scattering problem. The model is used to develop an understanding of the ground-trunk double-bounce scattering that is present in the data, which is seen to vary considerably as a function of incidence angle. Two parameters in the model fit appear to exhibit sensitivity to vegetation canopy structure, which is worth further exploration. Results from the model fit for the ground scattering term are compared with estimates from a forward model and shown to be in good agreement. The behavior of the scattering from the ground-trunk interaction is consistent with the presence of a pseudo-Brewster angle effect for the air-trunk scattering interface. If the Brewster angle is known, it is possible to directly estimate the real part of the dielectric constant of the trunks, a key variable in forward modeling of backscatter from forests. It is also shown how, with a prioriknowledge of the forest height, an estimate for th- e attenuation coefficient of the canopy can be obtained directly from the multi-incidence-angle polarimetric observations. This attenuation coefficient is another key variable in forward models and is generally related to the canopy density. [J1187]

## "Radio Echo Sounding of Pine Island Glacier, West Antarctica: Aperture Synthesis Processing and Analysis of Feasibility From Space"

Airborne radio echo sounding of the West Antarctic Ice Sheet over Pine Island Glacier was performed in the austral summer of 2004/2005 under the National Science Foundation's West Antarctic Ice Sheet Initiative. The British Antarctic Survey flew its newly developed 150-MHz ice-sounding radar over Pine Island Glacier and collected approximately 35 000 km of sounding data. The synthetic aperture radar (SAR) technique was applied to process those data in order to enhance radar signatures from the bed. As a matter of fact, airborne ice-sounding radar systems are generally affected by surface clutter returns, masking the echoes of internal layers and ice-bedrock transition at a large depth. Focused and unfocused (Doppler filtering) SAR techniques were compared, and their respective advantages/disadvantages were analyzed. Enhancement of bedrock detection at a large depth (> 2000 m) through SAR processing is demonstrated. Finally, a simulation analysis was performed for assessing the feasibility of ice-sheet sounding from space. It is shown that the gain in bed detection threshold is marginal in the satellite sounding geometry. Airborne radar, Antarctica, ice sounding, satellite remote sensing, subglacial topography, synthetic aperture radar (SAR) processing, West Antarctic Ice Sheet. [J1188]

## "Foreword to the Special Issue on Subsurface Sensing Using Ground-Penetrating Radar (GPR)"

The 17 papers in this special issue focus on subsurface sensing using ground-penetrating radar (GPR). These papers describe new approaches to subsurface sensing, including developments in electromagnetic wave propagation imaging/inversion of GPR data and antenna/radar technologies. Associated applications range from glaciology to pavement evaluation to landmine detection. [J1189]

## "Multistatic Ground-Penetrating Radar Experiments"

A multistatic ground-penetrating radar (GPR) system has been developed and used to measure the response of a number of targets to produce data for the investigation of multistatic inversion algorithms. The system consists of a linear array of resistive-vee antennas, microwave switches, a vector network analyzer, and a 3-D positioner, all under computer control. The array has two transmitters and four receivers which provide eight bistatic spacings from 12 to 96 cm in 12-cm increments. Buried targets are scanned with and without surface clutter, which is a layer of rocks whose spacing is empirically chosen to maximize the clutter effect. The measured responses are calibrated so that the direct coupling in the system is removed, and the signal reference point is

located at the antenna drive point. Images are formed using a frequency-domain beamforming algorithm that compensates for the phase response of the antennas. Images of targets in air validate the system calibration and the imaging algorithm. Bistatic and multistatic images for the buried targets are very good, and they show the effectiveness of the system and processing. [J1190]

## "MoM Analysis of Dipole Antennas in Crosshole Borehole Radar and Field Experiments"

In this paper, we propose a method-of-moments (MoM) analysis that includes the borehole effects on crosshole borehole radar, and we verify that the MoM represents the crosshole borehole radar data correctly. We derive the far-field approximation of an electric field radiated by an electric point source. In this derivation, we assume that the point source is in a cylindrically layered medium, while the observed electric field is in another cylindrically layered medium. The equations that are derived are used as a transfer function to connect the two impedance matrices-one for the transmitting antenna and the other one for the receiving one. In these matrices, the influence of the scattered field by the borehole is included completely. We conducted field experiments in granite with a controlled borehole medium in order to investigate the influence of the borehole. In this paper, we estimated the relative amplitude and the group delay of the received signals between the water-filled borehole case and the air-filled borehole case. This paper showed that the estimated amplitude and delay depend on the frequency and that the proposed MoM could predict these frequency dependencies. [J1191]

## "A Split-Based Approach to Unsupervised Change Detection in Large-Size Multitemporal Images: Application to Tsunami-Damage Assessment"

This paper presents a split-based approach (SBA) to automatic and unsupervised change detection in large-size multitemporal remote-sensing images. Unlike standard methods that are presented in the literature, the proposed approach can detect in a consistent and reliable way changes in images of large size also when the extension of the changed area is small (and, therefore, the prior probability of the class of changed pixels is very small). The method is based on the following: 1) a split of the large-size image into subimages; 2) an adaptive analysis of each subimage; and 3) an automatic split-based threshold-selection procedure. This general approach is used for defining a system for damage assessment in multitemporal synthetic aperture radar (SAR) images. The proposed system has been developed to properly identify different levels of damages that are induced by tsunamis along coastal areas. Experimental results that are obtained on multitemporal RADARSAT-1 SAR images of the Sumatra Island, Indonesia, confirm the effectiveness of both the proposed SBA and the presented system for tsunami-damage assessment [J1192]

## "A Multitemporal Method for Correction of Tropospheric Effects in Differential SAR Interferometry: Application to the Gulf of Corinth Earthquake"

Tropospheric inhomogeneities can form a major error source in differential synthetic aperture radar interferometry measurements, which are used in slow-deformation monitoring. Indeed, variations of atmospheric conditions between two radar acquisitions produce variations in the signal path of two images and, thus, additional fringes on differential interferograms. These effects have a strong influence on interferograms and must be compensated to obtain reliable deformation measurements. This paper presents a methodological approach to reduce at both global and local scales tropospheric contributions directly from differential interferograms. It first requires refined knowledge of the stable scatterers that can only be obtained from the analysis of a large population of multitemporal interferograms. The correction of global-scale atmospheric contribution exploits the correlation between phase and topography. The correction of local artifacts is based on the correlation between interferograms containing one common acquisition. This technique is validated on a database of 81 differential interferograms covering the Gulf of Corinth (Greece) and used to improve the measurements of ground deformation compared to global positioning system measurements [J1193]

## "A Novel Approach for Disaster Monitoring: Fractal Models and Tools"

In this paper, we present a complete framework to support the monitoring of natural and man-made disasters by means of synthetic aperture radar (SAR) images. The fractal geometry is the most appropriate mathematical instrument in describing the irregularity of a natural observed scene, by means of few effective and reliable parameters. Therefore, fractal concepts can be used to model and identify geometrical changes that occurred in areas hit by disasters. We present an overall framework employing fractal-based models, algorithms, and tools to support the identification of natural area changes due to natural or man-made disasters. Such a framework includes an algorithm used to extract fractal parameters from a 2-D signal, a fractal interpolation tool, and a SAR raw-signal simulator. The combined use of these tools provides an innovative instrument for disaster monitoring applications. In this paper, we implement the fractal framework to obtain a relation between the fractal parameters of a SAR image and those of the relative imaged area. In addition, a case study is discussed,

showing the potentiality of our framework for flooding detection [J1194]

## "A Portable Noncontact Heartbeat and Respiration Monitoring System Using 5-GHz Radar"

A portable noncontact heartbeat and respiration monitoring system operating in 5-GHz band is reported in this letter. Compared with the previously reported system operating at Ka-band, this system has been simplified to include only two PCB antennas, a palm-size PCB radio module, a data acquisition module, and a laptop. The system, powered by the laptop battery through USB connection, is compact, low-cost, and convenient for field test. A detection accuracy of better than 80% has been achieved at a distance of 2.8 m and at a low transmitted power of 20 muW. The system can be used for various applications in biology, medicine, and security. [J1195]

## "UWB short-range radar sensing-The architecture of a baseband, pseudo-noise UWB radar sensor"

The pioneers of radio science made their first trials of wireless information transmission and demonstrated localization of a steel vessel by radio waves more than 100 years ago. Back then, the world of radio frequencies was organized in a very simple way. The researchers could use any frequency band. There was no interference by others and no controlling government bodies. Since then, governmental authorities have established tight regulations that have split up the available frequency band into small partitions for exclusive use. This article discusses the architecture of a baseband, pseudo-noise UWB radar and gives some examples of applications [J1196]

## "Developing a Flood Monitoring System From Remotely Sensed Data for the Limpopo Basin"

This paper describes the application of remotely sensed precipitation to the monitoring of floods in a region that regularly experiences extreme precipitation and flood events, often associated with cyclonic systems. Precipitation data, which are derived from spaceborne radar aboard the National Aeronautics and Space Administration's Tropical Rainfall Measuring Mission and from National Oceanic and Atmospheric Administration's infrared-based products, are used to monitor areas experiencing extreme precipitation events that are defined as exceedance of a daily mean areal average value of 50 mm over a catchment. The remotely sensed precipitation data are also ingested into a hydrologic model that is parameterized using spatially distributed elevation, soil, and land cover data sets that are available globally from remote sensing and in situ sources. The resulting streamflow is classified as an extreme flood event when flow anomalies exceed 1.5 standard deviations above the short-term mean. In an application in the Limpopo basin, it is demonstrated that the use of satellite-derived precipitation allows for the identification of extreme precipitation and flood events, both in terms of relative intensity and spatial extent. The system is used by water authorities in Mozambique to proactively initiate independent flood hazard verification before generating flood warnings. The system also serves as a supplementary information source when in situ gauging systems are disrupted. This paper concludes that remotely sensed precipitation and derived products greatly enhance the ability of water managers in the Limpopo basin to monitor extreme flood events and provide at-risk communities with early warning information [J1197]

## "Rapid Damage Detection in the Bam Area Using Multitemporal SAR and Exploiting Ancillary Data"

In this paper, the problem of rapid earthquake damage detection in urban areas using multitemporal synthetic aperture radar data is addressed. It is shown that the combination of intensity and phase features enhances the damage pattern extracted from the data temporal stack using a spatially aware classifier. Moreover, the use of ancillary data, easily available for urban areas, further improves the accuracy by discarding uninteresting parts of the scene and forcing homogeneous classification within city blocks to avoid "class-blurring" effects consequential to the window-based computation of relevant measures. The procedure is validated based on results for the town of Bam, Iran, and compared with ground-based survey maps [J1198]

## "Estimation of Forest Fuel Load From Radar Remote Sensing"

Understanding fire behavior characteristics and planning for fire management require maps showing the distribution of wildfire fuel loads at medium to fine spatial resolution across large landscapes. Radar sensors from airborne or spaceborne platforms have the potential of providing quantitative information about the forest structure and biomass components that can be readily translated to meaningful fuel load estimates for fire management. In this paper, we used multifrequency polarimetric synthetic aperture radar (SAR) imagery acquired over a large area of the Yellowstone National Park by the Airborne SAR sensor to estimate the distribution of forest biomass and canopy fuel loads. Semiempirical algorithms were developed to estimate crown and stem biomass and three major fuel load parameters, namely: 1) canopy fuel weight; 2) canopy bulk density; and 3) foliage moisture content. These estimates, when compared directly to measurements made at plot and stand levels, provided more than 70% accuracy and, when partitioned into fuel load classes, provided more than

85% accuracy. Specifically, the radar-generated fuel parameters were in good agreement with the field-based fuel measurements, resulting in coefficients of determination of R2=85 for the canopy fuel weight, R2 =0.84 for canopy bulk density, and R2=0.78 for the foliage biomass [J1199]

## "High-Resolution 3-D Flood Information From Radar Imagery for Flood Hazard Management"

This paper presents a remote-sensing-based steady-state flood inundation model to improve preventive flood-management strategies and flood disaster management. The Regression and Elevation-based Flood Information eXtraction (REFIX) model is based on regression analysis and uses a remotely sensed flood extent and a high-resolution floodplain digital elevation model to compute flood depths for a given flood event. The root mean squared error of the REFIX, compared to ground-surveyed high water marks, is 18 cm for the January 2003 flood event on the River Alzette floodplain (G.D. of Luxembourg), on which the model is developed. Applying the same methodology on a reach of the River Mosel, France, shows that for some more complex river configurations (in this case, a meandering river reach that contains a number of hydraulic structures), piecewise regression is required to yield more accurate flood water-line estimations. A comparison with a simulation from the Hydrologic Engineering Centers River Analysis System hydraulic flood model, calibrated on the same events, shows that, for both events, the REFIX model approximates the water line reliably [J1200]

## "Comments on “Water Quality Retrievals From Combined Landsat TM Data and ERS-2 SAR Data in the Gulf of Finland”"

A paper by Zhang, using a feedforward artificial neural network (ANN) for water quality retrievals from combined Thematic Mapper data and synthetic aperture radar data in the Gulf of Finland, has been published in this journal. This correspondence attempts to discuss and comment on the paper by Zhang The amount of data used in the paper by Zhang is not enough to determine the number of fitting parameters in the networks. Therefore, the models are not mathematically sound or justified. The conclusion is that ANN modeling should be used with care and enough data [J1201]

## "Adaptive Multimodality Sensing of Landmines"

The problem of adaptive multimodality sensing of landmines is considered based on electromagnetic induction (EMI) and ground-penetrating radar (GPR) sensors. Two formulations are considered based on a partially observable Markov decision process (POMDP) framework. In the first formulation, it is assumed that sufficient training data are available, and a POMDP model is designed based on physics-based features, with model selection performed via a variational Bayes analysis of several possible models. In the second approach, the training data are assumed absent or insufficient, and a lifelong-learning approach is considered, in which exploration and exploitation are integrated. We provide a detailed description of both formulations, with example results presented using measured EMI and GPR data, for buried mines and clutter [J1202]

## "Characteristics of Tsunami-Affected Areas in Moderate-Resolution Satellite Images"

The massive 2004 Indian Ocean tsunami caused vast devastation along the coastal areas in countries around the Indian Ocean rim. Satellite images of various spatial resolutions could quickly capture the affected areas and were used for emergency response after the catastrophe occurred. To figure out the extent of affected areas, moderate-resolution satellites (e.g., Terra-ASTER) images are more suitable than high-resolution satellites (e.g., Ikonos) images. Basically, tsunami-affected areas can be observed and detected through land cover changes. Based on the nature of the tsunami attack, we chose the normalized difference vegetation index, soil index, and water index as indicators to help detect changes. This paper first investigates the fluctuations of these indexes and their differences using ASTER images of southern Thailand. The investigation is carried out in two cases: one using only the data acquired after the tsunami, and the other using both data acquired before and after the tsunami. Consequently, the thresholds of index differences are set up for the detection of tsunami-affected areas. In addition, since landform is a significant factor to determine the extent of tsunami runup, Shuttle Radar Topography Mission data are employed to perform geomorphological classification and to assess its relationship with the tsunami-affected areas [J1203]

## "MMW Polarimetric Radar Bistatic Scattering From a Random Surface"

This paper explores the nature of bistatic radar scattering from terrain by reporting the results of an investigation involving measurements of the hemispherical pattern of the field scattered by a random soil surface. The measurements were performed by a 35-GHz fully polarimetric radar system with transmitter and receiver modules mounted on separate rotatable arches. The acquired data were analyzed to determine the angular sensitivities of several attributes of the scattered field, including amplitudes and phase differences of the

polarized scattering coefficients, and their copolarized and cross-polarized ratios. Generally speaking, the scattering pattern exhibits a weak dependence on the scattering angle thetass(except along the backward direction and forward specular direction), but it exhibits a strong dependence on the azimuth angle phi, particularly for the cross-polarized components. Much of the dependence is attributed to the vectorial definition of polarization in a standard frame of reference. Comparison of the measured data with calculations based on the second-order physical optics model reveals reasonable overall agreement between theory and observations (typically within 4 dB) [J1204]

## "Measurement of radar signatures of passenger cars: airborne SAR multi-frequency and polarimetric experiment"

The launch of SAR satellites with high-resolution and dual-receive antenna capabilities opens new possibilities for traffic-monitoring applications on a global scale. Thus, it will be possible to detect cars and measure their speed from the acquired along track interferometric data. The development of vehicle-detection algorithms requires the knowledge of the radar signatures of vehicles, especially under consideration of the geometry of the radar look direction and the vehicle orientation. The radar signatures of the non-moving cars are presented. They are estimated experimentally from airborne E-SAR multi-frequency and polarimetric data, which have been collected during a flight campaign in 2003. Radar signatures are estimated for a considerable part of aspect angles ranging from 0deg to 180deg. The large synthetic aperture length of the E-SAR radar sensor allows the look processing of data and therefore allows an increase of the aspect angle resolution. The radar signature analysis for one type of passenger cars showed that the largest radar cross-section values and thus the greatest chance for high probability of detection are for cars standing in rear and front views of radar beam direction. This holds true for all frequencies and co-polarisations. Radar cross-section values for cross-polarisations and diagonal views are much lower and are therefore less suitable for car detection. The radar signature profile over a considerable range of aspect angles in fine resolution can be used further for the verification of simulation studies and for the performance prediction for traffic monitoring with a coming German TerraSAR-X satellite [J1205]

## "Comparisons Between SAR Backscattering Coefficient and Results of a Thermodynamic Snow/Ice Model for the Baltic Sea Land-Fast Sea Ice"

We have compared the time series of C-band HH-polarization backscattering coefficients (sigmadeg) of the Baltic Sea land-fast level ice with results from a 1-D high-resolution thermodynamic snow/ice model (HIGHTSI). The sigmadeg time series were obtained from ENVISAT synthetic aperture radar (SAR) images. The study period was from the middle of the winter to the early melt season, February 3-April 7, 2004. Due to the large incidence angle range of the SAR images, the sigmadeg values were divided into three subseries. In general, the HIGHTSI results greatly helped to interpret the sigmadeg behavior with changing ice and weather conditions. The modeled snow-surface temperature, cases of snow melting, and evolution of snow and ice thickness were related to the changes in sigmadeg. Equally useful information could not be obtained solely on the basis of large-scale atmospheric models. Realistic forcing data for HIGHTSI were available in the form of coastal-weather observations and model results of the European Centre of Medium-Range Weather Forecasts (ECMWF). The latter make it possible to apply HIGHTSI in the interpretation of SAR data from all ice-covered seas. There were some cases where detailed ground truth, combined with theoretical sigmadeg modeling, would have been needed for interpretation of the sigmadeg trends. A very interesting observation was the large variation of level ice sigmadeg with changing weather conditions, which complicates automatic classification of the SAR images, and thus, the algorithms must be tuned for different ice conditions. The HIGHTSI model could act as an indicator of various ice conditions for algorithm development [J1206]

## "Increasing the Existence of Very Shallow-Water LIDAR Measurements Using the Red-Channel Waveforms"

Mapping shallow-water bathymetry with acoustic techniques is complicated and expensive. The environmental parameters in shallow-water (<2 m) areas become more variable and greatly impact the depth extraction from the survey measurements. Current airborne light detection and ranging (LIDAR) bathymetry surveying in shallow-water depths uses green-channel waveforms to measure the water depth. Unfortunately, due to difficulties in distinguishing between the surface and bottom return of the water column, the timing of the bottom return is often ambiguous. Furthermore, the water often becomes optically "dirty" due to turbulence at these shallow depths. Therefore, it is common to find coastal areas that lack any measured depths. This paper presents a novel approach for measuring water depths in these shallow coastal waters with airborne LIDAR. Observations of the red-channel waveforms show that the waveforms are divided into two groups, namely: (1) waveforms in deep waters (>2 m) whose shape is invariant with respect to the water depth and (2) waveforms in shallow-water depths that show a change in shape as a function of the depth in the water column. The data for this study are

from the US Geological Survey LIDAR surveys of Lake Tahoe, CA, and Lake Michigan, using a SHOALS-400 LIDAR system [J1207]

## "Electromagnetic Propagation of GPR Signals in Martian Subsurface Scenarios Including Material Losses and Scattering"

A study on the electromagnetic propagation in various models of the Martian subsurface is performed with a relevance to ground penetrating radar (GPR) operating onboard rover missions. Measurements of the electromagnetic properties of Mars soil simulants are obtained; on this basis, the attenuation features of the GPR signals are estimated, including both electric and magnetic losses. The effect on propagation of inhomogeneities inside the soil is also taken into account by means of a specific model with randomly distributed scatterers. The GPR performance in terms of resolution and maximum penetration depth is evaluated in the considered scenarios for different operating frequencies, thus providing a basic information for the design of systems for future subsurface sounding investigations on Mars [J1208]

## "Use of C-Band Ground Penetrating Radar to Determine Backscatter Sources Within Glaciers"

The question of penetration of synthetic aperture radar (SAR) signals at C-band frequency into polar glaciers is addressed by comparing ground penetrating radar (GPR) and SAR backscatter signatures. Profiles of the Kongsvegen glacier, Svalbard, were obtained with a C-band GPR. The received signal is converted to the equivalent radar cross section using the standard radar equation, thus mapping the effective scattering sources within the glacier at this frequency. The depth of the observed scattering sources is greatest in the superimposed ice where layers are clearly seen to a depth of approximately 14 m. The very high scattering properties of the upper firn layers preclude layers deeper than approximately 6 m from being imaged. Integrating the radar cross sections over the depth gives a single backscatter value that we compare with the backscatter coefficient (scattering cross section per unit area) of the processed SAR data for the same profile. The comparison indicates that for coincidentally acquired GPR and SAR data, the radar cross section measured by the GPR does represent the features that contribute to the SAR signal [J1209]

## "Angular Dependence of -Distributed Sonar Data"

Backscattered signal statistics are widely used for target detection and seafloor characterization. The K-distribution shows interesting properties for describing experimental backscattered intensity statistics. In addition to the fact that its probability distribution function accurately fits actual sonar data, it advantageously provides a physical interpretation linked to the backscattering phenomenon. Sonar systems usually record backscattered signals from a wide angular range across the ship's track. In this context, previous studies have shown that backscatter statistics strongly depend on the incidence angle. In this paper, we propose an extension of previous works to model the angular evolution of the K-distribution shape parameter. This evolution is made clear and analyzed from experimental data recorded with two sonar systems: a 95-kHz multibeam echosounder and a 110-kHz sidescan sonar. Model fitting with data backscattered from six seafloor configurations shows the improvement provided by our extension as compared to two previous models [J1210]

## "SAR Imaging Degradation by Ionospheric Irregularities Based on TFTPCF Analysis"

The effects of ionospheric irregularities on spaceborne synthetic aperture radar (SAR) signal propagation with double path and multilook angle are studied in a model in which a two-frequency and two-position coherence function (TFTPCF) has been adopted for analysis. The TFTPCF is derived from the phase-screen principle. The ambiguity function based on TFTPCF has been used to analyze the effects of ionospheric turbulence on range resolution and cross resolution. The results show that, in some cases, the effects from the irregularities on SAR imaging can be very serious [J1211]

## "Analysis of the Effects of Faraday Rotation on Spaceborne Polarimetric SAR Observations at -Band"

Spaceborne microwave observation of subcanopy and subsurface requires the polarimetric synthetic aperture radar (SAR) technology at lower microwave frequencies, such as P-band. However, SAR observation at P-band is remarkably influenced by the Faraday rotation (FR) effect through the ionosphere. An example in this paper illustrates why the measured polarimetric data with FR at P-band cannot be directly applied to terrain surface classification. We further present that the parameters u, nu, H, alpha, A for terrain surface classification derived from the polarimetric data without FR, which are recovered from the data with FR, can be applied to the surface classification, there is a plusmnpi/2 ambiguity error unresolved. Based on gradual change of the FR degree along a geographical location, a method to eliminate the plusmnpi/2 ambiguity error is designed. Thus, the

polarimetric scattering vector and Mueller matrix without FR and plusmnpi/2 ambiguity can be fully inverted from the measured polarimetric data with FR [J1212]

## "Statistical Properties of Low-Grazing Range-Resolved Sea Surface Backscatter Generated Through Two-Dimensional Direct Numerical Simulations"

Statistical properties of the X-band sea clutter are studied using 2-D direct numerical simulations. Surfaces are modeled as realizations of a Gaussian random process with the Pierson-Moskowitz or Elfouhaily spectrum. The Creamer transform is further applied to account for the lowest-order surface nonlinearities. Backscattered field at a given frequency is found using the first-principles boundary integral equation (BIE) technique. Calculations are repeated at a number of frequencies, which allows synthesizing the surface response to a pulse as short as 2.2 ns (the corresponding spatial resolution is 0.33 m). Large-scale Monte Carlo trials are used to evaluate the correlation properties and to obtain the probability distributions for the vertically- and horizontally-polarized clutter. This paper concentrates on the incident angle of 85deg (5deg grazing), with a few results for moderate 60deg incidence also reported for comparison. The effects of variations in wind speed (sea state) and radar resolution on the clutter statistics are investigated. An L-band example (with proportionally longer pulse) helps explore the role of a different electromagnetic (e/m) wavelength. The simulation technique also allows for the isolation and examination of the impacts of certain e/m and hydrodynamic approximations, including the replacement of rigorous solution to the BIE by a simpler analytical scattering model. The amplitude statistics of the simulated backscatter are compared to the Weibull and K distributions that are often used to describe surface clutter [J1213]

## "A Takagi–Sugeno Fuzzy Rule-Based Model for Soil Moisture Retrieval From SAR Under Soil Roughness Uncertainty"

Radar remote sensing has shown its potential for retrieving soil moisture from bare soil surfaces. Since the backscattering process is also influenced by soil roughness, the characterization of this roughness is crucial for an accurate soil moisture retrieval. However, several field experiments have shown a large variability of the roughness parameters. Describing these parameters by means of possibility distributions allows to account for their uncertainty. Verhoest et al. introduced a retrieval procedure which calculates from these uncertain roughness parameters the possibility distribution of retrieved soil moisture, from which a soil moisture value and uncertainty upon the retrieval are estimated. The main disadvantage of their technique is the high computational demand, which hampers an operational application. In this paper, a fuzzy modeling approach, which is based on fuzzy rules of the Takagi-Sugeno type, is introduced that accurately simulates the soil moisture and the uncertainty upon its retrieved value as obtained by the possibilistic procedure [J1214]

## "**THIS ARTICLE HAS BEEN RETRACTED DUE TO A VIOLATION OF IET PUBLICATION PRINCIPLES** Specular and diffuse measurements of multipath from various terrain surfaces at 35 GHz"

Measurements of height-gain interference patterns at 35 GHz are carried out in order to obtain multipath interference data over various types of terrain viz. grass, road surface and concrete. The antenna with a beam width of 21deg is used both at transmitting and receiving ends to ensure full illumination of Fresnel zones. The transmitting antenna height is kept at 1 m and receiving antenna height is vertically translated from 1 through 4 m, with a horizontal range separation of 74 m. The polarisation combination is vertical transmit and vertical receive. The system geometry provides low-grazing angle incidence. The recorded height-gain curves indicate the presence of specular and diffuse multipath components. Specular and diffuse multipath components are separated out using discrete fourier transform-based filtering technique and reflection coefficients are computed for various types of terrain covers. The results can be vitally useful for millimetre wave radar, guidance, remote sensing and communication systems operating near the surface in arid conditions [J1215]

## "Data Fusion for Reconstruction of a DTM, Under a Woodland Canopy, From Airborne L-band InSAR"

This paper investigates the utility of different parameters from polarimetric interferometric synthetic aperture radar (InSAR) data for the identification of ground pixels in a woodland area to enable accurate digital terrain model (DTM) generation from the InSAR height of the selected ground hit pixels. The parameters assessed include radar backscatter, interferometric coherence, surface scattering proportion (based on Freeman-Durden decomposition), and standard deviation of the interferometric height. The method is applied to Monks Wood, a small seminatural deciduous woodland in Cambridgeshire, U.K., using airborne E-SAR data collected in June 2000. The 1428 variations of SAR-derived terrain models are validated with theodolite data and a light detection and ranging-derived DTM. The results show that increasing the amount of data used in the DTM creation does

not necessarily increase the accuracy of the final DTM. The most accurate method, for the whole wood, was a fixed-window minimum-filtering algorithm, followed by a mean filter. However, for a spatial subset of the area using the upsi3backscattering coefficient to identify ground pixels outperforms the minimum filtering method. The findings suggest that backscatter information may often be undervalued in estimating terrain height under forest canopies [J1216]

## "Spatial and Temporal Behavior of Microwave Backscatter Directional Modulation Over the Saharan Ergs"

Radar backscatter (sigmadeg) from ergs is modulated with view direction [incidence (thetas) and azimuth (phi) angles], where the modulation characteristics reflect the surface geometry. sigmadeg also varies spatially and reflects the spatial inhomogeneity of the sand surface. We use sigmadeg measurements at different thetas and phi angles from the NASA, European Remote Sensing satellite, and SeaWinds scatterometers to understand the relationship between wind and erg bedforms. A model incorporating the sigmadeg phi-modulation and spatial inhomogeneity is proposed. Surface slope variations are related to the sigmadeg spatial inhomogeneity. We compare the backscatter model results with numerically predicted wind direction data provided by the European Centre for Medium-Range Weather Forecasts (ECMWF) over the erg surfaces. We use the maxima of the phi-modulation at thetas=33deg to infer the orientation of the dominant slip-sides on the sand surface. These orientations are consistent with the ECMWF wind directions spatially and temporally [J1217]

## "Suppression of Surface Clutter Interference With Precipitation Measurements by Spaceborne Precipitation Radar"

The sidelobe surface clutter along the nadir direction severely interferes with the rain echo in the off-nadir angle observations made using a spaceborne Precipitation Radar (PR). A new method to suppress this sidelobe clutter interference is introduced. A characteristic of the 1-D phased array antenna system is that high sidelobes arise along the beam scan plane. The proposed method tilts the antenna beam scan plane from the nadir such that these high sidelobes would not be directed along the nadir direction, along which a specular component of the backscattering radar cross section of the Earth's surface is dominant. The simulation results using the designed parameters of a Ka-band spaceborne PR indicate the validity of this method, which is also quantitatively confirmed using Tropical Rainfall Measuring Mission/PR observation data sets [J1218]

## "Conceptual Case for Assimilating Interferometric Synthetic Aperture Radar Data Into the HAZUS-MH Earthquake Module"

The study of the Earth as a system is being adopted widely by geoscientists. Numerical models and simulations are providing the capability to rapidly test hypotheses and make forecasts of complex geophysical behavior. International efforts are seeking to integrate existing and emerging Earth observation systems into a global network, with enhanced data distribution, models, and decision support tools. Remote sensing is poised to fulfil the increasing need for a synoptic framework. However, the desire to improve the connection between scientific research and societal benefits has not been matched with resources and tools required to bridge the gap between research and applications. Natural hazards research and disaster management are a prime example. Here, we present a conceptual case for how interferometric synthetic aperture radar (InSAR) data could make a definitive contribution to understanding earthquake processes while simultaneously supporting policy- and decision-making. InSAR measurements derived from time series of radar observations from Earth orbit uniquely can provide geographically comprehensive maps of surface deformation. Observing system simulations are suggested to evaluate the potential contributions of a future system. Simulations would adopt an open seismic hazard analysis (SHA) framework, OpenSHA, recognizing the need for more physics-based modeling and computational infrastructure. SHA is employed by the HAZUS-MH earthquake module to estimate losses. InSAR measurements of strain accumulation would provide event magnitude recurrence bounds for probabilistic SHA, while coseismic InSAR measurements would add constraints on fault rupture models for deterministic approaches. Moreover, interferograms would be incorporated graphically as proxy seismic risk maps for planning and mitigation [J1219]

## "InSAR Elevation Bias Caused by Penetration Into Uniform Volumes"

Natural media like cold-land ice, vegetation, and dry sand are subject to a substantial penetration at microwave frequencies. For such media, the synthetic aperture radar (SAR) phase center is located below the surface, and consequently, the surface elevation determined with SAR interferometry (InSAR) is biased downward. For infinitely deep uniform volumes, the elevation bias is often equated with the penetration depth, but in this paper, it is shown that the two quantities generally differ. The interferometric bias is approximately equal to the two-way power-penetration depth if the latter is small compared to the ambiguity height, but for increasing penetration

depth, the bias approaches one quarter of the ambiguity height. Consequently, no phase wrapping results even if the penetration depth exceeds the ambiguity height. The ratio of the InSAR elevation bias to the ambiguity height depends only on the ratio of the penetration depth to the ambiguity height, and the bias can be expressed in terms of the InSAR coherence magnitude, which makes it possible to correct the InSAR surface elevation for the bias. The volume depth can be considered infinite if it exceeds the penetration depth by a factor of two to five and if the surface scattering from the top and the bottom of the volume is negligible. [J1220]

## "Sensitivity of Airborne 36.5-GHz Polarimetric Radiometer's Wind-Speed Measurement to Incidence Angle"

The Helsinki University of Technology's airborne fully polarimetric profiling radiometer at 36.5 GHz has been used for wind-vector measurements over the Gulf of Finland. The results, collected in a series of measurements over a period of two years, are presented in this paper. The Fourier coefficients of the harmonics of the first three modified Stokes parameters (in brightness temperature) have been solved, and their behavior as a function of the measurement incidence angle and the wind speed has been examined, resulting in a linear model in the measurement range. In this paper, we show a clear relationship between the incidence angle and the third modified Stokes parameter (in brightness temperature), which has been used to compensate for aircraft motion during measurements. Furthermore, the sensitivity of the wind-speed measurement to the incidence angle has been studied, and a model for wind-speed retrieval as a function of the harmonic coefficients and incidence angle was developed. [J1221]

## "Radar Signatures of Sahelian Surfaces in Mali Using ENVISAT-ASAR Data"

This paper presents an analysis of ENSIVAT advanced synthetic aperture radar data acquired over a Sahelian region located in Mali, West Africa. The considered period is 2004-2005 and includes two rainy seasons. Emphasis is put on two ScanSAR modes, namely, the global monitoring (GM) and the wide swath (WS) modes characterized by spatial resolutions of about 1 km and 150 m, respectively. Results show that the WS mode offers better performance in terms of radiometric resolution, radiometric stability, and speckle reduction than the GM mode. The latter is more appropriate for studies at large scale (> 10 times 10 km). In both modes, pronounced angular and temporal signatures are observed for most soil surfaces, and azimuthal effects are observed on markedly orientated rocky surfaces. In contrast, polarization differences (VV/HH) are small during the dry season except on flat loamy soil surfaces. Finally, a relationship is observed between the normalized WS backscattering signal at HH polarization and the surface soil moisture of sandy soils. [J1222]

## "Improvement of Satellite Radar Feature Tracking for Ice Velocity Derivation by Spatial Frequency Filtering"

Outlet glaciers of ice sheets are the primary means of transporting ice from the interior to the oceans, and their flow velocity is one control that determines the mass balance of ice sheets. Estimates of ice velocities, particularly for remote areas, are commonly based on satellite remote-sensing data. As radar-based systems emit energy at frequencies high enough to penetrate clouds, they can record backscatter signals from surfaces throughout the year. Radar data, which are collected with repeat-pass spaceborne platforms, are therefore good for extracting ice velocities using interferometry for slow-moving ice and the cross-correlation techniques for fast-moving ice. Here, we present an improvement on the cross-correlation technique that enables independent quality checks and enhances the spatial extent of the derived velocity fields. Filtering of ESA European remote sensing satellite scenes, based on a Butterworth high-pass spatial-frequency filter, focuses the cross-correlation technique on smaller, movable surface features, instead of large fixed features. It also allows a nonregional culling based on the signal-to-noise ratio of the velocities, with the effect of increasing the coverage of robust velocity estimates. [J1223]

## "Global Precipitation Map Using Satellite-Borne Microwave Radiometers by the GSMaP Project: Production and Validation"

This paper documents the production and validation of retrieved rainfall data obtained from satellite-borne microwave radiometers by the Global Satellite Mapping of Precipitation (GSMaP) Project. Using various attributes of precipitation derived from Tropical Rainfall Measuring Mission (TRMM) satellite data, the GSMaP has implemented hydrometeor profiles derived from Precipitation Radar (PR), statistical rain/no-rain classification, and scattering algorithms using polarization-corrected temperatures (PCTs) at 85.5 and 37 GHz. Combined scattering-based surface rainfalls are computed depending on rainfall intensities. PCT85 is not used for stronger rainfalls, because strong depressions of PCT85 are related to tall precipitation-top heights. Therefore, for stronger rainfalls, PCT37 is used, with PCT85 used for weaker rainfalls. With the suspiciously strong rainfalls retrieved from PCT85 deleted, the combined rainfalls correspond well to the PR rain rates over land. The

GSMaP algorithm for the TRMM Microwave Imager (TMI) is validated using the TRMM PR, ground radar [Kwajalein (KWAJ) radar and COBRA], and Radar Automated Meteorological Data Acquisition System (AMeDAS) precipitation analysis (RA). Monthly surface rainfalls retrieved from six microwave radiometers (GSMaP_MWR) are compared with the gauge-based dataset. Rain rates retrieved from the TMI (GSMaP_TMI) are in better agreement with the PR estimates over land everywhere except over tropical Africa in the boreal summer. Validation results of the KWAJ radar and COBRA show a good linear relationship for instantaneous rainfall rates, while validation around Japan using the RA shows a good relationship in the warm season. Poor results, connected to weak-precipitation cases, are found in the cold season around Japan. [J1224]

## "Effects of the Antenna Aperture on Remote Sensing of Sea Surface Salinity at L-Band"

Remote sensing of sea surface salinity can be performed by means of microwave radiometry at L-band, but it requires high radiometric accuracy (e.g., on the order of 0.1 K). Since the variability of salinity in the open ocean exhibits large spatial scales and long temporal scales, it is possible to use antennas with large footprints and averaging to meet this goal. However, antennas with large footprints introduce other problems such as variations of the incidence angle and direction of the polarization vectors over the footprint. Examples of these effects are computed here using antennas that are representative of those that will be flown on the Aquarius/SAC-D mission being developed for remote sensing of salinity from space. It is shown that the antenna temperature (i.e., integrated over the antenna pattern) is biased relative to the value at boresight. In part, this is due to change in incidence angles across the field of view. Polarization mixing, because of the variations of the local plane of incidence across the footprint, also induces bias (peculiarly for the third Stokes parameter). Finally, large antenna footprints limit how close to land measurements can be made. [J1225]

## "Sensitivity of the Kurtosis Statistic as a Detector of Pulsed Sinusoidal RFI"

A new type of microwave radiometer detector that is capable of identifying low-level pulsed radio frequency interference (RFI) has been developed. The Agile Digital Detector can discriminate between RFI and natural thermal emission signals by directly measuring other moments of the signal than the variance that is traditionally measured. The kurtosis is the ratio of the fourth central moment of the predetected voltage to the square of the second central moment. It can be an excellent indicator of the presence of RFI. A number of issues that are related to the proper calculation of the kurtosis are addressed. The mean and standard deviation of the kurtosis, in both the absence and the presence of pulsed sinusoidal RFI, are derived. The kurtosis is much more sensitive to short-pulsed RFI-such as from radars-than to continuous-wave RFI. The minimum detectable power for pulsed sinusoidal RFI is found to be proportional to (M3N)-1/4, where Nis the number of independent samples and Mis the number of frequency subbands in the receiver. [J1226]

## "A Review of Progress in FDTD Maxwell's Equations Modeling of Impulsive Subionospheric Propagation Below 300 kHz"

Wave propagation at the bottom of the electromagnetic spectrum (below 300 kHz) in the Earth-ionosphere waveguide system has been an interesting and important area of investigation for the last four decades. Such wave propagation is characterized by complex phenomena involving nonhomogeneous and anisotropic media, and can result in resonances of the entire Earth-ionosphere cavity. In the spirit of this Special Issue, the goal of this paper is to call attention to emerging finite-difference time-domain computational solutions of Maxwell's equations for wave propagation below 300 kHz which promise to complement and extend previous analyses by pioneers such as Profs. Wait and Felsen. The following topical areas are discussed: long-range two-dimensional propagation, lightning sources and radiation, global propagation, Schumann resonances, hypothesized pre-seismic lithosphere sources and radiation, detection of deep underground resource formations, and remote sensing of localized ionospheric anomalies. We conclude with a prospectus for future research, especially in incorporating the physics of the anisotropic, nonhomogeneous magnetized plasma in a global planetary ionosphere. [J1227]

## "Solution for the Fourth Moment Equation of Waves in Random Continuum Under Strong Fluctuations: General Theory and Plane Wave Solution"

The fourth moment plays an important role in wave propagation and scattering in random media. However, in the strong scattering regimes, it remains to be solved although a rich variety of methods have been proposed. The fourth moment equation is solved using the modified Gaussian solution method proposed in this paper. The fourth moment can be considered as a sum of the Gaussian solution and non-Gaussian correction term. The Gaussian solution is the fourth moment in the saturated regime, and can be obtained as a sum of products of the second-order moments. The derived equation of the non-Gaussian correction term is solved using the Rytov approximation and the Green's function. The fourth moment solution obtained is general for without restrictions

on incident wave forms. Specifically, the solution for a plane wave is derived and applied to study the amplitude scintillation and intensity correlation function of trans ionospheric radio signals. The theoretical calculation on the scintillation index agrees well with the experimental results, which confirms the fourth moment solution to some extent. [J1228]

## "R. Keith Raney Wins the 2007 IEEE Dennis J. Picard Medal for Radar Technologies and Applications"

R. Keith Raney is the recipient of the 2007 IEEE Dennis J. Picard Medal for Radar Technologies and Applications. A biography for Dr. Raney is provided. [J1229]

## "The Geoscience Laser Altimeter System (GLAS) Laser Transmitter"

The Geoscience Laser Altimeter System (GLAS), launched in January 2003, is a laser altimeter and lidar for the Earth Observing System's (EOS) ICESat mission. GLAS accommodates three, sequentially operated, diode-pumped, solid-state, Nd:YAG laser transmitters. The laser transmitter requirements, design, and qualification test results for this space-based remote-sensing instrument is summarized and presented. [J1230]

## "Recent Progress in the Development of Neodymium-Doped Ceramic Yttria"

Solid-state lasers play a significant role in providing the technology necessary for active remote sensing of the atmosphere. Neodymium-doped yttria (Nd:Y2O3) is considered to be an attractive material due to its possible lasing wavelengths of ~914 and ~946 nm for ozone profiling. These wavelengths, when frequency tripled, can generate ultraviolet (UV) light at ~305 and ~315 nm, which is particularly useful for ozone sensing using differential absorption light detection and ranging (LIDAR) technique. For practical realization of space-based UV transmitter technology, ceramic Nd:Y2O3material is considered to possess a great potential. A plasma melting and quenching method has been developed to produce Nd3+-doped powders for consolidation into Nd: Y2O3ceramic laser materials. This far-from-equilibrium processing methodology allows higher levels of rare earth doping than can be achieved by equilibrium methods. The method comprises two main steps: 1) plasma melting and quenching to generate dense, and homogeneous doped metastable powders and 2) pressure-assisted consolidation of these powders by hot isostatic pressing to make dense nanocomposite ceramics. Using this process, several in 1times1 ceramic cylinders have been produced. The infrared transmission of a 2-mm-thick undoped Y2O3ceramic was as high as ~75% without antireflection coating. In the case of Nd:Y2O3, ceramics infrared transmission values of ~50% were achieved for a similar sample thickness. Furthermore, Nd:Y2O3samples with dopant concentrations of up to ~2 at.% were prepared without significant emission quenching. [J1231]

## "Coherence- and Amplitude-Based Analysis of Seismogenic Damage in Bam, Iran, Using ENVISAT ASAR Data"

The sensitivity of synthetic aperture radar (SAR) and interferometric SAR (InSAR) to surface properties, especially changes in height and roughness, combined with an all-weather capability, makes radar remote sensing a potential tool for mapping urban damage caused by earthquakes. With InSAR, surface displacement has been mapped successfully and in detail, but for urban-damage mapping, results have so far been less conclusive. ENVISAT Advanced SAR images of Bam, Iran, that were acquired before and after the 2003 earthquake were used. Between preseismic and coseismic image pairs, coherence decreased with increasing damage levels. However, contrary to previous studies, earthquake damage caused both increases and decreases in amplitude. Therefore, its absolute value, which correlated with damage level, was used. Individually, coherence difference led to better results than absolute amplitude change, although still with limited accuracy. The combination of both resulted in an overall accuracy of 52%. Since vegetation causes decorrelation, a predisaster Advanced Spaceborne Thermal Emission and Reflection Radiometer image was used to mask out vegetated areas, which improved the accuracy by 4%. The ground-truth map showed damage levels per district instead of per pixel. Therefore, the ratio of pixels classified as "damage" and "nondamage" was calculated for each damage class of the map, and a clear relation was found. This shows that the aggregation level of the map partly explains the low-accuracy figures of the pixel-based evaluation. Although improvement was made, InSAR techniques for urban-damage mapping do not yet provide the accuracy levels needed for disaster mitigation. However, substantial improvements can be expected from instruments with higher spatial resolution, such as the recently launched Phased Array type L-band SAR and Terra SAR-X [J1232]

## "All Solid-State High-Efficiency Tunable UV Source for Airborne or Satellite-Based Ozone DIAL Systems"

We designed, built, and tested two laboratory prototype nanosecond UV sources for airborne or satellite-based ozone differential absorption lidar (DIAL) remote-sensing systems. Our prototypes use a 532-nm second-harmonic pulse from a Q-switched injection-seeded Nd:YAG laser to pump an optical parametric oscillator (OPO) that generates a tunable signal wavelength near 803 nm. The OPO signal is mixed with additional 532 nm light either inside the OPO cavity, or in a subsequent sum-frequency generation (SFG) stage, to generate 10-ns pulses at 320-nm. Our system designs result from an integrated, iterative approach where operating parameters including the pump-beam's spatial profile, the second harmonic generation efficiency, the OPO's cavity geometry, output coupling, crystal lengths, and the length of the SFG crystals, are all determined from numerical modeling. By using this approach, we obtained 320 nm pulse energies approaching 200 mJ with overall optical conversion efficiency-from 1064 to 320 nm-exceeding 20%. To optimize efficiency, we incorporate three important design characteristics: a pump beam having a high-quality flat-topped spatial profile, an image-rotating non-planar ring-cavity OPO capable of generating high-quality large-diameter flat-topped beams, and pulse injection seeding of the OPO to achieve near-zero cavity buildup time to enhance the efficiency of sum-frequency mining. We believe additional optimization of our designs may eventually yield UV pulse energies approaching 300 mJ with optical conversion efficiencies comparable to those of our current systems. [J1233]

## СПИСОК ЛИТЕРАТУРЫ

J1. Fan Wu. Rice Crop Monitoring in South China With RADARSAT-2 Quad-Polarization SAR Data. / Fan Wu, Chao Wang, Hong Zhang, Bo Zhang, Yixian Tang. // IEEE Geoscience and Remote Sensing Letters. - 2011. - Vol. 8, No. 2. - P. 196-200.

J2. Cristallini D. Exploiting MIMO SAR Potentialities With Efficient Cross-Track Constellation Configurations for Improved Range Resolution. / Cristallini D., Pastina D., Lombardo P. // IEEE Transactions on Geoscience and Remote Sensing. - 2011. - Vol. 49, No. 1. - P. 38-52.

J3. Pinsky M. Application of a Simple Adaptive Estimator for an Atmospheric Doppler Radar. / Pinsky M., Figueras i Ventura J., Otto T., Sterkin A., Khain A., Russchenberg H.W.J. // IEEE Transactions on Geoscience and Remote Sensing. - 2011. - Vol. 49, No. 1. - P. 115-127.

J4. McCarroll S. Approaches for Compression of Super-Resolution WSR-88D Data. / McCarroll S., Yeary M., Hougen D., Lakshmanan V., Smith S. // IEEE Geoscience and Remote Sensing Letters. - 2011. - Vol. 8, No. 2. - P. 191-195.

J5. Alvarez-Perez J.L. Coherence, Polarization, and Statistical Independence in Cloude-Pottier's Radar Polarimetry. IEEE Transactions on Geoscience and Remote Sensing. - 2011. - Vol. 49, No. 1. - P. 426-441.

J6. Shengqi Zhu. Ground Moving Targets Imaging Algorithm for Synthetic Aperture Radar. / Shengqi Zhu, Guisheng Liao, Yi Qu, Zhengguang Zhou, Xiangyang Liu. // IEEE Transactions on Geoscience and Remote Sensing. - 2011. - Vol. 49, No. 1. - P. 462-477.

J7. Hanwen Yu. A Cluster-Analysis-Based Efficient Multibaseline Phase-Unwrapping Algorithm. / Hanwen Yu, Zhenfang Li, Zheng Bao. // IEEE Transactions on Geoscience and Remote Sensing. - 2011. - Vol. 49, No. 1. - P. 478-487.

J8. Xiaofeng Yang. Comparison of Ocean-Surface Winds Retrieved From QuikSCAT Scatterometer and Radarsat-1 SAR in Offshore Waters of the U.S. West Coast. / Xiaofeng Yang, Xiaofeng Li, Quanan Zheng, Xingfa Gu, Pichel W.G., Ziwei Li. // IEEE Geoscience and Remote Sensing Letters. - 2011. - Vol. 8, No. 1. - P. 163-167.

J9. Soldovieri F. Combination of Advanced Inversion Techniques for an Accurate Target Localization via GPR for Demining Applications. / Soldovieri F., Lopera O., Lambot S. // IEEE Transactions on Geoscience and Remote Sensing. - 2011. - Vol. 49, No. 1. - P. 451-461.

J10. Tello Alonso M. Edge Enhancement Algorithm Based on the Wavelet Transform for Automatic Edge Detection in SAR Images. / Tello Alonso M., Lopez-Martinez C., Mallorqui J.J., Salembier P. // IEEE Transactions on Geoscience and Remote Sensing. - 2011. - Vol. 49, No. 1. - P. 222-235.

J11. Lijia Huang. Focusing of Medium-Earth-Orbit SAR With Advanced Nonlinear Chirp Scaling Algorithm. / Lijia Huang, Xiaolan Qiu, Donghui Hu, Chibiao Ding. // IEEE Transactions on Geoscience and Remote Sensing. - 2011. - Vol. 49, No. 1. - P. 500-508.

J12. Xiaozhen Ren. A New Three-Dimensional Imaging Algorithm for Airborne Forward-Looking SAR. / Xiaozhen Ren, Jiantao Sun, Ruliang Yang. // IEEE Geoscience and Remote Sensing Letters. - 2011. - Vol. 8, No. 1. - P. 153-157.

J13. Martinis S. Unsupervised Extraction of Flood-Induced Backscatter Changes in SAR Data Using Markov Image Modeling on Irregular Graphs. / Martinis S., Twele A., Voigt S. // IEEE Transactions on Geoscience and Remote Sensing. - 2011. - Vol. 49, No. 1. - P. 251-263.

J14. Xiaodong Zhuge. A Sparse Aperture MIMO-SAR-Based UWB Imaging System for Concealed Weapon Detection. / Xiaodong Zhuge, Yarovoy A.G. // IEEE Transactions on Geoscience and Remote Sensing. - 2011. - Vol. 49, No. 1. - P. 509-518.

J15. Moller D. The Glacier and Land Ice Surface Topography Interferometer: An Airborne Proof-of-Concept Demonstration of High-Precision Ka-Band Single-Pass Elevation Mapping. / Moller D., Hensley S., Sadowy G.A., Fisher C.D., Michel T., Zawadzki M., Rignot E. // IEEE Transactions on Geoscience and Remote Sensing. - 2011. - Vol. 49, No. 2. - P. 827-842.

J16. Liu G. Exploration of Subsidence Estimation by Persistent Scatterer InSAR on Time Series of High Resolution TerraSAR-X Images. / Liu G., Jia H., Zhang R., Zhang H., Jia H., Yu B., Sang M. // IEEE Journal of Selected Topics in Applied Earth Observations and Remote Sensing. - 2011. - Vol. 4, No. 1. - P. 159-170.

J17. Refaat T.F. Backscatter 2- Lidar Validation for Atmospheric Differential Absorption Lidar Applications. / Refaat T.F., Ismail S., Koch G.J., Rubio M., Mack T.L., Notari A., Collins J.E., Lewis J., De Young R., Yonghoon Choi, Abedin M.N., Singh U.N. // IEEE Transactions on Geoscience and Remote Sensing. - 2011. - Vol. 49, No. 1. - P. 572-580.

J18. Dengxin Dai. Multilevel Local Pattern Histogram for SAR Image Classification. / Dengxin Dai, Wen Yang, Hong Sun. // IEEE Geoscience and Remote Sensing Letters. - 2011. - Vol. 8, No. 2. - P. 225-229.

J19. Vernieuwe H. Possibilistic Soil Roughness Identification for Uncertainty Reduction on SAR-Retrieved Soil Moisture. / Vernieuwe H., Verhoest N.E.C., Lievens H., De Baets B. // IEEE Transactions on Geoscience and Remote Sensing. - 2011. - Vol. 49, No. 2. - P. 628-638.

J20. Hannuree Jang. Efficient Electromagnetic Imaging of an Artificial Infiltration Process in the Vadose Zone Using Cross-Borehole Radar. / Hannuree Jang, Kuroda S., Hee Joon Kim. // IEEE Geoscience and Remote Sensing Letters. - 2011. - Vol. 8, No. 2. - P. 243-247.

J21. Euillades L.D. On the Generation of Late ERS Deformation Time Series Through Small Doppler and Baseline Subsets Differential SAR Interferograms. / Euillades L.D., Euillades P.A., Pepe A., Blanco M.H., Baro,n J.H. // IEEE Geoscience and Remote Sensing Letters. - 2011. - Vol. 8, No. 2. - P. 238-242.

J22. Martinez-Lorenzo J.A. Physical Limitations on Detecting Tunnels Using Underground-Focusing Spotlight Synthetic Aperture Radar. / Martinez-Lorenzo J.A., Rappaport C.M., Quivira F. // IEEE Transactions on Geoscience and Remote Sensing. - 2011. - Vol. 49, No. 1. - P. 65-70.

J23. Wegner J. D. Building Detection From One Orthophoto and High-Resolution InSAR Data Using Conditional Random Fields. / Wegner J. D., Hansch R., Thiele A., Soergel U. // IEEE Journal of Selected Topics in Applied Earth Observations and Remote Sensing. - 2011. - Vol. 4, No. 1. - P. 83-91.

J24. Budillon A. Three-Dimensional SAR Focusing From Multipass Signals Using Compressive Sampling. / Budillon A., Evangelista A., Schirinzi G. // IEEE Transactions on Geoscience and Remote Sensing. - 2011. - Vol. 49, No. 1. - P. 488-499.

J25. Yang Jungang. An Interpolated Phase Adjustment by Contrast Enhancement Algorithm for SAR. / Yang Jungang, Huang Xiaotao, Jin Tian, Xue Guoyi, Zhou Zhimin. // IEEE Geoscience and Remote Sensing Letters. - 2011. - Vol. 8, No. 2. - P. 211-215.

J26. Sharma J.J. Polarimetric Decomposition Over Glacier Ice Using Long-Wavelength Airborne PolSAR. /

Sharma J.J., Hajnsek I., Papathanassiou K.P., Moreira A. // IEEE Transactions on Geoscience and Remote Sensing. - 2011. - Vol. 49, No. 1. - P. 519-535.

J27. Xiaofei Li. Scattering and Doppler Spectral Analysis for Two-Dimensional Linear and Nonlinear Sea Surfaces. / Xiaofei Li, Xiaojian Xu. // IEEE Transactions on Geoscience and Remote Sensing. - 2011. - Vol. 49, No. 2. - P. 603-611.

J28. Natsuaki R. SPEC Method-A Fine Coregistration Method for SAR Interferometry. / Natsuaki R., Hirose A. // IEEE Transactions on Geoscience and Remote Sensing. - 2011. - Vol. 49, No. 1. - P. 28-37.

J29. Gui Gao. An Improved Scheme for Target Discrimination in High-Resolution SAR Images. IEEE Transactions on Geoscience and Remote Sensing. - 2011. - Vol. 49, No. 1. - P. 277-294.

J30. Ming Yao. A Novel Radar Waveform for Monostatic Ionosonde. / Ming Yao, Zhengyu Zhao, Gang Chen, Guobin Yang, Shipeng Li, Fanfan Su, Ning Li, Shuo Huang, Ting Li, Zuowei He, Tianyao Pu. // IEEE Geoscience and Remote Sensing Letters. - 2011. - Vol. 8, No. 1. - P. 39-43.

J31. Stramondo S. X-, C-, and L-Band DInSAR Investigation of the April 6, 2009, Abruzzi Earthquake. / Stramondo S., Chini M., Bignami C., Salvi S., Atzori S. // IEEE Geoscience and Remote Sensing Letters. - 2011. - Vol. 8, No. 1. - P. 49-53.

J32. Bin Deng. Fast Raw-Signal Simulation of Extended Scenes for Missile-Borne SAR With Constant Acceleration. / Bin Deng, Xiang Li, Hongqiang Wang, Yuliang Qin, Jiantao Wang. // IEEE Geoscience and Remote Sensing Letters. - 2011. - Vol. 8, No. 1. - P. 44-48.

J33. Jung H.S. Mapping Three-Dimensional Surface Deformation by Combining Multiple-Aperture Interferometry and Conventional Interferometry: Application to the June 2007 Eruption of Kilauea Volcano, Hawaii. / Jung H.S., Lu Z., Won J.S., Poland M.P., Miklius A. // IEEE Geoscience and Remote Sensing Letters. - 2011. - Vol. 8, No. 1. - P. 34-38.

J34. Gamba P. Robust Extraction of Urban Area Extents in HR and VHR SAR Images. / Gamba P., Aldrighi M., Stasolla M. // IEEE Journal of Selected Topics in Applied Earth Observations and Remote Sensing. - 2011. - Vol. 4, No. 1. - P. 27-34.

J35. Xiao-Ming Li. Ocean Wave Integral Parameter Measurements Using Envisat ASAR Wave Mode Data. / Xiao-Ming Li, Lehner S., Bruns T. // IEEE Transactions on Geoscience and Remote Sensing. - 2011. - Vol. 49, No. 1. - P. 155-174.

J36. Stramondo S. Seismic Source Quantitative Parameters Retrieval From InSAR Data and Neural Networks. / Stramondo S., Del Frate F., Picchiani M., Schiavon G. // IEEE Transactions on Geoscience and Remote Sensing. - 2011. - Vol. 49, No. 1. - P. 96-104.

J37. Rodriguez-Alvarez N. Land Geophysical Parameters Retrieval Using the Interference Pattern GNSS-R Technique. / Rodriguez-Alvarez N., Camps A., Vall-llossera M., Bosch-Lluis X., Monerris A., Ramos-Perez I., Valencia E., Marchan-Hernandez J.F., Martinez-Fernandez J., Baroncini-Turricchia G., Pe,rez-Gutie,rrez C., Sa,nchez N. // IEEE Transactions on Geoscience and Remote Sensing. - 2011. - Vol. 49, No. 1. - P. 71-84.

J38. Shuo Wang. An Internal Calibration Scheme for Polarimetric Synthetic Aperture Radar System. / Shuo Wang, Haiming Qi, Weidong Yu. // IEEE Transactions on Geoscience and Remote Sensing. - 2011. - Vol. 49, No. 1. - P. 15-20.

J39. Perissin D. Time-Series InSAR Applications Over Urban Areas in China. / Perissin D., Wang T. // IEEE Journal of Selected Topics in Applied Earth Observations and Remote Sensing. - 2011. - Vol. 4, No. 1. - P. 92-100.

J40. Baghdadi N. Semiempirical Calibration of the Integral Equation Model for SAR Data in C-Band and Cross Polarization Using Radar Images and Field Measurements. / Baghdadi N., Chaaya J.A., Zribi M. // IEEE Geoscience and Remote Sensing Letters. - 2011. - Vol. 8, No. 1. - P. 14-18.

J41. Jong-Sen Lee. The Effect of Orientation Angle Compensation on Coherency Matrix and Polarimetric Target Decompositions. / Jong-Sen Lee, Ainsworth T.L. // IEEE Transactions on Geoscience and Remote Sensing. - 2011. - Vol. 49, No. 1. - P. 53-64.

J42. Va. Global CALIPSO Observations of Aerosol Changes Near Clouds. / Va,rnai T., Marshak A. // IEEE Geoscience and Remote Sensing Letters. - 2011. - Vol. 8, No. 1. - P. 19-23.

J43. Monsivais-Huertero A. Comparison of Backscattering Models at L-Band for Growing Corn. / Monsivais-Huertero A., Judge J. // IEEE Geoscience and Remote Sensing Letters. - 2011. - Vol. 8, No. 1. - P. 24-28.

J44. Li Wei. A New Improved Step Transform Algorithm for Highly Squint SAR Imaging. / Li Wei, Wang Jun. // IEEE Geoscience and Remote Sensing Letters. - 2011. - Vol. 8, No. 1. - P. 118-122.

J45. Krylov V.A. Enhanced Dictionary-Based SAR Amplitude Distribution Estimation and Its Validation With Very High-Resolution Data. / Krylov V.A., Moser G., Serpico S.B., Zerubia J. // IEEE Geoscience and Remote Sensing Letters. - 2011. - Vol. 8, No. 1. - P. 148-152.

J46. Lardeux C. Classification of Tropical Vegetation Using Multifrequency Partial SAR Polarimetry. / Lardeux C., Frison P.-L., Tison C., Souyris J.-C., Stoll B., Fruneau B., Rudant J.-P. // IEEE Geoscience and Remote Sensing Letters. - 2011. - Vol. 8, No. 1. - P. 133-137.

J47. Rambukkange M.P. Using Doppler Spectra to Separate Hydrometeor Populations and Analyze Ice Precipitation in Multilayered Mixed-Phase Clouds. / Rambukkange M.P., Verlinde J., Eloranta E.W., Flynn C.J., Clothiaux E.E. // IEEE Geoscience and Remote Sensing Letters. - 2011. - Vol. 8, No. 1. - P. 108-112.

J48. Onier C. Impact of Soil Structure on Microwave Volume Scattering Evaluated by a Two-Dimensional Numerical Model. / Onier C., Chanzy A., Chambarel A., Rouveure R., Chanet M., Bolvin H. // IEEE Transactions on Geoscience and Remote Sensing. - 2011. - Vol. 49, No. 1. - P. 415-425.

J49. Battaglia A. DOMUS: DOppler MUltiple-Scattering Simulator. / Battaglia A., Tanelli S. // IEEE Transactions on Geoscience and Remote Sensing. - 2011. - Vol. 49, No. 1. - P. 442-450.

J50. Soldovieri F. Validation of Microwave Tomographic Inverse Scattering Approach via Through-the-Wall Experiments in Semicontrolled Conditions. / Soldovieri F., Ahmad F., Solimene R. // IEEE Geoscience and Remote Sensing Letters. - 2011. - Vol. 8, No. 1. - P. 123-127.

J51. Wei Yang. Electromagnetic Modeling of Breaking Waves at Low Grazing Angles With Adaptive Higher Order Hierarchical Legendre Basis Functions. / Wei Yang, Zhiqin Zhao, Conghui Qi, Zaiping Nie. // IEEE Transactions on Geoscience and Remote Sensing. - 2011. - Vol. 49, No. 1. - P. 346-352.

J52. Xiaohui Yuan. Automatic Urban Water-Body Detection and Segmentation From Sparse ALSM Data via Spatially Constrained Model-Driven Clustering. / Xiaohui Yuan, Sarma V. // IEEE Geoscience and Remote Sensing Letters. - 2011. - Vol. 8, No. 1. - P. 73-77.

J53. Brunner D. Radar Imaging Simulation for Urban Structures. / Brunner D., Lemoine G., Greidanus H., Bruzzone L. // IEEE Geoscience and Remote Sensing Letters. - 2011. - Vol. 8, No. 1. - P. 68-72.

J54. Ballester-Berman J.D. Combination of Direct and Double-Bounce Ground Responses in the Homogeneous Oriented Volume Over Ground Model. / Ballester-Berman J.D., Lopez-Sanchez J.M. // IEEE Geoscience and Remote Sensing Letters. - 2011. - Vol. 8, No. 1. - P. 54-58.

J55. Lei Zhang. Modeling PSInSAR Time Series Without Phase Unwrapping. / Lei Zhang, Xiaoli Ding, Zhong Lu. // IEEE Transactions on Geoscience and Remote Sensing. - 2011. - Vol. 49, No. 1. - P. 547-556.

J56. Qisong Wu. Focusing of Tandem Bistatic-Configuration Data With Range Migration Algorithm. / Qisong Wu, Yi Liang, Mengdao Xing, Chengwei Qiu, Zheng Bao, Tat-Soon Yeo. // IEEE Geoscience and Remote Sensing Letters. - 2011. - Vol. 8, No. 1. - P. 88-92.

J57. Lauknes T.R. InSAR Deformation Time Series Using an -Norm Small-Baseline Approach. / Lauknes T.R., Zebker H.A., Larsen Y. // IEEE Transactions on Geoscience and Remote Sensing. - 2011. - Vol. 49, No. 1. - P. 536-546.

J58. Zrnic D.S. Bias Correction and Doppler Measurement for Polarimetric Phased-Array Radar. / Zrnic D.S., Guifu Zhang, Doviak R.J. // IEEE Transactions on Geoscience and Remote Sensing. - 2011. - Vol. 49, No. 2. - P. 843-853.

J59. Picco M. Unsupervised Classification of SAR Images Using Markov Random Fields and Model. / Picco M., Palacio G. // IEEE Geoscience and Remote Sensing Letters. - 2011. - Vol. 8, No. 2. - P. 350-353.

J60. Govindan R. Altimeter-Derived Ocean Wave Period Using Genetic Algorithm. / Govindan R., Kumar R., Basu S., Sarkar A. // IEEE Geoscience and Remote Sensing Letters. - 2011. - Vol. 8, No. 2. - P. 354-358.

J61. Marzano F.S. Remote Sensing of Volcanic Ash Cloud During Explosive Eruptions Using Ground-Based Weather RADAR Data Processing [In the Spotlight]. IEEE Signal Processing Magazine. - 2011. - Vol. 28, No. 2. - P. 128-126.

J62. Inggs M. Foreword to the Special Issue on the 2009 International Geoscience and Remote Sensing Symposium (IGARSS '09). / Inggs M., King R. L., Davis C. H. // IEEE Transactions on Geoscience and Remote Sensing. - 2011. - Vol. 49, No. 1. - P. 3-5.

J63. Refice A. On the Use of Anisotropic Covariance Models in Estimating Atmospheric DInSAR Contributions. / Refice A., Belmonte A., Bovenga F., Pasquariello G. // IEEE Geoscience and Remote Sensing Letters. - 2011. - Vol. 8, No. 2. - P. 341-345.

J64. Alpers W. On the Discrimination of Radar Signatures of Atmospheric Gravity Waves and Oceanic Internal Waves on Synthetic Aperture Radar Images of the Sea Surface. / Alpers W., Weigen Huang. // IEEE Transactions on Geoscience and Remote Sensing. - 2011. - Vol. 49, No. 3. - P. 1114-1126.

J65. Baek J. Electromagnetic Land Surface Classification Through Integration of Optical and Radar Remote Sensing Data. / Baek J., Kim J. W., Lim G. J., Lee D.-C. // IEEE Transactions on Geoscience and Remote Sensing. - 2011. - Vol. 49, No. 4. - P. 1214-1222.

J66. Shang X. Radar detection based on compound-gaussian model with inverse gamma texture. / Shang X., Song H. // IET Radar, Sonar & Navigation. - 2011. - Vol. 5, No. 3. - P. 315-321.

J67. Peeri S. The Seafloor: A Key Factor in Lidar Bottom Detection. / Peeri S., Gardner J.V., Ward L.G., Morrison J.R. // IEEE Transactions on Geoscience and Remote Sensing. - 2011. - Vol. 49, No. 3. - P. 1150-1157.

J68. Jezek K.C. Two-Frequency Radar Experiments for Sounding Glacier Ice and Mapping the Topography of the Glacier Bed. / Jezek K.C., Gogineni S., Wu X., Rodriguez E., Rodriguez-Morales F., Hoch A., Freeman A., Sonntag J.G. // IEEE Transactions on Geoscience and Remote Sensing. - 2011. - Vol. 49, No. 3. - P. 920-929.

J69. Brusch S. Ship Surveillance With TerraSAR-X. / Brusch S., Lehner S., Fritz T., Soccorsi M., Soloviev A., van Schie B. // IEEE Transactions on Geoscience and Remote Sensing. - 2011. - Vol. 49, No. 3. - P. 1092-1103.

J70. Biancheri-Astier M. Modeling the Configuration of HF Electrical Antennas for Deep Bistatic Subsurface Sounding. / Biancheri-Astier M., Ciarletti V., Reineix A., Corbel C. // IEEE Transactions on Geoscience and Remote Sensing. - 2011. - Vol. 49, No. 3. - P. 1082-1091.

J71. Merzouki A. Mapping Soil Moisture Using RADARSAT-2 Data and Local Autocorrelation Statistics. / Merzouki A., McNairn H., Pacheco A. // IEEE Journal of Selected Topics in Applied Earth Observations and Remote Sensing. - 2011. - Vol. 4, No. 1. - P. 128-137.

J72. Deledalle C.-A. NL-InSAR: Nonlocal Interferogram Estimation. / Deledalle C.-A., Denis L., Tupin F. // IEEE Transactions on Geoscience and Remote Sensing. - 2011. - Vol. 49, No. 4. - P. 1441-1452.

J73. Nitti D.O. Impact of DEM-Assisted Coregistration on High-Resolution SAR Interferometry. / Nitti D.O., Hanssen R.F., Refice A., Bovenga F., Nutricato R. // IEEE Transactions on Geoscience and Remote Sensing. - 2011. - Vol. 49, No. 3. - P. 1127-1143.

J74. Zhou G. Linear Feature Detection in Polarimetric SAR Images. / Zhou G., Cui Y., Chen Y., Yang J., Rashvand H., Yamaguchi Y. // IEEE Transactions on Geoscience and Remote Sensing. - 2011. - Vol. 49, No. 4. - P. 1453-1463.

J75. Shi Kuang. Differential Absorption Lidar to Measure Subhourly Variation of Tropospheric Ozone Profiles. / Shi Kuang, Burris J.F., Newchurch M.J., Johnson S., Long S. // IEEE Transactions on Geoscience and Remote

Sensing. - 2011. - Vol. 49, No. 1. - P. 557-571.

J76. Ebihara S. Mode Effect on Direct Wave in Single-Hole Borehole Radar. / Ebihara S., Sasakura A., Takemoto T. // IEEE Transactions on Geoscience and Remote Sensing. - 2011. - Vol. 49, No. 2. - P. 854-867.

J77. Li Z. A Microphysics-Based Simulator for Advanced Airborne Weather Radar Development. / Li Z., Zhang Y., Zhang G., Brewster K. A. // IEEE Transactions on Geoscience and Remote Sensing. - 2011. - Vol. 49, No. 4. - P. 1356-1373.

J78. Heping Zhong. An Improved Quality-Guided Phase-Unwrapping Algorithm Based on Priority Queue. / Heping Zhong, Jinsong Tang, Sen Zhang, Ming Chen. // IEEE Geoscience and Remote Sensing Letters. - 2011. - Vol. 8, No. 2. - P. 364-368.

J79. Wenchao Li. An Improved Radon-Transform-Based Scheme of Doppler Centroid Estimation for Bistatic Forward-Looking SAR. / Wenchao Li, Yulin Huang, Jianyu Yang, Junjie Wu, Lingjiang Kong. // IEEE Geoscience and Remote Sensing Letters. - 2011. - Vol. 8, No. 2. - P. 379-383.

J80. Julea A. Unsupervised Spatiotemporal Mining of Satellite Image Time Series Using Grouped Frequent Sequential Patterns. / Julea A., Meger N., Bolon P., Rigotti C., Doin M.-P., Lasserre C., Trouve E., Lazarescu V. N. // IEEE Transactions on Geoscience and Remote Sensing. - 2011. - Vol. 49, No. 4. - P. 1417-1430.

J81. Arii M. Adaptive Model-Based Decomposition of Polarimetric SAR Covariance Matrices. / Arii M., van Zyl J.J., Yunjin Kim. // IEEE Transactions on Geoscience and Remote Sensing. - 2011. - Vol. 49, No. 3. - P. 1104-1113.

J82. Huo K. A Novel Imaging Method for Fast Rotating Targets Based on the Segmental Pseudo Keystone Transform. / Huo K., Liu Y., Hu J., Jiang W., Li X. // IEEE Transactions on Geoscience and Remote Sensing. - 2011. - Vol. 49, No. 4. - P. 1464-1472.

J83. Kurekin A. New method for generating site-specific clutter map for land-based radar by using multimodal remote-sensing images and digital terrain data. / Kurekin A., Radford D., Lever K., Marshall D., Shark L.-K. // IET Radar, Sonar & Navigation. - 2011. - Vol. 5, No. 3. - P. 374-388.

J84. Rogers A.B. Complex Permittivity of Volcanic Rock and Ash at Millimeter Wave Frequencies. / Rogers A.B., Macfarlane D.G., Robertson D.A. // IEEE Geoscience and Remote Sensing Letters. - 2011. - Vol. 8, No. 2. - P. 298-302.

J85. Meneghini R. Standard Deviation of Spatially Averaged Surface Cross Section Data From the TRMM Precipitation Radar. / Meneghini R., Jones J.A. // IEEE Geoscience and Remote Sensing Letters. - 2011. - Vol. 8, No. 2. - P. 293-297.

J86. Root B. Consistent Clustering of Radar Reflectivities Using Strong Point Analysis: A Prelude to Storm Tracking. / Root B., Tian-You Yu, Yeary M. // IEEE Geoscience and Remote Sensing Letters. - 2011. - Vol. 8, No. 2. - P. 273-277.

J87. Taubenbojck H. Pattern-Based Accuracy Assessment of an Urban Footprint Classification Using TerraSAR-X Data. / Taubenbojck H., Esch T., Felbier A., Roth A., Dech S. // IEEE Geoscience and Remote Sensing Letters. - 2011. - Vol. 8, No. 2. - P. 278-282.

J88. Kainulainen J. Experimental Study on Radiometric Performance of Synthetic Aperture Radiometer HUT-2D-Measurements of Natural Targets. / Kainulainen J., Rautiainen K., Lemmetyinen J., Seppajnen J., Sievinen P., Takala M., Hallikainen M.T. // IEEE Transactions on Geoscience and Remote Sensing. - 2011. - Vol. 49, No. 2. - P. 814-826.

J89. Sixin Liu. Numerical Simulations of Borehole Radar Detection for Metal Ore. / Sixin Liu, Junjun Wu, Junfeng Zhou, Zhaofa Zeng. // IEEE Geoscience and Remote Sensing Letters. - 2011. - Vol. 8, No. 2. - P. 308-312.

J90. Eineder M. Imaging Geodesy-Toward Centimeter-Level Ranging Accuracy With TerraSAR-X. / Eineder M., Minet C., Steigenberger P., Xiaoying Cong, Fritz T. // IEEE Transactions on Geoscience and Remote Sensing. - 2011. - Vol. 49, No. 2. - P. 661-671.

J91. Bombrun L. Hierarchical Segmentation of Polarimetric SAR Images Using Heterogeneous Clutter Models. / Bombrun L., Vasile G., Gay M., Totir F. // IEEE Transactions on Geoscience and Remote Sensing. - 2011. - Vol. 49, No. 2. - P. 726-737.

J92. Sang-Hong Park. Cross-Range Scaling Algorithm for ISAR Images Using 2-D Fourier Transform and Polar Mapping. / Sang-Hong Park, Hyo-Tae Kim, Kyung-Tae Kim. // IEEE Transactions on Geoscience and Remote Sensing. - 2011. - Vol. 49, No. 2. - P. 868-877.

J93. Bin Liu. A Foreground/Background Separation Framework for Interpreting Polarimetric SAR Images. / Bin Liu, Huanyu Wang, Kaizhi Wang, Xingzhao Liu, Wenxian Yu. // IEEE Geoscience and Remote Sensing Letters. - 2011. - Vol. 8, No. 2. - P. 288-292.

J94. Yueqin Huang. Three-Dimensional GPR Ray Tracing Based on Wavefront Expansion With Irregular Cells. / Yueqin Huang, Jianzhong Zhang, Qing Huo Liu. // IEEE Transactions on Geoscience and Remote Sensing. - 2011. - Vol. 49, No. 2. - P. 679-687.

J95. Yunhua Wang. Investigation on Doppler Shift and Bandwidth of Backscattered Echoes From a Composite Sea Surface. / Yunhua Wang, Yanmin Zhang. // IEEE Transactions on Geoscience and Remote Sensing. - 2011. - Vol. 49, No. 3. - P. 1071-1081.

J96. Milla M.A. Incoherent Scatter Spectral Theories-Part II: Modeling the Spectrum for Modes Propagating Perpendicular to. / Milla M.A., Kudeki E. // IEEE Transactions on Geoscience and Remote Sensing. - 2011. - Vol. 49, No. 1. - P. 329-345.

J97. Vicen-Bueno R. Detection of Ships in Marine Environments by Square Integration Mode and Multilayer Perceptrons. / Vicen-Bueno R., Carrasco-A,lvarez R., Jarabo-Amores M.P., Nieto-Borge J.C., Alexandre-Cortizo E. // IEEE Transactions on Instrumentation and Measurement. - 2011. - Vol. 60, No. 3. - P. 712-724.

J98. Celik T. Multitemporal Image Change Detection Using Undecimated Discrete Wavelet Transform and Active Contours. / Celik T., Kai-Kuang Ma. // IEEE Transactions on Geoscience and Remote Sensing. - 2011. - Vol. 49, No. 2. - P. 706-716.

J99. Kudeki E. Incoherent Scatter Spectral Theories-Part I: A General Framework and Results for Small Magnetic Aspect Angles. / Kudeki E., Milla M.A. // IEEE Transactions on Geoscience and Remote Sensing. - 2011. - Vol. 49, No. 1. - P. 315-328.

J100. Wang W. Radio frequency interference cancellation for sea-state remote sensing by high-frequency radar. / Wang W., Wyatt L.R. // IET Radar, Sonar & Navigation. - 2011. - Vol. 5, No. 4. - P. 405-415.

J101. Samsonov S. Polarization Phase Difference Analysis for Selection of Persistent Scatterers in SAR Interferometry. / Samsonov S., Tiampo K. // IEEE Geoscience and Remote Sensing Letters. - 2011. - Vol. 8, No. 2. - P. 331-335.

J102. Brown C.G. Model-Based Estimation of Forest Canopy Height in Red and Austrian Pine Stands Using Shuttle Radar Topography Mission and Ancillary Data: A Proof-of-Concept Study. / Brown C.G., Sarabandi K., Pierce L.E. // IEEE Transactions on Geoscience and Remote Sensing. - 2010. - Vol. 48, No. 3. - P. 1105-1118.

J103. Carfantan H. Statistical Linear Destriping of Satellite-Based Pushbroom-Type Images. / Carfantan H., Idier J. // IEEE Transactions on Geoscience and Remote Sensing. - 2010. - Vol. 48, No. 4. - P. 1860-1871.

J104. Suri S. Mutual-Information-Based Registration of TerraSAR-X and Ikonos Imagery in Urban Areas. / Suri S., Reinartz P. // IEEE Transactions on Geoscience and Remote Sensing. - 2010. - Vol. 48, No. 2. - P. 939-949.

J105. Wong A. IceSynth II: Synthesis of SAR Sea-Ice Imagery Using Region-Based Posterior Sampling. / Wong A., Yu P., Wen Zhang, Clausi D.A. // IEEE Geoscience and Remote Sensing Letters. - 2010. - Vol. 7, No. 2. - P. 348-351.

J106. Shrestha K.Y. Performance Metrics for Single-Photon Laser Ranging. / Shrestha K.Y., Slatton K.C., Carter W.E., Cossio T.K. // IEEE Geoscience and Remote Sensing Letters. - 2010. - Vol. 7, No. 2. - P. 338-342.

J107. Cacciamano A. Contrast-Optimization-Based Range-Profile Autofocus for Polarimetric Stepped-Frequency Radar. / Cacciamano A., Giusti E., Capria A., Martorella M., Berizzi F. // IEEE Transactions on Geoscience and Remote Sensing. - 2010. - Vol. 48, No. 4. - P. 2049-2056.

J108. Saha S. Application of a Multiseed-Based Clustering Technique for Automatic Satellite Image Segmentation. / Saha S., Bandyopadhyay S. // IEEE Geoscience and Remote Sensing Letters. - 2010. - Vol. 7, No. 2. - P. 306-308.

J109. Steinbrecher U. TerraSAR-X Instrument Operations Rooted in the System Engineering and Calibration Project. / Steinbrecher U., Schulze D., Boer J., Mittermayer J. // IEEE Transactions on Geoscience and Remote Sensing. - 2010. - Vol. 48, No. 2. - P. 633-641.

J110. Gherboudj I. A Backscatter Modeling for River Ice: Analysis and Numerical Results. / Gherboudj I., Bernier M., Leconte R. // IEEE Transactions on Geoscience and Remote Sensing. - 2010. - Vol. 48, No. 4. - P. 1788-1798.

J111. Wang R. Focus FMCW SAR Data Using the Wavenumber Domain Algorithm. / Wang R., Loffeld O., Nies H., Knedlik S., Hagelen M., Essen H. // IEEE Transactions on Geoscience and Remote Sensing. - 2010. - Vol. 48, No. 4. - P. 2109-2118.

J112. Schwerdt M. Final TerraSAR-X Calibration Results Based on Novel Efficient Methods. / Schwerdt M., Brautigam B., Bachmann M., Doring B., Schrank D., Hueso Gonzalez J. // IEEE Transactions on Geoscience and Remote Sensing. - 2010. - Vol. 48, No. 2. - P. 677-689.

J113. Shimada M. Advanced Land Observing Satellite (ALOS) and Monitoring Global Environmental Change. / Shimada M., Tadono T., Rosenqvist A. // Proceedings of the IEEE. - 2010. - Vol. 98, No. 5. - P. 780-799.

J114. Bretar F. Terrain Modeling From Lidar Range Data in Natural Landscapes: A Predictive and Bayesian Framework. / Bretar F., Chehata N. // IEEE Transactions on Geoscience and Remote Sensing. - 2010. - Vol. 48, No. 3. - P. 1568-1578.

J115. Ying Luo. Micro-Doppler Effect Analysis and Feature Extraction in ISAR Imaging With Stepped-Frequency Chirp Signals. / Ying Luo, Qun Zhang, Cheng-wei Qiu, Xian-jiao Liang, Kai-ming Li. // IEEE Transactions on Geoscience and Remote Sensing. - 2010. - Vol. 48, No. 4. - P. 2087-2098.

J116. Junfeng Wang. Automatic Correction of Range Migration in SAR Imaging. / Junfeng Wang, Xingzhao Liu. // IEEE Geoscience and Remote Sensing Letters. - 2010. - Vol. 7, No. 2. - P. 256-260.

J117. Gabele M. Fore and Aft Channel Reconstruction in the TerraSAR-X Dual Receive Antenna Mode. / Gabele M., Brautigam B., Schulze D., Steinbrecher U., Tous-Ramon N., Younis M. // IEEE Transactions on Geoscience and Remote Sensing. - 2010. - Vol. 48, No. 2. - P. 795-806.

J118. Xiaoming Li. Investigation of Ocean Surface Wave Refraction Using TerraSAR-X Data. / Xiaoming Li, Lehner S., Rosenthal W. // IEEE Transactions on Geoscience and Remote Sensing. - 2010. - Vol. 48, No. 2. - P. 830-840.

J119. Fangyuan Nan. Reconstruction of GPR Signals by Spectral Analysis of the SVD Components of the Data Matrix. / Fangyuan Nan, Siyong Zhou, Yaonan Wang, Fuhai Li, Weifeng Yang. // IEEE Geoscience and Remote Sensing Letters. - 2010. - Vol. 7, No. 1. - P. 200-204.

J120. Knospe S. Covariance Estimation for dInSAR Surface Deformation Measurements in the Presence of Anisotropic Atmospheric Noise. / Knospe S., Jonsson S. // IEEE Transactions on Geoscience and Remote Sensing. - 2010. - Vol. 48, No. 4. - P. 2057-2065.

J121. Maurer E. TerraSAR-X Mission Planning System: Automated Command Generation for Spacecraft Operations. / Maurer E., Mrowka F., Braun A., Geyer M.P., Lenzen C., Wasser Y., Wickler M. // IEEE Transactions on Geoscience and Remote Sensing. - 2010. - Vol. 48, No. 2. - P. 642-648.

J122. Heygster G. Topographic Mapping of the German Tidal Flats Analyzing SAR Images With the Waterline Method. / Heygster G., Dannenberg J., Notholt J. // IEEE Transactions on Geoscience and Remote Sensing. - 2010. - Vol. 48, No. 3. - P. 1019-1030.

J123. Hai Li. An Estimation Method for InSAR Interferometric Phase Based on MMSE Criterion. / Hai Li, Guisheng Liao. // IEEE Transactions on Geoscience and Remote Sensing. - 2010. - Vol. 48, No. 3. - P. 1457-1469.

J124. Carretero-Moya J. Statistical Analysis of a High-Resolution Sea-Clutter Database. / Carretero-Moya J., Gismero-Menoyo J., Blanco-del-Campo A., Asensio-Lopez A. // IEEE Transactions on Geoscience and Remote Sensing. - 2010. - Vol. 48, No. 4. - P. 2024-2037.

J125. Durand M. Estimating River Depth From Remote Sensing Swath Interferometry Measurements of River Height, Slope, and Width. / Durand M., Rodriguez E., Alsdorf D.E., Trigg M. // IEEE Journal of Selected Topics in Applied Earth Observations and Remote Sensing. - 2010. - Vol. 3, No. 1. - P. 20-31.

J126. Soloviev A. Sonar Measurements in Ship Wakes Simultaneous With TerraSAR-X Overpasses. / Soloviev A., Gilman M., Young K., Brusch S., Lehner S. // IEEE Transactions on Geoscience and Remote Sensing. - 2010. - Vol. 48, No. 2. - P. 841-851.

J127. Werninghaus R. The TerraSAR-X Mission and System Design. / Werninghaus R., Buckreuss S. // IEEE Transactions on Geoscience and Remote Sensing. - 2010. - Vol. 48, No. 2. - P. 606-614.

J128. Liangbing Chen. One-Dimensional Mirrored Interferometric Aperture Synthesis. / Liangbing Chen, Qingxia Li, Wei Guo, Yaoting Zhu. // IEEE Geoscience and Remote Sensing Letters. - 2010. - Vol. 7, No. 2. - P. 357-361.

J129. Margarit G. Polarimetric Characterization and Temporal Stability Analysis of Urban Target Scattering. / Margarit G., Mallorqui J.J., Pipia L. // IEEE Transactions on Geoscience and Remote Sensing. - 2010. - Vol. 48, No. 4. - P. 2038-2048.

J130. D'Aria D. SAR Calibration Aided by Permanent Scatterers. / D'Aria D., Ferretti A., Guarnieri A.M., Tebaldini S. // IEEE Transactions on Geoscience and Remote Sensing. - 2010. - Vol. 48, No. 4. - P. 2076-2086.

J131. Balss U. Noise-Related Radiometric Correction in the TerraSAR-X Multimode SAR Processor. / Balss U., Breit H., Fritz T. // IEEE Transactions on Geoscience and Remote Sensing. - 2010. - Vol. 48, No. 2. - P. 741-750.

J132. Yong Bian. PolInSAR Statistical Analysis and Coherence Optimization Using Fractional Lower Order Statistics. / Yong Bian, Mercer B. // IEEE Geoscience and Remote Sensing Letters. - 2010. - Vol. 7, No. 2. - P. 314-318.

J133. Monsivais-Huertero A. Multipolarization Microwave Scattering Model for Sahelian Grassland. / Monsivais-Huertero A., Sarabandi K., Chenerie I. // IEEE Transactions on Geoscience and Remote Sensing. - 2010. - Vol. 48, No. 3. - P. 1416-1432.

J134. Wentao An. Fast Alternatives to for Polarimetric SAR. / Wentao An, Yi Cui, Jiang Yang, Hongji Zhang. // IEEE Geoscience and Remote Sensing Letters. - 2010. - Vol. 7, No. 2. - P. 343-347.

J135. Brunner D. Building Height Retrieval From VHR SAR Imagery Based on an Iterative Simulation and Matching Technique. / Brunner D., Lemoine G., Bruzzone L., Greidanus H. // IEEE Transactions on Geoscience and Remote Sensing. - 2010. - Vol. 48, No. 3. - P. 1487-1504.

J136. Petillot I. Radar-Coding and Geocoding Lookup Tables for the Fusion of GIS and SAR Data in Mountain Areas. / Petillot I., Trouve E., Bolon P., Julea A., Yajing Yan, Gay M., Vanpe J.-M. // IEEE Geoscience and Remote Sensing Letters. - 2010. - Vol. 7, No. 2. - P. 309-313.

J137. Fornaro G. 4-D SAR Imaging: The Case Study of Rome. / Fornaro G., Serafino F., Reale D. // IEEE Geoscience and Remote Sensing Letters. - 2010. - Vol. 7, No. 2. - P. 236-240.

J138. Baade J. Interferometric Microrelief Sensing With TerraSAR-X-First Results. / Baade J., Schmullius C.C. // IEEE Transactions on Geoscience and Remote Sensing. - 2010. - Vol. 48, No. 2. - P. 965-970.

J139. Cerutti-Maori D. Experimental Verification of SAR-GMTI Improvement Through Antenna Switching. / Cerutti-Maori D., Gierull C.H., Ender J.H.G. // IEEE Transactions on Geoscience and Remote Sensing. - 2010. - Vol. 48, No. 4. - P. 2066-2075.

J140. Seong-In Hwang. On a Novel Approach Using MLCC and CFAR for the Improvement of Ship Detection by Synthetic Aperture Radar. / Seong-In Hwang, Ouchi K. // IEEE Geoscience and Remote Sensing Letters. - 2010. - Vol. 7, No. 2. - P. 391-395.

J141. Yu Li. Segmentation of SAR Intensity Imagery With a Voronoi Tessellation, Bayesian Inference, and Reversible Jump MCMC Algorithm. / Yu Li, Li J., Chapman M.A. // IEEE Transactions on Geoscience and Remote Sensing. - 2010. - Vol. 48, No. 4. - P. 1872-1881.

J142. Tebaldini S. Single and Multipolarimetric SAR Tomography of Forested Areas: A Parametric Approach. IEEE Transactions on Geoscience and Remote Sensing. - 2010. - Vol. 48, No. 5. - P. 2375-2387.

J143. Mira M. Soil Moisture Effect on Thermal Infrared (8-13-µm) Emissivity. / Mira M., Valor E., Caselles V., Rubio E., Coll C., Galve J.M., Niclos R., Sanchez J.M., Boluda R. // IEEE Transactions on Geoscience and Remote Sensing. - 2010. - Vol. 48, No. 5. - P. 2251-2260.

J144. Esch T. Delineation of Urban Footprints From TerraSAR-X Data by Analyzing Speckle Characteristics and Intensity Information. / Esch T., Thiel M., Schenk A., Roth A., Muller A., Dech S. // IEEE Transactions on Geoscience and Remote Sensing. - 2010. - Vol. 48, No. 2. - P. 905-916.

J145. Anagnostou E.N. Benchmarking High-Resolution Global Satellite Rainfall Products to Radar and Rain-Gauge Rainfall Estimates. / Anagnostou E.N., Maggioni V., Nikolopoulos E.I., Meskele T., Hossain F., Papadopoulos A. // IEEE Transactions on Geoscience and Remote Sensing. - 2010. - Vol. 48, No. 4. - P. 1667-1683.

J146. Qisong Wu. Motion Parameter Estimation in the SAR System With Low PRF Sampling. / Qisong Wu, Mengdao Xing, Chengwei Qiu, Baochang Liu, Zheng Bao, Tat-Soon Yeo. // IEEE Geoscience and Remote Sensing Letters. - 2010. - Vol. 7, No. 3. - P. 450-454.

J147. Sugak V.G. Phase Spectrum of Signals in Ground-Penetrating Radar Applications. / Sugak V.G., Sugak A.V. // IEEE Transactions on Geoscience and Remote Sensing. - 2010. - Vol. 48, No. 4. - P. 1760-1767.

J148. Kidera S. Accurate UWB Radar Three-Dimensional Imaging Algorithm for a Complex Boundary Without Range Point Connections. / Kidera S., Sakamoto T., Sato T. // IEEE Transactions on Geoscience and Remote Sensing. - 2010. - Vol. 48, No. 4. - P. 1993-2004.

J149. Celik T. Change Detection in Satellite Images Using a Genetic Algorithm Approach. IEEE Geoscience and Remote Sensing Letters. - 2010. - Vol. 7, No. 2. - P. 386-390.

J150. Moreira A. Foreword to the Special Issue on TerraSAR-X: Mission, Calibration, and First Results. / Moreira A., Bamler R. // IEEE Transactions on Geoscience and Remote Sensing. - 2010. - Vol. 48, No. 2. - P. 603-604.

J151. Xueru Bai. Scaling the 3-D Image of Spinning Space Debris via Bistatic Inverse Synthetic Aperture Radar. / Xueru Bai, Feng Zhou, Mengdao Xing, Zheng Bao. // IEEE Geoscience and Remote Sensing Letters. - 2010. - Vol. 7, No. 3. - P. 430-434.

J152. Ram S.S. Simulation and Analysis of Human Micro-Dopplers in Through-Wall Environments. / Ram S.S., Christianson C., Youngwook Kim, Hao Ling. // IEEE Transactions on Geoscience and Remote Sensing. - 2010. - Vol. 48, No. 4. - P. 2015-2023.

J153. Pitz W. The TerraSAR-X Satellite. / Pitz W., Miller D. // IEEE Transactions on Geoscience and Remote Sensing. - 2010. - Vol. 48, No. 2. - P. 615-622.

J154. Marchant C.C. An Iterative Least Square Approach to Elastic-Lidar Retrievals for Well-Characterized Aerosols. / Marchant C.C., Moon T.K., Gunther J.H. // IEEE Transactions on Geoscience and Remote Sensing. - 2010. - Vol. 48, No. 5. - P. 2430-2444.

J155. Suchandt S. Automatic Extraction of Traffic Flows Using TerraSAR-X Along-Track Interferometry. / Suchandt S., Runge H., Breit H., Steinbrecher U., Kotenkov A., Balss U. // IEEE Transactions on Geoscience and Remote Sensing. - 2010. - Vol. 48, No. 2. - P. 807-819.

J156. Guang Qing Duan. Three-Dimensional Imaging via Wideband MIMO Radar System. / Guang Qing Duan,

Dang Wei Wang, Xiao Yan Ma, Yi Su. // IEEE Geoscience and Remote Sensing Letters. - 2010. - Vol. 7, No. 3. - P. 445-449.

J157. Sarmiento S.E. Spatial-Temporal Variability of Great Slave Lake Levels From Satellite Altimetry. / Sarmiento S.E., Khan S.D. // IEEE Geoscience and Remote Sensing Letters. - 2010. - Vol. 7, No. 3. - P. 426-429.

J158. Jorda G. Toward SMOS L4 SSS Products: Improving L3 SSS With Auxiliary SSS Data. / Jorda G., Gomis D. // IEEE Transactions on Geoscience and Remote Sensing. - 2010. - Vol. 48, No. 5. - P. 2204-2214.

J159. Yong Li. The Geometric-Distortion Correction Algorithm for Circular-Scanning SAR Imaging. / Yong Li, Daiyin Zhu. // IEEE Geoscience and Remote Sensing Letters. - 2010. - Vol. 7, No. 2. - P. 376-380.

J160. Bachmann M. TerraSAR-X Antenna Calibration and Monitoring Based on a Precise Antenna Model. / Bachmann M., Schwerdt M., Brautigam B. // IEEE Transactions on Geoscience and Remote Sensing. - 2010. - Vol. 48, No. 2. - P. 690-701.

J161. Anandan V.K. An Autonomous Interference Detection and Filtering Approach Applied to Wind Profilers. / Anandan V.K., Jagannatham D.B.V. // IEEE Transactions on Geoscience and Remote Sensing. - 2010. - Vol. 48, No. 4. - P. 1660-1666.

J162. Schubert A. Influence of Atmospheric Path Delay on the Absolute Geolocation Accuracy of TerraSAR-X High-Resolution Products. / Schubert A., Jehle M., Small D., Meier E. // IEEE Transactions on Geoscience and Remote Sensing. - 2010. - Vol. 48, No. 2. - P. 751-758.

J163. Marzano F.S. Evidence of Rainfall Signatures on X-Band Synthetic Aperture Radar Imagery Over Land. / Marzano F.S., Mori S., Weinman J.A. // IEEE Transactions on Geoscience and Remote Sensing. - 2010. - Vol. 48, No. 2. - P. 950-964.

J164. Kleynhans W. Improving Land Cover Class Separation Using an Extended Kalman Filter on MODIS NDVI Time-Series Data. / Kleynhans W., Olivier J.C., Wessels K.J., van den Bergh F., Salmon B.P., Steenkamp K.C. // IEEE Geoscience and Remote Sensing Letters. - 2010. - Vol. 7, No. 2. - P. 381-385.

J165. Gonzalez J.H. Development of the TanDEM-X Calibration Concept: Analysis of Systematic Errors. / Gonzalez J.H., Bachmann M., Krieger G., Fiedler H. // IEEE Transactions on Geoscience and Remote Sensing. - 2010. - Vol. 48, No. 2. - P. 716-726.

J166. Breit H. TerraSAR-X SAR Processing and Products. / Breit H., Fritz T., Balss U., Lachaise M., Niedermeier A., Vonavka M. // IEEE Transactions on Geoscience and Remote Sensing. - 2010. - Vol. 48, No. 2. - P. 727-740.

J167. Vasile G. Coherency Matrix Estimation of Heterogeneous Clutter in High-Resolution Polarimetric SAR Images. / Vasile G., Ovarlez J.-P., Pascal F., Tison C. // IEEE Transactions on Geoscience and Remote Sensing. - 2010. - Vol. 48, No. 4. - P. 1809-1826.

J168. Lopez-Dekker P. Capon- and APES-Based SAR Processing: Performance and Practical Considerations. / Lopez-Dekker P., Mallorqui J.J. // IEEE Transactions on Geoscience and Remote Sensing. - 2010. - Vol. 48, No. 5. - P. 2388-2402.

J169. Go. Modeling Envisat RA-2 Waveforms in the Coastal Zone: Case Study of Calm Water Contamination. / Go,mez-Enri J., Vignudelli S., Quartly G.D., Gommenginger C.P., Cipollini P., Challenor P.G., Benveniste J. // IEEE Geoscience and Remote Sensing Letters. - 2010. - Vol. 7, No. 3. - P. 474-478.

J170. Raggam H. Assessment of the Stereo-Radargrammetric Mapping Potential of TerraSAR-X Multibeam Spotlight Data. / Raggam H., Gutjahr K., Perko R., Schardt M. // IEEE Transactions on Geoscience and Remote Sensing. - 2010. - Vol. 48, No. 2. - P. 971-977.

J171. Gang Chen. HF Radio-Frequency Interference Mitigation. / Gang Chen, Zhengyu Zhao, Guoqiang Zhu, Yujie Huang, Ting Li. // IEEE Geoscience and Remote Sensing Letters. - 2010. - Vol. 7, No. 3. - P. 479-482.

J172. Nezirovic A. Signal Processing for Improved Detection of Trapped Victims Using UWB Radar. / Nezirovic A., Yarovoy A.G., Ligthart L.P. // IEEE Transactions on Geoscience and Remote Sensing. - 2010. - Vol. 48, No.

4. - P. 2005-2014.

J173. Santoro M. Signatures of ERS-Envisat Interferometric SAR Coherence and Phase of Short Vegetation: An Analysis in the Case of Maize Fields. / Santoro M., Wegmuller U., Askne J.I.H. // IEEE Transactions on Geoscience and Remote Sensing. - 2010. - Vol. 48, No. 4. - P. 1702-1713.

J174. Hosoi F. Estimation and Error Analysis of Woody Canopy Leaf Area Density Profiles Using 3-D Airborne and Ground-Based Scanning Lidar Remote-Sensing Techniques. / Hosoi F., Nakai Y., Omasa K. // IEEE Transactions on Geoscience and Remote Sensing. - 2010. - Vol. 48, No. 5. - P. 2215-2223.

J175. Kaasalainen S. Effect of Target Moisture on Laser Scanner Intensity. / Kaasalainen S., Niittymaki H., Krooks A., Koch K., Kaartinen H., Vain A., Hyyppa H. // IEEE Transactions on Geoscience and Remote Sensing. - 2010. - Vol. 48, No. 4. - P. 2128-2136.

J176. Zribi M. Numerical Backscattering Analysis for Rough Surfaces Including a Cloddy Structure. / Zribi M., Le Morvan-Quemener A., Dechambre M., Baghdadi N. // IEEE Transactions on Geoscience and Remote Sensing. - 2010. - Vol. 48, No. 5. - P. 2367-2374.

J177. Duk-jin Kim. Application of TerraSAR-X Data for Emergent Oil-Spill Monitoring. / Duk-jin Kim, Moon W.M., Youn-Soo Kim. // IEEE Transactions on Geoscience and Remote Sensing. - 2010. - Vol. 48, No. 2. - P. 852-863.

J178. Chini M. The May 12, 2008, (Mw 7.9) Sichuan Earthquake (China): Multiframe ALOS-PALSAR DInSAR Analysis of Coseismic Deformation. / Chini M., Atzori S., Trasatti E., Bignami C., Kyriakopoulos C., Tolomei C., Stramondo S. // IEEE Geoscience and Remote Sensing Letters. - 2010. - Vol. 7, No. 2. - P. 266-270.

J179. Rivas M.B. Bistatic Scattering of GPS Signals Off Arctic Sea Ice. / Rivas M.B., Maslanik J.A., Axelrad P. // IEEE Transactions on Geoscience and Remote Sensing. - 2010. - Vol. 48, No. 3. - P. 1548-1553.

J180. Kefeng Yang. A Two-Dimensional Spectrum for General Bistatic SAR Processing. / Kefeng Yang, Feng He, Diannong Liang. // IEEE Geoscience and Remote Sensing Letters. - 2010. - Vol. 7, No. 1. - P. 108-112.

J181. Feng Zhu. ISAR Imaging for Avian Species Identification With Frequency-Stepped Chirp Signals. / Feng Zhu, Ying Luo, Qun Zhang, You-Qian Feng, You-Qing Bai. // IEEE Geoscience and Remote Sensing Letters. - 2010. - Vol. 7, No. 1. - P. 151-155.

J182. Yuekui Yang. Uncertainties in Ice-Sheet Altimetry From a Spaceborne 1064-nm Single-Channel Lidar Due to Undetected Thin Clouds. / Yuekui Yang, Marshak A., Varnai T., Wiscombe W., Ping Yang. // IEEE Transactions on Geoscience and Remote Sensing. - 2010. - Vol. 48, No. 1. - P. 250-259.

J183. Bytheway J.L. A Physically Based Screen for Precipitation Over Complex Surfaces Using Passive Microwave Observations. / Bytheway J.L., Kummerow C.D. // IEEE Transactions on Geoscience and Remote Sensing. - 2010. - Vol. 48, No. 1. - P. 299-313.

J184. Habib A. Alternative Methodologies for the Internal Quality Control of Parallel LiDAR Strips. / Habib A., Kersting A.P., Ki In Bang, Dong-Cheon Lee. // IEEE Transactions on Geoscience and Remote Sensing. - 2010. - Vol. 48, No. 1. - P. 221-236.

J185. Marzano F.S. Monitoring Subglacial Volcanic Eruption Using Ground-Based C-Band Radar Imagery. / Marzano F.S., Barbieri S., Picciotti E., Karlsdottir S. // IEEE Transactions on Geoscience and Remote Sensing. - 2010. - Vol. 48, No. 1. - P. 403-414.

J186. Tanase M.A. TerraSAR-X Data for Burn Severity Evaluation in Mediterranean Forests on Sloped Terrain. / Tanase M.A., Perez-Cabello F., de la Riva J., Santoro M. // IEEE Transactions on Geoscience and Remote Sensing. - 2010. - Vol. 48, No. 2. - P. 917-929.

J187. Guarnieri A.M. ML-Based Fringe-Frequency Estimation for InSAR. / Guarnieri A.M., Tebaldini S. // IEEE Geoscience and Remote Sensing Letters. - 2010. - Vol. 7, No. 1. - P. 136-140.

J188. Teng Wang. InSAR Coherence-Decomposition Analysis. / Teng Wang, Mingsheng Liao, Perissin D. // IEEE Geoscience and Remote Sensing Letters. - 2010. - Vol. 7, No. 1. - P. 156-160.

J189. Prats P. Processing of Sliding Spotlight and TOPS SAR Data Using Baseband Azimuth Scaling. / Prats P., Scheiber R., Mittermayer J., Meta A., Moreira A. // IEEE Transactions on Geoscience and Remote Sensing. - 2010. - Vol. 48, No. 2. - P. 770-780.

J190. Wang R. Focusing Bistatic SAR Data in Airborne/Stationary Configuration. / Wang R., Loffeld O., Neo Y.L., Nies H., Walterscheid I., Espeter T., Klare J., Ender J. // IEEE Transactions on Geoscience and Remote Sensing. - 2010. - Vol. 48, No. 1. - P. 452-465.

J191. Pedros R. Climatology of the Aerosol Extinction-to-Backscatter Ratio from Sun-Photometric Measurements. / Pedros R., Estelles V., Sicard M., Gomez-Amo J.L., Utrillas M.P., Martinez-Lozano J.A., Rocadenbosch F., Perez C., Recio J.M.B. // IEEE Transactions on Geoscience and Remote Sensing. - 2010. - Vol. 48, No. 1. - P. 237-249.

J192. Shengqi Zhu. A New Slant-Range Velocity Ambiguity Resolving Approach of Fast Moving Targets for SAR System. / Shengqi Zhu, Guisheng Liao, Yi Qu, Xiangyang Liu, Zhengguang Zhou. // IEEE Transactions on Geoscience and Remote Sensing. - 2010. - Vol. 48, No. 1. - P. 432-451.

J193. Lo Monte L. Radio Frequency Tomography for Tunnel Detection. / Lo Monte L., Erricolo D., Soldovieri F., Wicks M.C. // IEEE Transactions on Geoscience and Remote Sensing. - 2010. - Vol. 48, No. 3. - P. 1128-1137.

J194. Verspeek J. Validation and Calibration of ASCAT Using CMOD5.n. / Verspeek J., Stoffelen A., Portabella M., Bonekamp H., Anderson C., Saldana J.F. // IEEE Transactions on Geoscience and Remote Sensing. - 2010. - Vol. 48, No. 1. - P. 386-395.

J195. Huaping Xu. Equivalence Analysis of Accuracy of Geolocation Models for Spaceborne InSAR. / Huaping Xu, Changhui Kang. // IEEE Transactions on Geoscience and Remote Sensing. - 2010. - Vol. 48, No. 1. - P. 480-490.

J196. Shkvarko Y.V. Unifying Experiment Design and Convex Regularization Techniques for Enhanced Imaging With Uncertain Remote Sensing Data-Part II: Adaptive Implementation and Performance Issues. IEEE Transactions on Geoscience and Remote Sensing. - 2010. - Vol. 48, No. 1. - P. 96-111.

J197. Shkvarko Y.V. Unifying Experiment Design and Convex Regularization Techniques for Enhanced Imaging With Uncertain Remote Sensing Data-Part I: Theory. IEEE Transactions on Geoscience and Remote Sensing. - 2010. - Vol. 48, No. 1. - P. 82-95.

J198. Ballester-Berman J.D. Applying the Freeman-Durden Decomposition Concept to Polarimetric SAR Interferometry. / Ballester-Berman J.D., Lopez-Sanchez J.M. // IEEE Transactions on Geoscience and Remote Sensing. - 2010. - Vol. 48, No. 1. - P. 466-479.

J199. Soccorsi M. Huber-Markov Model for Complex SAR Image Restoration. / Soccorsi M., Gleich D., Datcu M. // IEEE Geoscience and Remote Sensing Letters. - 2010. - Vol. 7, No. 1. - P. 63-67.

J200. Nascimento A.D.C. Hypothesis Testing in Speckled Data With Stochastic Distances. / Nascimento A.D.C., Cintra R.J., Frery A.C. // IEEE Transactions on Geoscience and Remote Sensing. - 2010. - Vol. 48, No. 1. - P. 373-385.

J201. Hedman K. Road Network Extraction in VHR SAR Images of Urban and Suburban Areas by Means of Class-Aided Feature-Level Fusion. / Hedman K., Stilla U., Lisini G., Gamba P. // IEEE Transactions on Geoscience and Remote Sensing. - 2010. - Vol. 48, No. 3. - P. 1294-1296.

J202. Thiele A. Analysis of Gable-Roofed Building Signature in Multiaspect InSAR Data. / Thiele A., Cadario E., Schulz K., Soergel U. // IEEE Geoscience and Remote Sensing Letters. - 2010. - Vol. 7, No. 1. - P. 83-87.

J203. Molina D.E. Gibbs Random Field Models for Model-Based Despeckling of SAR Images. / Molina D.E., Gleich D., Datcu M. // IEEE Geoscience and Remote Sensing Letters. - 2010. - Vol. 7, No. 1. - P. 73-77.

J204. Gleich D. Despeckling of TerraSAR-X Data Using Second-Generation Wavelets. / Gleich D., Kseneman M., Datcu M. // IEEE Geoscience and Remote Sensing Letters. - 2010. - Vol. 7, No. 1. - P. 68-72.

J205. McPherson C.J. Analysis of Optical Properties of Saharan Dust Derived From Dual-Wavelength Aerosol

Retrievals From CALIPSO Observations. / McPherson C.J., Reagan J.A. // IEEE Geoscience and Remote Sensing Letters. - 2010. - Vol. 7, No. 1. - P. 98-102.

J206. Chaabouni-Chouayakh H. Coarse-to-Fine Approach for Urban Area Interpretation Using TerraSAR-X Data. / Chaabouni-Chouayakh H., Datcu M. // IEEE Geoscience and Remote Sensing Letters. - 2010. - Vol. 7, No. 1. - P. 78-82.

J207. Sang-Hoon Hong. Evaluation of TerraSAR-X Observations for Wetland InSAR Application. / Sang-Hoon Hong, Wdowinski S., Sang-Wan Kim. // IEEE Transactions on Geoscience and Remote Sensing. - 2010. - Vol. 48, No. 2. - P. 864-873.

J208. Lianlin Li. Derivation and Discussion of the SAR Migration Algorithm Within Inverse Scattering Problem: Theoretical Analysis. / Lianlin Li, Wenji Zhang, Fang Li. // IEEE Transactions on Geoscience and Remote Sensing. - 2010. - Vol. 48, No. 1. - P. 415-422.

J209. Ersahin K. Segmentation and Classification of Polarimetric SAR Data Using Spectral Graph Partitioning. / Ersahin K., Cumming I.G., Ward R.K. // IEEE Transactions on Geoscience and Remote Sensing. - 2010. - Vol. 48, No. 1. - P. 164-174.

J210. Frankford M.T. Compensation of Faraday Rotation in Multipolarization Scatterometry. / Frankford M.T., Johnson J.T. // IEEE Transactions on Geoscience and Remote Sensing. - 2010. - Vol. 48, No. 1. - P. 358-364.

J211. Koskinen J.T. Monitoring of Snow-Cover Properties During the Spring Melting Period in Forested Areas. / Koskinen J.T., Pulliainen J.T., Luojus K.P., Takala M. // IEEE Transactions on Geoscience and Remote Sensing. - 2010. - Vol. 48, No. 1. - P. 50-58.

J212. Auer S. Ray-Tracing Simulation Techniques for Understanding High-Resolution SAR Images. / Auer S., Hinz S., Bamler R. // IEEE Transactions on Geoscience and Remote Sensing. - 2010. - Vol. 48, No. 3. - P. 1445-1456.

J213. Dawei Liu. Three-Dimensional Coherent Radar Backscatter Model and Simulations of Scattering Phase Center of Forest Canopies. / Dawei Liu, Guoqing Sun, Zhifeng Guo, Ranson K.J., Yang Du. // IEEE Transactions on Geoscience and Remote Sensing. - 2010. - Vol. 48, No. 1. - P. 349-357.

J214. Lianlin Li. A Novel Autofocusing Approach for Real-Time Through-Wall Imaging Under Unknown Wall Characteristics. / Lianlin Li, Wenji Zhang, Fang Li. // IEEE Transactions on Geoscience and Remote Sensing. - 2010. - Vol. 48, No. 1. - P. 423-431.

J215. Wenge Zhang. SAR Image Despeckling Using Edge Detection and Feature Clustering in Bandelet Domain. / Wenge Zhang, Fang Liu, Licheng Jiao, Biao Hou, Shuang Wang, Ronghua Shang. // IEEE Geoscience and Remote Sensing Letters. - 2010. - Vol. 7, No. 1. - P. 131-135.

J216. Pasolli E. Gaussian Process Approach to Buried Object Size Estimation in GPR Images. / Pasolli E., Melgani F., Donelli M. // IEEE Geoscience and Remote Sensing Letters. - 2010. - Vol. 7, No. 1. - P. 141-145.

J217. Dufva T. Scattering Model for a Pine Tree Employing VIE With a Broadband MLFMA and Comparison to ICA. / Dufva T., Praks J., Jarvenpaa S., Sarvas J. // IEEE Transactions on Geoscience and Remote Sensing. - 2010. - Vol. 48, No. 3. - P. 1119-1127.

J218. Yong Wang. ISAR Imaging of Maneuvering Target Based on the L-Class of Fourth-Order Complex-Lag PWVD. / Yong Wang, Yicheng Jiang. // IEEE Transactions on Geoscience and Remote Sensing. - 2010. - Vol. 48, No. 3. - P. 1518-1527.

J219. Buckreuss S. The TerraSAR-X Ground Segment. / Buckreuss S., Schattler B. // IEEE Transactions on Geoscience and Remote Sensing. - 2010. - Vol. 48, No. 2. - P. 623-632.

J220. Yeary M.B. Working Together for Better Student Learning: A Multi-University, Multi-Federal Partner Program for Asynchronous Learning Module Development for Radar-Based Remote Sensing Systems. / Yeary M.B., Yu T., Palmer R.D., Monroy H., Ruin I., Zhang G., Chilson P.B., Biggerstaff M.I., Weiss C., Mitchell K.A., Fink L.D. // IEEE Transactions on Education. - 2010. - Vol. 53, No. 3. - P. 504-515.

J221. Brautigam B. TerraSAR-X Instrument Calibration Results and Extension for TanDEM-X. / Brautigam B.,

Gonzalez J.H., Schwerdt M., Bachmann M. // IEEE Transactions on Geoscience and Remote Sensing. - 2010. - Vol. 48, No. 2. - P. 702-715.

J222. Neumann M. Estimation of Forest Structure, Ground, and Canopy Layer Characteristics From Multibaseline Polarimetric Interferometric SAR Data. / Neumann M., Ferro-Famil L., Reigber A. // IEEE Transactions on Geoscience and Remote Sensing. - 2010. - Vol. 48, No. 3. - P. 1086-1104.

J223. Rodriguez-Cassola M. Bistatic TerraSAR-X/F-SAR Spaceborne-Airborne SAR Experiment: Description, Data Processing, and Results. / Rodriguez-Cassola M., Baumgartner S.V., Krieger G., Moreira A. // IEEE Transactions on Geoscience and Remote Sensing. - 2010. - Vol. 48, No. 2. - P. 781-794.

J224. Navarro-Sanchez V.D. A Contribution of Polarimetry to Satellite Differential SAR Interferometry: Increasing the Number of Pixel Candidates. / Navarro-Sanchez V.D., Lopez-Sanchez J.M., Vicente-Guijalba F. // IEEE Geoscience and Remote Sensing Letters. - 2010. - Vol. 7, No. 2. - P. 276-280.

J225. Minet J. Soil Surface Water Content Estimation by Full-Waveform GPR Signal Inversion in the Presence of Thin Layers. / Minet J., Lambot S., Slob E.C., Vanclooster M. // IEEE Transactions on Geoscience and Remote Sensing. - 2010. - Vol. 48, No. 3. - P. 1138-1150.

J226. Sang-Hong Park. Segmentation of ISAR Images of Targets Moving in Formation. / Sang-Hong Park, Hyo-Tae Kim, Kyung-Tae Kim. // IEEE Transactions on Geoscience and Remote Sensing. - 2010. - Vol. 48, No. 4. - P. 2099-2108.

J227. Samczynski P. Coherent MapDrift Technique. / Samczynski P., Kulpa K.S. // IEEE Transactions on Geoscience and Remote Sensing. - 2010. - Vol. 48, No. 3. - P. 1505-1517.

J228. Dierking W. Mapping of Different Sea Ice Regimes Using Images From Sentinel-1 and ALOS Synthetic Aperture Radar. IEEE Transactions on Geoscience and Remote Sensing. - 2010. - Vol. 48, No. 3. - P. 1045-1058.

J229. Raucoules D. Assessing Ionospheric Influence on L-Band SAR Data: Implications on Coseismic Displacement Measurements of the 2008 Sichuan Earthquake. / Raucoules D., de Michele M. // IEEE Geoscience and Remote Sensing Letters. - 2010. - Vol. 7, No. 2. - P. 286-290.

J230. Viet Thuy Vu. Ultrawideband Chirp Scaling Algorithm. / Viet Thuy Vu, Sjogren T.K., Pettersson M.I. // IEEE Geoscience and Remote Sensing Letters. - 2010. - Vol. 7, No. 2. - P. 281-285.

J231. Wegmuller U. Nonuniform Ground Motion Monitoring With TerraSAR-X Persistent Scatterer Interferometry. / Wegmuller U., Walter D., Spreckels V., Werner C.L. // IEEE Transactions on Geoscience and Remote Sensing. - 2010. - Vol. 48, No. 2. - P. 895-904.

J232. Xiaolan Qiu. A Bistatic SAR Raw Data Simulator Based on Inverse Algorithm. / Xiaolan Qiu, Donghui Hu, Liangjiang Zhou, Chibiao Ding. // IEEE Transactions on Geoscience and Remote Sensing. - 2010. - Vol. 48, No. 3. - P. 1540-1547.

J233. Garestier F. Forest Modeling For Height Inversion Using Single-Baseline InSAR/Pol-InSAR Data. / Garestier F., Le Toan T. // IEEE Transactions on Geoscience and Remote Sensing. - 2010. - Vol. 48, No. 3. - P. 1528-1539.

J234. Laird C.M. Deep Ice Stratigraphy and Basal Conditions in Central West Antarctica Revealed by Coherent Radar. / Laird C.M., Blake W.A., Matsuoka K., Conway H., Allen C.T., Leuschen C.J., Gogineni S. // IEEE Geoscience and Remote Sensing Letters. - 2010. - Vol. 7, No. 2. - P. 246-250.

J235. Sampath A. Segmentation and Reconstruction of Polyhedral Building Roofs From Aerial Lidar Point Clouds. / Sampath A., Jie Shan. // IEEE Transactions on Geoscience and Remote Sensing. - 2010. - Vol. 48, No. 3. - P. 1554-1567.

J236. Willatt R.C. Field Investigations of Ku-Band Radar Penetration Into Snow Cover on Antarctic Sea Ice. / Willatt R.C., Giles K.A., Laxon S.W., Stone-Drake L., Worby A.P. // IEEE Transactions on Geoscience and Remote Sensing. - 2010. - Vol. 48, No. 1. - P. 365-372.

J237. Qiong Huang. UWB Through-Wall Imaging Based on Compressive Sensing. / Qiong Huang, Lele Qu,

Bingheng Wu, Guangyou Fang. // IEEE Transactions on Geoscience and Remote Sensing. - 2010. - Vol. 48, No. 3. - P. 1408-1415.

J238. Anguela T.P. Analysis of Local Variation of Soil Surface Parameters With TerraSAR-X Radar Data Over Bare Agricultural Fields. / Anguela T.P., Zribi M., Baghdadi N., Loumagne C. // IEEE Transactions on Geoscience and Remote Sensing. - 2010. - Vol. 48, No. 2. - P. 874-881.

J239. Mittermayer J. TerraSAR-X System Performance Characterization and Verification. / Mittermayer J., Younis M., Metzig R., Wollstadt S., Martinez J.M., Meta A. // IEEE Transactions on Geoscience and Remote Sensing. - 2010. - Vol. 48, No. 2. - P. 660-676.

J240. Changzhan Gu. Instrument-Based Noncontact Doppler Radar Vital Sign Detection System Using Heterodyne Digital Quadrature Demodulation Architecture. / Changzhan Gu, Changzhi Li, Jenshan Lin, Jiang Long, Jiangtao Huangfu, Lixin Ran. // IEEE Transactions on Instrumentation and Measurement. - 2010. - Vol. 59, No. 6. - P. 1580-1588.

J241. Meta A. TOPS Imaging With TerraSAR-X: Mode Design and Performance Analysis. / Meta A., Mittermayer J., Prats P., Scheiber R., Steinbrecher U. // IEEE Transactions on Geoscience and Remote Sensing. - 2010. - Vol. 48, No. 2. - P. 759-769.

J242. Munoz-Ferreras J.M. On the Doppler Spreading Effect for the Range-Instantaneous-Doppler Technique in Inverse Synthetic Aperture Radar Imagery. / Munoz-Ferreras J.M., Perez-Martinez F. // IEEE Geoscience and Remote Sensing Letters. - 2010. - Vol. 7, No. 1. - P. 180-184.

J243. Mason D.C. Flood Detection in Urban Areas Using TerraSAR-X. / Mason D.C., Speck R., Devereux B., Schumann G.J.-P., Neal J.C., Bates P.D. // IEEE Transactions on Geoscience and Remote Sensing. - 2010. - Vol. 48, No. 2. - P. 882-894.

J244. Mittermayer J. TerraSAR-X Commissioning Phase Execution Summary. / Mittermayer J., Schattler B., Younis M. // IEEE Transactions on Geoscience and Remote Sensing. - 2010. - Vol. 48, No. 2. - P. 649-659.

J245. Guarnieri A.M. Efficient Wavenumber Domain Focusing for Ground-Based SAR. / Guarnieri A.M., Scirpoli S. // IEEE Geoscience and Remote Sensing Letters. - 2010. - Vol. 7, No. 1. - P. 161-165.

J246. Josset D. Multi-Instrument Calibration Method Based on a Multiwavelength Ocean Surface Model. / Josset D., Pelon J., Yongxiang Hu. // IEEE Geoscience and Remote Sensing Letters. - 2010. - Vol. 7, No. 1. - P. 195-199.

J247. Yinghua Wang. PolSAR Data Segmentation by Combining Tensor Space Cluster Analysis and Markovian Framework. / Yinghua Wang, Chongzhao Han, Tupin F. // IEEE Geoscience and Remote Sensing Letters. - 2010. - Vol. 7, No. 1. - P. 210-214.

J248. Romeiser R. First Analysis of TerraSAR-X Along-Track InSAR-Derived Current Fields. / Romeiser R., Suchandt S., Runge H., Steinbrecher U., Grunler S. // IEEE Transactions on Geoscience and Remote Sensing. - 2010. - Vol. 48, No. 2. - P. 820-829.

J249. Serafino F. A Novel Strategy for the Surface Current Determination From Marine X-Band Radar Data. / Serafino F., Lugni C., Soldovieri F. // IEEE Geoscience and Remote Sensing Letters. - 2010. - Vol. 7, No. 2. - P. 231-235.

J250. Pan Cao. Minimum Entropy via Subspace for ISAR Autofocus. / Pan Cao, Mengdao Xing, Guangcai Sun, Yachao Li, Zheng Bao. // IEEE Geoscience and Remote Sensing Letters. - 2010. - Vol. 7, No. 1. - P. 205-209.

J251. Guida R. Assessment of TerraSAR-X Products with a New Feature Extraction Application: Monitoring of Cylindrical Tanks. / Guida R., Iodice A., Riccio D. // IEEE Transactions on Geoscience and Remote Sensing. - 2010. - Vol. 48, No. 2. - P. 930-938.

J252. Atzeni C. Remote Survey of the Leaning Tower of Pisa by Interferometric Sensing. / Atzeni C., Bicci A., Dei D., Fratini M., Pieraccini M. // IEEE Geoscience and Remote Sensing Letters. - 2010. - Vol. 7, No. 1. - P. 185-189.

J253. Shi Jun. APC Trajectory Design for "One-Active" Linear-Array Three-Dimensional Imaging SAR. / Shi Jun, Zhang Xiaoling, Yang Jianyu, Wen Chen. // IEEE Transactions on Geoscience and Remote Sensing. - 2010. - Vol. 48, No. 3. - P. 1470-1486.

J254. Ferraioli G. Multichannel InSAR Building Edge Detection. IEEE Transactions on Geoscience and Remote Sensing. - 2010. - Vol. 48, No. 3. - P. 1224-1231.

J255. Kobayashi T. Simultaneous Observation of Lunar Radar Sounder and Laser Altimeter of Kaguya for Lunar Regolith Layer Thickness Estimate. / Kobayashi T., Kim J.H., Lee S.R., Araki H., Ono T. // IEEE Geoscience and Remote Sensing Letters. - 2010. - Vol. 7, No. 3. - P. 435-439.

J256. Boniger U. On the Potential of Kinematic GPR Surveying Using a Self-Tracking Total Station: Evaluating System Crosstalk and Latency. / Boniger U., Tronicke J. // IEEE Transactions on Geoscience and Remote Sensing. - 2010. - Vol. 48, No. 10. - P. 3792-3798.

J257. Viet Thuy Vu. Detection of Moving Targets by Focusing in UWB SAR-Theory and Experimental Results. / Viet Thuy Vu, Sjogren T.K., Pettersson M.I., Gustavsson A., Ulander L.M.H. // IEEE Transactions on Geoscience and Remote Sensing. - 2010. - Vol. 48, No. 10. - P. 3799-3815.

J258. Ardila J.P. Angular Backscatter Variation in L-Band ALOS ScanSAR Images of Tropical Forest Areas. / Ardila J.P., Tolpekin V., Bijker W. // IEEE Geoscience and Remote Sensing Letters. - 2010. - Vol. 7, No. 4. - P. 821-825.

J259. Jiaqiu Ai. A New CFAR Ship Detection Algorithm Based on 2-D Joint Log-Normal Distribution in SAR Images. / Jiaqiu Ai, Xiangyang Qi, Weidong Yu, Yunkai Deng, Fan Liu, Li Shi. // IEEE Geoscience and Remote Sensing Letters. - 2010. - Vol. 7, No. 4. - P. 806-810.

J260. Zhuotong Nan. Analysis of Spatial Similarities Between NEXRAD and NLDAS Precipitation Data Products. / Zhuotong Nan, Shugong Wang, Xu Liang, Adams T.E., Teng W., Yao Liang. // IEEE Journal of Selected Topics in Applied Earth Observations and Remote Sensing. - 2010. - Vol. 3, No. 3. - P. 371-385.

J261. Elsherbini A. Mapping of Sand Layer Thickness in Deserts Using SAR Interferometry. / Elsherbini A., Sarabandi K. // IEEE Transactions on Geoscience and Remote Sensing. - 2010. - Vol. 48, No. 9. - P. 3550-3559.

J262. Arii M. A General Characterization for Polarimetric Scattering From Vegetation Canopies. / Arii M., van Zyl J.J., Yunjin Kim. // IEEE Transactions on Geoscience and Remote Sensing. - 2010. - Vol. 48, No. 9. - P. 3349-3357.

J263. Santoro M. Clear-Cut Detection in Swedish Boreal Forest Using Multi-Temporal ALOS PALSAR Backscatter Data. / Santoro M., Fransson J.E.S., Eriksson L.E.B., Ulander L.M.H. // IEEE Journal of Selected Topics in Applied Earth Observations and Remote Sensing. - 2010. - Vol. 3, No. 4. - P. 618-631.

J264. Moghaddam M. A Wireless Soil Moisture Smart Sensor Web Using Physics-Based Optimal Control: Concept and Initial Demonstrations. / Moghaddam M., Entekhabi D., Goykhman Y., Ke Li, Mingyan Liu, Mahajan A., Nayyar A., Shuman D., Teneketzis D. // IEEE Journal of Selected Topics in Applied Earth Observations and Remote Sensing. - 2010. - Vol. 3, No. 4. - P. 522-535.

J265. Zhiyong Suo. A New Strategy to Estimate Local Fringe Frequencies for InSAR Phase Noise Reduction. / Zhiyong Suo, Zhenfang Li, Zheng Bao. // IEEE Geoscience and Remote Sensing Letters. - 2010. - Vol. 7, No. 4. - P. 771-775.

J266. Baochang Liu. An Analytical Method of Updating the Range Derivatives and a Simple Image Registration Method for the MSR-Based Range Doppler Algorithm. / Baochang Liu, Tong Wang, Zheng Bao. // IEEE Geoscience and Remote Sensing Letters. - 2010. - Vol. 7, No. 4. - P. 831-835.

J267. Lojnnqvist A. Polarimetric SAR Data in Land Cover Mapping in Boreal Zone. / Lojnnqvist A., Rauste Y., Molinier M., Hajme T. // IEEE Transactions on Geoscience and Remote Sensing. - 2010. - Vol. 48, No. 10. - P. 3652-3662.

J268. Yong Bian. Interferometric SAR Extended Coherence Calculation Based on Fractional Lower Order Statistics. / Yong Bian, Mercer B. // IEEE Geoscience and Remote Sensing Letters. - 2010. - Vol. 7, No. 4. - P.

841-845.

J269. Meles G.A. A New Vector Waveform Inversion Algorithm for Simultaneous Updating of Conductivity and Permittivity Parameters From Combination Crosshole/Borehole-to-Surface GPR Data. / Meles G.A., Van der Kruk J., Greenhalgh S.A., Ernst J.R., Maurer H., Green A.G. // IEEE Transactions on Geoscience and Remote Sensing. - 2010. - Vol. 48, No. 9. - P. 3391-3407.

J270. Stiles B.W. A Neural Network Technique for Improving the Accuracy of Scatterometer Winds in Rainy Conditions. / Stiles B.W., Dunbar R.S. // IEEE Transactions on Geoscience and Remote Sensing. - 2010. - Vol. 48, No. 8. - P. 3114-3122.

J271. Attema E. Flexible Dynamic Block Adaptive Quantization for Sentinel-1 SAR Missions. / Attema E., Cafforio C., Gottwald M., Guccione P., Monti Guarnieri A., Rocca F., Snoeij P. // IEEE Geoscience and Remote Sensing Letters. - 2010. - Vol. 7, No. 4. - P. 766-770.

J272. Haipeng Wang. A Simple Moment Method of Forest Biomass Estimation From Non-Gaussian Texture Information by High-Resolution Polarimetric SAR. / Haipeng Wang, Ouchi K. // IEEE Geoscience and Remote Sensing Letters. - 2010. - Vol. 7, No. 4. - P. 811-815.

J273. Wilson J.J.W. Radiometric Calibration of the Advanced Wind Scatterometer Radar ASCAT Carried Onboard the METOP-A Satellite. / Wilson J.J.W., Anderson C., Baker M.A., Bonekamp H., Saldac,a J.F., Dyer R.G., Lerch J.A., Kayal G., Gelsthorpe R.V., Brown M.A., Schied E., Schutz-Munz S., Rostan F., Pritchard E.W., Wright N.G., King D., Onel U. // IEEE Transactions on Geoscience and Remote Sensing. - 2010. - Vol. 48, No. 8. - P. 3236-3255.

J274. Yimin Liu. Velocity Estimation and Range Shift Compensation for High Range Resolution Profiling in Stepped-Frequency Radar. / Yimin Liu, Huadong Meng, Gang Li, Xiqin Wang. // IEEE Geoscience and Remote Sensing Letters. - 2010. - Vol. 7, No. 4. - P. 791-795.

J275. Mills S.J. Evaluation of Aerial Remote Sensing Techniques for Vegetation Management in Power-Line Corridors. / Mills S.J., Castro M.P.G., Zhengrong Li, Jinhai Cai, Hayward R., Mejias L., Walker R.A. // IEEE Transactions on Geoscience and Remote Sensing. - 2010. - Vol. 48, No. 9. - P. 3379-3390.

J276. Lihua Liu. A Novel UWB Sampling Receiver and Its Applications for Impulse GPR Systems. / Lihua Liu, Guangyou Fang. // IEEE Geoscience and Remote Sensing Letters. - 2010. - Vol. 7, No. 4. - P. 690-693.

J277. Catapano I. A Qualitative Inverse Scattering Method for Through-the-Wall Imaging. / Catapano I., Crocco L. // IEEE Geoscience and Remote Sensing Letters. - 2010. - Vol. 7, No. 4. - P. 685-689.

J278. Aifei Liu. An Array Error Estimation Method for Constellation SAR Systems. / Aifei Liu, Guisheng Liao, Lun Ma, Qing Xu. // IEEE Geoscience and Remote Sensing Letters. - 2010. - Vol. 7, No. 4. - P. 731-735.

J279. Vu V.T. RFI Suppression in Ultrawideband SAR Using an Adaptive Line Enhancer. / Vu V.T., Sjojgren T.K., Pettersson M.I., He,kansson L., Gustavsson A., Ulander L.M.H. // IEEE Geoscience and Remote Sensing Letters. - 2010. - Vol. 7, No. 4. - P. 694-698.

J280. Byoung-Gyun Lim. Noniterative Super-Resolution Technique Combining SVA With Modified Geometric Mean Filter. / Byoung-Gyun Lim, Jae-Choon Woo, Young-Soo Kim. // IEEE Geoscience and Remote Sensing Letters. - 2010. - Vol. 7, No. 4. - P. 713-717.

J281. Mathews B. Effect of Rain Attenuation on Range Weighting in Weather Radar. IEEE Transactions on Aerospace and Electronic Systems. - 2010. - Vol. 46, No. 2. - P. 952-960.

J282. Durand M. The Surface Water and Ocean Topography Mission: Observing Terrestrial Surface Water and Oceanic Submesoscale Eddies. / Durand M., Lee-Lueng Fu, Lettenmaier D.P., Alsdorf D.E., Rodriguez E., Esteban-Fernandez D. // Proceedings of the IEEE. - 2010. - Vol. 98, No. 5. - P. 766-779.

J283. Zhigang Pan. A Lossless Compression Algorithm for SAR Amplitude Imagery Based on Modified Quadtree Coding of Bit Plane. / Zhigang Pan, Xin Gao, Xiumin Sun, Hongmei Song. // IEEE Geoscience and Remote Sensing Letters. - 2010. - Vol. 7, No. 4. - P. 723-726.

J284. Adi K. Phase Unwrapping by Markov Chain Monte Carlo Energy Minimization. / Adi K., Suksmono A.B.,

Mengko T.L.R., Gunawan H. // IEEE Geoscience and Remote Sensing Letters. - 2010. - Vol. 7, No. 4. - P. 704-707.

J285. Jen-Yu Han. A Noniterative Approach for the Quick Alignment of Multistation Unregistered LiDAR Point Clouds. IEEE Geoscience and Remote Sensing Letters. - 2010. - Vol. 7, No. 4. - P. 727-730.

J286. Dery B. Spectroscopic Calibration Correlation of Field and Lab-Sized Fluorescence LIDAR Systems. / Dery B., Buteau S., Simard J.-R., Bouchard J.-P., Vallee R. // IEEE Transactions on Geoscience and Remote Sensing. - 2010. - Vol. 48, No. 9. - P. 3580-3586.

J287. Stiles B.W. Obtaining Accurate Ocean Surface Winds in Hurricane Conditions: A Dual-Frequency Scatterometry Approach. / Stiles B.W., Hristova-Veleva S.M., Dunbar R.S., Chan S., Durden S.L., Esteban-Fernandez D., Rodriguez E., Poulsen W.L., Gaston R.W., Callahan P.S. // IEEE Transactions on Geoscience and Remote Sensing. - 2010. - Vol. 48, No. 8. - P. 3101-3113.

J288. Grosdidier S. HFSW Radar Model: Simulation and Measurement. / Grosdidier S., Baussard A., Khenchaf A. // IEEE Transactions on Geoscience and Remote Sensing. - 2010. - Vol. 48, No. 9. - P. 3539-3549.

J289. Garestier F. Estimation of the Backscatter Vertical Profile of a Pine Forest Using Single Baseline P-Band (Pol-)InSAR Data. / Garestier F., Le Toan T. // IEEE Transactions on Geoscience and Remote Sensing. - 2010. - Vol. 48, No. 9. - P. 3340-3348.

J290. Lucas R. An Evaluation of the ALOS PALSAR L-Band Backscatter-Above Ground Biomass Relationship Queensland, Australia: Impacts of Surface Moisture Condition and Vegetation Structure. / Lucas R., Armston J., Fairfax R., Fensham R., Accad A., Carreiras J., Kelley J., Bunting P., Clewley D., Bray S., Metcalfe D., Dwyer J., Bowen M., Eyre T., Laidlaw M., Shimada M. // IEEE Journal of Selected Topics in Applied Earth Observations and Remote Sensing. - 2010. - Vol. 3, No. 4. - P. 576-593.

J291. Paichard Y. Signal level Simulator for netted text radar waveforms evaluation. / Paichard Y., Brooker M., Inggs M. // IEEE Aerospace and Electronic Systems Magazine. - 2010. - Vol. 25, No. 3. - P. 27-29.

J292. Solberg S. Simulating X-Band Interferometric Height in a Spruce Forest From Airborne Laser Scanning. / Solberg S., Weydahl D.J., Nasset E. // IEEE Transactions on Geoscience and Remote Sensing. - 2010. - Vol. 48, No. 9. - P. 3369-3378.

J293. Marzano F.S. Iterative Bayesian Retrieval of Hydrometeor Content From X-Band Polarimetric Weather Radar. / Marzano F.S., Botta G., Montopoli M. // IEEE Transactions on Geoscience and Remote Sensing. - 2010. - Vol. 48, No. 8. - P. 3059-3074.

J294. Duchkov A.A. Discrete Almost-Symmetric Wave Packets and Multiscale Geometrical Representation of (Seismic) Waves. / Duchkov A.A., Andersson F., de Hoop M.V. // IEEE Transactions on Geoscience and Remote Sensing. - 2010. - Vol. 48, No. 9. - P. 3408-3423.

J295. Xiao Xiang Zhu. Tomographic SAR Inversion by -Norm Regularization-The Compressive Sensing Approach. / Xiao Xiang Zhu, Bamler R. // IEEE Transactions on Geoscience and Remote Sensing. - 2010. - Vol. 48, No. 10. - P. 3839-3846.

J296. Kersten P.R. Estimating surface water flow speeds using time-frequency methods. / Kersten P.R., Jansen R.W., Ainsworth T.L., Toporkov J.V., Sletten M.A. // IET Signal Processing. - 2010. - Vol. 4, No. 4. - P. 406-412.

J297. Moccia Antonio. Synthetic Aperture Radar for Earth Observation from a Lunar Base: Performance and Potential Applications. / Moccia Antonio, Renga Alfredo. // IEEE Transactions on Aerospace and Electronic Systems. - 2010. - Vol. 46, No. 3. - P. 1034-1051.

J298. Paillou P. Mapping Subsurface Geology in Sahara Using L-Band SAR: First Results From the ALOS/PALSAR Imaging Radar. / Paillou P., Lopez S., Farr T., Rosenqvist A. // IEEE Journal of Selected Topics in Applied Earth Observations and Remote Sensing. - 2010. - Vol. 3, No. 4. - P. 632-636.

J299. Evans T.L. Using ALOS/PALSAR and RADARSAT-2 to Map Land Cover and Seasonal Inundation in the Brazilian Pantanal. / Evans T.L., Costa M., Telmer K., Silva T.S.F. // IEEE Journal of Selected Topics in Applied Earth Observations and Remote Sensing. - 2010. - Vol. 3, No. 4. - P. 560-575.

J300. Chen Q. Polarimetric Scattering Similarity Between a Random Scatterer and a Canonical Scatterer. / Chen Q., Jiang Y.M., Zhao L.J., Kuang G.Y. // IEEE Geoscience and Remote Sensing Letters. - 2010. - Vol. 7, No. 4. - P. 866-869.

J301. Fritz J.P. Simultaneous Observations and Analysis of Severe Storms Using Polarimetric X-Band SAR and Ground-Based Weather Radar. / Fritz J.P., Chandrasekar V. // IEEE Transactions on Geoscience and Remote Sensing. - 2010. - Vol. 48, No. 10. - P. 3622-3637.

J302. Sen Zhang. Image Autocoregistration and Interferogram Estimation Using Extended COMET-EXIP Method. / Sen Zhang, Jinsong Tang, Ming Chen, Sanwen Zhu, Hailiang Yang. // IEEE Transactions on Geoscience and Remote Sensing. - 2010. - Vol. 48, No. 12. - P. 4204-4218.

J303. Touzi R. Requirement on Antenna Cross-Polarization Isolation for the Operational Use of C-Band SAR Constellations in Maritime Surveillance. / Touzi R., Vachon P.W., Wolfe J. // IEEE Geoscience and Remote Sensing Letters. - 2010. - Vol. 7, No. 4. - P. 861-865.

J304. Cossio T.K. Predicting Small Target Detection Performance of Low-SNR Airborne Lidar. / Cossio T.K., Slatton K.C., Carter W.E., Shrestha K.Y., Harding D. // IEEE Journal of Selected Topics in Applied Earth Observations and Remote Sensing. - 2010. - Vol. 3, No. 4. - P. 672-688.

J305. Cho M.A. Improving Discrimination of Savanna Tree Species Through a Multiple-Endmember Spectral Angle Mapper Approach: Canopy-Level Analysis. / Cho M.A., Debba P., Mathieu R., Naidoo L., van Aardt J., Asner G.P. // IEEE Transactions on Geoscience and Remote Sensing. - 2010. - Vol. 48, No. 11. - P. 4133-4142.

J306. Shimada M. Generating Large-Scale High-Quality SAR Mosaic Datasets: Application to PALSAR Data for Global Monitoring. / Shimada M., Ohtaki T. // IEEE Journal of Selected Topics in Applied Earth Observations and Remote Sensing. - 2010. - Vol. 3, No. 4. - P. 637-656.

J307. Hoekman D.H. PALSAR Wide-Area Mapping of Borneo: Methodology and Map Validation. / Hoekman D.H., Vissers M.A.M., Wielaard N. // IEEE Journal of Selected Topics in Applied Earth Observations and Remote Sensing. - 2010. - Vol. 3, No. 4. - P. 605-617.

J308. Rosenqvist A. The Kyoto & Carbon Initiative-A Brief Summary. / Rosenqvist A., Shimada M., Lucas R., Chapman B., Paillou P., Hess L., Lowry J. // IEEE Journal of Selected Topics in Applied Earth Observations and Remote Sensing. - 2010. - Vol. 3, No. 4. - P. 551-553.

J309. Simakov Evgenya I. First experimental demonstration of a photonic band gap channel-drop filter at 240 GHz. / Simakov Evgenya I., Earley Lawrence M., Heath Cynthia E., Shchegolkov Dmitry Yu., Schultz Brian D. // Review of Scientific Instruments. - 2010. - Vol. 81, No. 10. - P. 104701-104701-5.

J310. Shimada M. Ortho-Rectification and Slope Correction of SAR Data Using DEM and Its Accuracy Evaluation. IEEE Journal of Selected Topics in Applied Earth Observations and Remote Sensing. - 2010. - Vol. 3, No. 4. - P. 657-671.

J311. Vicen-Bueno R. Coherent Detection of Swerling 0 Targets in Sea-Ice Weibull-Distributed Clutter Using Neural Networks. / Vicen-Bueno R., Rosa-Zurera M., Jarabo-Amores M.P., de la Mata-Moya D. // IEEE Transactions on Instrumentation and Measurement. - 2010. - Vol. 59, No. 12. - P. 3139-3151.

J312. Chaabouni-Chouayakh H. Backscattering and Statistical Information Fusion for Urban Area Mapping Using TerraSAR-X Data. / Chaabouni-Chouayakh H., Datcu M. // IEEE Journal of Selected Topics in Applied Earth Observations and Remote Sensing. - 2010. - Vol. 3, No. 4. - P. 718-730.

J313. Cuozzo G. Random Walk Approach for Wave Propagation through Atmospheric Layers for DInSAR Applications. / Cuozzo G., Di Bisceglie M., Fusco A. // IEEE Transactions on Aerospace and Electronic Systems. - 2010. - Vol. 46, No. 4. - P. 1687-1698.

J314. Rebelo L.-S. Eco-Hydrological Characterization of Inland Wetlands in Africa Using L-Band SAR. IEEE Journal of Selected Topics in Applied Earth Observations and Remote Sensing. - 2010. - Vol. 3, No. 4. - P. 554-559.

J315. Liu A. Corrections to "An Array Error Estimation Method for Constellation SAR Systems" [Oct 10 731-

735]. / Liu A., Liao G., Ma L., Xu Q. // IEEE Geoscience and Remote Sensing Letters. - 2010. - Vol. 7, No. 4. - P. 880.

J316. Walsh J. The First-Order High Frequency Radar Ocean Surface Cross Section for an Antenna on a Floating Platform. / Walsh J., Weimin Huang, Gill E. // IEEE Transactions on Antennas and Propagation. - 2010. - Vol. 58, No. 9. - P. 2994-3003.

J317. Bouvet A. An End-to-End Error Model for Classification Methods Based on Temporal Change or Polarization Ratio of SAR Intensities. / Bouvet A., Thuy Le Toan, Floury N., Macklin T. // IEEE Transactions on Geoscience and Remote Sensing. - 2010. - Vol. 48, No. 9. - P. 3521-3538.

J318. Inggs M. Passive Coherent Location as Cognitive Radar. IEEE Aerospace and Electronic Systems Magazine. - 2010. - Vol. 25, No. 5. - P. 12-17.

J319. Foroozan F. Time-Reversal Ground-Penetrating Radar: Range Estimation With Cramйr-Rao Lower Bounds. / Foroozan F., Asif A. // IEEE Transactions on Geoscience and Remote Sensing. - 2010. - Vol. 48, No. 10. - P. 3698-3708.

J320. Marzano F.S. Model-Based Weather Radar Remote Sensing of Explosive Volcanic Ash Eruption. / Marzano F.S., Marchiotto S., Textor C., Schneider D.J. // IEEE Transactions on Geoscience and Remote Sensing. - 2010. - Vol. 48, No. 10. - P. 3591-3607.

J321. Saunier S. Radiometric, Geometric, and Image Quality Assessment of ALOS AVNIR-2 and PRISM Sensors. / Saunier S., Goryl P., Chander G., Santer R., Bouvet M., Collet B., Mambimba A., Aksakal S.K. // IEEE Transactions on Geoscience and Remote Sensing. - 2010. - Vol. 48, No. 10. - P. 3855-3866.

J322. Lei Zhang. Resolution Enhancement for Inversed Synthetic Aperture Radar Imaging Under Low SNR via Improved Compressive Sensing. / Lei Zhang, Mengdao Xing, Cheng-Wei Qiu, Jun Li, Jialian Sheng, Yachao Li, Zheng Bao. // IEEE Transactions on Geoscience and Remote Sensing. - 2010. - Vol. 48, No. 10. - P. 3824-3838.

J323. Kersten P.R. Estimating Surface Water Speeds With a Single-Phase Center SAR Versus an Along-Track Interferometric SAR. / Kersten P.R., Toporkov J.V., Ainsworth T.L., Sletten M.A., Jansen R.W. // IEEE Transactions on Geoscience and Remote Sensing. - 2010. - Vol. 48, No. 10. - P. 3638-3646.

J324. Jie Chen. Improved Estimators of Faraday Rotation in Spaceborne Polarimetric SAR Data. / Jie Chen, Shaun Quegan. // IEEE Geoscience and Remote Sensing Letters. - 2010. - Vol. 7, No. 4. - P. 846-850.

J325. Boccia L. L-band array for ground-based remote sensing of volcanic eruptions. / Boccia L., Di Massa G., Venneri I. // IET Microwaves, Antennas & Propagation. - 2010. - Vol. 4, No. 12. - P. 2062-2068.

J326. Nouguier F. Scattering From Nonlinear Gravity Waves: The "Choppy Wave" Model. / Nouguier F., Gue,rin C.-A., Chapron B. // IEEE Transactions on Geoscience and Remote Sensing. - 2010. - Vol. 48, No. 12. - P. 4184-4192.

J327. Tello Alonso M. A Novel Strategy for Radar Imaging Based on Compressive Sensing. / Tello Alonso M., Lo,pez-Dekker P., Mallorqui, J.J. // IEEE Transactions on Geoscience and Remote Sensing. - 2010. - Vol. 48, No. 12. - P. 4285-4295.

J328. Zebker H.A. Geodetically Accurate InSAR Data Processor. / Zebker H.A., Hensley S., Shanker P., Wortham C. // IEEE Transactions on Geoscience and Remote Sensing. - 2010. - Vol. 48, No. 12. - P. 4309-4321.

J329. Piedra-Ferna. Feature Selection in AVHRR Ocean Satellite Images by Means of Filter Methods. / Piedra-Ferna,ndez J.A., Canto,n-Garbi,n M., Wang J.Z. // IEEE Transactions on Geoscience and Remote Sensing. - 2010. - Vol. 48, No. 12. - P. 4193-4203.

J330. Woldemichael A.T. Role of Land-Water Classification and Manning's Roughness Parameter in Space-Borne Estimation of Discharge for Braided Rivers: A Case Study of the Brahmaputra River in Bangladesh. / Woldemichael A.T., Degu A.M., Siddique-E-Akbor A.H.M., Hossain F. // IEEE Journal of Selected Topics in Applied Earth Observations and Remote Sensing. - 2010. - Vol. 3, No. 3. - P. 395-403.

J331. Tanase M.A. Sensitivity of X-, C-, and L-Band SAR Backscatter to Burn Severity in Mediterranean Pine Forests. / Tanase M.A., Santoro M., de la Riva J., Pe,rez-Cabello F., Thuy Le Toan. // IEEE Transactions on Geoscience and Remote Sensing. - 2010. - Vol. 48, No. 10. - P. 3663-3675.

J332. Toutin T. Impact of Radarsat-2 SAR Ultrafine-Mode Parameters on Stereo-Radargrammetric DEMs. IEEE Transactions on Geoscience and Remote Sensing. - 2010. - Vol. 48, No. 10. - P. 3816-3823.

J333. Xiao Xiang Zhu. Very High Resolution Spaceborne SAR Tomography in Urban Environment. / Xiao Xiang Zhu, Bamler R. // IEEE Transactions on Geoscience and Remote Sensing. - 2010. - Vol. 48, No. 12. - P. 4296-4308.

J334. Walker W.S. Large-Area Classification and Mapping of Forest and Land Cover in the Brazilian Amazon: A Comparative Analysis of ALOS/PALSAR and Landsat Data Sources. / Walker W.S., Stickler C.M., Kellndorfer J.M., Kirsch K.M., Nepstad D.C. // IEEE Journal of Selected Topics in Applied Earth Observations and Remote Sensing. - 2010. - Vol. 3, No. 4. - P. 594-604.

J335. Mladenova I. Validation of the ASAR Global Monitoring Mode Soil Moisture Product Using the NAFE'05 Data Set. / Mladenova I., Lakshmi V., Walker J.P., Panciera R., Wagner W., Doubkova M. // IEEE Transactions on Geoscience and Remote Sensing. - 2010. - Vol. 48, No. 6. - P. 2498-2508.

J336. Jehle M. Measurement of Ionospheric TEC in Spaceborne SAR Data. / Jehle M., Frey O., Small D., Meier E. // IEEE Transactions on Geoscience and Remote Sensing. - 2010. - Vol. 48, No. 6. - P. 2460-2468.

J337. Krieger G. Interferometric Synthetic Aperture Radar (SAR) Missions Employing Formation Flying. / Krieger G., Hajnsek I., Papathanassiou K.P., Younis M., Moreira A. // Proceedings of the IEEE. - 2010. - Vol. 98, No. 5. - P. 816-843.

J338. Wentao An. Three-Component Model-Based Decomposition for Polarimetric SAR Data. / Wentao An, Yi Cui, Jian Yang. // IEEE Transactions on Geoscience and Remote Sensing. - 2010. - Vol. 48, No. 6. - P. 2732-2739.

J339. Heng-Chao Li. An Efficient and Flexible Statistical Model Based on Generalized Gamma Distribution for Amplitude SAR Images. / Heng-Chao Li, Wen Hong, Yi-Rong Wu, Ping-Zhi Fan. // IEEE Transactions on Geoscience and Remote Sensing. - 2010. - Vol. 48, No. 6. - P. 2711-2722.

J340. Lo Monte L. RF Tomography for Below-Ground Imaging of Extended Areas and Close-in Sensing. / Lo Monte L., Erricolo D., Soldovieri F., Wicks M.C. // IEEE Geoscience and Remote Sensing Letters. - 2010. - Vol. 7, No. 3. - P. 496-500.

J341. Xiaodong Zhuge. Modified Kirchhoff Migration for UWB MIMO Array-Based Radar Imaging. / Xiaodong Zhuge, Yarovoy A.G., Savelyev T., Ligthart L. // IEEE Transactions on Geoscience and Remote Sensing. - 2010. - Vol. 48, No. 6. - P. 2692-2703.

J342. Paes R.L. Ship Detection Using TerraSAR-X Images in the Campos Basin (Brazil). / Paes R.L., Lorenzzetti J.A., Gherardi D.F.M. // IEEE Geoscience and Remote Sensing Letters. - 2010. - Vol. 7, No. 3. - P. 545-548.

J343. Mironov V.L. Temperature-Dependable Microwave Dielectric Model for an Arctic Soil. / Mironov V.L., De Roo R.D., Savin I.V. // IEEE Transactions on Geoscience and Remote Sensing. - 2010. - Vol. 48, No. 6. - P. 2544-2556.

J344. Ranjani J.J. Dual-Tree Complex Wavelet Transform Based SAR Despeckling Using Interscale Dependence. / Ranjani J.J., Thiruvengadam S.J. // IEEE Transactions on Geoscience and Remote Sensing. - 2010. - Vol. 48, No. 6. - P. 2723-2731.

J345. Bruno D. Radar Imaging From Geosynchronous Orbit: Temporal Decorrelation Aspects. / Bruno D., Hobbs S.E. // IEEE Transactions on Geoscience and Remote Sensing. - 2010. - Vol. 48, No. 7. - P. 2924-2929.

J346. Gebert N. Multichannel Azimuth Processing in ScanSAR and TOPS Mode Operation. / Gebert N., Krieger G., Moreira A. // IEEE Transactions on Geoscience and Remote Sensing. - 2010. - Vol. 48, No. 7. - P. 2994-3008.

J347. Oliveri G. ADS-Based Guidelines for Thinned Planar Arrays. / Oliveri G., Manica L., Massa A. // IEEE Transactions on Antennas and Propagation. - 2010. - Vol. 58, No. 6. - P. 1935-1948.

J348. Ming Yao. Comparison of Radar Waveforms for a Low-Power Vertical-Incidence Ionosonde. / Ming Yao, Zhengyu Zhao, Gang Chen, Guobin Yang, Fanfan Su, Shipeng Li, Xinmiao Zhang. // IEEE Geoscience and Remote Sensing Letters. - 2010. - Vol. 7, No. 4. - P. 636-640.

J349. Amirmazlaghani M. Two Novel Bayesian Multiscale Approaches for Speckle Suppression in SAR Images. / Amirmazlaghani M., Amindavar H. // IEEE Transactions on Geoscience and Remote Sensing. - 2010. - Vol. 48, No. 7. - P. 2980-2993.

J350. Schleiss M. Identification of Dry and Rainy Periods Using Telecommunication Microwave Links. / Schleiss M., Berne A. // IEEE Geoscience and Remote Sensing Letters. - 2010. - Vol. 7, No. 3. - P. 611-615.

J351. Nezirovic A. Corrections to “Signal Processing for Improved Detection of Trapped Victims Using UWB Radar” [Apr 10 2005-2014]. / Nezirovic A., Yarovoy A.G., Ligthart L.P. // IEEE Transactions on Geoscience and Remote Sensing. - 2010. - Vol. 48, No. 4. - P. 2179.

J352. Wingham D.J. The Rough Surface Impulse Response of a Pulse-Limited Altimeter With an Elliptical Antenna Pattern. / Wingham D.J., Wallis D.W. // IEEE Antennas and Wireless Propagation Letters. - 2010. - Vol. 9, {no data available}. - P. 232-235.

J353. Duque S. Single-Pass Bistatic SAR Interferometry Using Fixed-Receiver Configurations: Theory and Experimental Validation. / Duque S., Lopez-Dekker P., Mallorqui J.J. // IEEE Transactions on Geoscience and Remote Sensing. - 2010. - Vol. 48, No. 6. - P. 2740-2749.

J354. Gonzalez J.H. Definition of ICESat Selection Criteria for Their Use as Height References for TanDEM-X. / Gonzalez J.H., Bachmann M., Scheiber R., Krieger G. // IEEE Transactions on Geoscience and Remote Sensing. - 2010. - Vol. 48, No. 6. - P. 2750-2757.

J355. Rabus B. The Importance of Soil Moisture and Soil Structure for InSAR Phase and Backscatter, as Determined by FDTD Modeling. / Rabus B., Wehn H., Nolan M. // IEEE Transactions on Geoscience and Remote Sensing. - 2010. - Vol. 48, No. 5. - P. 2421-2429.

J356. Marino A. A Polarimetric Target Detector Using the Huynen Fork. / Marino A., Cloude S.R., Woodhouse I.H. // IEEE Transactions on Geoscience and Remote Sensing. - 2010. - Vol. 48, No. 5. - P. 2357-2366.

J357. Hempel C.G. Sequential Track Initialization with Page's Test. IEEE Transactions on Aerospace and Electronic Systems. - 2010. - Vol. 46, No. 1. - P. 414-424.

J358. Partington K.C. Dual-Polarization C-Band Radar Observations of Sea Ice in the Amundsen Gulf. / Partington K.C., Flach J.D., Barber D., Isleifson D., Meadows P.J., Verlaan P. // IEEE Transactions on Geoscience and Remote Sensing. - 2010. - Vol. 48, No. 6. - P. 2685-2691.

J359. Viscardy S. Evaluation of Ozone Analyses From UARS MLS Assimilation by BASCOE Between 1992 and 1997. / Viscardy S., Errera Q., Christophe Y., Chabrillat S., Lambert J.-C. // IEEE Journal of Selected Topics in Applied Earth Observations and Remote Sensing. - 2010. - Vol. 3, No. 2. - P. 190-202.

J360. Zirizzotti A. Dry-Wet Bedrock Interface Detection by Radio Echo Sounding Measurements. / Zirizzotti A., Cafarella L., Baskaradas J.A., Tabacco I.E., Urbini S., Mangialetti M., Bianchi C. // IEEE Transactions on Geoscience and Remote Sensing. - 2010. - Vol. 48, No. 5. - P. 2343-2348.

J361. Brunner D. Earthquake Damage Assessment of Buildings Using VHR Optical and SAR Imagery. / Brunner D., Lemoine G., Bruzzone L. // IEEE Transactions on Geoscience and Remote Sensing. - 2010. - Vol. 48, No. 5. - P. 2403-2420.

J362. Reppucci A. Tropical Cyclone Intensity Estimated From Wide-Swath SAR Images. / Reppucci A., Lehner S., Schulz-Stellenfleth J., Brusch S. // IEEE Transactions on Geoscience and Remote Sensing. - 2010. - Vol. 48, No. 4. - P. 1639-1649.

J363. Gonzalez P.J. Coseismic Horizontal Offsets and Fault-Trace Mapping Using Phase Correlation of IRS Satellite Images: The 1999 Izmit (Turkey) Earthquake. / Gonzalez P.J., Chini M., Stramondo S., Fernandez J. //

IEEE Transactions on Geoscience and Remote Sensing. - 2010. - Vol. 48, No. 5. - P. 2242-2250.

J364. Titin-Schnaider C. Physical Meaning of Bistatic Polarimetric Parameters. IEEE Transactions on Geoscience and Remote Sensing. - 2010. - Vol. 48, No. 5. - P. 2349-2356.

J365. Fang Wang. A New Method of Deriving Spectrum for Bistatic SAR Processing. / Fang Wang, Xiang Li. // IEEE Geoscience and Remote Sensing Letters. - 2010. - Vol. 7, No. 3. - P. 483-486.

J366. Rott H. Cold Regions Hydrology High-Resolution Observatory for Snow and Cold Land Processes. / Rott H., Yueh S.H., Cline D.W., Duguay C., Essery R., Haas C., He,lie,re F., Kern M., Macelloni G., Malnes E., Nagler T., Pulliainen J., Rebhan H., Thompson A. // Proceedings of the IEEE. - 2010. - Vol. 98, No. 5. - P. 752-765.

J367. Vain A. Correcting Airborne Laser Scanning Intensity Data for Automatic Gain Control Effect. / Vain A., Xiaowei Yu, Kaasalainen S., Hyyppa J. // IEEE Geoscience and Remote Sensing Letters. - 2010. - Vol. 7, No. 3. - P. 511-514.

J368. Potter L.C. Sparsity and Compressed Sensing in Radar Imaging. / Potter L.C., Ertin E., Parker J.T., Cetin M. // Proceedings of the IEEE. - 2010. - Vol. 98, No. 6. - P. 1006-1020.

J369. Larsen K.W. Terrestrial Quadstatic Interferometric Radar Observations of Mars. / Larsen K.W., Jurgens R.F., Haldemann A.F.C., Slade M.A., Rumsey H.C. // IEEE Transactions on Geoscience and Remote Sensing. - 2010. - Vol. 48, No. 6. - P. 2670-2684.

J370. Bourlier C. Low-Frequency Limit of Unified Models for Backscattering From Oceanlike Surfaces. / Bourlier C., Pinel N. // IEEE Geoscience and Remote Sensing Letters. - 2010. - Vol. 7, No. 3. - P. 506-510.

J371. Reddy T.S. MST Radar Signal Processing Using Cepstral Thresholding. / Reddy T.S., Ramachandra Reddy G. // IEEE Transactions on Geoscience and Remote Sensing. - 2010. - Vol. 48, No. 6. - P. 2704-2710.

J372. Crow W.T. The Impact of Radar Incidence Angle on Soil-Moisture-Retrieval Skill. / Crow W.T., Wagner W., Naeimi V. // IEEE Geoscience and Remote Sensing Letters. - 2010. - Vol. 7, No. 3. - P. 501-505.

J373. Frigui H. Context-Dependent Multisensor Fusion and Its Application to Land Mine Detection. / Frigui H., Lijun Zhang, Gader P.D. // IEEE Transactions on Geoscience and Remote Sensing. - 2010. - Vol. 48, No. 6. - P. 2528-2543.

J374. Shaohui Chen. SAR and Multispectral Image Fusion Using Generalized IHS Transform Based on a Trous Wavelet and EMD Decompositions. / Shaohui Chen, Renhua Zhang, Hongbo Su, Jing Tian, Jun Xia. // IEEE Sensors Journal. - 2010. - Vol. 10, No. 3. - P. 737-745.

J375. Royer A. Monitoring Dry, Wet, and No-Snow Conditions From Microwave Satellite Observations. / Royer A., Goijta K., Kohn J., De Se,ve D. // IEEE Geoscience and Remote Sensing Letters. - 2010. - Vol. 7, No. 4. - P. 670-674.

J376. Yutao Zhu. An ISAR Imaging Method Based on MIMO Technique. / Yutao Zhu, Yi Su, Wenxian Yu. // IEEE Transactions on Geoscience and Remote Sensing. - 2010. - Vol. 48, No. 8. - P. 3290-3299.

J377. Le Vine D.M. Aquarius and Remote Sensing of Sea Surface Salinity from Space. / Le Vine D.M., Lagerloef G.S.E., Torrusio S.E. // Proceedings of the IEEE. - 2010. - Vol. 98, No. 5. - P. 688-703.

J378. Suksmono A.B. Compressive Stepped-Frequency Continuous-Wave Ground-Penetrating Radar. / Suksmono A.B., Bharata E., Lestari A.A., Yarovoy A.G., Ligthart L.P. // IEEE Geoscience and Remote Sensing Letters. - 2010. - Vol. 7, No. 4. - P. 665-669.

J379. Yueh S.H. Passive and Active L-Band Microwave Observations and Modeling of Ocean Surface Winds. / Yueh S.H., Dinardo S.J., Fore A.G., Li F.K. // IEEE Transactions on Geoscience and Remote Sensing. - 2010. - Vol. 48, No. 8. - P. 3087-3100.

J380. Isleifson D. C-Band Polarimetric Backscattering Signatures of Newly Formed Sea Ice During Fall Freeze-Up. / Isleifson D., Byongjun Hwang, Barber D.G., Scharien R.K., Shafai L. // IEEE Transactions on Geoscience and Remote Sensing. - 2010. - Vol. 48, No. 8. - P. 3256-3267.

J381. Campbell J.R. CALIOP Aerosol Subset Processing for Global Aerosol Transport Model Data Assimilation. / Campbell J.R., Reid J.S., Westphal D.L., Jianglong Zhang, Hyer E.J., Welton E.J. // IEEE Journal of Selected Topics in Applied Earth Observations and Remote Sensing. - 2010. - Vol. 3, No. 2. - P. 203-214.

J382. Palenichka R.M. Automatic Extraction of Control Points for the Registration of Optical Satellite and LiDAR Images. / Palenichka R.M., Zaremba M.B. // IEEE Transactions on Geoscience and Remote Sensing. - 2010. - Vol. 48, No. 7. - P. 2864-2879.

J383. Laupattarakasem P. Improved Hurricane Ocean Vector Winds Using SeaWinds Active/Passive Retrievals. / Laupattarakasem P., Jones W.L., Hennon C.C., Allard J.R., Harless A.R., Black P.G. // IEEE Transactions on Geoscience and Remote Sensing. - 2010. - Vol. 48, No. 7. - P. 2909-2923.

J384. Gifford C.M. Automated Polar Ice Thickness Estimation From Radar Imagery. / Gifford C.M., Finyom G., Jefferson M., Reid M., Akers E.L., Agah A. // IEEE Transactions on Image Processing. - 2010. - Vol. 19, No. 9. - P. 2456-2469.

J385. Entekhabi D. The Soil Moisture Active Passive (SMAP) Mission. / Entekhabi D., Njoku E.G., O'Neill P.E., Kellogg K.H., Crow W.T., Edelstein W.N., Entin J.K., Goodman S.D., Jackson T.J., Johnson J., Kimball J., Piepmeier J.R., Koster R.D., Martin N., McDonald K.C., Moghaddam M., Moran S., Reichle R., Shi J.C., Spencer M.W., Thurman S.W., Leung Tsang, Van Zyl J. // Proceedings of the IEEE. - 2010. - Vol. 98, No. 5. - P. 704-716.

J386. Guida R. Height Retrieval of Isolated Buildings From Single High-Resolution SAR Images. / Guida R., Iodice A., Riccio D. // IEEE Transactions on Geoscience and Remote Sensing. - 2010. - Vol. 48, No. 7. - P. 2967-2979.

J387. {no data available}. Correction to "A New Vector Waveform Inversion Algorithm for Simultaneous Updating of Conductivity and Permittivity Parameters From Combination Crosshole/Borehole-to-Surface GPR Data". IEEE Transactions on Geoscience and Remote Sensing. - 2010. - Vol. 48, No. 12. - P. 4329.

J388. Moon W.M. RADARSAT-2 and Coastal Applications: Surface Wind, Waterline, and Intertidal Flat Roughness. / Moon W.M., Staples G., Duk-jin Kim, Sang-Eun Park, Kyung-Ae Park. // Proceedings of the IEEE. - 2010. - Vol. 98, No. 5. - P. 800-815.

J389. Abdalati W. The ICESat-2 Laser Altimetry Mission. / Abdalati W., Zwally H.J., Bindschadler R., Csatho B., Farrell S.L., Fricker H.A., Harding D., Kwok R., Lefsky M., Markus T., Marshak A., Neumann T., Palm S., Schutz B., Smith B., Spinhirne J., Webb C. // Proceedings of the IEEE. - 2010. - Vol. 98, No. 5. - P. 735-751.

J390. Changren Zhu. A Novel Hierarchical Method of Ship Detection from Spaceborne Optical Image Based on Shape and Texture Features. / Changren Zhu, Hui Zhou, Runsheng Wang, Jun Guo. // IEEE Transactions on Geoscience and Remote Sensing. - 2010. - Vol. 48, No. 9. - P. 3446-3456.

J391. Fernandes M.J. GNSS-Derived Path Delay: An Approach to Compute the Wet Tropospheric Correction for Coastal Altimetry. / Fernandes M.J., Lazaro C., Nunes A.L., Pires N., Bastos L., Mendes V.B. // IEEE Geoscience and Remote Sensing Letters. - 2010. - Vol. 7, No. 3. - P. 596-600.

J392. Naenna P. A Monte Carlo Study of Altimeter Pulse Returns and the Electromagnetic Bias. / Naenna P., Johnson J.T. // IEEE Transactions on Geoscience and Remote Sensing. - 2010. - Vol. 48, No. 8. - P. 3218-3224.

J393. Yoshikawa E. Development and Initial Observation of High-Resolution Volume-Scanning Radar for Meteorological Application. / Yoshikawa E., Ushio T., Kawasaki Z., Mega T., Yoshida S., Morimoto T., Imai K., Nagayama S. // IEEE Transactions on Geoscience and Remote Sensing. - 2010. - Vol. 48, No. 8. - P. 3225-3235.

J394. Valencia E. Experimental Determination of the Sea Correlation Time Using GNSS-R Coherent Data. / Valencia E., Camps A., Marchan-Hernandez J.F., Rodriguez-Alvarez N., Ramos-Perez I., Bosch-Lluis X. // IEEE Geoscience and Remote Sensing Letters. - 2010. - Vol. 7, No. 4. - P. 675-679.

J395. Walterscheid I. Bistatic SAR Experiments With PAMIR and TerraSAR-X-Setup, Processing, and Image Results. / Walterscheid I., Espeter T., Brenner A.R., Klare J., Ender J.H.G., Nies H., Wang R., Loffeld O. // IEEE Transactions on Geoscience and Remote Sensing. - 2010. - Vol. 48, No. 8. - P. 3268-3279.

J396. Immoreev I.Y. Practical applications of UWB technology. IEEE Aerospace and Electronic Systems Magazine. - 2010. - Vol. 25, No. 2. - P. 36-42.

J397. Magruder L.A. ICESat Geolocation Validation Using Airborne Photography. / Magruder L.A., Ricklefs R.L., Silverberg E.C., Horstman M.F., Suleman M.A., Schutz B.E. // IEEE Transactions on Geoscience and Remote Sensing. - 2010. - Vol. 48, No. 6. - P. 2758-2766.

J398. Nwogu O.G. Surface-Wavefield Estimation From Coherent Marine Radars. / Nwogu O.G., Lyzenga D.R. // IEEE Geoscience and Remote Sensing Letters. - 2010. - Vol. 7, No. 4. - P. 631-635.

J399. Meng Wei. Decorrelation of L-Band and C-Band Interferometry Over Vegetated Areas in California. / Meng Wei, Sandwell D.T. // IEEE Transactions on Geoscience and Remote Sensing. - 2010. - Vol. 48, No. 7. - P. 2942-2952.

J400. Hongxian Wang. Single-Range Image Fusion for Spinning Space Debris Radar Imaging. / Hongxian Wang, Yinghui Quan, Mengdao Xing, Shouhong Zhang. // IEEE Geoscience and Remote Sensing Letters. - 2010. - Vol. 7, No. 4. - P. 626-630.

J401. Tebaldini S. On the Role of Phase Stability in SAR Multibaseline Applications. / Tebaldini S., Guarnieri A.M. // IEEE Transactions on Geoscience and Remote Sensing. - 2010. - Vol. 48, No. 7. - P. 2953-2966.

J402. Estephan H. Optimal Waveform Design for Improved Indoor Target Detection in Sensing Through-the-Wall Applications. / Estephan H., Amin M.G., Yemelyanov K.M. // IEEE Transactions on Geoscience and Remote Sensing. - 2010. - Vol. 48, No. 7. - P. 2930-2941.

J403. Gujner B. Performance Study of a Cross-Frequency Detection Algorithm for Pulsed Sinusoidal RFI in Microwave Radiometry. / Gujner B., Niamsuwan N., Johnson J.T. // IEEE Transactions on Geoscience and Remote Sensing. - 2010. - Vol. 48, No. 7. - P. 2899-2908.

J404. Samsonov S. Topographic Correction for ALOS PALSAR Interferometry. IEEE Transactions on Geoscience and Remote Sensing. - 2010. - Vol. 48, No. 7. - P. 3020-3027.

J405. Fujimura A. Numerical Simulation of the Wind-Stress Effect on SAR Imagery of Far Wakes of Ships. / Fujimura A., Soloviev A., Kudryavtsev V. // IEEE Geoscience and Remote Sensing Letters. - 2010. - Vol. 7, No. 4. - P. 646-649.

J406. Pastina D. Multistatic and MIMO Distributed ISAR for Enhanced Cross-Range Resolution of Rotating Targets. / Pastina D., Bucciarelli M., Lombardo P. // IEEE Transactions on Geoscience and Remote Sensing. - 2010. - Vol. 48, No. 8. - P. 3300-3317.

J407. Di Martino G. Imaging of Fractal Profiles. / Di Martino G., Iodice A., Riccio D., Ruello G. // IEEE Transactions on Geoscience and Remote Sensing. - 2010. - Vol. 48, No. 8. - P. 3280-3289.

J408. Fornaro G. Potentials and Limitations of Moon-Borne SAR Imaging. / Fornaro G., Franceschetti G., Lombardini F., Mori A., Calamia M. // IEEE Transactions on Geoscience and Remote Sensing. - 2010. - Vol. 48, No. 7. - P. 3009-3019.

J409. Sakamoto T. Code-Division Multiple Transmission for High-Speed UWB Radar Imaging With an Antenna Array. / Sakamoto T., Sato T. // IEEE Transactions on Geoscience and Remote Sensing. - 2009. - Vol. 47, No. 4. - P. 1179-1186.

J410. Chu P.C. Statistical Characteristics of the Global Surface Current Speeds Obtained From Satellite Altimetry and Scatterometer Data. IEEE Journal of Selected Topics in Applied Earth Observations and Remote Sensing. - 2009. - Vol. 2, No. 1. - P. 27-32.

J411. Askne J. Automatic Model-Based Estimation of Boreal Forest Stem Volume From Repeat Pass C-band InSAR Coherence. / Askne J., Santoro M. // IEEE Transactions on Geoscience and Remote Sensing. - 2009. - Vol. 47, No. 2. - P. 513-516.

J412. Ya-Qiu Jin. Automatic Detection of Terrain Surface Changes After Wenchuan Earthquake, May 2008, From ALOS SAR Images Using 2EM-MRF Method. / Ya-Qiu Jin, Dafang Wang. // IEEE Geoscience and Remote Sensing Letters. - 2009. - Vol. 6, No. 2. - P. 344-348.

J413. Oguchi T. Measurements of Dielectric Constant of Volcanic Ash Erupted From Five Volcanoes in Japan. / Oguchi T., Udagawa M., Nanba N., Maki M., Ishimine Y. // IEEE Transactions on Geoscience and Remote Sensing. - 2009. - Vol. 47, No. 4. - P. 1089-1096.

J414. Roy A. Genetic-Algorithm-Based Parameter Estimation Technique for Fragmenting Radar Meteor Head Echoes. / Roy A., Briczinski S.J., Doherty J.F., Mathews J.D. // IEEE Geoscience and Remote Sensing Letters. - 2009. - Vol. 6, No. 3. - P. 363-367.

J415. Fortuny-Guasch J. A Fast and Accurate Far-Field Pseudopolar Format Radar Imaging Algorithm. IEEE Transactions on Geoscience and Remote Sensing. - 2009. - Vol. 47, No. 4. - P. 1187-1196.

J416. Monsivais-Huertero A. Estimation of Sahelian-Grassland Parameters Using a Coherent Scattering Model and a Genetic Algorithm. / Monsivais-Huertero A., Chenerie I., Sarabandi K. // IEEE Transactions on Geoscience and Remote Sensing. - 2009. - Vol. 47, No. 4. - P. 999-1011.

J417. Maaref N. A Study of UWB FM-CW Radar for the Detection of Human Beings in Motion Inside a Building. / Maaref N., Millot P., Pichot C., Picon O. // IEEE Transactions on Geoscience and Remote Sensing. - 2009. - Vol. 47, No. 5. - P. 1297-1300.

J418. Kaijun Song. Empirically Adopted IEM for Retrieval of Soil Moisture From Radar Backscattering Coefficients. / Kaijun Song, Xiaobing Zhou, Yong Fan. // IEEE Transactions on Geoscience and Remote Sensing. - 2009. - Vol. 47, No. 6. - P. 1662-1672.

J419. Brautigam B. An Efficient Method for Performance Monitoring of Active Phased Array Antennas. / Brautigam B., Schwerdt M., Bachmann M. // IEEE Transactions on Geoscience and Remote Sensing. - 2009. - Vol. 47, No. 4. - P. 1236-1243.

J420. Folkesson K. Model-Based Compensation of Topographic Effects for Improved Stem-Volume Retrieval From CARABAS-II VHF-Band SAR Images. / Folkesson K., Smith-Jonforsen G., Ulander L.M.H. // IEEE Transactions on Geoscience and Remote Sensing. - 2009. - Vol. 47, No. 4. - P. 1045-1055.

J421. Margarit G. Exploitation of Ship Scattering in Polarimetric SAR for an Improved Classification Under High Clutter Conditions. / Margarit G., Mallorqui J.J., Fortuny-Guasch J., Lopez-Martinez C. // IEEE Transactions on Geoscience and Remote Sensing. - 2009. - Vol. 47, No. 4. - P. 1224-1235.

J422. Hostache R. Water Level Estimation and Reduction of Hydraulic Model Calibration Uncertainties Using Satellite SAR Images of Floods. / Hostache R., Matgen P., Schumann G., Puech C., Hoffmann L., Pfister L. // IEEE Transactions on Geoscience and Remote Sensing. - 2009. - Vol. 47, No. 2. - P. 431-441.

J423. Kumar R. Comparison of TRMM TMI and PR Version 5 and 6 Precipitation Data Products Under Cyclonic Weather Conditions. / Kumar R., Varma A.K., Mishra A., Gairola R.M., Das I.M.L., Sarkar A., Agarwal V.K. // IEEE Geoscience and Remote Sensing Letters. - 2009. - Vol. 6, No. 3. - P. 378-382.

J424. Lei Zhang. Two-Dimensional Spectrum Matched Filter Banks for High-Speed Spinning-Target Three-Dimensional ISAR Imaging. / Lei Zhang, Meng-dao Xing, Cheng-Wei Qiu, Zheng Bao. // IEEE Geoscience and Remote Sensing Letters. - 2009. - Vol. 6, No. 3. - P. 368-372.

J425. Hajnsek I. Tropical-Forest-Parameter Estimation by Means of Pol-InSAR: The INDREX-II Campaign. / Hajnsek I., Kugler F., Seung-Kuk Lee, Papathanassiou K.P. // IEEE Transactions on Geoscience and Remote Sensing. - 2009. - Vol. 47, No. 2. - P. 481-493.

J426. Hajnsek I. Potential of Estimating Soil Moisture Under Vegetation Cover by Means of PolSAR. / Hajnsek I., Jagdhuber T., Schon H., Papathanassiou K.P. // IEEE Transactions on Geoscience and Remote Sensing. - 2009. - Vol. 47, No. 2. - P. 442-454.

J427. Luzi G. Using a Ground-Based SAR Interferometer and a Terrestrial Laser Scanner to Monitor a Snow-Covered Slope: Results From an Experimental Data Collection in Tyrol (Austria). / Luzi G., Noferini L., Mecatti D., Macaluso G., Pieraccini M., Atzeni C., Schaffhauser A., Fromm R., Nagler T. // IEEE Transactions on Geoscience and Remote Sensing. - 2009. - Vol. 47, No. 2. - P. 382-393.

J428. Bignami C. Microwave Signature of the Greenland Ice Sheet at Ku- and S-Bands. / Bignami C., Pierdicca N., Pulvirenti L. // IEEE Geoscience and Remote Sensing Letters. - 2009. - Vol. 6, No. 2. - P. 322-326.

J429. Zheng Xiang. A Model-Spectrum-Based Flattening Algorithm for Airborne Single-Pass SAR Interferometry. / Zheng Xiang, Kaizhi Wang, Xingzhao Liu. // IEEE Geoscience and Remote Sensing Letters. - 2009. - Vol. 6, No. 2. - P. 307-311.

J430. Yong Wang. ISAR Imaging of a Ship Target Using Product High-Order Matched-Phase Transform. / Yong Wang, Yicheng Jiang. // IEEE Geoscience and Remote Sensing Letters. - 2009. - Vol. 6, No. 4. - P. 658-661.

J431. Bachmann C.M. Bathymetric Retrieval From Hyperspectral Imagery Using Manifold Coordinate Representations. / Bachmann C.M., Ainsworth T.L., Fusina R.A., Montes M.J., Bowles J.H., Korwan D.R., Gillis D.B. // IEEE Transactions on Geoscience and Remote Sensing. - 2009. - Vol. 47, No. 3. - P. 884-897.

J432. Guoqing Zhou. Near Real-Time Orthorectification and Mosaic of Small UAV Video Flow for Time-Critical Event Response. IEEE Transactions on Geoscience and Remote Sensing. - 2009. - Vol. 47, No. 3. - P. 739-747.

J433. Braun M. Recent Retreat of Wilkins Ice Shelf Reveals New Insights in Ice Shelf Breakup Mechanisms. / Braun M., Humbert A. // IEEE Geoscience and Remote Sensing Letters. - 2009. - Vol. 6, No. 2. - P. 263-267.

J434. West R.D. Cassini RADAR Sequence Planning and Instrument Performance. / West R.D., Anderson Y., Boehmer R., Borgarelli L., Callahan P., Elachi C., Yonggyu Gim, Hamilton G., Hensley S., Janssen M.A., Johnson W., Kelleher K., Lorenz R., Ostro S., Roth L., Shaffer S., Stiles B., Wall S., Wye L.C., Zebker H.A. // IEEE Transactions on Geoscience and Remote Sensing. - 2009. - Vol. 47, No. 6. - P. 1777-1795.

J435. Charalampidis D. Efficient Directional Gaussian Smoothers. IEEE Geoscience and Remote Sensing Letters. - 2009. - Vol. 6, No. 3. - P. 383-387.

J436. Agram P.S. Sparse Two-Dimensional Phase Unwrapping Using Regular-Grid Methods. / Agram P.S., Zebker H.A. // IEEE Geoscience and Remote Sensing Letters. - 2009. - Vol. 6, No. 2. - P. 327-331.

J437. Hee-Sub Shin. Omega-k Algorithm for Airborne Forward-Looking Bistatic Spotlight SAR Imaging. / Hee-Sub Shin, Jong-Tae Lim. // IEEE Geoscience and Remote Sensing Letters. - 2009. - Vol. 6, No. 2. - P. 312-316.

J438. Battaglia A. Rain Observations by a Multifrequency Dual-Polarized Radiometer. / Battaglia A., Saavedra P., Simmer C., Rose T. // IEEE Geoscience and Remote Sensing Letters. - 2009. - Vol. 6, No. 2. - P. 354-358.

J439. Martinez-Espla J.J. A Particle Filter Approach for InSAR Phase Filtering and Unwrapping. / Martinez-Espla J.J., Martinez-Marin T., Lopez-Sanchez J.M. // IEEE Transactions on Geoscience and Remote Sensing. - 2009. - Vol. 47, No. 4. - P. 1197-1211.

J440. Xueru Bai. High-Resolution Three-Dimensional Imaging of Spinning Space Debris. / Xueru Bai, Mengdao Xing, Feng Zhou, Zheng Bao. // IEEE Transactions on Geoscience and Remote Sensing. - 2009. - Vol. 47, No. 7. - P. 2352-2362.

J441. Mengdao Xing. A Matched-Filter-Bank-Based 3-D Imaging Algorithm for Rapidly Spinning Targets. / Mengdao Xing, Qi Wang, Genyuan Wang, Zheng Bao. // IEEE Transactions on Geoscience and Remote Sensing. - 2009. - Vol. 47, No. 7. - P. 2106-2113.

J442. Frey O. Focusing of Airborne Synthetic Aperture Radar Data From Highly Nonlinear Flight Tracks. / Frey O., Magnard C., Ruegg M., Meier E. // IEEE Transactions on Geoscience and Remote Sensing. - 2009. - Vol. 47, No. 6. - P. 1844-1858.

J443. Cossio T. Predicting Topographic and Bathymetric Measurement Performance for Low-SNR Airborne Lidar. / Cossio T., Slatton K.C., Carter W., Shrestha K., Harding D. // IEEE Transactions on Geoscience and Remote Sensing. - 2009. - Vol. 47, No. 7. - P. 2298-2315.

J444. Aldhubaib F.F.H. Characteristic Polarization States Estimation in an Ultrawideband Context: A Frequency Approach. / Aldhubaib F.F.H., Shuley N.V.Z. // IEEE Transactions on Geoscience and Remote Sensing. - 2009. - Vol. 47, No. 8. - P. 2808-2817.

J445. Feng Zhou. Narrow-Band Interference Suppression for SAR Based on Complex Empirical Mode Decomposition. / Feng Zhou, Mengdao Xing, Xueru Bai, Guangcai Sun, Zheng Bao. // IEEE Geoscience and Remote Sensing Letters. - 2009. - Vol. 6, No. 3. - P. 423-427.

J446. Dogaru T. SAR Images of Rooms and Buildings Based on FDTD Computer Models. / Dogaru T., Le C. // IEEE Transactions on Geoscience and Remote Sensing. - 2009. - Vol. 47, No. 5. - P. 1388-1401.

J447. Chang P.C. High-Frequency EM Characterization of Through-Wall Building Imaging. / Chang P.C., Burkholder R.J., Volakis J.L., Marhefka R.J., Bayram Y. // IEEE Transactions on Geoscience and Remote Sensing. - 2009. - Vol. 47, No. 5. - P. 1375-1387.

J448. Yunjin Kim. A Time-Series Approach to Estimate Soil Moisture Using Polarimetric Radar Data. / Yunjin Kim, van Zyl J.J. // IEEE Transactions on Geoscience and Remote Sensing. - 2009. - Vol. 47, No. 8. - P. 2519-2527.

J449. Storvik B. On the Combination of Multisensor Data Using Meta-Gaussian Distributions. / Storvik B., Storvik G., Fjortoft R. // IEEE Transactions on Geoscience and Remote Sensing. - 2009. - Vol. 47, No. 7. - P. 2372-2379.

J450. Flores A.N. Impact of Hillslope-Scale Organization of Topography, Soil Moisture, Soil Temperature, and Vegetation on Modeling Surface Microwave Radiation Emission. / Flores A.N., Ivanov V.Y., Entekhabi D., Bras R.L. // IEEE Transactions on Geoscience and Remote Sensing. - 2009. - Vol. 47, No. 8. - P. 2557-2571.

J451. Yisok Oh. Polarimetric Backscattering Coefficients of Flooded Rice Fields at L- and C-Bands: Measurements, Modeling, and Data Analysis. / Yisok Oh, Suk-Young Hong, Yunjin Kim, Jin-Young Hong, Yi-Hyun Kim. // IEEE Transactions on Geoscience and Remote Sensing. - 2009. - Vol. 47, No. 8. - P. 2714-2721.

J452. Miller P.E. Assessment of Glacier Volume Change Using ASTER-Based Surface Matching of Historical Photography. / Miller P.E., Kunz M., Mills J.P., King M.A., Murray T., James T.D., Marsh S.H. // IEEE Transactions on Geoscience and Remote Sensing. - 2009. - Vol. 47, No. 7. - P. 1971-1979.

J453. Yurchak B.S. Radar Volume Backscatter From Spatially Extended Geophysical Targets in a "Slice" Approach. IEEE Transactions on Geoscience and Remote Sensing. - 2009. - Vol. 47, No. 11. - P. 3690-3696.

J454. Debes C. Target Detection in Single- and Multiple-View Through-the-Wall Radar Imaging. / Debes C., Amin M.G., Zoubir A.M. // IEEE Transactions on Geoscience and Remote Sensing. - 2009. - Vol. 47, No. 5. - P. 1349-1361.

J455. Candy B. A Comparison of the Impact of QuikScat and WindSat Wind Vector Products on Met Office Analyses and Forecasts. / Candy B., English S.J., Keogh S.J. // IEEE Transactions on Geoscience and Remote Sensing. - 2009. - Vol. 47, No. 6. - P. 1632-1640.

J456. Wang R. Focusing Spaceborne/Airborne Hybrid Bistatic SAR Data Using Wavenumber-Domain Algorithm. / Wang R., Loffeld O., Nies H., Ender J. // IEEE Transactions on Geoscience and Remote Sensing. - 2009. - Vol. 47, No. 7. - P. 2275-2283.

J457. Amin M. Special Issue on Remote Sensing of Building Interior. / Amin M., Sarabandi K. // IEEE Transactions on Geoscience and Remote Sensing. - 2009. - Vol. 47, No. 5. - P. 1267-1268.

J458. Nunziata F. The Two-Scale BPM Scattering Model for Sea Biogenic Slicks Contrast. / Nunziata F., Sobieski P., Migliaccio M. // IEEE Transactions on Geoscience and Remote Sensing. - 2009. - Vol. 47, No. 7. - P. 1949-1956.

J459. Luojus K.P. Comparison of SAR-Based Snow-Covered Area Estimation Methods for the Boreal Forest Zone. / Luojus K.P., Pulliainen J.T., Blasco Cutrona A., Metsamaki S.J., Hallikainen M.T. // IEEE Geoscience and Remote Sensing Letters. - 2009. - Vol. 6, No. 3. - P. 403-407.

J460. Dehmollaian M. Through-the-Wall Imaging Using Differential SAR. / Dehmollaian M., Thiel M., Sarabandi K. // IEEE Transactions on Geoscience and Remote Sensing. - 2009. - Vol. 47, No. 5. - P. 1289-1296.

J461. Tournadre J. Cloud and Rain Effects on AltiKa/SARAL Ka-Band Radar Altimeter-Part II: Definition of a Rain/Cloud Flag. / Tournadre J., Lambin-Artru J., Steunou N. // IEEE Transactions on Geoscience and Remote Sensing. - 2009. - Vol. 47, No. 6. - P. 1818-1826.

J462. Tournadre J. Cloud and Rain Effects on AltiKa/SARAL Ka-Band Radar Altimeter-Part I: Modeling and Mean Annual Data Availability. / Tournadre J., Lambin-Artru J., Steunou N. // IEEE Transactions on Geoscience and Remote Sensing. - 2009. - Vol. 47, No. 6. - P. 1806-1817.

J463. Quartly G.D. Optimizing Information From the Jason-2 Altimeter. IEEE Geoscience and Remote Sensing Letters. - 2009. - Vol. 6, No. 3. - P. 398-402.

J464. Sauer S. Polarimetric Dual-Baseline InSAR Building Height Estimation at L-Band. / Sauer S., Ferro-Famil L., Reigber A., Pottier E. // IEEE Geoscience and Remote Sensing Letters. - 2009. - Vol. 6, No. 3. - P. 408-412.

J465. Cuizhen Wang. Characterizing L-Band Scattering of Paddy Rice in Southeast China With Radiative Transfer Model and Multitemporal ALOS/PALSAR Imagery. / Cuizhen Wang, Jiaping Wu, Yuan Zhang, Guangdong Pan, Jiaguo Qi, Salas W.A. // IEEE Transactions on Geoscience and Remote Sensing. - 2009. - Vol. 47, No. 4. - P. 988-998.

J466. Eineder M. Spaceborne Spotlight SAR Interferometry With TerraSAR-X. / Eineder M., Adam N., Bamler R., Yague-Martinez N., Breit H. // IEEE Transactions on Geoscience and Remote Sensing. - 2009. - Vol. 47, No. 5. - P. 1524-1535.

J467. Youngwook Kim. Human Activity Classification Based on Micro-Doppler Signatures Using a Support Vector Machine. / Youngwook Kim, Hao Ling. // IEEE Transactions on Geoscience and Remote Sensing. - 2009. - Vol. 47, No. 5. - P. 1328-1337.

J468. Pasolli E. Automatic Analysis of GPR Images: A Pattern-Recognition Approach. / Pasolli E., Melgani F., Donelli M. // IEEE Transactions on Geoscience and Remote Sensing. - 2009. - Vol. 47, No. 7. - P. 2206-2217.

J469. Ertin E. Through-the-Wall SAR Attributed Scattering Center Feature Estimation. / Ertin E., Moses R.L. // IEEE Transactions on Geoscience and Remote Sensing. - 2009. - Vol. 47, No. 5. - P. 1338-1348.

J470. Kokhanovsky A.A. Intercomparison of Ground-Based Radar and Satellite Cloud-Top Height Retrievals for Overcast Single-Layered Cloud Fields. / Kokhanovsky A.A., Naud C.M., Devasthale A. // IEEE Transactions on Geoscience and Remote Sensing. - 2009. - Vol. 47, No. 7. - P. 1901-1908.

J471. Cheng Wang. Separation of Ground and Low Vegetation Signatures in LiDAR Measurements of Salt-Marsh Environments. / Cheng Wang, Menenti M., Stoll M.-P., Feola A., Belluco E., Marani M. // IEEE Transactions on Geoscience and Remote Sensing. - 2009. - Vol. 47, No. 7. - P. 2014-2023.

J472. Yunqiang Yang. Development and Implementation of a Real-Time See-Through-Wall Radar System Based on FPGA. / Yunqiang Yang, Fathy A.E. // IEEE Transactions on Geoscience and Remote Sensing. - 2009. - Vol. 47, No. 5. - P. 1270-1280.

J473. Margarit G. Phenomenological Vessel Scattering Study Based on Simulated Inverse SAR Imagery. / Margarit G., Mallorqui J.J., Fortuny-Guasch J., Lopez-Martinez C. // IEEE Transactions on Geoscience and Remote Sensing. - 2009. - Vol. 47, No. 4. - P. 1212-1223.

J474. Cameron W.L. Polarization Symmetric Scatterer Metric Space. / Cameron W.L., Rais H. // IEEE Transactions on Geoscience and Remote Sensing. - 2009. - Vol. 47, No. 4. - P. 1097-1107.

J475. Fattahi H. Windowed Fourier Transform for Noise Reduction of SAR Interferograms. / Fattahi H., Zoej M.J.V., Mobasheri M.R., Dehghani M., Sahebi M.R. // IEEE Geoscience and Remote Sensing Letters. - 2009. - Vol. 6, No. 3. - P. 418-422.

J476. Sang-Eun Park. Estimation of Surface Roughness Parameter in Intertidal Mudflat Using Airborne Polarimetric SAR Data. / Sang-Eun Park, Moon W.M., Duk-jin Kim. // IEEE Transactions on Geoscience and Remote Sensing. - 2009. - Vol. 47, No. 4. - P. 1022-1031.

J477. Mattia F. Foreword to the Special Issue on Retrieval of Bio- and Geophysical Parameters From SAR

Data for Land Applications. / Mattia F., Floury N., Moreira A. // IEEE Transactions on Geoscience and Remote Sensing. - 2009. - Vol. 47, No. 2. - P. 379-380.

J478. Dong-Bin Shin. Variability of Passive Microwave Radiometric Signatures at Different Spatial Resolutions and Its Implication for Rainfall Estimation. / Dong-Bin Shin, Bowman K.P., Jung-Moon Yoo, Chiu L.S. // IEEE Transactions on Geoscience and Remote Sensing. - 2009. - Vol. 47, No. 6. - P. 1575-1584.

J479. Dehmollaian M. Optimum Polarizations for Discrimination of a Foliage-Camouflaged Target, Using Genetic Algorithms. / Dehmollaian M., Sarabandi K. // IEEE Geoscience and Remote Sensing Letters. - 2009. - Vol. 6, No. 1. - P. 82-86.

J480. Gonzalez-Partida J.-T. Through-the-Wall Surveillance With Millimeter-Wave LFMCW Radars. / Gonzalez-Partida J.-T., Almorox-Gonzalez P., Burgos-Garcia M., Dorta-Naranjo B.-P., Alonso J.I. // IEEE Transactions on Geoscience and Remote Sensing. - 2009. - Vol. 47, No. 6. - P. 1796-1805.

J481. Johnson J.T. A Numerical Study of the Retrieval of Sea Surface Height Profiles From Low Grazing Angle Radar Data. / Johnson J.T., Burkholder R.J., Toporkov J.V., Lyzenga D.R., Plant W.J. // IEEE Transactions on Geoscience and Remote Sensing. - 2009. - Vol. 47, No. 6. - P. 1641-1650.

J482. Tran N. Defining a Sea Ice Flag for Envisat Altimetry Mission. / Tran N., Girard-Ardhuin F., Ezraty R., Feng H., Femenias P. // IEEE Geoscience and Remote Sensing Letters. - 2009. - Vol. 6, No. 1. - P. 77-81.

J483. Le K.D. On the Use of Auxiliary Receive Channels for Clutter Mitigation With Phased Array Weather Radars. / Le K.D., Palmer R.D., Boon Leng Cheong, Tian-You Yu, Guifu Zhang, Torres S.M., Le K.D., Palmer R.D. // IEEE Transactions on Geoscience and Remote Sensing. - 2009. - Vol. 47, No. 1. - P. 272-284.

J484. Corbella I. Brightness-Temperature Retrieval Methods in Synthetic Aperture Radiometers. / Corbella I., Corbella I., Torres F., Torres F., Camps A., Camps A., Duffo N., Duffo N., Vall-llossera M., Vall-llossera M. // IEEE Transactions on Geoscience and Remote Sensing. - 2009. - Vol. 47, No. 1. - P. 285-294.

J485. Voge M. Installation of a Doppler Radar Monitoring System at Merapi Volcano, Indonesia. / Voge M., Hort M. // IEEE Transactions on Geoscience and Remote Sensing. - 2009. - Vol. 47, No. 1. - P. 251-271.

J486. Jehle M. Measurement of Ionospheric Faraday Rotation in Simulated and Real Spaceborne SAR Data. / Jehle M., Ruegg M., Zuberbuhler L., Small D., Meier E. // IEEE Transactions on Geoscience and Remote Sensing. - 2009. - Vol. 47, No. 5. - P. 1512-1523.

J487. Mar J. Implementation of SDR Digital Beamformer for Microsatellite SAR. / Mar J., You-Rong Lin. // IEEE Geoscience and Remote Sensing Letters. - 2009. - Vol. 6, No. 1. - P. 92-96.

J488. Liebe J.R. Suitability and Limitations of ENVISAT ASAR for Monitoring Small Reservoirs in a Semiarid Area. / Liebe J.R., van de Giesen N., Andreini M.S., Steenhuis T.S., Walter M.T. // IEEE Transactions on Geoscience and Remote Sensing. - 2009. - Vol. 47, No. 5. - P. 1536-1547.

J489. Fuller M.C. Surface-Based Polarimetric C-Band Microwave Scatterometer Measurements of Snow During a Chinook Event. / Fuller M.C., Geldsetzer T., Yackel J.J. // IEEE Transactions on Geoscience and Remote Sensing. - 2009. - Vol. 47, No. 6. - P. 1766-1776.

J490. Gui Gao. An Adaptive and Fast CFAR Algorithm Based on Automatic Censoring for Target Detection in High-Resolution SAR Images. / Gui Gao, Li Liu, Lingjun Zhao, Gongtao Shi, Gangyao Kuang. // IEEE Transactions on Geoscience and Remote Sensing. - 2009. - Vol. 47, No. 6. - P. 1685-1697.

J491. Ebihara S. Analysis of Eccentered Dipole Antenna for Borehole Radar. / Ebihara S., Inoue Y. // IEEE Transactions on Geoscience and Remote Sensing. - 2009. - Vol. 47, No. 4. - P. 1073-1088.

J492. Notarnicola C. Cassini Radar Data: Estimation of Titan's Lake Features by Means of a Bayesian Inversion Algorithm. / Notarnicola C., Ventura B., Casarano D., Posa F. // IEEE Transactions on Geoscience and Remote Sensing. - 2009. - Vol. 47, No. 5. - P. 1503-1511.

J493. Luojus K.P. Enhanced SAR-Based Snow-Covered Area Estimation Method for Boreal Forest Zone. / Luojus K.P., Pulliainen J.T., Metsamaki S.J., Hallikainen M.T. // IEEE Transactions on Geoscience and Remote Sensing. - 2009. - Vol. 47, No. 3. - P. 922-935.

J494. Prats P. Estimation of the Surface Velocity Field of the Aletsch Glacier Using Multibaseline Airborne SAR Interferometry. / Prats P., Scheiber R., Reigber A., Andres C., Horn R. // IEEE Transactions on Geoscience and Remote Sensing. - 2009. - Vol. 47, No. 2. - P. 419-430.

J495. De Grandi G.D. Analysis by Wavelet Frames of Spatial Statistics in SAR Data for Characterizing Structural Properties of Forests. / De Grandi G.D., Lucas R.M., Kropacek J. // IEEE Transactions on Geoscience and Remote Sensing. - 2009. - Vol. 47, No. 2. - P. 494-507.

J496. Khazaal A. On the Reduction of the Systematic Error in Imaging Radiometry by Aperture Synthesis: A New Approach for the SMOS Space Mission. / Khazaal A., Carfantan H., Anterrieu E. // IEEE Geoscience and Remote Sensing Letters. - 2009. - Vol. 6, No. 1. - P. 47-51.

J497. Zhijie Mao. Optimum Data Vector Approach to Multibaseline SAR Interferometry Phase Unwrapping. / Zhijie Mao, Guisheng Liao. // IEEE Geoscience and Remote Sensing Letters. - 2009. - Vol. 6, No. 1. - P. 42-46.

J498. Chini M. Exploiting SAR and VHR Optical Images to Quantify Damage Caused by the 2003 Bam Earthquake. / Chini M., Pierdicca N., Emery W.J. // IEEE Transactions on Geoscience and Remote Sensing. - 2009. - Vol. 47, No. 1. - P. 145-152.

J499. Pons Bernad G. Hierarchical Feature-Based Classification Approach for Fast and User-Interactive SAR Image Interpretation. / Pons Bernad G., Denise L., Refregier P. // IEEE Geoscience and Remote Sensing Letters. - 2009. - Vol. 6, No. 1. - P. 117-121.

J500. Xi Chen. DEM Generation Combining SAR Polarimetry and Shape-From-Shading Techniques. / Xi Chen, Chao Wang, Hong Zhang. // IEEE Geoscience and Remote Sensing Letters. - 2009. - Vol. 6, No. 1. - P. 28-32.

J501. Bin Deng. A Novel Approach to Range Doppler SAR Processing Based on Legendre Orthogonal Polynomials. / Bin Deng, Yuliang Qin, Yanpeng Li, Hongqiang Wang, Xiang Li. // IEEE Geoscience and Remote Sensing Letters. - 2009. - Vol. 6, No. 1. - P. 13-17.

J502. Yeary M.B. A Support-Vector-Machine-Based Approach to RF Sensor Spectral Signature Classifications. / Yeary M.B., Nemati S., Tian-You Yu, Yadong Wang, Yan Zhai. // IEEE Transactions on Instrumentation and Measurement. - 2009. - Vol. 58, No. 1. - P. 221-228.

J503. Xuan Feng. CMP Antenna Array GPR and Signal-to-Clutter Ratio Improvement. / Xuan Feng, Sato M., Yan Zhang, Cai Liu, Fusheng Shi, Yonghui Zhao. // IEEE Geoscience and Remote Sensing Letters. - 2009. - Vol. 6, No. 1. - P. 23-27.

J504. Yamaki R. Singular Unit Restoration in Interferograms Based on Complex-Valued Markov Random Field Model for Phase Unwrapping. / Yamaki R., Hirose A. // IEEE Geoscience and Remote Sensing Letters. - 2009. - Vol. 6, No. 1. - P. 18-22.

J505. Renga A. Performance of Stereoradargrammetric Methods Applied to Spaceborne Monostatic-Bistatic Synthetic Aperture Radar. / Renga A., Moccia A. // IEEE Transactions on Geoscience and Remote Sensing. - 2009. - Vol. 47, No. 2. - P. 544-560.

J506. Hee-Sub Shin. Omega-k Algorithm for Airborne Spatial Invariant Bistatic Spotlight SAR Imaging. / Hee-Sub Shin, Jong-Tae Lim. // IEEE Transactions on Geoscience and Remote Sensing. - 2009. - Vol. 47, No. 1. - P. 238-250.

J507. Jong-Sen Lee. Improved Sigma Filter for Speckle Filtering of SAR Imagery. / Jong-Sen Lee, Jong-Sen Lee, Jen-Hung Wen, Ainsworth T.L., Kun-Shan Chen, Chen A.J. // IEEE Transactions on Geoscience and Remote Sensing. - 2009. - Vol. 47, No. 1. - P. 202-213.

J508. Kaasalainen S. Radiometric Calibration of LIDAR Intensity With Commercially Available Reference Targets. / Kaasalainen S., Hyyppa H., Kukko A., Litkey P., Ahokas E., Hyyppa J., Lehner H., Jaakkola A., Suomalainen J., Akujarvi A., Kaasalainen M., Pyysalo U. // IEEE Transactions on Geoscience and Remote Sensing. - 2009. - Vol. 47, No. 2. - P. 588-598.

J509. Ferraiuolo G. DEM Reconstruction Accuracy in Multichannel SAR Interferometry. / Ferraiuolo G., Meglio F., Pascazio V., Schirinzi G. // IEEE Transactions on Geoscience and Remote Sensing. - 2009. - Vol. 47, No. 1.

- P. 191-201.

J510. Fornaro G. Four-Dimensional SAR Imaging for Height Estimation and Monitoring of Single and Double Scatterers. / Fornaro G., Reale D., Serafino F. // IEEE Transactions on Geoscience and Remote Sensing. - 2009. - Vol. 47, No. 1. - P. 224-237.

J511. Matsuoka K. Effects of Birefringence Within Ice Sheets on Obliquely Propagating Radio Waves. / Matsuoka K., Wilen L., Hurley S.P., Raymond C.F. // IEEE Transactions on Geoscience and Remote Sensing. - 2009. - Vol. 47, No. 5. - P. 1429-1443.

J512. Nord M.E. Comparison of Compact Polarimetric Synthetic Aperture Radar Modes. / Nord M.E., Nord M.E., Ainsworth T.L., Jong-Sen Lee, Stacy N.J.S. // IEEE Transactions on Geoscience and Remote Sensing. - 2009. - Vol. 47, No. 1. - P. 174-188.

J513. Fornaro G. LMMSE 3-D SAR Focusing. / Fornaro G., Pauciullo A. // IEEE Transactions on Geoscience and Remote Sensing. - 2009. - Vol. 47, No. 1. - P. 214-223.

J514. Longepe N. Snowpack Characterization in Mountainous Regions Using C-Band SAR Data and a Meteorological Model. / Longepe N., Allain S., Ferro-Famil L., Pottier E., Durand Y. // IEEE Transactions on Geoscience and Remote Sensing. - 2009. - Vol. 47, No. 2. - P. 406-418.

J515. Satalino G. Wheat Crop Mapping by Using ASAR AP Data. / Satalino G., Mattia F., Le Toan T., Rinaldi M. // IEEE Transactions on Geoscience and Remote Sensing. - 2009. - Vol. 47, No. 2. - P. 527-530.

J516. Bouvet A. Monitoring of the Rice Cropping System in the Mekong Delta Using ENVISAT/ASAR Dual Polarization Data. / Bouvet A., Le Toan T., Nguyen Lam-Dao. // IEEE Transactions on Geoscience and Remote Sensing. - 2009. - Vol. 47, No. 2. - P. 517-526.

J517. Trudel M. Application of Target Decomposition Theorems Over Snow-Covered Forested Areas. / Trudel M., Magagi R., Granberg H.B. // IEEE Transactions on Geoscience and Remote Sensing. - 2009. - Vol. 47, No. 2. - P. 508-512.

J518. Nannini M. Estimation of the Minimum Number of Tracks for SAR Tomography. / Nannini M., Scheiber R., Moreira A. // IEEE Transactions on Geoscience and Remote Sensing. - 2009. - Vol. 47, No. 2. - P. 531-543.

J519. Xuan Feng. Profiling the Rough Surface by Migration. / Xuan Feng, Sato M., Cai Liu, Yan Zhang. // IEEE Geoscience and Remote Sensing Letters. - 2009. - Vol. 6, No. 2. - P. 258-262.

J520. Chamundeeswari V.V. An Analysis of Texture Measures in PCA-Based Unsupervised Classification of SAR Images. / Chamundeeswari V.V., Singh D., Singh K. // IEEE Geoscience and Remote Sensing Letters. - 2009. - Vol. 6, No. 2. - P. 214-218.

J521. Toutin T. 3-D Radargrammetric Modeling of RADARSAT-2 Ultrafine Mode: Preliminary Results of the Geometric Calibration. / Toutin T., Chenier R. // IEEE Geoscience and Remote Sensing Letters. - 2009. - Vol. 6, No. 2. - P. 282-286.

J522. Xiangdong Meng. Short-Range Clutter Suppression for Airborne Radar by Utilizing Prefiltering in Elevation. / Xiangdong Meng, Tong Wang, Jianxin Wu, Zheng Bao. // IEEE Geoscience and Remote Sensing Letters. - 2009. - Vol. 6, No. 2. - P. 268-272.

J523. Isleifson D. C-Band Scatterometer Measurements of Multiyear Sea Ice Before Fall Freeze-Up in the Canadian Arctic. / Isleifson D., Langlois A., Barber D.G., Shafai L. // IEEE Transactions on Geoscience and Remote Sensing. - 2009. - Vol. 47, No. 6. - P. 1651-1661.

J524. Slob E. Interferometry by Deconvolution of Multicomponent Multioffset GPR Data. IEEE Transactions on Geoscience and Remote Sensing. - 2009. - Vol. 47, No. 3. - P. 828-838.

J525. Pathe C. Using ENVISAT ASAR Global Mode Data for Surface Soil Moisture Retrieval Over Oklahoma, USA. / Pathe C., Wagner W., Sabel D., Doubkova M., Basara J.B. // IEEE Transactions on Geoscience and Remote Sensing. - 2009. - Vol. 47, No. 2. - P. 468-480.

J526. Enjolras V.M. Using Altimetry Waveform Data and Ancillary Information From SRTM, Landsat, and

MODIS to Retrieve River Characteristics. / Enjolras V.M., Rodriguez E. // IEEE Transactions on Geoscience and Remote Sensing. - 2009. - Vol. 47, No. 6. - P. 1869-1881.

J527. Goller A. Radar image processing with clusters of computers. / Goller A., Leberl F. // IEEE Aerospace and Electronic Systems Magazine. - 2009. - Vol. 24, No. 1. - P. 18-22.

J528. Nakamura K. Observation of Sea-Ice Thickness Using ENVISAT Data From LЬtzow-Holm Bay, East Antarctica. / Nakamura K., Wakabayashi H., Uto S., Ushio S., Nishio F. // IEEE Geoscience and Remote Sensing Letters. - 2009. - Vol. 6, No. 2. - P. 277-281.

J529. Wen-Qin Wang. Waveform-Diversity-Based Millimeter-Wave UAV SAR Remote Sensing. / Wen-Qin Wang, Qicong Peng, Jingye Cai. // IEEE Transactions on Geoscience and Remote Sensing. - 2009. - Vol. 47, No. 3. - P. 691-700.

J530. Baselice F. DEM Reconstruction in Layover Areas From SAR and Auxiliary Input Data. / Baselice F., Ferraioli G., Pascazio V. // IEEE Geoscience and Remote Sensing Letters. - 2009. - Vol. 6, No. 2. - P. 253-257.

J531. Enjolras V.M. An Assessment of a Ka-Band Radar Interferometer Mission Accuracy Over Eurasian Rivers. / Enjolras V.M., Rodriguez E. // IEEE Transactions on Geoscience and Remote Sensing. - 2009. - Vol. 47, No. 6. - P. 1752-1765.

J532. Praks J. Using Multilook Averaging for Coherently Modeled Scattering From a Pine Tree at L-Band. / Praks J., Sarvas J., Hallikainen M., Pulliainen J. // IEEE Geoscience and Remote Sensing Letters. - 2009. - Vol. 6, No. 1. - P. 162-166.

J533. Jun S. Radix- Resolution-Fusion for LASAR via Orthogonal Complement Decomposition. / Jun S., Xiaoling Z., Jianyu Y., Junjie W. // IEEE Geoscience and Remote Sensing Letters. - 2009. - Vol. 6, No. 1. - P. 147-151.

J534. Zhang Zenghui. Local Degrees of Freedom of Airborne Array Radar Clutter for STAP. / Zhang Zenghui, Xie Wenchong, Hu Weidong, Yu Wenxian. // IEEE Geoscience and Remote Sensing Letters. - 2009. - Vol. 6, No. 1. - P. 97-101.

J535. Pipia L. Polarimetric Differential SAR Interferometry: First Results With Ground-Based Measurements. / Pipia L., Fabregas X., Aguasca A., Lopez-Martinez C., Duque S., Mallorqui J.J., Marturia J. // IEEE Geoscience and Remote Sensing Letters. - 2009. - Vol. 6, No. 1. - P. 167-171.

J536. Wei Jing. Unambiguous Reconstruction and High-Resolution Imaging for Multiple-Channel SAR and Airborne Experiment Results. / Wei Jing, Mengdao Xing, Cheng-Wei Qiu, Zheng Bao, Tat-Soon Yeo. // IEEE Geoscience and Remote Sensing Letters. - 2009. - Vol. 6, No. 1. - P. 102-106.

J537. Nielsen S.N. A Wind and Rain Backscatter Model Derived From AMSR and SeaWinds Data. / Nielsen S.N., Long D.G. // IEEE Transactions on Geoscience and Remote Sensing. - 2009. - Vol. 47, No. 6. - P. 1595-1606.

J538. Wang R. Chirp-Scaling Algorithm for Bistatic SAR Data in the Constant-Offset Configuration. / Wang R., Loffeld O., Nies H., Knedlik S., Ender J. // IEEE Transactions on Geoscience and Remote Sensing. - 2009. - Vol. 47, No. 3. - P. 952-964.

J539. Scialom G. RONSARD Radar: Implementation of Dual Polarization on a C-Band Doppler Weather Radar. / Scialom G., Faroux J., Giraud M., Ney R., Evaristo R., Lemaitre Y., Viltard N. // IEEE Geoscience and Remote Sensing Letters. - 2009. - Vol. 6, No. 1. - P. 132-136.

J540. King M.A. The GPS Contribution to the Error Budget of Surface Elevations Derived From Airborne LIDAR. IEEE Transactions on Geoscience and Remote Sensing. - 2009. - Vol. 47, No. 3. - P. 874-883.

J541. Antoniou M. Space-Surface Bistatic SAR Image Formation Algorithms. / Antoniou M., Cherniakov M., Cheng Hu. // IEEE Transactions on Geoscience and Remote Sensing. - 2009. - Vol. 47, No. 6. - P. 1827-1843.

J542. Eldhuset K. Spaceborne Bistatic SAR Processing Using the EETF4 Algorithm. IEEE Geoscience and Remote Sensing Letters. - 2009. - Vol. 6, No. 2. - P. 194-198.

J543. Erten E. Glacier Velocity Monitoring by Maximum Likelihood Texture Tracking. / Erten E., Reigber A., Hellwich O., Prats P. // IEEE Transactions on Geoscience and Remote Sensing. - 2009. - Vol. 47, No. 2. - P. 394-405.

J544. Yoon Y.T. TerraSAR-X Precise Trajectory Estimation and Quality Assessment. / Yoon Y.T., Eineder M., Yague-Martinez N., Montenbruck O. // IEEE Transactions on Geoscience and Remote Sensing. - 2009. - Vol. 47, No. 6. - P. 1859-1868.

J545. Daiyin Zhu. Robust ISAR Range Alignment via Minimizing the Entropy of the Average Range Profile. / Daiyin Zhu, Ling Wang, Yusheng Yu, Qingnian Tao, Zhaoda Zhu. // IEEE Geoscience and Remote Sensing Letters. - 2009. - Vol. 6, No. 2. - P. 204-208.

J546. Sandberg G. Measurements of Faraday Rotation Using Polarimetric PALSAR Images. / Sandberg G., Eriksson L., Ulander L. // IEEE Geoscience and Remote Sensing Letters. - 2009. - Vol. 6, No. 1. - P. 142-146.

J547. Wolfmuller M. Data Flow and Workflow Organization-The Data Management for the TerraSAR-X Payload Ground Segment. / Wolfmuller M., Dietrich D., Sireteanu E., Kiemle S., Mikusch E., Bottcher M. // IEEE Transactions on Geoscience and Remote Sensing. - 2009. - Vol. 47, No. 1. - P. 44-50.

J548. Pauwels V.R.N. Optimization of Soil Hydraulic Model Parameters Using Synthetic Aperture Radar Data: An Integrated Multidisciplinary Approach. / Pauwels V.R.N., Balenzano A., Satalino G., Skriver H., Verhoest N.E.C., Mattia F. // IEEE Transactions on Geoscience and Remote Sensing. - 2009. - Vol. 47, No. 2. - P. 455-467.

J549. Kaheil Y.H. Detecting and Downscaling Wet Areas on Boreal Landscapes. / Kaheil Y.H., Creed I.F. // IEEE Geoscience and Remote Sensing Letters. - 2009. - Vol. 6, No. 2. - P. 179-183.

J550. Buler J.J. Quantifying Bird Density During Migratory Stopover Using Weather Surveillance Radar. / Buler J.J., Diehl R.H. // IEEE Transactions on Geoscience and Remote Sensing. - 2009. - Vol. 47, No. 8. - P. 2741-2751.

J551. Shum C.K. Orbit Accuracy Requirement for ABYSS: The Space Station Radar Altimeter to Map Global Bathymetry. / Shum C.K., Abusali P.A.M., Chung-Yen Kuo, Hyongki Lee, Ogle J., Raney R.K., Ries J.C., Smith W.H.F., Svehla D., Changyin Zhao. // IEEE Geoscience and Remote Sensing Letters. - 2009. - Vol. 6, No. 4. - P. 653-657.

J552. Yonghong Zhang. A New Numerical Method for Calculating Extrema of Received Power for Polarimetric SAR. / Yonghong Zhang, Jixian Zhang, Zhong Lu, Wenyu Gong. // IEEE Geoscience and Remote Sensing Letters. - 2009. - Vol. 6, No. 4. - P. 666-670.

J553. Shimada M. PALSAR Radiometric and Geometric Calibration. / Shimada M., Isoguchi O., Tadono T., Isono K. // IEEE Transactions on Geoscience and Remote Sensing. - 2009. - Vol. 47, No. 12. - P. 3915-3932.

J554. Khwaja A.S. Efficient SAR Raw Data Generation for Anisotropic Urban Scenes Based on Inverse Processing. / Khwaja A.S., Ferro-Famil L., Pottier E. // IEEE Geoscience and Remote Sensing Letters. - 2009. - Vol. 6, No. 4. - P. 757-761.

J555. Green D. An Inversion Method for Extraction of Wind Speed From High-Frequency Ground-Wave Radar Oceanic Backscatter. / Green D., Gill E., Weimin Huang. // IEEE Transactions on Geoscience and Remote Sensing. - 2009. - Vol. 47, No. 10. - P. 3338-3346.

J556. Campbell B.A. Scale-Dependent Surface Roughness Behavior and Its Impact on Empirical Models for Radar Backscatter. IEEE Transactions on Geoscience and Remote Sensing. - 2009. - Vol. 47, No. 10. - P. 3480-3488.

J557. Qiang Chen. An Optimization Procedure of the Lagrange Multiplier Method for Polarimetric Power Optimization. / Qiang Chen, Yong-Mei Jiang, Ling-Jun Zhao, Gui Gao, Gang-Yao Kuang. // IEEE Geoscience and Remote Sensing Letters. - 2009. - Vol. 6, No. 4. - P. 699-702.

J558. Jiong Chen. Ship Detection Using Polarization Cross-Entropy. / Jiong Chen, Yilun Chen, Jian Yang. // IEEE Geoscience and Remote Sensing Letters. - 2009. - Vol. 6, No. 4. - P. 723-727.

J559. Villarini G. Inference of Spatial Scaling Properties of Rainfall: Impact of Radar Rainfall Estimation Uncertainties. / Villarini G., Krajewski W.F. // IEEE Geoscience and Remote Sensing Letters. - 2009. - Vol. 6, No. 4. - P. 812-815.

J560. Martinez-Espla J.J. An Optimized Algorithm for InSAR Phase Unwrapping Based on Particle Filtering, Matrix Pencil, and Region-Growing Techniques. / Martinez-Espla J.J., Martinez-Marin T., Lopez-Sanchez J.M. // IEEE Geoscience and Remote Sensing Letters. - 2009. - Vol. 6, No. 4. - P. 835-839.

J561. Kurum M. L-Band Radar Estimation of Forest Attenuation for Active/Passive Soil Moisture Inversion. / Kurum M., Lang R.H., O'Neill P.E., Joseph A.T., Jackson T.J., Cosh M.H. // IEEE Transactions on Geoscience and Remote Sensing. - 2009. - Vol. 47, No. 9. - P. 3026-3040.

J562. Yueh S.H. Airborne Ku-Band Polarimetric Radar Remote Sensing of Terrestrial Snow Cover. / Yueh S.H., Dinardo S.J., Akgiray A., West R., Cline D.W., Elder K. // IEEE Transactions on Geoscience and Remote Sensing. - 2009. - Vol. 47, No. 10. - P. 3347-3364.

J563. Sharma A.R. LIDAR Observations of Aerosol Properties Over Tropical Urban Region-A Case Study During a Low-Pressure System Over Bay of Bengal. / Sharma A.R., Kharol S.K., Badarinath K.V.S. // IEEE Geoscience and Remote Sensing Letters. - 2009. - Vol. 6, No. 4. - P. 807-811.

J564. Celik T. Multiscale Change Detection in Multitemporal Satellite Images. IEEE Geoscience and Remote Sensing Letters. - 2009. - Vol. 6, No. 4. - P. 820-824.

J565. Nakajima H. Nondestructive Sensor Using Microwaves From Laser Plasma by Subnanosecond Laser Pulses. / Nakajima H., Shimada Y., Somekawa T., Fujita M., Tanaka K.A. // IEEE Geoscience and Remote Sensing Letters. - 2009. - Vol. 6, No. 4. - P. 718-722.

J566. Wiebe H. Comparison of the ASI Ice Concentration Algorithm With Landsat-7 ETM+ and SAR Imagery. / Wiebe H., Heygster G., Markus T. // IEEE Transactions on Geoscience and Remote Sensing. - 2009. - Vol. 47, No. 9. - P. 3008-3015.

J567. Thatiparthi S.R. MST Radar Signal Processing Using Wavelet-Based Denoising. / Thatiparthi S.R., Gudheti R.R., Sourirajan V. // IEEE Geoscience and Remote Sensing Letters. - 2009. - Vol. 6, No. 4. - P. 752-756.

J568. Kern S. Multi Scat-A Helicopter-Based Scatterometer for Snow-Cover and Sea-Ice Investigations. / Kern S., Brath M., Fontes R., Gade M., Gurgel K.-W., Kaleschke L., Spreen G., Schulz S., Winderlich A., Stammer D. // IEEE Geoscience and Remote Sensing Letters. - 2009. - Vol. 6, No. 4. - P. 703-707.

J569. Dubey P. K. Depolarization ratio measurement using single photomultiplier tube in micropulse lidar. / Dubey P. K., Jain S. L., Arya B. C., Kulkarni Pavan S. // Review of Scientific Instruments. - 2009. - Vol. 80, No. 5. - P. 053111-053111-5.

J570. Harrison R. G. Comparison of balloon-carried atmospheric motion sensors with Doppler lidar turbulence measurements. / Harrison R. G., Heath A. M., Hogan R. J., Rogers G. W. // Review of Scientific Instruments. - 2009. - Vol. 80, No. 2. - P. 026108-026108-3.

J571. Sicard M. Aerosol Lidar Intercomparison in the Framework of SPALINET-The Spanish Lidar Network: Methodology and Results. / Sicard M., Molero F., Guerrero-Rascado J.L., Pedros R., Exposito F.J., Cordoba-Jabonero C., Bolarin J.M., Comeron A., Rocadenbosch F., Pujadas M., Alados-Arboledas L., Martinez-Lozano J.A., Diaz J.P., Gil M., Requena A., Navas-Guzman F., Moreno J.M. // IEEE Transactions on Geoscience and Remote Sensing. - 2009. - Vol. 47, No. 10. - P. 3547-3559.

J572. Tagawa T. Improved Correction of Beam Mismatch of the Precipitation Radar After Orbit Boost of the TRMM Satellite. / Tagawa T., Hanado H., Shimizu S., Oki R. // IEEE Transactions on Geoscience and Remote Sensing. - 2009. - Vol. 47, No. 10. - P. 3469-3479.

J573. Phillips R.D. An Adaptive Noise-Filtering Algorithm for AVIRIS Data With Implications for Classification Accuracy. / Phillips R.D., Blinn C.E., Watson L.T., Wynne R.H. // IEEE Transactions on Geoscience and Remote Sensing. - 2009. - Vol. 47, No. 9. - P. 3168-3179.

J574. Yeo-Sun Yoon. Spatial Filtering for Wall-Clutter Mitigation in Through-the-Wall Radar Imaging. / Yeo-

Sun Yoon, Amin M.G. // IEEE Transactions on Geoscience and Remote Sensing. - 2009. - Vol. 47, No. 9. - P. 3192-3208.

J575. Toutin T. 3-D Radargrammetric Modeling of RADARSAT-2 Ultrafine Mode: Preliminary Results of the Geometric Calibration. / Toutin T., Chenier R. // IEEE Geoscience and Remote Sensing Letters. - 2009. - Vol. 6, No. 3. - P. 611-615.

J576. Kameyama S. Performance of Discrete-Fourier-Transform-Based Velocity Estimators for a Wind-Sensing Coherent Doppler Lidar System in the Kolmogorov Turbulence Regime. / Kameyama S., Ando T., Asaka K., Hirano Y., Wadaka S. // IEEE Transactions on Geoscience and Remote Sensing. - 2009. - Vol. 47, No. 10. - P. 3560-3569.

J577. Piles M. A Change Detection Algorithm for Retrieving High-Resolution Soil Moisture From SMAP Radar and Radiometer Observations. / Piles M., Entekhabi D., Camps A. // IEEE Transactions on Geoscience and Remote Sensing. - 2009. - Vol. 47, No. 12. - P. 4125-4131.

J578. Garestier F. Forest Biophysical Parameter Estimation Using L- and P-Band Polarimetric SAR Data. / Garestier F., Dubois-Fernandez P.C., Guyon D., Le Toan T. // IEEE Transactions on Geoscience and Remote Sensing. - 2009. - Vol. 47, No. 10. - P. 3379-3388.

J579. Collins M.J. Modeling and Simulation of SAR Image Texture. / Collins M.J., Allan J.M. // IEEE Transactions on Geoscience and Remote Sensing. - 2009. - Vol. 47, No. 10. - P. 3530-3546.

J580. Roca M. The EnviSat RA-2 Instrument Design and Tracking Performance. / Roca M., Laxon S., Zelli C. // IEEE Transactions on Geoscience and Remote Sensing. - 2009. - Vol. 47, No. 10. - P. 3489-3506.

J581. Reale D. An Accurate Strategy for 3-D Ground-Based SAR Imaging. / Reale D., Serafino F., Pascazio V. // IEEE Geoscience and Remote Sensing Letters. - 2009. - Vol. 6, No. 4. - P. 681-685.

J582. de Queiroz da Silva A. Relationship Between PALSAR Backscatter and Surface-Roughness Parameters From Iron Laterites in CarajЂs, Amazon Region. / de Queiroz da Silva A., Paradella W.R., Freitas C.C., de Oliveira C.G. // IEEE Transactions on Geoscience and Remote Sensing. - 2009. - Vol. 47, No. 12. - P. 4027-4031.

J583. Danklmayer A. Assessment of Atmospheric Propagation Effects in SAR Images. / Danklmayer A., Doring B.J., Schwerdt M., Chandra M. // IEEE Transactions on Geoscience and Remote Sensing. - 2009. - Vol. 47, No. 10. - P. 3507-3518.

J584. Balz T. Hybrid GPU-Based Single- and Double-Bounce SAR Simulation. / Balz T., Stilla U. // IEEE Transactions on Geoscience and Remote Sensing. - 2009. - Vol. 47, No. 10. - P. 3519-3529.

J585. Thiel C.J. Operational Large-Area Forest Monitoring in Siberia Using ALOS PALSAR Summer Intensities and Winter Coherence. / Thiel C.J., Thiel C., Schmullius C.C. // IEEE Transactions on Geoscience and Remote Sensing. - 2009. - Vol. 47, No. 12. - P. 3993-4000.

J586. Qiuzhao Dong. Microwave Subsurface Imaging Using Direct Finite-Difference Frequency-Domain-Based Inversion. / Qiuzhao Dong, Rappaport C.M. // IEEE Transactions on Geoscience and Remote Sensing. - 2009. - Vol. 47, No. 11. - P. 3664-3670.

J587. Bindlish R. Combined Passive and Active Microwave Observations of Soil Moisture During CLASIC. / Bindlish R., Jackson T., Ruijing Sun, Cosh M., Yueh S., Dinardo S. // IEEE Geoscience and Remote Sensing Letters. - 2009. - Vol. 6, No. 4. - P. 644-648.

J588. Ngheim S.V. Arctic sea ice mapping with satellite radars. / Ngheim S.V., Clemete-Colon P. // IEEE Aerospace and Electronic Systems Magazine. - 2009. - Vol. 24, No. 11. - P. 41-44.

J589. Guifu Zhang. Phased Array Radar Polarimetry for Weather Sensing: A Theoretical Formulation for Bias Corrections. / Guifu Zhang, Doviak R.J., Zrnic D.S., Crain J., Staiman D., Al-Rashid Y. // IEEE Transactions on Geoscience and Remote Sensing. - 2009. - Vol. 47, No. 11. - P. 3679-3689.

J590. Wen-Qin Wang. GPS-Based Time & Phase Synchronization Processing for Distributed SAR. IEEE Transactions on Aerospace and Electronic Systems. - 2009. - Vol. 45, No. 3. - P. 1040-1051.

J591. Edenhofer P. Space-borne technology and inversion techniques for radar. IEEE Aerospace and Electronic Systems Magazine. - 2009. - Vol. 24, No. 8. - P. 43-44.

J592. Migliaccio M. The PALSAR Polarimetric Mode for Sea Oil Slick Observation. / Migliaccio M., Gambardella A., Nunziata F., Shimada M., Isoguchi O. // IEEE Transactions on Geoscience and Remote Sensing. - 2009. - Vol. 47, No. 12. - P. 4032-4041.

J593. Shimada M. A New Method for Correcting ScanSAR Scalloping Using Forests and Inter-SCAN Banding Employing Dynamic Filtering. IEEE Transactions on Geoscience and Remote Sensing. - 2009. - Vol. 47, No. 12. - P. 3933-3942.

J594. My-Linh Truong-Loi. Estimation of Soil Moisture and Faraday Rotation From Bare Surfaces Using Compact Polarimetry. / My-Linh Truong-Loi, Freeman A., Dubois-Fernandez P.C., Pottier E. // IEEE Transactions on Geoscience and Remote Sensing. - 2009. - Vol. 47, No. 11. - P. 3608-3615.

J595. Shimada M. Foreword to the Special Issue on Calibration and Validation of ALOS Sensors (PALSAR, AVNIR-2, and PRISM) and Their Use for Bio- and Geophysical Parameter Retrievals. / Shimada M, Touzi R, Tadono T, Smith A. // IEEE Transactions on Geoscience and Remote Sensing. - 2009. - Vol. 47, No. 12. - P. 3911-3913.

J596. Touzi R. Polarimetric PALSAR Calibration. / Touzi R., Shimada M. // IEEE Transactions on Geoscience and Remote Sensing. - 2009. - Vol. 47, No. 12. - P. 3951-3959.

J597. Buckreuss S. The German satellite mission TerraSAR-X. / Buckreuss S., Werninghaus R., Pitz W. // IEEE Aerospace and Electronic Systems Magazine. - 2009. - Vol. 24, No. 11. - P. 4-9.

J598. Shih-Hsun Hsu. A Dual-Polarized Planar-Array Antenna for S-Band and X-Band Airborne Applications. / Shih-Hsun Hsu, Yu-Jiun Ren, Kai Chang. // IEEE Antennas and Propagation Magazine. - 2009. - Vol. 51, No. 4. - P. 70-78.

J599. Shunguang Wu. Collision Sensing by Stereo Vision and Radar Sensor Fusion. / Shunguang Wu, Decker S., Peng Chang, Camus T., Eledath J. // IEEE Transactions on Intelligent Transportation Systems. - 2009. - Vol. 10, No. 4. - P. 606-614.

J600. Surussavadee C. Satellite Retrievals of Arctic and Equatorial Rain and Snowfall Rates Using Millimeter Wavelengths. / Surussavadee C., Staelin D.H. // IEEE Transactions on Geoscience and Remote Sensing. - 2009. - Vol. 47, No. 11. - P. 3697-3707.

J601. Takeshiro A. Verification of Polarimetric Calibration Method Including Faraday Rotation Compensation Using PALSAR Data. / Takeshiro A., Furuya T., Fukuchi H. // IEEE Transactions on Geoscience and Remote Sensing. - 2009. - Vol. 47, No. 12. - P. 3960-3968.

J602. Amini J. Employing a Method on SAR and Optical Images for Forest Biomass Estimation. / Amini J., Sumantyo J.T.S. // IEEE Transactions on Geoscience and Remote Sensing. - 2009. - Vol. 47, No. 12. - P. 4020-4026.

J603. Kimura H. Calibration of Polarimetric PALSAR Imagery Affected by Faraday Rotation Using Polarization Orientation. IEEE Transactions on Geoscience and Remote Sensing. - 2009. - Vol. 47, No. 12. - P. 3943-3950.

J604. Lombardini F. Linear and adaptive spaceborne threedimensional SAR tomography: a comparison on real data. / Lombardini F., Pardini M., Fornaro G., Serafino F., Verrazzani L., Costantini M. // IET Radar, Sonar & Navigation. - 2009. - Vol. 3, No. 4. - P. 424-436.

J605. Corbane C. Comparative Study on the Performance of Multiparameter SAR Data for Operational Urban Areas Extraction Using Textural Features. / Corbane C., Baghdadi N., Descombes X., Wilson G., Villeneuve N., Petit M. // IEEE Geoscience and Remote Sensing Letters. - 2009. - Vol. 6, No. 4. - P. 728-732.

J606. Gebert N. Azimuth Phase Center Adaptation on Transmit for High-Resolution Wide-Swath SAR Imaging. / Gebert N., Krieger G. // IEEE Geoscience and Remote Sensing Letters. - 2009. - Vol. 6, No. 4. - P. 782-786.

J607. Guoxiang Liu. Estimating Spatiotemporal Ground Deformation With Improved Persistent-Scatterer Radar Interferometry. / Guoxiang Liu, Buckley S.M., Xiaoli Ding, Qiang Chen, Xiaojun Luo. // IEEE Transactions on

Geoscience and Remote Sensing. - 2009. - Vol. 47, No. 9. - P. 3209-3219.

J608. Zaugg E.C. Generalized Frequency-Domain SAR Processing. / Zaugg E.C., Long D.G. // IEEE Transactions on Geoscience and Remote Sensing. - 2009. - Vol. 47, No. 11. - P. 3761-3773.

J609. Santoro M. Signatures of ALOS PALSAR L-Band Backscatter in Swedish Forest. / Santoro M., Fransson J.E.S., Eriksson L.E.B., Magnusson M., Ulander L.M.H., Olsson H. // IEEE Transactions on Geoscience and Remote Sensing. - 2009. - Vol. 47, No. 12. - P. 4001-4019.

J610. Bellez S. Analysis of the Main Scattering Mechanisms in Forested Areas: An Integral Representation Approach for Monostatic Radar Configurations. / Bellez S., Dahon C., Roussel H. // IEEE Transactions on Geoscience and Remote Sensing. - 2009. - Vol. 47, No. 12. - P. 4153-4166.

J611. Denis L. Joint Regularization of Phase and Amplitude of InSAR Data: Application to 3-D Reconstruction. / Denis L., Tupin F., Darbon J., Sigelle M. // IEEE Transactions on Geoscience and Remote Sensing. - 2009. - Vol. 47, No. 11. - P. 3774-3785.

J612. Sagnard F.-M. Design of Compact UWB Planar Monopole Antennas for Cross-Hole Radar Application. IEEE Geoscience and Remote Sensing Letters. - 2009. - Vol. 6, No. 4. - P. 816-819.

J613. Martorella M. Automatic Target Recognition by Means of Polarimetric ISAR Images and Neural Networks. / Martorella M., Giusti E., Capria A., Berizzi F., Bates B. // IEEE Transactions on Geoscience and Remote Sensing. - 2009. - Vol. 47, No. 11. - P. 3786-3794.

J614. Massagram W. Assessment of Heart Rate Variability and Respiratory Sinus Arrhythmia via Doppler Radar. / Massagram W., Lubecke V.M., Host-Madsen A., Boric-Lubecke O. // IEEE Transactions on Microwave Theory and Techniques. - 2009. - Vol. 57, No. 10. - P. 2542-2549.

J615. Lardeux C. Support Vector Machine for Multifrequency SAR Polarimetric Data Classification. / Lardeux C., Frison P.-L., Tison C., Souyris J.-C., Stoll B., Fruneau B., Rudant J.-P. // IEEE Transactions on Geoscience and Remote Sensing. - 2009. - Vol. 47, No. 12. - P. 4143-4152.

J616. Xin Nie. The Application of the Principle of Chirp Scaling in Processing Stepped Chirps in Spotlight SAR. / Xin Nie, Daiyin Zhu, Xinhua Mao, Zhaoda Zhu. // IEEE Geoscience and Remote Sensing Letters. - 2009. - Vol. 6, No. 4. - P. 860-864.

J617. Tebaldini S. Algebraic Synthesis of Forest Scenarios From Multibaseline PolInSAR Data. IEEE Transactions on Geoscience and Remote Sensing. - 2009. - Vol. 47, No. 12. - P. 4132-4142.

J618. Bombrun L. DEM Error Retrieval by Analyzing Time Series of Differential Interferograms. / Bombrun L., Gay M., Trouve E., Vasile G., Mars J. // IEEE Geoscience and Remote Sensing Letters. - 2009. - Vol. 6, No. 4. - P. 830-834.

J619. Cheng-Yen Chiang. Feature Enhancement of Stripmap-Mode SAR Images Based on an Optimization Scheme. / Cheng-Yen Chiang, Kun-Shan Chen, Chih-Tien Wang, Nien-Shiang Chou. // IEEE Geoscience and Remote Sensing Letters. - 2009. - Vol. 6, No. 4. - P. 870-874.

J620. McNairn H. The Contribution of ALOS PALSAR Multipolarization and Polarimetric Data to Crop Classification. / McNairn H., Jiali Shang, Xianfeng Jiao, Champagne C. // IEEE Transactions on Geoscience and Remote Sensing. - 2009. - Vol. 47, No. 12. - P. 3981-3992.

J621. Disney M.I. Quantifying Surface Reflectivity for Spaceborne Lidar via Two Independent Methods. / Disney M.I., Lewis P.E., Bouvet M., Prieto-Blanco A., Hancock S. // IEEE Transactions on Geoscience and Remote Sensing. - 2009. - Vol. 47, No. 9. - P. 3262-3271.

J622. Moser G. Unsupervised Change Detection From Multichannel SAR Data by Markovian Data Fusion. / Moser G., Serpico S.B. // IEEE Transactions on Geoscience and Remote Sensing. - 2009. - Vol. 47, No. 7. - P. 2114-2128.

J623. Mengdao Xing. Motion Compensation for UAV SAR Based on Raw Radar Data. / Mengdao Xing, Xiuwei Jiang, Renbiao Wu, Feng Zhou, Zheng Bao. // IEEE Transactions on Geoscience and Remote Sensing. - 2009. - Vol. 47, No. 8. - P. 2870-2883.

J624. Drews R. A Spatially Adjusted Elevation Model in Dronning Maud Land, Antarctica, Based on Differential SAR Interferometry. / Drews R., Rack W., Wesche C., Helm V. // IEEE Transactions on Geoscience and Remote Sensing. - 2009. - Vol. 47, No. 8. - P. 2501-2509.

J625. Silveira M. Separation Between Water and Land in SAR Images Using Region-Based Level Sets. / Silveira M., Heleno S. // IEEE Geoscience and Remote Sensing Letters. - 2009. - Vol. 6, No. 3. - P. 471-475.

J626. Panciera R. Improved Understanding of Soil Surface Roughness Parameterization for L-Band Passive Microwave Soil Moisture Retrieval. / Panciera R., Walker J.P., Merlin O. // IEEE Geoscience and Remote Sensing Letters. - 2009. - Vol. 6, No. 4. - P. 625-629.

J627. Sabry R. A New Coherency Formalism for Change Detection and Phenomenology in SAR Imagery: A Field Approach. IEEE Geoscience and Remote Sensing Letters. - 2009. - Vol. 6, No. 3. - P. 458-462.

J628. Baochang Liu. Bistatic SAR Data Focusing Using an Omega-K Algorithm Based on Method of Series Reversion. / Baochang Liu, Tong Wang, Qisong Wu, Zheng Bao. // IEEE Transactions on Geoscience and Remote Sensing. - 2009. - Vol. 47, No. 8. - P. 2899-2912.

J629. Hyung-Sup Jung. An Improvement of the Performance of Multiple-Aperture SAR Interferometry (MAI). / Hyung-Sup Jung, Joong-Sun Won, Sang-Wan Kim. // IEEE Transactions on Geoscience and Remote Sensing. - 2009. - Vol. 47, No. 8. - P. 2859-2869.

J630. Alberti G. A Waveform Model for Near-Nadir Radar Altimetry Applied to the Cassini Mission to Titan. / Alberti G., Festa L., Papa C., Vingione G. // IEEE Transactions on Geoscience and Remote Sensing. - 2009. - Vol. 47, No. 7. - P. 2252-2261.

J631. Wei-Lwun Lu. A Hybrid Conditional Random Field for Estimating the Underlying Ground Surface From Airborne LiDAR Data. / Wei-Lwun Lu, Murphy K.P., Little J.J., Sheffer A., Hongbo Fu. // IEEE Transactions on Geoscience and Remote Sensing. - 2009. - Vol. 47, No. 8. - P. 2913-2922.

J632. Wojcik R. Conditioning Stochastic Rainfall Replicates on Remote Sensing Data. / Wojcik R., McLaughlin D., Konings A.G., Entekhabi D. // IEEE Transactions on Geoscience and Remote Sensing. - 2009. - Vol. 47, No. 8. - P. 2436-2449.

J633. Haddadi K. A New Range Finder Based on a Four-Port Junction. / Haddadi K., Wang M.M., Glay D., Lasri T. // IEEE Sensors Journal. - 2009. - Vol. 9, No. 6. - P. 697-698.

J634. Belli K. Effectiveness of 2-D and 2.5-D FDTD Ground-Penetrating Radar Modeling for Bridge-Deck Deterioration Evaluated by 3-D FDTD. / Belli K., Rappaport C.M., He Zhan, Wadia-Fascetti S. // IEEE Transactions on Geoscience and Remote Sensing. - 2009. - Vol. 47, No. 11. - P. 3656-3663.

J635. Gorgucci E. An Examination of the Validity of the Mean Raindrop-Shape Model for Dual-Polarization Radar Rainfall Retrievals. / Gorgucci E., Baldini L. // IEEE Transactions on Geoscience and Remote Sensing. - 2009. - Vol. 47, No. 8. - P. 2752-2761.

J636. Schumann G. The Utility of Spaceborne Radar to Render Flood Inundation Maps Based on Multialgorithm Ensembles. / Schumann G., Di Baldassarre G., Bates P.D. // IEEE Transactions on Geoscience and Remote Sensing. - 2009. - Vol. 47, No. 8. - P. 2801-2807.

J637. Maestri T. Retrieval of Cloud Optical Properties From Multiple Infrared Hyperspectral Measurements: A Methodology Based on a Line-by-Line Multiple-Scattering Code. / Maestri T., Holz R.E. // IEEE Transactions on Geoscience and Remote Sensing. - 2009. - Vol. 47, No. 8. - P. 2413-2426.

J638. Brandt O. Radar Response of Firn Exposed to Seasonal Percolation, Validation Using Cores and FDTD Modeling. / Brandt O., Langley K., Giannopoulos A., Hamran S.-E., Kohler J. // IEEE Transactions on Geoscience and Remote Sensing. - 2009. - Vol. 47, No. 8. - P. 2773-2786.

J639. Xiaofeng Li. Sea Surface Manifestation of Along-Tidal-Channel Underwater Ridges Imaged by SAR. / Xiaofeng Li, Chunyan Li, Qing Xu, Pichel W.G. // IEEE Transactions on Geoscience and Remote Sensing. - 2009. - Vol. 47, No. 8. - P. 2467-2477.

J640. Isoguchi O. An L-Band Ocean Geophysical Model Function Derived From PALSAR. / Isoguchi O.,

Shimada M. // IEEE Transactions on Geoscience and Remote Sensing. - 2009. - Vol. 47, No. 7. - P. 1925-1936.

J641. Dragosevic M.V. Space-Based Motion Estimators-Evaluation With the First RADARSAT-2 MODEX Data. / Dragosevic M.V., Shen Chiu. // IEEE Geoscience and Remote Sensing Letters. - 2009. - Vol. 6, No. 3. - P. 438-442.

J642. Lasne Y. Study of Hypersaline Deposits and Analysis of Their Signature in Airborne and Spaceborne SAR Data: Example of Death Valley, California. / Lasne Y., Paillou P., Freeman A., Farr T., McDonald K., Ruffie G., Malezieux J.-M., Chapman B. // IEEE Transactions on Geoscience and Remote Sensing. - 2009. - Vol. 47, No. 8. - P. 2581-2598.

J643. Jones T.A. Injection Heights of Biomass Burning Debris Estimated From WSR-88D Radar Observations. / Jones T.A., Christopher S.A. // IEEE Transactions on Geoscience and Remote Sensing. - 2009. - Vol. 47, No. 8. - P. 2599-2605.

J644. De Maio A. Detection of Single Scatterers in Multidimensional SAR Imaging. / De Maio A., Fornaro G., Pauciullo A. // IEEE Transactions on Geoscience and Remote Sensing. - 2009. - Vol. 47, No. 7. - P. 2284-2297.

J645. Naeimi V. An Improved Soil Moisture Retrieval Algorithm for ERS and METOP Scatterometer Observations. / Naeimi V., Scipal K., Bartalis Z., Hasenauer S., Wagner W. // IEEE Transactions on Geoscience and Remote Sensing. - 2009. - Vol. 47, No. 7. - P. 1999-2013.

J646. Le C. Ultrawideband (UWB) Radar Imaging of Building Interior: Measurements and Predictions. / Le C., Dogaru T., Lam Nguyen, Ressler M.A. // IEEE Transactions on Geoscience and Remote Sensing. - 2009. - Vol. 47, No. 5. - P. 1409-1420.

J647. Galland F. Unsupervised Synthetic Aperture Radar Image Segmentation Using Fisher Distributions. / Galland F., Nicolas J.-M., Sportouche H., Roche M., Tupin F., Refregier P. // IEEE Transactions on Geoscience and Remote Sensing. - 2009. - Vol. 47, No. 8. - P. 2966-2972.

J648. Hui Lin. Monitoring Sugarcane Growth Using ENVISAT ASAR Data. / Hui Lin, Jinsong Chen, Zhiyuan Pei, Songling Zhang, Xianzhi Hu. // IEEE Transactions on Geoscience and Remote Sensing. - 2009. - Vol. 47, No. 8. - P. 2572-2580.

J649. Makynen M.P. Simulation of ASIRAS Altimeter Echoes for Snow-Covered First-Year Sea Ice. / Makynen M.P., Hallikainen M.T. // IEEE Geoscience and Remote Sensing Letters. - 2009. - Vol. 6, No. 3. - P. 486-490.

J650. Praks J. Alternatives to Target Entropy and Alpha Angle in SAR Polarimetry. / Praks J., Koeniguer E.C., Hallikainen M.T. // IEEE Transactions on Geoscience and Remote Sensing. - 2009. - Vol. 47, No. 7. - P. 2262-2274.

J651. Wentao An. Data Compression for Multilook Polarimetric SAR Data. / Wentao An, Yi Cui, Weijie Zhang, Jian Yang. // IEEE Geoscience and Remote Sensing Letters. - 2009. - Vol. 6, No. 3. - P. 476-480.

J652. Cheng Wang. Integrating LiDAR Intensity and Elevation Data for Terrain Characterization in a Forested Area. / Cheng Wang, Glenn N.F. // IEEE Geoscience and Remote Sensing Letters. - 2009. - Vol. 6, No. 3. - P. 463-466.

J653. Corbella I. On-Ground Characterization of the SMOS Payload. / Corbella I., Torres F., Duffo N., Martin-Neira M., Gonzalez-Gambau V., Camps A., Vall-llossera M. // IEEE Transactions on Geoscience and Remote Sensing. - 2009. - Vol. 47, No. 9. - P. 3123-3133.

J654. Hunt A.R. Use of a Frequency-Hopping Radar for Imaging and Motion Detection Through Walls. IEEE Transactions on Geoscience and Remote Sensing. - 2009. - Vol. 47, No. 5. - P. 1402-1408.

J655. Fruehauf F. Experiments and Algorithms to Detect Snow Avalanche Victims Using Airborne Ground-Penetrating Radar. / Fruehauf F., Heilig A., Schneebeli M., Fellin W., Scherzer O. // IEEE Transactions on Geoscience and Remote Sensing. - 2009. - Vol. 47, No. 7. - P. 2240-2251.

J656. Se Young Kim. Antenna Mask Design for SAR Performance Optimization. / Se Young Kim, Noh Hoon Myung, Min Jeong Kang. // IEEE Geoscience and Remote Sensing Letters. - 2009. - Vol. 6, No. 3. - P. 443-447.

J657. Lei Zhang. Achieving Higher Resolution ISAR Imaging With Limited Pulses via Compressed Sampling. / Lei Zhang, Mengdao Xing, Cheng-Wei Qiu, Jun Li, Zheng Bao. // IEEE Geoscience and Remote Sensing Letters. - 2009. - Vol. 6, No. 3. - P. 567-571.

J658. Hua Zhong. An Extended Nonlinear Chirp-Scaling Algorithm for Focusing Large-Baseline Azimuth-Invariant Bistatic SAR Data. / Hua Zhong, Xingzhao Liu. // IEEE Geoscience and Remote Sensing Letters. - 2009. - Vol. 6, No. 3. - P. 548-552.

J659. Gaffar M.Y.A. Selecting Suitable Coherent Processing Time Window Lengths for Ground-Based ISAR Imaging of Cooperative Sea Vessels. / Gaffar M.Y.A., Nel W.A.J., Inggs M.R. // IEEE Transactions on Geoscience and Remote Sensing. - 2009. - Vol. 47, No. 9. - P. 3231-3240.

J660. Chun-Mao Yeh. Cross-Range Scaling for ISAR Based on Image Rotation Correlation. / Chun-Mao Yeh, Jia Xu, Ying-Ning Peng, Xiu-Tan Wang. // IEEE Geoscience and Remote Sensing Letters. - 2009. - Vol. 6, No. 3. - P. 597-601.

J661. Quartly G.D. Improving the Intercalibration of Values for the Jason-1 and Jason-2 Altimeters. IEEE Geoscience and Remote Sensing Letters. - 2009. - Vol. 6, No. 3. - P. 538-542.

J662. Shuo Wang. Polarimetric SAR Internal Calibration Scheme Based on T/R Module Orthogonal Phase Coding. / Shuo Wang, Haiming Qi, Weidong Yu. // IEEE Transactions on Geoscience and Remote Sensing. - 2009. - Vol. 47, No. 12. - P. 3969-3980.

J663. Bo Guan. Electromagnetic Scattering From Objects Above a Rough Surface Using the Method of Moments With Half-Space Green's Function. / Bo Guan, Jian Feng Zhang, Xiao Yang Zhou, Tie Jun Cui. // IEEE Transactions on Geoscience and Remote Sensing. - 2009. - Vol. 47, No. 10. - P. 3399-3405.

J664. Sagnard F.-M. Design of a Wideband Antenna for a Narrow Borehole Radar Using FDTD Modeling. IEEE Geoscience and Remote Sensing Letters. - 2009. - Vol. 6, No. 3. - P. 553-557.

J665. Georgiev G.T. BRDF Analysis of Savanna Vegetation and Salt-Pan Samples. / Georgiev G.T., Gatebe C.K., Butler J.J., King M.D. // IEEE Transactions on Geoscience and Remote Sensing. - 2009. - Vol. 47, No. 8. - P. 2546-2556.

J666. Baselice F. Layover Solution in SAR Imaging: A Statistical Approach. / Baselice F., Budillon A., Ferraioli G., Pascazio V. // IEEE Geoscience and Remote Sensing Letters. - 2009. - Vol. 6, No. 3. - P. 577-581.

J667. Williams D.P. Mine Classification With Imbalanced Data. / Williams D.P., Myers V., Silvious M.S. // IEEE Geoscience and Remote Sensing Letters. - 2009. - Vol. 6, No. 3. - P. 528-532.

J668. Touzi R. Phase of Target Scattering for Wetland Characterization Using Polarimetric C-Band SAR. / Touzi R., Deschamps A., Rother G. // IEEE Transactions on Geoscience and Remote Sensing. - 2009. - Vol. 47, No. 9. - P. 3241-3261.

J669. Ferraioli G. Multichannel Phase Unwrapping With Graph Cuts. / Ferraioli G., Shabou A., Tupin F., Pascazio V. // IEEE Geoscience and Remote Sensing Letters. - 2009. - Vol. 6, No. 3. - P. 562-566.

J670. Ji Siwei. Comments on "Modified Hough Transform for Searching Radar Detection". / Ji Siwei, He Mingxing. // IEEE Geoscience and Remote Sensing Letters. - 2009. - Vol. 6, No. 3. - P. 616.

J671. Gebert N. Digital Beamforming on Receive: Techniques and Optimization Strategies for High-Resolution Wide-Swath SAR Imaging. / Gebert N., Krieger G., Moreira A. // IEEE Transactions on Aerospace and Electronic Systems. - 2009. - Vol. 45, No. 2. - P. 564-592.

J672. Anfinsen S.N. Estimation of the Equivalent Number of Looks in Polarimetric Synthetic Aperture Radar Imagery. / Anfinsen S.N., Doulgeris A.P., Eltoft T. // IEEE Transactions on Geoscience and Remote Sensing. - 2009. - Vol. 47, No. 11. - P. 3795-3809.

J673. Xu F. Raw signal processing of stripmap bistatic synthetic aperture radar. / Xu F., Jin Y.-Q. // IET Radar, Sonar & Navigation. - 2009. - Vol. 3, No. 3. - P. 233-244.

J674. Shu-zhu Shi. A Low-Power and Small-Size HF Backscatter Radar for Ionospheric Sensing. / Shu-zhu Shi, Zheng-yu Zhao, Fan-fan Su, Gang Chen. // IEEE Geoscience and Remote Sensing Letters. - 2009. - Vol. 6, No. 3. - P. 504-508.

J675. Guoxiang Liu. Estimating Spatiotemporal Ground Deformation With Improved Permanent-Scatterer Radar Interferometry. / Guoxiang Liu, Buckley S.M., Xiaoli Ding, Qiang Chen, Xiaojun Luo. // IEEE Transactions on Geoscience and Remote Sensing. - 2009. - Vol. 47, No. 8. - P. 2762-2772.

J676. Srivastava H.S. Large-Area Soil Moisture Estimation Using Multi-Incidence-Angle RADARSAT-1 SAR Data. / Srivastava H.S., Patel P., Sharma Y., Navalgund R.R. // IEEE Transactions on Geoscience and Remote Sensing. - 2009. - Vol. 47, No. 8. - P. 2528-2535.

J677. Hebar M. Autobinomial Model for SAR Image Despeckling and Information Extraction. / Hebar M., Gleich D., Cucej Z. // IEEE Transactions on Geoscience and Remote Sensing. - 2009. - Vol. 47, No. 8. - P. 2818-2835.

J678. Kassab R. Performance analysis of interrupted sparse HFSWR waveform coded with successive fast Fourier transforms. / Kassab R., Lesturgie M., Fiorina J. // Electronics Letters. - 2009. - Vol. 45, No. 10. - P. 525-527.

J679. Imperatore P. Transmission Through Layered Media With Rough Boundaries: First-Order Perturbative Solution. / Imperatore P., Iodice A., Riccio D. // IEEE Transactions on Antennas and Propagation. - 2009. - Vol. 57, No. 5. - P. 1481-1494.

J680. Zhenhong Li. Integration of InSAR Time-Series Analysis and Water-Vapor Correction for Mapping Postseismic Motion After the 2003 Bam (Iran) Earthquake. / Zhenhong Li, Fielding E.J., Cross P. // IEEE Transactions on Geoscience and Remote Sensing. - 2009. - Vol. 47, No. 9. - P. 3220-3230.

J681. Peterson E.H. A Feasibility Assessment for Low-Cost InSAR Formation-Flying Microsatellites. / Peterson E.H., Fotopoulos G., Zee R.E. // IEEE Transactions on Geoscience and Remote Sensing. - 2009. - Vol. 47, No. 8. - P. 2847-2858.

J682. Lakshmivarahan S. Ensemble Kalman filter. / Lakshmivarahan S., Stensrud D. // IEEE Control Systems Magazine. - 2009. - Vol. 29, No. 3. - P. 34-46.

J683. Davidson M. A Closed-Form Expression Relating Classification Accuracy to SAR System Calibration Uncertainty. / Davidson M., Attema E., Floury N., Rommen B., Snoeij P. // IEEE Geoscience and Remote Sensing Letters. - 2009. - Vol. 6, No. 3. - P. 467-470.

J684. Perkovic D. Longshore Surface Currents Measured by Doppler Radar and Video PIV Techniques. / Perkovic D., Lippmann T.C., Frasier S.J. // IEEE Transactions on Geoscience and Remote Sensing. - 2009. - Vol. 47, No. 8. - P. 2787-2800.

J685. Shanker A.P. Sparse Two-Dimensional Phase Unwrapping Using Regular Grid Methods. / Shanker A.P., Zebker H.A. // IEEE Geoscience and Remote Sensing Letters. - 2009. - Vol. 6, No. 3. - P. 519-522.

J686. Denis L. SAR Image Regularization With Fast Approximate Discrete Minimization. / Denis L., Tupin F., Darbon J., Sigelle M. // IEEE Transactions on Image Processing. - 2009. - Vol. 18, No. 7. - P. 1588-1600.

J687. Mladenova I. Terrain: Slope Influence on QuikSCAT Backscatter. / Mladenova I., Lakshmi V. // IEEE Transactions on Geoscience and Remote Sensing. - 2009. - Vol. 47, No. 8. - P. 2722-2732.

J688. Jinyun Guo. Lake Level Variations Monitored With Satellite Altimetry Waveform Retracking. / Jinyun Guo, Xiaotao Chang, Yonggang Gao, Jialong Sun, Cheinway Hwang. // IEEE Journal of Selected Topics in Applied Earth Observations and Remote Sensing. - 2009. - Vol. 2, No. 2. - P. 80-86.

J689. Pettinelli E. GPR Response From Buried Pipes: Measurement on Field Site and Tomographic Reconstructions. / Pettinelli E., Di Matteo A., Mattei E., Crocco L., Soldovieri F., Redman J.D., Annan A.P. // IEEE Transactions on Geoscience and Remote Sensing. - 2009. - Vol. 47, No. 8. - P. 2639-2645.

J690. Xiaolei Lv. Coherence-Improving Algorithm for Image Pairs of Bistatic SARs With Nonparallel Trajectories. / Xiaolei Lv, Mengdao Xing, Yunkai Deng, Shouhong Zhang, Yirong Wu. // IEEE Transactions on Geoscience and Remote Sensing. - 2009. - Vol. 47, No. 8. - P. 2884-2898.

J691. Xianjie Zha. Noise Reduction in Interferograms Using the Wavelet Packet Transform and Wiener Filtering. / Xianjie Zha, Rongshan Fu, Zhiyang Dai, Bin Liu. // IEEE Geoscience and Remote Sensing Letters. - 2008. - Vol. 5, No. 3. - P. 404-408.

J692. Mohr J.J. An Error Prediction Framework for Interferometric SAR Data. / Mohr J.J., Boncori J.P.M. // IEEE Transactions on Geoscience and Remote Sensing. - 2008. - Vol. 46, No. 6. - P. 1600-1613.

J693. Sarma D.K. An Artificial-Neural-Network-Based Integrated Regional Model for Rain Retrieval Over Land and Ocean. / Sarma D.K., Konwar M., Sharma S., Pal S., Das J., De U.K., Viswanathan G. // IEEE Transactions on Geoscience and Remote Sensing. - 2008. - Vol. 46, No. 6. - P. 1689-1696.

J694. Yajima Y. POLSAR Image Analysis of Wetlands Using a Modified Four-Component Scattering Power Decomposition. / Yajima Y., Yamaguchi Y., Sato R., Yamada H., Boerner W.-M. // IEEE Transactions on Geoscience and Remote Sensing. - 2008. - Vol. 46, No. 6. - P. 1667-1673.

J695. Yongwei Sheng. Quantifying the Size of a Lidar Footprint: A Set of Generalized Equations. IEEE Geoscience and Remote Sensing Letters. - 2008. - Vol. 5, No. 3. - P. 419-422.

J696. Capus C.G. Data correction for visualisation and classification of sidescan SONAR imagery. / Capus C.G., Banks A.C., Coiras E., Ruiz I.T., Smith C.J., Petillot Y.R. // IET Radar, Sonar & Navigation. - 2008. - Vol. 2, No. 3. - P. 155-169.

J697. Gnanaseelan C. Impact of Biannual Rossby Waves on the Indian Ocean Dipole. / Gnanaseelan C., Vaid B.H., Polito P.S. // IEEE Geoscience and Remote Sensing Letters. - 2008. - Vol. 5, No. 3. - P. 427-429.

J698. Naftaly U. Overview of the TECSAR Satellite Hardware and Mosaic Mode. / Naftaly U., Levy-Nathansohn R. // IEEE Geoscience and Remote Sensing Letters. - 2008. - Vol. 5, No. 3. - P. 423-426.

J699. Bachmann S.M. Using the Existing Spectral Clutter Filter With the Nonuniformly Spaced Time Series Data in Weather Radar. IEEE Geoscience and Remote Sensing Letters. - 2008. - Vol. 5, No. 3. - P. 400-403.

J700. Collins M.J. On the Design and Evaluation of Multiobjective Single-Channel SAR Image Segmentation Algorithms. / Collins M.J., Kopp E.B. // IEEE Transactions on Geoscience and Remote Sensing. - 2008. - Vol. 46, No. 6. - P. 1836-1846.

J701. Daiyin Zhu. Some Aspects of Improving the Frequency Scaling Algorithm for Dechirped SAR Data Processing. / Daiyin Zhu, Mingwei Shen, Zhaoda Zhu. // IEEE Transactions on Geoscience and Remote Sensing. - 2008. - Vol. 46, No. 6. - P. 1579-1588.

J702. Mercier G. Conditional Copulas for Change Detection in Heterogeneous Remote Sensing Images. / Mercier G., Moser G., Serpico S.B. // IEEE Transactions on Geoscience and Remote Sensing. - 2008. - Vol. 46, No. 5. - P. 1428-1441.

J703. Zhixi Li. Data-Level Fusion of Multilook Inverse Synthetic Aperture Radar Images. / Zhixi Li, Papson S., Narayanan R.M. // IEEE Transactions on Geoscience and Remote Sensing. - 2008. - Vol. 46, No. 5. - P. 1394-1406.

J704. Titin-Schnaider C. Polarimetric Characterization of Bistatic Coherent Mechanisms. IEEE Transactions on Geoscience and Remote Sensing. - 2008. - Vol. 46, No. 5. - P. 1535-1546.

J705. Bogdanov A.V. Neuroinspired Architecture for Robust Classifier Fusion of Multisensor Imagery. IEEE Transactions on Geoscience and Remote Sensing. - 2008. - Vol. 46, No. 5. - P. 1467-1487.

J706. Waske B. Classifying Multilevel Imagery From SAR and Optical Sensors by Decision Fusion. / Waske B., van der Linden S. // IEEE Transactions on Geoscience and Remote Sensing. - 2008. - Vol. 46, No. 5. - P. 1457-1466.

J707. Ho K.C. An Investigation of Using the Spectral Characteristics From Ground Penetrating Radar for Landmine/Clutter Discrimination. / Ho K.C., Carin L., Gader P.D., Wilson J.N. // IEEE Transactions on Geoscience and Remote Sensing. - 2008. - Vol. 46, No. 4. - P. 1177-1191.

J708. Wessel J. Calibration and Validation of DMSP SSMIS Lower Atmospheric Sounding Channels. / Wessel

J., Farley R.W., Fote A., Ye Hong, Poe G.A., Swadley S.D., Thomas B., Boucher D.J. // IEEE Transactions on Geoscience and Remote Sensing. - 2008. - Vol. 46, No. 4. - P. 946-961.

J709. Pacifici F. Urban Mapping Using Coarse SAR and Optical Data: Outcome of the 2007 GRSS Data Fusion Contest. / Pacifici F., Del Frate F., Emery W.J., Gamba P., Chanussot J. // IEEE Geoscience and Remote Sensing Letters. - 2008. - Vol. 5, No. 3. - P. 331-335.

J710. Koh G. Extinction Behavior of Soil at 26.5 to 110 GHz. IEEE Geoscience and Remote Sensing Letters. - 2008. - Vol. 5, No. 3. - P. 346-348.

J711. Budillon A. Estimation of Radial Velocity of Moving Targets by Along-Track Interferometric SAR Systems. / Budillon A., Pascazio V., Schirinzi G. // IEEE Geoscience and Remote Sensing Letters. - 2008. - Vol. 5, No. 3. - P. 349-353.

J712. Dalponte M. Fusion of Hyperspectral and LIDAR Remote Sensing Data for Classification of Complex Forest Areas. / Dalponte M., Bruzzone L., Gianelle D. // IEEE Transactions on Geoscience and Remote Sensing. - 2008. - Vol. 46, No. 5. - P. 1416-1427.

J713. Gohil B.S. A New Algorithm for Wind-Vector Retrieval From Scatterometers. / Gohil B.S., Sarkar A., Agarwal V.K. // IEEE Geoscience and Remote Sensing Letters. - 2008. - Vol. 5, No. 3. - P. 387-391.

J714. Jinshan Ding. A New Look at the Bistatic-to-Monostatic Conversion for Tandem SAR Image Formation. / Jinshan Ding, Zhenhua Zhang, Mengdao Xing, Zheng Bao. // IEEE Geoscience and Remote Sensing Letters. - 2008. - Vol. 5, No. 3. - P. 392-395.

J715. Battaglia A. How Does Multiple Scattering Affect the Spaceborne W-Band Radar Measurements at Ranges Close to and Crossing the Sea-Surface Range?. / Battaglia A., Simmer C. // IEEE Transactions on Geoscience and Remote Sensing. - 2008. - Vol. 46, No. 6. - P. 1644-1651.

J716. Noferini L. Analysis of Ground-Based SAR Data With Diverse Temporal Baselines. / Noferini L., Takayama T., Pieraccini M., Mecatti D., Macaluso G., Luzi G., Atzeni C. // IEEE Transactions on Geoscience and Remote Sensing. - 2008. - Vol. 46, No. 6. - P. 1614-1623.

J717. Dehmollaian M. Refocusing Through Building Walls Using Synthetic Aperture Radar. / Dehmollaian M., Sarabandi K. // IEEE Transactions on Geoscience and Remote Sensing. - 2008. - Vol. 46, No. 6. - P. 1589-1599.

J718. Liang Liao. Retrieval of Snow and Rain From Combined X- and W-Band Airborne Radar Measurements. / Liang Liao, Meneghini R., Lin Tian, Heymsfield G.M. // IEEE Transactions on Geoscience and Remote Sensing. - 2008. - Vol. 46, No. 5. - P. 1514-1524.

J719. Gupta P. Multisensor Data Product Fusion for Aerosol Research. / Gupta P., Patadia F., Christopher S.A. // IEEE Transactions on Geoscience and Remote Sensing. - 2008. - Vol. 46, No. 5. - P. 1407-1415.

J720. Milisavljevic N. Possibilistic Versus Belief Function Fusion for Antipersonnel Mine Detection. / Milisavljevic N., Bloch I. // IEEE Transactions on Geoscience and Remote Sensing. - 2008. - Vol. 46, No. 5. - P. 1488-1498.

J721. Lei Yang. Ground Moving Target Indication Using an InSAR System With a Hybrid Baseline. / Lei Yang, Tong Wang, Zheng Bao. // IEEE Geoscience and Remote Sensing Letters. - 2008. - Vol. 5, No. 3. - P. 373-377.

J722. McMahon J.M. Fiber lasers: A future technology for lasers in space. IEEE Aerospace and Electronic Systems Magazine. - 2008. - Vol. 23, No. 4. - P. 25-30.

J723. Lambers M. Interactive Dynamic Range Reduction for SAR Images. / Lambers M., Nies H., Kolb A. // IEEE Geoscience and Remote Sensing Letters. - 2008. - Vol. 5, No. 3. - P. 507-511.

J724. Bombrun L. Fisher Distribution for Texture Modeling of Polarimetric SAR Data. / Bombrun L., Beaulieu J.-M. // IEEE Geoscience and Remote Sensing Letters. - 2008. - Vol. 5, No. 3. - P. 512-516.

J725. Wang R. A Bistatic Point Target Reference Spectrum for General Bistatic SAR Processing. / Wang R., Loffeld O., Ul-Ann Q., Nies H., Ortiz A.M., Samarah A. // IEEE Geoscience and Remote Sensing Letters. - 2008.

- Vol. 5, No. 3. - P. 517-521.

J726. Perissin D. Validation of the Submetric Accuracy of Vertical Positioning of PSs in C-Band. IEEE Geoscience and Remote Sensing Letters. - 2008. - Vol. 5, No. 3. - P. 502-506.

J727. Zhi-Wei Li. Least Squares-Based Filter for Remote SensingImage Noise Reduction. / Zhi-Wei Li, Xiao-Li Ding, Da-Wei Zheng, Cheng Huang. // IEEE Transactions on Geoscience and Remote Sensing. - 2008. - Vol. 46, No. 7. - P. 2044-2049.

J728. Jun-Qi Duan. A New Approach for Simultaneous Range Measurement and Doppler Estimation. / Jun-Qi Duan, Zi-Shu He, Ling Qin. // IEEE Geoscience and Remote Sensing Letters. - 2008. - Vol. 5, No. 3. - P. 492-496.

J729. Kon Joon Bhang. Limitations in the Hydrologic Applications of C-Band SRTM DEMs in Low-Relief Settings. / Kon Joon Bhang, Schwartz F. // IEEE Geoscience and Remote Sensing Letters. - 2008. - Vol. 5, No. 3. - P. 497-501.

J730. Xiangrong Zhang. Spectral Clustering Ensemble Applied to SAR Image Segmentation. / Xiangrong Zhang, Licheng Jiao, Fang Liu, Liefeng Bo, Maoguo Gong. // IEEE Transactions on Geoscience and Remote Sensing. - 2008. - Vol. 46, No. 7. - P. 2126-2136.

J731. Xupu Geng. A Two-Dimensional Spectrum Model for General Bistatic SAR. / Xupu Geng, Honghui Yan, Yanfei Wang. // IEEE Transactions on Geoscience and Remote Sensing. - 2008. - Vol. 46, No. 8. - P. 2216-2223.

J732. Senet C.M. Determination of Bathymetric and Current Maps by the Method DiSC Based on the Analysis of Nautical X-Band Radar Image Sequences of the Sea Surface (November 2007). / Senet C.M., Seemann J., Flampouris S., Ziemer F. // IEEE Transactions on Geoscience and Remote Sensing. - 2008. - Vol. 46, No. 8. - P. 2267-2279.

J733. Ram S.S. Through-Wall Tracking of Human Movers Using Joint Doppler and Array Processing. / Ram S.S., Hao Ling. // IEEE Geoscience and Remote Sensing Letters. - 2008. - Vol. 5, No. 3. - P. 537-541.

J734. Gupta M. Radar Revisited (review of "Radar Handbook, 3rd ed." by Merrill Skolnik) [Book Reviews]. IEEE Microwave Magazine. - 2008. - Vol. 9, No. 4. - P. 129-130.

J735. Zheng-Wen Xu. Potential Effects of the Ionosphere on Space-Based SAR Imaging. / Zheng-Wen Xu, Jian Wu, Zhen-Sen Wu. // IEEE Transactions on Antennas and Propagation. - 2008. - Vol. 56, No. 7. - P. 1968-1975.

J736. Yu Wang. Squint Spotlight SAR Raw Signal Simulation in the Frequency Domain Using Optical Principles. / Yu Wang, Zhimin Zhang, Yunkai Deng. // IEEE Transactions on Geoscience and Remote Sensing. - 2008. - Vol. 46, No. 8. - P. 2208-2215.

J737. Dierking W. Sea Ice Deformation State From Synthetic Aperture Radar Imagery-Part II: Effects of Spatial Resolution and Noise Level. / Dierking W., Dall J. // IEEE Transactions on Geoscience and Remote Sensing. - 2008. - Vol. 46, No. 8. - P. 2197-2207.

J738. Hongbo Su. Spatial and Temporal Scaling Behavior of Surface Shortwave Downward Radiation Based on MODIS and In Situ Measurements. / Hongbo Su, Wood E.F., Wang H., Pinker R.T. // IEEE Geoscience and Remote Sensing Letters. - 2008. - Vol. 5, No. 3. - P. 542-546.

J739. Xiaolan Qiu. An Omega-K Algorithm With Phase Error Compensation for Bistatic SAR of a Translational Invariant Case. / Xiaolan Qiu, Donghui Hu, Chibiao Ding. // IEEE Transactions on Geoscience and Remote Sensing. - 2008. - Vol. 46, No. 8. - P. 2224-2232.

J740. Takahashi N. Characteristics of TRMM/PR System Noise and Their Application to the Rain Detection Algorithm. / Takahashi N., Iguchi T. // IEEE Transactions on Geoscience and Remote Sensing. - 2008. - Vol. 46, No. 6. - P. 1697-1704.

J741. Nebuloni R. Quantifying Bird Migration by a High-Resolution Weather Radar. / Nebuloni R., Capsoni C., Vigorita V. // IEEE Transactions on Geoscience and Remote Sensing. - 2008. - Vol. 46, No. 6. - P. 1867-1875.

J742. Ferraioli G. Phase-Offset Estimation in Multichannel SAR Interferometry. / Ferraioli G., Ferraiuolo G., Pascazio V. // IEEE Geoscience and Remote Sensing Letters. - 2008. - Vol. 5, No. 3. - P. 458-462.

J743. Bamler R. The Pyramids of Gizeh Seen by TerraSAR-X-A Prime Example for Unexpected Scattering Mechanisms in SAR. / Bamler R., Eineder M. // IEEE Geoscience and Remote Sensing Letters. - 2008. - Vol. 5, No. 3. - P. 468-470.

J744. Casu F. SBAS-DInSAR Analysis of Very Extended Areas: First Results on a 60 000- Test Site. / Casu F., Manzo M., Pepe A., Lanari R. // IEEE Geoscience and Remote Sensing Letters. - 2008. - Vol. 5, No. 3. - P. 438-442.

J745. Vallecchi A. Physical Optics Curved-Boundary Dielectric Plate Scattering Formulas for an Accurate and Efficient Electromagnetic Characterization of a Class of Natural Targets. IEEE Transactions on Geoscience and Remote Sensing. - 2008. - Vol. 46, No. 6. - P. 1657-1666.

J746. Munoz-Ferreras J.M. Traffic Surveillance System Based on a High-Resolution Radar. / Munoz-Ferreras J.M., Perez-Martinez F., Calvo-Gallego J., Asensio-Lopez A., Dorta-Naranjo B.P., Blanco-del-Campo A. // IEEE Transactions on Geoscience and Remote Sensing. - 2008. - Vol. 46, No. 6. - P. 1624-1633.

J747. Changzheng Ma. Three-Dimensional ISAR Imaging Using a Two-Dimensional Sparse Antenna Array. / Changzheng Ma, Tat Soon Yeo, Hwee Siang Tan, Jun Wang, Baixiao Chen. // IEEE Geoscience and Remote Sensing Letters. - 2008. - Vol. 5, No. 3. - P. 378-382.

J748. Esch T. Improvement of Image Segmentation Accuracy Based on Multiscale Optimization Procedure. / Esch T., Thiel M., Bock M., Roth A., Dech S. // IEEE Geoscience and Remote Sensing Letters. - 2008. - Vol. 5, No. 3. - P. 463-467.

J749. Rico-Ramirez M.A. Classification of Ground Clutter and Anomalous Propagation Using Dual-Polarization Weather Radar. / Rico-Ramirez M.A., Cluckie I.D. // IEEE Transactions on Geoscience and Remote Sensing. - 2008. - Vol. 46, No. 7. - P. 1892-1904.

J750. Leung H. Distributed sensing based on intelligent sensor networks. / Leung H., Chandana S., Shuang Wei. // IEEE Circuits and Systems Magazine. - 2008. - Vol. 8, No. 2. - P. 38-52.

J751. Bachmann S.M. Phase-Based Clutter Identification in Spectra of Weather Radar Signals. IEEE Geoscience and Remote Sensing Letters. - 2008. - Vol. 5, No. 3. - P. 487-491.

J752. Feng Li. Focusing Azimuth-Invariant Bistatic SAR Data With Chirp Scaling. / Feng Li, Shu Li, Yigong Zhao. // IEEE Geoscience and Remote Sensing Letters. - 2008. - Vol. 5, No. 3. - P. 484-486.

J753. Lasne Y. Effect of Salinity on the Dielectric Properties of Geological Materials: Implication for Soil Moisture Detection by Means of Radar Remote Sensing. / Lasne Y., Paillou P., Freeman A., Farr T., McDonald K.C., Ruffie G., Malezieux J.-M., Chapman B., Demontoux F. // IEEE Transactions on Geoscience and Remote Sensing. - 2008. - Vol. 46, No. 6. - P. 1674-1688.

J754. Daum F. Radar Handbook, 3rd Edition (M.I. Skolnik, Ed; 2008) [Book Review]. IEEE Aerospace and Electronic Systems Magazine. - 2008. - Vol. 23, No. 5. - P. 41.

J755. Xin Guo. Interference Cancellation for High-Frequency Surface Wave Radar. / Xin Guo, Hongbo Sun, Tat Soon Yeo. // IEEE Transactions on Geoscience and Remote Sensing. - 2008. - Vol. 46, No. 7. - P. 1879-1891.

J756. Williams M.L. Potential for Surface Parameter Estimation Using Compact Polarimetric SAR. IEEE Geoscience and Remote Sensing Letters. - 2008. - Vol. 5, No. 3. - P. 471-473.

J757. Freeman A. Response to “Corrections to ‘Calibration of Linearly Polarized Polarimetric SAR Data Subject to Faraday Rotation’” [orig. paper Aug 04 1617-1624]. IEEE Transactions on Geoscience and Remote Sensing. - 2008. - Vol. 46, No. 4. - P. 1279.

J758. Zribi M. A Method for Soil Moisture Estimation in Western Africa Based on the ERS Scatterometer. / Zribi M., Andre C., Decharme B. // IEEE Transactions on Geoscience and Remote Sensing. - 2008. - Vol. 46,

No. 2. - P. 438-448.

J759. Notarnicola C. Soil Moisture Retrieval From Remotely Sensed Data: Neural Network Approach Versus Bayesian Method. / Notarnicola C., Angiulli M., Posa F. // IEEE Transactions on Geoscience and Remote Sensing. - 2008. - Vol. 46, No. 2. - P. 547-557.

J760. Pinel N. Modeling of the Bistatic Electromagnetic Scattering From Sea Surfaces Covered in Oil for Microwave Applications. / Pinel N., Dechamps N., Bourlier C. // IEEE Transactions on Geoscience and Remote Sensing. - 2008. - Vol. 46, No. 2. - P. 385-392.

J761. Changzheng Ma. Three-Dimensional ISAR Imaging Based on Antenna Array. / Changzheng Ma, Tat Soon Yeo, Qun Zhang, Hwee Siang Tan, Jun Wang. // IEEE Transactions on Geoscience and Remote Sensing. - 2008. - Vol. 46, No. 2. - P. 504-515.

J762. Yew Lam Neo. Processing of Azimuth-Invariant Bistatic SAR Data Using the Range Doppler Algorithm. / Yew Lam Neo, Wong F.H., Cumming I.G. // IEEE Transactions on Geoscience and Remote Sensing. - 2008. - Vol. 46, No. 1. - P. 14-21.

J763. Loffeld O. Phase Unwrapping for SAR Interferometry-A Data Fusion Approach by Kalman Filtering. / Loffeld O., Nies H., Knedlik S., Yu Wang. // IEEE Transactions on Geoscience and Remote Sensing. - 2008. - Vol. 46, No. 1. - P. 47-58.

J764. Lang M.W. Using C-Band Synthetic Aperture Radar Data to Monitor Forested Wetland Hydrology in Maryland's Coastal Plain, USA. / Lang M.W., Kasischke E.S. // IEEE Transactions on Geoscience and Remote Sensing. - 2008. - Vol. 46, No. 2. - P. 535-546.

J765. Qi Wang. High-Resolution Three-Dimensional Radar Imaging for Rapidly Spinning Targets. / Qi Wang, Mengdao Xing, Guangyue Lu, Zheng Bao. // IEEE Transactions on Geoscience and Remote Sensing. - 2008. - Vol. 46, No. 1. - P. 22-30.

J766. Perna S. X-Band Airborne Differential Interferometry: Results of the OrbiSAR Campaign Over the Perugia Area. / Perna S., Wimmer C., Moreira J., Fornaro G. // IEEE Transactions on Geoscience and Remote Sensing. - 2008. - Vol. 46, No. 2. - P. 489-503.

J767. Montopoli M. Analysis and Synthesis of Raindrop Size Distribution Time Series From Disdrometer Data. / Montopoli M., Marzano F.S., Vulpiani G. // IEEE Transactions on Geoscience and Remote Sensing. - 2008. - Vol. 46, No. 2. - P. 466-478.

J768. Leducq P. Matching-Pursuit-Based Analysis of Moving Objects in Polarimetric SAR Images. / Leducq P., Ferro-Famil L., Pottier E. // IEEE Geoscience and Remote Sensing Letters. - 2008. - Vol. 5, No. 2. - P. 123-127.

J769. Vasile G. High-Resolution SAR Interferometry: Estimation of Local Frequencies in the Context of Alpine Glaciers. / Vasile G., Trouve E., Petillot I., Bolon P., Nicolas J.-M., Gay M., Chanussot J., Landes T., Grussenmeyer P., Buzuloiu V., Hajnsek I., Andres C., Keller M., Horn R. // IEEE Transactions on Geoscience and Remote Sensing. - 2008. - Vol. 46, No. 4. - P. 1079-1090.

J770. Bradley C.J. Evaluation of a Near-Field Monostatic-to-Bistatic Equivalence Theorem. / Bradley C.J., Collins P.J., Falconer D.G., Fortuny-Guasch J., Terzuoli A.J. // IEEE Transactions on Geoscience and Remote Sensing. - 2008. - Vol. 46, No. 2. - P. 449-457.

J771. Piepmeier J.R. Stokes Antenna Temperatures. / Piepmeier J.R., Long D.G., Njoku E.G. // IEEE Transactions on Geoscience and Remote Sensing. - 2008. - Vol. 46, No. 2. - P. 516-527.

J772. Kaasalainen S. Brightness Measurements and Calibration With Airborne and Terrestrial Laser Scanners. / Kaasalainen S., Kukko A., Lindroos T., Litkey P., Kaartinen H., Hyyppa J., Ahokas E. // IEEE Transactions on Geoscience and Remote Sensing. - 2008. - Vol. 46, No. 2. - P. 528-534.

J773. Shenbin Yang. Rice Mapping and Monitoring Using ENVISAT ASAR Data. / Shenbin Yang, Shuanghe Shen, Bingbai Li, Thuy Le Toan, Wei He. // IEEE Geoscience and Remote Sensing Letters. - 2008. - Vol. 5, No. 1. - P. 108-112.

J774. Greenhalgh S.A. Authors' Reply to Comments by Takuya Sakamoto, Shouhei Kidera, and Toru Sato on

“Seabed Algorithm and Comments on ‘Modeling and Migration of 2-D Georadar Data: A Stationary Phase Approach’”. / Greenhalgh S.A., Marescot L. // IEEE Transactions on Geoscience and Remote Sensing. - 2008. - Vol. 46, No. 1. - P. 300.

J775. Vandewal M. Efficient SAR Raw Data Generation Including Low Squint Angles and Platform Instabilities. / Vandewal M., Speck R., Suess H. // IEEE Geoscience and Remote Sensing Letters. - 2008. - Vol. 5, No. 1. - P. 26-30.

J776. Pieraccini M. Detection of Breathing and Heartbeat Through Snow Using a Microwave Transceiver. / Pieraccini M., Luzi G., Dei D., Pieri L., Atzeni C. // IEEE Geoscience and Remote Sensing Letters. - 2008. - Vol. 5, No. 1. - P. 57-59.

J777. Neumann M. Multibaseline Polarimetric SAR Interferometry Coherence Optimization. / Neumann M., Ferro-Famil L., Reigber A. // IEEE Geoscience and Remote Sensing Letters. - 2008. - Vol. 5, No. 1. - P. 93-97.

J778. Brekke C. Classifiers and Confidence Estimation for Oil Spill Detection in ENVISAT ASAR Images. / Brekke C., Solberg A.H.S. // IEEE Geoscience and Remote Sensing Letters. - 2008. - Vol. 5, No. 1. - P. 65-69.

J779. Zhengzhao Luo. On the Use of CloudSat and MODIS Data for Estimating Hurricane Intensity. / Zhengzhao Luo, Stephens G.L., Emanuel K.A., Vane D.G., Tourville N.D., Haynes J.M. // IEEE Geoscience and Remote Sensing Letters. - 2008. - Vol. 5, No. 1. - P. 13-16.

J780. Sabry R. Basic Slant Range-Doppler Modeling of Moving Scatterers for SAR Applications. IEEE Geoscience and Remote Sensing Letters. - 2008. - Vol. 5, No. 1. - P. 8-12.

J781. Nekrasov A. Measurement of the Wind Vector Over Sea by an Airborne Radar Altimeter Using an Antenna Characterized by Different Beamwidth in the Vertical and Horizontal Planes. IEEE Geoscience and Remote Sensing Letters. - 2008. - Vol. 5, No. 1. - P. 31-33.

J782. Yanping Li. Bistatic Spotlight SAR Processing Using the Frequency-Scaling Algorithm. / Yanping Li, Zhenhua Zhang, Mengdao Xing, Zheng Bao. // IEEE Geoscience and Remote Sensing Letters. - 2008. - Vol. 5, No. 1. - P. 48-52.

J783. Marzano F.S. Supervised Classification and Estimation of Hydrometeors From C-Band Dual-Polarized Radars: A Bayesian Approach. / Marzano F.S., Scaranari D., Montopoli M., Vulpiani G. // IEEE Transactions on Geoscience and Remote Sensing. - 2008. - Vol. 46, No. 1. - P. 85-98.

J784. Zare A. Vegetation Mapping for Landmine Detection Using Long-Wave Hyperspectral Imagery. / Zare A., Bolton J., Gader P., Schatten M. // IEEE Transactions on Geoscience and Remote Sensing. - 2008. - Vol. 46, No. 1. - P. 172-178.

J785. Xudong Jiang. Afterpulsing Effects in Free-Running InGaAsP Single-Photon Avalanche Diodes. / Xudong Jiang, Itzler M.A., Ben-Michael R., Slomkowski K., Krainak M.A., Wu S., Xiaoli Sun. // IEEE Journal of Quantum Electronics. - 2008. - Vol. 44, No. 1. - P. 3-11.

J786. Krieger G. Multidimensional Waveform Encoding: A New Digital Beamforming Technique for Synthetic Aperture Radar Remote Sensing. / Krieger G., Gebert N., Moreira A. // IEEE Transactions on Geoscience and Remote Sensing. - 2008. - Vol. 46, No. 1. - P. 31-46.

J787. Garestier F. Pine Forest Height Inversion Using Single-Pass X-Band PolInSAR Data. / Garestier F., Dubois-Fernandez P.C., Papathanassiou K.P. // IEEE Transactions on Geoscience and Remote Sensing. - 2008. - Vol. 46, No. 1. - P. 59-68.

J788. Pipia L. Atmospheric Artifact Compensation in Ground-Based DInSAR Applications. / Pipia L., Fabregas X., Aguasca A., Lopez-Martinez C. // IEEE Geoscience and Remote Sensing Letters. - 2008. - Vol. 5, No. 1. - P. 88-92.

J789. Tong Wang. Improving Coherence of Complex Image Pairs Obtained by Along-Track Bistatic SARs Using Range-Azimuth Prefiltering. / Tong Wang, Zheng Bao, Zhen-hua Zhang, Jin-shan Ding. // IEEE Transactions on Geoscience and Remote Sensing. - 2008. - Vol. 46, No. 1. - P. 3-13.

J790. Kononov A.A. Model-Associated Forest Parameter Retrieval Using VHF SAR Data at the Individual Tree Level. / Kononov A.A., Min-Ho Ka. // IEEE Transactions on Geoscience and Remote Sensing. - 2008. - Vol. 46, No. 1. - P. 69-84.

J791. Persico R. Effects of Background Removal in Linear Inverse Scattering. / Persico R., Soldovieri F. // IEEE Transactions on Geoscience and Remote Sensing. - 2008. - Vol. 46, No. 4. - P. 1104-1114.

J792. Bin Cai. A New Adaptive Multiresolution Noise-Filtering Approach for SAR Interferometric Phase Images. / Bin Cai, Diannong Liang, Zhen Dong. // IEEE Geoscience and Remote Sensing Letters. - 2008. - Vol. 5, No. 2. - P. 266-270.

J793. Kerekes J. Receiver Operating Characteristic Curve Confidence Intervals and Regions. IEEE Geoscience and Remote Sensing Letters. - 2008. - Vol. 5, No. 2. - P. 251-255.

J794. Prats P. Estimation of the Temporal Evolution of the Deformation Using Airborne Differential SAR Interferometry. / Prats P., Mallorqui J.J., Reigber A., Scheiber R., Moreira A. // IEEE Transactions on Geoscience and Remote Sensing. - 2008. - Vol. 46, No. 4. - P. 1065-1078.

J795. Xiaowei Li. Processing of Envisat Alternating Polarization Data for Vessel Detection. / Xiaowei Li, Jinsong Chong. // IEEE Geoscience and Remote Sensing Letters. - 2008. - Vol. 5, No. 2. - P. 271-275.

J796. Cochin V. Sea Surface Current-Wave-Wind Interactions Measured by Coastal Ground Wave HF Radars. / Cochin V., Mariette V., Garello R. // IEEE Geoscience and Remote Sensing Letters. - 2008. - Vol. 5, No. 2. - P. 227-230.

J797. Merryman Boncori J.P. A Tunable Closed-Form Model for the Structure Function of Tropospheric Delay. / Merryman Boncori J.P., Mohr J.J. // IEEE Geoscience and Remote Sensing Letters. - 2008. - Vol. 5, No. 2. - P. 222-226.

J798. Kimura H. Radar Polarization Orientation Shifts in Built-Up Areas. IEEE Geoscience and Remote Sensing Letters. - 2008. - Vol. 5, No. 2. - P. 217-221.

J799. Eryan Dai. Three-Dimensional Stereo Reconstruction of Buildings Using Polarimetric SAR Images Acquired in Opposite Directions. / Eryan Dai, Ya-Qiu Jin, Hamasaki T., Sato M. // IEEE Geoscience and Remote Sensing Letters. - 2008. - Vol. 5, No. 2. - P. 236-240.

J800. Mason I.M. The Effect of Conduction on VHF Radar Images Shot in Water-Filled Boreholes. / Mason I.M., Bray A.J., Sindle T.G., Simmat C.M., Cloete J.H. // IEEE Geoscience and Remote Sensing Letters. - 2008. - Vol. 5, No. 2. - P. 304-307.

J801. Hongxing Liu. Simultaneous Least Squares Adjustment of Multiframe Velocities Derived From Interferometric and Speckle-Tracking Methods. / Hongxing Liu, Zhiyuan Zhao, Jaehyung Yu, Ken Jezek. // IEEE Geoscience and Remote Sensing Letters. - 2008. - Vol. 5, No. 2. - P. 289-293.

J802. Durden S.L. Predicted Effects of Nonuniform Beam Filling on GPM Radar Data. / Durden S.L., Tanelli S. // IEEE Geoscience and Remote Sensing Letters. - 2008. - Vol. 5, No. 2. - P. 308-310.

J803. Pardini M. The Hybrid CramЙr-Rao Bound on Broadside DOA Estimation of Extended Sources in Presence of Array Errors. / Pardini M., Lombardini F., Gini F. // IEEE Transactions on Signal Processing. - 2008. - Vol. 56, No. 4. - P. 1726-1730.

J804. Zhishun She. Autofocus for ISAR Imaging Using Higher Order Statistics. / Zhishun She, Liu Y. // IEEE Geoscience and Remote Sensing Letters. - 2008. - Vol. 5, No. 2. - P. 299-303.

J805. Bao-Quan Liu. Analytic Search Method for Interferometric SAR Image Registration. / Bao-Quan Liu, Da-Zheng Feng, Peng-Lang Shui, Nan Wu. // IEEE Geoscience and Remote Sensing Letters. - 2008. - Vol. 5, No. 2. - P. 294-298.

J806. Haipeng Wang. Accuracy of the -Distribution Regression Model for Forest Biomass Estimation by High-Resolution Polarimetric SAR: Comparison of Model Estimation and Field Data. / Haipeng Wang, Ouchi K. // IEEE Transactions on Geoscience and Remote Sensing. - 2008. - Vol. 46, No. 4. - P. 1058-1064.

J807. Turner D.D. Validating Mixed-Phase Cloud Optical Depth Retrieved From Infrared Observations With High Spectral Resolution Lidar. / Turner D.D., Eloranta E.W. // IEEE Geoscience and Remote Sensing Letters. - 2008. - Vol. 5, No. 2. - P. 285-288.

J808. Bachmann S.M. Three-Dimensional Attributes of Clear-Air Scatterers Observed With the Polarimetric Weather Radar. / Bachmann S.M., Zrnic D.S. // IEEE Geoscience and Remote Sensing Letters. - 2008. - Vol. 5, No. 2. - P. 231-235.

J809. Giusti E. Equivalence Between Cameron's Unit Disc and PoincarЙ's Sphere for Symmetric Scattering Characterization and Classification. / Giusti E., Martorella M., Petronio C., Berizzi F. // IEEE Geoscience and Remote Sensing Letters. - 2008. - Vol. 5, No. 2. - P. 152-156.

J810. Gill E. The Effect of the Bistatic Scattering Angle on the High-Frequency Radar Cross Sections of the Ocean Surface. / Gill E., Weimin Huang, Walsh J. // IEEE Geoscience and Remote Sensing Letters. - 2008. - Vol. 5, No. 2. - P. 143-146.

J811. Ahmad F. Three-Dimensional Wideband Beamforming for Imaging Through a Single Wall. / Ahmad F., Yimin Zhang, Amin M.G. // IEEE Geoscience and Remote Sensing Letters. - 2008. - Vol. 5, No. 2. - P. 176-179.

J812. Martinez-Espla J.J. Using a Grid-Based Filter to Solve InSAR Phase Unwrapping. / Martinez-Espla J.J., Martinez-Marin T., Lopez-Sanchez J.M. // IEEE Geoscience and Remote Sensing Letters. - 2008. - Vol. 5, No. 2. - P. 147-151.

J813. Loew A. On the Disaggregation of Passive Microwave Soil Moisture Data Using A Priori Knowledge of Temporally Persistent Soil Moisture Fields. / Loew A., Mauser W. // IEEE Transactions on Geoscience and Remote Sensing. - 2008. - Vol. 46, No. 3. - P. 819-834.

J814. Boncori J.P.M. Signal Processing Issues for the Exploitation of Pulse-to-Pulse Encoding SAR Transponders. / Boncori J.P.M., Schiavon G. // IEEE Transactions on Geoscience and Remote Sensing. - 2008. - Vol. 46, No. 4. - P. 1048-1057.

J815. Bachmann S.M. Suppression of Clutter Residue in Weather Radar Reveals Birds' Corridors Over Urban Area. / Bachmann S.M., Zrnic D.S. // IEEE Geoscience and Remote Sensing Letters. - 2008. - Vol. 5, No. 2. - P. 128-132.

J816. Braun N. Sea-Surface Current Features Observed by Doppler Radar. / Braun N., Ziemer F., Bezuglov A., Cysewski M., Schymura G. // IEEE Transactions on Geoscience and Remote Sensing. - 2008. - Vol. 46, No. 4. - P. 1125-1133.

J817. Solbo S. A Stationary Wavelet-Domain Wiener Filter for Correlated Speckle. / Solbo S., Eltoft T. // IEEE Transactions on Geoscience and Remote Sensing. - 2008. - Vol. 46, No. 4. - P. 1219-1230.

J818. Ubolkosold P. A Method to Extend the Estimation Range of the Existing Time-Domain Doppler Centroid Estimators. / Ubolkosold P., Knedlik S., Loffeld O. // IEEE Geoscience and Remote Sensing Letters. - 2008. - Vol. 5, No. 2. - P. 185-188.

J819. Hernandez-Marin S. Multilayered 3D LiDAR Image Construction Using Spatial Models in a Bayesian Framework. / Hernandez-Marin S., Wallace A.M., Gibson G.J. // IEEE Transactions on Pattern Analysis and Machine Intelligence. - 2008. - Vol. 30, No. 6. - P. 1028-1040.

J820. Matrosov S.Y. Assessment of Radar Signal Attenuation Caused by the Melting Hydrometeor Layer. IEEE Transactions on Geoscience and Remote Sensing. - 2008. - Vol. 46, No. 4. - P. 1039-1047.

J821. Mingsheng Liao. Using SAR Images to Detect Ships From Sea Clutter. / Mingsheng Liao, Changcheng Wang, Yong Wang, Liming Jiang. // IEEE Geoscience and Remote Sensing Letters. - 2008. - Vol. 5, No. 2. - P. 194-198.

J822. Xiong W. Corrections to “Calibration of Linearly Polarized Polarimetric SAR Data Subject to Faraday Rotation” [Aug 04 1617-1624]. IEEE Transactions on Geoscience and Remote Sensing. - 2008. - Vol. 46, No. 4. - P. 1278.

J823. Ghoggali N. Genetic SVM Approach to Semisupervised Multitemporal Classification. / Ghoggali N.,

Melgani F. // IEEE Geoscience and Remote Sensing Letters. - 2008. - Vol. 5, No. 2. - P. 212-216.

J824. Anterrieu E. Brightness Temperature Map Reconstruction from Dual-Polarimetric Visibilities in Synthetic Aperture Imaging Radiometry. / Anterrieu E., Khazaal A. // IEEE Transactions on Geoscience and Remote Sensing. - 2008. - Vol. 46, No. 3. - P. 606-612.

J825. Guccione P. Comparison of Processing Algorithms for a Delay/Doppler Altimeter. IEEE Geoscience and Remote Sensing Letters. - 2008. - Vol. 5, No. 4. - P. 764-768.

J826. Ngan Tran. Validation of Envisat Rain Detection and Rain Rate Estimates by Comparing With TRMM Data. / Ngan Tran, Tournadre J., Femenias P. // IEEE Geoscience and Remote Sensing Letters. - 2008. - Vol. 5, No. 4. - P. 658-662.

J827. Xiaolan Qiu. Some Reflections on Bistatic SAR of Forward-Looking Configuration. / Xiaolan Qiu, Donghui Hu, Chibiao Ding. // IEEE Geoscience and Remote Sensing Letters. - 2008. - Vol. 5, No. 4. - P. 735-739.

J828. Parinussa R.M. Comparison of Microwave and Infrared Land Surface Temperature Products Over the NAFE'06 Research Sites. / Parinussa R.M., de Jeu R., Holmes T., Walker J.P. // IEEE Geoscience and Remote Sensing Letters. - 2008. - Vol. 5, No. 4. - P. 783-787.

J829. Lamei Zhang. Multiple-Component Scattering Model for Polarimetric SAR Image Decomposition. / Lamei Zhang, Bin Zou, Hongjun Cai, Ye Zhang. // IEEE Geoscience and Remote Sensing Letters. - 2008. - Vol. 5, No. 4. - P. 603-607.

J830. Yonghui Wu. Region-Based Classification of Polarimetric SAR Images Using Wishart MRF. / Yonghui Wu, Kefeng Ji, Wenxian Yu, Yi Su. // IEEE Geoscience and Remote Sensing Letters. - 2008. - Vol. 5, No. 4. - P. 668-672.

J831. Dragosevic M.V. Estimation of Ship Radial Speed by Adaptive Processing of RADARSAT-1 Fine Mode Data. / Dragosevic M.V., Vachon P.W. // IEEE Geoscience and Remote Sensing Letters. - 2008. - Vol. 5, No. 4. - P. 678-682.

J832. Abdul Gaffar M.Y. Quaternion-Based Transformation for Extraction of Image-Generating Doppler for ISAR. / Abdul Gaffar M.Y., Nel W., Inggs M.R. // IEEE Geoscience and Remote Sensing Letters. - 2008. - Vol. 5, No. 4. - P. 560-563.

J833. Zhe Liu. Study on Spaceborne/Airborne Hybrid Bistatic SAR Image Formation in Frequency Domain. / Zhe Liu, Jianyu Yang, Xiaoling Zhang, Yiming Pi. // IEEE Geoscience and Remote Sensing Letters. - 2008. - Vol. 5, No. 4. - P. 578-582.

J834. Zeng Jiankui. Modified Hough Transform for Searching Radar Detection. / Zeng Jiankui, He Zishu, Sellathurai M., Liu Hongming. // IEEE Geoscience and Remote Sensing Letters. - 2008. - Vol. 5, No. 4. - P. 683-686.

J835. Le Gall A. An Imaging HF GPR Using Stationary Antennas: Experimental Validation Over the Antarctic Ice Sheet. / Le Gall A., Ciarletti V., Berthelier J.-J., Reineix A., Guiffaut C., Ney R., Dolon F., Bonaime S. // IEEE Transactions on Geoscience and Remote Sensing. - 2008. - Vol. 46, No. 12. - P. 3975-3986.

J836. Yang D.K. GPS Reflections for Sea Surface Wind Speed Measurement. / Yang D.K., Zhang Y.Q., Lu Y., Zhang Q.S. // IEEE Geoscience and Remote Sensing Letters. - 2008. - Vol. 5, No. 4. - P. 569-572.

J837. Yongmin Shuai. SAR Image Segmentation Based on Level Set With Stationary Global Minimum. / Yongmin Shuai, Hong Sun, Ge Xu. // IEEE Geoscience and Remote Sensing Letters. - 2008. - Vol. 5, No. 4. - P. 644-648.

J838. Yun-Woong Choi. Three-Dimensional LiDAR Data Classifying to Extract Road Point in Urban Area. / Yun-Woong Choi, Young-Woon Jang, Hyo-Jong Lee, Gi-Sung Cho. // IEEE Geoscience and Remote Sensing Letters. - 2008. - Vol. 5, No. 4. - P. 725-729.

J839. Yong Wang. A Novel Algorithm for Estimating the Rotation Angle in ISAR Imaging. / Yong Wang, Yicheng Jiang. // IEEE Geoscience and Remote Sensing Letters. - 2008. - Vol. 5, No. 4. - P. 608-609.

J840. Yu Tang. The Polar Format Imaging Algorithm Based on Double Chirp-Z Transforms. / Yu Tang, Meng-Dao Xing, Zheng Bao. // IEEE Geoscience and Remote Sensing Letters. - 2008. - Vol. 5, No. 4. - P. 610-614.

J841. Jong-Suk Yoon. Land Cover Characteristics of Airborne LiDAR Intensity Data: A Case Study. / Jong-Suk Yoon, Jung-Il Shin, Kyu-Sung Lee. // IEEE Geoscience and Remote Sensing Letters. - 2008. - Vol. 5, No. 4. - P. 801-805.

J842. Masuyama S. Multiple-Mode Selection of Walled-LTSA Array Elements for High-Resolution Imaging to Visualize Antipersonnel Plastic Landmines. / Masuyama S., Yasuda K., Hirose A. // IEEE Geoscience and Remote Sensing Letters. - 2008. - Vol. 5, No. 4. - P. 745-749.

J843. Gambardella A. On the Superresolution of Microwave Scanning Radiometer Measurements. / Gambardella A., Migliaccio M. // IEEE Geoscience and Remote Sensing Letters. - 2008. - Vol. 5, No. 4. - P. 796-800.

J844. Ozyavas A. Assessment of Recent Short-Term Water-Level Fluctuations in Caspian Sea Using Topex/Poseidon. / Ozyavas A., Khan S.D. // IEEE Geoscience and Remote Sensing Letters. - 2008. - Vol. 5, No. 4. - P. 720-724.

J845. Martinez-Vazquez A. Averaging and Formulation Impact on GB-SAR Topographic Mapping. / Martinez-Vazquez A., Fortuny-Guasch J. // IEEE Geoscience and Remote Sensing Letters. - 2008. - Vol. 5, No. 4. - P. 635-639.

J846. Chao Chen. Sifting Through the Jungle of Sensor Standards. / Chao Chen, Helal S. // IEEE Pervasive Computing. - 2008. - Vol. 7, No. 4. - P. 84-88.

J847. Zaugg E.C. Theory and Application of Motion Compensation for LFM-CW SAR. / Zaugg E.C., Long D.G. // IEEE Transactions on Geoscience and Remote Sensing. - 2008. - Vol. 46, No. 10. - P. 2990-2998.

J848. Gambardella A. A Physical Full-Resolution SAR Ship Detection Filter. / Gambardella A., Nunziata F., Migliaccio M. // IEEE Geoscience and Remote Sensing Letters. - 2008. - Vol. 5, No. 4. - P. 760-763.

J849. Camps A. Angular and Radiometric Resolution of Y-Shaped Nonuniform Synthetic Aperture Radiometers for Earth Observation. / Camps A., Vall-llossera M., Corbella I., Torres F., Duffo N. // IEEE Geoscience and Remote Sensing Letters. - 2008. - Vol. 5, No. 4. - P. 793-795.

J850. Schumann G. Conditioning Water Stages From Satellite Imagery on Uncertain Data Points. / Schumann G., Matgen P., Pappenberger F. // IEEE Geoscience and Remote Sensing Letters. - 2008. - Vol. 5, No. 4. - P. 810-813.

J851. Gang Li. Doppler Keystone Transform: An Approach Suitable for Parallel Implementation of SAR Moving Target Imaging. / Gang Li, Xiang-Gen Xia, Ying-Ning Peng. // IEEE Geoscience and Remote Sensing Letters. - 2008. - Vol. 5, No. 4. - P. 573-577.

J852. Jinfeng Wang. Level Set Method for SAR Image Coregistration. / Jinfeng Wang, Yiming Pi, Zongjie Cao. // IEEE Geoscience and Remote Sensing Letters. - 2008. - Vol. 5, No. 4. - P. 615-619.

J853. Jiao Guo. Using Multibaseline InSAR to Recover Layovered Terrain Considering Wideband Array Problem. / Jiao Guo, Zhenfang Li, Zheng Bao. // IEEE Geoscience and Remote Sensing Letters. - 2008. - Vol. 5, No. 4. - P. 583-587.

J854. Gierull C.H. Ground Moving Target Indication With Tandem Satellite Constellations. / Gierull C.H., Cerutti-Maori D., Ender J. // IEEE Geoscience and Remote Sensing Letters. - 2008. - Vol. 5, No. 4. - P. 710-714.

J855. Rigling B.D. Image-Quality Focusing of Rotating SAR Targets. IEEE Geoscience and Remote Sensing Letters. - 2008. - Vol. 5, No. 4. - P. 750-754.

J856. Nunziata F. On the Mueller Scattering Matrix for SAR Sea Oil Slick Observation. / Nunziata F., Gambardella A., Migliaccio M. // IEEE Geoscience and Remote Sensing Letters. - 2008. - Vol. 5, No. 4. - P. 691-695.

J857. Lombardini F. 3-D SAR Tomography: The Multibaseline Sector Interpolation Approach. / Lombardini F., Pardini M. // IEEE Geoscience and Remote Sensing Letters. - 2008. - Vol. 5, No. 4. - P. 630-634.

J858. Ender J.H.G. Improved Space-Based Moving Target Indication via Alternate Transmission and Receiver Switching. / Ender J.H.G., Gierull C.H., Cerutti-Maori D. // IEEE Transactions on Geoscience and Remote Sensing. - 2008. - Vol. 46, No. 12. - P. 3960-3974.

J859. Lopez-Martinez C. Model-Based Polarimetric SAR Speckle Filter. / Lopez-Martinez C., Fabregas X. // IEEE Transactions on Geoscience and Remote Sensing. - 2008. - Vol. 46, No. 11. - P. 3894-3907.

J860. Wong A. Efficient FFT-Accelerated Approach to Invariant Optical-LIDAR Registration. / Wong A., Orchard J. // IEEE Transactions on Geoscience and Remote Sensing. - 2008. - Vol. 46, No. 11. - P. 3917-3925.

J861. Della Vecchia A. Observing and Modeling Multifrequency Scattering of Maize During the Whole Growth Cycle. / Della Vecchia A., Ferrazzoli P., Guerriero L., Ninivaggi L., Strozzi T., Wegmuller U. // IEEE Transactions on Geoscience and Remote Sensing. - 2008. - Vol. 46, No. 11. - P. 3709-3718.

J862. Ng W. Particle Filtering Based Approach for Landmine Detection Using Ground Penetrating Radar. / Ng W., Chan T., So H.C., Ho K.C. // IEEE Transactions on Geoscience and Remote Sensing. - 2008. - Vol. 46, No. 11. - P. 3739-3755.

J863. Xueru Bai. Imaging of Micromotion Targets With Rotating Parts Based on Empirical-Mode Decomposition. / Xueru Bai, Mengdao Xing, Feng Zhou, Guangyue Lu, Zheng Bao. // IEEE Transactions on Geoscience and Remote Sensing. - 2008. - Vol. 46, No. 11. - P. 3514-3523.

J864. Guarnieri A.M. On the Exploitation of Target Statistics for SAR Interferometry Applications. / Guarnieri A.M., Tebaldini S. // IEEE Transactions on Geoscience and Remote Sensing. - 2008. - Vol. 46, No. 11. - P. 3436-3443.

J865. Chubb S.R. Ocean Surface Currents From AVHRR Imagery: Comparison With Land-Based HF Radar Measurements. / Chubb S.R., Mied R.P., Shen C.Y., Wei Chen, Evans T.E., Kohut J. // IEEE Transactions on Geoscience and Remote Sensing. - 2008. - Vol. 46, No. 11. - P. 3647-3660.

J866. Zhi-Hong Jiang. Squint LFMCW SAR Data Processing Using Doppler-Centroid-Dependent Frequency Scaling Algorithm. / Zhi-Hong Jiang, Kan Huang-Fu. // IEEE Transactions on Geoscience and Remote Sensing. - 2008. - Vol. 46, No. 11. - P. 3535-3543.

J867. Martinez-Vazquez A. A GB-SAR Processor for Snow Avalanche Identification. / Martinez-Vazquez A., Fortuny-Guasch J. // IEEE Transactions on Geoscience and Remote Sensing. - 2008. - Vol. 46, No. 11. - P. 3948-3956.

J868. Jin T. Feature Extraction and Discriminator Design for Landmine Detection on Double-Hump Signature in Ultrawideband SAR. / Jin T., Zhou Z. // IEEE Transactions on Geoscience and Remote Sensing. - 2008. - Vol. 46, No. 11. - P. 3783-3791.

J869. Aspey R. A. LABVIEW graphical user interface for precision multichannel alignment of Raman lidar at Jet Propulsion Laboratory, Table Mountain Facility. / Aspey R. A., McDermid I. S., Leblanc T., Howe J. W., Walsh T. D. // Review of Scientific Instruments. - 2008. - Vol. 79, No. 9. - P. 094502-094502-9.

J870. Oh Y. Effect of standing stubble on radar backscatter from harvested rice fields. Electronics Letters. - 2008. - Vol. 44, No. 24. - P. 1423-1424.

J871. Ngan Tran. Snow Facies Over Ice Sheets Derived From Envisat Active and Passive Observations. / Ngan Tran, Remy F., Hui Feng, Femenias P. // IEEE Transactions on Geoscience and Remote Sensing. - 2008. - Vol. 46, No. 11. - P. 3694-3708.

J872. Pierdicca N. Comparing Scatterometric and Radiometric Simulations With Geophysical Model Functions to Tune a Sea Wave Spectrum Model. / Pierdicca N., Pulvirenti L. // IEEE Transactions on Geoscience and Remote Sensing. - 2008. - Vol. 46, No. 11. - P. 3756-3767.

J873. Shi Jun. Surface-Tracing-Based LASAR 3-D Imaging Method via Multiresolution Approximation. / Shi Jun, Zhang Xiaoling, Jianyu Yang, Wang Yinbo. // IEEE Transactions on Geoscience and Remote Sensing. -

2008. - Vol. 46, No. 11. - P. 3719-3730.

J874. Hecht R. Estimation of Urban Green Volume Based on Single-Pulse LiDAR Data. / Hecht R., Meinel G., Buchroithner M.F. // IEEE Transactions on Geoscience and Remote Sensing. - 2008. - Vol. 46, No. 11. - P. 3832-3840.

J875. Tanelli S. CloudSat's Cloud Profiling Radar After Two Years in Orbit: Performance, Calibration, and Processing. / Tanelli S., Durden S.L., Im E., Pak K.S., Reinke D.G., Partain P., Haynes J.M., Marchand R.T. // IEEE Transactions on Geoscience and Remote Sensing. - 2008. - Vol. 46, No. 11. - P. 3560-3573.

J876. Blaes X. Characterizing Bidimensional Roughness of Agricultural Soil Surfaces for SAR Modeling. / Blaes X., Defourny P. // IEEE Transactions on Geoscience and Remote Sensing. - 2008. - Vol. 46, No. 12. - P. 4050-4061.

J877. Nishizawa T. Algorithm to Retrieve Aerosol Optical Properties From High-Spectral-Resolution Lidar and Polarization Mie-Scattering Lidar Measurements. / Nishizawa T., Sugimoto N., Matsui I., Shimizu A., Tatarov B., Okamoto H. // IEEE Transactions on Geoscience and Remote Sensing. - 2008. - Vol. 46, No. 12. - P. 4094-4103.

J878. Congling Nie. A C-Band Scatterometer Simultaneous Wind/Rain Retrieval Method. / Congling Nie, Long D.G. // IEEE Transactions on Geoscience and Remote Sensing. - 2008. - Vol. 46, No. 11. - P. 3618-3631.

J879. Liu B. Doppler Ambiguity Resolving in Compressed Azimuth Time and Range Frequency Domain. / Liu B., Wang T., Bao Z. // IEEE Transactions on Geoscience and Remote Sensing. - 2008. - Vol. 46, No. 11. - P. 3444-3458.

J880. Farah I.R. Multiapproach System Based on Fusion of Multispectral Images for Land-Cover Classification. / Farah I.R., Boulila W., Ettabaa K.S., Ben Ahmed M. // IEEE Transactions on Geoscience and Remote Sensing. - 2008. - Vol. 46, No. 12. - P. 4153-4161.

J881. Farah I.R. Interpretation of Multisensor Remote Sensing Images: Multiapproach Fusion of Uncertain Information. / Farah I.R., Boulila W., Ettabaa K.S., Solaiman B., Ben Ahmed M. // IEEE Transactions on Geoscience and Remote Sensing. - 2008. - Vol. 46, No. 12. - P. 4142-4152.

J882. Nguyen Trung Thanh. Infrared Thermography for Buried Landmine Detection: Inverse Problem Setting. / Nguyen Trung Thanh, Sahli H., Dinh Nho Hao. // IEEE Transactions on Geoscience and Remote Sensing. - 2008. - Vol. 46, No. 12. - P. 3987-4004.

J883. de Lange R. Scatterometer-Derived Soil Moisture Calibrated for Soil Texture With a One-Dimensional Water-Flow Model. / de Lange R., Beck R., van de Giesen N., Friesen J., de Wit A., Wagner W. // IEEE Transactions on Geoscience and Remote Sensing. - 2008. - Vol. 46, No. 12. - P. 4041-4049.

J884. Jia Xu. Parametric Velocity Synthetic Aperture Radar: Multilook Processing and Its Applications. / Jia Xu, Gang Li, Ying-Ning Peng, Xiang-Gen Xia, Yong-Liang Wang. // IEEE Transactions on Geoscience and Remote Sensing. - 2008. - Vol. 46, No. 11. - P. 3488-3502.

J885. Johnsen H. Sea-Surface Polarization Ratio From Envisat ASAR AP Data. / Johnsen H., Engen G., Guitton G. // IEEE Transactions on Geoscience and Remote Sensing. - 2008. - Vol. 46, No. 11. - P. 3637-3646.

J886. Kidera S. High-Resolution and Real-Time Three-Dimensional Imaging Algorithm With Envelopes of Spheres for UWB Radars. / Kidera S., Sakamoto T., Sato T. // IEEE Transactions on Geoscience and Remote Sensing. - 2008. - Vol. 46, No. 11. - P. 3503-3513.

J887. Lopez-Dekker P. Phase Synchronization and Doppler Centroid Estimation in Fixed Receiver Bistatic SAR Systems. / Lopez-Dekker P., Mallorqui J.J., Serra-Morales P., Sanz-Marcos J. // IEEE Transactions on Geoscience and Remote Sensing. - 2008. - Vol. 46, No. 11. - P. 3459-3471.

J888. Garestier F. Forest Height Inversion Using High-Resolution P-Band Pol-InSAR Data. / Garestier F., Dubois-Fernandez P.C., Champion I. // IEEE Transactions on Geoscience and Remote Sensing. - 2008. - Vol. 46, No. 11. - P. 3544-3559.

J889. Sandwell D.T. Accuracy and Resolution of ALOS Interferometry: Vector Deformation Maps of the

Father's Day Intrusion at Kilauea. / Sandwell D.T., Myer D., Mellors R., Shimada M., Brooks B., Foster J. // IEEE Transactions on Geoscience and Remote Sensing. - 2008. - Vol. 46, No. 11. - P. 3524-3534.

J890. Guangdong Pan. A Numerical Method for Studying Modulation Effects in Radar Observations of the Sea Surface. / Guangdong Pan, Johnson J.T. // IEEE Transactions on Geoscience and Remote Sensing. - 2008. - Vol. 46, No. 11. - P. 3632-3636.

J891. Marzano F.S. Inversion of Spaceborne X-Band Synthetic Aperture Radar Measurements for Precipitation Remote Sensing Over Land. / Marzano F.S., Weinman J.A. // IEEE Transactions on Geoscience and Remote Sensing. - 2008. - Vol. 46, No. 11. - P. 3472-3487.

J892. Langley K. From Glacier Facies to SAR Backscatter Zones via GPR. / Langley K., Hamran S.-E., Hogda K.A., Storvold R., Brandt O., Kohler J., Hagen J.O. // IEEE Transactions on Geoscience and Remote Sensing. - 2008. - Vol. 46, No. 9. - P. 2506-2516.

J893. Hallberg B. A Physical-Optics Model for Double-Bounce Scattering From Tree Stems Standing on an Undulating Ground Surface. / Hallberg B., Smith-Jonforsen G., Ulander L.M.H., Sandberg G. // IEEE Transactions on Geoscience and Remote Sensing. - 2008. - Vol. 46, No. 9. - P. 2607-2621.

J894. Rao I. Bispectral analysis of atmospheric radar signals. / Rao I., Anandan V.K. // IEEE Aerospace and Electronic Systems Magazine. - 2008. - Vol. 23, No. 8. - P. 38-41.

J895. Mcmahon J.M. Fiber lasers: A future space technology [same article as "Fiber lasers: A future technology for lasers in space", ibid, vol. 23, n. 4, pp. 25-30, 08]. IEEE Aerospace and Electronic Systems Magazine. - 2008. - Vol. 23, No. 8. - P. 32-37.

J896. Boon Leng Cheong. Refractivity Retrieval Using the Phased-Array Radar: First Results and Potential for Multimission Operation. / Boon Leng Cheong, Palmer R.D., Curtis C.D., Tian-You Yu, Zrnic D.S., Forsyth D. // IEEE Transactions on Geoscience and Remote Sensing. - 2008. - Vol. 46, No. 9. - P. 2527-2537.

J897. Yew Lam Neo. A Comparison of Point Target Spectra Derived for Bistatic SAR Processing. / Yew Lam Neo, Wong F.H., Cumming I.G. // IEEE Transactions on Geoscience and Remote Sensing. - 2008. - Vol. 46, No. 9. - P. 2481-2492.

J898. Collin A. Mapping the Shallow Water Seabed Habitat With the SHOALS. / Collin A., Archambault P., Long B. // IEEE Transactions on Geoscience and Remote Sensing. - 2008. - Vol. 46, No. 10. - P. 2947-2955.

J899. Jia Xu. Parametric Velocity Synthetic Aperture Radar:Signal Modeling and Optimal Methods. / Jia Xu, Gang Li, Ying-Ning Peng, Xiang-Gen Xia, Yong-Liang Wang. // IEEE Transactions on Geoscience and Remote Sensing. - 2008. - Vol. 46, No. 9. - P. 2463-2480.

J900. Del Frate F. Monitoring Urban Land Cover in Rome, Italy, and Its Changes by Single-Polarization Multitemporal SAR Images. / Del Frate F., Pacifici F., Solimini D. // IEEE Journal of Selected Topics in Applied Earth Observations and Remote Sensing. - 2008. - Vol. 1, No. 2. - P. 87-97.

J901. Rigling B.D. Urban RF multipath mitigation. IET Radar, Sonar & Navigation. - 2008. - Vol. 2, No. 6. - P. 419-425.

J902. Jaruwatanadilok S. Electromagnetic Coherent Tomography Array Imaging in Random Scattering Media. / Jaruwatanadilok S., Ishimaru A. // IEEE Antennas and Wireless Propagation Letters. - 2008. - Vol. 7, {no data available}. - P. 524-527.

J903. Brusch S. Synergetic Use of Radar and Optical Satellite Images to Support Severe Storm Prediction for Offshore Wind Farming. / Brusch S., Lehner S., Schulz-Stellenfleth J. // IEEE Journal of Selected Topics in Applied Earth Observations and Remote Sensing. - 2008. - Vol. 1, No. 1. - P. 57-66.

J904. Beaucage P. Regional Mapping of the Offshore Wind Resource: Towards a Significant Contribution From Space-Borne Synthetic Aperture Radars. / Beaucage P., Bernier M., Lafrance G., Choisnard J. // IEEE Journal of Selected Topics in Applied Earth Observations and Remote Sensing. - 2008. - Vol. 1, No. 1. - P. 48-56.

J905. Frehlich R. Measurements of Wind and Turbulence Profiles With Scanning Doppler Lidar for Wind Energy Applications. / Frehlich R., Kelley N. // IEEE Journal of Selected Topics in Applied Earth Observations

and Remote Sensing. - 2008. - Vol. 1, No. 1. - P. 42-47.

J906. del Rio V.S. Reply to “Comments on `Statistics of the Degree of Polarization'”. / del Rio V.S., Mosquera J.M.P., Isasa M.V., de Lorenzo M.E. // IEEE Transactions on Antennas and Propagation. - 2008. - Vol. 56, No. 9. - P. 3086.

J907. Stasolla M. Spatial Indexes for the Extraction of Formal and Informal Human Settlements From High-Resolution SAR Images. / Stasolla M., Gamba P. // IEEE Journal of Selected Topics in Applied Earth Observations and Remote Sensing. - 2008. - Vol. 1, No. 2. - P. 98-106.

J908. Guccione P. Beam Sharpening of Delay/Doppler Altimeter Data Through Chirp Zeta Transform. IEEE Transactions on Geoscience and Remote Sensing. - 2008. - Vol. 46, No. 9. - P. 2517-2526.

J909. Hefner E. Whitening Dual-Polarized Weather Radar Signals With a Hermitian Transformation. / Hefner E., Chandrasekar V. // IEEE Transactions on Geoscience and Remote Sensing. - 2008. - Vol. 46, No. 8. - P. 2357-2364.

J910. Borgioli G. The Detection of Buried Pipes From Time-of-Flight Radar Data. / Borgioli G., Capineri L., Falorni P.L., Matucci S., Windsor C.G. // IEEE Transactions on Geoscience and Remote Sensing. - 2008. - Vol. 46, No. 8. - P. 2254-2266.

J911. Joseph A.T. Soil Moisture Retrieval During a Corn Growth Cycle Using L-Band (1.6 GHz) Radar Observations. / Joseph A.T., van der Velde R., O'Neill P.E., Lang R.H., Gish T. // IEEE Transactions on Geoscience and Remote Sensing. - 2008. - Vol. 46, No. 8. - P. 2365-2374.

J912. Feng Xu. Imaging Simulation of Bistatic Synthetic Aperture Radar and Its Polarimetric Analysis. / Feng Xu, Ya-Qiu Jin. // IEEE Transactions on Geoscience and Remote Sensing. - 2008. - Vol. 46, No. 8. - P. 2233-2248.

J913. Branch R. Relating Microwave Modulation to Microbreaking Observed in Infrared Imagery. / Branch R., Plant W.J., Gade M., Jessup A.T. // IEEE Geoscience and Remote Sensing Letters. - 2008. - Vol. 5, No. 3. - P. 364-367.

J914. Schneider S.W. AMTA Corner. / Schneider S.W., Kemp J. // IEEE Antennas and Propagation Magazine. - 2008. - Vol. 50, No. 2. - P. 210-211.

J915. Schuhmacher D. A Consistent Metric for Performance Evaluation of Multi-Object Filters. / Schuhmacher D., Vo B.-T., Vo B.-N. // IEEE Transactions on Signal Processing. - 2008. - Vol. 56, No. 8. - P. 3447-3457.

J916. Jangal F. Wavelet Contribution to Remote Sensing of the Sea and Target Detection for a High-Frequency Surface Wave Radar. / Jangal F., Saillant S., Helier M. // IEEE Geoscience and Remote Sensing Letters. - 2008. - Vol. 5, No. 3. - P. 552-556.

J917. Bera R. Sikkim's Teesta River fog, mist and dust particle monitoring using monostatic LiDAR. / Bera R., Paul B.D., Sinha N.B., Guchhait A., Maity G. // IEEE Aerospace and Electronic Systems Magazine. - 2008. - Vol. 23, No. 7. - P. 25-27.

J918. Wong F.H. Focusing Bistatic SAR Data Using the Nonlinear Chirp Scaling Algorithm. / Wong F.H., Cumming I.G., Yew Lam Neo. // IEEE Transactions on Geoscience and Remote Sensing. - 2008. - Vol. 46, No. 9. - P. 2493-2505.

J919. Bianchi T. Segmentation-Based MAP Despeckling of SAR Images in the Undecimated Wavelet Domain. / Bianchi T., Argenti F., Alparone L. // IEEE Transactions on Geoscience and Remote Sensing. - 2008. - Vol. 46, No. 9. - P. 2728-2742.

J920. Morio J. Information Theory-Based Approach for Contrast Analysis in Polarimetric and/or Interferometric SAR Images. / Morio J., Refregier P., Goudail F., Dubois-Fernandez P.C., Dupuis X. // IEEE Transactions on Geoscience and Remote Sensing. - 2008. - Vol. 46, No. 8. - P. 2185-2196.

J921. Zhong Lu. Radarsat-1 and ERS InSAR Analysis Over Southeastern Coastal Louisiana: Implications for Mapping Water-Level Changes Beneath Swamp Forests. / Zhong Lu, Oh-ig Kwoun. // IEEE Transactions on Geoscience and Remote Sensing. - 2008. - Vol. 46, No. 8. - P. 2167-2184.

J922. Lindgren T. A Multistatic GNSS Synthetic Aperture Radar for Surface Characterization. / Lindgren T., Akos D.M. // IEEE Transactions on Geoscience and Remote Sensing. - 2008. - Vol. 46, No. 8. - P. 2249-2253.

J923. Marquart N.P. A Refined GTD Ray System for an Embedded Object and Its Polarimetric Behavior. / Marquart N.P., Molinet F., Pottier E. // IEEE Transactions on Geoscience and Remote Sensing. - 2008. - Vol. 46, No. 9. - P. 2538-2546.

J924. Wenbo Sun. Side-Face Effect of a Dielectric Strip on Its Optical Properties. / Wenbo Sun, Bing Lin, Yongxiang Hu, Zhenhui Wang, Yunfei Fu, Qian Feng, Ping Yang. // IEEE Transactions on Geoscience and Remote Sensing. - 2008. - Vol. 46, No. 8. - P. 2337-2344.

J925. Filali B. Design and Calibration of a Large Open-Ended Coaxial Probe for the Measurement of the Dielectric Properties of Concrete. / Filali B., Boone F., Rhazi J., Ballivy G. // IEEE Transactions on Microwave Theory and Techniques. - 2008. - Vol. 56, No. 10. - P. 2322-2328.

J926. Montopoli M. Statistical Characterization and Modeling of Raindrop Spectra Time Series for Different Climatological Regions. / Montopoli M., Marzano F.S., Vulpiani G., Anagnostou M.N., Anagnostou E.N. // IEEE Transactions on Geoscience and Remote Sensing. - 2008. - Vol. 46, No. 10. - P. 2778-2787.

J927. Williams B.A. Estimation of Hurricane Winds From SeaWinds at Ultrahigh Resolution. / Williams B.A., Long D.G. // IEEE Transactions on Geoscience and Remote Sensing. - 2008. - Vol. 46, No. 10. - P. 2924-2935.

J928. Paloscia S. A Comparison of Algorithms for Retrieving Soil Moisture from ENVISAT/ASAR Images. / Paloscia S., Pampaloni P., Pettinato S., Santi E. // IEEE Transactions on Geoscience and Remote Sensing. - 2008. - Vol. 46, No. 10. - P. 3274-3284.

J929. Jiang Xiao. Additional Corrections to “Unconstrained Inversion of Waveheight Spectra From SAR Image” [Feb 02 261-270]. / Jiang Xiao, Minhui Zhu, Xiaoqing Wang, Yongqiang Chen. // IEEE Transactions on Geoscience and Remote Sensing. - 2008. - Vol. 46, No. 10. - P. 3359.

J930. Jong-Sen Lee. Evaluation and Bias Removal of Multilook Effect on Entropy/Alpha/Anisotropy in Polarimetric SAR Decomposition. / Jong-Sen Lee, Ainsworth T.L., Kelly J.P., Lopez-Martinez C. // IEEE Transactions on Geoscience and Remote Sensing. - 2008. - Vol. 46, No. 10. - P. 3039-3052.

J931. Kaab A. Glacier Volume Changes Using ASTER Satellite Stereo and ICESat GLAS Laser Altimetry. A Test Study on EdgeШуа, Eastern Svalbard. IEEE Transactions on Geoscience and Remote Sensing. - 2008. - Vol. 46, No. 10. - P. 2823-2830.

J932. Meyer F.J. Prediction, Detection, and Correction of Faraday Rotation in Full-Polarimetric L-Band SAR Data. / Meyer F.J., Nicoll J.B. // IEEE Transactions on Geoscience and Remote Sensing. - 2008. - Vol. 46, No. 10. - P. 3076-3086.

J933. Marchan-Hernandez J.F. Correction of the Sea State Impact in the L-Band Brightness Temperature by Means of Delay-Doppler Maps of Global Navigation Satellite Signals Reflected Over the Sea Surface. / Marchan-Hernandez J.F., Rodriguez-Alvarez N., Camps A., Bosch-Lluis X., Ramos-Perez I., Valencia E. // IEEE Transactions on Geoscience and Remote Sensing. - 2008. - Vol. 46, No. 10. - P. 2914-2923.

J934. Pierdicca N. Radar Bistatic Configurations for Soil Moisture Retrieval: A Simulation Study. / Pierdicca N., Pulvirenti L., Ticconi F., Brogioni M. // IEEE Transactions on Geoscience and Remote Sensing. - 2008. - Vol. 46, No. 10. - P. 3252-3264.

J935. Freitas C. Land Use and Land Cover Mapping in the Brazilian Amazon Using Polarimetric Airborne P-Band SAR Data. / Freitas C., Soler L., Sant'Anna S.J.S., Dutra L.V., dos Santos J.R., Mura J.C., Correia A.H. // IEEE Transactions on Geoscience and Remote Sensing. - 2008. - Vol. 46, No. 10. - P. 2956-2970.

J936. Solimene R. Imaging Small PEC Spheres by a Linear Approach. / Solimene R., Buonanno A., Pierri R. // IEEE Transactions on Geoscience and Remote Sensing. - 2008. - Vol. 46, No. 10. - P. 3010-3018.

J937. Savtchenko A. A-Train Data Depot: Bringing Atmospheric Measurements Together. / Savtchenko A., Kummerer R., Smith P., Gopalan A., Kempler S., Leptoukh G. // IEEE Transactions on Geoscience and Remote Sensing. - 2008. - Vol. 46, No. 10. - P. 2788-2795.

J938. Soldovieri F. A Kirchhoff-Based Shape Reconstruction Algorithm for the Multimonostatic Configuration: The Realistic Case of Buried Pipes. / Soldovieri F., Brancaccio A., Prisco G., Leone G., Pierri R. // IEEE Transactions on Geoscience and Remote Sensing. - 2008. - Vol. 46, No. 10. - P. 3031-3038.

J939. Jinzheng Peng. Calibration Method for Fully Polarimetric Microwave Radiometers Using the Correlated Noise Calibration Standard. / Jinzheng Peng, Ruf C.S. // IEEE Transactions on Geoscience and Remote Sensing. - 2008. - Vol. 46, No. 10. - P. 3087-3097.

J940. Xiaolan Qiu. An Improved NLCS Algorithm With Capability Analysis for One-Stationary BiSAR. / Xiaolan Qiu, Donghui Hu, Chibiao Ding. // IEEE Transactions on Geoscience and Remote Sensing. - 2008. - Vol. 46, No. 10. - P. 3179-3186.

J941. Weissman D.E. Measurements of the Effect of Rain-Induced Sea Surface Roughness on the QuikSCAT Scatterometer Radar Cross Section. / Weissman D.E., Bourassa M.A. // IEEE Transactions on Geoscience and Remote Sensing. - 2008. - Vol. 46, No. 10. - P. 2882-2894.

J942. Saqellari-Likoka A. An Approach for Solving Rank-Deficient Systems That Enable Atmospheric Path Delay and Water Vapor Content Estimation. / Saqellari-Likoka A., Karathanassi V. // IEEE Transactions on Geoscience and Remote Sensing. - 2008. - Vol. 46, No. 10. - P. 3187-3195.

J943. Shi Jun. Principle and Methods on Bistatic SAR Signal Processing via Time Correlation. / Shi Jun, Xiaoling Zhang, Jianyu Yang. // IEEE Transactions on Geoscience and Remote Sensing. - 2008. - Vol. 46, No. 10. - P. 3163-3178.

J944. Anagnostou M.N. Evaluation of Underwater Rainfall Measurements During the Ionian Sea Rainfall Experiment. / Anagnostou M.N., Nystuen J.A., Anagnostou E.N., Nikolopoulos E.I., Amitai E. // IEEE Transactions on Geoscience and Remote Sensing. - 2008. - Vol. 46, No. 10. - P. 2936-2946.

J945. Soergel U. Feature Extraction and Visualization of Bridges Over Water From High-Resolution InSAR Data and One Orthophoto. / Soergel U., Cadario E., Thiele A., Thoennessen U. // IEEE Journal of Selected Topics in Applied Earth Observations and Remote Sensing. - 2008. - Vol. 1, No. 2. - P. 147-153.

J946. Berizzi F. A Contrast-Based Algorithm For Synthetic Range-Profile Motion Compensation. / Berizzi F., Martorella M., Cacciamano A., Capria A. // IEEE Transactions on Geoscience and Remote Sensing. - 2008. - Vol. 46, No. 10. - P. 3053-3062.

J947. Anagnostou M.N. Evaluation of X-Band Polarimetric-Radar Estimates of Drop-Size Distributions From Coincident S-Band Polarimetric Estimates and Measured Raindrop Spectra. / Anagnostou M.N., Anagnostou E.N., Vulpiani G., Montopoli M., Marzano F.S., Vivekanandan J. // IEEE Transactions on Geoscience and Remote Sensing. - 2008. - Vol. 46, No. 10. - P. 3067-3075.

J948. Zecchetto S. A Wavelet-Based Technique for Sea Wind Extraction from SAR Images. / Zecchetto S., De Biasio F. // IEEE Transactions on Geoscience and Remote Sensing. - 2008. - Vol. 46, No. 10. - P. 2983-2989.

J949. Flampouris S. Accuracy of Bathymetric Assessment by Locally Analyzing Radar Ocean Wave Imagery (February 2008). / Flampouris S., Ziemer F., Seemann J. // IEEE Transactions on Geoscience and Remote Sensing. - 2008. - Vol. 46, No. 10. - P. 2906-2913.

J950. Guida R. Model-Based Interpretation of High-Resolution SAR Images of Buildings. / Guida R., Iodice A., Riccio D., Stilla U. // IEEE Journal of Selected Topics in Applied Earth Observations and Remote Sensing. - 2008. - Vol. 1, No. 2. - P. 107-119.

J951. Hasager C.B. Remote Sensing Observation Used in Offshore Wind Energy. / Hasager C.B., Pena A., Christiansen M.B., Astrup P., Nielsen M., Monaldo F., Thompson D., Nielsen P. // IEEE Journal of Selected Topics in Applied Earth Observations and Remote Sensing. - 2008. - Vol. 1, No. 1. - P. 67-79.

J952. Doulgeris A.P. Classification With a Non-Gaussian Model for PolSAR Data. / Doulgeris A.P., Anfinsen S.N., Eltoft T. // IEEE Transactions on Geoscience and Remote Sensing. - 2008. - Vol. 46, No. 10. - P. 2999-3009.

J953. Dinnat E.P. Impact of Sun Glint on Salinity Remote Sensing: An Example With the Aquarius Radiometer.

/ Dinnat E.P., Le Vine D.M. // IEEE Transactions on Geoscience and Remote Sensing. - 2008. - Vol. 46, No. 10. - P. 3137-3150.

J954. Dubois-Fernandez P.C. The Compact Polarimetry Alternative for Spaceborne SAR at Low Frequency. / Dubois-Fernandez P.C., Souyris J.-C., Angelliaume S., Garestier F. // IEEE Transactions on Geoscience and Remote Sensing. - 2008. - Vol. 46, No. 10. - P. 3208-3222.

J955. Galletti M. Measurement and Characterization of Entropy and Degree of Polarization of Weather Radar Targets. / Galletti M., Bebbington D.H.O., Chandra M., Borner T. // IEEE Transactions on Geoscience and Remote Sensing. - 2008. - Vol. 46, No. 10. - P. 3196-3207.

J956. Brenner A.R. Radar Imaging of Urban Areas by Means of Very High-Resolution SAR and Interferometric SAR. / Brenner A.R., Roessing L. // IEEE Transactions on Geoscience and Remote Sensing. - 2008. - Vol. 46, No. 10. - P. 2971-2982.

J957. Cerutti-Maori D. Wide-Area Traffic Monitoring With the SAR/GMTI System PAMIR. / Cerutti-Maori D., Klare J., Brenner A.R., Ender J.H.G. // IEEE Transactions on Geoscience and Remote Sensing. - 2008. - Vol. 46, No. 10. - P. 3019-3030.

J958. de Macedo K.A.C. An Autofocus Approach for Residual Motion Errors With Application to Airborne Repeat-Pass SAR Interferometry. / de Macedo K.A.C., Scheiber R., Moreira A. // IEEE Transactions on Geoscience and Remote Sensing. - 2008. - Vol. 46, No. 10. - P. 3151-3162.

J959. Thirion-Lefevre L.. Investigating Attenuation, Scattering Phase Center, and Total Height Using Simulated Interferometric SAR Images of Forested Areas. / Thirion-Lefevre L.., Colin-Koeniguer E.. // IEEE Transactions on Geoscience and Remote Sensing. - 2007. - Vol. 45, No. 10. - P. 3172-3179.

J960. Yongxiang Hu. Retrieving Optical Depths and Lidar Ratios for Transparent Layers Above Opaque Water Clouds From CALIPSO Lidar Measurements. / Yongxiang Hu, Vaughan M., Zhaoyan Liu, Powell K., Rodier S. // IEEE Geoscience and Remote Sensing Letters. - 2007. - Vol. 4, No. 4. - P. 523-526.

J961. Karjalainen M. Geocoding of Synthetic Aperture Radar Images Using Digital Vector Maps. IEEE Geoscience and Remote Sensing Letters. - 2007. - Vol. 4, No. 4. - P. 616-620.

J962. Yamaki R. Singularity-Spreading Phase Unwrapping. / Yamaki R., Hirose A. // IEEE Transactions on Geoscience and Remote Sensing. - 2007. - Vol. 45, No. 10. - P. 3240-3251.

J963. D'Aria D. High-Resolution Spaceborne SAR Focusing by SVD-Stolt. / D'Aria D., Guarnieri A.M. // IEEE Geoscience and Remote Sensing Letters. - 2007. - Vol. 4, No. 4. - P. 639-643.

J964. Anagnostou M.N. Comparison of Raindrop Size Distribution Estimates From X-Band and S-Band Polarimetric Observations. / Anagnostou M.N., Anagnostou E.N., Vivekanandan J., Ogden F.L. // IEEE Geoscience and Remote Sensing Letters. - 2007. - Vol. 4, No. 4. - P. 601-605.

J965. Wilheit T.T. Impact of Uncertainty in the Drop Size Distribution on Oceanic Rainfall Retrievals From Passive Microwave Observations. / Wilheit T.T., Chandrasekar V., Wanyu Li. // IEEE Transactions on Geoscience and Remote Sensing. - 2007. - Vol. 45, No. 10. - P. 3160-3164.

J966. Frezza F. Short-Pulse Electromagnetic Scattering by Buried Perfectly Conducting Cylinders. / Frezza F., Martinelli P., Pajewski L., Schettini G. // IEEE Geoscience and Remote Sensing Letters. - 2007. - Vol. 4, No. 4. - P. 611-615.

J967. Kersten P.R. Motion Analysis in SAR Images of Unfocused Objects Using Time-Frequency Methods. / Kersten P.R., Jansen R.W., Luc K., Ainsworth T.L. // IEEE Geoscience and Remote Sensing Letters. - 2007. - Vol. 4, No. 4. - P. 527-531.

J968. Richards M.A. A Beginner's Guide to Interferometric SAR Concepts and Signal Processing [AESS Tutorial IV]. IEEE Aerospace and Electronic Systems Magazine. - 2007. - Vol. 22, No. 9. - P. 5-29.

J969. Gui-Song Xia. A Rapid and Automatic MRF-Based Clustering Method for SAR Images. / Gui-Song Xia, Chu He, Hong Sun. // IEEE Geoscience and Remote Sensing Letters. - 2007. - Vol. 4, No. 4. - P. 596-600.

J970. Qi Wang. Single Range Matching Filtering for Space Debris Radar Imaging. / Qi Wang, Mengdao Xing, Guangyue Lu, Zheng Bao. // IEEE Geoscience and Remote Sensing Letters. - 2007. - Vol. 4, No. 4. - P. 576-580.

J971. Dierking W. Sea-Ice Deformation State From Synthetic Aperture Radar Imagery-Part I: Comparison of C- and L-Band and Different Polarization. / Dierking W., Dall J. // IEEE Transactions on Geoscience and Remote Sensing. - 2007. - Vol. 45, No. 11. - P. 3610-3622.

J972. Santalla del Rio V. Least Squares Estimation of Doppler and Polarimetric Parameters for Weather Targets. IEEE Transactions on Geoscience and Remote Sensing. - 2007. - Vol. 45, No. 11. - P. 3760-3772.

J973. Kovalenko V. A Novel Clutter Suppression Algorithm for Landmine Detection With GPR. / Kovalenko V., Yarovoy A.G., Ligthart L.P. // IEEE Transactions on Geoscience and Remote Sensing. - 2007. - Vol. 45, No. 11. - P. 3740-3751.

J974. Venkatasubramanian V. An Interacting Multiple-Model-Based Abrupt Change Detector for Ground-Penetrating Radar. / Venkatasubramanian V., Leung H., Moorman B. // IEEE Geoscience and Remote Sensing Letters. - 2007. - Vol. 4, No. 4. - P. 634-638.

J975. Palubinskas G. Radar Signatures of a Passenger Car. / Palubinskas G., Runge H. // IEEE Geoscience and Remote Sensing Letters. - 2007. - Vol. 4, No. 4. - P. 644-648.

J976. Noferini L. DEM by Ground-Based SAR Interferometry. / Noferini L., Pieraccini M., Mecatti D., Macaluso G., Luzi G., Atzeni C. // IEEE Geoscience and Remote Sensing Letters. - 2007. - Vol. 4, No. 4. - P. 659-663.

J977. Heng-Chao Li. Texture-Preserving Despeckling of SAR Images Using Evidence Framework. / Heng-Chao Li, Wen Hong, Yi-Rong Wu, Heng-Ming Tai. // IEEE Geoscience and Remote Sensing Letters. - 2007. - Vol. 4, No. 4. - P. 537-541.

J978. Ngan Tran. Effect of Long Waves on Ku-Band Ocean Radar Backscatter at Low Incidence Angles Using TRMM and Altimeter Data. / Ngan Tran, Chapron B., Vandemark D. // IEEE Geoscience and Remote Sensing Letters. - 2007. - Vol. 4, No. 4. - P. 542-546.

J979. Suksmono A.B. Signal Representation and the Nonlinear Property of Phase Images. IEEE Geoscience and Remote Sensing Letters. - 2007. - Vol. 4, No. 4. - P. 606-610.

J980. Smith-Jonforsen G. Effects of Forest Biomass and Stand Consolidation on P-Band Backscatter. / Smith-Jonforsen G., Folkesson K., Hallberg B., Ulander L.M.H. // IEEE Geoscience and Remote Sensing Letters. - 2007. - Vol. 4, No. 4. - P. 669-673.

J981. Soisuvarn S.. An Ocean Surface Wind Vector Model Function for a Spaceborne Microwave Radiometer. / Soisuvarn S.., Jelenak Z.., Jones W.L. // IEEE Transactions on Geoscience and Remote Sensing. - 2007. - Vol. 45, No. 10. - P. 3119-3130.

J982. Berry P.A.M. Global Analysis of Envisat RA-2 Burst Mode Echo Sequences. / Berry P.A.M., Freeman J.A., Rogers C., Benveniste J. // IEEE Transactions on Geoscience and Remote Sensing. - 2007. - Vol. 45, No. 9. - P. 2869-2874.

J983. Barnes C.F. Image-Driven Data Mining for Image Content Segmentation, Classification, and Attribution. IEEE Transactions on Geoscience and Remote Sensing. - 2007. - Vol. 45, No. 9. - P. 2964-2978.

J984. Addesso P. Correlation Properties of Signals Backscattered From Fractal Profiles. / Addesso P., Marano S., Restaino R., Tesauro M. // IEEE Transactions on Geoscience and Remote Sensing. - 2007. - Vol. 45, No. 9. - P. 2859-2868.

J985. Jun-Yi Koay. Paddy Fields as Electrically Dense Media: Theoretical Modeling and Measurement Comparisons. / Jun-Yi Koay, Chue-Poh Tan, Ka-Sing Lim, Saiful Bahari bin Abu Bakar, Hong-Tat Ewe, Hean-Teik Chuah, Jin-Au Kong. // IEEE Transactions on Geoscience and Remote Sensing. - 2007. - Vol. 45, No. 9. - P. 2837-2849.

J986. Kanagaratnam P. Ultrawideband Radar Measurements of Thickness of Snow Over Sea Ice. / Kanagaratnam P., Markus T.., Lytle V.., Heavey B.., Jansen P.., Prescott G.., Gogineni S.P. // IEEE Transactions

on Geoscience and Remote Sensing. - 2007. - Vol. 45, No. 9. - P. 2715-2724.

J987. Ernst J.R. Full-Waveform Inversion of Crosshole Radar Data Based on 2-D Finite-Difference Time-Domain Solutions of Maxwell's Equations. / Ernst J.R., Maurer H.., Green A.G., Holliger K.. // IEEE Transactions on Geoscience and Remote Sensing. - 2007. - Vol. 45, No. 9. - P. 2807-2828.

J988. He Zhan. Scale Model Experimental Validation and Calibration of the Half-Space Green's Function Born Approximation Model Applied to Cross-Well Radar Sensing. / He Zhan, Farid A.M., Alshawabkeh A.N., Raemer H.R., Rappaport C.M. // IEEE Transactions on Geoscience and Remote Sensing. - 2007. - Vol. 45, No. 8. - P. 2423-2428.

J989. Wilson J.N. A Large-Scale Systematic Evaluation of Algorithms Using Ground-Penetrating Radar for Landmine Detection and Discrimination. / Wilson J.N., Gader P., Wen-Hsiung Lee, Frigui H., Ho K.C. // IEEE Transactions on Geoscience and Remote Sensing. - 2007. - Vol. 45, No. 8. - P. 2560-2572.

J990. van der Kruk J. Fundamental and Higher Mode Inversion of Dispersed GPR Waves Propagating in an Ice Layer. / van der Kruk J., Arcone S.A., Lanbo Liu. // IEEE Transactions on Geoscience and Remote Sensing. - 2007. - Vol. 45, No. 8. - P. 2483-2491.

J991. {no data available}. Instructions for AP-S and URSI Authors. IEEE Antennas and Propagation Magazine. - 2007. - Vol. 49, No. 3. - P. 11.

J992. Le Caillec J.-M. SAR Remote Sensing Analysis of the Sea Surface by Polynomial Filtering [Applications Corner]. IEEE Signal Processing Magazine. - 2007. - Vol. 24, No. 4. - P. 105-107.

J993. Palacin J. Real-Time Tree-Foliage Surface Estimation Using a Ground Laser Scanner. / Palacin J., Palleja T., Tresanchez M., Sanz R., Llorens J., Ribes-Dasi M., Masip J., Arno J., Escola A., Rosell J. R. // IEEE Transactions on Instrumentation and Measurement. - 2007. - Vol. 56, No. 4. - P. 1377-1383.

J994. Jacobson N.P. Linear Fusion of Image Sets for Display. / Jacobson N.P., Gupta M.R., Cole J.B. // IEEE Transactions on Geoscience and Remote Sensing. - 2007. - Vol. 45, No. 10. - P. 3277-3288.

J995. Haarpaintner J. Use of Enhanced-Resolution QuikSCAT/SeaWinds Data for Operational Ice Services and Climate Research: Sea Ice Edge, Type, Concentration, and Drift. / Haarpaintner J., Spreen G. // IEEE Transactions on Geoscience and Remote Sensing. - 2007. - Vol. 45, No. 10. - P. 3131-3137.

J996. Frery A.C. Classifying Multifrequency Fully Polarimetric Imagery With Multiple Sources of Statistical Evidence and Contextual Information. / Frery A.C., Correia A.H., da Freitas C.d. // IEEE Transactions on Geoscience and Remote Sensing. - 2007. - Vol. 45, No. 10. - P. 3098-3109.

J997. Sakamoto T. SEABED Algorithm and Comments on “Modeling and Migration of 2-D Georadar Data: A Stationary Phase Approach”. / Sakamoto T., Kidera S., Sato T. // IEEE Transactions on Geoscience and Remote Sensing. - 2007. - Vol. 45, No. 10. - P. 3300.

J998. Rocca F. Modeling Interferogram Stacks. IEEE Transactions on Geoscience and Remote Sensing. - 2007. - Vol. 45, No. 10. - P. 3289-3299.

J999. Notarnicola C. Inferring Vegetation Water Content From C- and L-Band SAR Images. / Notarnicola C., Posa F. // IEEE Transactions on Geoscience and Remote Sensing. - 2007. - Vol. 45, No. 10. - P. 3165-3171.

J1000. Peters M.E. Along-Track Focusing of Airborne Radar Sounding Data From West Antarctica for Improving Basal Reflection Analysis and Layer Detection. / Peters M.E., Blankenship D.D., Carter S.P., Kempf S.D., Young D.A., Holt J.W. // IEEE Transactions on Geoscience and Remote Sensing. - 2007. - Vol. 45, No. 9. - P. 2725-2736.

J1001. Martinez-Lozano J.A. Atmospheric Components Determination From Ground-Level Measurements During the Spectra Barax Campaigns (SPARC) Field Campaigns. / Martinez-Lozano J.A., Estelles V., Molero F., Gomez-Amo J.L., Utrillas M.P., Pujadas M., Fortea J.C., Guanter L. // IEEE Transactions on Geoscience and Remote Sensing. - 2007. - Vol. 45, No. 9. - P. 2778-2793.

J1002. Le Vine D.M. The Influence of Antenna Pattern on Faraday Rotation in Remote Sensing at L-Band. / Le Vine D.M., Jacob S.D., Dinnat E.P., de Matthaeis P., Abraham S. // IEEE Transactions on Geoscience and

Remote Sensing. - 2007. - Vol. 45, No. 9. - P. 2737-2746.

J1003. Ferraro P.B. A System for the Measurement of the Amazon. / Ferraro P.B., Bauersachs M., Burns J., Bataller G. // IEEE Aerospace and Electronic Systems Magazine. - 2007. - Vol. 22, No. 8. - P. 9-19.

J1004. Wenqin Wang. Approach of Adaptive Synchronization for Bistatic SAR Real-Time Imaging. IEEE Transactions on Geoscience and Remote Sensing. - 2007. - Vol. 45, No. 9. - P. 2695-2700.

J1005. Souyris J.-C. Polarimetric Analysis of Bistatic SAR Images From Polar Decomposition: A Quaternion Approach. / Souyris J.-C., Tison C. // IEEE Transactions on Geoscience and Remote Sensing. - 2007. - Vol. 45, No. 9. - P. 2701-2714.

J1006. Le Vine D.M. Initial Images of the Synthetic Aperture Radiometer 2D-STAR. / Le Vine D.M., Jackson T.J., Haken M. // IEEE Transactions on Geoscience and Remote Sensing. - 2007. - Vol. 45, No. 11. - P. 3623-3632.

J1007. Mason D.C. Improving River Flood Extent Delineation From Synthetic Aperture Radar Using Airborne Laser Altimetry. / Mason D.C., Horritt M.S., Dall'Amico J.T., Scott T.R., Bates P.D. // IEEE Transactions on Geoscience and Remote Sensing. - 2007. - Vol. 45, No. 12. - P. 3932-3943.

J1008. Clausi D. A. Foreword to the Special Issue on Pattern Recognition in Remote Sensing. / Clausi D. A., Aksoy S., Tilton J. C. // IEEE Transactions on Geoscience and Remote Sensing. - 2007. - Vol. 45, No. 12. - P. 3855-3856.

J1009. D'Hondt O. Spatially Nonstationary Anisotropic Texture Analysis in SAR Images. / D'Hondt O., Lopez-Martinez C., Ferro-Famil L., Pottier E. // IEEE Transactions on Geoscience and Remote Sensing. - 2007. - Vol. 45, No. 12. - P. 3905-3918.

J1010. Ping Zhong. A Multiple Conditional Random Fields Ensemble Model for Urban Area Detection in Remote Sensing Optical Images. / Ping Zhong, Runsheng Wang. // IEEE Transactions on Geoscience and Remote Sensing. - 2007. - Vol. 45, No. 12. - P. 3978-3988.

J1011. Qiyao Yu. SAR Sea-Ice Image Analysis Based on Iterative Region Growing Using Semantics. / Qiyao Yu, Clausi D.A. // IEEE Transactions on Geoscience and Remote Sensing. - 2007. - Vol. 45, No. 12. - P. 3919-3931.

J1012. Palenichka R.M. Multiscale Isotropic Matched Filtering for Individual Tree Detection in LiDAR Images. / Palenichka R.M., Zaremba M.B. // IEEE Transactions on Geoscience and Remote Sensing. - 2007. - Vol. 45, No. 12. - P. 3944-3956.

J1013. Chen Liu. A New Application for PolSAR Imagery in the Field of Moving Target Indication/Ship Detection. / Chen Liu, Gierull C.H. // IEEE Transactions on Geoscience and Remote Sensing. - 2007. - Vol. 45, No. 11. - P. 3426-3436.

J1014. Krieger G. TanDEM-X: A Satellite Formation for High-Resolution SAR Interferometry. / Krieger G., Moreira A., Fiedler H., Hajnsek I., Werner M., Younis M., Zink M. // IEEE Transactions on Geoscience and Remote Sensing. - 2007. - Vol. 45, No. 11. - P. 3317-3341.

J1015. Jager M. A Self-Initializing PolInSAR Classifier Using Interferometric Phase Differences. / Jager M., Neumann M., Guillaso S., Reigber A. // IEEE Transactions on Geoscience and Remote Sensing. - 2007. - Vol. 45, No. 11. - P. 3503-3518.

J1016. Morio J. Polarimetric and Interferometric SAR Image Partition Into Statistically Homogeneous Regions Based on the Minimization of the Stochastic Complexity. / Morio J., Goudail F., Dupuis X., Dubois-Fernandez P.C., Refregier P. // IEEE Transactions on Geoscience and Remote Sensing. - 2007. - Vol. 45, No. 11. - P. 3599-3609.

J1017. Meta A. Signal Processing for FMCW SAR. / Meta A., Hoogeboom P., Ligthart L.P. // IEEE Transactions on Geoscience and Remote Sensing. - 2007. - Vol. 45, No. 11. - P. 3519-3532.

J1018. Marzano F.S. Supervised Fuzzy-Logic Classification of Hydrometeors Using C-Band Weather Radars. / Marzano F.S., Scaranari D., Vulpiani G. // IEEE Transactions on Geoscience and Remote Sensing. - 2007. - Vol.

45, No. 11. - P. 3784-3799.

J1019. Martini A. Percolation-Based Models for Ray-Optical Propagation in Stochastic Distributions of Scatterers With Random Shape. / Martini A., Caramanica F., Franceschetti M., Massa A. // IEEE Antennas and Wireless Propagation Letters. - 2007. - Vol. 6, {no data available}. - P. 639-642.

J1020. {no data available}. Instructions for AP-S and URSI Authors. IEEE Antennas and Propagation Magazine. - 2007. - Vol. 49, No. 4. - P. 11.

J1021. Pastina D. Effect of Apodization on SAR Image Understanding. / Pastina D., Colone F., Lombardo P. // IEEE Transactions on Geoscience and Remote Sensing. - 2007. - Vol. 45, No. 11. - P. 3533-3551.

J1022. Migliaccio M. A Physically Consistent Speckle Model for Marine SLC SAR Images. / Migliaccio M., Ferrara G., Gambardella A., Nunziata F., Sorrentino A. // IEEE Journal of Oceanic Engineering. - 2007. - Vol. 32, No. 4. - P. 839-847.

J1023. Vanjari S.V. Remote data sensing using SAR and harmonic reradiators. / Vanjari S.V., Krogmeier J.V., Bell M.R. // IEEE Transactions on Aerospace and Electronic Systems. - 2007. - Vol. 43, No. 4. - P. 1426-1440.

J1024. Baker C.J. Editorial Electro-Magnetic Remote Sensing Defence Technology Centre (EMRS-DTC). / Baker C.J., Mulgrew B. // IET Radar, Sonar & Navigation. - 2007. - Vol. 1, No. 6. - P. 397.

J1025. Tian Jin. Refraction and Dispersion Effects Compensation for UWB SAR Subsurface Object Imaging. / Tian Jin, Zhimin Zhou. // IEEE Transactions on Geoscience and Remote Sensing. - 2007. - Vol. 45, No. 12. - P. 4059-4066.

J1026. Gleich D. Wavelet-Based Despeckling of SAR Images Using Gauss-Markov Random Fields. / Gleich D., Datcu M. // IEEE Transactions on Geoscience and Remote Sensing. - 2007. - Vol. 45, No. 12. - P. 4127-4143.

J1027. Campbell B.A. Focused 70-cm Wavelength Radar Mapping of the Moon. / Campbell B.A., Campbell D.B., Margot J.L., Ghent R.R., Nolan M., Chandler J., Carter L.M., Stacy N.J.S. // IEEE Transactions on Geoscience and Remote Sensing. - 2007. - Vol. 45, No. 12. - P. 4032-4042.

J1028. Shih-Hsun Hsu. An Offset Linear-Array-Fed Ku /Ka Dual-Band Reflectarray for Planet Cloud/Precipitation Radar. / Shih-Hsun Hsu, Chulmin Han, Huang J., Kai Chang. // IEEE Transactions on Antennas and Propagation. - 2007. - Vol. 55, No. 11. - P. 3114-3122.

J1029. Romeiser R. Current Measurements in Rivers by Spaceborne Along-Track InSAR. / Romeiser R., Runge H., Suchandt S., Sprenger J., Weilbeer H., Sohrmann A., Stammer D. // IEEE Transactions on Geoscience and Remote Sensing. - 2007. - Vol. 45, No. 12. - P. 4019-4031.

J1030. Perissin D. Urban-Target Recognition by Means of Repeated Spaceborne SAR Images. / Perissin D., Ferretti A. // IEEE Transactions on Geoscience and Remote Sensing. - 2007. - Vol. 45, No. 12. - P. 4043-4058.

J1031. Iribe K. Analysis of Polarization Orientation Angle Shifts by Artificial Structures. / Iribe K., Sato M. // IEEE Transactions on Geoscience and Remote Sensing. - 2007. - Vol. 45, No. 11. - P. 3417-3425.

J1032. Martorella M. Statistical CLEAN Technique for ISAR Imaging. / Martorella M., Acito N., Berizzi F. // IEEE Transactions on Geoscience and Remote Sensing. - 2007. - Vol. 45, No. 11. - P. 3552-3560.

J1033. Margarit G. Single-Pass Polarimetric SAR Interferometry for Vessel Classification. / Margarit G., Mallorqui J.J., Fabregas X. // IEEE Transactions on Geoscience and Remote Sensing. - 2007. - Vol. 45, No. 11. - P. 3494-3502.

J1034. Arnold-Bos A. Bistatic Radar Imaging of the Marine Environment-Part I: Theoretical Background. / Arnold-Bos A., Khenchaf A., Martin A. // IEEE Transactions on Geoscience and Remote Sensing. - 2007. - Vol. 45, No. 11. - P. 3372-3383.

J1035. Arnold-Bos A. Bistatic Radar Imaging of the Marine Environment-Part II: Simulation and Results Analysis. / Arnold-Bos A., Khenchaf A., Martin A. // IEEE Transactions on Geoscience and Remote Sensing. -

2007. - Vol. 45, No. 11. - P. 3384-3396.

J1036. Waske B. Fusion of Support Vector Machines for Classification of Multisensor Data. / Waske B., Benediktsson J.A. // IEEE Transactions on Geoscience and Remote Sensing. - 2007. - Vol. 45, No. 12. - P. 3858-3866.

J1037. Thiele A. Building Recognition From Multi-Aspect High-Resolution InSAR Data in Urban Areas. / Thiele A., Cadario E., Schulz K., Thonnessen U., Soergel U. // IEEE Transactions on Geoscience and Remote Sensing. - 2007. - Vol. 45, No. 11. - P. 3583-3593.

J1038. Geldsetzer T. Surface-Based Polarimetric C-Band Scatterometer for Field Measurements of Sea Ice. / Geldsetzer T., Mead J.B., Yackel J.J., Scharien R.K., Howell S.E.L. // IEEE Transactions on Geoscience and Remote Sensing. - 2007. - Vol. 45, No. 11. - P. 3405-3416.

J1039. Tian Jin. Ultrawideband Synthetic Aperture Radar Landmine Detection. / Tian Jin, Zhimin Zhou. // IEEE Transactions on Geoscience and Remote Sensing. - 2007. - Vol. 45, No. 11. - P. 3561-3573.

J1040. De Grandi G.D. Target Detection and Texture Segmentation in Polarimetric SAR Images Using a Wavelet Frame: Theoretical Aspects. / De Grandi G.D., Jong-Sen Lee, Schuler D.L. // IEEE Transactions on Geoscience and Remote Sensing. - 2007. - Vol. 45, No. 11. - P. 3437-3453.

J1041. Bertran Ortiz A. ScanSAR-to-Stripmap Mode Interferometry Processing Using ENVISAT/ASAR Data. / Bertran Ortiz A., Zebker H. // IEEE Transactions on Geoscience and Remote Sensing. - 2007. - Vol. 45, No. 11. - P. 3468-3480.

J1042. Raney R.K. Hybrid-Polarity SAR Architecture. IEEE Transactions on Geoscience and Remote Sensing. - 2007. - Vol. 45, No. 11. - P. 3397-3404.

J1043. Bamler R. Processing of Bistatic SAR Data From Quasi-Stationary Configurations. / Bamler R., Meyer F., Liebhart W. // IEEE Transactions on Geoscience and Remote Sensing. - 2007. - Vol. 45, No. 11. - P. 3350-3358.

J1044. Atwood D.K. DEM Control in Arctic Alaska With ICESat Laser Altimetry. / Atwood D.K., Guritz R.M., Muskett R.R., Lingle C.S., Sauber J.M., Freymueller J.T. // IEEE Transactions on Geoscience and Remote Sensing. - 2007. - Vol. 45, No. 11. - P. 3710-3720.

J1045. Antoniou M. Results of a Space-Surface Bistatic SAR Image Formation Algorithm. / Antoniou M., Saini R., Cherniakov M. // IEEE Transactions on Geoscience and Remote Sensing. - 2007. - Vol. 45, No. 11. - P. 3359-3371.

J1046. Zhenhua Zhang. Focusing Parallel Bistatic SAR Data Using the Analytic Transfer Function in the Wavenumber Domain. / Zhenhua Zhang, Mengdao Xing, Jinshan Ding, Zheng Bao. // IEEE Transactions on Geoscience and Remote Sensing. - 2007. - Vol. 45, No. 11. - P. 3633-3645.

J1047. Moreira A. Foreword to the Special Issue on Synthetic Aperture Radar (SAR) Technologies and Techniques. / Moreira A., Hounam D., Wiesbeck W. // IEEE Transactions on Geoscience and Remote Sensing. - 2007. - Vol. 45, No. 11. - P. 3303-3305.

J1048. Fang Cao. An Unsupervised Segmentation With an Adaptive Number of Clusters Using the SPAN/H/α/A Space and the Complex Wishart Clustering for Fully Polarimetric SAR Data Analysis. / Fang Cao, Wen Hong, Yirong Wu, Pottier E. // IEEE Transactions on Geoscience and Remote Sensing. - 2007. - Vol. 45, No. 11. - P. 3454-3467.

J1049. Bezvesilniy O.O. Retrieving 3-D Topography by Using a Single-Antenna Squint-Mode Airborne SAR. / Bezvesilniy O.O., Dukhopelnykova I.V., Vynogradov V.V., Vavriv D.M. // IEEE Transactions on Geoscience and Remote Sensing. - 2007. - Vol. 45, No. 11. - P. 3574-3582.

J1050. Rosenqvist A. ALOS PALSAR: A Pathfinder Mission for Global-Scale Monitoring of the Environment. / Rosenqvist A., Shimada M., Ito N., Watanabe M. // IEEE Transactions on Geoscience and Remote Sensing. - 2007. - Vol. 45, No. 11. - P. 3307-3316.

J1051. Lopez-Sanchez J.M. Model Limitations and Parameter-Estimation Methods for Agricultural Applications

of Polarimetric SAR Interferometry. / Lopez-Sanchez J.M., Ballester-Berman J.D., Marquez-Moreno Y. // IEEE Transactions on Geoscience and Remote Sensing. - 2007. - Vol. 45, No. 11. - P. 3481-3493.

J1052. Nies H. Analysis and Focusing of Bistatic Airborne SAR Data. / Nies H., Loffeld O., Natroshvili K. // IEEE Transactions on Geoscience and Remote Sensing. - 2007. - Vol. 45, No. 11. - P. 3342-3349.

J1053. Makkapati V.V. Extreme Compression of Weather Radar Data. / Makkapati V.V., Mahapatra P.R. // IEEE Transactions on Geoscience and Remote Sensing. - 2007. - Vol. 45, No. 11. - P. 3773-3783.

J1054. Titin-Schnaider C. Power Optimization for Polarimetric Bistatic Random Mechanisms. IEEE Transactions on Geoscience and Remote Sensing. - 2007. - Vol. 45, No. 11. - P. 3646-3660.

J1055. Yonghong Wang. Evaluation of a New Airborne Microwave Remote Sensing Radiometer by Measuring the Salinity Gradients Across the Shelf of the Great Barrier Reef Lagoon. / Yonghong Wang, Heron M.L., Prytz A., Ridd P.V., Steinberg C.R., Hacker J.M. // IEEE Transactions on Geoscience and Remote Sensing. - 2007. - Vol. 45, No. 11. - P. 3701-3709.

J1056. Takayama T. A Novel Direction-Finding Algorithm for Directional Borehole Radar. / Takayama T., Sato M. // IEEE Transactions on Geoscience and Remote Sensing. - 2007. - Vol. 45, No. 8. - P. 2520-2528.

J1057. Hui Zhou. Reconstruction From Antenna-Transformed Radar Data Using a Time-Domain Reconstruction Method. / Hui Zhou, Motoyuki Sato, Takashi Takenaka, Guofa Li. // IEEE Transactions on Geoscience and Remote Sensing. - 2007. - Vol. 45, No. 3. - P. 689-696.

J1058. Bustos J.P. Matching radar and satellite images for ship trajectory estimation using the Hausdorff distance. / Bustos J.P., Donoso F., Guesalaga A., Torres M. // IET Radar, Sonar & Navigation. - 2007. - Vol. 1, No. 1. - P. 50-58.

J1059. David A. Yocky. Shift–Scale Complex Correlation for Wide-Angle Coherent Cross-Track SAR Stereo Processing. / David A. Yocky, Charles V. Jakowatz. // IEEE Transactions on Geoscience and Remote Sensing. - 2007. - Vol. 45, No. 3. - P. 576-583.

J1060. Anne H. S. Solberg. Oil Spill Detection in Radarsat and Envisat SAR Images. / Anne H. S. Solberg, Camilla Brekke, Per Ove Husoy. // IEEE Transactions on Geoscience and Remote Sensing. - 2007. - Vol. 45, No. 3. - P. 746-755.

J1061. Tsaipei Wang. Frequency Subband Processing and Feature Analysis of Forward-Looking Ground-Penetrating Radar Signals for Land-Mine Detection. / Tsaipei Wang, James M. Keller, Paul D. Gader, Ozy Sjahputera. // IEEE Transactions on Geoscience and Remote Sensing. - 2007. - Vol. 45, No. 3. - P. 718-729.

J1062. MacDonald A. Binary Weighted Averaging of an Ensemble of Coherently Collected Image Frames. / MacDonald A., Cain S., Oxley M. // IEEE Transactions on Image Processing. - 2007. - Vol. 16, No. 4. - P. 1085-1100.

J1063. Evans J.S. A Multiscale Curvature Algorithm for Classifying Discrete Return LiDAR in Forested Environments. / Evans J.S., Hudak A.T. // IEEE Transactions on Geoscience and Remote Sensing. - 2007. - Vol. 45, No. 4. - P. 1029-1038.

J1064. Luojus K.P. Snow-Covered Area Estimation Using Satellite Radar Wide-Swath Images. / Luojus K.P., Pulliainen J.T., Metsamaki S.J., Hallikainen M.T. // IEEE Transactions on Geoscience and Remote Sensing. - 2007. - Vol. 45, No. 4. - P. 978-989.

J1065. Dunne S.C. Impact of Multiresolution Active and Passive Microwave Measurements on Soil Moisture Estimation Using the Ensemble Kalman Smoother. / Dunne S.C., Entekhabi D., Njoku E.G. // IEEE Transactions on Geoscience and Remote Sensing. - 2007. - Vol. 45, No. 4. - P. 1016-1028.

J1066. Anterrieu E. On the Reduction of the Reconstruction Bias in Synthetic Aperture Imaging Radiometry (Corrected) . IEEE Transactions on Geoscience and Remote Sensing. - 2007. - Vol. 45, No. 4. - P. 1084-1093.

J1067. Axelsson S.R.J. Analysis of Random Step Frequency Radar and Comparison With Experiments. IEEE Transactions on Geoscience and Remote Sensing. - 2007. - Vol. 45, No. 4. - P. 890-904.

J1068. Michele D'Urso. Effective Solution of 3-D Scattering Problems via Series Expansions: Applicability and a New Hybrid Scheme. / Michele D'Urso, Ilaria Catapano, Lorenzo Crocco, Tommaso Isernia. // IEEE Transactions on Geoscience and Remote Sensing. - 2007. - Vol. 45, No. 3. - P. 639-648.

J1069. Maria S. Greco. Statistical Analysis of High-Resolution SAR Ground Clutter Data. / Maria S. Greco, Fulvio Gini. // IEEE Transactions on Geoscience and Remote Sensing. - 2007. - Vol. 45, No. 3. - P. 566-575.

J1070. Xudong Chen. Spheroidal Mode Approach for the Characterization of Metallic Objects Using Electromagnetic Induction. / Xudong Chen, Kevin O'Neill, Tomasz M. Grzegorczyk, Jin Au Kong. // IEEE Transactions on Geoscience and Remote Sensing. - 2007. - Vol. 45, No. 3. - P. 697-706.

J1071. Cong S. Iterative robust filtering for ground target tracking. / Cong S., Hong L., Layne J.R. // IET Control Theory & Applications. - 2007. - Vol. 1, No. 1. - P. 372-380.

J1072. Eric Anterrieu. On the Reduction of the Reconstruction Bias in Synthetic Aperture Imaging Radiometry. IEEE Transactions on Geoscience and Remote Sensing. - 2007. - Vol. 45, No. 3. - P. 592-601.

J1073. Zhenfang Li. A Joint Image Coregistration, Phase Noise Suppression, and Phase Unwrapping Method Based on Subspace Projection for Multibaseline InSAR Systems. / Zhenfang Li, Zheng Bao, Zhiyong Suo. // IEEE Transactions on Geoscience and Remote Sensing. - 2007. - Vol. 45, No. 3. - P. 584-591.

J1074. Maurice Ruegg. Capabilities of Dual-Frequency Millimeter Wave SAR With Monopulse Processing for Ground Moving Target Indication. / Maurice Ruegg, Erich Meier, Daniel Nuesch. // IEEE Transactions on Geoscience and Remote Sensing. - 2007. - Vol. 45, No. 3. - P. 539-553.

J1075. Rashmi Sharma. A New Technique for Forecasting Surface Wind Field From Scatterometer Observations: A Case Study for the Arabian Sea. / Rashmi Sharma, Abhijit Sarkar, Neeraj Agarwal, Raj Kumar, Sujit Basu. // IEEE Transactions on Geoscience and Remote Sensing. - 2007. - Vol. 45, No. 3. - P. 613-620.

J1076. Congling Nie. A C-Band Wind/Rain Backscatter Model. / Congling Nie, David G. Long. // IEEE Transactions on Geoscience and Remote Sensing. - 2007. - Vol. 45, No. 3. - P. 621-631.

J1077. Gang Li. Bistatic Linear Antenna Array SAR for Moving Target Detection, Location, and Imaging With Two Passive Airborne Radars. / Gang Li, Jia Xu, Ying-Ning Peng, Xiang-Gen Xia. // IEEE Transactions on Geoscience and Remote Sensing. - 2007. - Vol. 45, No. 3. - P. 554-565.

J1078. Olga Lopera. Filtering Soil Surface and Antenna Effects From GPR Data to Enhance Landmine Detection. / Olga Lopera, Evert C. Slob, Nada Milisavljevic, Sbastien Lambot. // IEEE Transactions on Geoscience and Remote Sensing. - 2007. - Vol. 45, No. 3. - P. 707-717.

J1079. Zhigang Su. Feature-Independent Aperture Evaluator for the Curvilinear SAR. / Zhigang Su, Yingning Peng, Xiutan Wang. // IEEE Geoscience and Remote Sensing Letters. - 2007. - Vol. 4, No. 2. - P. 191-195.

J1080. Wang K. Quartic-Phase Algorithm for Highly Squinted SAR Data Processing. / Wang K., Liu X. // IEEE Geoscience and Remote Sensing Letters. - 2007. - Vol. 4, No. 2. - P. 246-250.

J1081. Secord J. Tree Detection in Urban Regions Using Aerial Lidar and Image Data. / Secord J., Zakhor A. // IEEE Geoscience and Remote Sensing Letters. - 2007. - Vol. 4, No. 2. - P. 196-200.

J1082. Moser G. Unsupervised Change Detection From Multichannel SAR Images. / Moser G., Serpico S., Vernazza G. // IEEE Geoscience and Remote Sensing Letters. - 2007. - Vol. 4, No. 2. - P. 278-282.

J1083. Sanz-Marcos J. SABRINA: A SAR Bistatic Receiver for Interferometric Applications. / Sanz-Marcos J., Lopez-Dekker P., Mallorqui J.J., Aguasca A., Prats P. // IEEE Geoscience and Remote Sensing Letters. - 2007. - Vol. 4, No. 2. - P. 307-311.

J1084. Waske B. A Segment-Based Speckle Filter Using Multisensoral Remote Sensing Imagery. / Waske B., Braun M., Menz G. // IEEE Geoscience and Remote Sensing Letters. - 2007. - Vol. 4, No. 2. - P. 231-235.

J1085. Ferretti A. Submillimeter Accuracy of InSAR Time Series: Experimental Validation. / Ferretti A., Savio G., Barzaghi R., Borghi A., Musazzi S., Novali F., Prati C., Rocca F. // IEEE Transactions on Geoscience and Remote Sensing. - 2007. - Vol. 45, No. 5. - P. 1142-1153.

J1086. Inglada J. A New Statistical Similarity Measure for Change Detection in Multitemporal SAR Images and Its Extension to Multiscale Change Analysis. / Inglada J., Mercier G. // IEEE Transactions on Geoscience and Remote Sensing. - 2007. - Vol. 45, No. 5. - P. 1432-1445.

J1087. Axelsson S.R.J. Random Noise Radar/Sodar With Ultrawideband Waveforms. IEEE Transactions on Geoscience and Remote Sensing. - 2007. - Vol. 45, No. 5. - P. 1099-1114.

J1088. Zhiwei Yang. Reduced-Dimensional Processing for Ground Moving Target Detection in Distributed Space-Based Radar. / Zhiwei Yang, Guisheng Liao, Cao Zeng. // IEEE Geoscience and Remote Sensing Letters. - 2007. - Vol. 4, No. 2. - P. 256-259.

J1089. Yu Q. Coregistration Based on Three Parts of Two Complex Images and Contoured Windows for Synthetic Aperture Radar Interferometry. / Yu Q., Fu S., Mayer H., Liu X., Yang X. // IEEE Geoscience and Remote Sensing Letters. - 2007. - Vol. 4, No. 2. - P. 288-292.

J1090. Yackel J.J. Observations of Snow Water Equivalent Change on Landfast First-Year Sea Ice in Winter Using Synthetic Aperture Radar Data. / Yackel J.J., Barber D.G. // IEEE Transactions on Geoscience and Remote Sensing. - 2007. - Vol. 45, No. 4. - P. 1005-1015.

J1091. Ballester-Berman J.D. Coherence Loci for a Homogeneous Volume Over a Double-Bounce Ground Return. / Ballester-Berman J.D., Lopez-Sanchez J.M. // IEEE Geoscience and Remote Sensing Letters. - 2007. - Vol. 4, No. 2. - P. 317-321.

J1092. Moreno-Galbis P. Experimental Demonstration of the Corbella Equation for Aperture Synthesis Microwave Radiometry. / Moreno-Galbis P., Kainulainen J., Martin-Neira M. // IEEE Transactions on Geoscience and Remote Sensing. - 2007. - Vol. 45, No. 4. - P. 945-957.

J1093. Ruf C.S. GEOSAT Follow-On Water Vapor Radiometer: Performance With a Shared Active/Passive Antenna. / Ruf C.S., Warnock A.M. // IEEE Transactions on Geoscience and Remote Sensing. - 2007. - Vol. 45, No. 4. - P. 970-977.

J1094. Trouve E. Combining Airborne Photographs and Spaceborne SAR Data to Monitor Temperate Glaciers: Potentials and Limits. / Trouve E., Vasile G., Gay M., Bombrun L., Grussenmeyer P., Landes T., Nicolas J.-M., Bolon P., Petillot I., Julea A., Valet L., Chanussot J., Koehl M. // IEEE Transactions on Geoscience and Remote Sensing. - 2007. - Vol. 45, No. 4. - P. 905-924.

J1095. Gorgucci E. Attenuation and Differential Attenuation Correction of C-Band Radar Observations Using a Fully Self-Consistent Methodology. / Gorgucci E., Baldini L. // IEEE Geoscience and Remote Sensing Letters. - 2007. - Vol. 4, No. 2. - P. 326-330.

J1096. Meng D. A Novel Technique for Noise Reduction in InSAR Images. / Meng D., Sethu V., Ambikairajah E., Ge L. // IEEE Geoscience and Remote Sensing Letters. - 2007. - Vol. 4, No. 2. - P. 226-230.

J1097. Minghelli-Roman A. Bathymetric Estimation Using MERIS Images in Coastal Sea Waters. / Minghelli-Roman A., Polidori L., Mathieu S., Loubersac L., Cauneau F. // IEEE Geoscience and Remote Sensing Letters. - 2007. - Vol. 4, No. 2. - P. 274-277.

J1098. Luc K. A Novel Method for Removal of Emitter Noise in SAR Images. / Luc K., Jansen R.W., Kersten P.R., Fiedler R.L. // IEEE Geoscience and Remote Sensing Letters. - 2007. - Vol. 4, No. 2. - P. 265-268.

J1099. Kaasalainen S. Toward Hyperspectral Lidar: Measurement of Spectral Backscatter Intensity With a Supercontinuum Laser Source. / Kaasalainen S., Lindroos T., Hyyppa J. // IEEE Geoscience and Remote Sensing Letters. - 2007. - Vol. 4, No. 2. - P. 211-215.

J1100. Duk-jin Kim. Dependence of Waterline Mapping on Radar Frequency Used for SAR Images in Intertidal Areas. / Duk-jin Kim, Moon W.M., Sang-Eun Park, Ji-Eun Kim, Hyo-Sung Lee. // IEEE Geoscience and Remote Sensing Letters. - 2007. - Vol. 4, No. 2. - P. 269-273.

J1101. Tison C. A Fusion Scheme for Joint Retrieval of Urban Height Map and Classification From High-Resolution Interferometric SAR Images. / Tison C., Tupin F., Maitre H. // IEEE Transactions on Geoscience and Remote Sensing. - 2007. - Vol. 45, No. 2. - P. 496-505.

J1102. Cloude S.R. Dual-Baseline Coherence Tomography. IEEE Geoscience and Remote Sensing Letters. - 2007. - Vol. 4, No. 1. - P. 127-131.

J1103. Durden S.L. On the Use of Multiantenna Radars for Spaceborne Doppler Precipitation Measurements. / Durden S.L., Siqueira P.R., Tanelli S. // IEEE Geoscience and Remote Sensing Letters. - 2007. - Vol. 4, No. 1. - P. 181-183.

J1104. Bryant R. Measuring Surface Roughness Height to Parameterize Radar Backscatter Models for Retrieval of Surface Soil Moisture. / Bryant R., Moran M. S., Thoma D. P., Holifield Collins C. D., Skirvin S., Rahman M., Slocum K., Starks P., Bosch D., Gonzalez Dugo M. P. // IEEE Geoscience and Remote Sensing Letters. - 2007. - Vol. 4, No. 1. - P. 137-141.

J1105. Qiaoping Zhang. Accurate Centerline Detection and Line Width Estimation of Thick Lines Using the Radon Transform. / Qiaoping Zhang, Couloigner I. // IEEE Transactions on Image Processing. - 2007. - Vol. 16, No. 2. - P. 310-316.

J1106. Askne J. Selection of Forest Stands for Stem Volume Retrieval From Stable ERS Tandem InSAR Observations. / Askne J., Santoro M. // IEEE Geoscience and Remote Sensing Letters. - 2007. - Vol. 4, No. 1. - P. 46-50.

J1107. Grant M.S. Terrain Moisture Classification Using GPS Surface-Reflected Signals. / Grant M.S., Acton S.T., Katzberg S.J. // IEEE Geoscience and Remote Sensing Letters. - 2007. - Vol. 4, No. 1. - P. 41-45.

J1108. Min-Ho Ka. Effect of Look Angle on the Accuracy Performance of Fixed-Baseline Interferometric SAR. / Min-Ho Ka, Kononov A.A. // IEEE Geoscience and Remote Sensing Letters. - 2007. - Vol. 4, No. 1. - P. 65-69.

J1109. Liu H. Synergistic Fusion of Interferometric and Speckle-Tracking Methods for Deriving Surface Velocity From Interferometric SAR Data. / Liu H., Zhao Z., Jezek K. C. // IEEE Geoscience and Remote Sensing Letters. - 2007. - Vol. 4, No. 1. - P. 102-106.

J1110. Jimenez-Munoz J.C. Feasibility of Retrieving Land-Surface Temperature From ASTER TIR Bands Using Two-Channel Algorithms: A Case Study of Agricultural Areas. / Jimenez-Munoz J.C., Sobrino J.A. // IEEE Geoscience and Remote Sensing Letters. - 2007. - Vol. 4, No. 1. - P. 60-64.

J1111. Hofierka J. Spatial Interpolation of Elevation Data With Variable Density: A New Methodology to Derive Quality DEMs. / Hofierka J., Cebecauer T. // IEEE Geoscience and Remote Sensing Letters. - 2007. - Vol. 4, No. 1. - P. 117-121.

J1112. Ito S. Multiple-Scattering Formulation of Pulsed Beam Waves in Hydrometeors and Its Application to Millimeter-Wave Weather Radar. / Ito S., Kobayashi S., Oguchi T. // IEEE Geoscience and Remote Sensing Letters. - 2007. - Vol. 4, No. 1. - P. 13-17.

J1113. Grasmueck M. Integration of Ground-Penetrating Radar and Laser Position Sensors for Real-Time 3-D Data Fusion. / Grasmueck M., Viggiano D. A. // IEEE Transactions on Geoscience and Remote Sensing. - 2007. - Vol. 45, No. 1. - P. 130-137.

J1114. Nogues-Correig O. A GPS-Reflections Receiver That Computes Doppler/Delay Maps in Real Time. / Nogues-Correig O., Cardellach Gali E., Sanz Campderros J., Rius A. // IEEE Transactions on Geoscience and Remote Sensing. - 2007. - Vol. 45, No. 1. - P. 156-174.

J1115. Fischer C. Detection of Antipersonnel Mines by Using the Factorization Method on Multistatic Ground-Penetrating Radar Measurements. / Fischer C., Herschlein A., Younis M., Wiesbeck W. // IEEE Transactions on Geoscience and Remote Sensing. - 2007. - Vol. 45, No. 1. - P. 85-92.

J1116. Bhang K. J. Verification of the Vertical Error in C-Band SRTM DEM Using ICESat and Landsat-7, Otter Tail County, MN. / Bhang K. J., Schwartz F. W., Braun A. // IEEE Transactions on Geoscience and Remote Sensing. - 2007. - Vol. 45, No. 1. - P. 36-44.

J1117. Firoozabadi R. Subsurface Sensing of Buried Objects Under a Randomly Rough Surface Using Scattered Electromagnetic Field Data. / Firoozabadi R., Miller E. L., Rappaport C. M., Morgenthaler A. W. // IEEE Transactions on Geoscience and Remote Sensing. - 2007. - Vol. 45, No. 1. - P. 104-117.

J1118. Oveisgharan S. Estimating Snow Accumulation From InSAR Correlation Observations. / Oveisgharan S., Zebker H. A. // IEEE Transactions on Geoscience and Remote Sensing. - 2007. - Vol. 45, No. 1. - P. 10-20.

J1119. Suwa K. A Two-Dimensional Bandwidth Extrapolation Technique for Polarimetric Synthetic Aperture Radar Images. / Suwa K., Iwamoto M. // IEEE Transactions on Geoscience and Remote Sensing. - 2007. - Vol. 45, No. 1. - P. 45-54.

J1120. Touzi R. Target Scattering Decomposition in Terms of Roll-Invariant Target Parameters. IEEE Transactions on Geoscience and Remote Sensing. - 2007. - Vol. 45, No. 1. - P. 73-84.

J1121. Streich R. Accurate Imaging of Multicomponent GPR Data Based on Exact Radiation Patterns. / Streich R., Kruk J. V. D. // IEEE Transactions on Geoscience and Remote Sensing. - 2007. - Vol. 45, No. 1. - P. 93-103.

J1122. Romeiser R. Theoretical Evaluation of Several Possible Along-Track InSAR Modes of TerraSAR-X for Ocean Current Measurements. / Romeiser R., Runge H. // IEEE Transactions on Geoscience and Remote Sensing. - 2007. - Vol. 45, No. 1. - P. 21-35.

J1123. Savelyev T. G. Investigation of Time–Frequency Features for GPR Landmine Discrimination. / Savelyev T. G., van Kempen L., Sahli H., Sachs J., Sato M. // IEEE Transactions on Geoscience and Remote Sensing. - 2007. - Vol. 45, No. 1. - P. 118-129.

J1124. Lee W.-H. Optimizing the Area Under a Receiver Operating Characteristic Curve With Application to Landmine Detection. / Lee W.-H., Gader P. D., Wilson J. N. // IEEE Transactions on Geoscience and Remote Sensing. - 2007. - Vol. 45, No. 2. - P. 389-397.

J1125. Liao Y. Decision Fusion of Ground-Penetrating Radar and Metal Detector Algorithms—A Robust Approach. / Liao Y., Nolte L. W., Collins L. M. // IEEE Transactions on Geoscience and Remote Sensing. - 2007. - Vol. 45, No. 2. - P. 398-409.

J1126. Kuo C.-h. Electromagnetic Scattering From Multilayer Rough Surfaces With Arbitrary Dielectric Profiles for Remote Sensing of Subsurface Soil Moisture. / Kuo C.-h., Moghaddam M. // IEEE Transactions on Geoscience and Remote Sensing. - 2007. - Vol. 45, No. 2. - P. 349-366.

J1127. Cumming I. G. Adding Sensitivity to the MLBF Doppler Centroid Estimator. / Cumming I. G., Li S. // IEEE Transactions on Geoscience and Remote Sensing. - 2007. - Vol. 45, No. 2. - P. 279-292.

J1128. Ioannidou M. P. Depolarization, Scattering, and Attenuation of Circularly Polarized Radio Waves by Spherically Asymmetric Melting Ice Particles. / Ioannidou M. P., Chrissoulidis D. P. // IEEE Transactions on Geoscience and Remote Sensing. - 2007. - Vol. 45, No. 2. - P. 367-375.

J1129. Lopez-Martinez C. On the Extension of Multidimensional Speckle Noise Model From Single-Look to Multilook SAR Imagery. / Lopez-Martinez C., Pottier E. // IEEE Transactions on Geoscience and Remote Sensing. - 2007. - Vol. 45, No. 2. - P. 305-320.

J1130. Samsonov S. Application of DInSAR-GPS Optimization for Derivation of Fine-Scale Surface Motion Maps of Southern California. / Samsonov S., Tiampo K., Rundle J., Li Z. // IEEE Transactions on Geoscience and Remote Sensing. - 2007. - Vol. 45, No. 2. - P. 512-521.

J1131. Stephens P. J. Geometrical Variations of Gain Patterns. / Stephens P. J., Jones A. S. // IEEE Transactions on Geoscience and Remote Sensing. - 2007. - Vol. 45, No. 2. - P. 376-382.

J1132. Ruegg M. Vibration and Rotation in Millimeter-Wave SAR. / Ruegg M., Meier E., Nuesch D. // IEEE Transactions on Geoscience and Remote Sensing. - 2007. - Vol. 45, No. 2. - P. 293-304.

J1133. Migliaccio M. SAR Polarimetry to Observe Oil Spills. / Migliaccio M., Gambardella A., Tranfaglia M. // IEEE Transactions on Geoscience and Remote Sensing. - 2007. - Vol. 45, No. 2. - P. 506-511.

J1134. Rose C. R. Systems Engineering Analysis of a TRMM PR-Like Rainfall Retrieval Algorithm. / Rose C. R., Chandrasekar V. // IEEE Transactions on Geoscience and Remote Sensing. - 2007. - Vol. 45, No. 2. - P. 426-434.

J1135. Peters M.E. The Distribution and Classification of Bottom Crevasses From Radar Sounding of a Large Tabular Iceberg. / Peters M.E., Blankenship D.D., Smith D.E., Holt J.W., Kempf S.D. // IEEE Geoscience and Remote Sensing Letters. - 2007. - Vol. 4, No. 1. - P. 142-146.

J1136. Wenqin Wang. A Technique for Jamming Bi- and Multistatic SAR Systems. / Wenqin Wang, Jingye Cai. // IEEE Geoscience and Remote Sensing Letters. - 2007. - Vol. 4, No. 1. - P. 80-82.

J1137. Yew Lam Neo. A Two-Dimensional Spectrum for Bistatic SAR Processing Using Series Reversion. / Yew Lam Neo, Wong F., Cumming I.G. // IEEE Geoscience and Remote Sensing Letters. - 2007. - Vol. 4, No. 1. - P. 93-96.

J1138. Meincke P. Efficient Calculation of Born Scattering for Fixed-Offset Ground-Penetrating Radar Surveys. IEEE Geoscience and Remote Sensing Letters. - 2007. - Vol. 4, No. 1. - P. 88-92.

J1139. Morales C.A. Evaluation of Peak Current Polarity Retrieved by the ZEUS Long-Range Lightning Monitoring System. / Morales C.A., Anagnostou E.N., Williams E., Kriz J.S. // IEEE Geoscience and Remote Sensing Letters. - 2007. - Vol. 4, No. 1. - P. 32-36.

J1140. Qifeng Yu. An Adaptive Contoured Window Filter for Interferometric Synthetic Aperture Radar. / Qifeng Yu, Xia Yang, Sihua Fu, Xiaolin Liu, Xiangyi Sun. // IEEE Geoscience and Remote Sensing Letters. - 2007. - Vol. 4, No. 1. - P. 23-26.

J1141. Aly Z. Analysis of the Backscattering Coefficient of Salt-Affected Soils Using Modeling and RADARSAT-1 SAR Data. / Aly Z., Bonn F. J., Magagi R. // IEEE Transactions on Geoscience and Remote Sensing. - 2007. - Vol. 45, No. 2. - P. 332-341.

J1142. Brenner A. C. Precision and Accuracy of Satellite Radar and Laser Altimeter Data Over the Continental Ice Sheets. / Brenner A. C., DiMarzio J. P., Zwally H. J. // IEEE Transactions on Geoscience and Remote Sensing. - 2007. - Vol. 45, No. 2. - P. 321-331.

J1143. Qingping Zou. Wind-Vector Estimation for RADARSAT-1 SAR Images: Validation of Wind-Direction Estimates Based Upon Geometry Diversity. / Qingping Zou, Yijun He, Perrie W., Vachon P.W. // IEEE Geoscience and Remote Sensing Letters. - 2007. - Vol. 4, No. 1. - P. 176-180.

J1144. Zhou F. Eigensubspace-Based Filtering With Application in Narrow-Band Interference Suppression for SAR. / Zhou F., Wu R., Xing M., Bao Z. // IEEE Geoscience and Remote Sensing Letters. - 2007. - Vol. 4, No. 1. - P. 75-79.

J1145. Daiyin Zhu. A Keystone Transform Without Interpolation for SAR Ground Moving-Target Imaging. / Daiyin Zhu, Yong Li, Zhaoda Zhu. // IEEE Geoscience and Remote Sensing Letters. - 2007. - Vol. 4, No. 1. - P. 18-22.

J1146. Mega T. A Low-Power High-Resolution Broad-Band Radar Using a Pulse Compression Technique for Meteorological Application. / Mega T., Monden K., Ushio T., Okamoto K., Kawasaki Z.-I., Morimoto T. // IEEE Geoscience and Remote Sensing Letters. - 2007. - Vol. 4, No. 3. - P. 392-396.

J1147. Migliaccio M. Knab Sampling Window for InSAR Data Interpolation. / Migliaccio M., Nunziata F., Bruno F., Casu F. // IEEE Geoscience and Remote Sensing Letters. - 2007. - Vol. 4, No. 3. - P. 397-400.

J1148. Marmorino G.O. Ocean Mixed-Layer Depth and Current Variation Estimated From Imagery of Surfactant Streaks. / Marmorino G.O., Toporkov J.V., Smith G.B., Sletten M.A., Perkovic D., Frasier S., Judd K.P. // IEEE Geoscience and Remote Sensing Letters. - 2007. - Vol. 4, No. 3. - P. 364-367.

J1149. Jaebin Lee. Adjustment of Discrepancies Between LIDAR Data Strips Using Linear Features. / Jaebin Lee, Kiyun Yu, Yongil Kim, Habib A.F. // IEEE Geoscience and Remote Sensing Letters. - 2007. - Vol. 4, No. 3. - P. 475-479.

J1150. Luzi G. Monitoring of an Alpine Glacier by Means of Ground-Based SAR Interferometry. / Luzi G., Pieraccini M., Mecatti D., Noferini L., Macaluso G., Tamburini A., Atzeni C. // IEEE Geoscience and Remote Sensing Letters. - 2007. - Vol. 4, No. 3. - P. 495-499.

J1151. Nadarajah S. On the Distribution of the Estimated Coherence. IEEE Geoscience and Remote Sensing

Letters. - 2007. - Vol. 4, No. 3. - P. 368-371.

J1152. Selva J. Efficient Interpolation of SAR Images for Coregistration in SAR Interferometry. / Selva J., Lopez-Sanchez J.M. // IEEE Geoscience and Remote Sensing Letters. - 2007. - Vol. 4, No. 3. - P. 411-415.

J1153. Stathakis D. Feature Evolution for Classification of Remotely Sensed Data. / Stathakis D., Perakis K. // IEEE Geoscience and Remote Sensing Letters. - 2007. - Vol. 4, No. 3. - P. 354-358.

J1154. Prats P. Comparison of Topography- and Aperture-Dependent Motion Compensation Algorithms for Airborne SAR. / Prats P., Camara de Macedo K.A., Reigber A., Scheiber R., Mallorqui J.J. // IEEE Geoscience and Remote Sensing Letters. - 2007. - Vol. 4, No. 3. - P. 349-353.

J1155. Nico G. On the Existence of Coverage and Integration Time Regimes in Bistatic SAR Configurations. / Nico G., Tesauro M. // IEEE Geoscience and Remote Sensing Letters. - 2007. - Vol. 4, No. 3. - P. 426-430.

J1156. Praks J. Height Estimation of Boreal Forest: Interferometric Model-Based Inversion at L- and X-Band Versus HUTSCAT Profiling Scatterometer. / Praks J., Kugler F., Papathanassiou K.P., Hajnsek I., Hallikainen M. // IEEE Geoscience and Remote Sensing Letters. - 2007. - Vol. 4, No. 3. - P. 466-470.

J1157. Min-Ho Ka. Selection of Pulse Repetition Frequency in High-Precision Oceanographic Radar Altimeters. / Min-Ho Ka, Baskakov A.I. // IEEE Geoscience and Remote Sensing Letters. - 2007. - Vol. 4, No. 3. - P. 345-348.

J1158. Feng Xu. Automatic Reconstruction of Building Objects From Multiaspect Meter-Resolution SAR Images. / Feng Xu, Ya-Qiu Jin. // IEEE Transactions on Geoscience and Remote Sensing. - 2007. - Vol. 45, No. 7. - P. 2336-2353.

J1159. Amitai E. Comparison of Deep Underwater Measurements and Radar Observations of Rainfall. / Amitai E., Nystuen J.A., Anagnostou E.N., Anagnostou M.N. // IEEE Geoscience and Remote Sensing Letters. - 2007. - Vol. 4, No. 3. - P. 406-410.

J1160. Torrione P. Texture Features for Antitank Landmine Detection Using Ground Penetrating Radar. / Torrione P., Collins L.M. // IEEE Transactions on Geoscience and Remote Sensing. - 2007. - Vol. 45, No. 7. - P. 2374-2382.

J1161. Mingsheng Liao. Reconstruction of DEMs From ERS-1/2 Tandem Data in Mountainous Area Facilitated by SRTM Data. / Mingsheng Liao, Teng Wang, Lijun Lu, Wenjun Zhouzhou, Deren Li. // IEEE Transactions on Geoscience and Remote Sensing. - 2007. - Vol. 45, No. 7. - P. 2325-2335.

J1162. Montopoli M. Maximum-Likelihood Retrieval of Modeled Convective Rainfall Patterns from Midlatitude C-Band Weather Radar Data. / Montopoli M., Marzano F.S. // IEEE Transactions on Geoscience and Remote Sensing. - 2007. - Vol. 45, No. 7. - P. 2403-2416.

J1163. Bhattacharya C. A Discrete Wavelet Transform Approach to Multiresolution Complex SAR Image Generation. / Bhattacharya C., Mahapatra P.R. // IEEE Geoscience and Remote Sensing Letters. - 2007. - Vol. 4, No. 3. - P. 416-420.

J1164. Crow W.T. Continental-Scale Evaluation of Remotely Sensed Soil Moisture Products. / Crow W.T., Xiwu Zhan. // IEEE Geoscience and Remote Sensing Letters. - 2007. - Vol. 4, No. 3. - P. 451-455.

J1165. Zhi-Hong Jiang. A Chirp Transform Algorithm for Processing Squint Mode FMCW SAR Data. / Zhi-Hong Jiang, Kan Huang-Fu, Jian-Wei Wan. // IEEE Geoscience and Remote Sensing Letters. - 2007. - Vol. 4, No. 3. - P. 377-381.

J1166. Chiu J.C. Cloud Optical Depth Retrievals From Solar Background "Signals" of Micropulse Lidars. / Chiu J.C., Marshak A., Wiscombe W.J., Valencia S., Welton E.J. // IEEE Geoscience and Remote Sensing Letters. - 2007. - Vol. 4, No. 3. - P. 456-460.

J1167. Chander G. Revised Landsat-5 Thematic Mapper Radiometric Calibration. / Chander G., Markham B.L., Barsi J.A. // IEEE Geoscience and Remote Sensing Letters. - 2007. - Vol. 4, No. 3. - P. 490-494.

J1168. Jinsong Chen. Application of ENVISAT ASAR Data in Mapping Rice Crop Growth in Southern China. /

Jinsong Chen, Hui Lin, Zhiyuan Pei. // IEEE Geoscience and Remote Sensing Letters. - 2007. - Vol. 4, No. 3. - P. 431-435.

J1169. Moghaddam M. Microwave Observatory of Subcanopy and Subsurface (MOSS): A Mission Concept for Global Deep Soil Moisture Observations. / Moghaddam M., Rahmat-Samii Y., Rodriguez E., Entekhabi D., Hoffman J., Moller D., Pierce L.E., Saatchi S., Thomson M. // IEEE Transactions on Geoscience and Remote Sensing. - 2007. - Vol. 45, No. 8. - P. 2630-2643.

J1170. Oden C.P. Improving GPR Image Resolution in Lossy Ground Using Dispersive Migration. / Oden C.P., Powers M.H., Wright D.L., Olhoeft G.R. // IEEE Transactions on Geoscience and Remote Sensing. - 2007. - Vol. 45, No. 8. - P. 2492-2500.

J1171. Masuyama S. Walled LTSA Array for Rapid, High Spatial Resolution, and Phase-Sensitive Imaging to Visualize Plastic Landmines. / Masuyama S., Hirose A. // IEEE Transactions on Geoscience and Remote Sensing. - 2007. - Vol. 45, No. 8. - P. 2536-2543.

J1172. Le Bastard C. Thin-Pavement Thickness Estimation Using GPR With High-Resolution and Superresolution Methods. / Le Bastard C., Baltazart V., Yide Wang, Saillard J. // IEEE Transactions on Geoscience and Remote Sensing. - 2007. - Vol. 45, No. 8. - P. 2511-2519.

J1173. Lanbo Liu. Wave Interferometry Applied to Borehole Radar: Virtual Multioffset Reflection Profiling. / Lanbo Liu, Kuang He. // IEEE Transactions on Geoscience and Remote Sensing. - 2007. - Vol. 45, No. 8. - P. 2554-2559.

J1174. Sang-Eun Park. Unsupervised Classification of Scattering Mechanisms in Polarimetric SAR Data Using Fuzzy Logic in Entropy and Alpha Plane. / Sang-Eun Park, Moon W.M. // IEEE Transactions on Geoscience and Remote Sensing. - 2007. - Vol. 45, No. 8. - P. 2652-2664.

J1175. Slob E. GPR Without a Source: Cross-Correlation and Cross-Convolution Methods. / Slob E., Wapenaar K. // IEEE Transactions on Geoscience and Remote Sensing. - 2007. - Vol. 45, No. 8. - P. 2501-2510.

J1176. Soldovieri F. Localization of the Interfaces of a Slab Hidden Behind a Wall. / Soldovieri F., Solimene R., Brancaccio A., Pierri R. // IEEE Transactions on Geoscience and Remote Sensing. - 2007. - Vol. 45, No. 8. - P. 2471-2482.

J1177. Sato M. A Novel Directional Borehole Radar System Using Optical Electric Field Sensors. / Sato M., Takayama T. // IEEE Transactions on Geoscience and Remote Sensing. - 2007. - Vol. 45, No. 8. - P. 2529-2535.

J1178. Rappaport C.M. Accurate Determination of Underground GPR Wavefront and B-Scan Shape From Above-Ground Point Sources. IEEE Transactions on Geoscience and Remote Sensing. - 2007. - Vol. 45, No. 8. - P. 2429-2434.

J1179. Santoro M. Observations, Modeling, and Applications of ERS-ENVISAT Coherence Over Land Surfaces. / Santoro M., Askne J.I.H., Wegmiiller U., Werner C.L. // IEEE Transactions on Geoscience and Remote Sensing. - 2007. - Vol. 45, No. 8. - P. 2600-2611.

J1180. Chien-Ping Kao. Measurement of Layer Thickness and Permittivity Using a New Multilayer Model From GPR Data. / Chien-Ping Kao, Jing Li, Ying Wang, Huichun Xing, Ce Richard Liu. // IEEE Transactions on Geoscience and Remote Sensing. - 2007. - Vol. 45, No. 8. - P. 2463-2470.

J1181. Jian-guo Zhao. Consistency Analysis of Subsurface Fracture Characterization Using Different Polarimetry Techniques by a Borehole Radar. / Jian-guo Zhao, Sato M. // IEEE Geoscience and Remote Sensing Letters. - 2007. - Vol. 4, No. 3. - P. 359-363.

J1182. Min Zhu. High-Resolution Forecast Models of Water Vapor Over Mountains: Comparison With MERIS and Meteosat Data. / Min Zhu, Wadge G., Holley R.J., James I.N., Clark P.A., Changgui Wang, Woodage M.J. // IEEE Geoscience and Remote Sensing Letters. - 2007. - Vol. 4, No. 3. - P. 401-405.

J1183. Yeary M. Tornadic Time-Series Detection Using Eigen Analysis and a Machine Intelligence-Based Approach. / Yeary M., Nemati S., Yu T.-Y., Wang Y. // IEEE Geoscience and Remote Sensing Letters. - 2007. -

Vol. 4, No. 3. - P. 335-339.

J1184. Qi Wang. A New Algorithm for Sparse Aperture Interpolation. / Qi Wang, Renbiao Wu, Mengdao Xing, Zheng Bao. // IEEE Geoscience and Remote Sensing Letters. - 2007. - Vol. 4, No. 3. - P. 480-484.

J1185. Weizu Xiong. Polarimetric Calibration Using a Genetic Algorithm. IEEE Geoscience and Remote Sensing Letters. - 2007. - Vol. 4, No. 3. - P. 421-425.

J1186. Adhikari N.B. Rain Retrieval Performance of a Dual-Frequency Precipitation Radar Technique With Differential-Attenuation Constraint. / Adhikari N.B., Iguchi T., Seto S., Takahashi N. // IEEE Transactions on Geoscience and Remote Sensing. - 2007. - Vol. 45, No. 8. - P. 2612-2618.

J1187. Freeman A. Fitting a Two-Component Scattering Model to Polarimetric SAR Data From Forests. IEEE Transactions on Geoscience and Remote Sensing. - 2007. - Vol. 45, No. 8. - P. 2583-2592.

J1188. Heliere F. Radio Echo Sounding of Pine Island Glacier, West Antarctica: Aperture Synthesis Processing and Analysis of Feasibility From Space. / Heliere F., Chung-Chi Lin, Corr H., Vaughan D. // IEEE Transactions on Geoscience and Remote Sensing. - 2007. - Vol. 45, No. 8. - P. 2573-2582.

J1189. Chen C.-C. Foreword to the Special Issue on Subsurface Sensing Using Ground-Penetrating Radar (GPR). / Chen C.-C., Johnson J. T., Sato M., Yarovoy A. G. // IEEE Transactions on Geoscience and Remote Sensing. - 2007. - Vol. 45, No. 8. - P. 2419-2421.

J1190. Counts T. Multistatic Ground-Penetrating Radar Experiments. / Counts T., Gurbuz A.C., Scott W.R., McClellan J.H., Kangwook Kim. // IEEE Transactions on Geoscience and Remote Sensing. - 2007. - Vol. 45, No. 8. - P. 2544-2553.

J1191. Ebihara S. MoM Analysis of Dipole Antennas in Crosshole Borehole Radar and Field Experiments. / Ebihara S., Hashimoto Y. // IEEE Transactions on Geoscience and Remote Sensing. - 2007. - Vol. 45, No. 8. - P. 2435-2450.

J1192. Bovolo F. A Split-Based Approach to Unsupervised Change Detection in Large-Size Multitemporal Images: Application to Tsunami-Damage Assessment. / Bovolo F., Bruzzone L. // IEEE Transactions on Geoscience and Remote Sensing. - 2007. - Vol. 45, No. 6. - P. 1658-1670.

J1193. Chaabane F. A Multitemporal Method for Correction of Tropospheric Effects in Differential SAR Interferometry: Application to the Gulf of Corinth Earthquake. / Chaabane F., Avallone A., Tupin F., Briole P., Maitre H. // IEEE Transactions on Geoscience and Remote Sensing. - 2007. - Vol. 45, No. 6. - P. 1605-1615.

J1194. Di Martino G. A Novel Approach for Disaster Monitoring: Fractal Models and Tools. / Di Martino G., Iodice A., Riccio D., Ruello G. // IEEE Transactions on Geoscience and Remote Sensing. - 2007. - Vol. 45, No. 6. - P. 1559-1570.

J1195. Yanming Xiao. A Portable Noncontact Heartbeat and Respiration Monitoring System Using 5-GHz Radar. / Yanming Xiao, Changzhi Li, Jenshan Lin. // IEEE Sensors Journal. - 2007. - Vol. 7, No. 7. - P. 1042-1043.

J1196. Zetik R. UWB short-range radar sensing-The architecture of a baseband, pseudo-noise UWB radar sensor. / Zetik R., Sachs J., Thoma R.S. // IEEE Instrumentation & Measurement Magazine. - 2007. - Vol. 10, No. 2. - P. 39-45.

J1197. Asante K.O. Developing a Flood Monitoring System From Remotely Sensed Data for the Limpopo Basin. / Asante K.O., Macuacua R.D., Artan G.A., Lietzow R.W., Verdin J.P. // IEEE Transactions on Geoscience and Remote Sensing. - 2007. - Vol. 45, No. 6. - P. 1709-1714.

J1198. Gamba P. Rapid Damage Detection in the Bam Area Using Multitemporal SAR and Exploiting Ancillary Data. / Gamba P., Dell'Acqua F., Trianni G. // IEEE Transactions on Geoscience and Remote Sensing. - 2007. - Vol. 45, No. 6. - P. 1582-1589.

J1199. Saatchi S. Estimation of Forest Fuel Load From Radar Remote Sensing. / Saatchi S., Halligan K., Despain D.G., Crabtree R.L. // IEEE Transactions on Geoscience and Remote Sensing. - 2007. - Vol. 45, No. 6. - P. 1726-1740.

J1200. Schumann G. High-Resolution 3-D Flood Information From Radar Imagery for Flood Hazard Management. / Schumann G., Hostache R., Puech C., Hoffmann L., Matgen P., Pappenberger F., Pfister L. // IEEE Transactions on Geoscience and Remote Sensing. - 2007. - Vol. 45, No. 6. - P. 1715-1725.

J1201. Sha W. Comments on “Water Quality Retrievals From Combined Landsat TM Data and ERS-2 SAR Data in the Gulf of Finland”. IEEE Transactions on Geoscience and Remote Sensing. - 2007. - Vol. 45, No. 6. - P. 1896-1897.

J1202. He L. Adaptive Multimodality Sensing of Landmines. / He L., Shihao Ji, Scott W.R., Carin L. // IEEE Transactions on Geoscience and Remote Sensing. - 2007. - Vol. 45, No. 6. - P. 1756-1774.

J1203. Kouchi K. Characteristics of Tsunami-Affected Areas in Moderate-Resolution Satellite Images. / Kouchi K., Yamazaki F. // IEEE Transactions on Geoscience and Remote Sensing. - 2007. - Vol. 45, No. 6. - P. 1650-1657.

J1204. Nashashibi A.Y. MMW Polarimetric Radar Bistatic Scattering From a Random Surface. / Nashashibi A.Y., Ulaby F.T. // IEEE Transactions on Geoscience and Remote Sensing. - 2007. - Vol. 45, No. 6. - P. 1743-1755.

J1205. Palubinskas G. Measurement of radar signatures of passenger cars: airborne SAR multi-frequency and polarimetric experiment. / Palubinskas G., Runge H., Reinartz P. // IET Radar, Sonar & Navigation. - 2007. - Vol. 1, No. 2. - P. 164-169.

J1206. Makynen M.P. Comparisons Between SAR Backscattering Coefficient and Results of a Thermodynamic Snow/Ice Model for the Baltic Sea Land-Fast Sea Ice. / Makynen M.P., Bin Cheng, Simila M.H., Vihma T., Hallikainen M.T. // IEEE Transactions on Geoscience and Remote Sensing. - 2007. - Vol. 45, No. 5. - P. 1131-1141.

J1207. Pe'eri S. Increasing the Existence of Very Shallow-Water LIDAR Measurements Using the Red-Channel Waveforms. / Pe'eri S., Philpot W. // IEEE Transactions on Geoscience and Remote Sensing. - 2007. - Vol. 45, No. 5. - P. 1217-1223.

J1208. Pettinelli E. Electromagnetic Propagation of GPR Signals in Martian Subsurface Scenarios Including Material Losses and Scattering. / Pettinelli E., Burghignoli P., Pisani A.R., Ticconi F., Galli A., Vannaroni G., Bella F. // IEEE Transactions on Geoscience and Remote Sensing. - 2007. - Vol. 45, No. 5. - P. 1271-1281.

J1209. Langley K. Use of C-Band Ground Penetrating Radar to Determine Backscatter Sources Within Glaciers. / Langley K., Hamran S.-E., Hogda K.A., Storvold R., Brandt O., Hagen J.O., Kohler J. // IEEE Transactions on Geoscience and Remote Sensing. - 2007. - Vol. 45, No. 5. - P. 1236-1246.

J1210. Le Chenadec G. Angular Dependence of -Distributed Sonar Data. / Le Chenadec G., Boucher J.-M., Lurton X. // IEEE Transactions on Geoscience and Remote Sensing. - 2007. - Vol. 45, No. 5. - P. 1224-1235.

J1211. Lianlin Li. SAR Imaging Degradation by Ionospheric Irregularities Based on TFTPCF Analysis. / Lianlin Li, Fang Li. // IEEE Transactions on Geoscience and Remote Sensing. - 2007. - Vol. 45, No. 5. - P. 1123-1130.

J1212. Ren-Yuan Qi. Analysis of the Effects of Faraday Rotation on Spaceborne Polarimetric SAR Observations at -Band. / Ren-Yuan Qi, Ya-Qiu Jin. // IEEE Transactions on Geoscience and Remote Sensing. - 2007. - Vol. 45, No. 5. - P. 1115-1122.

J1213. Toporkov J.V. Statistical Properties of Low-Grazing Range-Resolved Sea Surface Backscatter Generated Through Two-Dimensional Direct Numerical Simulations. / Toporkov J.V., Sletten M.A. // IEEE Transactions on Geoscience and Remote Sensing. - 2007. - Vol. 45, No. 5. - P. 1181-1197.

J1214. Verhoest N.E.C. A Takagi–Sugeno Fuzzy Rule-Based Model for Soil Moisture Retrieval From SAR Under Soil Roughness Uncertainty. / Verhoest N.E.C., Bernard De Baets, Vernieuwe H. // IEEE Transactions on Geoscience and Remote Sensing. - 2007. - Vol. 45, No. 5. - P. 1351-1360.

J1215. Joshi S. **THIS ARTICLE HAS BEEN RETRACTED DUE TO A VIOLATION OF IET PUBLICATION PRINCIPLES** Specular and diffuse measurements of multipath from various terrain surfaces at 35 GHz. / Joshi S., Sancheti S., Goyal A. // IET Microwaves, Antennas & Propagation. - 2007. - Vol. 1, No. 2. - P. 496-500.

J1216. Rowland C.S. Data Fusion for Reconstruction of a DTM, Under a Woodland Canopy, From Airborne L-band InSAR. / Rowland C.S., Balzter H. // IEEE Transactions on Geoscience and Remote Sensing. - 2007. - Vol. 45, No. 5. - P. 1154-1163.

J1217. Stephen H. Spatial and Temporal Behavior of Microwave Backscatter Directional Modulation Over the Saharan Ergs. / Stephen H., Long D.G. // IEEE Transactions on Geoscience and Remote Sensing. - 2007. - Vol. 45, No. 5. - P. 1164-1173.

J1218. Tagawa T. Suppression of Surface Clutter Interference With Precipitation Measurements by Spaceborne Precipitation Radar. / Tagawa T., Hanado H., Okamoto K., Kozu T. // IEEE Transactions on Geoscience and Remote Sensing. - 2007. - Vol. 45, No. 5. - P. 1324-1331.

J1219. Tralli D.M. Conceptual Case for Assimilating Interferometric Synthetic Aperture Radar Data Into the HAZUS-MH Earthquake Module. / Tralli D.M., Blom R.G., Fielding E.J., Donnellan A., Evans D.L. // IEEE Transactions on Geoscience and Remote Sensing. - 2007. - Vol. 45, No. 6. - P. 1595-1604.

J1220. Dall J. InSAR Elevation Bias Caused by Penetration Into Uniform Volumes. IEEE Transactions on Geoscience and Remote Sensing. - 2007. - Vol. 45, No. 7. - P. 2319-2324.

J1221. Colliander A. Sensitivity of Airborne 36.5-GHz Polarimetric Radiometer's Wind-Speed Measurement to Incidence Angle. / Colliander A., Lahtinen J., Tauriainen S., Pihlflyckt J., Lemmetyinen J., Hallikainen M.T. // IEEE Transactions on Geoscience and Remote Sensing. - 2007. - Vol. 45, No. 7. - P. 2122-2129.

J1222. Baup F. Radar Signatures of Sahelian Surfaces in Mali Using ENVISAT-ASAR Data. / Baup F., Mougin E., Hiernaux P., Lopes A., De Rosnay P., Chenerie I. // IEEE Transactions on Geoscience and Remote Sensing. - 2007. - Vol. 45, No. 7. - P. 2354-2363.

J1223. de Lange R. Improvement of Satellite Radar Feature Tracking for Ice Velocity Derivation by Spatial Frequency Filtering. / de Lange R., Luckman A., Murray T. // IEEE Transactions on Geoscience and Remote Sensing. - 2007. - Vol. 45, No. 7. - P. 2309-2318.

J1224. Kubota T. Global Precipitation Map Using Satellite-Borne Microwave Radiometers by the GSMaP Project: Production and Validation. / Kubota T., Shige S., Hashizume H., Aonashi K., Takahashi N., Seto S., Takayabu Y.N., Ushio T., Nakagawa K., Iwanami K., Kachi M., Okamoto K. // IEEE Transactions on Geoscience and Remote Sensing. - 2007. - Vol. 45, No. 7. - P. 2259-2275.

J1225. Dinnat E.P. Effects of the Antenna Aperture on Remote Sensing of Sea Surface Salinity at L-Band. / Dinnat E.P., Le Vine D.M. // IEEE Transactions on Geoscience and Remote Sensing. - 2007. - Vol. 45, No. 7. - P. 2051-2060.

J1226. De Roo R.D. Sensitivity of the Kurtosis Statistic as a Detector of Pulsed Sinusoidal RFI. / De Roo R.D., Misra S.., Ruf C.S. // IEEE Transactions on Geoscience and Remote Sensing. - 2007. - Vol. 45, No. 7. - P. 1938-1946.

J1227. Simpson J.J. A Review of Progress in FDTD Maxwell's Equations Modeling of Impulsive Subionospheric Propagation Below 300 kHz. / Simpson J.J., Taflove A. // IEEE Transactions on Antennas and Propagation. - 2007. - Vol. 55, No. 6. - P. 1582-1590.

J1228. Zheng-Wen Xu. Solution for the Fourth Moment Equation of Waves in Random Continuum Under Strong Fluctuations: General Theory and Plane Wave Solution. / Zheng-Wen Xu, Jian Wu, Zhen-Sen Wu, Qiang Li. // IEEE Transactions on Antennas and Propagation. - 2007. - Vol. 55, No. 6. - P. 1613-1621.

J1229. {no data available}. R. Keith Raney Wins the 2007 IEEE Dennis J. Picard Medal for Radar Technologies and Applications. IEEE Antennas and Propagation Magazine. - 2007. - Vol. 49, No. 1. - P. 190-191.

J1230. Afzal R.S. The Geoscience Laser Altimeter System (GLAS) Laser Transmitter. / Afzal R.S., Yu A.W., Dallas J.L., Melak A., Lukemire A.T.L., Ramos-Izqueirdo L., Mamakos W. // IEEE Journal of Selected Topics in Quantum Electronics. - 2007. - Vol. 13, No. 3. - P. 511-536.

J1231. Prasad N.S. Recent Progress in the Development of Neodymium-Doped Ceramic Yttria. / Prasad N.S., Edwards W.C., Trivedi S.B., Kutcher S.W., Chen-Chia Wang, Joo-Soo Kim, Hommerich U., Shukla V., Sadangi

R., Kear B.H. // IEEE Journal of Selected Topics in Quantum Electronics. - 2007. - Vol. 13, No. 3. - P. 831-837.

J1232. Arciniegas G.A. Coherence- and Amplitude-Based Analysis of Seismogenic Damage in Bam, Iran, Using ENVISAT ASAR Data. / Arciniegas G.A., Bijker W., Kerle N., Tolpekin V.A. // IEEE Transactions on Geoscience and Remote Sensing. - 2007. - Vol. 45, No. 6. - P. 1571-1581.

J1233. Armstrong D.J. All Solid-State High-Efficiency Tunable UV Source for Airborne or Satellite-Based Ozone DIAL Systems. / Armstrong D.J., Smith A.V. // IEEE Journal of Selected Topics in Quantum Electronics. - 2007. - Vol. 13, No. 3. - P. 721-731.